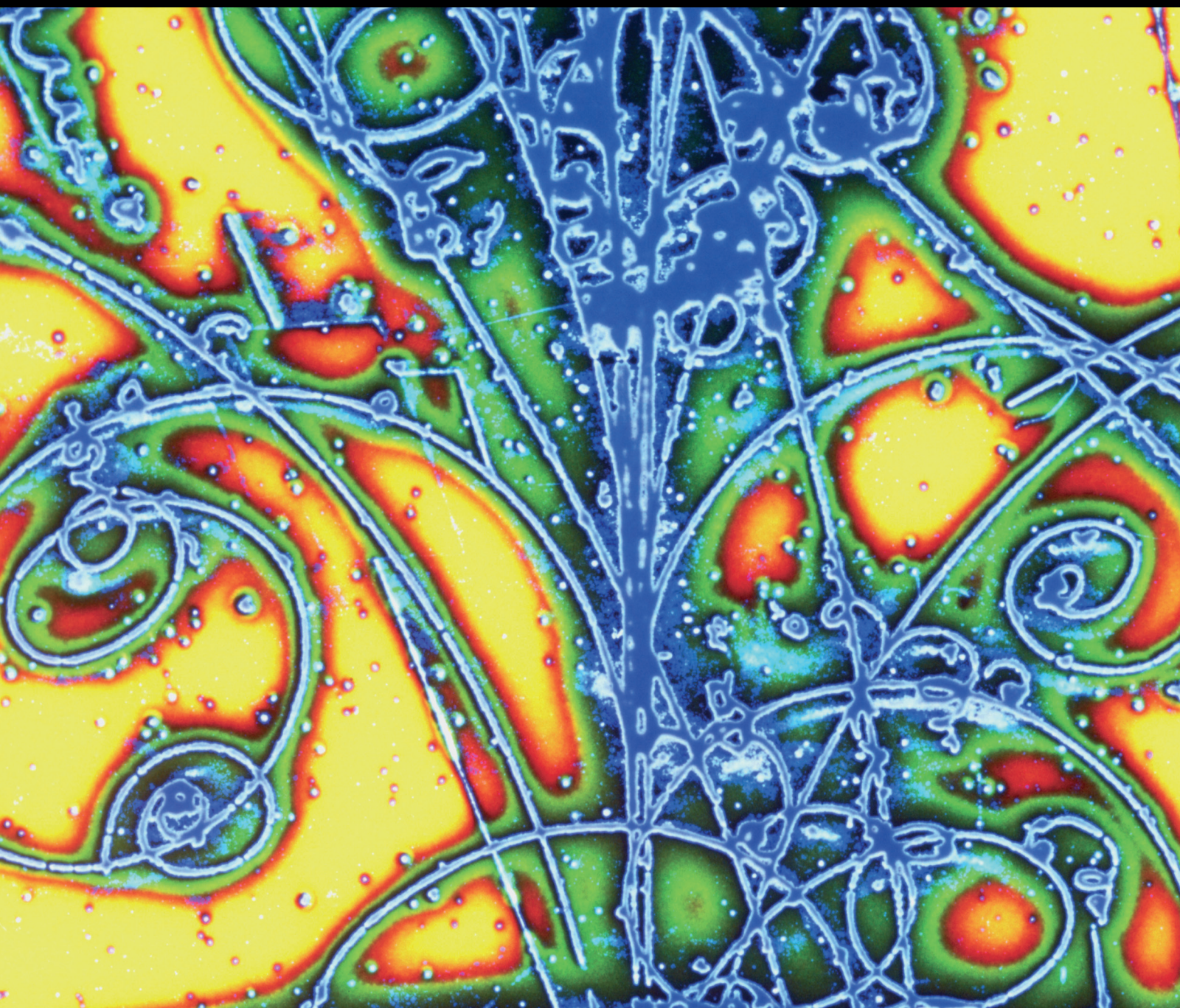


Advances in High Energy Physics

Analytical Methods for High Energy Physics

Lead Guest Editor: Saber Zarrinkamar

Guest Editors: Andrzej Okniński and Chun-Sheng Jia






Analytical Methods for High Energy Physics

Advances in High Energy Physics

Analytical Methods for High Energy Physics

Lead Guest Editor: Saber Zarrinkamar

Guest Editors: Andrzej Okniński and Chun-Sheng Jia



Copyright © 2019 Hindawi. All rights reserved.

This is a special issue published in “Advances in High Energy Physics.” All articles are open access articles distributed under the Creative Commons Attribution License, which permits unrestricted use, distribution, and reproduction in any medium, provided the original work is properly cited.

Editorial Board

Antonio J. Accioly, Brazil
Giovanni Amelino-Camelia, Italy
Luis A. Anchordoqui, USA
Michele Arzano, Italy
T. Asselmeyer-Maluga, Germany
Alessandro Baldini, Italy
Marco Battaglia, Switzerland
Lorenzo Bianchini, Switzerland
Roelof Bijker, Mexico
Burak Bilki, USA
Rong-Gen Cai, China
Anna Cimmino, France
Osvaldo Civitarese, Argentina
Andrea Coccaro, Italy
Shi-Hai Dong, Mexico
Lorenzo Fortunato, Italy
Mariana Frank, Canada
Ricardo G. Felipe, Portugal

Chao-Qiang Geng, Taiwan
Philippe Gras, France
Xiaochun He, USA
Luis Herrera, Spain
Filipe R. Joaquim, Portugal
Aurelio Juste, Spain
Theocharis Kosmas, Greece
Ming Liu, USA
Enrico Lunghi, USA
Salvatore Mignemi, Italy
Omar G. Miranda, Mexico
Grégory Moreau, France
Piero Nicolini, Germany
Carlos Pajares, Spain
Sergio Palomares-Ruiz, Spain
Giovanni Pauletta, Italy
Yvonne Peters, UK
Anastasios Petkou, Greece

Alexey A. Petrov, USA
Thomas Rössler, Sweden
Diego Saez-Chillon Gomez, Spain
Takao Sakaguchi, USA
Juan José Sanz-Cillero, Spain
Edward Sarkisyan-Grinbaum, USA
Sally Seidel, USA
George Siopsis, USA
Luca Stanco, Italy
Jouni Suhonen, Finland
Mariam Tórtola, Spain
Smarajit Triambak, South Africa
Jose M. Udías, Spain
Elias C. Vagenas, Kuwait
Sunny Vagnozzi, Sweden
Yau W. Wah, USA

Contents

Analytical Methods for High Energy Physics

Saber Zarrinkamar , Andrzej Okniński , and Chun-Sheng Jia 

Editorial (2 pages), Article ID 2758906, Volume 2019 (2019)

Double Charmonium Productions in Electron-Positron Annihilation Using Bethe-Salpeter Approach

Hluf Negash  and Shashank Bhatnagar 



Research Article (6 pages), Article ID 4029356, Volume 2019 (2019)

The Third Five-Parametric Hypergeometric Quantum-Mechanical Potential

T. A. Ishkhanyan and A. M. Ishkhanyan 



Research Article (8 pages), Article ID 2769597, Volume 2018 (2019)

Exact Solutions of the Razavy Cosine Type Potential

Shishan Dong , Qian Dong, Guo-Hua Sun, S. Femmam, and Shi-Hai Dong 

Research Article (5 pages), Article ID 5824271, Volume 2018 (2019)

Semiexact Solutions of the Razavy Potential

Qian Dong, F. A. Serrano, Guo-Hua Sun, Jian Jing , and Shi-Hai Dong 

Research Article (7 pages), Article ID 9105825, Volume 2018 (2019)

A New Model for Calculating the Ground and Excited States Masses Spectra of Doubly Heavy Ξ Baryons

Neda Mohajery, Nasrin Salehi , and Hassan Hassanabadi

Research Article (11 pages), Article ID 1326438, Volume 2018 (2019)

Heun Functions and Some of Their Applications in Physics

M. Hortaçsu 

Review Article (14 pages), Article ID 8621573, Volume 2018 (2019)

Dirac Equation in the Presence of Hartmann and Ring-Shaped Oscillator Potentials

Zahra Bakhshi 

Research Article (9 pages), Article ID 1940925, Volume 2018 (2019)

Heavy-Light Mesons in the Nonrelativistic Quark Model Using Laplace Transformation Method

M. Abu-Shady  and E. M. Khokha

Research Article (12 pages), Article ID 7032041, Volume 2018 (2019)

Bottomonium Suppression in Nucleus-Nucleus Collisions Using Effective Fugacity Quasi-Particle Model

Indrani Nilima and Vineet Kumar Agotiya 

Research Article (12 pages), Article ID 8965413, Volume 2018 (2019)

New Possibilities of Hybrid Texture of Neutrino Mass Matrix

Madan Singh 

Research Article (24 pages), Article ID 1056472, Volume 2018 (2019)

Expansions of the Solutions of the General Heun Equation Governed by Two-Term Recurrence Relations for Coefficients

T. A. Ishkhanyan, T. A. Shahverdyan, and A. M. Ishkhanyan 
Research Article (9 pages), Article ID 4263678, Volume 2018 (2019)

Integrable and Superintegrable Systems with Higher Order Integrals of Motion: Master Function Formalism

Z. Alizadeh and H. Panahi 
Research Article (7 pages), Article ID 5647148, Volume 2018 (2019)


Heun Functions Describing Bosons and Fermions on Melvin's Spacetime

Marina-Aura Dariescu  and Ciprian Dariescu
Research Article (7 pages), Article ID 1953586, Volume 2018 (2019)

Nonrelativistic Arbitrary l -States of Quarkonium through Asymptotic Iteration Method

Hakan Ciftci  and Hasan Fatih Kisoglu 
Research Article (7 pages), Article ID 4549705, Volume 2018 (2019)

Solutions of the D -Dimensional Schrödinger Equation with the Hyperbolic Pöschl-Teller Potential plus Modified Ring-Shaped Term

Ibsal A. Assi, Akpan N. Ikot , and E. O. Chukwuocha
Research Article (9 pages), Article ID 4536543, Volume 2018 (2019)

Spinors and Rodrigues Representations Associated with Orthogonal Polynomials

Zahra Bakhshi 
Research Article (8 pages), Article ID 6405784, Volume 2018 (2019)

Energy Dependence of Particle Ratios in High Energy Nucleus-Nucleus Collisions: A USTFM Approach

Inam-ul Bashir, Rameez Ahmad Parra , Hamid Nanda, and Saeed Uddin
Research Article (9 pages), Article ID 9285759, Volume 2018 (2019)

Hermitian–Non-Hermitian Interfaces in Quantum Theory

Miloslav Znojil 
Research Article (12 pages), Article ID 7906536, Volume 2018 (2019)

The Visualization of the Space Probability Distribution for a Particle Moving in a Double Ring-Shaped Coulomb Potential

Yuan You , Fa-Lin Lu, Dong-Sheng Sun, Chang-Yuan Chen , and Shi-Hai Dong 
Research Article (20 pages), Article ID 8307486, Volume 2018 (2019)

The Texture One-Zero Neutrino Mass Matrix with Vanishing Trace

Madan Singh 
Research Article (13 pages), Article ID 2863184, Volume 2018 (2019)

Study of Rare Semileptonic $B_c^+ \rightarrow D^+ \nu \bar{\nu}$ Decay in the Light-Cone Quark Model

Nisha Dhiman and Harleen Dahiya 
Research Article (7 pages), Article ID 2943406, Volume 2018 (2019)

Standard Model Effective Potential from Trace Anomalies

Renata Jora 
Research Article (8 pages), Article ID 5294394, Volume 2018 (2019)

Editorial

Analytical Methods for High Energy Physics

Saber Zarrinkamar ¹, Andrzej Okniński ² and Chun-Sheng Jia ³

¹Department of Basic Sciences, Garmsar Branch, Islamic Azad University, Garmsar, Iran

²Chair of Mathematics and Physics, Politechnika Świętokrzyska, Kielce, Poland

³State Key Laboratory of Oil and Gas Reservoir Geology and Exploitation, Southwest Petroleum University, Chengdu, China

Correspondence should be addressed to Saber Zarrinkamar; zarrinkamar.s@gmail.com

Received 3 December 2018; Accepted 3 December 2018; Published 5 March 2019

Copyright © 2019 Saber Zarrinkamar et al. This is an open access article distributed under the Creative Commons Attribution License, which permits unrestricted use, distribution, and reproduction in any medium, provided the original work is properly cited.

High energy physics is an exciting field of experimental and theoretical research. While the important stimulus comes from the experiment, analytical methods are gaining importance. For example, new analytical approaches, such as Lie groups, path integrals, integrable and superintegrable systems, renormalization methods, factorization methods, Green functions, special functions, homotopy method, integral transforms, and approximate methods based on perturbative or variational treatments to solve differential equations of high energy physics, are becoming more useful. Moreover, there is a significant input of new formulations of quantum mechanics and field theory used in particle physics such as new kinds of interactions, wave equations in curved spaces, fractional order wave equations, noncommutative quantum mechanics, or quantum deformed algebras which may lead to better understanding of high energy physics.

In this special issue we propose a selection of papers, devoted to mathematical problems of high energy and particle physics, where analytical approaches and ideas are used as the main tool to study particle physics.

Several authors studied applications of special functions. The useful review paper by M. Hortaçsu concentrates on properties of the Heun equation and Heun functions which find applications in General Relativity and astrophysics.

There were several papers in which the Schrödinger equation and the Dirac equation were solved in various potentials. For example, S. Dong et al. found exact solutions of the Schrödinger equation in Razavy Cosine Type equation. I. A. Assi et al. obtained solutions for D-dimensional

Schrödinger equation in Pöschl-Teller type potential. Y. You et al. solved the Schrödinger equation in Double Ring-Shaped Coulomb Potential and computed several space probability distributions of the solutions.

N. Mohajery et al. solved the six-dimensional hyperradial Schrödinger equation describing baryons consisting of two heavy quarks and one light quark to compute the mass spectra. This result may be particularly useful since masses of majority of such baryons are unknown.

There are also several interesting papers exploring less standard problems. M.-A. Dariescu and C. Dariescu solve the Klein-Gordon and the Dirac equations in the Melvin space-time in terms of Heun functions. These solutions describe particles moving in the neighbourhood of magnetars. M. Singh studies in two papers the neutrino mass matrix. R. Jora constructs the effective Standard Model potential based on the requirement that the tree level and quantum level trace anomalies must be satisfied. M. Znojil studies in his paper the important problem of quasi-Hermitian formulation of Quantum Mechanics. He demonstrates that for weakly non-local interaction potentials non-Hermitian and Hermitian formulations describe the same dynamics.

We do hope that the readers will find the present special issue interesting and useful.

Conflicts of Interest

The authors declare that there are no conflicts of interest.

Acknowledgments

The guest editors congratulate the authors who contributed to this special issue and express their gratitude to the reviewers who devoted their time to improve the issue.

Saber Zarrinkamar

Andrzej Okniński

Chun-Sheng Jia

Research Article

Double Charmonium Productions in Electron-Positron Annihilation Using Bethe-Salpeter Approach

Hluf Negash ¹ and Shashank Bhatnagar ²

¹Department of Physics, Samara University, P.O. Box 132, Samara, Ethiopia

²Department of Physics, University Institute of Sciences, Chandigarh University, Mohali 140413, India

Correspondence should be addressed to Hluf Negash; h2002hluf@yahoo.com and Shashank Bhatnagar; shashank_bhatnagar@yahoo.com

Received 21 May 2018; Accepted 26 June 2018; Published 3 March 2019

Academic Editor: Andrzej Okniński

Copyright © 2019 Hluf Negash and Shashank Bhatnagar. This is an open access article distributed under the Creative Commons Attribution License, which permits unrestricted use, distribution, and reproduction in any medium, provided the original work is properly cited. The publication of this article was funded by SCOAP³.

We calculate the double charmonium production cross-section within the framework of 4×4 Bethe-Salpeter Equation in the electron-positron annihilation, at center of mass energy $\sqrt{s} = 10.6\text{GeV}$, that proceeds through the exchange of a single virtual photon. In this calculation, we make use of the full Dirac structure of 4D BS wave functions of these charmonia, with the incorporation of all the Dirac covariants (both leading and subleading). The calculated cross-sections for the double charmonium productions for final states, $(J/\Psi, \eta_c)$, (Ψ', η_c) , $(J/\Psi, \eta'_c)$, and (Ψ', η'_c) , are close to experimental data and in broad agreement with results of other theoretical models.

1. Introduction

One of the challenging problems in heavy-quark physics is the process of double charmonium production in electron-positron annihilation at B-factories [1–4]. Many studies of double quarkonium production process [5–9] have been performed in order to understand this process and thereby the internal structures of quarkonia and interactions of the quark and antiquark inside the quarkonium. In recent years, the quarkonium production has been studied in various process at B-factories whose measurements were made by Babar and Belle collaborations [1–4]. Among them, the study of charmonium production in e^+e^- annihilation is particularly interesting in testing the quarkonium production mechanisms at center of mass energies $\sqrt{s} = 10.6\text{GeV}$. The investigation of double charmonium production is very important since these charmonium can be easily produced in experiments and hence their theoretical prediction can verify the discrepancy between different theoretical models and experimental data. As regards the dynamical framework, to investigate the double charmonium production concerned, many approaches have been proposed to deal with the cross-section of double charmonium production [5–9] and the

pseudoscalar and vector charmonium production process has been recently studied in a Bethe-Salpeter formalism [10, 11]. However, in these studies the complete Dirac structure of P (pseudoscalar) and V (vector) quarkonia was not taken into account, and calculations were performed by taking only the leading Dirac structures, γ_5 , and $i\gamma_5 \epsilon$ in the BS wave functions of pseudoscalar and vector charmonia respectively.

In these calculations, we make use of the Bethe-Salpeter Equation (BSE) approach [12–16], which is a conventional approach in dealing with relativistic bound state problems. Due to its firm base in quantum field theory and being a dynamical equation based approach, it provides a realistic description for analyzing hadrons as composite objects and can be applied to study not only the low energy hadronic processes but also the high energy production processes involving quarkonia as well.

In our recent works [17–20], we employed BSE under Covariant Instantaneous Ansatz, which is a Lorentz-invariant generalization of Instantaneous Approximation, to investigate the mass spectra and the transition amplitudes for various processes involving charmonium and bottomonium. The BSE framework using phenomenological potentials can give consistent theoretical predictions as more and more data

are being accumulated. In our studies on 4×4 BSE, in all processes except in [19], the quark–antiquark loop involved a single hadron-quark vertex, which was simple to handle. However for the transitions such as $V \rightarrow P + \gamma$ (where V vector and P pseudoscalar quarkonium), which we have studied in [19] and for the process of double charmonium production, $e^+e^- \rightarrow V + P$, we will study in present work the process requires calculation involving two hadron-quark vertices, due to which the calculation becomes more and more difficult to handle. However in the present work, we demonstrate an explicit mathematical procedure for handling this problem using the formulation of 4×4 Bethe-Salpeter Equation under Covariant Instantaneous Ansatz. We will use this framework for the calculation of cross-section for the production of double charmonia, $(J/\psi, \eta_c), (J/\psi, \eta'_c), (\psi', \eta_c)$, and (ψ', η'_c) in electron-positron annihilation that proceeds through a single virtual photon at center of mass energies, $\sqrt{s} = 10.6$ GeV., where such problems do not enter our previous papers on 4×4 BSE [17–22].

This paper is organized as follows. In Section 2, we introduce the detailed formulation of the transition amplitudes for the process of double charmonium production and the numerical results of cross-sections. Finally, we give the discussions and conclusions in Section 3.

2. Formulation of Double Charmonium Production Amplitude

We start from the lowest-order Feynman diagrams for the process, $e^+e^- \rightarrow V + P$, as given in Figure 1. There are four Feynman diagrams for the production of double charmonium, one of which is shown in Figure 1, while the other three can be obtained by reversing the arrows of the quark lines.

The relativistic amplitude M_{fi}^1 for double charmonium production, corresponding to Figure 1, is given by the one-loop momentum integral as

$$M_{fi}^1 = \frac{2^7 \pi^2 \alpha_{em} \alpha_s}{3^2 s} [\bar{v}(p_2) \gamma_\mu u(p_1)] \int \frac{d^4 q_a}{(2\pi)^4} \int \frac{d^4 q_b}{(2\pi)^4} \cdot Tr \left[\bar{\Psi}(P_a, q_a) \gamma_\beta S_F(q_1) \gamma_\mu \bar{\Psi}(P_b, q_b) \gamma_\beta \right] \frac{1}{k^2} \quad (1)$$

where s is the Mandelstam variable defined as $s = -(p_1 + p_2)^2$, $\alpha_{em} = e^2/4\pi$ is called the electromagnetic coupling constant, $\alpha_s = g_s^2/4\pi$ is the strong coupling strength, and $\bar{\Psi}(P_a, q_a)$ and $\bar{\Psi}(P_b, q_b)$ are the conjugations of the BS wave function of vector and pseudoscalar charmonium, respectively. From the figure, we can relate the momenta of the quark and antiquark, respectively, as

$$\begin{aligned} q'_1 &= \frac{1}{2}P_a + q_a \\ q_3 &= \frac{1}{2}P_a - q_a \\ q_4 &= \frac{1}{2}P_b + q_b \\ q_2 &= \frac{1}{2}P_b - q_b \end{aligned} \quad (2)$$

and the momenta for the propagators of gluon and quark are given, respectively, by

$$\begin{aligned} k &= \frac{1}{2}(P_a + P_b) - q_a + q_b \\ q_1 &= P_a + \frac{1}{2}P_b + q_b \end{aligned} \quad (3)$$

As the quark and gluon propagators depend upon the internal hadron momenta q_a and q_b , the calculation of amplitude is going to involve integrations over these internal momenta and will be quite complex. Hence following [17–19], we simplify the calculation, by reducing the 4-dimensional expression of BS amplitude, M_{fi}^1 into 3-dimensional expression of BS amplitude, M_{fi}^1 , and employing the heavy-quark approximation on the propagators, the momenta k and q_1 can be written as $k \approx (1/2)(P_a + P_b)$ and $q_1 \approx P_a + (1/2)P_b$, which leads to $k^2 \approx s/4$ and $q_1^2 \approx s/2 + m_c^2$ [10, 11]. Then, with the above approximation and applying the definition of 3D BS wave function in [17–20] $\psi(\hat{q}_a) = (i/2\pi) \int M_a d\sigma \Psi(P_a, q_a)$ and $\psi(\hat{q}_b) = (i/2\pi) \int M_b d\sigma \Psi(P_b, q_b)$, the double charmonium production BS amplitude, M_{fi}^1 , can be written in the instantaneous Bethe-Salpeter amplitude form as

$$\begin{aligned} M_{fi}^1 &= -\frac{2^{10} \pi^2 \alpha_{em} \alpha_s}{3^2 s^3} [\bar{v}(p_2) \gamma_\mu u(p_1)] \\ &\cdot \int \frac{d^3 \hat{q}_a}{(2\pi)^3} \int \frac{d^3 \hat{q}_b}{(2\pi)^3} \\ &\cdot Tr \left[\bar{\Psi}(\hat{q}_a) \gamma_\beta \left(-i\not{P}_a - \frac{i}{2}\not{P}_b + m_c \right) \gamma_\mu \bar{\Psi}(\hat{q}_b) \gamma_\beta \right] \end{aligned} \quad (4)$$

where $\psi(\hat{q}_a)$ and $\psi(\hat{q}_b)$ are the relativistic BS wave function of pseudoscalar and vector charmonium, respectively. We now give details of calculation of double charmonium production for the process, $e^+e^- \rightarrow V + P$ in the next section.

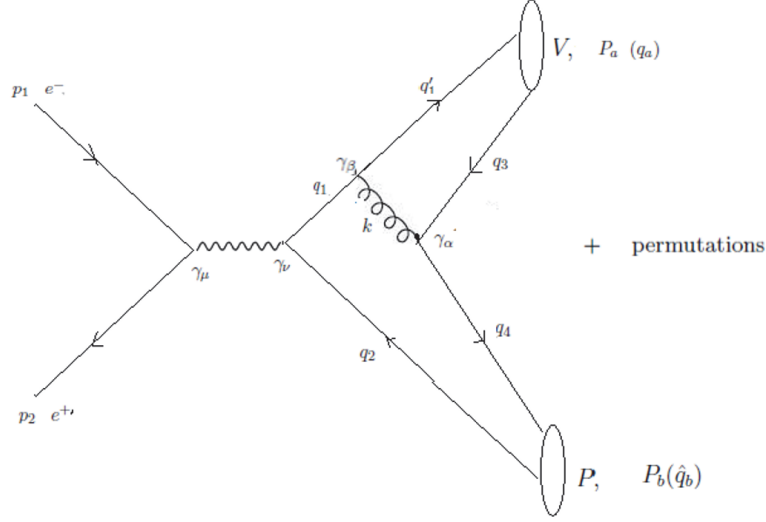
(i) *For the production process, $e^+ + e^- \rightarrow V + P$*

The relativistic BS wave function of pseudoscalar and vector charmonium is taken from our recent papers [17–19], respectively, as

$$\psi_P(\hat{q}_b) = N_P \left[M_b + \not{P}_b + \frac{\not{q}_b \not{P}_b}{m_c} \right] \gamma_5 \phi_P(\hat{q}_b) \quad (5)$$

for P_b and M_b are the momentum and mass of the pseudoscalar charmonium, respectively, and N_P is the BS normalization of the pseudoscalar charmonium, which is given in a simple form as

$$N_P = \left[\frac{16M_b}{m_c} \int \frac{d^3 \hat{q}_b}{(2\pi)^3} \frac{\hat{q}_b^2}{\omega_b} \phi_P^2(\hat{q}_b) \right]^{-1/2} \quad (6)$$

FIGURE 1: Leading-order Feynman diagrams for the production of double charmonium in e^+e^- -annihilation.

and

$$\begin{aligned} & \psi_V(\hat{q}_a) \\ &= N_V \left[M_a \not{\epsilon} + \hat{q}_a \cdot \epsilon \frac{M_a}{m_c} + \not{\epsilon} \not{P}_a + \frac{\not{P}_a \hat{q}_a \cdot \epsilon}{m_c} - \frac{\not{P}_a \not{\not{\epsilon}}}{m_c} \right] \quad (7) \\ & \cdot \phi_V(\hat{q}_a) \end{aligned}$$

where ϵ is the polarization vector of the vector quarkonia, P_a and M_a are the momentum and mass of the vector quarkonia, respectively, and N_V is the BS normalization of the vector quarkonia, which is given in a simple form as

$$N_V = \left[16m_c M_a \int \frac{d^3 \hat{q}_a}{(2\pi)^3} \frac{\hat{q}_a^2}{\omega_a^3} \phi_V^2(\hat{q}_a) \right]^{-1/2} \quad (8)$$

where $\phi_P(\hat{q}_b)$ and $\phi_V(\hat{q}_a)$ are the radial wave functions of P and V , which are solutions of the 3D BSE for pseudoscalar and vector quarkonia, respectively (see [18]). The adjoint BS wave functions for pseudoscalar and vector charmonia are obtained from $\bar{\psi}_{P,V}(\hat{q}_{b,a}) = \gamma^0 (\psi_{P,V}(\hat{q}_{b,a}))^+ \gamma^0$. With the substitution of adjoint BS wave functions of P and V charmoni into the 3D amplitude (4), M_{fi}^1 becomes

$$\begin{aligned} M_{fi}^1 &= -\frac{2^{10} \pi^2 \alpha_{em} \alpha_s}{3^2 s^3} [\bar{v}(p_2) \gamma_\mu u(p_1)] \\ & \cdot \int \frac{d^3 \hat{q}_a}{(2\pi)^3} N_V \phi_V(\hat{q}_a) \int \frac{d^3 \hat{q}_b}{(2\pi)^3} N_P \phi_P(\hat{q}_b) [TR] \quad (9) \end{aligned}$$

where

$$[TR] = Tr \left[\left(-M_a \not{\epsilon} + \hat{q}_a \cdot \epsilon \frac{M_a}{m_c} - \not{\epsilon} \not{P}_a - \frac{\not{P}_a \hat{q}_a \cdot \epsilon}{m_c} \right. \right.$$

$$\begin{aligned} & \left. + \frac{\not{\hat{q}}_a \not{\not{P}}_a}{m_c} \right) \gamma_\beta \left(-i \not{P}_a - \frac{i}{2} \not{P}_b + m_c \right) \gamma_\mu \left(M_b + \not{P}_b \right. \\ & \left. + \frac{\not{\hat{q}}_b \not{\not{P}}_b}{m_c} \right) \gamma_5 \gamma_\beta \left. \right]. \quad (10) \end{aligned}$$

Applying the trace theorem and evaluating trace over the gamma matrices, one can obtain the expression:

$$\begin{aligned} [TR] &= -8M_a \epsilon_{\nu\delta\mu\lambda} \epsilon_\nu P_{a\lambda} P_{b\delta} \\ & + \frac{8i}{m_c} [(\hat{q}_a \cdot \epsilon) \epsilon_{\lambda\delta\sigma\mu} P_{a\lambda} P_{b\beta} \hat{q}_{b\sigma} \\ & + \epsilon_{\rho\nu\lambda\phi} (P_{b\phi} \hat{q}_{b\mu} - P_{b\mu} \hat{q}_{b\phi})] \\ & \cdot \frac{8(\hat{q}_a \cdot \epsilon) M_a}{m_c^2} [\epsilon_{\mu\sigma\beta\delta} P_{a\beta} P_{b\delta} \hat{q}_{b\sigma} + \epsilon_{\lambda\beta\mu\sigma} P_{a\lambda} P_{b\beta} \hat{q}_{b\sigma}] \quad (11) \\ & + \frac{16M_b^2}{m_c} \epsilon_{\nu\delta\sigma\mu} \epsilon_\nu P_{b\delta} \hat{q}_{b\sigma} - \frac{8(\hat{q}_a \cdot \epsilon)}{m_c} \epsilon_{\lambda\delta\sigma\mu} P_{a\lambda} P_{b\delta} \hat{q}_{b\sigma} \\ & + 8iM_b \epsilon_{\rho\nu\lambda\mu} \epsilon_\nu P_{a\lambda} \hat{q}_{a\rho} \end{aligned}$$

After some mathematical steps, we can get the following expression:

$$[TR] = -16m_c \epsilon_{\mu\nu\rho\sigma} \epsilon_\mu P_a^\rho P_b^\sigma \quad (12)$$

Thus we can express the amplitude M_{fi}^1 for the vector and pseudoscalar charmonium production as

$$\begin{aligned} M_{fi}^1 &= \frac{2^{14} \pi^2 \alpha_{em} \alpha_s m_c}{3^2 s^3} [\bar{v}(p_2) \gamma_\mu u(p_1)] \\ & \cdot \epsilon_{\mu\nu\rho\sigma} \epsilon_\mu P_a^\rho P_b^\sigma \int \frac{d^3 \hat{q}_a}{(2\pi)^3} N_V \phi_V(\hat{q}_a) \end{aligned}$$

$$\cdot \int \frac{d^3 \hat{q}_b}{(2\pi)^3} N_P \phi_P(\hat{q}_b) \quad (13)$$

The full amplitude for the process $e^+ + e^- \rightarrow V + P$ can be obtained by summing over the amplitudes of all the possibilities in Figure 1. Then, the unpolarized total cross-section is obtained by summing over various $V + P$, spin-states, and averaging over those of the initial state $e^+ e^-$, which is given as

$$\sigma = \frac{1}{32\pi} \frac{\sqrt{s - 16m_c^2}}{s^{3/2}} \int \frac{1}{4} \sum_{spin} |M_{total}|^2 d \cos \theta \quad (14)$$

The total amplitude, $|M_{total}|^2$, is given as

$$\begin{aligned} & \frac{1}{4} \sum_{spin} |M_{total}|^2 \\ &= \frac{2^{30} \pi^4 \alpha_{em}^2 \alpha_s^2 m_c^2}{3^4 s^5} \left[\int \frac{d^3 \hat{q}_a}{(2\pi)^3} N_V \phi_V(\hat{q}_a) \right]^2 \\ & \cdot \left[\int \frac{d^3 \hat{q}_b}{(2\pi)^3} N_P \phi_P(\hat{q}_b) \right]^2 \end{aligned} \quad (15)$$

After integration over the phase space, the total cross-section for vector and pseudoscalar charmonium production is

$$\begin{aligned} \sigma_{e^+ e^- \rightarrow VP} &= \frac{2^{27} \pi^3 \alpha_{em}^2 \alpha_s^2 m_c^2}{3^4 s^4} \left(1 - \frac{16m_c^2}{s} \right)^{3/2} \\ & \cdot \left[\int \frac{d^3 \hat{q}_a}{(2\pi)^3} N_V \phi_V(\hat{q}_a) \right]^2 \\ & \cdot \left[\int \frac{d^3 \hat{q}_b}{(2\pi)^3} N_P \phi_P(\hat{q}_b) \right]^2 \end{aligned} \quad (16)$$

The algebraic expressions of the wave functions of pseudoscalar and vector charmonium, $\phi_{P(V)}(\hat{q}_{b(a)})$, for ground (1S) and first excited (2S) states, respectively, that are obtained as analytic solutions of the corresponding mass spectral equations of these quarkonia in an approximate harmonic oscillator basis are [18]

$$\begin{aligned} \phi_{P(V)}(1S, \hat{q}) &= \frac{1}{\pi^{3/4} \beta_{P(V)}^{3/2}} e^{-\hat{q}^2/2\beta_{P(V)}^2} \\ \phi_{P(V)}(2S, \hat{q}) &= \frac{\sqrt{3/2}}{3\pi^{3/4} \beta_{P(V)}^{7/2}} (3\beta_{P(V)}^2 - 2\hat{q}^2) e^{-\hat{q}^2/2\beta_{P(V)}^2}, \end{aligned} \quad (17)$$

where the inverse range parameter β_P for pseudoscalar charmonium is $\beta_P = (4(m_c \omega_{\hat{q}\bar{q}}^2 / \sqrt{1 + 2A_0(N + 3/2)}))^{1/4}$, while

β_V for vector charmonium is $\beta_V = (2(m_c \omega_{\hat{q}\bar{q}}^2 / \sqrt{1 + 2A_0(N + 3/2)}))^{1/4}$, and these two constants depend on the input parameters and contain the dynamical information, and they differ from each other due to spin-spin interactions. It can be checked that our cross-sectional formula is in (16) scales as $\alpha_{em}^2 \alpha_s^2 m^6 / s^4$, with m being the mass of c -quark, where in (16), the wave functions, $\phi_{(P,V)}$, involve the inverse range parameters, $\beta_{P,V} \sim m^{1/2}$.

Numerical Results. We had calculated recently the mass spectrum and various decays of ground and excited states of pseudoscalar and vector quarkonia in [18–20]. The same input parameters are employed in this calculation as in our recent works, given in Table 1.

Using these input parameters listed in Table 1, we calculate the cross-sections of pseudoscalar and vector charmonium production in our framework listed in Table 2.

We wish to mention here that the $b\bar{b}b\bar{b}$ as well as $b\bar{b}c\bar{c}$ production has not been observed so far, but cross-sections have been predicted for $e^- e^+ \rightarrow \Upsilon + \eta_b$ at center of mass energy, $\sqrt{s} = 25 - 30$ GeV. We thus wished to check our calculations for double bottomonium (Υ, η_b) production in electron-positron annihilation for sake of completeness. The same can be studied with our framework used in this work with little modifications. Taking the mass of the b -quark that is fixed from our recent work on spectroscopy of $b\bar{b}$ states as $m_b = 5.07$ GeV [18] and other input parameters the same, the cross-section for production of ground states of η_b and Υ for energy range ($\sqrt{s} = 28 - 30$) GeV is given in Table 3.

3. Discussions and Conclusion

Our main aim in this paper was to study the cross-section for double charmonium production in electron-positron collisions at center of mass energies, $\sqrt{s} = 10.6$ GeV., having successfully studied the mass spectrum and a range of low energy processes using an analytic treatment of 4×4 Bethe-Salpeter Equation (BSE) [18–22]. This is due to the fact any quark model should successfully describe a range of processes—not only the mass spectra and low energy hadronic decay constants/decay widths, but also the high energy production processes involving these hadrons and all within a common dynamical framework and with a single set of input parameters that are calibrated to the mass spectrum.

Further, the exclusive production of double heavy charmonia in $e^+ e^-$ annihilation has been a challenge to understand in heavy-quark physics and has received considerable attention in recent years, due to the fact that there is a significant discrepancy in the data of Babar [2] and Belle [1] and the calculations performed in NRQCD [5, 6] of this process at $\sqrt{s} = 10.6$ GeV., where using leading order (LO) QCD diagrams alone leads to cross-sections that are an order of magnitude smaller than data [1, 2, 4]. These discrepancies were then resolved by taking into account the Next-to-Leading-Order (NLO) QCD corrections combined with relativistic corrections [23, 24]), though the

TABLE 1: Input parameters for this study.

C_0	$\omega_0(\text{GeV})$	$\Lambda(\text{GeV})$	A_0	$m_c(\text{GeV})$
0.210	0.150	0.200	0.010	1.490

TABLE 2: The total cross-sections of pseudoscalar and vector charmonium production for ground and first excited states with experimental data and other theoretical models (in units of fb).

Production Process	σ (Our result)	σ [1]	σ [2]	σ [8]	σ [9]	σ [10]	σ [11]
$e^+e^- \rightarrow J/\psi\eta_c$	20.770	25.6±2.8	17.6±2.8	26.7	22.2±4.2	22.3	21.75
$e^+e^- \rightarrow \psi'\eta_c$	11.643	16.3±4.6		16.3	15.3±2.9		
$e^+e^- \rightarrow J/\psi\eta'_c$	11.177	16.5±3.0	16.4±3.7	26.6	16.4±3.1		
$e^+e^- \rightarrow \psi'\eta'_c$	6.266	16.0±5.1		14.5	9.6±1.8		

TABLE 3: The total cross-sections of pseudoscalar and vector bottomonium production for their ground states with predictions of other theoretical models (in units of fb).

Production Process	σ (Our result)	σ [1]	σ [2]	σ [10] for ($\sqrt{s} = 25 - 30$)GeV
$\sigma[e^+e^- \rightarrow \Upsilon\eta_b]$	0.155-0.058			0.16-0.06

NLO contributions were larger than the LO contributions [10].

This process has also been studied in Relativistic Quark Model [7, 9], Light Cone formalism [8], and Bethe-Salpeter Equation [10, 11]. Relativistic corrections to cross-section in Light Cone formalism (in [8]) were considered to eliminate the discrepancy between theory and experiment. Further in an attempt to explain a part of this discrepancy, [25] even suggested that processes proceeding through two virtual photons may be important. In Relativistic Quark Model [7], which incorporated relativistic treatment of internal motion of quarks and bound states, improvements in the results were obtained.

We wish to mention that, in our framework of 4×4 Bethe-Salpeter Equation (BSE) using the Covariant Instantaneous Ansatz, where we treat the internal motion of quarks and the bound states in a relativistically covariant manner, we obtained results on cross-sections (in Table 2) for production of opposite parity $c\bar{c}$ states such as, $(J/\Psi, \eta_c)$; (Ψ', η_c) ; $(J/\Psi, \eta'_c)$; (Ψ', η'_c) , which are close to central values of data [1, 2, 4] using leading-order (LO) QCD diagrams alone. This validates the fact that relativistic quark models such as BSE are strong candidates for treating not only the low energy processes but also the high energy production processes involving double heavy quarkonia, due to their consistent relativistic treatment of internal motion of quarks in the hadrons, where our BS wave functions that take into account all the Dirac structures in pseudoscalar and vector mesons in a mathematically consistent manner play a vital role in the dynamics of the process. We also give our predictions on cross-section for double $b\bar{b}$ production at energies 28-30 GeV. in Table 3 for future experiments at colliders.

The main objective of this study was to test the validation of our approach, which provides a much deeper insight than the purely numerical calculations in 4×4 BSE that are very common in the literature. We wish to mention that we have not encountered any work in 4×4 representation of BSE

that treats this problem analytically. On the contrary, all the other 4×4 BSE approaches adopt a purely numerical approach of solving the BSE. We are also not aware of any other BSE framework, involving 4×4 BS amplitude, and with all the Dirac structures incorporated in the 4D hadronic BS wave functions (in fact many works used only the leading Dirac structures; for instance, see [10, 11]) for calculations of this production process. We treat this problem analytically by making use of the algebraic forms of wave functions, $\phi_{(P,V)}$ derived analytically from mass spectral equations [18], for calculation of cross-section of this double charmonium production process.

This calculation involving production of double charmonia in electron-positron annihilation can be easily extended to studies on other processes (involving the exchange of a single virtual photon) observed at B-factories such as $e^-e^+ \rightarrow \Psi(2S)\gamma$, $e^-e^+ \rightarrow J/\Psi\chi_{c0}$, and $e^-e^+ \rightarrow \Psi(2S)\chi_{c0}$. We further wish to extend this study to processes involving two virtual photons, such as the production of double charmonia in final states with $C = +1$ such as $e^-e^+ \rightarrow J/\Psi J/\Psi$, recently observed at BABAR.

These processes that we intend to study next are quite involved, and the dynamical equation based approaches such as BSE are a promising approach. And since these processes involve quark-triangle diagrams, we make use of the techniques we used for handling such diagrams recently done in [19, 26, 27]. Such analytic approaches not only lead to better insight into the mass spectra and low energy decay processes involving charmonia but also their high energy production processes such as the one studied here.

Note Added in Proofs. We have just now come to know about the recent experimental observation by CMS collaboration [28] of two excited $B_c^+(2S)$, and $B_c^{*+}(2S)$ states in pp collisions at $\sqrt{s} = 13$ TeV. at Large Hadron Collider (LHC). The theoretical study of this process will be a challenge to hadronic physics.

Data Availability

The data used to support the findings of this study are available from the corresponding author upon request.

Conflicts of Interest

The authors declare that they have no conflicts of interest.

Acknowledgments

This work was carried out at Samara University, Ethiopia, and at Chandigarh University, India. The authors thank these institutions for the facilities provided during the course of this work.

References

- [1] K.-F. Chen, W.-S. Hou, I. Adachi et al., "Observation of an enhancement in $e^+e^- \rightarrow Y(1S)\pi^+\pi^-$, $Y(2S)\pi^+\pi^-$, and $Y(3S)\pi^+\pi^-$, production near $\sqrt{s} = 10.6$ GeV," *Physical Review*, vol. 82, Article ID 091106, 2010, <https://arxiv.org/abs/0810.3829>.
- [2] B. Aubert, M. Bona, Y. Karyotakis et al., "Evidence for the $\eta_b(1S)$ meson in radiative $Y(2S)$ decay," *Physical Review Letters*, vol. 103, Article ID 161801, 2009.
- [3] K. W. Edwards, R. Janicek, P. M. Patel et al., "Study of B Decays to Charmonium States: $B \rightarrow \eta_c K$ and $B \rightarrow \eta_b K$," *Physical Review Letters*, vol. 86, no. 30, 2001.
- [4] K. Olive, K. Agashe, and C. Amsler, "Review of particle physics," *Chinese Physics C*, vol. 38, no. 9, Article ID 090001, 2014.
- [5] G. T. Bodwin, E. Braaten, J. Lee, and C. Yu, "Exclusive two-vector-meson production from e^+e^- annihilation," *Physical Review D*, vol. 74, no. 7, Article ID 074014, 2006.
- [6] G. T. Bodwin, D. Kang, T. Kim, J. Lee, and C. Yu, "Relativistic Corrections to $e^+e^- \rightarrow J/\psi + \eta_c$ in a Potential Model," in *Proceedings of the AIP Conference*, vol. 892, 2007.
- [7] D. Ebert and A. P. Martynenko, "Relativistic effects in the production of pseudoscalar and vector doubly heavy mesons from e^+e^- annihilation," *Physical Review D*, Article ID 054008, 2006.
- [8] V. V. Braguta, A. K. Likhoded, and A. V. Luchinsky, "Excited charmonium mesons production in e^+e^- annihilation at $\sqrt{s}=10.6$ GeV," *Physical Review D*, vol. 72, Article ID 074019, 2005.
- [9] D. Ebert, R. N. Faustov, and V. O. Galkin, "Relativistic model of hidden bottom tetraquarks," *Modern Physics Letters A*, vol. 24, no. 08, pp. 567–573, 2009.
- [10] X.-H. Guo, H.-W. Ke, X.-Q. Li et al., "Double heavy-quarkonium production from electron-positron annihilation in the Bethe-Salpeter formalism," <https://arxiv.org/abs/0804.0949>.
- [11] E. Mengesha and S. Bhatnagar, "Cross section for double charmonium production in electron-positron annihilation at energy $\sqrt{s} = 10.6$ GeV," *International Journal of Modern Physics*, vol. E20, pp. 2521–2533, 2011.
- [12] A. N. Mitra and B. M. Sodermark, "A dynamical principle for 3D–4D interlinkage in Salpeter-like equations," *Nuclear Physics A*, vol. 695, pp. 328–352, 2001.
- [13] A. N. Mitra and S. Bhatnagar, "A hadron-quark vertex function: interconnection between 3D and 4D wave functions," *International Journal of Modern Physics A*, vol. 7, p. 121, 1992.
- [14] A. N. Mitra, "QCD motivated BSE SDE framework for quark dynamics under Markov-Yukawa transversality: A Unified view of q anti- q and $q q q$ systems. 1," in *Proceedings of the Indian National Science Academy*, vol. 65, pp. 527–584, 1999.
- [15] S. Bhatnagar, D. S. Kulshreshtha, and A. N. Mitra, "How big are the decay constants f_p of heavy-light mesons?" *Physics Letters B*, vol. 263, no. 3-4, pp. 485–490, 1991.
- [16] S. Bhatnagar, J. Mahecha, and Y. Mengesha, "Relevance of various Dirac covariants in hadronic Bethe-Salpeter wave functions in electromagnetic decays of ground state vector mesons," *Physical Review D: Particles, Fields, Gravitation and Cosmology*, vol. 90, Article ID 014034, 2014.
- [17] H. Negash and S. Bhatnagar, "Mass spectrum and leptonic decay constants of ground and radially excited states of η_c and η_b in a Bethe-Salpeter equation framework," *International Journal of Modern Physics E*, vol. 24, no. 4, Article ID 1550030, 2015.
- [18] H. Negash and S. Bhatnagar, "Spectroscopy of ground and excited states of pseudoscalar and vector charmonium and bottomonium," *International Journal of Modern Physics E*, vol. 25, no. 8, Article ID 1650059, 2016.
- [19] H. Negash and S. Bhatnagar, "Radiative decay widths of ground and excited states of vector charmonium and bottomonium," <https://arxiv.org/abs/1703.06082>.
- [20] H. Negash and S. Bhatnagar, "Analytical calculations of ground and excited states of unequal mass heavy pseudoscalar and vector mesons mass spectra using Bethe-Salpeter formalism," <https://arxiv.org/abs/1711.07036>.
- [21] E. Gebrehana, S. Bhatnagar, and H. Negash, "Analytic approach to calculations of mass spectra and decay constants of heavy-light quarkonia in the framework of Bethe-Salpeter equation," <https://arxiv.org/abs/1901.01888>.
- [22] S. Bhatnagar and L. Alemu, "Approach to calculation of mass spectra and two-photon decays of cc mesons in the framework of Bethe-Salpeter equation," *Physical Review D*, vol. 97, Article ID 034021, 2018.
- [23] E. Braaten and J. Lee, "Exclusive double-charmonium production from e^+e^- annihilation into a virtual photon," *Physical Review D*, vol. 67, Article ID 054007, 2003.
- [24] Y. J. Zhang, Y. J. Gao, and K. T. Chao, "Next-to-leading-order QCD correction to $e^+e^- \rightarrow J/\psi + \eta_c$ at $\sqrt{s}=10.6$ GeV," *Physical Review Letters*, vol. 96, Article ID 092001, 2008.
- [25] G. T. Bodwin, J. Lee, and E. Braaten, " e^+e^- annihilation into $J/\psi + J/\psi$," *Physical Review Letters*, vol. 90, Article ID 162001, 2005.
- [26] E. Mengesha and S. Bhatnagar, "Radiative decays of equal mass vector mesons in a Bethe-Salpeter equation framework," *International Journal of Modern Physics E*, vol. 21, Article ID 1250084, 2012.
- [27] E. Mengesha and S. Bhatnagar, "Strong decays of first radial excitations of lightest vector meson states," *International Journal of Modern Physics E*, vol. 22, no. 7, Article ID 1350046, p. 15, 2013.
- [28] A. M. Sirunyan et al., "Observation of two excited B_c^+ states and measurement of the $B_c^+(2S)$ mass in pp collisions at $\sqrt{s} = 13$ TeV," <https://arxiv.org/abs/1902.00571>, 2019.

Research Article

The Third Five-Parametric Hypergeometric Quantum-Mechanical Potential

T. A. Ishkhanyan^{1,2,3} and A. M. Ishkhanyan ^{1,2}

¹Russian-Armenian University, Yerevan 0051, Armenia

²Institute for Physical Research, Ashtarak 0203, Armenia

³Moscow Institute of Physics and Technology, Dolgoprudny 141700, Russia

Correspondence should be addressed to A. M. Ishkhanyan; aishkhanyan@gmail.com

Received 12 August 2018; Revised 25 September 2018; Accepted 27 September 2018; Published 17 October 2018

Guest Editor: Andrzej Okniński

Copyright © 2018 T. A. Ishkhanyan and A. M. Ishkhanyan. This is an open access article distributed under the Creative Commons Attribution License, which permits unrestricted use, distribution, and reproduction in any medium, provided the original work is properly cited. The publication of this article was funded by SCOAP³.

We introduce the third *five-parametric* ordinary hypergeometric energy-independent quantum-mechanical potential, after the Eckart and Pöschl-Teller potentials, which is proportional to an arbitrary variable parameter and has a shape that is independent of that parameter. Depending on an involved parameter, the potential presents either a short-range singular well (which behaves as inverse square root at the origin and vanishes exponentially at infinity) or a smooth asymmetric step-barrier (with variable height and steepness). The general solution of the Schrödinger equation for this potential, which is a member of a general Heun family of potentials, is written through fundamental solutions each of which presents an irreducible linear combination of two Gauss ordinary hypergeometric functions.

1. Introduction

The solutions of the Schrödinger equation in terms of special mathematical functions for energy-independent potentials which are proportional to an arbitrary variable parameter and have a shape independent of that parameter are very rare [1–10] (see the discussion in [11]). It is a common convention to refer to such potentials as *exactly* solvable in order to distinguish them from the *conditionally* integrable ones for which a condition is imposed on the potential parameters such that the shape of the potential is not independent of the potential strength (e.g., a parameter is fixed to a constant or different term-strengths are not varied independently). While there is a relatively large set of potentials of the latter type (see, e.g., [12–20] for some examples discussed in the past and [21–25] for some recent examples), the list of the known exactly integrable potentials is rather limited even for the potentials of the most flexible *hypergeometric* class. The list of the exactly solvable hypergeometric potentials currently involves only ten items [1–10]. Six of these potentials are solved in terms of the confluent hypergeometric functions [1–6]. These are the classical Coulomb [1], harmonic oscillator [2], and Morse

[3] potentials and the three recently derived potentials, which are the inverse square root [4], the Lambert-W step [5], and Lambert-W singular [6] potentials. The remaining four exactly integrable potentials which are solved in terms of the Gauss ordinary hypergeometric functions are the classical Eckart [7] and Pöschl-Teller [8] potentials and the two new potentials that we have introduced recently [9, 10].

An observation worth mentioning here is that all five classical hypergeometric potentials, both confluent and ordinary, involve *five* arbitrary variable parameters, while all new potentials are four-parametric. In this communication we show that the two four-parametric ordinary hypergeometric potentials [9, 10] are in fact particular cases of a more general five-parametric potential which is solved in terms of the hypergeometric functions. This generalization thus suggests the third five-parametric ordinary hypergeometric quantum-mechanical potential after the ones by Eckart [7] and Pöschl-Teller [8].

The potential we introduce belongs to one of the eleven independent eight-parametric general Heun families [25] (see also [26]). From the mathematical point of view, a peculiarity of the potential is that this is the only known

case when the location of a singularity of the equation to which the Schrödinger equation is reduced is not fixed to a particular point but stands for a variable potential-parameter. Precisely, in our case the third finite singularity of the Heun equation, located at a point $z = a$ of the complex z -plane (that is, the singularity which is additional if compared with the ordinary hypergeometric equation), is not fixed but is variable; it stands for the fifth free parameter of the potential.

The potential is in general defined parametrically as a pair of functions $V(z), x(z)$. However, in several cases the coordinate transformation $x(z)$ is inverted thus producing explicitly written potentials given as $V = V(z(x))$ through an elementary function $z = z(x)$. All these cases are achieved by fixing the parameter a to a particular value; hence, all these particular potentials are four-parametric. The mentioned two recently presented four-parametric ordinary hypergeometric potentials [9, 10] are just such cases.

The potential we present is either a singular well (which behaves as the inverse square root in the vicinity of the origin and exponentially vanishes at infinity) or a smooth asymmetric step-barrier (with variable height, steepness, and asymmetry). The general solution of the Schrödinger equation for this potential is written through fundamental solutions each of which presents an irreducible linear combination of two ordinary hypergeometric functions ${}_2F_1$. The singular version of the potential describes a short-range interaction and for this reason supports only a finite number of bound states. We derive the exact equation for energy spectrum and estimate the number of bound states.

2. The Potential

The potential is given parametrically as

$$V(z) = V_0 + \frac{V_1}{z}, \quad (1)$$

$$x(z) = x_0 + \sigma(a \ln(z - a) - \ln(z - 1)), \quad (2)$$

where $a \neq 0, 1$ and x_0, σ, V_0, V_1 are arbitrary (real or complex) constants. Rewriting the coordinate transformation as

$$\frac{(z - a)^a}{z - 1} = e^{(x - x_0)/\sigma}, \quad (3)$$

it is seen that for real rational a the transformation is rewritten as a polynomial equation for z ; hence, in several cases it can be inverted.

Since $a \neq 0, 1$, the possible simplest case is when the polynomial equation is quadratic. This is achieved for $a = -1, 1/2, 2$. It is checked, however, that these three cases lead to four-parametric subpotentials which are equivalent in the sense that each is derived from another by specifications of the involved parameters. For $a = -1$ the potential reads [9]

$$V(x) = V_0 + \frac{V_1}{\sqrt{1 + e^{(x - x_0)/\sigma}}}, \quad (4)$$

where we have changed $\sigma \rightarrow -\sigma$.

The next are the cubic polynomial reductions which are achieved in six cases: $a = -2, -1/2, 1/3, 2/3, 3/2, 3$. It is

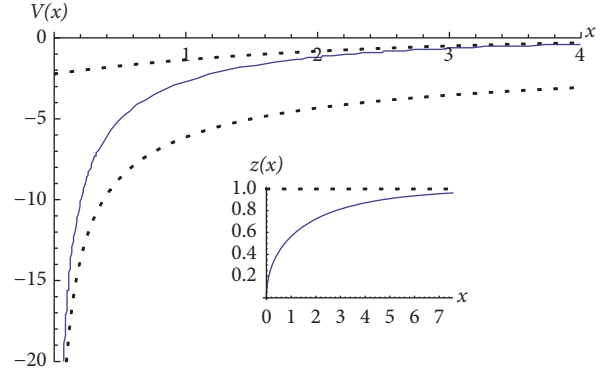


FIGURE 1: Potential (1), (2) for $a = -2$ and $(\sigma, x_0, V_0, V_1) = (2, 0, 5, -5)$. The inset presents the coordinate transformation $z(x) \in (0, 1)$ for $x \in (0, \infty)$.

again checked, however, that these choices produce only one independent potential. This is the four-parametric potential presented in [10]:

$$V = V_0 + \frac{V_1}{z},$$

$$z = -1 + \frac{1}{\left(e^{x/(2\sigma)} + \sqrt{1 + e^{x/\sigma}}\right)^{2/3} + \left(e^{x/(2\sigma)} + \sqrt{1 + e^{x/\sigma}}\right)^{2/3}}, \quad (5)$$

where one should replace x by $x - x_0$. Similar potentials in terms of elementary functions through quartic and quintic reductions of (3) are rather cumbersome; we omit those.

For arbitrary real $a \neq 0, 1$, assuming $z \in (0, 1)$ and shifting

$$x_0 \rightarrow x_0 - \sigma a \ln(-a) + i\pi\sigma, \quad (6)$$

the potential (1), (2) presents a singular well. In the vicinity of the origin it behaves as $x^{-1/2}$,

$$V|_{x \rightarrow 0} \sim \sqrt{\frac{(a - 1)\sigma}{2a}} \frac{V_1}{\sqrt{x}}, \quad (7)$$

and exponentially approaches a constant, $V_0 + V_1$, at infinity,

$$V|_{x \rightarrow +\infty} \sim \left(\frac{a - 1}{a}\right)^a V_1 e^{-x/\sigma}. \quad (8)$$

The potential and the two asymptotes are shown in Figure 1.

A potential of a different type is constructed if one allows the parameterization variable z to vary within the interval $z \in (1, \infty)$ for $a < 1$ or within the interval $z \in (1, a)$ for $a > 1$. This time, shifting (compare with (6))

$$x_0 \rightarrow x_0 - \sigma a \ln(1 - a), \quad (9)$$

we derive an asymmetric step-barrier the height of which depends on V_0 and V_1 , while the asymmetry and steepness

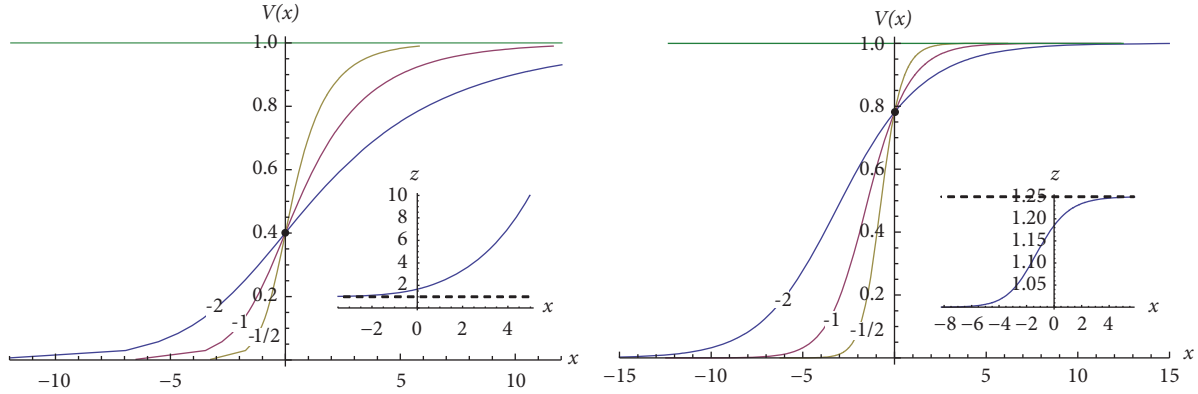


FIGURE 2: Potential (1), (2) for $a = -2$ and $(x_0, V_0, V_1) = (0, 1, -1)$ (left figure) and for $a = 1.25$ and $(x_0, V_0, V_1) = (0.5, 5, -5)$ (right figure); $\sigma = -2, -1, -1/2$. The fixed points are marked by filled circles. The insets present the coordinate transformation $z(x)$ for $\sigma = -1$.

are controlled by the parameters a and σ . The shape of the potential is shown in Figure 2 for $a = -2$ and $a = 1.25$. We note that in the limit $\sigma \rightarrow 0$ the potential turns into the abrupt-step potential and that the subfamily of barriers generated by variation of σ at constant V_0 and V_1 has a σ -independent fixed point located at $x = x_0$ (marked in Figure 2 by filled circles).

3. Reduction to the General Heun Equation

The solution of the one-dimensional Schrödinger equation for potential (1), (2),

$$\frac{d^2\psi}{dx^2} + \frac{2m}{\hbar^2} (E - V(x))\psi = 0, \quad (10)$$

is constructed via reduction to the general Heun equation [27–29]

$$\frac{d^2u}{dz^2} + \left(\frac{\gamma}{z-a_1} + \frac{\delta}{z-a_2} + \frac{\varepsilon}{z-a_3} \right) \frac{du}{dz} + \frac{\alpha\beta z - q}{(z-a_1)(z-a_2)(z-a_3)} u = 0. \quad (11)$$

The details of the technique are presented in [11, 25]. It has been shown that the energy-independent general-Heun potentials, which are proportional to an arbitrary variable parameter and have shapes which are independent of that parameter, are constructed by the coordinate transformation $z = z(x)$ of the Manning form [30] given as

$$\frac{dz}{dx} = \frac{(z-a_1)^{m_1} (z-a_2)^{m_2} (z-a_3)^{m_3}}{\sigma}, \quad (12)$$

where $m_{1,2,3}$ are integers or half-integers and σ is an arbitrary scaling constant. As it is seen, the coordinate transformation is solely defined by the singularities $a_{1,2,3}$ of the general Heun equation. The canonical form of the Heun equation assumes two of the three finite singularities at 0 and 1, and the third one at a point a , so that $a_{1,2,3} = (0, 1, a)$ [27–29]. However, it may be convenient for practical purposes to apply a different

specification of the singularities, so for a moment we keep the parameters $a_{1,2,3}$ unspecified.

The coordinate transformation is followed by the change of the dependent variable

$$\psi = (z-a_1)^{\alpha_1} (z-a_2)^{\alpha_2} (z-a_3)^{\alpha_3} u(z) \quad (13)$$

and application of the ansatz

$$V(z) = \frac{v_0 + v_1 z + v_2 z^2 + v_3 z^3 + v_4 z^4}{(z-a_1)^2 (z-a_2)^2 (z-a_3)^2} \left(\frac{dz}{dx} \right)^2, \quad (14)$$

$v_{0,1,2,3,4} = \text{const.}$

The form of this ansatz and the permissible sets of the parameters $m_{1,2,3}$ are revealed through the analysis of the behavior of the solution in the vicinity of the finite singularities of the general Heun equation [11]. This is a crucial point which warrants that all the parameters involved in the resulting potentials can be varied independently.

It has been shown that there exist in total thirty-five permissible choices for the coordinate transformation each being defined by a triad (m_1, m_2, m_3) satisfying the inequalities $-1 \leq m_{1,2,3} \leq 1$ and $1 \leq m_1 + m_2 + m_3 \leq 3$ [25]. However, because of the symmetry of the general Heun equation with respect to the transpositions of its singularities, only eleven of the resultant potentials are independent [25]. The potential (1), (2) belongs to the fifth independent family with $m_{1,2,3} = (1, 1, -1)$ for which from (14) we have

$$V(z) = \frac{V_4 + V_3 z + V_2 z^2 + V_1 z^3 + V_0 z^4}{(z-a_3)^4} \quad (15)$$

with arbitrary $V_{0,1,2,3,4} = \text{const}$, and, from (12),

$$\frac{x-x_0}{\sigma} = \frac{a_1-a_3}{a_1-a_2} \ln(z-a_1) + \frac{a_3-a_2}{a_1-a_2} \ln(z-a_2). \quad (16)$$

It is now convenient to have a potential which does not explicitly involve the singularities. Hence, we put $a_3 = 0$ and apply the specification $a_{1,2,3} = (a, 1, 0)$ to derive the potential

$$V(z) = V_0 + \frac{V_1}{z} + \frac{V_2}{z^2} + \frac{V_3}{z^3} + \frac{V_4}{z^4} \quad (17)$$

$$\text{with } \frac{(x - x_0)}{\sigma/(a-1)} = a \ln(z-a) - \ln(z-1). \quad (18)$$

The solution of the Schrödinger equation (10) for this potential is written in terms of the general Heun function H_G as

$$\psi = (z-a)^{\alpha_1} z^{\alpha_2} (z-1)^{\alpha_3} \cdot H_G(a_1, a_2, a_3; q; \alpha, \beta, \gamma, \delta, \varepsilon; z), \quad (19)$$

where the involved parameters $\alpha, \beta, \gamma, \delta, \varepsilon$, and q are given through the parameters $V_{0,1,2,3,4}$ of potential (17) and the exponents $\alpha_{1,2,3}$ of the prefactor by the equations [25]

$$(\gamma, \delta, \varepsilon) = (1 + 2\alpha_1, 1 + 2\alpha_2, -1 + 2\alpha_3), \quad (20)$$

$$1 + \alpha + \beta = \gamma + \delta + \varepsilon,$$

$$\alpha\beta = (\alpha_1 + \alpha_2 + \alpha_3)^2 + \frac{2m\sigma^2(E - V_0)}{\hbar^2}, \quad (21)$$

$$q = \frac{2m\sigma^2}{\hbar^2} (V_1 - (1+a)(E - V_0)) + (-\alpha_2^2 + (-1 + \alpha_1 + \alpha_3)(\alpha_1 + \alpha_3)) + a(-\alpha_1^2 + (-1 + \alpha_2 + \alpha_3)(\alpha_2 + \alpha_3)); \quad (22)$$

the exponents $\alpha_{1,2,3}$ of the prefactor are defined by the equations

$$\alpha_1^2 = \frac{2m\sigma^2}{a^2(a-1)^2\hbar^2} (V_4 + aV_3 + a^2V_2 + a^3V_1 + a^4(V_0 - E)), \quad (23)$$

$$\alpha_2^2 = -\frac{2m\sigma^2}{(a-1)^2\hbar^2} (E - V_0 - V_1 - V_2 - V_3 - V_4), \quad (24)$$

$$\alpha_3(\alpha_3 - 2) = \frac{2m\sigma^2 V_4}{a^2\hbar^2}. \quad (25)$$

4. The Solution of the Schrödinger Equation in Terms of the Gauss Functions

Having determined the parameters of the Heun equation, the next step is to examine the cases when the general Heun function H_G is written in terms of the Gauss hypergeometric functions ${}_2F_1$. An observation here is that the direct one-term Heun-to-hypergeometric reductions discussed by many authors (see, e.g., [27, 28, 31–34]) are achieved by such restrictions and imposed on the involved parameters (three or more conditions), which are either not satisfied by the

Heun potentials or produce very restrictive potentials. It is checked that the less restrictive reductions reproduce the classical Eckart and Pöschl-Teller potentials, while the other reductions result in conditionally integrable potentials.

More advanced are the finite-sum solutions achieved by termination of the series expansions of the general Heun function in terms of the hypergeometric functions [35–39]. For such reductions, only two restrictions are imposed on the involved parameters and, notably, these restrictions are such that in many cases they are satisfied. The solutions for the above-mentioned four-parametric subpotentials [9, 10] have been constructed right in this way. Other examples achieved by termination of the hypergeometric series expansions of the functions of the Heun class include the recently reported inverse square root [4], Lambert-W step [5], and Lambert-W singular [6] potentials.

The series expansions of the general Heun function in terms of the Gauss ordinary hypergeometric functions are governed by three-term recurrence relations for the coefficients of the successive terms of the expansion. A useful particular expansion in terms of the functions of the form ${}_2F_1(\alpha, \beta; \gamma_0 - n; z)$ which leads to simpler coefficients of the recurrence relation is presented in [25, 39]. If the expansion functions are assumed irreducible to simpler functions, the termination of this series occurs if $\varepsilon = -N$, $n = 0, 1, 2, \dots$, and a $(N+1)$ th degree polynomial equation for the accessory parameter q is satisfied. For $\varepsilon = 0$ the latter equation is $q = a\alpha\beta$, which corresponds to the trivial direct reduction of the general Heun equation to the Gauss hypergeometric equation. This case reproduces the classical Eckart and Pöschl-Teller potentials [25]. For the first nontrivial case $\varepsilon = -1$ the termination condition for singularities $a_{1,2,3} = (a, 1, 0)$ takes a particularly simple form:

$$q^2 + q(\gamma - 1 + a(\delta - 1)) + a\alpha\beta = 0. \quad (26)$$

The solution of the Heun equation for a root of this equation is written as [39]

$$u = {}_2F_1\left(\alpha, \beta; \gamma; \frac{a-z}{a-1}\right) + \frac{\gamma-1}{q+a(\delta-1)} \cdot {}_2F_1\left(\alpha, \beta; \gamma-1; \frac{a-z}{a-1}\right), \quad (27)$$

This solution has a representation through Clausen's generalized hypergeometric function ${}_3F_2$ [40, 41].

Consider if the termination condition (26) for $\varepsilon = -1$ is satisfied for the parameters given by (20)–(25). From (20) we find that for $\varepsilon = -1$ holds $\alpha_3 = 0$. It then follows from (25) that $V_4 = 0$. With this, (26) is reduced to

$$V_2 + V_3 \left(\frac{1+a}{a} - \frac{2m\sigma^2}{a^2\hbar^2} V_3 \right) = 0. \quad (28)$$

This equation generally defines a conditionally integrable potential in that the potential parameters V_2 and V_3 are not varied independently. Alternatively, if the potential parameters are assumed independent, the equation is satisfied only if $V_2 = V_3 = 0$. Thus, we put $V_{2,3,4} = 0$ and potential

(17) is reduced to that given by (1). Furthermore, since σ is arbitrary, in order for (18) to exactly reproduce the coordinate transformation (2), we replace $\sigma/(1-a) \rightarrow \sigma$.

With this, the solution of the Schrödinger equation (10) for potential (1) is written as

$$\begin{aligned} \psi = & (z-a)^{\alpha_1} (z-1)^{\alpha_2} \left({}_2F_1 \left(\alpha, \beta; \gamma; \frac{a-z}{a-1} \right) \right. \\ & \left. + \frac{2\alpha_1}{a\alpha_2 - \alpha_1} \cdot {}_2F_1 \left(\alpha, \beta; \gamma-1; \frac{a-z}{a-1} \right) \right) \end{aligned} \quad (29)$$

$$\text{with } (\alpha, \beta, \gamma) = (\alpha_1 + \alpha_2 + \alpha_0, \alpha_1 + \alpha_2 - \alpha_0, 1 + 2\alpha_1), \quad (30)$$

$$\begin{aligned} \alpha_{0,1,2} = & \left(\pm \sqrt{\frac{2m\sigma^2(a-1)^2}{\hbar^2} (V_0 - E)}, \right. \\ & \pm \sqrt{\frac{2m\sigma^2 a^2}{\hbar^2} \left(V_0 - E + \frac{V_1}{a} \right)}, \\ & \left. \pm \sqrt{\frac{2m\sigma^2}{\hbar^2} (V_0 - E + V_1)} \right). \end{aligned} \quad (31)$$

This solution applies for any real or complex set of the involved parameters. Furthermore, we note that any combination for the signs of $\alpha_{1,2}$ is applicable. Hence, by choosing different combinations, one can construct different independent fundamental solutions. Thus, this solution supports the general solution of the Schrödinger equation.

A final remark is that using the contiguous functions relations for the hypergeometric functions one can replace the second hypergeometric function in (29) by a linear combination of the first hypergeometric function and its derivative. In this way we arrive at the following representation of the general solution of the Schrödinger equation:

$$\psi = (z-a)^{\alpha_1} (z-1)^{\alpha_2} \left(F + \frac{z-a}{\alpha_1 + \alpha\alpha_2} \frac{dF}{dz} \right), \quad (32)$$

$$\begin{aligned} \text{where } F = & c_1 \cdot {}_2F_1 \left(\alpha, \beta; \gamma; \frac{a-z}{a-1} \right) + c_2 \\ & \cdot {}_2F_1 \left(\alpha, \beta; 1 + \alpha + \beta - \gamma; \frac{z-1}{a-1} \right). \end{aligned} \quad (33)$$

5. Bound States

Consider the bound states supported by the singular version of potential (1), (2), achieved by shifting $x_0 \rightarrow x_0 - \sigma a \ln(-a) + i\pi\sigma$ in (2). Since the potential vanishes at infinity exponentially, it is understood that this is a short-range potential. The integral of the function $xV(x)$ over the semiaxis $x \in (0, +\infty)$ is finite, hence, according to the general criterion [42–46], the potential supports only a finite number of bound states. These states are derived by demanding the wave function to vanish both at infinity and in the origin (see the discussion in [47]). We recall that for this potential the coordinate transformation maps the interval $x \in (0, +\infty)$ onto the interval $z \in (0, 1)$. Thus, we demand $\psi(z=0) = \psi(z=1) = 0$.

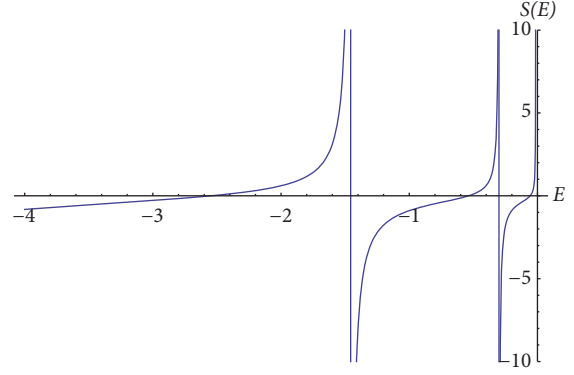


FIGURE 3: Graphical representation of the spectrum equation (35) for $m, \hbar, V_0, \sigma, a = 1, 1, 5, 2, -2$.

The condition $V(+\infty) = 0$ assumes $V_0 + V_1 = 0$; hence, α_2 is real for negative energy. Choosing, for definiteness, the plus signs in (31), we have $\alpha_2 > 0$. Then, examining the equation $\psi(z=1) = 0$, we find that

$$\psi|_{z \rightarrow 1} \sim c_1 A_1 (1-z)^{-\alpha_2} + c_2 A_2 (1-z)^{\alpha_2} \quad (34)$$

with some constants $A_{1,2}$. Since for positive α_2 the first term diverges, we conclude $c_1 = 0$. The condition $\psi(z=0) = 0$ then gives the following exact equation for the spectrum:

$$\begin{aligned} S(E) \equiv & 1 + \frac{\alpha_1 + a\alpha_2}{2(1-a)\alpha_2} \\ & \cdot \frac{{}_2F_1(\alpha+1, \beta+1; 1+2\alpha_2; 1/(1-a))}{{}_2F_1(\alpha, \beta; 2\alpha_2; 1/(1-a))} = 0. \end{aligned} \quad (35)$$

The graphical representation of this equation is shown in Figure 3. The function $S(E)$ has a finite number of zeros. For the parameters $m, \hbar, V_0, \sigma, a = 1, 1, 5, 2, -2$ applied in the figure there are just three bound states.

According to the general theory, the number of bound states is equal to the number of zeros (not counting $x=0$) of the zero-energy solution, which vanishes at the origin [42–46]. We note that for $E=0$ the lower parameter of the second hypergeometric function in (33) vanishes: $1 + \alpha + \beta - \gamma = 0$. Hence, a different second independent solution should be applied. This solution is constructed by using the first hypergeometric function with α_1 everywhere replaced by $-\alpha_1$. The result is rather cumbersome. It is more conveniently written in terms of the Clausen functions as

$$\begin{aligned} \psi_{E=0} = & c_1 (z-a)^{\alpha_1} {}_3F_2 \left(-\sqrt{\frac{a-1}{a}}\alpha_1 + \alpha_1, \sqrt{\frac{a-1}{a}}\alpha_1 \right. \\ & \left. + \alpha_1, 1 + \alpha_1; \alpha_1, 1 + 2\alpha_1; \frac{a-z}{a-1} \right) + c_2 (z-a)^{-\alpha_1} \\ & \cdot {}_3F_2 \left(-\sqrt{\frac{a-1}{a}}\alpha_1 - \alpha_1, \sqrt{\frac{a-1}{a}}\alpha_1 - \alpha_1, 1 - \frac{\alpha_1}{a}; \right. \\ & \left. -\frac{\alpha_1}{a}, 1; \frac{z-1}{a-1} \right), \end{aligned} \quad (36)$$

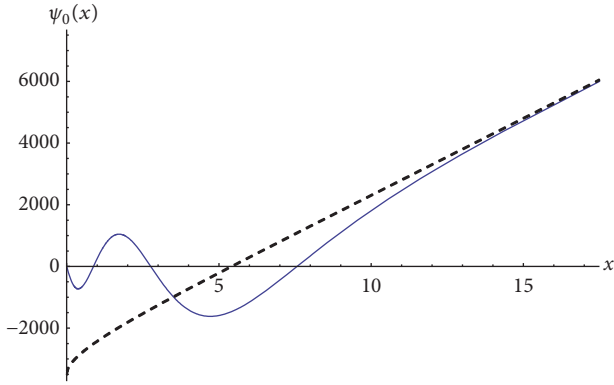


FIGURE 4: The zero-energy solution for $m, \hbar, V_0, \sigma, a = 1, 1, 5, 2, -2$. The dashed line shows the logarithmic asymptote at infinity: $\psi_0|_{x \rightarrow \infty} \sim A + B \ln(1 - z)$.

where $\alpha_1 = \sqrt{2a(a-1)m\sigma^2 V_0/\hbar^2}$ and the relation between c_1 and c_2 is readily derived from the condition $\psi_{E=0}(0) = 0$. This solution is shown in Figure 4. It is seen that for parameters $m, \hbar, V_0, \sigma, a = 1, 1, 5, 2, -2$ used in Figure 3 the number of zeros (excluded the origin) is indeed 3.

For practical purposes, it is useful to have an estimate for the number of bound states. The absolute upper limit for this number is given by the integral [42, 43]

$$I_B = \int_0^\infty r \left| V \left(x \rightarrow \frac{r\hbar}{\sqrt{2m}} \right) \right| dr = (1-a) \cdot \left(Li_2 \left(\frac{1}{1-a} \right) + 2a \coth^{-1} (1-2a)^2 \right) \frac{2m\sigma^2 V_0}{\hbar^2}. \quad (37)$$

where Li_2 is Jonquière's polylogarithm function of order 2 [48, 49]. Though of general importance, however, in many cases this is a rather overestimating limit. Indeed, for the parameters applied in Figure 3 it gives $n \leq I_B \approx 24$.

More stringent are the estimates by Calogero [44] and Chadan [45] which are specialized for everywhere monotonically nondecreasing attractive central potentials. Calogero's estimate reads $n \leq I_C$ with [44]

$$I_C = \frac{2/\pi}{\hbar/\sqrt{2m}} \int_0^\infty \sqrt{-V(x)} dx = \left(1 + (\sqrt{1-a} - \sqrt{-a})^2 \right) \sqrt{\frac{2m\sigma^2 V_0}{\hbar^2}}, \quad (38)$$

We note that $I_C \approx \sqrt{2I_B}$. The result by Chadan further tunes the upper limit for the number of bound states to the half of that by Calogero; that is $n \leq I_C/2$ [45]. For the parameters applied in Figure 3 this gives $n \leq 3.48$, which is, indeed, an accurate estimate. The dependence of the function $n_c = I_C/2$ on the parameter a for $a \in (-\infty, 0) \cup (1, +\infty)$ is shown in Figure 5. It is seen that more bound states are available for a close to zero. The maximum number achieved in the limit $a \rightarrow 0$ is $\sqrt{2m\sigma^2 V_0/\hbar^2}$; hence, for sufficiently small V_0 or σ such that $2m\sigma^2 V_0 < \hbar^2$, bound states are not possible at all.

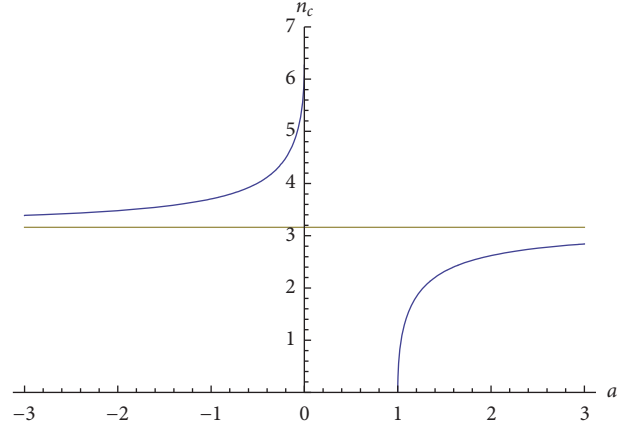


FIGURE 5: The dependence of Chadan's estimate $n_c = I_C/2$ for the number of bound states on the parameter a ($m, \hbar, V_0, \sigma = 1, 1, 5, 2$).

6. Discussion

Thus, we have presented the third five-parametric quantum-mechanical potential for which the solution of the Schrödinger equation is written in terms of the Gauss ordinary hypergeometric functions. The potential involves five (generally complex) parameters which are varied independently. Depending on the particular specifications of these parameters, the potential suggests two different appearances. In one version we have a smooth step-barrier with variable height, steepness, and asymmetry, while in the other version this is a singular potential-well which behaves as the inverse square root in the vicinity of the origin and exponentially vanishes at infinity.

The potential is in general given parametrically; however, in several cases the involved coordinate transformation allows inversion thus leading to particular potentials which are explicitly written in terms of elementary functions. These reductions are achieved by particular specifications of a parameter standing for the third finite singularity of the general Heun equation. The resultant subpotentials all are four-parametric (see, e.g., [9, 10]). These particular cases are defined by coordinate transformations which are roots of polynomial equations. It turns out that different polynomial equations of the same degree produce the same potential (with altered parameters). The reason for this is well understood in the case of quadratic equations. In that case the third singularity of the general Heun equation, to which the Schrödinger equation is reduced, is specified as $a = -1, 1/2$ or 2 . We then note that the form-preserving transformations of the independent variable map the four singularities of the Heun equation, $z = 0, 1, a, \infty$, onto the points $z = 0, 1, a_1, \infty$ with a_1 adopting one of the six possible values $a, 1/a, 1-a, 1/(1-a), a/(1-a), (a-1)/a$ [27–29]. It is seen that the triad $(-1, 1/2, 2)$ is a specific set which remains invariant at form-preserving transformations of the independent variable.

The potential belongs to the general Heun family $m_{1,2,3} = (1, 1, -1)$. This family allows several conditionally integrable reductions too [25]. A peculiarity of the exactly integrable potential that we have presented here is that the location of

a finite singularity of the general Heun equation is not fixed to a particular point of the complex z -plane but serves as a variable potential-parameter. In the step-barrier version of the potential, this parameter stands for the asymmetry of the potential.

The solution of the Schrödinger equation for the potential we have presented is constructed via termination of a series expansion of the general Heun equation in terms of the Gauss ordinary hypergeometric functions. The general solution of the problem is composed of fundamental solutions each of which is an *irreducible* combination of two hypergeometric functions. Several other potentials allowing solutions of this type have been reported recently [4–6, 9, 10, 23–25]. Further cases involve the solutions for supersymmetric partner potentials much discussed in the past [15, 50, 51] and for several nonanalytic potentials discussed recently [52–54]. One should distinguish these solutions from the case of reducible hypergeometric functions [55–59] when the solutions eventually reduce to quasi-polynomials, e.g., discussed in the context of quasi-exactly solvability [57–59]. We note that, owing to the contiguous functions relations [60], the two-term structure of the solution is a general property of all finite-sum hypergeometric reductions of the general Heun functions achieved via termination of series solutions. It is checked that in our case the linear combination of the involved Gauss functions is expressed through a single generalized hypergeometric function ${}_3F_2$ [40, 41].

We have presented the explicit solution of the problem and discussed the bound states supported by the singular version of the potential. We have derived the exact equation for the energy spectrum and estimated the number of bound states. The exact number of bound states is given by the number of zeros of the zero-energy solution which we have also presented.

Data Availability

No data were used to support this study.

Conflicts of Interest

The authors declare that they have no conflicts of interest.

Acknowledgments

The research was supported by the Russian-Armenian (Slavonic) University at the expense of the Ministry of Education and Science of the Russian Federation, the Armenian Science Committee (SC Grants no. 18RF-139 and no. 18T-1C276), and the Armenian National Science and Education Fund (ANSEF Grant no. PS-4986). T. A. Ishkhanyan acknowledges the support from SPIE through a 2017 Optics and Photonics Education Scholarship and thanks the French Embassy in Armenia for a doctoral grant as well as the Agence universitaire de la Francophonie with Armenian Science Committee for a Scientific Mobility grant.

References

- [1] E. Schrödinger, “Quantisierung als eigenwertproblem,” *Annalen der Physik*, vol. 384, no. 4, pp. 361–376, 1926.
- [2] E. Schrödinger, “Quantisierung als Eigenwertproblem. Zweite Mitteilung,” *Annalen der Physik*, vol. 384, no. 6, pp. 489–527, 1926.
- [3] P. M. Morse, “Diatomic molecules according to the wave mechanics. II. Vibrational levels,” *Physical Review A: Atomic, Molecular and Optical Physics*, vol. 34, no. 1, pp. 57–64, 1929.
- [4] A. M. Ishkhanyan, “Exact solution of the Schrödinger equation for the inverse square root potential V_0/\sqrt{x} ,” *EPL (Europhysics Letters)*, vol. 112, no. 1, 2015.
- [5] A. M. Ishkhanyan, “The Lambert- W step-potential – an exactly solvable confluent hypergeometric potential,” *Physics Letters A*, vol. 380, no. 5-6, pp. 640–644, 2016.
- [6] A. M. Ishkhanyan, “A singular Lambert- W Schrödinger potential exactly solvable in terms of the confluent hypergeometric functions,” *Modern Physics Letters A*, vol. 31, no. 33, 1650177, 11 pages, 2016.
- [7] C. Eckart, “The penetration of a potential barrier by electrons,” *Physical Review A: Atomic, Molecular and Optical Physics*, vol. 35, no. 11, article 1303, 1930.
- [8] G. Pöschl and E. Teller, “Bemerkungen zur Quantenmechanik des anharmonischen Oszillators,” *Zeitschrift für Physik*, vol. 83, no. 3-4, pp. 143–151, 1933.
- [9] A. Ishkhanyan, “The third exactly solvable hypergeometric quantum-mechanical potential,” *EPL (Europhysics Letters)*, vol. 115, no. 2, 2016.
- [10] T. A. Ishkhanyan, V. A. Manukyan, A. H. Harutyunyan, and A. M. Ishkhanyan, “A new exactly integrable hypergeometric potential for the Schrödinger equation,” *AIP Advances*, vol. 8, no. 3, 2018.
- [11] A. Ishkhanyan and V. Krainov, “Discretization of Natanzon potentials,” *The European Physical Journal Plus*, vol. 131, no. 9, 2016.
- [12] F. H. Stillinger, “Solution of a quantum mechanical eigenvalue problem with long range potentials,” *Journal of Mathematical Physics*, vol. 20, no. 9, pp. 1891–1895, 1979.
- [13] G. P. Flessas and A. Watt, “An exact solution of the Schrödinger equation for a multiterm potential,” *Journal of Physics A: Mathematical and General*, vol. 14, no. 9, pp. L315–L318, 1981.
- [14] J. N. Ginocchio, “A class of exactly solvable potentials. I. One-dimensional Schrödinger equation,” *Annals of Physics*, vol. 152, no. 1, pp. 203–219, 1984.
- [15] F. Cooper, J. N. Ginocchio, and A. Khare, “Relationship between supersymmetry and solvable potentials,” *Physical Review D: Particles, Fields, Gravitation and Cosmology*, vol. 36, no. 8, pp. 2458–2473, 1987.
- [16] A. De Souza Dutra, “Conditionally exactly soluble class of quantum potentials,” *Physical Review A: Atomic, Molecular and Optical Physics*, vol. 47, no. 4, pp. R2435–R2437, 1993.
- [17] R. Dutt, A. Khare, and Y. P. Varshni, “New class of conditionally exactly solvable potentials in quantum mechanics,” *Journal of Physics A: Mathematical and General*, vol. 28, no. 3, pp. L107–L113, 1995.
- [18] C. Grosche, “Conditionally solvable path integral problems,” *Journal of Physics A: Mathematical and General*, vol. 28, no. 20, pp. 5889–5902, 1995.
- [19] H. Exton, “The exact solution of two new types of Schrödinger equation,” *Journal of Physics A: Mathematical and General*, vol. 28, no. 23, pp. 6739–6741, 1995.

- [20] G. Junker and P. Roy, "Conditionally exactly solvable problems and non-linear algebras," *Physics Letters A*, vol. 232, no. 3-4, pp. 155-161, 1997.
- [21] B. W. Williams, "Exact solutions of a Schrödinger equation based on the Lambert function," *Physics Letters A*, vol. 334, no. 2-3, pp. 117-122, 2005.
- [22] A. López-Ortega, "New conditionally exactly solvable inverse power law potentials," *Physica Scripta*, vol. 90, no. 8, p. 085202, 2015.
- [23] G. Junker and P. Roy, "Conditionally exactly solvable potentials: a supersymmetric construction method," *Annals of Physics*, vol. 270, no. 1, pp. 155-177, 1998.
- [24] A. M. Ishkhanyan, "A conditionally exactly solvable generalization of the inverse square root potential," *Physics Letters A*, vol. 380, pp. 3786-3790, 2016.
- [25] A. M. Ishkhanyan, "Schrödinger potentials solvable in terms of the general Heun functions," *Annals of Physics*, vol. 388, pp. 456-471, 2018.
- [26] A. Lemieux and A. K. Bose, *Construction de Potentiels Pour Lesquels L'équation De Schrödinger Est Soluble*, vol. 10, Annales de l'Institut Henri Poincaré, 1969.
- [27] A. Ronveaux, *Heun's Differential Equations*, Oxford University Press, Oxford, UK, 1995.
- [28] S. Y. Slavyanov and W. Lay, *Special Functions, A Unified Theory Based on Singularities*, Oxford Mathematical Monographs, Oxford, 2000.
- [29] F. W. J. Olver, D. W. Lozier, R. F. Boisvert, and C. W. Clark, *NIST Handbook of Mathematical Functions*, Cambridge University Press, 2010.
- [30] M. F. Manning, "Exact solutions of the schrödinger equation," *Physical Review A: Atomic, Molecular and Optical Physics*, vol. 48, no. 2, pp. 161-164, 1995.
- [31] R. S. Maier, "On reducing the Heun equation to the hypergeometric equation," *Journal of Differential Equations*, vol. 213, no. 1, pp. 171-203, 2005.
- [32] R. Vidunas and G. Filipuk, "Parametric transformations between the Heun and Gauss hypergeometric functions," *Funkcialaj Ekvacioj. Serio Internacia*, vol. 56, no. 2, pp. 271-321, 2013.
- [33] R. Vidunas and G. Filipuk, "A classification of coverings yielding Heun-to-hypergeometric reductions," *Osaka Journal of Mathematics*, vol. 51, no. 4, pp. 867-903, 2014.
- [34] M. van Hoeij and R. Vidunas, "Belyi functions for hyperbolic hypergeometric-to-Heun transformations," *Journal of Algebra*, vol. 441, pp. 609-659, 2015.
- [35] N. Svartholm, "Die Lösung der Fuchs'schen Differentialgleichung zweiter Ordnung durch Hypergeometrische Polynome," *Mathematische Annalen*, vol. 116, no. 1, pp. 413-421, 1939.
- [36] A. Erdélyi, "The Fuchsian equation of second order with four singularities," *Duke Mathematical Journal*, vol. 9, pp. 48-58, 1942.
- [37] A. Erdélyi, "Certain expansions of solutions of the Heun equation," *Quarterly Journal of Mathematics*, vol. 15, pp. 62-69, 1944.
- [38] E. G. Kalnins and J. Miller, "Hypergeometric expansions of Heun polynomials," *SIAM Journal on Mathematical Analysis*, vol. 22, no. 5, pp. 1450-1459, 1991.
- [39] T. A. Ishkhanyan, T. A. Shahverdyan, and A. M. Ishkhanyan, "Expansions of the Solutions of the General Heun Equation Governed by Two-Term Recurrence Relations for Coefficients," *Advances in High Energy Physics*, vol. 2018, Article ID 4263678, 9 pages, 2018.
- [40] J. Letessier, G. Valent, and J. Wimp, "Some differential equations satisfied by hypergeometric functions," in *Approximation and computation (West Lafayette, IN, 1993)*, vol. 119 of *Internat. Ser. Numer. Math.*, pp. 371-381, Birkhauser Boston, Boston, Mass, USA, 1994.
- [41] R. S. Maier, "P-symbols, Heun identities, and 3 F2 identities," in *Special Functions and Orthogonal Polynomials*, vol. 471 of *Contemp. Math.*, pp. 139-159, Amer. Math. Soc., Providence, RI, 2008.
- [42] V. Bargmann, "On the number of bound states in a central field of force," *Proceedings of the National Academy of Sciences of the United States of America*, vol. 38, pp. 961-966, 1952.
- [43] J. Schwinger, "On the bound states of a given potential," *Proceedings of the National Academy of Sciences of the United States of America*, vol. 47, pp. 122-129, 1961.
- [44] F. Calogero, "Upper and lower limits for the number of bound states in a given central potential," *Communications in Mathematical Physics*, vol. 1, pp. 80-88, 1965.
- [45] K. Chadan, "The asymptotic behaviour of the number of bound states of a given potential in the limit of large coupling," *Il Nuovo Cimento A*, vol. 58, no. 1, pp. 191-204, 1968.
- [46] F. Brau, "Limits on the number of bound states and conditions for their existence," in *Studies in mathematical physics research*, pp. 1-54, Nova Sci. Publ., New York, 2004.
- [47] M. Znojil, "Comment on 'Conditionally exactly soluble class of quantum potentials'," *Physical Review A: Atomic, Molecular and Optical Physics*, vol. 61, no. 6, 2000.
- [48] L. Euler, "Institutiones Calculi Integralis," *Opera Omnia*, vol. 11, pp. 110-113, 1768.
- [49] A. Jonquière, "Note sur la série," *Bulletin de la Société Mathématique de France*, vol. 17, pp. 142-152, 1889.
- [50] F. Cooper, A. Khare, and U. Sukhatme, "Supersymmetry and quantum mechanics," *Physics Reports*, vol. 251, no. 5-6, pp. 267-385, 1995.
- [51] B. K. Bagchi, *Supersymmetry in Quantum And Classical Mechanics*, Chapman & Hall/CRC, 2000.
- [52] R. Sasaki and M. Znojil, "One-dimensional Schrödinger equation with non-analytic potential and its exact Bessel-function solvability," *Journal of Physics A: Mathematical and General*, vol. 49, no. 44, Article ID 445303, 2016.
- [53] M. Znojil, "Symmetrized exponential oscillator," *Modern Physics Letters A*, vol. 31, no. 34, 1650195, 11 pages, 2016.
- [54] M. Znojil, "Morse potential, symmetric Morse potential and bracketed bound-state energies," *Modern Physics Letters A*, vol. 31, no. 14, p. 1650088, 2016.
- [55] S. K. Bose, "Exact bound states for the central fraction power singular potential," *Nuovo Cimento*, vol. 109, no. 11, pp. 1217-1220, 1994.
- [56] J. Karwowski and H. A. Witek, "Biconfluent Heun equation in quantum chemistry: Harmonium and related systems," *Theoretical Chemistry Accounts*, vol. 133, no. 7, 2014.
- [57] A. G. Ushveridze, *Quasi-Exactly Solvable Models in Quantum Mechanics*, IOP, Bristol, UK, 1994.
- [58] C. M. Bender and M. Monou, "New quasi-exactly solvable sextic polynomial potentials," *Journal of Physics A: Mathematical and General*, vol. 38, no. 10, pp. 2179-2187, 2005.
- [59] A. V. Turbiner, "One-dimensional quasi-exactly solvable Schrödinger equations," *Physics Reports*, vol. 642, pp. 1-71, 2016.
- [60] M. Abramowitz and I. A. Stegun, *Handbook of Mathematical Functions, with Formulas, Graphs, and Mathematical Tables*, Dover, New York, NY, USA, 1972.

Research Article

Exact Solutions of the Razavy Cosine Type Potential

Shishan Dong ¹, Qian Dong,² Guo-Hua Sun,³ S. Femmam,⁴ and Shi-Hai Dong ²

¹Information and Engineering College, Dalian University, Dalian 116622, China

²Laboratorio de Información Cuántica, CIDETEC, Instituto Politécnico Nacional, UPALM, CDMX 07700, Mexico

³Catedrática CONACYT, CIC, Instituto Politécnico Nacional, CDMX 07738, Mexico

⁴UHA University and Polytechnic Engineers School, Sceaux, France

Correspondence should be addressed to Shi-Hai Dong; dongsh2@yahoo.com

Received 5 June 2018; Revised 3 August 2018; Accepted 5 August 2018; Published 2 October 2018

Academic Editor: Chun-Sheng Jia

Copyright © 2018 Shishan Dong et al. This is an open access article distributed under the Creative Commons Attribution License, which permits unrestricted use, distribution, and reproduction in any medium, provided the original work is properly cited. The publication of this article was funded by SCOAP³.

We solve the quantum system with the symmetric Razavy cosine type potential and find that its exact solutions are given by the confluent Heun function. The eigenvalues are calculated numerically. The properties of the wave functions, which depend on the potential parameter a , are illustrated for a given potential parameter ξ . It is shown that the wave functions are shrunk to the origin when the potential parameter a increases. We note that the energy levels ϵ_i ($i \in [1, 3]$) decrease with the increasing potential parameter a but the energy levels ϵ_i ($i \in [4, 7]$) first increase and then decrease with the increasing a .

1. Introduction

As we know, the exact solutions of quantum systems have been playing an important role since the foundation of quantum mechanics. The hydrogen atom and harmonic oscillator have been taken as typical and seminal examples to explain the classic quantum phenomena in almost all quantum mechanics textbooks [1, 2]. Generally speaking, some popular methods are used to solve these quantum soluble systems. First, we call the functional analysis method, with which one solves the second-order differential equation and obtains their solutions [3] expressed by some well-known special functions. Second, it is called the algebraic method and can be realized by analyzing the Hamiltonian of quantum system. This method is relevant for the SUSYQM [4] and essentially connected to the factorization method [5]. Third, we call the exact quantization rule method [6] and further developed as the proper quantization rule method [7]. The latter approach shows more beauty and symmetry than the former one. It should be recognized that almost all soluble potentials mentioned above belong to single well potentials except for the double well potentials [8–10].

More than thirty years ago, Razavy proposed a cosine type potential [11, 12]

$$V(m, x) = \frac{\hbar^2}{2\mu} \left\{ \frac{1}{8} \xi^2 [1 - \cos(2mx)] - (a + 1) \xi \cos(mx) \right\}, \quad (1)$$

with $V(m, -x) = V(m, x)$ and $V(-m, x) = V(-m, x)$. Here the parameters a, m are positive integers and ξ is a positive real number. (The potential taken here is slightly different from original expression [11, 12], in which a proportional coefficient was included. In addition, the factor $(a + 1)\xi$ is extracted from the originally proposed Razavy potential [11, 12] to incorporate the energy level E . Such a treatment does not affect the property of the quantum system.) In Figure 1, we plot it as a function of the variable x with various a , in which we take $\xi = 3$ and $m = 1$ for simplicity. We find that the minimum value of the potential $V_{\min}(m, x) = -(a + 1)\xi$, which is independent of the parameter m . Razavy presented the so-called exact solutions by using the series method [11, 12]. After studying it carefully, it is found that the solutions cannot be given exactly due to the complicated three-term recurrence relation. The method used by him is nothing but the Bethe ansatz method as summarized in [13]. In this case the solutions cannot be expressed as

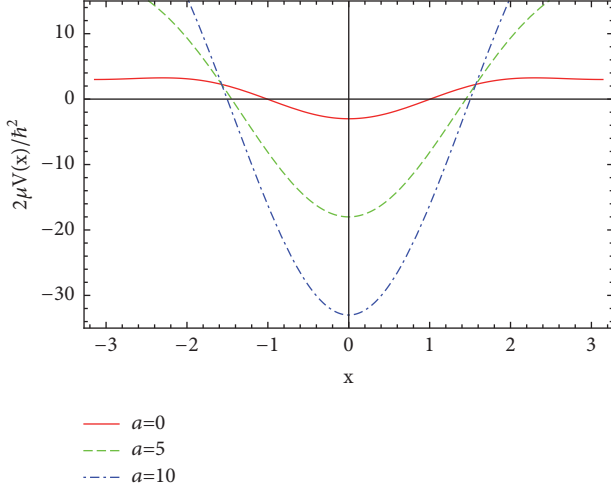


FIGURE 1: A plot of potential as function of the variables x and a .

one of the special functions due to the complicated three-term recurrence relations. One must take some constraints on the coefficients in the recurrence relations as shown in [11, 12] to obtain *quasi*-exact solutions. Recently it is found that the solutions of the hyperbolic type potentials [14–21] are given explicitly by the confluent Heun function [22]. Just recently, we have carried out the Razavy cosine hyperbolic type $V(x) = (\hbar^2 \beta^2 / 2\mu)[(1/8)\xi^2 \cosh(4\beta x) - (m+1)\xi \cosh(2\beta x) - (1/8)\xi^2]$, which was studied by Razavy in [11, 12] and found that its solutions can be written as the confluent Heun function [23]. The purpose of this work is to study the solutions of the Razavy cosine type potential (1) [11, 12] and to see whether its solutions can be written as the confluent Heun function or not. The answer is yes, but the energy spectra must be calculated numerically since the energy level term is involved inside the parameter η of the confluent Heun function $H_c(\alpha, \beta, \gamma, \delta, \eta; z)$. Even though the Heun functions have been studied well since 1889, its main topics are focused on the mathematical area. The reason why Razavy did not find its solutions related to this function is that only recent connections with the physical problems have been discovered, in particular for those hyperbolic type potentials [14–21].

This paper is organized as follows. In Section 2, we show how to obtain the solutions of the Schrödinger equation with the Razavy cosine type potential. This is realized by transforming the Schrödinger equation into a confluent Heun differential equation through taking some variable transformations. In Section 3, some fundamental properties of the solutions are studied and illustrated graphically. The energy levels for different parameter values a are calculated numerically. We summarize our results and conclusions in Section 4.

2. Exact Solutions

Let us consider the one-dimensional Schrödinger equation,

$$-\frac{\hbar^2}{2\mu} \frac{d^2}{dx^2} \psi(x) + V(x) \psi(x) = E \psi(x). \quad (2)$$

Substituting potential (1) into (2), we have

$$\begin{aligned} \frac{d^2}{dx^2} \psi(x) + \left\{ \epsilon \right. \\ \left. - \left[\frac{1}{8} \xi^2 (1 - \cos(2mx)) - (a+1) \xi \cos(mx) \right] \right\} \\ \cdot \psi(x) = 0, \\ \epsilon = \frac{2\mu E}{\hbar^2} - (a+1) \xi. \end{aligned} \quad (3)$$

Take the wave functions of the form

$$\psi(x) = \exp\left[\frac{\xi \cos(mx)}{2m}\right] \phi(x). \quad (4)$$

Substituting this into (3) yields

$$\begin{aligned} \phi''(x) - \xi \sin(mx) \phi'(x) \\ + \frac{1}{2} [\xi(2a - m + 2) \cos(mx) + 2\epsilon] \phi(x) = 0. \end{aligned} \quad (5)$$

Choose a new variable $z = \cos^2(mx/2)$. The above equation becomes

$$\begin{aligned} (z-1)z\phi''(z) + \frac{1}{2} \left(\frac{4\xi(z-1)z}{m} + 2z-1 \right) \phi'(z) \\ - \frac{\phi(z) [\xi(2z-1)(2a-m+2) + 2\epsilon]}{2m^2} = 0, \end{aligned} \quad (6)$$

which can be rearranged as

$$\begin{aligned} \phi''(z) + \left[\frac{2\xi}{m} + \frac{1}{2} \left(\frac{1}{z-1} + \frac{1}{z} \right) \right] \phi'(z) \\ - \frac{\xi(2z-1)(2a-m+2) + 2\epsilon}{2m^2(z-1)z} \phi(z) = 0. \end{aligned} \quad (7)$$

Compared this with the confluent Heun differential equation in the simplest uniform form [22]

$$\begin{aligned} \frac{d^2 H(z)}{dz^2} + \left(\alpha + \frac{1+\beta}{z} + \frac{1+\gamma}{z-1} \right) \frac{dH(z)}{dz} \\ + \left(\frac{\mu}{z} + \frac{\nu}{z-1} \right) H(z) = 0, \end{aligned} \quad (8)$$

we find the solution to (7) is given by the acceptable confluent Heun function $H_c(\alpha, \beta, \gamma, \delta, \eta; z)$ with the following parameters:

$$\begin{aligned} \alpha &= \frac{2\xi}{m}, \\ \beta &= -\frac{1}{2}, \\ \gamma &= -\frac{1}{2}, \end{aligned} \quad (9)$$

$$\mu_{\pm} = \frac{\xi(-2a+m-2) \pm 2\epsilon}{2m^2},$$

$$\nu = \mu_-$$

TABLE I: Spectra of the Schrödinger equation with potential (1).

a	ϵ_1	ϵ_2	ϵ_3	ϵ_4	ϵ_5	ϵ_6	ϵ_7
$a = 0$	-1.25000	1.79206	3.88549	5.52599	7.571	10.2587	13.4768
$a = 1$	-3.85555	0.105572	3.35555	5.88783	8.10716	10.6369	13.7448
$a = 2$	-6.5289	-1.86011	2.22966	5.68013	8.54924	11.2207	14.2107
$a = 3$	-9.2426	-3.97095	0.793349	5.00238	8.62128	11.7636	14.8280
$a = 4$	-11.9842	-6.17622	-0.831098	4.01497	8.31808	12.0716	15.4571
$a = 5$	-14.7467	-8.44991	-2.58550	2.81773	7.72170	12.0880	15.9545
$a = 6$	-17.5255	-10.7764	-4.43719	1.46786	6.90679	11.8388	16.2407
$a = 7$	-20.3178	-13.1452	-6.36553	0.00034	5.92502	11.3718	16.3004
$a = 8$	-23.1212	-15.5492	-8.35647	-1.56169	4.81114	10.7299	16.1532
$a = 9$	-25.9342	-17.9829	-10.3999	-3.20197	3.58925	9.94554	15.8289
$a = 10$	-28.7554	-20.4422	-12.4881	-4.90854	2.27678	9.04264	15.3551

from which we are able to calculate the parameters δ and η as

$$\begin{aligned}\delta &= \mu_+ + \mu_- - \frac{1}{2}\alpha(\beta + \gamma + 2) = -\frac{2(a+1)\xi}{m^2}, \\ \eta &= \frac{1}{2}\alpha(\beta + 1) - \mu_+ - \frac{1}{2}(\beta + \gamma + \beta\gamma) \\ &= \frac{8(a+1)\xi + 3m^2 - 8\epsilon}{8m^2},\end{aligned}\quad (10)$$

which implies the parameter η involved in the confluent Heun function is related to energy levels. The wave function given by this Heun function seems to be analytical, but the key issue is how to first get the energy levels. Otherwise, the solution becomes unsolvable. Generally, the confluent Heun function can be expressed as a series expansion

$$H_C(\alpha, \beta, \gamma, \delta, \eta; z) = \sum_{n=0}^{\infty} v_n(\alpha, \beta, \gamma, \delta, \eta, \xi) z^n, \quad (11)$$

$$|z| < 1.$$

The coefficients v_n are given by a three-term recurrence relation

$$\begin{aligned}A_n v_n - B_n v_{n-1} - C_n v_{n-2} &= 0, \\ v_{-1} &= 0, \\ v_0 &= 1,\end{aligned}\quad (12)$$

with

$$\begin{aligned}A_n &= 1 + \frac{\beta}{n} = 1 - \frac{1}{2n}, \\ B_n &= 1 + \frac{1}{n}(\beta + \gamma - \alpha - 1) \\ &\quad + \frac{1}{n^2} \left\{ \eta - \frac{1}{2}(\beta + \gamma - \alpha) - \frac{\alpha\beta}{2} + \frac{\beta\gamma}{2} \right\}, \\ &= \frac{2(a\xi + \xi - \epsilon) + 2m^2(n-1)^2 + m(3-4n)\xi}{2m^2n^2}\end{aligned}$$

$$\begin{aligned}C_n &= \frac{\alpha}{n^2} \left(\frac{\delta}{\alpha} + \frac{\beta + \gamma}{2} + n - 1 \right) \\ &= \frac{\xi(-2a + m(2n-3) - 2)}{m^2n^2}\end{aligned}\quad (13)$$

To make the confluent Heun function reduce to polynomials, two termination conditions have to be satisfied [22]

$$\begin{aligned}\mu_+ + \mu_- + N\alpha &= 0, \\ \Delta_{N+1}(\mu_+) &= 0.\end{aligned}\quad (14)$$

The second condition is a tridiagonal determinant and can be constructed by the matrix elements

$$\begin{aligned}a_{ii} &= \mu_+ - s_i + (i-1)\alpha, \\ a_{ii+1} &= i(i+\beta), \\ a_{i+1i} &= (N-i+1)\alpha, \\ s_i &= (i-1)(i+\beta+\gamma),\end{aligned}\quad (15)$$

$$i = 1, 2, \dots, N, N+1.$$

The explicit expression of this determinant can refer to [16–19] for some detail.

For present case, there is a problem for the first condition. That is, $\mu_+ + \mu_- + \alpha = 0$ when $N = 1$. From this we have $m = 2(1+a)/(1+4\xi)$. This is contrary to the assumption m is positive integer. Therefore, how to obtain the eigenvalues becomes a challenging task. Due to $z \in [0, 1]$ we would like to solve this problem via series expansion method as shown in [15]. Unfortunately, the calculation results are not ideal. We have to solve it in another way as shown in [14].

3. Fundamental Properties

Now, let us study some basic properties of the solutions as shown in Figures 2 and 3. We find that the wave functions are shrunk to the origin when the potential parameter a increases. This makes the amplitude of the wave function be increased. We list the energy levels ϵ_i ($i \in [1, 7]$) in Table I and illustrate them in Figure 3. We notice that the energy levels ϵ_i

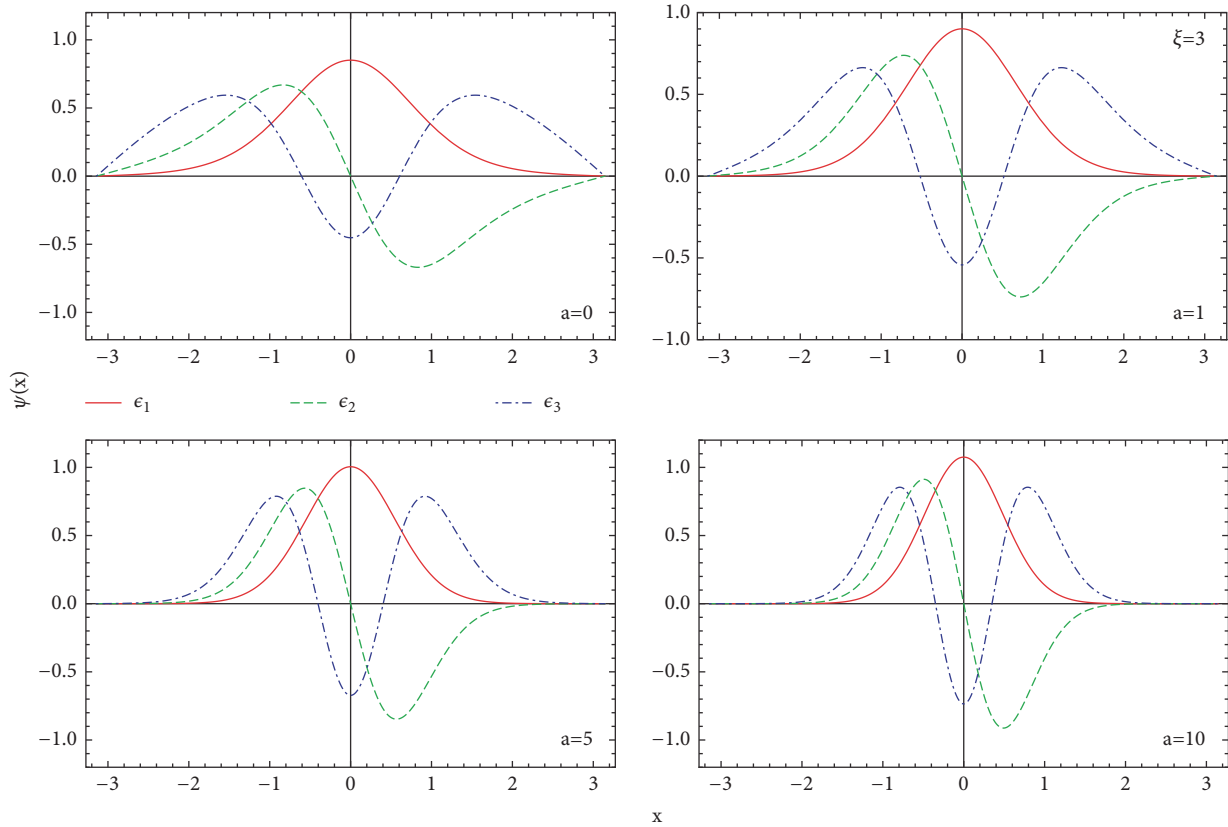


FIGURE 2: The characteristics of wave functions as a function of the position x . We take $\xi = 3$.

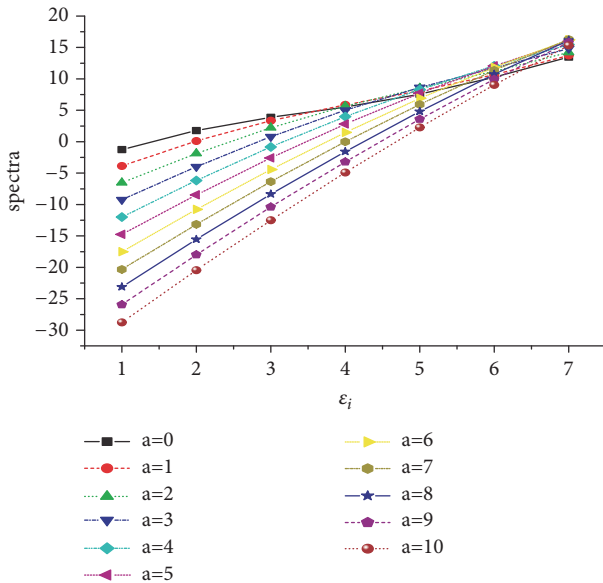


FIGURE 3: The variation of the energy spectra ϵ_i and $\xi = 3$.

$(i \in [1, 3])$ decrease with the increasing potential parameter a but ϵ_i ($i \in [4, 7]$) first increase and then decrease with the increasing potential parameter a .

4. Conclusions

In this work we have studied the quantum system with the Razavy cosine type potential and found that its exact solutions are given by confluent Heun function $\psi(z) = \exp[(2z - 1)\xi/2]H_c(\alpha, \beta, \gamma, \delta, \eta; z)$ by transforming the original differential equation into a confluent type Heun differential equation. The fact that the energy levels are involved inside the parameter η makes us calculate the eigenvalues numerically. The properties of the wave functions depending on the potential parameter a have been illustrated graphically for a given potential parameter ξ . We have also noticed that the energy levels ϵ_i ($i \in [1, 3]$) decrease with the increasing potential parameter a but ϵ_i ($i \in [4, 7]$) first increase and then decrease with the increasing a .

Data Availability

The data used to support the findings of this study are available from the corresponding author upon request.

Conflicts of Interest

The authors declare that there are no conflicts of interest regarding the publication of this paper.

Acknowledgments

This work is supported by project 20180677-SIP-IPN, COFAA-IPN, Mexico, and partially by the CONACYT project under grant No. 288856-CB-2016.

References

- [1] L. D. Landau and E. M. Lifshitz, *Quantum mechanics: non-relativistic theory*, Pergamon, New York, NY, USA, 1977.
- [2] L. I. Schiff, *Quantum Mechanics*, McGraw-Hill Book Co., New York, NY, USA, 3rd edition, 1955.
- [3] D. ter Haar, *Problems in Quantum Mechanics*, Pion Ltd, London, 3rd edition, 1975.
- [4] F. Cooper, A. Khare, and U. Sukhatme, "Supersymmetry and quantum mechanics," *Physics Reports*, vol. 251, no. 5-6, pp. 267–385, 1995.
- [5] S. H. Dong, *Factorization Method in Quantum Mechanics*, vol. 150, Springer, Kluwer Academic Publisher, 2007.
- [6] Z. Q. Ma and B. W. Xu, "Quantum correction in exact quantization rules," *EPL (Europhysics Letters)*, vol. 69, p. 685, 2005.
- [7] W. C. Qiang and S. H. Dong, "Proper quantization rule," *EPL*, vol. 89, article 10003, 2010.
- [8] H. Konwent, P. Machnikowski, and A. Radosz, "A certain double-well potential related to SU(2) symmetry," *Journal of Physics A: Mathematical and General*, vol. 28, no. 13, pp. 3757–3762, 1995.
- [9] Q.-T. Xie, "New quasi-exactly solvable double-well potentials," *Journal of Physics A: Mathematical and General*, vol. 45, no. 17, Article ID 175302, 2012.
- [10] B. Chen, Y. Wu, and Q. Xie, "Heun functions and quasi-exactly solvable double-well potentials," *Journal of Physics A: Mathematical and Theoretical*, vol. 46, no. 3, 2013.
- [11] M. Razavy, "A potential model for torsional vibrations of molecules," *Physics Letters A*, vol. 82, no. 1, pp. 7–9, 1981.
- [12] M. Razavy, "An exactly soluble Schrödinger equation with a bistable potential," *American Journal of Physics*, vol. 48, no. 4, p. 285, 1980.
- [13] S.-H. Dong, *Wave Equation in Higher Dimensions*, Springer, Berlin, Germany, 2011.
- [14] S. Dong, Q. Fang, B. J. Falaye, G. Sun, C. Yáñez-Márquez, and S. Dong, "Exact solutions to solitonic profile mass Schrödinger problem with a modified Pöschl–Teller potential," *Modern Physics Letters A*, vol. 31, no. 04, p. 1650017, 2016.
- [15] S. Dong, G. H. Sun, B. J. Falaye, and S. H. Dong, "Semi-exact solutions to position-dependent mass Schrödinger problem with a class of hyperbolic potential $V_0 \tanh(ax)$," *The European Physical Journal Plus*, vol. 131, no. 5, p. 176, 2016.
- [16] G. H. Sun, S. H. Dong, K. D. Launey, T. Dytrych, J. P. Draayer, and J. Quan, "Shannon information entropy for a hyperbolic double-well potential," *International Journal of Quantum Chemistry*, vol. 115, no. 14, article 891, 2015.
- [17] C. A. Downing, "On a solution of the Schrödinger equation with a hyperbolic double-well potential," *Journal of Mathematical Physics*, vol. 54, no. 7, 072101, 8 pages, 2013.
- [18] P. P. Fiziev, "Novel relations and new properties of confluent Heun's functions and their derivatives of arbitrary order," *Journal of Physics A: Mathematical and General*, vol. 43, no. 3, article 035203, 2010.
- [19] R. R. Hartmann and M. E. Portnoi, "Quasi-exact solution to the Dirac equation for the hyperbolic-secant potential," *Physical Review A: Atomic, Molecular and Optical Physics*, vol. 89, no. 1, 2014.
- [20] D. Agboola, "On the solvability of the generalized hyperbolic double-well models," *Journal of Mathematical Physics*, vol. 55, no. 5, Article ID 052102, 8 pages, 2014.
- [21] F.-K. Wen, Z.-Y. Yang, C. Liu, W.-L. Yang, and Y.-Z. Zhang, "Exact Polynomial Solutions of Schrödinger equation with various hyperbolic potentials," *Communications in Theoretical Physics*, vol. 61, no. 2, pp. 153–159, 2014.
- [22] A. Ronveaux, Ed., *Heun's Differential Equations*, Oxford University Press, Oxford, 1995.
- [23] Q. Dong, F. Serrano, G. H. Sun, J. Jing, and S. H. Dong, "Semi-exact solutions of the Razavy potential," *Advances in High Energy Physics*.

Research Article

Semiexact Solutions of the Razavy Potential

Qian Dong,¹ F. A. Serrano,² Guo-Hua Sun,³ Jian Jing ,⁴ and Shi-Hai Dong ¹

¹Laboratorio de Información Cuántica, CIDETEC, Instituto Politécnico Nacional, UPALM, CDMX 07700, Mexico

²Escuela Superior de Ingeniería Mecánica y Eléctrica UPC, Instituto Politécnico Nacional, Av. Santa Ana 1000, México, D. F. 04430, Mexico

³Catedrática CONACYT, CIC, Instituto Politécnico Nacional, CDMX 07738, Mexico

⁴Department of Physics and Electronic, School of Science, Beijing University of Chemical Technology, Beijing 100029, China

Correspondence should be addressed to Shi-Hai Dong; dongsh2@yahoo.com

Received 9 May 2018; Accepted 10 June 2018; Published 28 August 2018

Academic Editor: Saber Zarrinkamar

Copyright © 2018 Qian Dong et al. This is an open access article distributed under the Creative Commons Attribution License, which permits unrestricted use, distribution, and reproduction in any medium, provided the original work is properly cited. The publication of this article was funded by SCOAP³.

In this work, we study the quantum system with the symmetric Razavy potential and show how to find its exact solutions. We find that the solutions are given by the confluent Heun functions. The eigenvalues have to be calculated numerically. The properties of the wave functions depending on m are illustrated graphically for a given potential parameter ξ . We find that the even and odd wave functions with definite parity are changed to odd and even wave functions when the potential parameter m increases. This arises from the fact that the parity, which is a defined symmetry for very small m , is completely violated for large m . We also notice that the energy levels ϵ_i decrease with the increasing potential parameter m .

1. Introduction

It is well-known that the exact solutions of quantum systems play an important role since the early foundation of the quantum mechanics. Generally speaking, two typical examples are studied for the hydrogen atom and harmonic oscillator in classical quantum mechanics textbooks [1, 2]. Up till now, there are a few main methods to solve the quantum soluble systems. The first is called the functional analysis method. That is to say, one solves the second-order differential equation and obtains their solutions [3], which are expressed by some well-known special functions. The second is called the algebraic method, which is realized by studying the Hamiltonian of quantum system. This method is also related to supersymmetric quantum mechanics (SUSYQM) [4], further closely with the factorization method [5]. The third is called the exact quantization rule method [6], from which we proposed proper quantization rule [7], which shows more beauty and symmetry than exact quantization rule. It should be recognized that almost all soluble potentials mentioned above belong to single well potentials. The double-well potentials have not been studied well due to their complications [8–17],

in which many authors have been searching the solutions of the double-well potentials for a long history. This is because the double-well potentials could be used in the quantum theory of molecules to describe the motion of the particle in the presence of two centers of force, the heterostructures, Bose-Einstein condensates, superconducting circuits, etc.

Almost forty years ago, Razavy proposed a bistable potential [18]:

$$V(x) = \frac{\hbar^2 \beta^2}{2\mu} \left[\frac{1}{8} \xi^2 \cosh(4\beta x) - (m+1) \xi \cosh(2\beta x) - \frac{1}{8} \xi^2 \right], \quad (1)$$

which depends on three potential parameters β , ξ , and a positive integer m . In Figure 1 we plot it as the function of the variables x with various m , in which we take $\beta = 1$ and $\xi = 3$. Choose atomic units $\hbar = \mu = 1$ and also take $\mathcal{V}(x) = 2V(x)$. Using series expansion around the origin, we have

$$\mathcal{V}(x) = (-m\xi - \xi) + x^2(-2m\xi + \xi^2 - 2\xi)$$

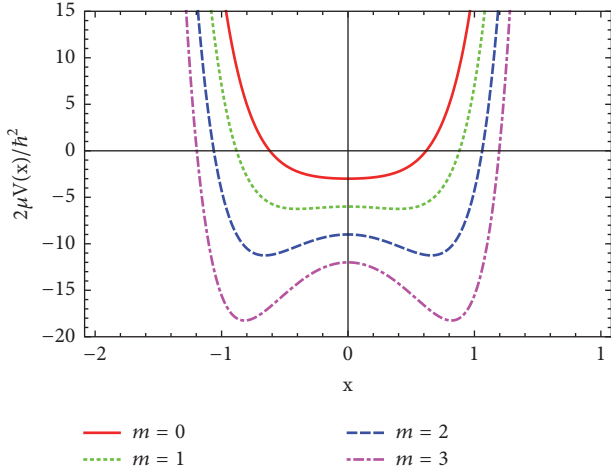


FIGURE 1: (Color online) A plot of potential as function of the variables x and m .

$$\begin{aligned}
 & + \frac{2}{3}x^4(-m\xi + 2\xi^2 - \xi) \\
 & + \frac{4}{45}x^6(-m\xi + 8\xi^2 - \xi) + O(x^7),
 \end{aligned} \tag{2}$$

which shows that $\mathcal{V}(x)$ is symmetric to variable x . We find that the minimum value of the potential $\mathcal{V}_{\min}(x) = -(m+1)^2 - \xi^2/4$ at two minimum values $x = \pm(1/2)\cosh^{-1}[2(m+1)/\xi]$. For a given value $\xi = 3$, we find that the potential has a flat bottom for $n = 0$, but for $n > 1$ it takes the form of a double-well. Razavy presented the so-called exact solutions by using the ‘‘polynomial method’’ [18]. After studying it carefully, we find that the solutions cannot be given exactly due to the complicated three-term recurrence relation. The method presented there [18] is more like the Bethe Ansatz method as summarized in our recent book [19]. That is, the solutions cannot be expressed as one of special functions because of three-term recurrence relations. In order to obtain some so-called exact solutions, the author has to take some constraints on the coefficients in the recurrence relations as shown in [18]. Inspired by recent study of the hyperbolic type potential well [20–28], in which we have found that their solutions can be exactly expressed by the confluent Heun functions [23], in this work we attempt to study the solutions of the Razavy potential. We shall find that the solutions can be written as the confluent Heun functions but their energy levels have to be calculated numerically since the energy term is involved within the parameter η of the confluent Heun functions $H_c(\alpha, \beta, \gamma, \delta, \eta, z)$. This constraints us to use the traditional Bethe Ansatz method to get the energy levels. Even though the Heun functions have been studied well, its main topics are focused in the mathematical area. Only recent connections with the physical problems have been discovered; in particular the quantum systems for those hyperbolic type potential have been studied [20–28]. The terminology ‘‘semiexact’’ solutions used in [21] arise from

the fact that the wave functions can be obtained analytically, but the eigenvalues cannot be written out explicitly.

This paper is organized as follows. In Section 2, we present the solutions of the Schrödinger equation with the Razavy potential. It should be recognized that the Razavy potential is single or double-well depends on the potential parameter m . In Section 3 some fundamental properties of the solutions are studied. The energy levels for different m are calculated numerically. Some concluding remarks are given in Section 4.

2. Semiexact Solutions

Let us consider the one-dimensional Schrödinger equation:

$$-\frac{\hbar^2}{2\mu} \frac{d^2}{dx^2} \psi(x) + V(x) \psi(x) = E \psi(x). \tag{3}$$

Substituting potential (1) into (3), we have

$$\begin{aligned}
 & \frac{d^2}{dx^2} \psi(x) + \left\{ \epsilon \right. \\
 & \left. - \left[\frac{1}{8} \xi^2 \cosh(4x) - (m+1) \xi \cosh(2x) - \frac{1}{8} \xi^2 \right] \right\} \\
 & \cdot \psi(x) = 0, \\
 & \epsilon = 2E.
 \end{aligned} \tag{4}$$

Take the wave functions of the form

$$\psi(x) = e^{\xi \cosh^2(x)/2} y(x). \tag{5}$$

Substituting this into (4) allows us to obtain

$$\begin{aligned}
 & y''(x) + \xi \sinh(2x) y'(x) \\
 & + [(m+2) \xi \cosh(2x) + \epsilon] y(x) = 0.
 \end{aligned} \tag{6}$$

Take a new variable $z = \cosh^2(x)$. The above equation becomes

$$\begin{aligned}
 & 4(z-1)zy''(z) + [4z(\xi(z-1)+1)-2]y'(z) \\
 & + ((m+2)\xi(2z-1)+\epsilon)y(z) = 0
 \end{aligned} \tag{7}$$

which can be rearranged as

$$\begin{aligned}
 & y''(z) + \left[\xi + \frac{1}{2} \left(\frac{1}{z} + \frac{1}{z-1} \right) \right] y'(z) \\
 & + \frac{(m+2)\xi(2z-1)+\epsilon}{4(z-1)z} y(z) = 0.
 \end{aligned} \tag{8}$$

When comparing this with the confluent Heun differential equation in the simplest uniform form [13]

$$\begin{aligned}
 & \frac{d^2 H(z)}{dz^2} + \left(\alpha + \frac{1+\beta}{z} + \frac{1+\gamma}{z-1} \right) \frac{dH(z)}{dz} \\
 & + \left(\frac{\mu}{z} + \frac{\nu}{z-1} \right) H(z) = 0,
 \end{aligned} \tag{9}$$

we find the solution to (8) is given by the acceptable confluent Heun function $H_c(\alpha, \beta, \gamma, \delta, \eta; z)$ with

$$\begin{aligned} \alpha &= \xi, \\ \beta &= -\frac{1}{2}, \\ \gamma &= -\frac{1}{2}, \\ \mu &= \frac{\xi(m+2) - \varepsilon}{4}, \\ \nu &= \frac{\xi(m+2) + \varepsilon}{4}, \end{aligned} \quad (10)$$

from which we are able to calculate the parameters δ and η involved in $H_c(\alpha, \beta, \gamma, \delta, \eta; z)$ as

$$\begin{aligned} \delta &= \mu + \nu - \frac{1}{2}\alpha(\beta + \gamma + 2) = \frac{1}{2}(m+1)\xi, \\ \eta &= \frac{1}{2}\alpha(\beta + 1) - \mu - \frac{1}{2}(\beta + \gamma + \beta\gamma) \\ &= \frac{1}{8}[-2(m+1)\xi + 2\varepsilon + 3]. \end{aligned} \quad (11)$$

It is found that the parameter η related to energy levels is involved in the confluent Heun function. The wave function given by this function seems to be analytical, but the key issue is how to first get the energy levels. Otherwise, the solution becomes unsolvable. Generally, the confluent Heun function can be expressed as a series of expansions:

$$H_C(\alpha, \beta, \gamma, \delta, \eta, z) = \sum_{n=0}^{\infty} v_n(\alpha, \beta, \gamma, \delta, \eta, \xi) z^n,$$

$$\begin{vmatrix} \mu - p_1 & (1 + \beta) & 0 & \dots & 0 & 0 & 0 \\ N\alpha & \mu - p_2 + \alpha & 2(2 + \beta) & \dots & 0 & 0 & 0 \\ 0 & (N - 1)\alpha & \mu - p_3 + 2\alpha & \dots & 0 & 0 & 0 \\ \vdots & \vdots & \vdots & \ddots & \vdots & \vdots & \vdots \\ 0 & 0 & 0 & \dots & \mu - p_{N-1} + (N - 2)\alpha & (N - 1)(N - 1 + \beta) & 0 \\ 0 & 0 & 0 & \dots & 2\alpha & \mu - p_N + (N - 1)\alpha & N(N + \beta) \\ 0 & 0 & 0 & \dots & 0 & \alpha & \mu - p_{N+1} + N\alpha \end{vmatrix} = 0 \quad (16)$$

with

$$p_N = (N - 1)(N + \beta + \gamma). \quad (17)$$

For present problem, it is not difficult to see that the first condition is violated. That is, $\mu + \nu + \alpha = 0$ when $N = 1$. From this we have $m = -4$. This is contrary to the fact that m is a positive integer. Therefore, we cannot use this method to obtain the eigenvalues. On the other hand, we know that $z \in [1, \infty)$. Thus, the series expansion method is invalid. This is unlike previous study [22, 24], in which the quasixact wave

$$|z| < 1. \quad (12)$$

The coefficients v_n are given by a three-term recurrence relation:

$$\begin{aligned} A_n v_n - B_n v_{n-1} - C_n v_{n-2} &= 0, \\ v_{-1} &= 0, \\ v_0 &= 1, \end{aligned} \quad (13)$$

with

$$\begin{aligned} A_n &= 1 + \frac{\beta}{n}, \\ B_n &= 1 + \frac{1}{n}(\beta + \gamma - \alpha - 1) \\ &\quad + \frac{1}{n^2} \left\{ \eta - \frac{1}{2}(\beta + \gamma - \alpha) - \frac{\alpha\beta}{2} + \frac{\beta\gamma}{2} \right\}, \\ C_n &= \frac{\alpha}{n^2} \left(\frac{\delta}{\alpha} + \frac{\beta + \gamma}{2} + n - 1 \right). \end{aligned} \quad (14)$$

To make the confluent Heun functions reduce to polynomials, two termination conditions have to be satisfied [13, 14]:

$$\begin{aligned} \mu + \nu + N\alpha &= 0, \\ \Delta_{N+1}(\mu) &= 0, \end{aligned} \quad (15)$$

where

functions and eigenvalues can be obtained by studying those two constraints. The present case is similar to our previous study [20, 21], in which some constraint is violated. We have to choose other approach to study the eigenvalues as used in [20, 21].

3. Fundamental Properties

In this section we are going to study some basic properties of the wave functions as shown in Figures 2–4. We first consider the positive integer m . Since the energy spectrum

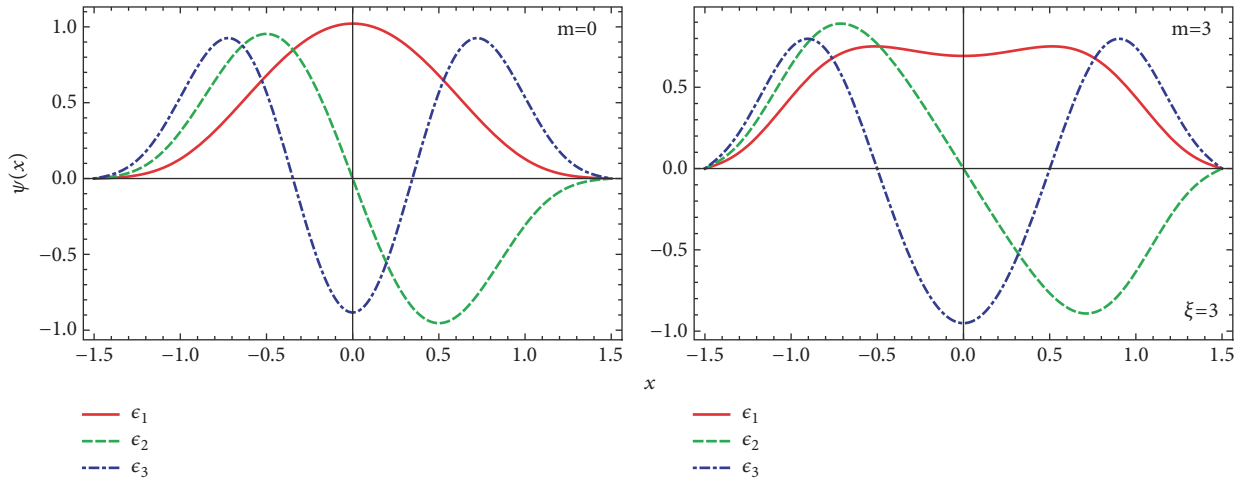


FIGURE 2: (Color online) The characteristics of the potential $V(z)$ as a function of the position z . We take $m = 0, 1$ and $\xi = 3$.

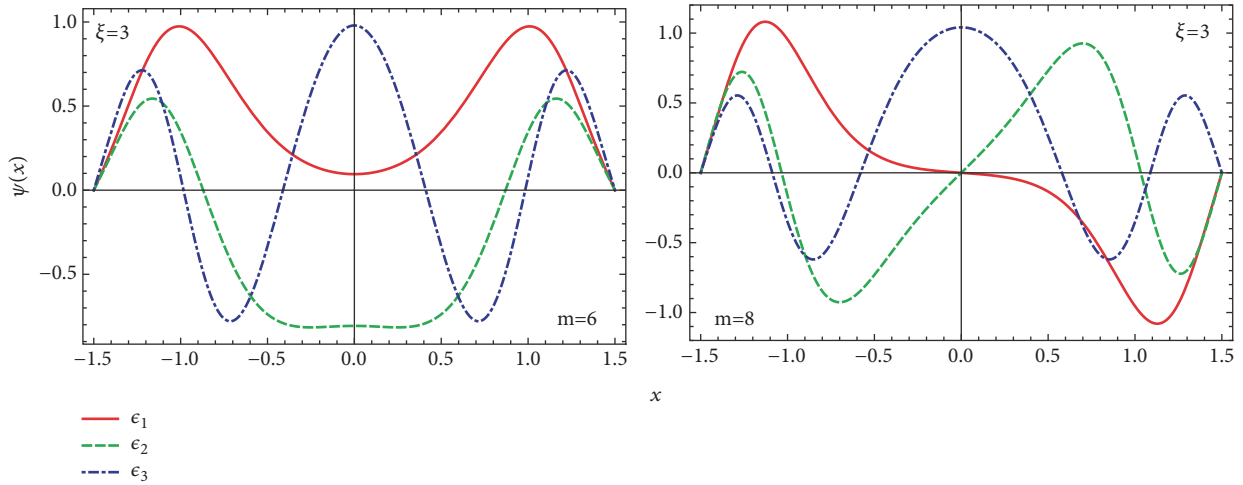


FIGURE 3: (Color online) The characteristics of the potential $V(z)$ as a function of the position z . We take $m = 6, 8$ and $\xi = 3$.

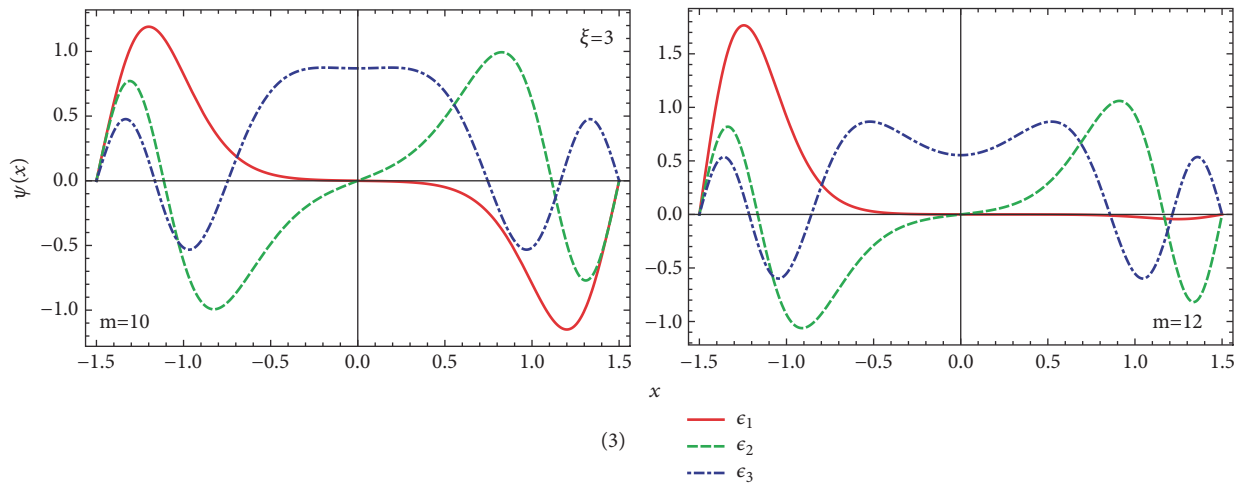


FIGURE 4: (Color online) The same as the above case but $m = 10, 12$.

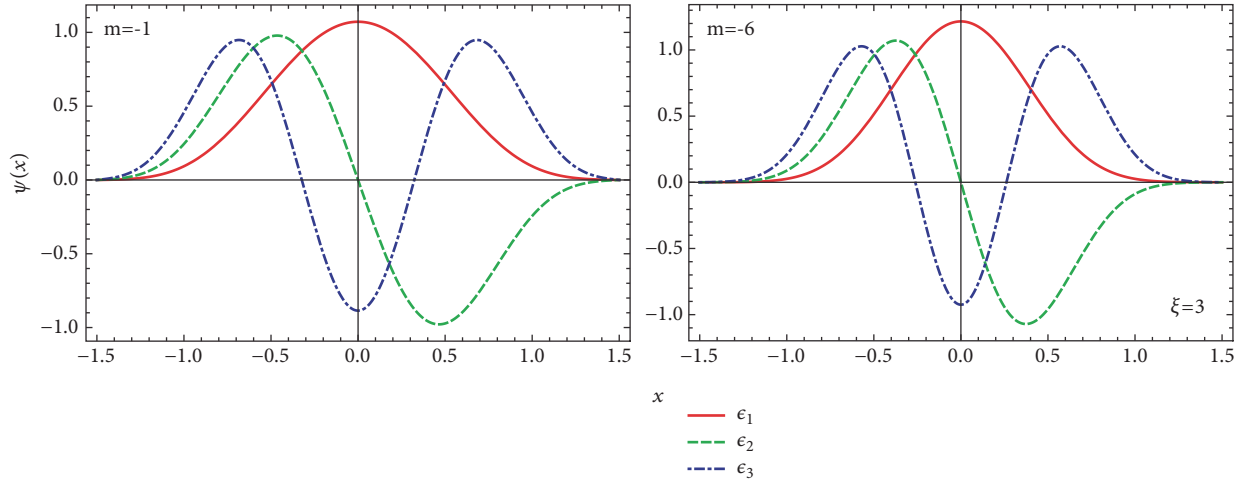


FIGURE 5: (Color online) The characteristics of the potential $V(z)$ as a function of the position z . We take $m = -1, -6$ and $\xi = 3$.

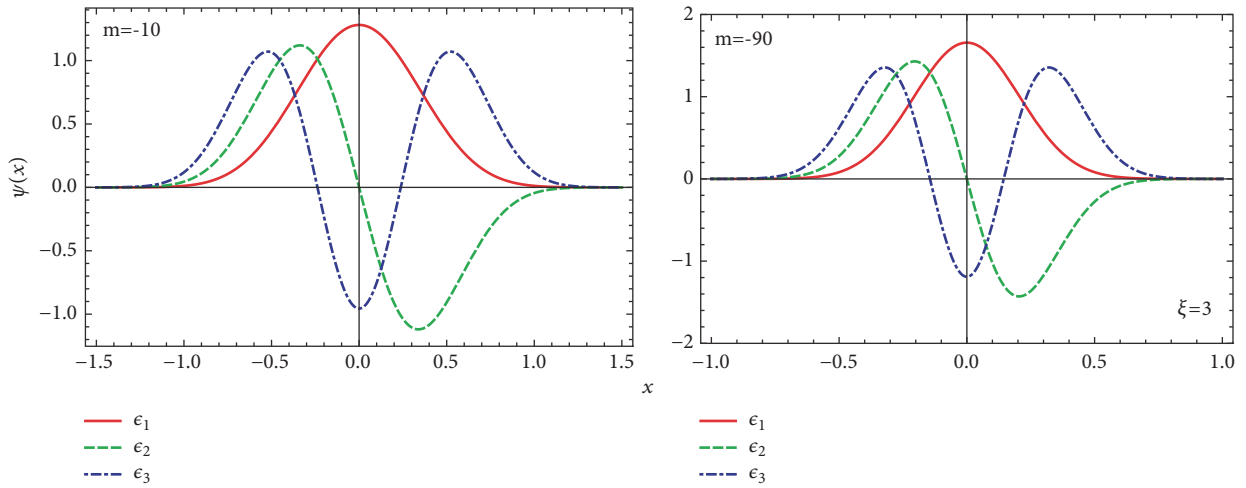


FIGURE 6: (Color online) The same as the above case but $m = -10, -90$.

cannot be given explicitly we have to solve the second-order differential equation (4) numerically. We denote the energy levels as ϵ_i ($i \in [1, 6]$) in Table 1. We find that the energy levels ϵ_i decrease with the increasing m . Originally, we wanted to calculate the energy levels numerically by using powerful MAPLE, which includes some special functions such as the confluent Heun function that cannot be found in MATHEMATICA. As we know, the wave function is given by $\psi(z) = \exp(z\xi/2)H_c(\alpha, \beta, \gamma, \delta, \eta, z)$. Generally speaking, the wave function requires $\psi(z) \rightarrow 0$ when $z \rightarrow \infty$; i.e., $x \rightarrow \infty$. Unfortunately, the present study is unlike our previous study [20, 21], in which $z \rightarrow 1$ when x goes to infinity. The energy spectra can be calculated by series expansions through taking $z \rightarrow 1$. On the other hand, the wave functions have a definite parity; e.g., for $m = 0$ some wave functions are symmetric. It is found that such properties are violated when the potential parameter m becomes larger as shown in Figure 4. That is, the wave functions for $m = 12$ are nonsymmetric. In addition, on the contrary to the case discussed by Razavy [18], in which he supposed the m is taken

as positive integers, we are going to show what happens to the negative m case. We display the graphics in Figures 5 and 6 for this case. We find that the wave functions are shrunk towards the origin. This makes the amplitude of the wave function increase.

4. Conclusions

In this work we have studied the quantum system with the Razavy potential, which is symmetric with respect to the variable x and showed how its exact solutions are found by transforming the original differential equation into a confluent type Heun differential equation. It is found that the solutions can be expressed by the confluent Heun functions $H_c(\alpha, \beta, \gamma, \delta, \eta)$, in which the energy levels are involved inside the parameter η . This makes us calculate the eigenvalues numerically. The properties of the wave functions depending on m are illustrated graphically for a given potential parameter ξ . We have found that the even and odd wave functions with definite parity are changed to odd and even

TABLE 1: Energy levels of the Schrödinger equation with potential (1).

ν	ϵ_1	ϵ_2	ϵ_3	ϵ_4	ϵ_5	ϵ_6
$m = -6$	21.6608	35.7557	51.3448	68.3341	86.6500	106.233
$m = -5$	18.1891	31.3844	46.1503	62.3746	79.9715	98.8740
$m = -4$	14.6806	26.9167	40.8214	56.2549	73.1150	91.3249
$m = -3$	11.1259	22.3314	35.3346	49.9525	66.0599	83.5680
$m = -2$	7.51110	17.5996	29.6610	43.4412	58.7838	75.5860
$m = -1$	3.81463	12.6800	23.7644	36.6914	51.2639	67.3635
$m = 0$	0.00007	7.51170	17.6027	29.6729	43.4799	58.8919
$m = 1$	-3.99968	2.00200	11.1343	22.3606	35.4208	50.1750
$m = 2$	-8.32288	-3.99300	4.34771	14.7494	27.0959	41.2385
$m = 3$	-13.2815	-10.6927	-2.64788	6.87526	18.5501	32.1389
$m = 4$	-19.5196	-9.46859	-1.17161	9.87916	22.9677	38.0537
$m = 5$	-27.7547	-15.7094	-9.29612	1.24110	13.8439	28.5940
$m = 6$	-38.0314	-21.6913	-17.5131	-7.12621	4.89289	19.3065
$m = 7$	-49.9928	-28.2027	-25.9897	-14.8827	-3.78434	10.2625
$m = 8$	-63.3335	-35.8866	-21.7455	-12.1464	1.51447	17.5661
$m = 9$	-77.8339	-44.5255	-27.8571	-20.2355	-6.89162	8.76577
$m = 10$	-93.3024	-54.9017	-33.6970	-28.1690	-14.8944	0.229704
$m = 11$	-109.592	-65.743	-39.7373	-36.1005	-22.4007	-8.04337
$m = 12$	-126.580	-77.2416	-46.3335	-29.3139	-16.0647	1.06475

wave functions when the potential parameter m increases. This arises from the fact that the parity, which is a defined symmetry for very small m , is completely violated for large m . We have also noticed that the energy levels ϵ_i decrease with the increasing potential parameter m .

Data Availability

No data were used to support this study.

Conflicts of Interest

The authors declare that there are no conflicts of interest regarding the publication of this paper.

Acknowledgments

This work is supported by Project 20180677-SIP-IPN, COFAA-IPN, Mexico, and partially by the CONACYT project under Grant no. 288856-CB-2016 and partially by NSFC with Grant no. 11465006.

References

- [1] L. I. Schiff, *Quantum Mechanics*, McGraw-Hill Book Co, New York, NY, USA, 3rd edition, 1955.
- [2] L. D. Landau and E. M. Lifshitz, *Quantum Mechanics (Non-Relativistic Theory)*, Pergamon, New York, NY, USA, 3rd edition, 1977.
- [3] D. ter Haar, *Problems in Quantum Mechanics*, Pion Ltd, London, UK, 3rd edition, 1975.
- [4] F. Cooper, A. Khare, and U. Sukhatme, "Supersymmetry and quantum mechanics," *Physics Reports*, vol. 251, no. 5-6, pp. 267–385, 1995.
- [5] S. H. Dong, *Factorization Method in Quantum Mechanics*, Springer, Kluwer Academic Publisher, 2007.
- [6] Z. Q. Ma and B. W. Xu, "Quantum correction in exact quantization rules," *Europhys. Lett*, vol. 69, no. 5, 685 pages, 2005.
- [7] W. C. Qiang and S. H. Dong, "Proper quantization rule," *EPL*, vol. 89, no. 1, Article ID 10003, 2010.
- [8] N. Rosen and P. M. Morse, "On the vibrations of polyatomic molecules," *Physical Review A: Atomic, Molecular and Optical Physics*, vol. 42, no. 2, pp. 210–217, 1932.
- [9] M. F. Manning, "Energy levels of a symmetrical double minima problem with applications to the NH_3 and ND_3 molecules," *The Journal of Chemical Physics*, vol. 3, no. 3, pp. 136–138, 1935.
- [10] M. Baradaran and H. Panahi, "Lie Symmetry and the Bethe Ansatz Solution of a New Quasi-Exactly Solvable Double-Well Potential," *Advances in High Energy Physics*, vol. 2017, Article ID 2181532, 8 pages, 2017.
- [11] H. Konwent, "One-dimensional Schrödinger equation with a new type double-well potential," *Physics Letters A*, vol. 118, no. 9, pp. 467–470, 1986.
- [12] H. Konwent, P. Machnikowski, and A. Radosz, "A certain double-well potential related to $\text{SU}(2)$ symmetry," *Journal of Physics A: Mathematical and General*, vol. 28, no. 13, pp. 3757–3762, 1995.
- [13] Q.-T. Xie, "New quasi-exactly solvable double-well potentials," *Journal of Physics A: Mathematical and General*, vol. 45, no. 17, Article ID 175302, 2012.
- [14] B. Chen, Y. Wu, and Q. Xie, "Heun functions and quasi-exactly solvable double-well potentials," *Journal of Physics A: Mathematical and Theoretical*, vol. 46, no. 3, Article ID 035301, 2013.
- [15] R. R. Hartmann, "Bound states in a hyperbolic asymmetric double-well," *Journal of Mathematical Physics*, vol. 55, no. 1, 012105, 6 pages, 2014.

- [16] A. E. Sitniksky, "Exactly solvable Schrödinger equation with double-well potential for hydrogen bond," *Chemical Physics Letters*, vol. 676, pp. 169–173, 2017.
- [17] D.-N. Le, N. D. Hoang, and V.-H. Le, "Exact analytical solutions of the Schrödinger equation for a two dimensional purely sextic double-well potential," *Journal of Mathematical Physics*, vol. 59, no. 3, 032101, 15 pages, 2018.
- [18] M. Razavy and Am. J. Phys, "An exactly soluble Schrödinger equation with a bistable potential," *American Journal of Physics*, vol. 48, no. 4, 285 pages, 1980.
- [19] S.-H. Dong, *Wave Equation in Higher Dimensions*, Springer, Berlin, Germany, 2011.
- [20] S. Dong, Q. Fang, B. J. Falaye, G. Sun, C. Yáñez-Márquez, and S. Dong, "Exact solutions to solitonic profile mass Schrödinger problem with a modified Pöschl–Teller potential," *Modern Physics Letters A*, vol. 31, no. 04, p. 1650017, 2016.
- [21] S. Dong, G. H. Sun, B. J. Falaye, and S. H. Dong, "Semi-exact solutions to position-dependent mass Schrödinger problem with a class of hyperbolic potential $V_0 \tanh(ax)$," *The European Physical Journal Plus*, vol. 131, no. 176, 2016.
- [22] G. H. Sun, S. H. Dong, K. D. Launey et al., "Shannon information entropy for a hyperbolic double-well potential," *International Journal of Quantum Chemistry*, vol. 115, no. 14, pp. 891–899, 2015.
- [23] N. Ainsworth-Vaughn, *Heun's Differential Equations*, A. Ronveaux, Ed., Oxford University Press, Oxford, UK, 1995.
- [24] C. A. Downing, "On a solution of the Schrödinger equation with a hyperbolic double-well potential," *Journal of Mathematical Physics*, vol. 54, no. 7, 072101, 8 pages, 2013.
- [25] P. P. Fiziev, "Novel relations and new properties of confluent Heun's functions and their derivatives of arbitrary order," *Journal of Physics A: Mathematical and General*, vol. 43, no. 3, article 035203, 2010.
- [26] R. Hartmann and M. E. Portnoi, "Quasi-exact solution to the Dirac equation for the hyperbolic-secant potential," *Physical Review A*, vol. 89, Article ID 012101, 2014.
- [27] D. Agboola, "On the solvability of the generalized hyperbolic double-well models," *Journal of Mathematical Physics*, vol. 55, no. 5, 052102, 8 pages, 2014.
- [28] F.-K. Wen, Z.-Y. Yang, C. Liu, W.-L. Yang, and Y.-Z. Zhang, "Exact polynomial solutions of Schrödinger equation with various hyperbolic potentials," *Communications in Theoretical Physics*, vol. 61, no. 2, pp. 153–159, 2014.

Research Article

A New Model for Calculating the Ground and Excited States Masses Spectra of Doubly Heavy Ξ Baryons

Neda Mohajery,¹ Nasrin Salehi ,¹ and Hassan Hassanabadi²

¹Department of Basic Sciences, Shahrood Branch, Islamic Azad University, Shahrood, Iran

²Faculty of Physics, Shahrood University of Technology, Shahrood, Iran

Correspondence should be addressed to Nasrin Salehi; salehi@shahroodut.ac.ir

Received 9 March 2018; Revised 31 May 2018; Accepted 11 June 2018; Published 26 July 2018

Academic Editor: Chun-Sheng Jia

Copyright © 2018 Neda Mohajery et al. This is an open access article distributed under the Creative Commons Attribution License, which permits unrestricted use, distribution, and reproduction in any medium, provided the original work is properly cited. The publication of this article was funded by SCOAP³.

Since the doubly heavy baryons masses are experimentally unknown (except Ξ_{cc}^+ and Ξ_{cc}^{++}), we present the ground state masses and the positive and negative parity excited state masses of doubly heavy Ξ baryons. For this purpose, we have solved the six-dimensional hyperradial Schrödinger equation analytically for three particles under the hypercentral potential by using the ansatz approach. In this paper, the hypercentral potential is regarded as a combination of the color Coulomb plus linear confining term and the six-dimensional harmonic oscillator potential. We also added the first-order correction and the spin-dependent part contains three types of interaction terms (the spin-spin term, spin-orbit term, and tensor term) to the hypercentral potential. Our obtained masses for the radial excited states and orbital excited states of Ξ_{ccd} , Ξ_{ccu} , Ξ_{bbd} , Ξ_{bbu} , Ξ_{bcd} , and Ξ_{bcu} systems are compared with other theoretical reports, which could be a beneficial tool for the interpretation of experimentally unknown doubly heavy baryons spectrum.

1. Introduction

The doubly heavy baryons have two heavy quarks (c and b) with a light quark (d or u or s). The doubly heavy Ξ baryons family have up or down quarks but Ω family has a light strange quark and their masses spectra have been predicted in the quark model [1]. The SELEX collaboration announced only the experimental mass for the ground state of Ξ_{cc}^+ baryon and LHCb has determined the ground state of Ξ_{cc}^{++} baryon mass while no triply heavy baryons have been observed yet [2]. Recently experiments and theoretical outcomes have been used in studying the heavy baryons. A lot of new experimental results have been reported by various experimental facilities like CLEO, Belle, BaBar, LHCb, and so forth [3, 4] on ground states and many new excited states of heavy flavor baryons. Bottom baryons are investigated at LHC and Lattice QCD whereas charm baryons are announced at the B-factories [5, 6]. On the other hand, the theoretical works are providing new results for doubly heavy baryons like the Hamiltonian model [7], relativistic quark model [8], the chiral unitary model [9], QCD sum rule [10, 11], and many more. Single- and double- heavy baryons in the constituent

quark model were studied by Yoshida et al. They used a model in which there were two exceptions, a color Coulomb term depending on quark masses and an antisymmetric L.S force. They studied the low-lying negative parity states and structures within the framework of a constituent quark model [7]. In [12], the authors calculated the masses of baryons with the quadratic mass relations for ground and orbitally excited states. Wei et al. estimated the masses of singly, doubly, and triply bottom baryons in [13]. Then they studied the linear mass relations and quadratic mass relations.

The light flavor dependence of the singly and doubly charmed states is investigated by Rubio et al. They focused on searching the masses of charmed baryons with positive and negative parity [5]. In [14], the authors used lattice QCD for baryons containing one, two, or three heavy quarks. They applied nonrelativistic QCD for the bottom quarks and relativistic heavy-quark action for the charm quarks. Padmanath et al. determined the ground and excited state spectra of doubly charmed baryons from lattice QCD with dynamical quark fields [15]. The mass of the heavy baryons with two heavy b or c quarks for spin 1/2 in the framework of

QCD sum rules is estimated by Aliev et al. They use the most general form of the interpolating current in its symmetric and antisymmetric forms with respect to the exchange of heavy quarks, to calculate the two point correlation functions describing the baryons under consideration [16]. The authors calculated the masses and residues of the spin 3/2 doubly heavy baryons within the QCD sum rules method. In [17], Eakins et al. ignored all spin-dependent interactions and assume a flavor independent potential, working in the limit where the two heavy quarks are massive enough that their motion can be treated as essentially nonrelativistic, and QCD interactions can be well described by an adiabatic potential [18]. The three-quark problem was solved by Valcarce et al. by means of the Faddeev method in momentum space [19].

The masses of the ground and excited states of the doubly heavy baryons were calculated by Ebert et al. baryons on the basis of the quark-diquark approximation in the framework of the relativistic quark model [20]. In [21], the authors, in the model with the quark-diquark factorization of wave functions, estimated the spectroscopic characteristics of baryons containing two heavy quarks. Albertus et al. used five different quark-quark potentials that include a confining term plus Coulomb and hyperfine terms coming from one-gluon exchange. They solved the three-body problem by means of a variational ansatz made possible by heavy-quark spin symmetry constraints [22].

In this study, we have used the hypercentral constituent quark model (hCQM) with Coulombic-like term plus a linear confining term and the harmonic oscillator potential [23]. We also added the first-order correction and the spin-dependent part to the potential and calculation has been performed by solving six-dimensional hyperradial Schrödinger equations by using the ansatz method. We have obtained the mass spectra of radial excited states up to 5S and orbital excited states for 1P-5P, 1D-4D, and 1F-2F states.

This paper is organized as follows: we briefly present the hypercentral constituent quark model and introduce the interaction potentials between three quarks in doubly heavy baryons in Section 2. In Section 3, we present the exact analytical solution of the hyperradial Schrödinger equation for our proposed potential. In Section 4, our masses spectra results for ground, radial, and orbital excited states of baryon family with six members are given and compared with other predictions. We present the conclusions in Section 5.

2. Theoretical Framework: The HCQM Model and Hypercentral Potential

The hypercentral model has been applied to solve bound states and scattering problems in many various fields of physics. In this model, we consider baryons as three-body systems of constituent quarks. In the center of mass frame, the internal quark motion is described by the Jacobi coordinates (ρ and λ) [37] and the respective reduced masses are given by

$$m_\rho = \frac{2m_1m_2}{m_1 + m_2}, \quad (1)$$

$$m_\lambda = \frac{2m_3(m_1^2 + m_2^2 + m_1m_2)}{(m_1 + m_2)(m_1 + m_2 + m_3)}$$

Here m_1 , m_2 , and m_3 are the current quark masses. In order to describe three-quark dynamics, we define hyperradius $x = \sqrt{\rho^2 + \lambda^2}$ and hyperangle $\xi = \arctan(\rho/\lambda)$ [38]. In present work, the confining three-body potential is regarded as a combination of three hypercentral interacting potentials. First, the six-dimensional hyper-Coulomb potential $V_{hyc}(x) = \tau/x$, which is attractive for small separations [39–41], while at large separations a hyper-linear term, $V_{con} = \beta x$, gives rise to quark confinement [42], where β corresponds to the string tension of the confinement [43]. Third, the six-dimension harmonic oscillator potential $V_{h.o.} = px^2$, which has a two-body character and turns out to be exactly hypercentral [44], where p is constant. The solution of the hypercentral Schrödinger equation with Coulombic-like term plus a linear confining term potential cannot be obtained analytically [45]; therefore, Giannini et al. used the dynamic symmetry O(7) of the hyper-Coulomb problem to obtain the hyper-Coulomb Hamiltonian and eigenfunctions analytically and they regarded the linear term as a perturbation. Combination of the color Coulomb plus linear confining term and the six-dimensional harmonic oscillator potential has interesting properties since it can be solved analytically, with a good correspondence to physical results. The first-order correction $V^{(1)}(x)$ can be written as [44–47]

$$V^1(x) = -C_F C_A \frac{\alpha_s^2}{4x^2} \quad (2)$$

The parameters $C_F = 2/3$ and $C_A = 3$ are the Casimir charges of the fundamental and adjoint representation. The hyper-Coulomb strength $\tau = -(2/3)\alpha_s$, $2/3$ is the color factor for the baryon. α_s is the strong running coupling constant, which is written as

$$\alpha_s = \frac{\alpha_s(\mu_0)}{1 + ((33 - 2n_f)/12\pi)\alpha_s(\mu_0)\ln((m_1 + m_2 + m_3)/\mu_0)} \quad (3)$$

The spin-dependent part $V_{SD}(x)$ is given as

$$V_{SD}(x) = V_{SS}(x) (\vec{S}_\rho \cdot \vec{S}_\lambda) + V_{\gamma S}(x) (\vec{\gamma} \cdot \vec{S}) + V_T(x) \left[S^2 - \frac{3(\vec{S} \cdot \vec{x})(\vec{S} \cdot \vec{x})}{x^2} \right] \quad (4)$$

The spin-dependent potential, $V_{SD}(x)$, contains three types of the interaction terms [48], such as the spin-spin term $V_{SS}(x)$, the spin-orbit term $V_{\gamma S}(x)$, and tensor term $V_T(x)$ described as [35]. Here $S = S_\rho + S_\lambda$, where S_ρ and S_λ are the spin vectors associated with the ρ and λ variables, respectively. The coefficient of these spin-dependent terms of the above equation can be written in terms of the vector, $V_V(x) = \tau/x$, and scalar, $V_S(x) = \beta x + px^2$ parts of the static potential as [38]

$$V_{\gamma S} = \frac{1}{2m_\rho m_\lambda x} \left(3 \frac{dV_V}{dx} - \frac{dV_S}{dx} \right) \quad (5)$$

TABLE 1: The quark mass (in GeV) and the fitted values of the parameters used in our calculations.

m_b	m_c	m_d	m_u	α_s	C_F	C_A	β	ω
4.750	1.348	0.35	0.34	0.340	$\frac{2}{3}$	3	0.02	0.11 fm^{-1}

TABLE 2: The outcomes ground state masses of Ξ are listed with other theoretical predictions (in GeV). Standard deviation of the result is 0.350.

Baryon J^P	Ξ_{ccd} / Ξ_{ccu}		Ξ_{bbd} / Ξ_{bbu}		Ξ_{bcd} / Ξ_{bcu}	
	$\frac{1^+}{2}$	$\frac{3^+}{2}$	$\frac{1^+}{2}$	$\frac{3^+}{2}$	$\frac{1^+}{2}$	$\frac{3^+}{2}$
Our Calc	3.522 / 3.515	3.696 / 3.689	9.716 / 9.711	9.894 / 9.889	6.628 / 6.622	6.688 / 6.682
Ref.[1]	3.520 / 3.511	3.695 / 3.687	10.317 / 10.312	10.340 / 10.335	6.920 / 6.914	6.986 / 6.980
Ref.[24]	3.519					
Ref.[7]	3.685	3.754	10.314			
Ref.[12, 13]	3.520	3.695	10.199	10.316		
Ref.[5]	3.610	3.694				
Ref.[14]	3.610	3.692	10.143	10.178	6.943	6.985
Ref.[25]	3.561	3.642				
Ref.[17]	3.720		9.960		6.720	
Ref.[18]	3.687	3.752	10.322	10.352	7.014	7.064
Ref.[26]	3.676	3.753	10.340	10.367	7.011	7.074
Ref.[27]	3.547	3.719	10.185	10.216	6.904	6.936
Ref.[19]	3.579	3.656	10.189	10.218		
Ref.[20]	3.620	3.727	10.202	10.237	6.933	6.980
Ref.[21]	3.478	3.610	10.093	10.133	6.820	6.900
Ref.[28]	3.627	3.690	10.162	10.184	6.914	
Ref.[29]	3.519	3.620	9.800	9.980	6.650	6.690
Ref.[22]	3.612	3.706	10.197	10.136	6.919	6.986
Ref.[30]	3.510	3.548	10.130	10.144	6.792	6.827
Ref.[31]	3.570	3.610	10.170	10.220		

$$V_T(x) = \frac{1}{6m_\rho m_\lambda} \left(\frac{3d^2 V_V}{d^2 x} - \frac{1}{x} \frac{dV_V}{dx} \right) \quad (6)$$

$$V_{SS}(x) = \frac{1}{3m_\rho m_\lambda} \nabla^2 V_V \quad (7)$$

In our model, the hypercentral interaction potential is assumed as follows [48]:

$$V(x) = V^{(0)}(x) + \left(\frac{1}{m_\rho} + \frac{1}{m_\lambda} \right) V^{(1)}(x) + V_{SD}(x) \quad (8)$$

where $V^{(0)}(x)$ is given by

$$\begin{aligned} V^{(0)}(x) &= V_{hyc}(x) + V_{con}(x) + V_{h.o.}(x) \\ &= \frac{\tau}{x} + \beta x + px^2 \end{aligned} \quad (9)$$

The baryons masses are determined by the sum of the model quark masses plus kinetic energy, potential energy, and the spin-dependent interaction as $M_B = \sum m_i + \langle H \rangle$ [49]. First, we have solved the hyperradial Schrödinger equation exactly and find eigenvalue under the proposed potential by using the ansatz approach.

3. The Exact Analytical Solution of the Hyperradial Schrödinger Equation under the Hypercentral Potential

The Hamiltonian of three bodies' baryonic system in the hypercentral constituent quark model is expressed as [50]

$$H = \frac{P_\rho^2}{2m} + \frac{P_\lambda^2}{2m} + V(x) \quad (10)$$

and the hyperradial wave function $\psi_{\nu\gamma}(x)$ is determined by the hypercentral Schrödinger equation. The hyperradial Schrödinger equation corresponding to the above Hamiltonian can be written as [51]

$$\begin{aligned} &\left(\frac{d^2}{dx^2} + \frac{5}{x} \frac{d}{dx} - \frac{\gamma(\gamma+4)}{x^2} \right) \psi_{\nu\gamma}(x) \\ &= -2m [E - V(x)] \psi_{\nu\gamma}(x) \end{aligned} \quad (11)$$

where γ is the grand angular quantum number and given by $\gamma = 2n + l_\rho + l_\lambda$, $n = 0, 1, \dots$; l_ρ and l_λ are the angular momenta associated with the $\vec{\rho}$ and $\vec{\lambda}$ variable and ν denotes the number of nodes of the space three-quark wave function [36]. In (11), m is the reduced mass which is defined as $m =$

TABLE 3: The masses of radial excited states for doubly heavy Ξ baryons (in GeV). Standard deviations of the result are 0.435 and 0.434.

Baryon	State	J^P	Our Calc	Our Calc	[1]	[1]	[7]	[26]	[27]	[19]	[20]	[18]
Ξ_{ccd} and Ξ_{ccu}	2S		3.905	3.901	3.925	3.920	4.079	4.029	4.183	3.976	3.910	4.030
	3S	$\frac{1}{2}^+$	4.185	4.118	4.233	4.159	4.206		4.640		4.154	
	4S	$\frac{2}{2}$	4.430	4.429	4.502	4.501						
	5S		4.653	4.653	4.748	4.748						
	2S		3.962	3.958	3.988	3.983	4.114	4.042	4.282	4.025	4.027	4.078
	3S	$\frac{3}{2}^+$	4.213	4.211	4.264	4.261	4.131		4.719			
Ξ_{bbd} and Ξ_{bbu}	4S	$\frac{2}{2}$	4.446	4.445	4.520	4.519						
	5S		4.663	4.663	4.759	4.759						
	2S		9.984	9.981	10.612	10.609	10.571	10.576	10.751	10.482	10.441	10.551
	3S	$\frac{1}{2}^+$	10.211	10.211	10.862	10.862	10.612		11.170		10.630	
	4S	$\frac{2}{2}$	10.417	10.418	11.088	11.090					10.812	
	5S		10.606	10.610	11.297	11.301						
Ξ_{bcd} and Ξ_{bcu}	2S		9.990	9.988	10.619	10.617	10.592	10.578	10.770	10.501	10.482	10.574
	3S	$\frac{3}{2}^+$	10.205	10.233	10.855	10.866	10.593		11.184		10.673	
	4S	$\frac{2}{2}$	10.418	10.420	11.090	11.092					10.856	
	5S		10.607	10.611	11.298	11.302						
	2S		6.922	6.919	7.244	7.240			7.478			7.321
	3S	$\frac{1}{2}^+$	7.163	7.161	7.509	7.507			7.904			
Ξ_{bcd} and Ξ_{bcu}	4S	$\frac{2}{2}$	7.379	7.377	7.746	7.744						
	5S		7.576	7.581	7.963	7.964						
	2S		6.943	6.939	7.267	7.263			7.495			7.353
	3S	$\frac{3}{2}^+$	7.174	7.171	7.521	7.518			7.917			
	4S	$\frac{2}{2}$	7.384	7.384	7.752	7.752						
	5S		7.580	7.581	7.968	7.969						

$2m_\rho m_\lambda / (m_\rho + m_\lambda)$ [32]. By regarding $\psi_{\gamma\gamma}(x) = x^{-5/2} \varphi_{\gamma\gamma}$ [20, 35], (11) reduces to the following form:

$$\varphi''_{\gamma\gamma}(x) + \left[\varepsilon - r_1 x^2 - r_2 x - \frac{r_3}{x} - \frac{r_4}{x^2} - \frac{r_5}{x^3} + \frac{r_6}{x^5} + r_7 - \frac{(2\gamma + 3)(2\gamma + 5)}{4x^2} \right] \varphi_{\gamma\gamma}(x) = 0 \quad (12)$$

The hyperradial wave function $\varphi_{\gamma\gamma}(x)$ is a solution of the reduced Schrödinger equation for each of the three identical particles with the mass m and interacting potential (8), where

$$\varepsilon = 2mE,$$

$$r_1 = 2mp,$$

$$r_2 = 2m\beta,$$

$$r_3 = 2m\tau,$$

$$r_4 = 2m \left(\frac{1}{m_\rho} + \frac{1}{m_\lambda} \right) \left(-C_f C_A \frac{\alpha_s^2}{4} \right),$$

$$r_5 = 2m \left[\frac{2\tau}{3m_\rho m_\lambda} (S_\rho \cdot S_\lambda) - \frac{3\tau}{2m_\rho m_\lambda} (\vec{\gamma} \cdot \vec{s}) + \frac{7\tau}{6m_\rho m_\lambda} s^2 \right],$$

$$r_6 = 2m \frac{21\tau}{6m_\rho m_\lambda} (\vec{s} \cdot \vec{x}) (\vec{s} \cdot \vec{x}),$$

$$r_7 = 2m \left(\frac{(\beta + 2p)}{2m_\rho m_\lambda} (\vec{\gamma} \cdot \vec{s}) \right).$$

(13)

We suppose the $\varphi_{\gamma\gamma} = h(x)e^{g(x)}$ form for the wave function. Now we make use of the ansatz for $h(x)$ and $g(x)$ [33, 34]:

$$h(x) = \Pi(x - a_i^\nu) \quad \nu = 1, 2, \dots,$$

$$h(x) = 1 \quad \nu = 0$$

(14)

$$g(x) = a \ln x + qx^2 + cx + \frac{d}{x}$$

(b) Continued.

State	Our Cal Ξ_{cc}^+	Our Cal Ξ_{cc}^{++}	[1] Ξ_{cc}^+	[1] Ξ_{cc}^{++}	[7]	[32]	[33]	[34]	[35]	[33]	[36]	[5]
($4^2 D_{5/2}$)	4.690	4.690	4.788	4.788								
($4^4 D_{5/2}$)	4.696	4.696	4.795	4.795								
($4^4 D_{7/2}$)	4.675	4.675	4.772	4.772								
($1^4 F_{3/2}$)	4.198	4.193	4.247	4.242								
($1^2 F_{5/2}$)	4.169	4.164	4.215	4.210								
($1^4 F_{5/2}$)	4.142	4.172	4.186	4.219								
($1^4 F_{7/2}$)	4.150	4.147	4.194	4.191								
($1^2 F_{7/2}$)	4.178	4.139	4.225	4.182					4.267			
($1^4 F_{9/2}$)	4.118	4.115	4.159	4.156					4.413			
($2^4 F_{3/2}$)	4.422	4.425	4.494	4.497								
($2^2 F_{5/2}$)	4.399	4.399	4.468	4.468								
($2^4 F_{5/2}$)	4.405	4.406	4.475	4.476								
($2^4 F_{7/2}$)	4.378	4.382	4.445	4.450								
($2^2 F_{7/2}$)	4.384	4.376	4.452	4.443								
($2^4 F_{9/2}$)	4.359	4.355	4.424	4.420								

where a , q , c , and d are positive. From (14), we obtain

$$\begin{aligned} \varphi''(x) &= \left[g''(x) + g'^2(x) + \left(\frac{h''(x) + 2h'(x)g'(x)}{h(x)} \right) \right] \cdot \varphi(x) \end{aligned} \quad (15)$$

Comparing (12) and (15), it can be found that

$$\begin{aligned} \left[r_1 x^2 + r_2 x + \frac{r_3}{x} + \frac{r_4}{x^2} + \frac{r_5}{x^3} - \frac{r_6}{x^5} - r_7 \right. \\ \left. + \frac{(2\gamma + 3)(2\gamma + 5)}{4x^2} - \varepsilon \right] &= \left[g''(x) + g'^2(x) \right. \\ \left. + \frac{h''(x) + 2h'(x)g'(x)}{h(x)} \right] \end{aligned} \quad (16)$$

By substituting (14) into (16), we obtained the following equation:

$$\begin{aligned} -\varepsilon + r_1 x^2 + r_2 x + \frac{r_3}{x} + \frac{r_4}{x^2} + \frac{r_5}{x^3} - \frac{r_6}{x^5} - r_7 \\ + \frac{(2\gamma + 3)(2\gamma + 5)}{4x^2} \\ = 4q^2 x^2 + 4cqx + \frac{(2ac - 4dq)}{x} + \frac{(a^2 - a - 2cd)}{x^2} \\ + \frac{2d(1-a)}{x^3} + \frac{d^2}{x^4} + (c^2 + 2q + 4ac) \end{aligned} \quad (17)$$

By equating the corresponding powers of x on both sides of (17), we can obtain

$$\begin{aligned} a &= \frac{2\tau}{\beta} \sqrt{\frac{mp}{2}}, \\ c &= \frac{m\beta}{2} \sqrt{\frac{2}{mp}}, \\ q &= \sqrt{\frac{mp}{2}}, \\ \varepsilon &= - \left[\frac{m\beta^2}{2p} + 2\sqrt{\frac{mp}{2}} + \frac{4mp\tau}{\beta} \right. \\ &\quad \left. + 2m \left(\frac{(\beta + 2p)}{2m_\rho m_\lambda} (\vec{\gamma} \cdot \vec{s}) \right) \right] \end{aligned} \quad (18)$$

Since $p = m\omega^2/2$, we have $a = 2m\omega/2\beta$, $c = \beta/\omega$, $q = m\omega/2$. The energy eigenvalues for the mode $\nu = 0$ and grand angular momentum γ from (13) and (18) are given as follows:

$$\begin{aligned} E &= - \left[\frac{\beta^2}{2m\omega} + \frac{\omega}{2} + \frac{m\omega^2\tau}{\beta} \right. \\ &\quad \left. + \left(\frac{(\beta + m\omega^2)}{2m_\rho m_\lambda} (\vec{\gamma} \cdot \vec{s}) \right) \right] \end{aligned} \quad (19)$$

At last for the best doubly heavy baryons masses (Ξ_{ccd} , Ξ_{ccu} , Ξ_{bbd} , Ξ_{bbu} , Ξ_{bcd} , Ξ_{bcu}) predictions, the values of m_u , m_d , m_c , m_b , α_S , ω , and β (which are listed in Table 1) are selected using genetic algorithm. The cost function of a genetic algorithm is the minimum difference between our calculated baryon mass and the reported baryons mass of other works.

TABLE 5: The masses of orbital excited states for Ξ_{bb} baryon (in GeV).

State	Our cal Ξ_{bb}^-	Our Cal Ξ_{bb}^0	[1] Ξ_{bb}^-	[1] Ξ_{bb}^0	[7]	[26]	[19]	[20]	[12]	[18]	Others
$(1^2 P_{1/2})$	9.895	9.892	10.514	10.511	10.476	10.493	10.406	10.368		10.691	
$(1^2 P_{3/2})$	9.890	9.887	10.509	10.506	10.476	10.495		10.408	10.474	10.692	10.390 [31]
$(1^4 P_{1/2})$	9.897	9.895	10.517	10.514							
$(1^4 P_{3/2})$	9.893	9.890	10.512	10.509							10.430 [17]
$(1^4 P_{5/2})$	9.901	9.898	10.521	10.518	10.759				10.588	10.695	
$(2^2 P_{1/2})$	10.127	10.127	10.77	10.77	10.703	10.710	10612	10.563			
$(2^2 P_{3/2})$	10.124	10.120	10.766	10.762	10.704	10.713		10.607			
$(2^4 P_{1/2})$	10.129	10.129	10.772	10.772							
$(2^4 P_{3/2})$	10.126	10.125	10.768	10.767							
$(2^4 P_{5/2})$	10.121	10.133	10.763	10.776	10.973	10.713					
$(3^2 P_{1/2})$	10.337	10.338	11.001	11.002	10.740			10.744			
$(3^2 P_{3/2})$	10.334	10.335	10.997	10.998	10.742			10.788			
$(3^4 P_{1/2})$	10.339	10.340	11.003	11.004							
$(3^4 P_{3/2})$	10.336	10.337	10.999	11.000							
$(3^4 P_{5/2})$	10.331	10.343	10.994	11.007	11.004						
$(4^2 P_{1/2})$	10.531	10.534	11.214	11.217				10.900			
$(4^2 P_{3/2})$	10.527	10.530	11.21	11.213							
$(4^4 P_{1/2})$	10.533	10.536	11.216	11.219							
$(4^4 P_{3/2})$	10.529	10.532	11.212	11.215							
$(4^4 P_{5/2})$	10.526	10.538	11.208	11.222							
$(5^2 P_{1/2})$	10.712	10.716	11.413	11.418							
$(5^2 P_{3/2})$	10.709	10.714	11.41	11.415							
$(5^4 P_{1/2})$	10.714	10.718	11.415	11.420							
$(5^4 P_{3/2})$	10.711	10.716	11.412	11.417							
$(5^4 P_{5/2})$	10.706	10.721	11.407	11.423							
$(1^4 D_{1/2})$	10.043	10.041	10.677	10.675							
$(1^2 D_{3/2})$	10.037	10.035	10.670	10.668							
$(1^4 D_{3/2})$	10.038	10.037	10.672	10.670						11.011	
$(1^2 D_{5/2})$	10.030	10.028	10.663	10.661	10.592	10.676			10.742	11.002	
$(1^4 D_{5/2})$	10.033	10.031	10.666	10.664							
$(1^4 D_{7/2})$	10.026	10.024	10.658	10.656		10.608			10.853	11.011	
$(2^4 D_{1/2})$	10.257	10.257	10.913	10.913							
$(2^2 D_{3/2})$	10.252	10.252	10.907	10.907							
$(2^4 D_{3/2})$	10.254	10.254	10.909	10.909							
$(2^2 D_{5/2})$	10.247	10.247	10.901	10.901		10.712					
$(2^4 D_{5/2})$	10.248	10.248	10.903	10.903	10.613						
$(2^4 D_{7/2})$	10.242	10.242	10.896	10.896		11.057					
$(3^4 D_{1/2})$	10.455	10.457	11.13	11.133			4.592	4.592			
$(3^2 D_{3/2})$	10.450	10.452	11.125	11.127			4.571	4.570			
$(3^4 D_{3/2})$	10.451	10.454	11.126	11.129							
$(3^2 D_{5/2})$	10.446	10.447	11.120	11.122							
$(3^4 D_{5/2})$	10.447	10.449	11.122	11.124	10.809						
$(3^4 D_{7/2})$	10.442	10.444	11.116	11.118							
$(4^4 D_{1/2})$	10.639	10.643	11.333	11.337							
$(4^2 D_{3/2})$	10.635	10.638	11.328	11.332							
$(4^4 D_{3/2})$	10.636	10.640	11.330	11.334							
$(4^2 D_{5/2})$	10.631	10.635	11.324	11.328							

TABLE 5: Continued.

State	Our cal Ξ_{bb}^-	Our Cal Ξ_{bb}^0	[1] Ξ_{bb}^-	[1] Ξ_{bb}^0	[7]	[26]	[19]	[20]	[12]	[18]	Others
$(4^4 D_{5/2})$	10.632	10.636	11.325	11.33							
$(4^4 D_{7/2})$	10.627	10.631	11.320	11.324							
$(1^4 F_{3/2})$	10.173	10.172	10.82	10.819							
$(1^2 F_{5/2})$	10.166	10.165	10.812	10.811							
$(1^4 F_{5/2})$	10.158	10.167	10.804	10.813							
$(1^4 F_{7/2})$	10.167	10.160	10.814	10.806							
$(1^2 F_{7/2})$	10.160	10.157	10.806	10.803						11.004	
$(1^4 F_{9/2})$	10.152	10.152	10.797	10.797						11.112	
$(2^4 F_{3/2})$	10.357	10.376	11.022	11.043							
$(2^2 F_{5/2})$	10.368	10.369	11.035	11.036							
$(2^4 F_{5/2})$	10.369	10.371	11.036	11.038							
$(2^4 F_{7/2})$	10.362	10.365	11.028	11.031							
$(2^2 F_{7/2})$	10.364	10.363	11.030	11.029							
$(2^4 F_{9/2})$	10.357	10.357	11.022	11.023							

4. Results and Discussions: Mass Spectrum

The ground and excited states of doubly heavy Ξ baryons are unclear to us experimentally (except Ξ_{cc}^+ and Ξ_{cc}^{++}). Hence, we have obtained the ground and excited state masses of Ξ_{cc}^+ , Ξ_{cc}^{++} , Ξ_{bb}^- , Ξ_{bb}^0 , Ξ_{bc}^0 , and Ξ_{bc}^+ (see Tables 2, 3, 4, 5, and 6, respectively). These mass spectra are estimated by using the hypercentral potential equation (8) in the hypercentral constituent quark model. We begin with the ground state 1S; the masses are computed for both parities $J^P = (1/2)^+$ and $J^P = (3/2)^+$. Our predicted ground state masses of doubly heavy Ξ baryons are compared with other predictions in Table 2.

We can observe that, in the case of Ξ_{cc} baryon, for 2S states $J^P = (1/2)^+$ and $J^P = (3/2)^+$, our predictions are close to [34] and [1], respectively. Our outcomes for 3S state $J^P = (1/2)^+$ of Ξ_{cc} baryon show 21 MeV (with [7]) and $J^P = (3/2)^+$ shows 51 MeV (with [1]) difference. Analyzing the 2S and 3S states masses for Ξ_{bb} and Ξ_{bc} baryons (with both parities) shows that our masses have a difference in the range of ≈ 0.5 GeV with [1, 7, 20, 32–34, 36].

To calculate the orbital excited state masses (1P–5P, 1D–4D, 1F–2F), we have considered all possible isospin splitting and all combinations of total spin S and total angular momentum J . Our outcomes and the comparison of masses with other approaches are also tabulated in Tables 4, 5, and 6.

Our obtained orbital excited masses for Ξ_{cc} , 1P state $J^P = (1/2)^-$ show a difference of 14 MeV (with [1]), 29 MeV (with [33]), 13 MeV (with [34]), and 41 MeV (with [5]), while 1P state $J^P = (3/2)^-$ shows 14 MeV (with [1]), 48 MeV (with [35]), and 0 MeV (with [33]). Our 2P state $J^P = (1/2)^-$ shows a difference of 15 MeV (with [7]), 35 MeV (with [34]), and 41 MeV (with [1]), while 2P state $J^P = (3/2)^-$ shows 26 MeV (with [32]), 33 MeV (with [7]), and 40 MeV (with [1]). Results for 3P states $J^P = (1/2)^-$ and $J^P = (3/2)^-$ show a difference in the range of ≈ 60 MeV with [1]. We can easily observe that our calculated masses for 4P–5P, 1D–3D, and 1F–2F are matched with [1]. Our outcome for 3D state $J^P = (3/2)^+$ is quite

equal to the predictions of [7, 32, 33, 35]. For the ground and excited states of doubly heavy baryons (Ξ_{cc}^+), the minimum and maximum percentage of relative error values are 0% and 3.53% between our calculations and the masses reported by Shah et al. [1].

For Ξ_{bb} and Ξ_{bc} baryons, the mass difference from our calculations and other references is large.

Comparing our findings with the masses reported by Shah et al. [1], the minimum and maximum percentage of relative error values are 1.2% (0.8%) and 10.317% (6.92%) for the ground and excited states of doubly heavy baryons Ξ_{bb} and Ξ_{bc} , respectively.

5. Conclusion

In this study, we have computed the mass spectra of ground and excited states for doubly heavy Ξ baryons by using a hypercentral constituent quark model. For this goal, we have analytically solved the hyperradial Schrödinger equation for three identical interacting particles under the effective hypercentral potential by using the ansatz method. Our proposed potential is regarded as a combination of the Coulombic-like term plus a linear confining term and the harmonic oscillator potential. We also added the first-order correction and the spin-dependent part to the potential. In our calculations, the u and d quarks have 10 MeV difference mass, so there is a very small mass difference between Ξ_{ccd} and Ξ_{ccu} , Ξ_{bbd} and Ξ_{bbu} , Ξ_{bcd} and Ξ_{bcu} . Our model has succeeded to assign the J^P values to the excited states of doubly heavy baryons (Ξ_{ccd} , Ξ_{ccu} , Ξ_{bbd} , Ξ_{bbu} , Ξ_{bcd} , and Ξ_{bcu}). Comparison of the results with other predictions revealed that they are in agreement and our proposed model can be useful to investigate the doubly heavy baryons states masses. For example, for the ground, radial, and orbital excited states masses of doubly heavy Ξ baryons the minimum and the maximum percentage of relative error values are 0% and 6% between our calculations and the masses reported by Shah et al. [1].

TABLE 6: The masses of orbital excited states for Ξ_{bc} baryon (in GeV).

State	Our cal Ξ_{bc}^0	Our Cal Ξ_{bc}^+	[1] Ξ_{bc}^0	[1] Ξ_{bc}^+	[18]
$(1^2 P_{1/2})$	6.846	6.842	7.16	7.156	7.390
$(1^2 P_{3/2})$	6.836	6.831	7.149	7.144	7.394
$(1^4 P_{1/2})$	6.851	6.847	7.166	7.161	7.399
$(1^4 P_{3/2})$	6.841	6.837	7.155	7.15	
$(1^4 P_{5/2})$	6.859	6.856	7.175	7.171	
$(2^2 P_{1/2})$	7.087	7.084	7.425	7.422	
$(2^2 P_{3/2})$	7.078	7.075	7.415	7.412	
$(2^4 P_{1/2})$	7.091	7.088	7.43	7.426	
$(2^4 P_{3/2})$	7.082	7.079	7.42	7.417	
$(2^4 P_{5/2})$	7.071	7.095	7.408	7.434	
$(3^2 P_{1/2})$	7.304	7.302	7.664	7.662	
$(3^2 P_{3/2})$	7.296	7.295	7.655	7.654	
$(3^4 P_{1/2})$	7.308	7.306	7.668	7.666	
$(3^4 P_{3/2})$	7.299	7.299	7.659	7.658	
$(3^4 P_{5/2})$	7.289	7.312	7.648	7.673	
$(4^2 P_{1/2})$	7.504	7.623	7.884	8.015	
$(4^2 P_{3/2})$	7.497	7.498	7.876	7.877	
$(4^4 P_{1/2})$	7.508	7.508	7.888	7.888	
$(4^4 P_{3/2})$	7.500	7.500	7.88	7.88	
$(4^4 P_{5/2})$	7.491	7.514	7.87	7.895	
$(5^2 P_{1/2})$	7.692	7.693	8.091	8.092	
$(5^2 P_{3/2})$	7.686	7.687	8.084	8.085	
$(5^4 P_{1/2})$	7.695	7.697	8.094	8.096	
$(5^4 P_{3/2})$	7.689	7.689	8.087	8.088	
$(5^4 P_{5/2})$	7.680	7.681	8.078	8.079	
$(1^4 D_{1/2})$	7.006	7.004	7.336	7.334	
$(1^2 D_{3/2})$	6.992	6.989	7.321	7.318	
$(1^4 D_{3/2})$	6.997	6.980	7.326	7.308	7.324
$(1^2 D_{5/2})$	6.980	6.977	7.308	7.304	
$(1^4 D_{5/2})$	6.985	6.969	7.313	7.295	7.309
$(1^4 D_{7/2})$	6.969	6.953	7.296	7.278	7.292
$(2^4 D_{1/2})$	7.087	7.227	7.425	7.579	7.579
$(2^2 D_{3/2})$	7.216	7.214	7.567	7.565	
$(2^4 D_{3/2})$	7.219	7.219	7.571	7.57	
$(2^2 D_{5/2})$	7.205	7.203	7.555	7.553	7.538
$(2^4 D_{5/2})$	7.209	7.208	7.559	7.558	
$(2^4 D_{7/2})$	7.196	7.195	7.545	7.544	
$(3^4 D_{1/2})$	7.431	7.431	7.804	7.804	
$(3^2 D_{3/2})$	7.420	7.420	7.792	7.792	
$(3^4 D_{3/2})$	7.411	7.424	7.782	7.796	
$(3^2 D_{5/2})$	7.415	7.410	7.786	7.781	
$(3^4 D_{5/2})$	7.402	7.414	7.772	7.785	
$(3^4 D_{7/2})$	7.402	7.402	7.772	7.772	
$(4^4 D_{1/2})$	7.429	7.504	7.801	7.884	7.797
$(4^2 D_{3/2})$	7.611	7.613	8.002	8.004	
$(4^4 D_{3/2})$	7.615	7.617	8.006	8.008	
$(4^2 D_{5/2})$	7.603	7.604	7.993	7.994	
$(4^4 D_{5/2})$	7.606	7.608	7.996	7.998	
$(4^4 D_{7/2})$	7.596	7.597	7.985	7.986	
$(1^4 F_{3/2})$	7.143	7.141	7.487	7.485	
$(1^2 F_{5/2})$	7.127	7.125	7.469	7.467	

TABLE 6: Continued.

State	Our cal	Our Cal	[1]	[1]	[18]
	Ξ_{bc}^0	Ξ_{bc}^+	Ξ_{bc}^0	Ξ_{bc}^+	
$(1^4 F_{5/2})$	7.131	7.129	7.474	7.472	
$(1^4 F_{7/2})$	7.117	7.114	7.458	7.455	
$(1^2 F_{7/2})$	7.112	7.109	7.453	7.45	
$(1^4 F_{9/2})$	7.099	7.097	7.439	7.436	
$(2^4 F_{3/2})$	7.350	7.350	7.715	7.715	
$(2^2 F_{5/2})$	7.337	7.336	7.7	7.699	
$(2^4 F_{5/2})$	7.340	7.339	7.704	7.703	
$(2^4 F_{7/2})$	7.328	7.327	7.69	7.689	
$(2^2 F_{7/2})$	7.324	7.323	7.686	7.685	
$(2^4 F_{9/2})$	7.313	7.311	7.674	7.672	

Data Availability

The data used to support the findings of this study are included within the article.

Conflicts of Interest

The authors declare that they have no conflicts of interest.

References

- [1] Z. Shah and A. K. Rai, "Excited state mass spectra of doubly heavy Ξ baryons," *The European Physical Journal C*, vol. 77, no. 2, 2017.
- [2] SELEX Collaboration, A. Ocherashvili, M. A. Moinester, J. Russ et al., "Confirmation of the doubly charmed baryon Ξ_{cc}^+ (3520) via its decay to pD^+K^- ," *Physics Letters B*, vol. 628, article 18, 2005.
- [3] K. A. Olive, K. Agashe, and C. Amsler, "Review of particle physics," *Chinese Physics C*, vol. 38, no. 9, Article ID 090001, 2014.
- [4] S. Koshkarev and V. Anikeev, "Production of the doubly charmed baryons at the SELEX experiment – The double intrinsic charm approach," *Physics Letters B*, vol. 765, pp. 171–174, 2017.
- [5] P. P. Rubio, S. Collins, and G. S. Baliy, "Charmed baryon spectroscopy and light flavor symmetry from lattice QCD," *Physical Review D*, vol. 92, article 034504, 2015.
- [6] R. M. Woloshyn and M. Wurtz, "Systematics of radial excitations in heavy-light hadrons," <https://arxiv.org/abs/1601.01925>.
- [7] T. Yoshida, E. Hiyama, A. Hosaka, M. Oka, and K. Sadato, "Spectrum of heavy baryons in the quark model," *Physical Review D: Particles, Fields, Gravitation and Cosmology*, vol. 92, no. 11, 2015.
- [8] D. Ebert, R. N. Faustov, and V. O. Galkin, "Spectroscopy and Regge trajectories of heavy baryons in the relativistic quark-diquark picture," *Physical Review D: Particles, Fields, Gravitation and Cosmology*, vol. 84, no. 1, 2011.
- [9] C. García-Recio, J. Nieves, O. Romanets, L. L. Salcedo, and L. Tolos, "Hidden charm N and Δ resonances with heavy-quark symmetry," *Physical Review D: Particles, Fields, Gravitation and Cosmology*, vol. 87, no. 7, article 034032, 2013.
- [10] Q. Mao, H. X. Chen, W. Chen et al., "QCD sum rule calculation for P -wave bottom baryons," *Physical Review D*, vol. 92, article 114007, 2015.
- [11] Y. Yamaguchi, S. Ohkoda, A. Hosaka, T. Hyodo, and S. Yasui, "Heavy quark symmetry in multihadron systems," *Physical Review D: Particles, Fields, Gravitation and Cosmology*, vol. 91, no. 3, 2015.
- [12] K. W. Wei, B. Chen, and X. H. Guo, "Masses of doubly and triply charmed baryons," *Physical Review D*, vol. 92, article 076008, 2015.
- [13] K. W. Wei, B. Chen, N. Liu et al., "Spectroscopy of singly, doubly, and triply bottom baryons," *Physical Review D*, vol. 95, article 116005, 2016.
- [14] Z. S. Brown, W. Detmold, S. Meinel, and K. Orginos, "Charmed bottom baryon spectroscopy from lattice QCD," *Physical Review D*, vol. 90, article 094507, Article ID 094507, 2014.
- [15] M. Padmanath, R. G. Edwards, N. Mathur, and M. Peardon, "Spectroscopy of doubly charmed baryons from lattice QCD," *Physical Review D: Particles, Fields, Gravitation and Cosmology*, vol. 91, no. 9, 2015.
- [16] T. M. Aliev, K. Azizi, and M. Savei, "Doubly heavy spin-1/2 baryon spectrum in QCD," *Nuclear Physics A*, vol. 895, article 59, 2012.
- [17] T. M. Aliev, K. Azizi, and M. Savci, "The masses and residues of doubly heavy spin-3/2 baryons," *Journal of Physics G: Nuclear and Particle Physics*, vol. 40, article 065003, 2013.
- [18] B. Eakins and W. Roberts, "Symmetries and Systematics of Doubly Heavy Hadrons," *International Journal of Modern Physics A*, vol. 27, article 1250039, 2012.
- [19] A. Valcarce, H. Garcilazo, and J. Vijande, "Towards an understanding of heavy baryon spectroscopy," *The European Physical Journal A*, vol. 37, article 217, 2008.
- [20] D. Ebert, R. N. Faustov, V. O. Galkin, and A. P. Martynenko, "Mass spectra of doubly heavy baryons in the relativistic quark model," *Physical Review D: Particles, Fields, Gravitation and Cosmology*, vol. 66, no. 1, 2002.
- [21] S. S. Gershtein, V. V. Kiselev, A. K. Likhoded, and A. I. Onishchenko, "Spectroscopy of doubly heavy baryons," *Physical Review D: Particles, Fields, Gravitation and Cosmology*, vol. 62, no. 5, 2000.
- [22] C. Albertus, E. Hernandez, J. Nieves, and J. M. Verde-Velasco, "Static properties and semileptonic decays of doubly heavy baryons in a nonrelativistic quark model," *The European Physical Journal A*, vol. 32, article 183, 2007.

- [23] N. Salehi, A. A. Rajabi, and Z. Ghalenovi, "Spectrum of strange and nonstrange baryons by using generalized gürsey radicati mass formula and hypercentral potential," *Acta Physica Polonica*, vol. 42, 2011.
- [24] C. Patrignani and Particle Data Group, "Review of Particle Physics," *Chinese Physics C*, vol. 40, article 100001, 2016.
- [25] C. Alexandrou, V. Drach, K. Jansen, C. Kallidonis, and G. Koutsou, "Baryon spectrum with," *Physical Review D: Particles, Fields, Gravitation and Cosmology*, vol. 90, no. 7, 2014.
- [26] W. Roberts and M. Pervin, "Heavy Baryons in a Quark Model," *International Journal of Modern Physics A*, vol. 23, article 2817, 2008.
- [27] F. Giannuzzi, "Doubly heavy baryons in a Salpeter model with AdS/QCD inspired potential," *Physical Review D: Particles, Fields, Gravitation and Cosmology*, vol. 79, no. 9, 2009.
- [28] M. Karliner and J. L. Rosner, "Baryons with two heavy quarks: Masses, production, decays, and detection," *Physical Review D: Particles, Fields, Gravitation and Cosmology*, vol. 90, no. 9, 2014.
- [29] L. Tang, X.-H. Yuan, C.-F. Qiao, and X.-Q. Li, "Study of Doubly Heavy Baryon Spectrum via QCD Sum Rules," *Communications in Theoretical Physics*, vol. 57, article 435, 2012.
- [30] A. P. Martynenko, "Ground-state triply and doubly heavy baryons in a relativistic three-quark model," *Physics Letters B*, vol. 663, article 317, 2008.
- [31] Z. G. Wang, "Analysis of the $(1/2)^-$ and $(3/2)^-$ heavy and doubly heavy baryon states with QCD sum rules," *The European Physical Journal A*, vol. 47, article 267, 2010.
- [32] U. Loring, K. Kretzschmar, B. C. Metsch, and H. R. Petry, "Relativistic quark models of baryons with instantaneous forces," *The European Physical Journal A*, vol. 10, article 309, 2001.
- [33] A. A. Rajabi and N. Salehi, "Mesons states and their dependence on spin and isospin," *Iranian Journal of Physics Research*, vol. 8, no. 3, pp. 169–175, 2008.
- [34] N. Salehi, "A New Method for Obtaining the Baryons Mass under the Killingbeck Plus Isotonic Oscillator Potentials," *Advances in High Energy Physics*, vol. 2016, Article ID 5054620, 9 pages, 2016.
- [35] Z. Shah, K. Thakkar, A. K. Rai et al., "Mass spectra and Regge trajectories of Λ_c^+ , Σ_c^0 , Ξ_c^0 and Ω_c^0 baryons*," *Chinese Physics C*, vol. 40, article 123102, 2016.
- [36] N. Salehi, H. Hassanabadi, and A. A. Rajabi, "The light and strange baryon spectrum in a non-relativistic hypercentral quark potential model and algebraic framework," *The European Physical Journal Plus*, vol. 128, p. 27, 2013.
- [37] L. I. Abou-Salem, "Study of baryon spectroscopy using a new potential form," *Advances in High Energy Physics*, vol. 2014, Article ID 196484, 5 pages, 2014.
- [38] Z. Shah, K. Thakkar, A. Kumar Rai, and P. C. Vinodkumar, "Excited state mass spectra of singly charmed baryons," *The European Physical Journal A*, vol. 52, article 313, 2016.
- [39] H. Garcila, J. Vijande, and A. Valcarce, "Faddeev study of heavy-baryon spectroscopy," *Journal of Physics G: Nuclear and Particle Physics*, vol. 34, article 961, 2007.
- [40] E. Santopinto, M. M. Giannini, and F. Iachello, *Symmetries in Science VII*, B. Gruber, Ed., Plenum Press, New York, NY, USA, 1995.
- [41] F. Iachello, *Symmetries in Science VII*, B. Gruber, Ed., Plenum Press, New York, NY, USA, 1995.
- [42] L. Y. Glozman and D. O. Riska, "The spectrum of the nucleons and the strange hyperons and chiral dynamics," *Physics Reports*, vol. 268, article 263, 1996.
- [43] K. Thakkar, Z. Shah, A. K. Rai et al., "Excited state mass spectra and Regge trajectories of bottom baryons," *Nuclear Physics A*, vol. 965, pp. 57–73, 2017.
- [44] Y. Koma, M. Koma, and H. Wittig, "Nonperturbative Determination of the QCD Potential at," *Physical Review Letters*, vol. 97, no. 12, 2006.
- [45] E. Santopinto, F. Iachello, and M. M. Giannini, "Nucleon form factors in a simple three-body quark model," *The European Physical Journal A*, vol. 1, p. 307, 1998.
- [46] A. K. Rai and D. P. Rathaud, "The mass spectra and decay properties of dimesonic states, using the Hellmann potential," *The European Physical Journal C*, vol. 75, no. 9, 2015.
- [47] H. Mariji, "Imposing Fermi momentum cut-off on the channel- and density-dependent effective interaction and the ground-state properties of closed shell nuclei," *The European Physical Journal A*, vol. 50, no. 3, article 56, 2014.
- [48] Z. Shah and A. K. Rai, "Masses and electromagnetic transitions of the B_c mesons," *The European Physical Journal A*, vol. 53, article 195, 2017.
- [49] W. Lucha and F. F. Schoberl, "Solving the Schrodinger equation for bound states with Mathematica 3.0," *International Journal of Modern Physics C*, vol. 10, no. 4, pp. 607–619, 1999.
- [50] J. Ballot and M. Fabre de la Ripelle, "Application of the hyperspherical formalism to the trinucleon bound state problems," *Annals of Physics*, vol. 127, article 62, 1980.
- [51] Z. Shah, K. Thakkar, and A. K. Rai, "Excited state mass spectra of doubly heavy baryons Ω_{cc} , Ω_{bb} , and Ω_{bc} ," *The European Physical Journal C*, vol. 76, article 530, 2016.

Review Article

Heun Functions and Some of Their Applications in Physics

M. Hortaçsu 

Department of Physics, Mimar Sinan Fine Arts University, Istanbul, Turkey

Correspondence should be addressed to M. Hortaçsu; hortacsu@itu.edu.tr

Received 3 May 2018; Accepted 27 May 2018; Published 19 July 2018

Academic Editor: Saber Zarrinkamar

Copyright © 2018 M. Hortaçsu. This is an open access article distributed under the Creative Commons Attribution License, which permits unrestricted use, distribution, and reproduction in any medium, provided the original work is properly cited. The publication of this article was funded by SCOAP³.

Most of the theoretical physics known today is described by using a small number of differential equations. For linear systems, different forms of the hypergeometric or the confluent hypergeometric equations often suffice to describe the system studied. These equations have power series solutions with simple relations between consecutive coefficients and/or can be represented in terms of simple integral transforms. If the problem is nonlinear, one often uses one form of the Painlevé equations. There are important examples, however, where one has to use higher order equations. Heun equation is one of these examples, which recently is often encountered in problems in general relativity and astrophysics. Its special and confluent forms take names as Mathieu, Lamé, and Coulomb spheroidal equations. For these equations whenever a power series solution is written, instead of a two-way recursion relation between the coefficients in the series, we find one between three or four different ones. An integral transform solution using simpler functions also is not obtainable. The use of this equation in physics and mathematical literature exploded in the later years, more than doubling the number of papers with these solutions in the last decade, compared to time period since this equation was introduced in 1889 up to 2008. We use SCI data to conclude this statement, which is not precise, but in the correct ballpark. Here this equation will be introduced and examples for its use, especially in general relativity literature, will be given.

1. Introduction

Most of the theoretical physics known today is described by using a small number of differential equations. If we study only linear systems, different forms of the hypergeometric or the confluent hypergeometric equations often suffice to describe the system studied. These equations have power series solutions with simple relations between consecutive coefficients and/or can be represented in terms of simple integral transforms. If the problem is described in terms of nonlinear differential equations, then one often uses one form of the Painlevé equations.

There are important examples, however, where one has to use higher order equations. Such an equation was proposed by Karl Heun in 1889 [1]. This equation and its confluent forms become indispensable in general relativity if one studies exact solutions of wave equations in the background of certain metrics. A well-known example is the Kerr metric [2]. Although it is possible to solve the wave equations in the background of some metrics in terms of hypergeometric functions or its confluent forms, this is not possible for the

much studied Kerr metric. If we also study even the trivially extended forms of some metrics by adding a flat dimension to the existing metric, we may have to solve the Heun equation to obtain the exact solution.

Here we will introduce the Heun equation and its confluent forms and mention some of the properties of the Heun equation. Then we will give some examples in physics, mainly in gravitational physics, where one can find many recent papers. This part is meant to be a survey of the work done in the field of *General Relativity and Quantum Gravity* concentrating on the last decades. In another section we will give an example where the Heun equation emerges from a trivial extension of a wave equation in the background of the Eguchi-Hanson instanton metric [3]. We will end with some concluding remarks.

2. Heun Equation

Let us review some well-known facts about second-order differential equations. Differential equations are classified

according to their singularity structure [4, 5]. If a differential equation has no singularities over the full complex plane, it can only be a constant. Singularities are classified as regular singular and irregular singular points. If the coefficient of the first derivative has at most single poles and the coefficient of the term without a derivative has at most double poles when the coefficient of the second derivative is unity, this second-order differential equation has regular singularities, which gives us one regular solution while expanding around this singular point. In general the second solution has a pole or a branch point singularity. If the poles of these coefficients are higher, we have irregular singularities and the general solution has an essential singularity [6].

As stated in Morse and Feshbach [4] an example of a second-order differential equation with one regular singular point is

$$\frac{d^2 w}{dz^2} = 0. \quad (1)$$

This equation has one solution which is constant. The second solution blows up at infinity. The differential equation

$$\frac{d^2 w}{dz^2} + k^2 w = 0 \quad (2)$$

has one irregular singularity at infinity which gives an essential singularity at this point. The equation

$$z \frac{d^2 w}{dz^2} + (1+a) \frac{dw}{dz} = 0 \quad (3)$$

has two regular singular points, at zero and at infinity.

In physics an often used equation is the hypergeometric equation

$$z(1-z) \frac{d^2 w}{dz^2} + [c - (1+a+b)z] \frac{dw}{dz} - abw = 0. \quad (4)$$

This equation has three regular singular points, at zero, one, and infinity. Jacobi, Legendre, Gegenbauer, and Tchebycheff equations are special forms of this equation. When the singular points at $z=1$ and z which equal infinity are "coalesced" at infinity, we get the confluent hypergeometric equation

$$z \frac{d^2 w}{dz^2} + (c-z) \frac{dw}{dz} - aw = 0 \quad (5)$$

with an essential singularity at infinity and a regular singularity at zero. Bessel, Laguerre, and Hermite equations can be reduced to this form.

An important property of all these equations is that they allow infinite series solutions about one of their regular singular points where a recursion relation can be found between two consecutive coefficients. This fact allows one to have an idea about the general properties of the solution, as the asymptotic behaviour at distant points, the radius of convergence of the series, etc.

A new equation was introduced in 1889 by Karl M. W. L. Heun [1]. This is an equation with four regular singular points at zero and one and an arbitrary point f between zero

and one and infinity. This equation is discussed in the book edited by Ronveaux [7]. Most of the general information we give below is taken from this book. As discussed there, any equation with four regular singular points can be transformed to the equation given below:

$$\frac{d^2 w}{dz^2} + \left[\frac{c}{z} + \frac{d}{z-1} + \frac{e}{z-f} \right] \frac{dw}{dz} - \frac{abz - q}{z(z-1)(z-f)} w = 0. \quad (6)$$

There is a relation between the constants given as $a + b + 1 = c + d + e$. This relation is not related to the regularity of the singularity at infinity. It just gives the exponents of the term multiplying the series solution around infinity in terms of $u = 1/z$ as a, b .

If we try to obtain a solution in terms of a power series, one cannot get a recursion relation between two consecutive coefficients. We have a relation at least between three coefficients.

It is known that [8] any second-order differential equation with n regular singular points has a family of $2^{n-1}n!$ local solutions, which splits into $2n$ sets of

$$2^{n-2}(n-1)! \quad (7)$$

equivalent expressions, each set defining one of the two Frobenius solutions in the neighborhood of a singular point. The $n!$ factor comes from permuting the n singular points and the 2^{n-1} factor from negating exponent differences. Maier [8] gave the list of 192 local solutions for the Heun equation.

The set of transformations that can be applied to the Fuchian equation with n singular points to generate alternative expressions for this equation has order $2^{n-1}n!$ and acts on the parameter space of the equation. This group of transformations is isomorphic to the Coxeter group D_n . These transformations generate $2^{n-2}(n-1)!$ solutions. For the Heun case $n=4$, and this group is isomorphic to D_4 , a group of order 192. These transformations will be the combination of Mobius transformations and transformations which multiply the desired solution by powers.

It turns out that the Mobius group $\text{PGL}(2, \mathbb{C})$, which takes x to $(Ax + B)/(Cx + D)$, for nonvanishing $AD-BC$, can be used where x takes values from the different singular points. For Heun equation with four regular singular points, this transformation takes each singular point to five other points, which have zeroes at the same value. These points are given below:

$$\begin{aligned} &x, x/(x-1), x/f, x/(x-f), (1-f)x/(x-f), (f-1)x/f(x-1), \\ &1-x, (x-1)/x, (x-1)/(x-f), (x-1)/(f-1), d(x-1)/(x-f), f(x-1)/(f-1)x, \\ &1/x, 1/(1-x), f/x, f/(f-x), (f-1)/(x-1), (1-f)/(x-f), \\ &(x-f)/x, (f-x)/a, (x-f)/(x-1), (f-x)/(f-1), (x-f)/f(x-1), (f-x)/(f-1)x. \end{aligned}$$

Any one of these transformations maps three of the four points, 0, 1, f , and infinity, into 0, 1, and infinity but generally changes the value of f , which takes one of the six possible values: $f_1 = f$, $f_2 = 1 - f$, $f_3 = 1/f$, $f_4 = 1/(1 - f)$, $f_5 = f/(f - 1)$, and $f_6 = (f - 1)/f$. Each value is taken four times.

Just recall the Heun equation:

$$\frac{d^2 w}{dx^2} + \left[\frac{c}{x} + \frac{d}{x-1} + \frac{e}{x-f} \right] \frac{dw}{dx} - \frac{abx - q}{x(x-1)(x-f)} w = 0, \quad (8)$$

written in terms of the real variable x . One writes the solution to the Heun equation in the form

$$y(x) = x^r (x-1)^s \left(1 - \frac{x}{f}\right)^t u(x). \quad (9)$$

This changes the form of the differential equation. For (i) $r = 0$ or $1 - c$, (ii) $s = 0$ or $1 - d$, and (iii) $t = 0$ or $1 - e$, however, the resulting equation has the Heun form. The values given above are the exponents at the singularities [9, 10].

Of course, the parameters of the equations change. For each such combination, say for $r = 0$, there are four possible values s and t can take, namely, both equal to zero; $s = 1 - d$, and $t = 0$; $s = 0$, and $t = 1 - d$; $s = 1 - d$, and $t = 1 - e$. Thus we get three more solutions for each solution. Another factor of six comes from the six different possible values f can take. In total for expansions around a single regular singular point, we have twenty-four equivalent solutions, obtained by simply transforming the original equation.

The presence of two different indices for expansion around each singular point doubles the number of equivalent solutions, resulting in 48 solutions for expansions around each singular point. Four singular points multiply this number by four giving the total of 192 local solutions.

It turns out that, for infinite set of values of the parameter q , there are solutions which are analytic at 0 and at 1. These are called *Heun functions*, whereas those which are analytic only at one point are called *local Heun functions* [11].

For integer values of one of $a, c - a, d - a, e - a$ and for special finite values of q , solutions analytic at three singularities exist, the so-called *Heun polynomials*. A special case is for $a = -n, n = 0, 1, 2$ and $q_{n,m}, m = 0, 1, \dots, n$, where $q_{n,m}$ are eigenvalues of a tridiagonal matrix, we get the solution as a polynomial of degree n , which is analytic at three singular points, 0, 1, and f [12].

“No example has been given of a solution of Heun’s equation expressed in the form of a definite integral or contour integral involving only functions which are, in some sense, simpler” [13]. This statement does not exclude the possibility of having an infinite series of integrals with “simpler” integrands.

One can obtain different confluent forms of this equation. When we “coalesce” two regular singular points, we get the

confluent Heun equation: the standard form of the confluent form equation is given as [14]

$$\frac{d^2 w}{dz^2} + \left(\alpha + \frac{\gamma + 1}{z-1} + \frac{\beta + 1}{z} \right) \frac{dw}{dz} + \left(\frac{\nu}{z-1} + \frac{\mu}{z} \right) w = 0 \quad (10)$$

with solution

$$\begin{aligned} & \text{HeunC}(\alpha, \beta, \gamma, \delta, \eta, z). \\ & \delta = \mu + \nu - \alpha \left(\frac{\beta + \gamma + 2}{2} \right), \\ & \eta = \frac{\alpha(\beta + 1)}{2} - \mu - \left(\frac{\beta + \gamma + \beta\gamma}{2} \right). \end{aligned} \quad (11)$$

Another version of this equation can be written as

$$\begin{aligned} & \frac{d}{dz} \left((z^2 - 1) \frac{dw}{dz} \right) \\ & + \left[-p^2 (z^2 - 1) + 2p\beta z - \lambda - \frac{m^2 + s^2 + 2msz}{(z^2 - 1)} \right] w = 0. \end{aligned} \quad (12)$$

Special forms of this equation are obtained in problems with two Coulombic centers,

$$\begin{aligned} & \frac{d}{dz} \left((z^2 - 1) \frac{dw}{dz} \right) \\ & + \left[-p^2 (z^2 - 1) + 2p\beta z - \lambda - \frac{m^2}{(z^2 - 1)} \right] w = 0, \end{aligned} \quad (13)$$

whose special form, when $b = 0$, is the spheroidal equation

$$\begin{aligned} & \frac{d}{dz} \left((z^2 - 1) \frac{dw}{dz} \right) \\ & + \left[-p^2 (z^2 - 1) - \lambda - \frac{m^2}{(z^2 - 1)} \right] w = 0. \end{aligned} \quad (14)$$

Another form is the algebraic form of the Mathieu equation is

$$\begin{aligned} & \frac{d}{dz} \left((z^2 - 1) \frac{dw}{dz} \right) \\ & + \left[-p^2 (z^2 - 1) - \lambda - \frac{1}{4(z^2 - 1)} \right] w = 0. \end{aligned} \quad (15)$$

If we coalesce two regular singular points pairwise, we obtain the double confluent form

$$\begin{aligned} & D^2 w + \left(\alpha_1 z + \frac{\alpha_{-1}}{z} \right) Dw + \left[\left(B_1 + \frac{\alpha_1}{2} \right) z \right. \\ & \left. + \left(B_0 + \frac{\alpha_1 \alpha_{-1}}{2} \right) + \left(B_{-1} - \frac{\alpha_{-1}}{2} \right) \frac{1}{z} \right] w = 0. \end{aligned} \quad (16)$$

Here $D = z(d/dz)$. We can reduce the new equation to the Mathieu equation, an equation with two irregular singularities at zero and at infinity if we reduce this equation to the form

$$D^2 y + (Bz^2 + B_0 + Bz^{-2}) y = 0. \quad (17)$$

Another form is the biconfluent form, where three regular singularities are coalesced. The result is an equation with a regular singularity at zero and an irregular singularity at infinity of higher order:

$$z^2 \frac{d^2 w}{dz^2} + z \frac{dw}{dz} w + (A_0 + A_1 z + A_2 z^2 + A_3 z^3 - z^4) w = 0. \quad (18)$$

The anharmonic equation in three dimensions can be reduced to this equation:

$$\frac{d^2 w}{dz^2} + \left(E - \frac{\nu}{r^2} - \mu r^2 - \lambda r^4 - \eta r^6 \right) w = 0. \quad (19)$$

In the triconfluent case, all regular singular points are “coalesced” at infinity which gives the equation below:

$$\frac{d^2 w}{dz^2} + \left(A_0 + A_1 z + A_2 z^2 - \frac{9}{4} z^4 \right) w = 0. \quad (20)$$

These different forms are used in different problems in physics.

3. Some Examples of the Heun Equation in Physical Applications

In SCI we found about one hundred thirty papers when Heun functions were searched in the summer of 2010. Now, at the end of April 2018, the number exceeded 330. The number of published articles in SCI more than doubled in the last eight years. More than three fourths of these papers were published in the last ten years. The rest of the papers were published between 1990 and 2005, except a single paper in 1986 [15]. These numbers may differ depending on the institution where one uses the SCI, since different universities in Turkey start their search from different dates. We think we are still in the correct *ball park*. This shows that although the Heun equation was found in 1889, it was largely neglected in the physics literature until recently. Earlier papers on this topic are mostly articles in mathematics journals. If one looks for books on this topic, published before the year 2000, one finds out the list of books is not very long. There is a book edited by A. Ronveaux, which is a collection of papers presented in the “Centennial Workshop on Heun’s Equations: Theory and Application. Sept. 3–8 1989, Schloss Ringberg.” It was published by the Oxford University Press in 1995 by the title *Heun’s Differential Equations* [7]. There are two books on functions which are special cases of the Heun Equation: *Mathiesche Funktionen und Sphaeroidfunktionen mit anwendungen auf physikalische und technische Probleme* by Joseph Meixner and Friedrich Wilhelm Schaeffe, published by Springer Verlag in 1954 [16]

and a Dover reprint of a book first published in 1946, *Theory and Applications of Mathieu Functions* by N. W. McLachlan in 1963 [17]. Classical mathematical physics books, such as Morse and Feshbach [4], Whittaker and Watson [18], or the Batemann Manuscript [19], have sections or chapters on the special forms of the Heun equation like Mathieu, Lamé, or spheroidal functions. Some papers on different mathematical properties of these functions can be found in [8, 20–25].

A reason why more physicists are interested in the Heun equation recently may be, perhaps, a demonstration of the fact that we do not have simple problems in theoretical physics anymore. Mathematical physicists have to tackle more difficult problems, either with more difficult metrics or in higher dimensions. Both of these extensions may necessitate the use of the Heun functions among the solutions. We can give the Eguchi-Hanson case as an example. The wave equation for the scalar particle in the background of the Eguchi-Hanson metric [3] in four dimensions has hypergeometric functions as solutions [26], whereas the Nutku helicoid [27, 28] metric, the next higher one, gives us Mathieu functions [29], a member of the Heun function set, if the method of separation of variables is used to get a solution. We also find that the scalar particle, in the background of the Eguchi-Hanson metric, trivially extended to five dimensions gives Heun type solutions. [30].

Note that the problem does not need to be very complicated to work with these equations. We encounter Mathieu functions if we consider two-dimensional problems with elliptical shapes [31]. Let us use $x = (1/2)a \cosh \mu \cos \theta$ and $y = (1/2)a \sinh \mu \sin \theta$, where a is the distance from the origin to the focal point. Then the Helmholtz equation can be written as

$$\partial_{\mu\mu} \psi + \partial_{\theta\theta} \psi + \frac{1}{4} a^2 k^2 [\cosh^2 \mu - \cos^2 \theta] \psi = 0 \quad (21)$$

which separates into two equations

$$\frac{d^2 H}{d\theta^2} + (b - h^2 \cos^2 \theta) H = 0, \quad (22)$$

$$-\frac{d^2 M}{d\mu^2} + (b - h^2 \cosh^2 \mu) M = 0. \quad (23)$$

The solutions to these two equations can be represented as Mathieu and modified Mathieu functions.

If we combine different inverse powers of r , starting from first up to the fourth, or if we combine the quadratic potentials with inverse even powers of two, four and six, we see that the solution of the Schrodinger equation involves Heun functions [23]. Solution to symmetric double Morse potentials also needs these functions, like $V(x) = B^2/4 \sinh 2x - (s + 1/2)B \cosh x$, where $s = (0, 1/2, 1, \dots)$ [23]. Similar problems are treated in [32–34]

In atomic physics further problems such as separated double wells, Stark effect, and hydrogen molecule ion use these functions. Physics problems which end up with these equations are given in the book by S. Y. Slavyanov and S. Lay [35]. Here we see that even the Stark effect, hydrogen atom in the presence of an external electric field, gives rise to this

equation. As described in page 166 of Slavyanov's book, cited above (original reference is Epstein [36], also treated by S. Yu Slavyanov [37]), when all the relevant constants, namely, Planck constant over 2π , electron mass, and electron charge, are set to unity, the Schrodinger equation for the hydrogen atom in a constant electric field of magnitude F in the z direction is given by

$$\left(\Delta + 2\left[E - \left(Fz - \frac{1}{r}\right)\right]\right)\Psi = 0. \quad (24)$$

Here Δ is the Laplacian operator. Using parabolic coordinates, where the Cartesian ones are given in terms of the new coordinates by $x = \sqrt{\xi\eta} \cos \phi$, $y = \sqrt{\xi\eta} \sin \phi$, and $z = (\xi - \eta)/2$ and writing the wave function in the product form

$$\Psi = \frac{1}{\sqrt{\xi\eta}} V(\xi) U(\eta) \exp(im\phi), \quad (25)$$

we get two separated equations:

$$\frac{d^2V}{d\xi^2} + \left(\frac{E}{2} + \frac{\beta_1}{\xi} - \frac{F}{4}\xi + \frac{1-m^2}{4\xi^2}\right)V(\xi) = 0, \quad (26)$$

$$\frac{d^2U}{d\eta^2} + \left(\frac{E}{2} + \frac{\beta_2}{\eta} + \frac{F}{4}\eta + \frac{1-m^2}{4\eta^2}\right)U(\eta) = 0. \quad (27)$$

Here β_1 and β_2 are separation constants that must add to one. We note that these equations are of the biconfluent Heun form.

The hydrogen molecule also is treated in [38]. When the hydrogen-molecule ion is studied in the Born-Oppenheimer approximation, where the ratio of the electron mass to the proton mass is very small, one gets two singly confluent Heun equations if the prolate spheroidal coordinates $\xi = (r_1 + r_2)/2c$ and $\eta = (r_1 - r_2)/2c$ are used. Here c is the distance between the two centers. Assuming

$$\psi = \sqrt{\xi\eta} V(\xi) U(\eta) \exp(im\phi), \quad (28)$$

we get two confluent Heun equations:

$$\frac{d}{d\xi} \left((1-\xi^2) \frac{dV}{d\xi} \right) + \left(\lambda^2 \xi^2 - \kappa \xi - \frac{m^2}{1-\xi^2} + \mu \right) V = 0, \quad (29)$$

$$\frac{d}{d\eta} \left((1-\eta^2) \frac{dU}{d\eta} \right) + \left(\lambda^2 \eta^2 - \frac{m^2}{1-\eta^2} + \mu \right) U = 0. \quad (30)$$

Some additional physics papers with Heun type solutions include the following:

Three relatively recent papers which treat atoms in magnetic fields are as follows.

Exact low-lying states of two interacting equally charged particles in a magnetic field are studied by Truong and Bazzali [39].

The energy spectrum of a charged particle on a sphere under a magnetic field and Coulomb force are studied by Ralko and Truong [40].

B. S. Kandemir presented an analytical analysis of the two-dimensional Schrodinger equation for two interacting electrons subjected to a homogeneous magnetic field and confined by a two-dimensional external parabolic potential. Here a biconfluent Heun (BHE) equation is used [41].

Arda and Sever in one instance with Aydoğdu studied Schrodinger equation with different potentials and in two cases found Heun and confluent Heun solutions [42, 43].

In two papers Hammann et al. [44, 45] solved the one-dimensional Schrodinger equation for position-dependent masses and obtained Heun solutions. The importance of these papers is the derivation and use of relations between Heun functions which are functions of z and $1-z$, which can be used for obtaining the reflection and transition amplitudes for scattering problems for waves described in terms of Heun functions.

Recently Ishkhanyan showed that the solution of the Schrodinger equation for V_0/\sqrt{x} can be given as a derivative of a triconfluent Heun function [46]. In another paper, solution for the same potential is given [47] as a linear combination of two confluent hypergeometric functions. For another potential which is an inverse square root near the origin and vanishes exponentially at infinity, solution is given in terms of linear combination of Gauss hypergeometric functions [48]. These potentials belong to the Heun class.

Downing showed that the solution to the one-dimensional Schrodinger equation with a hyperbolic double well potential is obtained by a transformation of the confluent Heun equation [49].

Hartmann and Portnoi calculated the bound modes of two-dimensional massless Dirac fermions confined within a hyperbolic secant potential [50].

Portnoi et al. continued studying the two-dimensional Dirac particles in two papers, first confined in nonuniform magnetic fields and second in Poschl-Teller waveguide [51, 52] in terms of confluent Heun functions.

In a relatively recent work P. Dorey [53] showed that equations in finite lattice systems also reduce to Heun equations.

Dislocation movement in crystalline materials and quantum diffusion of kinks along dislocations are some solid state applications of this equation. The book by S. Y. Slavyanov and S. Lay [35] is a general reference on problems solved before 2000.

We also cite a recent mathematical application by A. M. Ishkhanyan et al. where "total fifteen potentials for which the stationary Klein-Gordon equation is solvable in terms of the confluent Heun functions are presented.. Only nine of the potentials are independent due to the transposition symmetry of regular singular points of the equation. Four of these equations can be reduced to the hypergeometric form. The remaining five independent Heun potentials are four-parametric and have solutions only in terms of irreducible confluent Heun functions [54]. Prof Ishkhanyan expands the Heun solution in terms of hypergeometric functions and shows that the sum has only finite number of terms in his cases. Prof. Ishkhanyan wrote additional papers after this one using the same method for other potentials. We will not comment on them, however, since from this point on, we

will confine ourselves only to papers on general relativity and cosmology.

Among the papers in general relativity, we also will not be able to comment on all the works of some experts like Prof Fiziev on this field, who wrote scores of papers on Heun equations. We will give only the earlier papers and leave the reader to investigate the later ones in the ArXiv.

In general relativity, in a relatively early work, Teukolsky studied the perturbations of the Kerr metric [55]. If we take

$$\Psi = \exp(-i\omega t) \exp(im\phi) S(\theta) R(r), \quad (31)$$

for the scalar particle we get two equations.

$$\begin{aligned} & \frac{d}{dr} \left(\Delta \frac{dR}{dr} \right) \\ & + \left(\left[(r^2 + a^2) \omega^2 - 4aMr\omega m + a^2 m^2 \right] \Delta^{-1} - A \right. \\ & \left. - a^2 \omega^2 \right) R = 0, \end{aligned} \quad (32)$$

$$\begin{aligned} & \frac{1}{\sin\theta} \left(\frac{d}{d\theta} \sin\theta \frac{dS}{d\theta} \right) + \left(a^2 \omega^2 \cos^2\theta - \frac{m^2}{\sin^2\theta} + A \right) S \\ & = 0. \end{aligned} \quad (33)$$

Here A is the separation constant, $\Delta = r^2 - 2Mr + a^2$.

Teukolsky just stated these equations [55]. Later these equations were found to be two coupled singly confluent Heun equations [56].

Quasi-normal modes of rotational gravitational singularities were also studied by solving these equations by E.W. Leaver [57].

In recent applications in general relativity, Heun type equations become indispensable when one studies phenomena in higher dimensions, or in different geometries. We must note that even the simplest black hole metric, the Schwarzschild, has solutions in the Heun form [58, 59].

Some other references for general relativity applications are:

D. Batic, H. Schmid, M. Winklmeier where the Dirac equation in the Kerr-Newman metric and static perturbations of the non-extremal Reisner-Nordstrom solution are studied [60]. D. Batic and H. Schmid also studied the Dirac equation for the Kerr-Newman metric and looked for its propagator [61]. They found that the equation satisfied is a form of a general Heun equation described in Reference [60]. In later work Batic, with collaborators continued studying Heun equations and their generalizations [62]. In his most recent paper Batic, with collaborators studied *Semi commuting and commuting operators for the Heun family* [63].

Prof. P.P. Fiziev studied problems whose solutions are Heun equations extensively.

In a paper published in gr-qc/0603003, he studied the exact solutions of the Regge-Wheeler equation in the Schwarzschild black hole interior [58].

He presented a novel derivation of the Teukolsky-Starobinsky identities, based on properties of the confluent Heun functions [64]. These functions define analytically all

exact solutions to the Teukolsky master equation, as well as to the Regge-Wheeler and Zerilli ones.

In a talk given at 29th Spanish Relativity Meeting (ERE 2006), he depicted in more detail the exact solutions of Regge-Wheeler equation, which described the axial perturbations of Schwarzschild metric in linear approximation, in the Schwarzschild black hole interior and on Kruskal-Szekeres manifold in terms of the confluent Heun functions [65].

All classes of exact solutions to the Teukolsky master equation were described in terms of confluent Heun functions in Reference [66, 67].

In reference [68] he reveals important properties of the confluent Heun's functions by deriving a set of novel relations for confluent Heun's functions and their derivatives of arbitrary order. Specific new sub classes of confluent Heun's functions are introduced and studied. A new alternative derivation of confluent Heun's polynomials is presented.

In another paper [69] he, with a collaborator, noted that weak gravitational, electromagnetic, neutrino and scalar fields, considered as perturbations on Kerr background satisfied Teukolsky Master Equation. The two non-trivial equations were obtained after separating the variables, one equation only with the polar angle and another using only the radial variable. These were solved by transforming each one into the form of a confluent Heun equation.

Fiziev is an expert in this topic. Two further articles by him and his collaborator are *Solving systems of transcendental equations involving the Heun functions*, [70] and *Application of the confluent Heun functions for finding the quasinormal modes of non rotating black holes* [71].

We also cite one of the last papers of Fiziev on the mathematical properties of this subject which can have applications in physics. In [72], the author "introduces and studies a novel type of solutions to the general Heun equation." His approach is based "on the symmetric form of the Heun differential equation yielded by development of the Papperitz-Klein symmetric form of the Fuchsian equations with an arbitrary number of regular singular points greater than 4. The symmetry group of these equations turns to be a proper extension of the Mobius group." He also introduces and studies "new series solutions and derives solutions for the four singular point case which treats simultaneously and on an equal footing all singular points."

Among other papers on this subject one may cite the following papers.

R. Manvelyan, H. J. W. Muller Kirsten, J. Q. Liang, and Y. Zhang calculated the absorption rate of a scalar by a D3 brane in ten dimensions in terms of modified Mathieu functions and obtained the S-matrix in [73].

T.Oota and Y.Yasui studied the scalar Laplacian on a wide class of five-dimensional toric Sasaki-Einstein manifolds, ending in two Heun's differential equations in [74].

S. Musiri and G. Siopsis found out that the wave equation, obtained in calculating the asymptotic form of the quasinormal frequencies for large AdS black holes in five dimensions, reduces to a Heun equation, in [75].

A. Al-Badawi and I. Sakalli studied the Dirac equation in the rotating Bertotti-Robinson space-time [76] ending up with a Heun type equation.

I first *encountered* this type of equation when we tried to solve the scalar wave in the background of the Nutku helicoid instanton [29]. In this case, for a scalar particle in this background metric, one gets the Mathieu equation which is a special case of the Heun equation. In the same paper, the solutions in four dimensions involve the product of two exponentials and two Heun functions. These solutions can be summed to give Green's function for this problem in a closed form. We could not succeed in obtaining a closed form solution for the Green function when the similar problem is studied in five dimensions [77, 78].

The helicoid instanton is a double-centered solution. As remarked above, for the simpler instanton solution of Eguchi-Hanson [3] hypergeometric solutions are sufficient [26]. Here one must remark that another paper using the Eguchi-Hanson metric ends up with the confluent Heun equation [79]. These two papers show that sometimes judicious choice of the coordinate system and separation ansatz matters.

Sucu and Ünal also obtained closed solutions for the spinor particle written in the background of the Nutku helicoid instanton [26], whereas using the separation of variables method gives us an infinite series of product of two Mathieu functions [77].

One can show that the solutions of Sucu and Ünal can be expanded in terms of Mathieu functions if one attempts to use the separation of variables method, as described by L. Chaos-Cador and E. Ley-Koo [80].

Tolga Birkandan and I also found an extension of the Heun equation with five singular points [30] and calculated the solution of a scalar field in the background of the Eguchi-Hanson equation trivially extended to five dimensions [30]. Then the solution for the radial component turned out to be given in terms of the confluent Heun equation.

Mirjam Cvetič and Finn Larsen studied grey body factors and event horizons for rotating black holes with two rotation parameters and five charges in five dimensions. When the Klein-Gordon equation for a scalar particle in this background is written, one gets a confluent Heun equation. In the asymptotic region this equation turns into the hypergeometric form [81]. When they studied the similar problem for the rotating black hole with four $U(1)$ charges, they again obtained a confluent Heun equation for the radial component of the Klein-Gordon equation, which they reduce to the hypergeometric form by making approximations [82]. These two papers are partly repeated in [83]. The same equations were obtained which were reduced to approximate forms which gave solutions in the hypergeometric form.

M. Cvetič encounters this function in several of her publications and reduces them to the hypergeometric form by giving physical arguments to drop certain terms in the equation. The hypergeometric solution points to the presence of conformal symmetry in the reduced model [84, 85]. The method is going to the extreme and near-extreme (Kerr/CFT correspondence) limits, going to the boundary and in some cases using a “subtracted metric” using a warp factor which preserves all the near-horizon properties of the black hole such as the entropy and the thermodynamic potentials, and if necessary dropping certain terms which are negligible in these limits [86–88].

“In general, conformal symmetry does not exist in the non-extremal cases. The solutions often turn out to be of the Heun form. In the extremal case two horizons overlap. In the near extremal case they are very close to each other. In these two cases and in the near horizon limit, we find conformal symmetry, resulting in solutions which are hypergeometric functions, or one of its confluent forms. If we want conformal symmetry without going to the extremal or the near horizon limit, we have to change the ‘warp factor’. When the warp factor is changed, the rest of the metric preserves its initial form. The thermodynamic potentials and entropy do not change. You have to drop some terms resulting in solutions in the hypergeometric form. This is equivalent to putting the black hole into a conic box. If you go to the asymptotic or to the scaling limit, this is seen clearly. In these limits the Einstein equations are not satisfied unless the energy-momentum tensor, on the right side of the Einstein equations are also changed, to account for putting the system into the conic box.” [89]

Cvetič also studied black holes in supergravity with Birkandan. Heun solutions also exist for the Wu Black Hole which is the most general solution of maximally supersymmetric gauged supergravity in $D=5$ [90]. Here they did not study the limiting cases. For the massless Klein-Gordon equation in the background of the most general black hole in four dimensions and $N=2$ gauge supersymmetry with $U(1)^2$ gauge symmetry (Chow-Compere solution [91]), the angular equation gives Heun type solutions. The radial equation has five regular singularities, which reduce to hypergeometric functions in the near-horizon extremal limit [92].

We should also mention two papers by H. R. Christiansen and M. S. Cunha with Heun type solutions. These are *Confluent Heun Functions in Gauge Theories on Thick Braneworlds* [93] and *Kalb-Ramond Excitations in a Thick-Brane Scenario with Dilaton* [94]. In the first paper, the propagation modes of gauge fields in an infinite Randall-Sundrum scenario are investigated. Here a sine-Gordon soliton represents the thick four-dimensional braneworld while an exponentially coupled scalar field acts for the dilaton. For the gauge field motion a differential equation is found which can be transformed into a confluent Heun equation. In the second paper a similar scenario is used. Here a bulk Kalb-Ramond field is coupled to a dilaton, in a warped space-time in the presence of a brane field in five dimensions. Full spectrum and eigenstates are studied. In the general case, the solutions to the field equations are given in terms of the confluent Heun function, which reduces to the confluent hypergeometric function for special values of the parameters.

Other relevant references I could find are listed as [95–102].

The more recent papers on this subject include *The Quantum Treatment of the 5D-Warped Friedman-Robertson-Walker Universe in Schrodinger Picture* [103]. Here the time-evolving Schrodinger version of the Wheeler-De Witt equation, written for the five-dimensional warped $k=0$ -FRW Universe, is studied. For small values of the cosmological scale factor, a , the wave function of the Universe is expressed in terms of the Heun Double Confluent functions, whereas for large values of this parameter the solution becomes the Hermite

associated functions. Two papers by the same authors using Heun type functions are *Fermions in Magnetar's Crust in terms of Heun Double Confluent Functions* [104] and *The Approximative Analytic Study of Fermions in Magnetar's Crust; Ultra-Relativistic Plane Waves, Heun and Mathieu Solutions and Beyond* [105].

In *Fermi Surfaces and Analytic Green's Functions from Conformal Gravity* [106], T2-symmetric charged AdS black holes are constructed in conformal gravity. The most general solution up to an overall conformal factor contains three non-trivial parameters: the mass, electric charge, and a quantity that can be identified as the massive spin-2 hair. The Dirac equation for the charged massless spinor in this background can be solved in terms of the general Heun function for generic frequency ω and wave number k . This allows us to obtain the analytic Green function $G(\omega, k)$ for both extremal and nonextremal black holes. For some special choice of black hole parameters, the Green function reduces to simpler hypergeometric or confluent hypergeometric functions.

Two of the authors of the paper quoted above had calculated Green's functions in terms of the Heun function in an earlier paper, *Exact Green's Functions from Conformal Gravity* [107].

Another paper is *Quantized Black Hole and Heun Function* by D. Momeni, K. Yerzhanov, and R. Myrzakulov [108] where a black hole is quantized using the Bohr method. The solution turns to be of the Heun type.

In *On an Approach to Constructing Static Ball Models in General Relativity* by A. M. Baranov, some solutions of the Einstein equation were described by Heun functions [109].

In an paper on analytic solutions of wave equations in regular coordinate systems on Schwarzschild background Dennis Philipp and Volker Perlick claim that they find "the wave equation for the propagation of (massless) scalar, electromagnetic and gravitational waves on fixed Schwarzschild background spacetime, which is described by the general time-dependent Regge-Wheeler equation, can be transformed to usual Schwarzschild, Eddington-Finkelstein, Painleve Gullstrand and Kruskal-Szekeres coordinates. In the first three cases, but not in the last one, it is possible to separate a harmonic time-dependence. Then the resulting radial equations belong to the class of confluent Heun equations" [59].

Among additional papers we can also cite the article of Bezerra et al., *Exact Solutions of the Klein-Gordon Equation in the Kerr-Newman Background and Hawking Radiation*, where both the radial and angular solutions are given in terms of confluent Heun functions [110]. In the particular case corresponding to an extreme Kerr-Newman black hole, the solution is given by the double confluent Heun functions [111]. Biconfluent Heun functions were obtained for the exact solution of the Schrodinger equation for a particle (galaxy) moving in a Newtonian universe with a cosmological constant [112].

Other papers on general relativity written in 2015 also include *New Results for Electromagnetic Quasinormal and Quasibound Modes of Kerr Black Holes*, by D. Staicova and P. Fiziev [113], where the authors solve Teukolsky equations with confluent Heun solutions numerically. In *Heun Functions Describing Fermions Evolving in Parallel and Magnetic Fields*,

by C. Dariescu and M. A. Dariescu [114], the solutions are in terms of double confluent Heun functions. The same authors also published *Quantum Analysis of $k=-1$ Robert-Walker Universe*, where they solved the Wheeler-DeWitt equation [115]. The solutions turned out to be Heun functions. M. C. E. Cedeno and J. C. N. Araujo show that, for Master equation solutions in the linear regime of characteristic formulation of general relativity, the solution is in terms of confluent Heun's functions for radiative case in the Schwarzschild's background [116]. In *Massless Dirac Particles in the Vacuum C-Metric*, D. Bini et al. show that the Dirac equation, written in the background of the C-metric, can be reduced to a radial and an angular equation, both of which can be solved in terms of general Heun functions [117]. Vieira et al. [118] show that for *Charged Massive Scalar Fields are Considered in the Gravitational and Electromagnetic Field Produced by a Dyonic Black Hole with a Cosmic String along its Axis of Symmetry* "exact solutions of both angular and radial parts of the covariant Klein-Gordon equation in this background can be obtained, and are given in terms of the confluent Heun functions." In [119], Kofron separates test fields equations on the nonrotating C-metric background. He finds that the resulting equations are of the Heun or confluent Heun form for the general case. These equations, however, can be reduced to hypergeometric functions in the static, axial symmetric, and the extremal case where the inner and outer horizons coalesce. In another paper [120], the same author studies the similar phenomena on the background of the rotating C-metric. For the general case, the radial equation has five regular singularities. In the extremal, static, and axial symmetric cases, one obtains a polynomial solution.

Some other papers published in 2016 in the field of general relativity where solutions to field equations are in the background of different metrics are as follows.

Valtancoli [121] found Heun solutions for the radial part of the Klein-Gordon equation when the scalar field is conformally coupled to a charged BTZ black hole.

Vieira and Bezerra [122] study "resonant frequencies, Hawking radiation and scattering of scalar waves. . ." and find confluent Heun solutions. They also study [123] the class of solutions of the Wheeler-DeWitt equation in the Friedmann-Robertson-Walker universe. In still another paper [124], these authors find confluent Heun solutions for the massless Klein-Gordon equation in the background metric of the three-dimensional rotating and four-dimensional canonical acoustic black holes.

Sakalli [125] finds analytical solutions in rotating linear dilaton black holes.

Kraniotis [126] studies the Klein-Gordon equation in the background metric of the Kerr-Newman (anti-)de Sitter black hole. He first reduces the radial and angular equations to the Heun form and writes the solution in terms of local Heun and confluent Heun functions. In my opinion this paper should be also praised for the introduction of the "false singular point" concept, which reduces the solution to hypergeometric functions for certain values of the physical parameters in the equation.

Since we updated this paper in February 2017, we find close to thirty new publications if one searches for the word

Heun Functions in the index Web of Knowledge in April 2018. Many of these papers are on the mathematical aspects of the equation and solving Schrodinger equations for different new potentials in terms of Heun or linear combinations of Heun functions. There are also solutions in terms of Heun functions for equations used in different branches of physics. Here we will attempt to review only the papers for applications in physics related to general relativity.

In [127], Arda et al. solve the energy relations obtained with the help of the quantization rule for the Klein-Gordon equation with a linear plus an inverse-linear potential in terms of biconfluent Heun equations. Vieira wrote two papers [128, 129] where he first studied *Resonant Frequencies of a Hydrodynamic Vortex*. The radial equation has solutions in terms of double confluent Heun functions. In the second paper, analytic solutions for sound perturbations in the presence of a rotating acoustic black hole which is an analogue of the conical Kerr metric were studied. In the massless case, the radial equation has Heun type solutions. Vieira also wrote another paper with coauthors [130], where *massive scalar fields are considered in the gravitational field produced by a Schwarzschild black hole with a global monopole in $f(R)$ gravity*. The exact solution of the radial part of the Klein-Gordon equation in this background is given in terms of the general Heun functions. The properties of the general Heun functions are applied to study the Hawking radiation and the resonant frequencies of scalar particles.

Ciprian Dariescu wrote two papers with collaborators [131, 132]. In the first paper, using a perturbative method, Klein-Gordon equation for a charged massive field in the background of a magnetar is solved both in the interior solution and outside the star. Equations can be separated with general and confluent Heun function solutions. With special conditions on parameters, polynomial solutions can be found and first-order transition amplitudes are computed [131]. In the second paper, for the spatially open Friedmann-Robertson-Walker (FRW) Universe with stiff matter and radiation as noninteracting matter sources, the scale function coming from the integration of the Friedmann equation is expressed in terms of elliptic integrals. For a negative cosmological constant, the allowed ranges for the models parameters are identified. Within the quantum analysis, the Wheeler-DeWitt (WDW) equation turns into a modified Morse equation whose solutions are Mathieu and Heun functions. [132].

Sobhani et al. [133] wrote a paper where the thermodynamic properties of the anharmonic oscillator cosmic string framework are studied. The Schrodinger equation is written in the cosmic string framework and anharmonic oscillations are investigated. The wave function and energy spectrum are derived using confluent Heun functions.

Birkandan was also active in this period. He wrote four papers. In the first paper, with Bouaziz, he showed that the deformed Schrodinger equation for a singular inverse square potential in coordinate space with a minimal length is solved in terms of Heun functions [134]. In his second paper with a collaborator, confluent Heun solutions to the radial equations of two Halilsoy-Badawi metrics are found. For the first metric, the radial part of the massless Dirac equation

and, for the second case, the radial part of the massless Klein-Gordon equation are studied [135], both with Heun type solutions. In the third paper, he and his collaborator showed that Heun-type exact solutions emerged for both the radial and the angular equations for the case of a scalar particle coupled to the zero-mass limit of both the Kerr and Kerr-(anti-)de-Sitter space-times. Since any type D metric has Heun-type solutions, it is interesting that this property is retained when the black hole has a zero-mass limit. This work further refuted the claims that mass of the black hole, going to zero limit of the Kerr metric, was both locally and globally the same as the Minkowski metric [136]. We comment on the fourth paper in the Conclusion.

A comprehensive bibliography can be found at the bibliography section of <http://tcpa.uni-sofia.bg/heun/home.html>, compiled by Professors Plamen Fiziev and Denitsa Staicova.

Just to give an example of how the Heun function emerges in a simple problem, in the next section, our work in [30] for the scalar particle in the background metric of the extended Eguchi-Hanson solution will be sketched.

4. Scalar Field in the Background of the Extended Eguchi-Hanson Solution

To go to five dimensions, we can add a time component to the Eguchi-Hanson [3] metric so that we have

$$ds^2 = -dt^2 + \frac{1}{1 - a^4/r^4} dr^2 + r^2 (\sigma_x^2 + \sigma_y^2) + r^2 \left(1 - \frac{a^4}{r^4}\right) \sigma_z^2 \quad (34)$$

where

$$\sigma_x = \frac{1}{2} (-\cos \xi d\theta - \sin \theta \sin \xi d\phi) \quad (35)$$

$$\sigma_y = \frac{1}{2} (\sin \xi d\theta - \sin \theta \cos \xi d\phi) \quad (36)$$

$$\sigma_z = \frac{1}{2} (-d\xi - \cos \theta d\phi). \quad (37)$$

This is a vacuum solution. If we take

$$\Phi = e^{ikt} e^{im\phi} e^{i(m+1/2)\xi} \varphi(r, \theta), \quad (38)$$

we find the scalar equation as

$$\varphi(r, \theta) = \left(\frac{r^4 - a^4}{r^2} \partial_{rr} + \frac{3r^4 + a^4}{r^3} \partial_r + k^2 r^2 + \frac{4a^4 m^2}{a^4 - r^4} + 4\partial_{\theta\theta} + 4 \cot \theta \partial_\theta + \frac{8mn \cos \theta - 4(m^2 + n^2)}{\sin^2 \theta} \right) \cdot \varphi(r, \theta). \quad (39)$$

If we take $\varphi(r, \theta) = f(r)g(\theta)$, the solution of the radial part is expressed in terms of confluent Heun (H_C) functions.

$$f(r) = (-a^4 + r^4)^{(1/2)m} H_C \left(0, m, m, \frac{1}{2}k^2 a^2, \frac{1}{2}m^2 - \frac{1}{4}\lambda - \frac{1}{4}k^2 a^2, \frac{a^2 + r^2}{2a^2} \right) + (a^2 + r^2)^{-(1/2)m} \left(r^2 - a^2 \right)^{1/2m} H_C \left(0, -m, m, \frac{1}{2}k^2 a^2, \frac{1}{2}m^2 - \frac{1}{4}\lambda - \frac{1}{4}k^2 a^2, \frac{a^2 + r^2}{2a^2} \right). \quad (40)$$

If the variable transformation $r = a\sqrt{\cosh x}$ is made, one solution can be expressed as

$$f(x) = (\sinh(x))^m H_C \left(0, m, m, \frac{1}{2}k^2 a^2, \frac{1}{2}m^2 - \frac{1}{4}\lambda - \frac{1}{4}k^2 a^2, \frac{1}{2}\cosh^2\left(\frac{x}{2}\right) \right). \quad (41)$$

$$g(\theta) = \sin(\theta)^m \cot\left(\frac{\theta}{2}\right)^n \times {}_2F_1 \left(\left(\left[m + \frac{1}{2}\sqrt{\lambda+1} + \frac{1}{2}, m - \frac{1}{2}\sqrt{\lambda+1} + \frac{1}{2} \right], \right) [1+n+m], \frac{(1/2)\cos^2(\theta)}{2} \right). \quad (43)$$

5. Conclusion

In this paper, first the Heun function is introduced; then some of its uses in physics, especially in the field of general relativity and gravitation, are demonstrated. We have to note that most of the physicists that bluntly state their solution is in terms of Heun functions are mainly from the third world. We see physicists from Bulgaria, Romania, Brazil, Armenia, and even Turkey in this group. There are mathematicians from the western world, though, who are experts in this field. Batic, a mathematician, although he now works in UAE may be considered from the western world. Ronveaux from Belgium and many other mathematicians are from the western world.

They are not really many exceptions to this observation. Cvetič and Larsen demonstrate what the physicists from the western world do. They try to express their solutions in terms of hypergeometric functions, by going to the asymptotics, to the extremal, or to the near-extremal limit, or putting the solution into a conic box, by changing the energy momentum term if necessary, but keeping the thermodynamic potentials the same. A long endeavor was necessary to label *Teukolsky Master Equations* as belonging to the Heun class [56]. Only recently was the equation given by 't Hooft [137] shown to belong to the Heun class if it were not modified [138]. When modified the solution is the manageable hypergeometric function. We agree that this impression may be wrong, but it is just an observation.

The first version of this paper was submitted to the 13th Regional Conference on Mathematical Physics, which was

We tried to express the equation for the radial part in terms of $u = (a^2 + r^2)/2a^2$ to see the singularity structure more clearly. Then the radial differential operator reads

$$4 \frac{d^2}{du^2} + 4 \left(\frac{1}{u-1} + \frac{1}{u} \right) \frac{d}{du} + k^2 a^2 \left(\frac{1}{u-1} + \frac{1}{u} \right) + \frac{m^2}{u^2(1-u)^2}. \quad (42)$$

This operator has two regular singularities at zero and one and an irregular singularity at infinity, the singularity structure of the confluent Heun equation. This is different from the hypergeometric equation, which has regular singularities at zero, one and infinity.

The solution of the angular equation which is regular at $\theta = \pi$ for m greater than n is given below in terms of hypergeometric functions.

held in Antalya, Turkey, on 27–31 October 2010 and printed in [139].

Disclosure

This paper is a revised and many-times-updated version of the conference talk by the same author, published in *Proceedings of the 13th Regional Conference on Mathematical Physics, Antalya, Turkey, 27–31 October 2010*, edited by Uğur Camcı and Ibrahim Semiz, pp. 23–39, World Scientific (2013).

Conflicts of Interest

The author declares that they have no conflicts of interest.

Acknowledgments

The author is grateful to Professors Cemsinan Deliduman and Kayhan Ülker for providing the author with a shelter at Mimar Sinan Fine Arts University during the author's days in retirement. The author is indebted to Tolga Birkandan for collaboration and technical assistance and is grateful to Professor Dr. André Ronveaux for informing the author of a slight error in [9]. The author thanks Science Academy, Turkey, for support.

References

- [1] K. Heun, "Zur Theorie der Riemann'schen Functionen zweiter Ordnung mit vier Verzweigungspunkten," *Mathematische Annalen*, vol. 33, no. 2, pp. 161–179, 1888.

- [2] R. P. Kerr, "Gravitational field of a spinning mass as an example of algebraically special metrics," *Physical Review Letters*, vol. 11, pp. 237-238, 1963.
- [3] T. Eguchi and A. J. Hanson, "Asymptotically flat self-dual solutions to euclidean gravity," *Physics Letters*, vol. 74B, p. 249, 1978.
- [4] P. M. Morse and H. Feshbach, *Methods of Theoretical Physics*, McGraw-Hill, New York, NY, USA, 1953.
- [5] E. L. Ince, *Ordinary Differential Equations*, Dover Publications, (1926, 1956).
- [6] P. M. Morse and H. Feshbach, *Methods of Theoretical Physics*, p. 532, McGraw-Hill, New York, NY, USA, 1953.
- [7] A. Ronveaux, *Heun's Differential Equations*, Oxford University Press, Oxford, UK, 1995.
- [8] R. S. Maier, "On reducing the Heun equation to the hypergeometric equation," *Journal of Differential Equations*, vol. 213, no. 1, pp. 171-203, 2005.
- [9] F. M. Arscott, *Heun's Differential Equations*, A. Ronveaux, Ed., Oxford University Press, 1995.
- [10] A. Ronveaux, "Factorization of the Heun's differential operator," *Applied Mathematics and Computation*, vol. 141, no. 1, pp. 177-184, 2003.
- [11] F. M. Arscott, *Heun's Differential Equations*, A. Ronveaux, Ed., pp. 11-12, 39-41, Oxford University Press, 1995.
- [12] F. M. Arscott, "Heun's Differential Equations," A. A. Ronveaux, Ed., pp. 12, 41-44, Oxford University Press, 1995.
- [13] F. M. Arscott, *Heun's Differential Equation*, A. Ronveaux, Ed., p. 65, Oxford University Press, 1995.
- [14] P. P. Fiziev, "Classes of exact solutions to the Teukolsky master equation," *Classical and Quantum Gravity*, vol. 27, article 135001, 2010.
- [15] G. Valent, "An integral transform involving Heun functions and a related eigenvalue problem," *SIAM Journal on Mathematical Analysis*, vol. 17, no. 3, pp. 688-703, 1986.
- [16] J. Meixner and F. W. Schafke, *Mathieu'sche Funktionen und Sphaeroidfunktionen mit anwendungen auf physikalische und technische Probleme*, Springer, 1954.
- [17] N. W. McLachlan, "Theory and applications of mathieu functions," *Dover reprint from 1946 edition*, 1964.
- [18] E. T. Whittaker and G. N. Watson, *A Course of Modern Analysis*, Cambridge University Press, 1963.
- [19] A. Erdelyi, W. Magnus, F. Oberhettinger, and F. G. Tricomi, *Bateman Manuscript, Higher Transcendental Functions*, vol. III, Mc.Graw Hil, 1995.
- [20] R. Schafke and D. Schmidt, "The connection problem for general linear ordinary differential equations at two regular singular points with applications in the theory of special functions," *SIAM Journal on Mathematical Analysis*, vol. 11, no. 5, pp. 848-862, 1980.
- [21] N. Gurappa and P. K. Panigrahi, "On polynomial solutions of the Heun equation," *Journal of Physics A: Mathematical and General*, vol. 37, no. 46, pp. L605-L608, 2004.
- [22] K. Kuiken, "Heun's equation and the hypergeometric equation," *SIAM Journal on Mathematical Analysis*, vol. 10, no. 3, pp. 655-657, 1979.
- [23] B. D. B. Figueiredo, "Ince's limits for confluent and double-confluent Heun equations," *Journal of Mathematical Physics*, vol. 46, no. 11, Article ID 113503, 2005.
- [24] S. Bellucci and V. Yeghikyan, "The Coulomb problem on a 3-sphere and Heun polynomials," *Journal of Mathematical Physics*, vol. 54, no. 8, article 082103, 8 pages, 2013.
- [25] P. Aydiner and T. Birkandan, "Physical problems admitting Heun-to-hypergeometric reduction," in *Proceedings of the International Conference DAYS on DIFFRACTION 2015*, pp. 27-33, St. Petersburg, Russia, May 2015.
- [26] Y. Sucu and N. Ünal, "Dirac equation in Euclidean Newman-Penrose formalism with applications to instanton metrics," *Classical and Quantum Gravity*, vol. 21, no. 6, pp. 1443-1451, 2004.
- [27] Y. Nutku, "Gravitational instantons and minimal surfaces," *Physical Review Letters*, vol. 77, no. 23, pp. 4702-4703, 1996.
- [28] D. Lorenz-Petzold, "Positive-definite self-dual solutions of Einstein's field equations," *Journal of Mathematical Physics*, vol. 24, article 2632, 1983.
- [29] A. N. Aliev, M. Hortaçsu, J. Kalayci, and Y. Nutku, "Gravitational instantons from minimal surfaces," *Classical and Quantum Gravity*, vol. 16, no. 2, pp. 631-642, 1999.
- [30] T. Birkandan and M. Hortaçsu, "Singularity structure and stability analysis of the dirac equation on the boundary of the nutku helicoid solution," *Journal of Mathematical Physics*, vol. 49, article 054101, 2008.
- [31] P. M. Morse and H. Feshbach, *Methods of Theoretical Physics*, p. 1407, McGraw-Hill, New York, NY, USA, 1953.
- [32] B. D. B. Figueiredo, "Generalized spheroidal wave equation and limiting cases," *Journal of Mathematical Physics*, vol. 48, article 013503, 2007.
- [33] L. J. El-Jaick and B. D. Figueiredo, "Solutions for confluent and double-confluent Heun equations," *Journal of Mathematical Physics*, vol. 49, no. 8, article 083508, 2008.
- [34] L. J. El-Jaick and B. D. Figueiredo, "A limit of the confluent Heun equation and the Schrödinger equation for an inverted potential and for an electric dipole," *Journal of Mathematical Physics*, vol. 50, no. 12, article 123511, 2009.
- [35] S. Y. Slavyanov and W. Lay, *Special Functions, A Unified Theory Based on Singularities*, Oxford University Press, 2000.
- [36] P. S. Epstein, "The Stark effect from the point of view of schrodinger's quantum theory," *Physical Review A: Atomic, Molecular and Optical Physics*, vol. 28, no. 4, pp. 695-710, 1926.
- [37] S. Y. Slavyanov, "Asymptotic Solutions of the One-dimensional Schrodinger Equation," (Leningrad University Press) (in Russian) (1991), Translation into English: S. Y. Slavyanov, *Asymptotic Solutions of the One-dimensional Schrodinger Equation* (American Mathematical Society Transactions of Math. Monographs) 151, 1996.
- [38] A. H. Wilson, "A generalised spheroidal wave equation," in *Proceedings of the Royal Society of London*, vol. A118 of also reference [37], pp. 617-635, 1928.
- [39] T. T. Truong and D. Bazzali, "Exact low-lying states of two interacting equally charged particles in a magnetic field," *Physics Letters A*, vol. 269, pp. 186-193, 2000.
- [40] A. Ralko and T. T. Truong, "Heun functions and the energy spectrum of a charged particle on a sphere under a magnetic field and Coulomb force," *Journal of Physics A: Mathematical and General*, vol. 35, no. 45, pp. 9573-9583, 2002.
- [41] B. S. Kandemir, "Two interacting electrons in a uniform magnetic field and a parabolic potential: the general closed-form solution," *Journal of Mathematical Physics*, vol. 46, no. 3, article 032110, 2005.
- [42] A. Arda, O. Aydoğdu, and R. Sever, "Scattering of the Woods-Saxon potential in the Schrödinger equation," *Journal of Physics A: Mathematical and Theoretical*, vol. 43, article 425204, 2010.

- [43] A. Arda and R. Sever, "Approximate solutions of Dirac equation with hyperbolic-type potential," *Communications in Theoretical Physics*, vol. 64, no. 3, pp. 269–273, 2015.
- [44] L. Dekar, L. Chetouani, and T. F. Hammann, "An exactly soluble Schrödinger equation with smooth position-dependent mass," *Journal of Mathematical Physics*, vol. 39, no. 5, pp. 2551–2563, 1998.
- [45] L. Dekar, L. Chetouani, and T. F. Hammann, "Wave function for smooth potential and mass step," *Physical Review A: Atomic, Molecular and Optical Physics*, vol. 59, no. 1, pp. 107–112, 1999.
- [46] A. M. Ishkhanyan, "Exact solution of the Schrödinger equation for the inverse square root potential V_0/\sqrt{x} ," *Europhysics Letters*, vol. 112, article 10006, 2015.
- [47] A. M. Ishkhanyan, "The Lambert- W step-potential – an exactly solvable confluent hypergeometric potential," *Physics Letters A*, vol. 380, no. 5–6, pp. 640–644, 2016.
- [48] A. M. Ishkhanyan, "Exact solution of the Schrödinger equation for a short-range exponential potential with inverse square root singularity," *The European Physical Journal Plus*, vol. 133, article 83, 2018.
- [49] C. A. Downing, "On a solution of the Schrodinger equation with a hyperbolic double-well potential," *Journal of Mathematical Physics*, vol. 54, no. 89, article 072101, 2013.
- [50] R. R. Hartmann and M. E. Portnoi, "Quasi-exact solution to the Dirac equation for the hyperbolic-secant potential," *Physical Review A*, vol. 89, article 012101, 2014.
- [51] C. A. Downing and M. E. Portnoi, "Massless Dirac fermions in two dimensions: Confinement in nonuniform magnetic fields," *Physical Review B*, vol. 94, article 165404, 2016.
- [52] R. R. Hartmann and M. E. Portnoi, "Two-dimensional Dirac particles in a Pöschl-Teller waveguide," *Scientific Reports*, vol. 7, no. 1, article 11599, 2017.
- [53] P. Dorey, J. Suzuki, and R. Tateo, "Finite lattice Bethe ansatz systems and the Heun equation," *Journal of Physics A: Mathematical and General*, vol. 37, no. 6, pp. 2047–2061, 2004.
- [54] A. S. Tarloyan, T. A. Ishkhanyan, and A. M. Ishkhanyan, "Four five-parametric and five four-parametric independent confluent Heun potentials for the stationary Klein-Gordon equation," *Annalen der Physik*, vol. 528, no. 3–4, pp. 264–271, 2016.
- [55] S. A. Teukolsky, "Rotating Black Holes: Separable Wave Equations for Gravitational and Electromagnetic Perturbations," *Physical Review Letters*, vol. 29, no. 16, pp. 1114–1118, 1972.
- [56] D. Batic and H. Schmid, "Heun equation, Teukolsky equation, and type-D metrics," *Journal of Mathematical Physics*, vol. 48, no. 4, article 042502, 2007.
- [57] E. W. Leaver, "An analytic representation for the quasinormal modes of Kerr black holes," *Proceedings of the Royal Society A Mathematical, Physical and Engineering Sciences*, vol. 402, no. 1823, pp. 285–298, 1985.
- [58] P. P. Fiziev, "Exact solutions of Regge-Wheeler equation and quasi-normal modes of compact objects," *Classical and Quantum Gravity*, vol. 23, no. 7, pp. 2447–2468, 2006.
- [59] D. Philipp and V. Perlick, "On analytic solutions of wave equations in regular coordinate systems on Schwarzschild background," *General Relativity and Quantum Cosmology (gr-qc)*, 2015.
- [60] D. Batic, H. Schmid, and M. Winklmeier, "The generalized Heun equation in QFT in curved spacetimes," *Journal of Physics A: Mathematical and General*, vol. 39, no. 40, pp. 12559–12564, 2006.
- [61] D. Batic and H. Schmid, "The Dirac propagator in the Kerr-Newman metric," *Progress of Theoretical and Experimental Physics*, vol. 116, no. 3, pp. 517–544, 2006.
- [62] D. Batic and M. Sandoval, "The hypergeneralized Heun equation in QFT in curved space-times," *General Relativity and Quantum Cosmology (gr-qc)*, 2008.
- [63] D. Batic, D. Mills, and M. Nowakowski, "Semicommuting and commuting operators for the Heun family," *Theoretical and Mathematical Physics*, vol. 195, no. 1, pp. 6–26, 2018.
- [64] P. P. Fiziev, "Teukolsky-Starobinsky identities: a novel derivation and generalizations," *Physical Review D: Particles, Fields, Gravitation and Cosmology*, vol. 80, no. 12, article 124001, 2009.
- [65] P. P. Fiziev, "Exact solutions of Regge-Wheeler equation," *Journal of Physics: Conference Series*, vol. 66, no. 1, article 012016, 2007.
- [66] P. P. Fiziev, "Classes of exact solutions to the Teukolsky master equation," *Classical and Quantum Gravity*, vol. 27, no. 13, article 135001, 2010.
- [67] D. R. Staicova and P. P. Fiziev, "The spectrum of electromagnetic jets from Kerr black holes and naked singularities in the Teukolsky perturbation theory," *Astrophysics and Space Science*, vol. 332, no. 2, pp. 385–401, 2011.
- [68] P. P. Fiziev, "Novel relations and new properties of confluent Heun's functions and their derivatives of arbitrary order," *Journal of Physics A: Mathematical and General*, vol. 43, no. 3, article 035203, 2010.
- [69] R. S. Borissov and P. P. Fiziev, "Exact Solutions of Teukolsky Master Equation with Continuous Spectrum," *Bulgarian Journal of Physics*, vol. 37, pp. 65–89, 2010.
- [70] P. Fiziev and D. Staicova, "Towards New Paradigms: Proceeding of the Spanish Relativity Meeting 2011," I. B. Jimenez, J. S. R. Cembranos, A. Dobado et al., Eds., vol. 1458 of *AIP Conference Proceedings*, pp. 395–398, 2011.
- [71] P. Fiziev and D. Staicova, "Application of the confluent Heun functions for finding the quasinormal modes of nonrotating black holes," *Physical Review D: Particles, Fields, Gravitation and Cosmology*, vol. 84, article 127502, 2011.
- [72] P. Fiziev, "Novel representation of the general fuchsian and heun equations and their solutions," *International frontier science letters*, vol. 7, pp. 11–24, 2016.
- [73] R. Manvelyan, H. J. W. Muller-Kirsten, J. Q. Liang, and Y. Zhang, "Absorption Cross Section of Scalar Field in Supergravity Background," *Nuclear Physics B*, vol. 579, pp. 177–208, 2000.
- [74] T. Oota and Y. Yasui, "Toric Sasaki-Einstein manifolds and Heun equations," *Nuclear Physics. B. Theoretical, Phenomenological, and Experimental High Energy Physics. Quantum Field Theory and Statistical Systems*, vol. 742, no. 1–3, pp. 275–294, 2006.
- [75] S. Musiri and G. Siopsis, "Asymptotic form of quasi-normal modes of large AdS black holes," *Physics Letters B*, vol. 576, no. 3–4, pp. 309–313, 2003.
- [76] A. Al-Badawi and I. Sakalli, "Solution of the Dirac equation in the rotating Bertotti-Robinson spacetime," *Journal of Mathematical Physics*, vol. 49, article 052501, 2008.
- [77] T. Birkandan and Hortaçsu M., "Examples of Heun and Mathieu functions as solutions of wave equations in curved spaces," *Journal of Physics A: Mathematical and General*, vol. 40, no. 5, pp. 1105–1116, 2007.
- [78] T. Birkandan and M. Hortaçsu, "Dirac equation in the background of the Nutku helicoid metric," *Journal of Mathematical Physics*, vol. 48, article 092301, 2007.

- [79] A. Malmendier, “The eigenvalue equation on the Eguchi-Hanson space,” *Journal of Mathematical Physics*, vol. 44, no. 9, pp. 4308–4343, 2003.
- [80] L. Chaos-Cador and E. Ley-Koo, “Mathieu functions revisited: matrix evaluation and generating functions,” *Revista Mexicana de Fisica*, vol. 48, no. 1, pp. 67–75, 2002.
- [81] M. Cvetič and F. Larsen, “General rotating black holes in string theory: greybody factors and event horizons,” *Physical Review D: Particles, Fields, Gravitation and Cosmology*, vol. 56, no. 8, pp. 4994–5007, 1997.
- [82] M. Cvetič and F. Larsen, “Greybody factors for rotating black holes in four dimensions,” *Nuclear Physics. B. Theoretical, Phenomenological, and Experimental High Energy Physics. Quantum Field Theory and Statistical Systems*, vol. 506, no. 1-2, pp. 107–120, 1997.
- [83] M. Cvetič and F. Larsen, “Greybody Factors and Charges in Kerr/CFT,” *Journal of High Energy Physics*, vol. 0909, article 088, 2009.
- [84] T. Birkandan and M. Cvetič, “Conformal invariance and near-extreme rotating AdS black holes,” *Physical Review D: Particles, Fields, Gravitation and Cosmology*, vol. 84, article 044018, 2011.
- [85] M. Cvetič and F. Larsen, “Conformal symmetry for general black holes,” *Journal of High Energy Physics*, vol. 1202, no. 122, 2012.
- [86] M. Cvetič and F. Larsen, “Conformal symmetry for black holes in four dimensions,” *Journal of High Energy Physics*, vol. 1209, no. 076, 2012.
- [87] M. Cvetič and F. Larsen, “Black holes with intrinsic spin,” *Journal of High Energy Physics*, vol. 1411, no. 033, 2014.
- [88] M. Cvetič and G. Gibbons, “Conformal symmetry of a black hole as a scaling limit: a black hole in an asymptotically conical box,” *Journal of High Energy Physics*, vol. 1207, 2012.
- [89] “Tolga Birkandan (Private communication).”
- [90] T. Birkandan and M. Cvetič, “Wave equation for the wu black hole,” *Journal of High Energy Physics*, vol. 1409, no. 121, p. 121, 2014.
- [91] D. D. Chow and G. Compère, “Seed for general rotating non-extremal black holes of $N = 8$ supergravity,” *Classical and Quantum Gravity*, vol. 31, article 022001, 2014.
- [92] T. Birkandan and M. Cvetič, “An analysis of the wave equation for the $U(1)_2$ gauged supergravity black hole,” *Classical and Quantum Gravity*, vol. 32, article 085007, 2015.
- [93] M. S. Cunha and H. R. Christiansen, “Confluent Heun functions in gauge theories on thick braneworlds,” *Physical Review D: Particles, Fields, Gravitation and Cosmology*, vol. 84, no. 8, article 085002, 2011.
- [94] H. R. Christiansen and M. S. Cunha, “Kalb–Ramond excitations in a thick-brane scenario with dilaton,” *The European Physical Journal C*, vol. 72, no. 1942, pp. 1203–2172, 2012.
- [95] G. Siopsis, “On quasi-normal modes and the AdS_5/CFT_4 correspondence,” *Nuclear Physics B*, vol. B715, no. 483, 2005.
- [96] L. Anguelova and P. Langfelder, “Massive gravitino propagator in maximally symmetric spaces and fermions in dS/CFT,” *Journal of High Energy Physics*, vol. 0303, no. 057, 2003.
- [97] S. R. Lau, “Rapid evaluation of radiation boundary kernels for time-domain wave propagation on black holes: Implementation and numerical tests,” *Classical and Quantum Gravity*, vol. 21, no. 4147, 2004, also *Journal of Computational Physics*, 199 (2004) 376.
- [98] H. Suzuki, E. Takasugi, and H. Umetsu, “Perturbations of Kerr-de Sitter black holes and Heun’s equations,” *Progress of Theoretical and Experimental Physics*, vol. 100, no. 3, pp. 491–505, 1998.
- [99] A. Zecca, “Solution of radial spin-1 field equation in Robertson-Walker space-time via Heun’s equation,” *Nuovo Cimento B*, vol. 125, pp. 191–199, 2010.
- [100] A. Enciso and N. Kamran, “Green’s function for the Hodge Laplacian on some classes of Riemannian and Lorentzian symmetric spaces,” *Communications in Mathematical Physics*, vol. 290, no. 1, pp. 105–127, 2009.
- [101] G. Esposito and R. Roychowdhury, “On the complete analytic structure of the massive gravitino propagator in four-dimensional de Sitter space,” *General Relativity and Gravitation*, vol. 42, no. 5, pp. 1221–1238, 2010.
- [102] S. Yoshida, N. Uchikata, and T. Futamase, “Quasinormal modes of Kerr-de Sitter black holes,” *Physical Review D: Particles, Fields, Gravitation and Cosmology*, vol. 81, article 044005, 2010.
- [103] C. Dariescu, M.-A. Dariescu, and C. Cretu, “The quantum treatment of the 5D-warped friedmann–robertson–walker universe in schrödinger picture,” *International Journal of Theoretical Physics*, vol. 52, no. 4, pp. 1345–1353, 2013.
- [104] C. Dariescu and M. A. Dariescu, “Fermions in magnetar’s crust in terms of heun double confluent functions,” *Modern Physics Letters*, vol. 27, no. 32, article 1250184, 2012.
- [105] M.-A. Dariescu and C. Dariescu, “Approximative analytic study of fermions in magnetar’s crust; ultra-relativistic plane waves, Heun and Mathieu solutions and beyond,” *Astrophysics and Space Science*, vol. 341, no. 2, pp. 429–435, 2012.
- [106] Li. Jun, Liu. Hai-Shan, H. Lu, and Z.-L. Wang, “Fermi surfaces and analytic Green’s functions for conformal gravity,” *Journal of High Energy Physics*, vol. 1302, p. 109, 2013.
- [107] H. Lu and Z.-L. Wang, “Exact Green’s function and Fermi surfaces from conformal gravity,” *Physics Letters. B. Particle Physics, Nuclear Physics and Cosmology*, vol. 718, no. 4-5, pp. 1536–1542, 2013.
- [108] D. Momeni, K. Yerzhanov, and R. Myrzakulov, “Quantized black hole and Heun function,” *Canadian Journal of Physics*, vol. 90, no. 9, pp. 877–881, 2012.
- [109] A. M. Baranov, “On an approach to constructing static ball models in general relativity,” *Gravitation & Cosmology*, vol. 18, no. 3, pp. 201–203, 2012.
- [110] H. S. Vieira, V. B. Bezerra, and C. R. Muniz, “Exact solutions of the Klein-Gordon equation in the Kerr-Newman background and Hawking radiation,” *Annals of Physics*, vol. 350, pp. 14–28, 2014.
- [111] V. B. Bezerra, H. S. Vieira, and A. Costa, “The Klein-Gordon equation in the spacetime of a charged and rotating black hole,” *Classical and Quantum Gravity*, vol. 31, no. 4, article 045003, 2014.
- [112] H. S. Vieira and V. B. Bezerra, “Quantum Newtonian cosmology and the biconfluent Heun functions,” *Journal of Mathematical Physics*, vol. 56, article 092501, 2015.
- [113] D. Staicova and P. Fiziev, “New results for electromagnetic quasinormal and quasibound modes of Kerr black holes,” *Astrophysics and Space Science*, vol. 358, no. 1, p. 10, 2015.
- [114] M. A. Dariescu and C. Dariescu, “Heun functions describing fermions evolving in parallel electric and magnetic fields,” *Chinese Physics Letters*, vol. 32, no. 7, article 071101, 2015.
- [115] C. Dariescu and M.-A. Dariescu, “Quantum analysis of $k = -1$ $k = -1$ robertson–walker universe,” *Foundations of Physics*, vol. 45, no. 11, pp. 1495–1513, 2015.

- [116] C. E. Cedeño and J. C. de Araujo, “Master equation solutions in the linear regime of characteristic formulation of general relativity,” *Physical Review D: Particles, Fields, Gravitation and Cosmology*, vol. 92, article 124015, 2015.
- [117] D. Bini, E. Bittencourt, and A. Geralico, “Massless Dirac particles in the vacuum C -metric,” *Classical and Quantum Gravity*, vol. 32, article 215010, 2015.
- [118] H. S. Vieira, V. B. Bezerra, and G. V. Silva, “Analytic solutions in the dyon black hole with a cosmic string: scalar fields, Hawking radiation and energy flux,” *Annals of Physics*, vol. 362, pp. 576–592, 2015.
- [119] D. Kofron, “Separability of test fields equations on the C -metric background,” *Physical Review D*, vol. 92, article 124064, 2015.
- [120] D. Kofron, “Separability of test fields equations on the C -metric background. II. Rotating case and the Meissner effect,” *Physical Review D*, vol. 93, article 104012, 2016.
- [121] P. Valtancoli, “Scalar field conformally coupled to a charged BTZ black hole,” *Annals of Physics*, vol. 369, pp. 161–167, 2016.
- [122] H. S. Vieira and V. B. Bezerra, “Acoustic black holes: massless scalar field analytic solutions and analogue Hawking radiation,” *General Relativity and Gravitation*, vol. 48, no. 7, article 88, 2016.
- [123] H. S. Vieira and V. B. Bezerra, “Class of solutions of the Wheeler-DeWitt equation in the Friedmann-Robertson-Walker universe,” *Physical Review D: Particles, Fields, Gravitation and Cosmology*, vol. 94, article 023511, 2016.
- [124] H. S. Vieira and V. B. Bezerra, “Confluent Heun functions and the physics of black holes: resonant frequencies, Hawking radiation and scattering of scalar waves,” *Annals of Physics*, vol. 373, pp. 28–42, 2016.
- [125] I. Sakalli, “Analytical solutions in rotating linear dilaton black holes: resonant frequencies, quantization, greybody factor, and Hawking radiation,” *Physical Review D: Particles, Fields, Gravitation and Cosmology*, vol. 94, article 084040, 2016.
- [126] G. V. Kraniotis, “The Klein-Gordon-Fock equation in the curved spacetime of the Kerr-Newman (anti) de Sitter black hole,” *Classical and Quantum Gravity*, vol. 33, article 225011, 2016.
- [127] A. Arda, C. Tezcan, and R. Sever, “Thermodynamics Quantities for the Klein-Gordon Equation with a Linear plus Inverse-linear Potential: Biconfluent Heun functions,” *PRAMANA-Journal of Physics*, vol. 88, article 39, 2017.
- [128] H. S. Vieira, “Resonant frequencies of the hydrodynamic vortex,” *International Journal of Modern Physics D*, vol. 26, no. 4, article 1750035, 2017.
- [129] H. S. Vieira, “Analytic solutions in the acoustic black hole analogue of the conical Kerr metric,” *Chinese Physics C*, vol. 41, article 043105, 2017.
- [130] H. S. Vieira, J. P. Morais Graça, and V. B. Bezerra, “Scalar resonant frequencies and Hawking effect of an $f(R)$ global monopole,” *Chinese Physics C*, vol. 41, article 095102, 2017.
- [131] C. Dariescu, M.-A. Dariescu, and C. Stelea, “The $SO(3,1) \times U(1)$ -gauge invariant approach to charged bosons in relativistic magnetars,” *General Relativity and Gravitation*, vol. 49, no. 12, p. 153, 2017.
- [132] M. A. Dariescu and C. Dariescu, “Mathieu and Heun Solutions to the Wheeler-De Witt Equation for Hyperbolic Universes,” *International Journal of Theoretical Physics*, vol. 57, no. 3, pp. 652–663, 2018.
- [133] H. Sobhani, H. Hassanabdi, and W. S. Chung, “Effects of cosmic-string framework on the thermodynamical properties of anharmonic oscillator using the ordinary statistics and the q -deformed superstatistics approaches,” *The European Physical Journal C*, vol. 78, p. 106, 2018.
- [134] D. Bouaziz and T. Birkandan, “Singular inverse square potential in coordinate space with a minimal length,” *Annals of Physics*, vol. 387, pp. 62–74, 2017.
- [135] T. Birkandan and M. Hortaçsu, “Heun-type solutions for Schwarzschild metric with electromagnetic fields,” *Europhysics Letters*, vol. 119, no. 2, article 20002, 2017.
- [136] T. Birkandan and M. Hortaçsu, “The zero mass limit of Kerr and Kerr-(anti-)de-Sitter space-times: exact solutions and wormholes,” *General Relativity and Gravitation*, vol. 50, no. 3, article 28, 2018.
- [137] G. ’t Hooft, “Computation of the quantum effects due to a four-dimensional pseudoparticle,” *Physical Review D*, vol. 14, article 3432, 1976.
- [138] T. Birkandan and M. Hortaçsu, “Quantum field theory applications of Heun type functions,” *Reports on Mathematical Physics*, vol. 79, no. 1, pp. 81–87, 2017.
- [139] M. Hortaçsu, “Heun functions and their uses in physics,” in *Proceedings of the 13th Regional Conference on Mathematical Physics*, U. Camcı and I. Semiz, Eds., pp. 23–39, World Scientific, Antalya, Turkey, October, 2010.

Research Article

Dirac Equation in the Presence of Hartmann and Ring-Shaped Oscillator Potentials

Zahra Bakhshi 

Department of Physics, Faculty of Basic Sciences, Shahed University, Tehran, Iran

Correspondence should be addressed to Zahra Bakhshi; z.bakhshi@shahed.ac.ir

Received 26 December 2017; Revised 26 April 2018; Accepted 31 May 2018; Published 18 July 2018

Academic Editor: Saber Zarrinkamar

Copyright © 2018 Zahra Bakhshi. This is an open access article distributed under the Creative Commons Attribution License, which permits unrestricted use, distribution, and reproduction in any medium, provided the original work is properly cited. The publication of this article was funded by SCOAP³.

The importance of the energy spectrum of bound states and their restrictions in quantum mechanics due to the different methods have been used for calculating and determining the limit of them. Comparison of Schrödinger-like equation obtained by Dirac equation with the nonrelativistic solvable models is the most efficient method. By this technique, the exact relativistic solutions of Dirac equation for Hartmann and Ring-Shaped Oscillator Potentials are accessible, when the scalar potential is equal to the vector potential. Using solvable nonrelativistic quantum mechanics systems as a basic model and considering the physical conditions provide the changes in the restrictions of relativistic parameters based on the nonrelativistic definitions of parameters.

1. Introduction

Since the advent of quantum mechanics, several methods have been developed in order to find the exact energy spectrum of bound states in stationary quantum systems. The knowledge of these spectrums is necessary for several applications in many fields of physics and theoretical chemistry [1–4]. Such encouraging results have arisen some studies on the potential within the frame work of common wave equations of both nonrelativistic and relativistic wave equations, that is, including Schrödinger, Duffin-Kemmer-Petiau (DKP), Klein-Gordon, or Dirac equations [5–10]. There are some noncentral separable potentials in spherical coordinates which are of considerable interest and are practical in the branches of science such as chemistry and nuclear physics. Hartmann potential introduced by Hartmann is one of the noncentral potentials, which can be realized by adding a potential proportional to Coulomb potential [11–16]. This potential was suggested to describe the energy spectrum of Ring-Shaped Potential obtained by replacing the Coulomb part of Hartmann potential with a Harmonic Oscillator term and that is called a Ring-Shaped Oscillator Potential, which is investigated to find discrete spectrum and integrals of motions [17–22]. The relativistic linear interaction, which is

called the relativistic oscillator due to the similarity with the nonrelativistic harmonic oscillator, has been subject of many successful theoretical studies. Such a space has interesting property and algebra; for example, there are some articles in which a free particle has been studied in different situations; Dirac oscillator system that is initiated by a relativistic fermion is subjected to linear vector potential [23–25]. In this article, for solving Dirac equation with Hartmann and Ring-Shaped Oscillator Potentials in three dimensions, equality of scalar and vector potentials can constitute a couple of differential equations for the spinor components [26, 27]. One of them is the second-order differential equation for the upper spinor and the lower spinor can be gotten from the first-order differential equation based on the upper spinor. Since Hartmann and Ring-Shaped Oscillator Potentials contained two radial and angular parts, the second-order differential equation is considered in the spherical polar coordinates. With separation of the second-order differential equation, there are two Schrödinger-like equations in r and θ coordinates. Moreover, the normalized solution of the polar angular part is considered as an exponential function based on φ coordinate and separating constant, because there is not any part of φ coordinate in the potential function. There exists one-dimensional solvable Schrödinger equation

in the nonrelativistic quantum mechanics for the determined potential which can be expanded to the Schrödinger-like equation and is derived from Dirac equation [28, 29]. In the radial part of differential equation, the relativistic energy spectrum can be gotten by comparison with the nonrelativistic solvable Schrödinger equation. In this comparison, the relativistic energy spectrum is obtained based on the nonrelativistic energy spectrum and the wave function of the nonrelativistic space will be considered for calculation of the relations between nonrelativistic and relativistic parameters. The mentioned method can be used on the angular part of differential equation. The relations of parameters between the two models are confirmed to the changes in the restriction of parameters. The new restriction of parameters and separating constants ensure the physical conditions. The paper is organized as follows: assuming $V(\vec{r}) = S(\vec{r})$, the couple of differential equations can be obtained for the spinor components and the second-order differential equation can be separated to the three coordinates in Section 2. The radial part of Dirac equation and the relativistic energy spectrum that is associated with the radial part have been investigated in Section 3. The angular part of Dirac equation for the potential that is related to θ coordinate according to different function of θ and the relativistic parameters have been paid attention in Section 4. Finally, in Section 5, the brief of method has been presented.

2. The General Form of Hartmann and Ring-Shaped Oscillator Potentials in Dirac Equation

The generalized Hartmann and Ring-Shaped Oscillator Potentials are defined as follows [27]:

$$V(r, \theta) = V(r) + \frac{f(\theta)}{2r^2}. \quad (1)$$

The radial part of potential can be considered as Coulomb and harmonic oscillator potentials [17, 18]:

$$\begin{aligned} V(r) &= -\frac{1}{2} \left(\frac{V_0 \lambda}{r} \right), \\ V(r) &= Kr^2, \end{aligned} \quad (2)$$

where V_0 , λ , and K are free parameters with respect to the relevant potentials. Different types of functions are assumed for the angular part of potential so that the exact solvable models can be provided from Dirac equation. In (1), θ and r are polar angular and radial in spherical coordinates of hydrogen atom.

Time-independent Dirac equation for arbitrary scalar and vector potentials is given by differential equation:

$$\begin{aligned} & \left[c\vec{\alpha} \cdot \vec{P} + \beta \left(Mc^2 + \vec{S}(\vec{r}) \right) \right] \psi(\vec{r}) \\ & = \left[\varepsilon - V(\vec{r}) \right] \psi(\vec{r}). \end{aligned} \quad (3)$$

The following parameters are defined in (3):

$$\begin{aligned} \vec{P} &= -i\hbar\vec{\nabla}, \\ \alpha &\equiv \begin{pmatrix} 0 & \vec{\sigma} \\ \vec{\sigma} & 0 \end{pmatrix}, \\ \beta &\equiv \begin{pmatrix} I & 0 \\ 0 & -I \end{pmatrix}, \end{aligned} \quad (4)$$

where $\vec{\sigma}$ and I are vector Pauli spin matrix and the identity matrix, respectively. Use the Pauli-Dirac representation as

$$\psi(\vec{r}) = \begin{pmatrix} \varphi(\vec{r}) \\ \chi(\vec{r}) \end{pmatrix}, \quad (5)$$

where $\varphi(r)$ and $\psi(r)$ are spinor components. The following set of coupled equations for the spinor components can be gotten:

$$c\vec{\sigma} \cdot \vec{P} \chi(\vec{r}) = \left[\varepsilon - V(\vec{r}) - Mc^2 - S(\vec{r}) \right] \varphi(\vec{r}), \quad (6)$$

$$c\vec{\sigma} \cdot \vec{P} \varphi(\vec{r}) = \left[\varepsilon - V(\vec{r}) + Mc^2 + S(\vec{r}) \right] \chi(\vec{r}). \quad (7)$$

Assume that $S(\vec{r}) = V(\vec{r})$ and $S(\vec{r}) = -V(\vec{r})$ due to combining (6) and (7) and provide the situations for obtaining the second-order differential equations according to one of the components so that another component can be gotten by using the first differential equation based on the determined component. Since in the case where $S(\vec{r}) = -V(\vec{r})$ the treatment of (6) and (7) is quite equivalent to the case where $S(\vec{r}) = V(\vec{r})$, the case where $S(\vec{r}) = V(\vec{r})$ is considered and then the results of that case will be expanded to the second case [26, 27].

The state $S(\vec{r}) = V(\vec{r})$ allows making two differential equations for each component:

$$\chi(\vec{r}) = \left[\frac{c\vec{\sigma} \cdot \vec{P}}{\varepsilon + Mc^2} \right] \varphi(\vec{r}), \quad (8)$$

$$\begin{aligned} & \left[c^2 \vec{P}^2 + 2(\varepsilon + Mc^2)V(\vec{r}) \right] \varphi(\vec{r}) \\ & = \left[\varepsilon^2 - M^2 c^4 \right] \varphi(\vec{r}). \end{aligned} \quad (9)$$

Schrödinger-like equation is obtained for the component $\varphi(\vec{r})$ by considering the definitions of \vec{P} and $V(\vec{r})$ in (9):

$$\begin{aligned} & \left[-\hbar^2 c^2 \vec{\nabla}^2 - (\varepsilon + Mc^2) \left(\frac{V_0 \lambda}{r} - \frac{f(\theta)}{r^2} \right) \right] \varphi(\vec{r}) \\ & = \left[\varepsilon^2 - M^2 c^4 \right] \varphi(\vec{r}). \end{aligned} \quad (10)$$

Assuming a solution as

$$\varphi(\vec{r}) = \frac{1}{r} u(r) \Theta(\theta) \Phi(\varphi), \quad (11)$$

(10) can be separated to three differential equations in the three dimensions φ , r , and θ :

$$\frac{1}{\Phi} \frac{d^2 \Phi}{d\varphi^2} = -m^2, \quad (12)$$

$$-\frac{d^2 u(r)}{dr^2} + \left[\frac{\rho}{r^2} + 2 \frac{(\varepsilon + Mc^2)}{\hbar^2 c^2} V(r) \right] u(r) = \frac{(\varepsilon^2 - M^2 c^4)}{\hbar^2 c^2} u(r), \quad (13)$$

$$\frac{1}{\sin \theta} \frac{d}{d\theta} \left(\sin \theta \frac{d\Theta(\theta)}{d\theta} \right) - \left[\frac{m^2}{\sin^2 \theta} + (\varepsilon + M^2 c^4) f(\theta) - s \right] \Theta(\theta) = 0, \quad (14)$$

where m and ρ/r^2 are separation factors.

The normalized solution of (12) which satisfies the boundary conditions becomes

$$\Phi(\varphi) = -\frac{1}{\sqrt{2\pi}} e^{im\varphi}, \quad m = 0, \pm 1, \pm 2, \dots \quad (15)$$

3. The Radial Part Solutions of Dirac Equation

In this section, radial part of wave function (13) will be analyzed by corresponding to Generalized Laguerre differential equation. Coulomb and harmonic oscillator potentials are two potentials that are considered in (13), respectively. For these potentials, (13) can be converted to Generalized Laguerre differential equation with exact solution of Generalized Laguerre polynomials. In the first case, substituting the radial part of potential as Coulomb potential in (13) [26, 27],

$$\frac{d^2 u(r)}{dr^2} + \left[\frac{(\varepsilon^2 - M^2 c^4)}{\hbar^2 c^2} - \frac{\rho}{r^2} + \left(\frac{\varepsilon + Mc^2}{\hbar^2 c^2} \right) \frac{V_0 \lambda}{r} \right] u(r) = 0, \quad (16)$$

and considering units system ($\hbar = 2m = 1$), (16) can be compared to the following nonrelativistic solvable model [28, 29]:

$$\frac{d^2 u_{n,l}(r)}{dr^2} + (E - V(r)) u_{n,l}(r) = 0. \quad (17)$$

Indeed, comparing radial Schrödinger-like equation to nonrelativistic Schrödinger equation according to Coulomb potential with exact solution based on Generalized Laguerre polynomials, the results of nonrelativistic equation can be expanded to relativistic models. Nonrelativistic model for Coulomb potential has the following form:

$$\frac{d^2 u(r)}{dr^2} + \left[-\frac{e^4}{4(n+l+1)} - \frac{l(l+1)}{r^2} + \frac{e^2}{r} \right] u(r) = 0. \quad (18)$$

Therefore, relativistic parameters can be connected to nonrelativistic parameters as follows:

$$\rho = l(l+1), \quad (19)$$

$$\left(\frac{\varepsilon + Mc^2}{c^2} \right) V_0 \lambda = e^2, \quad (20)$$

$$\frac{\varepsilon^2 - M^2 c^4}{c^2} = -\frac{e^4}{4(n+l+1)^2}. \quad (21)$$

Since $e^2 c^2 / 4(n+l+1)^2 > 0$, relation of parameters (20) causes the condition $|\varepsilon| < M^2 c^2$. Relativistic energy can be calculated based on defined parameters in nonrelativistic solvable model by Combining above relations of parameters. Assuming that $\tau = V_0 \lambda / 2c(n+l+1)$, relativistic energy can be obtained as follows [26, 27]:

$$\varepsilon = Mc^2 \frac{1 - \tau^2}{1 + \tau^2}. \quad (22)$$

In nonrelativistic model, the exact solution is considered for (17) as [28, 29]

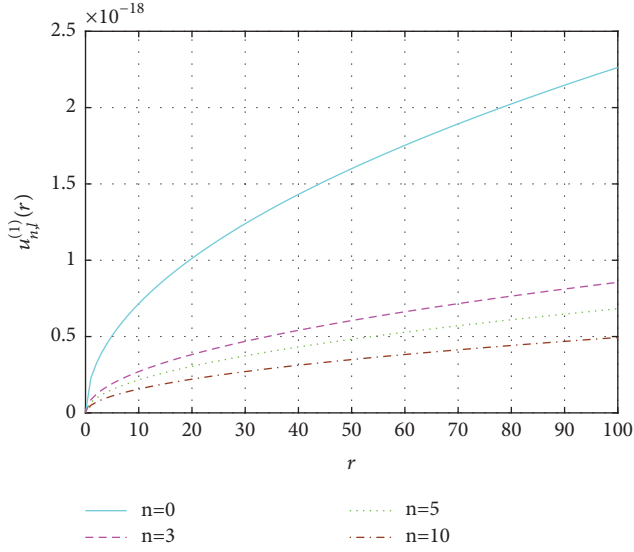
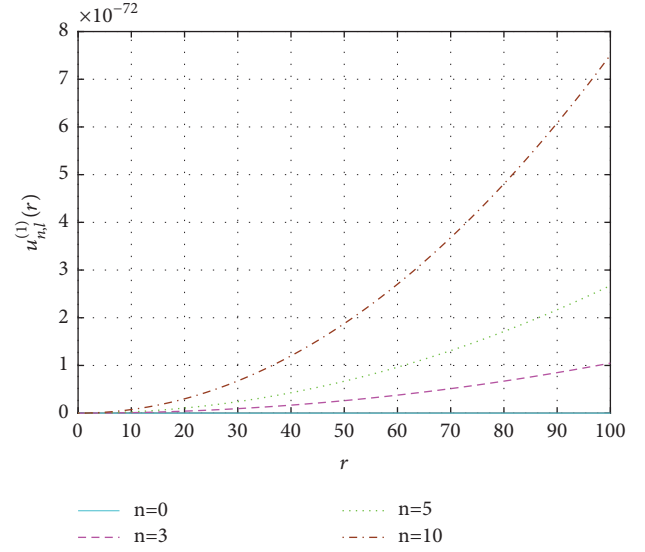
$$u_{n,l}(r) = f(r) F(g(r)), \quad (23)$$

where $F(g(r))$ is a special function based on the internal function $g(r)$. Generalized Laguerre polynomials are orthogonal polynomials that are satisfied in (18). Therefore, that function can be expanded to Schrödinger-like equation (16) of radial part. Since $\alpha > -1$ in Generalized Laguerre polynomials $L_n^\alpha(g(r))$ and $\alpha = 2l+1$ in nonrelativistic model, condition of $l > -1$ is satisfied in Generalized Laguerre polynomials. Therefore, according to relation of $\alpha = 2l+1$ in relativistic model, $\rho < 0$ and $\rho > 0$ are considered for $-1 < l < 0$ and $l > 0$, respectively. In the last angular part section, it will be shown that relativistic energy is calculated based on nonrelativistic energy and term of $\rho + 1/4$. Since the sign of nonrelativistic energy term is cleared, determining term of $\rho + 1/4$ is very important because of the condition $|\varepsilon| < M^2 c^2$. The term of $\rho + 1/4$ should be signed for defined different l parameter. According to parametric relation of $\rho = l(l+1)$, $\rho + 1/4$ will be positive for each l that is defined in the problem. It means that the sign of term $\rho = l(l+1)$ separated the limit of l parameter. The ρ relativistic parameter will be restricted by $\rho \geq 0$ for $l > 0$ and $-1/4 \leq \rho \leq 0$ for $-1 < l < 0$. Since there is term of $n+l+1$ in energy spectrum and for $n = l+1$ singularity happens in the wave function, in Generalized Laguerre polynomials related to differential equation (16), parameter n is transformed to $n-l-1$. Thus energy spectrum will be restricted and the problem of singularity will disappear. If the following nonnormalized wave function is associated with differential equation (18) for internal function $g(r) = ((e^2/(n+l+1))r)$ [28, 29]:

$$u_{n,l}(r) \propto g^{(l+1)} \exp\left(-\frac{g}{2}\right) L_n^{2l+1}(g(r)), \quad (24)$$

the radial wave function is considered to differential equation (16) as follows:

$$u_{n,l}^{(1)}(r) \propto (2kr)^{l+1} \exp(-kr) L_{n-l-1}^{2l+1}(2kr), \quad (25)$$

FIGURE 1: $u_{n,l}^{(1)}(r)$ versus r with $l = -0.5$.FIGURE 2: $u_{n,l}^{(1)}(r)$ versus r with $l = 1$.

where $k = e^2/2(n+l+1)$ and $0 < r < +\infty$. The wave function that is satisfied in Schrödinger-like equation must be physically acceptable. Physical wave functions are satisfied in the usual square-integrability condition as $\int_{x_1}^{x_2} |\Psi_n(x)|^2 dx < \infty$ for energy bound state to ensure Hermiticity of Hamiltonian in Hilbert space spanned by its eigenfunctions. Since this integral must be finite, the wave functions have a constant value or zero at the endpoints of definition interval of \vec{V} potential. Therefore, solutions of Schrödinger-like equation should be checked at the endpoints of $[x_1, x_2]$ interval, therefore providing square-integrability condition and investigating physical situations in the wave functions. It is seen that wave function (25) is a square-integrability function at the endpoints of $[0, +\infty]$ interval, so that $u_{n,l}(r) \rightarrow 0$ when $r \rightarrow 0$ and $r \rightarrow +\infty$ for the range $l > 0$ and $-1 < l < 0$. Thus it will be physically acceptable wave function in restriction of l parameter. $u_{n,l}^{(1)}(r)$ wave function in restriction of l parameter for $l = -0.5$ and $l = 1$ based on r is displaced in Figures 1 and 2.

In the second case, the following differential equation is obtained from (13) for harmonic oscillator as radial part of potential:

$$\frac{d^2 u(r)}{dr^2} + \left[\frac{(\varepsilon^2 - M^2 c^4)}{\hbar^2 c^2} - \frac{\rho}{r^2} - \left(\frac{\varepsilon + M c^2}{\hbar^2 c^2} \right) (2kr^2) \right] u(r) = 0, \quad (26)$$

where $k > 0$. Nonrelativistic solvable model based on (17) which can be compared to (26) has the following form ($\hbar = 2m = 1$) [28, 29]:

$$\frac{d^2 u(r)}{dr^2} + \left[2n\omega + \left(l + \frac{3}{2} \right) \omega - \frac{l(l+1)}{r^2} - \frac{1}{4} \omega^2 r^2 \right] u(r) = 0, \quad (27)$$

where $\omega > 0$. The relations of parameters between (26) and (27) are as follows:

$$\rho = l(l+1), \quad (28)$$

$$\frac{2k(\varepsilon + M c^2)}{c^2} = \frac{1}{4} \omega^2, \quad (29)$$

$$\frac{\varepsilon^2 - M^2 c^4}{c^2} = 2n\omega + \left(l + \frac{3}{2} \right) \omega. \quad (30)$$

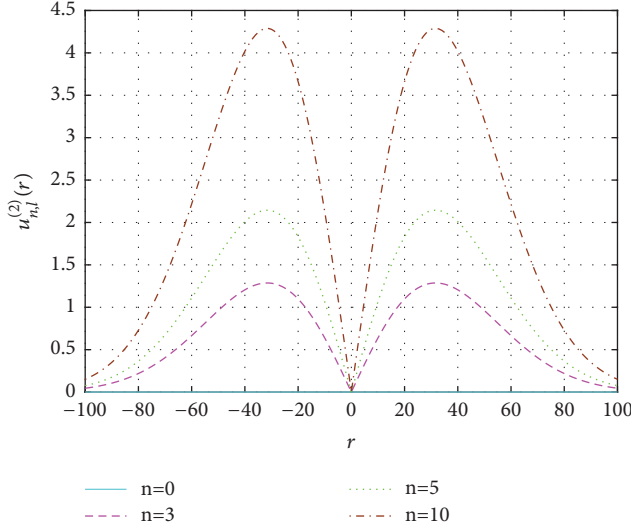
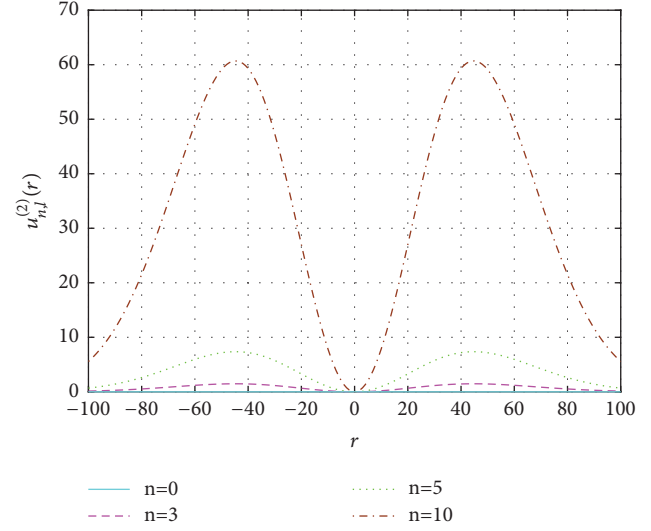
Since $L_n^\alpha(g(r))$ Generalized Laguerre polynomials for $\alpha > -1$ are related to (27) as an exact solution and α parameter is defined as $\alpha = l + 1/2$, l parameter will be restricted by $l > -3/2$. The relations of parameters (28) and (30) emphasize the conditions of $\rho + 1/4 \geq 0$ and $|\varepsilon| < M c^2$. Relativistic energy that is related to nonrelativistic energy for harmonic oscillator can be gotten by combining relations (29) and (30) as follows:

$$(\varepsilon - M c^2)^2 (\varepsilon + M c^2) = 8k c^2 \left(2n + l + \frac{3}{2} \right), \quad (31)$$

where (31) is a third-order equation of ε . In nonrelativistic solvable model, the wave function that is associated with (27) is [28, 29]

$$u_{n,l}(r) \propto g^{(l+1)/2} \exp\left(-\frac{g}{2}\right) L_n^{(l+1/2)}(g(r)), \quad (32)$$

where $g(r) = (1/2)\omega r^2$. By comparing two nonrelativistic and relativistic models, the wave function (32) can be expanded


 FIGURE 3: $u_{n,l}^{(2)}(r)$ versus r with $l = 0$ and $\omega = 10^{-3}$.

 FIGURE 4: $u_{n,l}^{(2)}(r)$ versus r with $l = 1$ and $\omega = 10^{-3}$.

to (26). Therefore, radial part of spinor wave function can be corresponded to (26) as follows:

$$u_{n,l}^{(2)}(r) \propto \left(\frac{1}{2}\omega r^2\right)^{(l+1)/2} \exp\left(-\frac{1}{4}\omega r^2\right) L_n^{(l+1/2)}\left(\frac{1}{2}\omega r^2\right), \quad (33)$$

where $-\infty < r < +\infty$. In the investigation of square-integrability condition, it is obvious that wave function (33) is limited as $u_{n,l}(r) \rightarrow 0$ when $r \rightarrow -\infty$ and $r \rightarrow +\infty$ in restriction of l parameter that has been introduced as $l > -3/2$. $u_{n,l}^{(2)}(r)$ wave function for $\omega = 10^{-3}$ and in restriction of l parameter for $l = 0$ and $l = 1$ is indicated in Figures 3 and 4.

4. The Angular Part Solutions of Dirac Equation

As mentioned before, for Hartmann and Ring-Shaped Oscillator Potentials, angular part of Dirac equation is [26, 27]

$$\frac{1}{\sin\theta} \frac{d}{d\theta} \left(\sin\theta \frac{d\Theta(\theta)}{d\theta} \right) - \left[\frac{m^2}{\sin^2\theta} + (\varepsilon + M^2 c^4) f(\theta) - s \right] \Theta(\theta) = 0. \quad (34)$$

Assuming that $\Theta(\theta) = H(\theta)/\sin^{1/2}\theta$, first-order differential term can be vanished from differential equation (34). This transformation can provide the condition that Schrödinger-like equation is accessible from (34). Considering the mentioned transformation, (34) can be converted to

$$\frac{d^2 H(\theta)}{d\theta^2} + \left[-\frac{(m^2 - 1/4)}{\sin^2\theta} - (\varepsilon + Mc^2) f(\theta) + \rho + \frac{1}{4} \right] H(\theta) = 0. \quad (35)$$

In comparing (35) with the following Schrödinger solvable equation ($\hbar = 2m = 1$) [28, 29],

$$\frac{d^2 H(x)}{dx^2} + [E - V(x)] H(x) = 0, \quad (36)$$

(35) will be solvable according to different types of $f(\theta)$. It means that the solution of (36) for nonrelativistic energy spectrum and different potentials will be expanded to Schrödinger-like equation obtained from Dirac equation. In this comparison, relativistic parameters can be connected to nonrelativistic parameters. Furthermore, it should be mentioned that this method is useable for special functions of $f(\theta)$. Therefore, $f(\theta)$ functions that can be solved in these techniques are as follows [26, 27]:

$$f_1(\theta) = \frac{\gamma + \beta \cos\theta + \alpha \cos^2\theta}{\sin^2\theta}, \quad (37)$$

$$f_2(\theta) = \frac{\gamma + \beta \cos^2\theta + \alpha \cos^4\theta}{\sin^2\theta \cos^2\theta}, \quad (38)$$

$$f_3(\theta) = \gamma + \beta \cot\theta + \alpha \cot^2\theta, \quad (39)$$

where α , β , and γ are arbitrary constant values. In other words, above functions are solvable functions that are considered as Hartmann and Ring-Shaped Oscillator Potentials. If $f_1(\theta)$ is substituted in (35) as

$$\frac{d^2 H(\theta)}{d\theta^2} + \left\{ \left[\left(-m^2 + \frac{1}{4} \right) - \eta(\gamma + \alpha) \right] \csc^2 \theta - \eta\beta \csc \theta \cot \theta + \eta\alpha + \rho + \frac{1}{4} \right\} H(\theta) = 0, \quad (40)$$

where $\eta = \varepsilon + Mc^2$, (40) can be compared to the following Schrödinger equation ($\hbar = 2m = 1$) [28, 29]:

$$\frac{d^2 H(x)}{dx^2} + \left[-(\lambda^2 + s^2 - s) \csc^2 x + \lambda(2s - 1) \csc x \cot x + (s + n)^2 \right] H(x) = 0. \quad (41)$$

The relations of parameters between nonrelativistic solvable model and relativistic model will be obtained by comparing between (40) and (41) as

$$\eta\alpha + \rho + \frac{1}{4} = (s + n)^2, \quad (42)$$

$$\eta(\gamma + \alpha) + m^2 - \frac{1}{4} = \lambda^2 + s^2 - s, \quad (43)$$

$$\eta\beta = -\lambda(2s - 1). \quad (44)$$

The wave function that is related to (40) is written based on Jacobi polynomials $P_n^{(\mu, \nu)}(g(x))$, where $\mu > -1$, $\nu > -1$, and $n = 0, 1, 2, \dots$ According to parameter definitions of $\mu = -\lambda + s - 1/2$ and $\nu = \lambda + s - 1/2$ in Jacobi polynomials, restrictions of s and λ parameters will be as $s > -1/2$ and $-(s + 1/2) < \lambda < (s + 1/2)$.

The relation between nonrelativistic energy and relativistic energy according to (42) causes ρ separation constant to be calculated as $\rho = (s + n)^2 - \alpha(\varepsilon + Mc^2) - 1/4$, so that condition of $\rho + 1/4 \geq 0$ causes

$$\varepsilon \leq \frac{1}{\alpha} (s + n)^2 - Mc^2. \quad (45)$$

Positive values may be provided for relativistic energy, if $\alpha > 0$. Nonnormalized wave function that is associated with the solvable differential equation (41) is [28, 29]

$$H(x) = (1 - g)^{(s-\lambda)/2} (1 + g)^{(s+\lambda)/2} \cdot P_n^{(-\lambda+s-1/2, \lambda+s-1/2)}(g(x)), \quad (46)$$

where $g(x) = \cos x$. Considering function (46), the wave function is obtained for differential equation (40) as follows:

$$H(\theta) = (1 - \cos \theta)^{(s-\lambda)/2} (1 + \cos \theta)^{(s+\lambda)/2} \cdot P_n^{(-\lambda+s-1/2, \lambda+s-1/2)}(\cos \theta). \quad (47)$$

According to $\Theta(\theta) = H(\theta)/\sin^{1/2} \theta$, angular part of Dirac equation is gotten as

$$\Theta^{(1)}(\theta) = 2^{s-1} (\sin \theta)^{s-\lambda-1/2} (\cos \theta)^{s+\lambda-1/4} \cdot P_n^{(-\lambda+s-1/2, \lambda+s-1/2)}(\cos \theta), \quad (48)$$

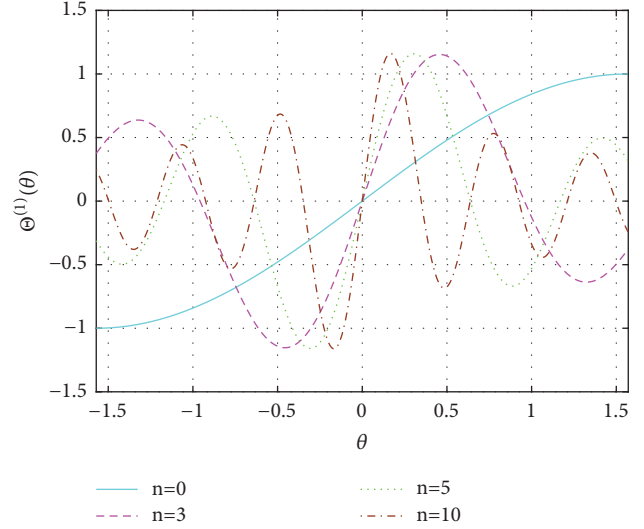


FIGURE 5: $\Theta^{(2)}(\theta)$ versus θ with $s = 1$ and $\lambda = -0.5$.

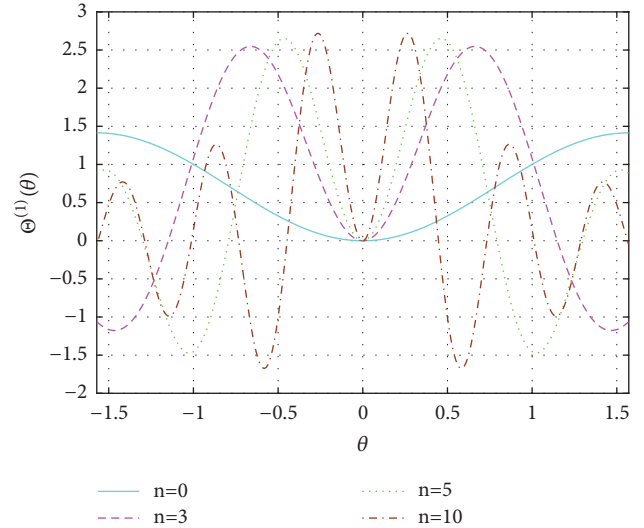


FIGURE 6: $\Theta^{(1)}(\theta)$ versus θ with $s = 1.5$ and $\lambda = -1$.

where $-\pi/2 \leq \theta \leq \pi/2$. Wave function (48) will be zero, if θ variable is limited to the endpoints of interval; it means that when $\theta \rightarrow \mp\pi/2$, the wave function is restricted as $\Theta(\theta) \rightarrow 0$, although establishing of mentioned physical situations and also avoiding divergence of wave function (48) at $\theta = 0$ will cause restriction of λ and s parameters changing to $-(s+1/4) < \lambda < (s-1/2)$ for $s > 3/8$. $\Theta^{(1)}(\theta)$ wave function based on θ is depicted in restriction of λ and s parameters for $\lambda = -0.5$ and $s = 1$ in Figure 5 and $\lambda = -1$ and $s = 1.5$ in Figure 6.

The illustrated technique can be expanded to other functions of θ . For $f_2(\theta)$ function, angular part of Dirac equation has the following form:

$$\frac{d^2 H(\theta)}{d\theta^2} + \left\{ \left[\left(-m^2 + \frac{1}{4} \right) - \eta(\gamma + \beta + \alpha) \right] \csc^2 \theta - \eta\gamma \sec^2 \theta + \eta\alpha + \rho + \frac{1}{4} \right\} H(\theta) = 0. \quad (49)$$

Perfect differential solvable equation ($\hbar = 2m = 1$) that can be used for this method is [28, 29]

$$\frac{d^2 H(x)}{dx^2} + \left[-\lambda(\lambda - 1) \csc^2 x - s(s - 1) \sec^2 x + (\lambda + s + 2n)^2 \right] H(x) = 0. \quad (50)$$

The following parameter relations are made by comparison between (49) and (50):

$$\eta\alpha + \rho + \frac{1}{4} = (\lambda + s + 2n)^2, \quad (51)$$

$$\eta(\gamma + \beta + \alpha) + m^2 - \frac{1}{4} = \lambda(\lambda - 1), \quad (52)$$

$$\eta\gamma = s(s - 1). \quad (53)$$

Since Jacobi polynomials $P_n^{(\mu, \nu)}$ are associated with (50) for $\mu > -1$ and $\nu > -1$, λ and s will be restricted by $\lambda > -1/2$ and $s > -1/2$. Relation (51) confirms ρ parameter as $\rho = (\lambda + s + 2n)^2 - \eta\alpha - 1/4$ which can connect relativistic energy to perfect nonrelativistic parameters. The condition of $\rho + 1/4 \geq 0$ creates the following range of relativistic energy spectrum:

$$\varepsilon \leq \frac{1}{\alpha} (\lambda + s + 2n)^2 - Mc^2. \quad (54)$$

If α parameter is considered as $\alpha > 0$, positive values may be gotten for relativistic energy spectrum.

Nonnormalized wave function that is satisfied in differential equation (50) for $g(x) = \cos(2x)$ is [28, 29]

$$H(x) = (1 - g)^{\lambda/2} (1 + g)^{s/2} P_n^{(\lambda-1/2, s-1/2)}(g(x)). \quad (55)$$

Function (55) can be expanded to differential equation (49) and considered as the exact solution of differential equation. The mentioned solution based on Jacobi polynomials is considered as

$$H(\theta) = (1 - \cos 2\theta)^{\lambda/2} (1 + \cos 2\theta)^{s/2} \cdot P_n^{(\lambda-1/2, s-1/2)}(\cos 2\theta), \quad (56)$$

so that angular part solution of Dirac equation can be constituted as

$$\Theta^{(2)}(\theta) = 2^{(\lambda+s)/2} (\sin \theta)^{\lambda-1/2} (\cos \theta)^s P_n^{(\lambda-1/2, s-1/2)}(\cos 2\theta), \quad (57)$$

where $-\pi/4 \leq \theta \leq \pi/4$. Wave function (57) will be always constant value at the endpoints of defined interval for θ variable, but divergence of the wave function at $\theta = 0$ converts the restriction of λ parameter to $\lambda > 1/2$. Therefore, wave function (57) will be physical solution, if s and λ parameters are considered as $s > -1/2$ and $\lambda > 1/2$. In restriction $\lambda = 0.6$ and $s = -0.2$ and also $\lambda = 0.55$ and $s = 1$; $\Theta^{(2)}(\theta)$ wave function is performed in Figures 7 and 8, respectively.

Another function of $f_3(\theta)$ can be also analyzed by this method because there is a nonrelativistic solvable model that

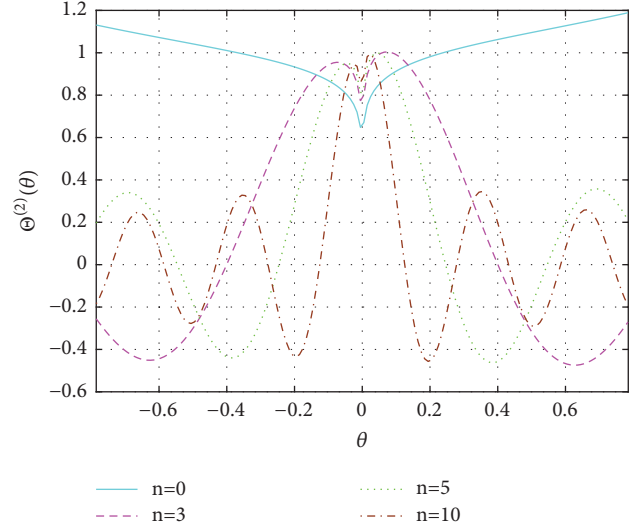


FIGURE 7: $\Theta^{(2)}(\theta)$ versus θ with $s = -0.2$ and $\lambda = 0.6$.

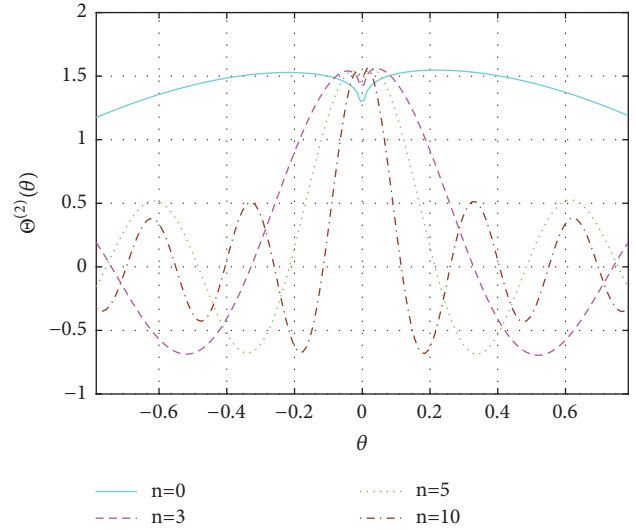


FIGURE 8: $\Theta^{(2)}(\theta)$ versus θ with $s = 1$ and $\lambda = 0.55$.

can correspond to this function as angular part solution of Dirac equation. Angular part of Dirac equation with $f_3(\theta)$ according to (35) is

$$\frac{d^2 H(\theta)}{d\theta^2} + \left\{ \left[\left(-m^2 + \frac{1}{4} \right) - \eta\alpha \right] \csc^2 \theta - \eta\beta \cot \theta - \eta(\gamma - \alpha) + \rho + \frac{1}{4} \right\} H(\theta) = 0. \quad (58)$$

For corresponding to nonrelativistic solvable model, the following Schrödinger equation ($\hbar = 2m = 1$) is considered [28, 29]:

$$\frac{d^2 H(x)}{dx^2} + \left[-s(s + 1) \csc^2 x + 2\lambda \cot \theta + (s - n)^2 - \frac{\lambda^2}{(s - n)^2} \right] H(x) = 0. \quad (59)$$

The relativistic parameters in (58) connected to the nonrelativistic parameters in (59) are as follows:

$$\eta(\gamma - \alpha) - \left(\rho + \frac{1}{4}\right) = \frac{\lambda^2}{(s-n)^2} - (s-n)^2, \quad (60)$$

$$\eta\alpha + m^2 - \frac{1}{4} = s(s+1), \quad (61)$$

$$\eta\beta = -2\lambda. \quad (62)$$

In the assumed solvable model, the limits of s and λ parameters are considered as $s > n-1$ and $-i(s-n)(s-n+1) < \lambda < i(s-n)(s-n+1)$. By using relation (60) ρ separation constant can be obtained as $\rho = \eta(\gamma - \alpha) + (s-n)^2 - \lambda^2/(s-n)^2 - 1/4$. The range of relativistic energy will be of the following form, if the condition $\rho + 1/4 \geq 0$ is considered:

$$\varepsilon \leq \left(\frac{1}{\alpha - \gamma}\right) \left[(s-n)^2 - \frac{\lambda^2}{(s-n)^2} \right] - Mc^2. \quad (63)$$

If $\alpha > \gamma$ is considered, it will be possible to calculate positive value for relativistic energy spectrum. The following nonnormalized wave function that is associated with Jacobi polynomials in the solvable model (59), for $g(x) = -i \cot x$, is [28, 29]

$$H(x) = (g^2 - 1)^{(s-n)/2} \cdot \exp\left(\frac{\lambda}{s-n}x\right) P_n^{(s-n+i(\lambda/(s-n)), s-n-i(\lambda/(s-n)))}(g(x)). \quad (64)$$

The above nonnormalized function based on Jacobi polynomials can be applied for differential equation (58) as follows:

$$H(\theta) = (-1)^{(s-n)/2} (\csc \theta)^{s-n} \exp\left(\frac{\lambda}{s-n}\theta\right) \cdot P_n^{(s-n+i(\lambda/(s-n)), s-n-i(\lambda/(s-n)))}(-i \cot \theta). \quad (65)$$

Finally, angular part solution of Dirac equation which was called $\Theta(\theta)$ is gotten as

$$\Theta^{(3)}(\theta) = (-1)^{(s-n)/2} (\csc \theta)^{s-n+1/2} \exp\left(\frac{\lambda}{s-n}\theta\right) \cdot P_n^{(s-n+i(\lambda/(s-n)), s-n-i(\lambda/(s-n)))}(-i \cot \theta), \quad (66)$$

where $0 \leq \theta \leq \pi$. Restriction of s parameter will be $s < n-1/2$, if the boundary situations are considered for wave function (66) in the endpoints of interval as $\theta \rightarrow 0$ and $\theta \rightarrow \pi$ with no divergence at $\theta = \pi/2$. Therefore, wave function (66) is physically acceptable by providing the range of s and λ parameters as $n-1 < s < n-1/2$ and $-i(s-n)(s-n+1) < \lambda < i(s-n)(s-n+1)$. $\Theta^{(3)}(\theta)$ wave function in restriction $\lambda = 0.1i$ and $s = 9.5$ and also $\lambda = 1i$ and $s = 9.5$ is displayed in Figures 9 and 10.

5. Conclusion

The energy spectrum of bound states and spinor wave function of Dirac equation for Hartmann and Ring-Shaped

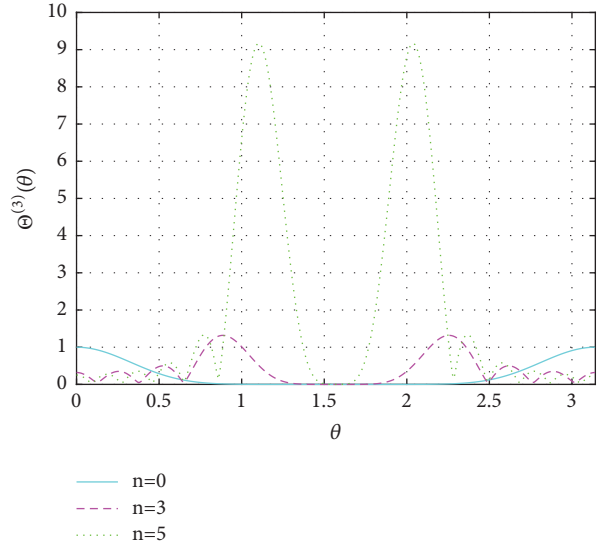


FIGURE 9: $\Theta^{(3)}(\theta)$ versus θ with $s = 9.5$ and $\lambda = 0.1i$.

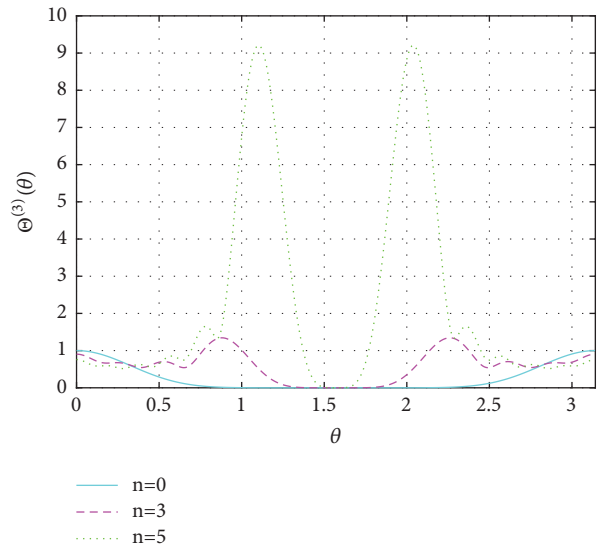


FIGURE 10: $\Theta^{(3)}(\theta)$ versus θ with $s = 9.5$ and $\lambda = 1i$.

Oscillator Potentials have been calculated by comparing the mentioned relativistic models with nonrelativistic systems. In radial and angular parts of Dirac equation, relativistic parameters and their restrictions have been investigated by considering the solutions of nonrelativistic models related to the problem and restrictions of nonrelativistic parameters. By this method, spinor wave functions are associated with orthogonal polynomials such as Generalized Laguerre polynomials and Jacobi polynomials in radial and angular parts of Dirac equation, respectively.

Conflicts of Interest

The author declares that she has no conflicts of interest.

References

- [1] B. Bentag and L. Chetouani, "Path integral treatment of a noncentral potential," *Czechoslovak Journal of Physics*, vol. 50, no. 5, pp. 593–606, 2000.
- [2] Z. Q. Ma and B. W. Xu, "Quantum correction in exact quantization rules," *EPL (Europhysics Letters)*, vol. 69, p. 685, 2005.
- [3] S.-A. Yahiaoui and M. Bentaiba, "A group-theoretical method for Natanzon potentials in position-dependent mass background by means of conformal mappings," *International Journal of Theoretical Physics*, vol. 48, no. 2, pp. 315–322, 2009.
- [4] A. Gharbi and A. Bouda, "Energy spectra of Hartmann and ring-shaped oscillator potentials using the quantum Hamilton–Jacobi formalism," *Physica Scripta*, vol. 88, Article ID 045007, 2013.
- [5] H. Hassanabadi, B. H. Yazarloo, S. Zarrinkamar, and A. A. Rajabi, "Duffin-Kemmer-Petiau equation under a scalar Coulomb interaction," *Physical Review C*, vol. 84, Article ID 064003, 2011.
- [6] B. H. Yazarloo, H. Hassanabadi, and S. Zarrinkamar, "Oscillator strengths based on the Möbius square potential under Schrödinger equation," *The European Physical Journal Plus*, vol. 127, p. 51, 2012.
- [7] G. F. Wei and S. H. Dong, "Algebraic approach to pseudospin symmetry for the Dirac equation with scalar and vector modified Pöschl-Teller potentials," *EPL (Europhysics Letters)*, vol. 87, Article ID 40004, 2009.
- [8] S. Zarrinkamar, A. A. Rajabi, B. H. Yazarloo, and H. Hassanabadi, "Quasi-Analytical Solutions of DKP Equation under the Deng-Fan Interaction," *Advances in High Energy Physics*, vol. 2012, 13 pages, 2012.
- [9] S.-H. Dong, "Exact solutions of the two-dimensional Schrödinger equation with certain central potentials," *International Journal of Theoretical Physics*, vol. 39, no. 4, pp. 1119–1128, 2000.
- [10] H. Hassanabadi, A. N. Ikot, and S. Zarrinkamar, "Exact Solution of Klein-Gordon with the Pöschl-Teller Double-Ring-Shaped Coulomb Potential," *Acta Physica Polonica A*, vol. 126, p. 647, 2014.
- [11] H. Hartmann, "Die Bewegung eines Körpers in einem ringförmigen Potentialfeld," *Theoretical Chemistry Accounts*, vol. 24, no. 2-3, pp. 201–206, 1972.
- [12] A. Hautot, "Exact motion in noncentral electric fields," *Journal of Mathematical Physics*, vol. 14, 1973.
- [13] M. Kibler and P. Winternitz, "Dynamical invariance algebra of the Hartmann potential," *Journal of Physics A: Mathematical and General*, vol. 20, no. 13, pp. 4097–4108, 1987.
- [14] M. Kibler and P. Winternitz, "Periodicity and quasi-periodicity for super-integrable Hamiltonian systems," *Physics Letters A*, vol. 147, no. 7, pp. 338–342, 1990.
- [15] M. Kibler, G. H. Lamot, and P. Winternitz, "Classical trajectories for two ring-shaped potentials," *International Journal of Quantum Chemistry*, vol. 43, p. 625, 1992.
- [16] M. Hamzavi, H. Hassanabadi, and A. A. Rajabi, "Exact solutions of dirac equation with hartmann potential by nikiforov–uvarov method," *International Journal of Modern Physics E*, vol. 19, p. 2189, 2010.
- [17] S. W. Qian, B. W. Huang, D. Y. Wang, and Z. Y. Gu, "Supersymmetry and shape invariance of Hartmann potential and ring-shaped oscillator potential in the r and theta dimensions of spherical polar coordinates," *Communications in Theoretical Physics*, vol. 38, p. 139, 2002.
- [18] C. Berkdemir, "A novel angle-dependent potential and its exact solution," *Journal of Mathematical Chemistry*, vol. 46, no. 1, pp. 139–154, 2009.
- [19] C. Quesne, "A new ring-shaped potential and its dynamical invariance algebra," *Journal of Physics A: Mathematical and General*, vol. 21, no. 14, pp. 3093–3101, 1988.
- [20] S. H. Dong, C. Y. Chen, and M. Lozada-Cassou, "Quantum properties of complete solutions for a new noncentral ring-shaped potential," *International Journal of Quantum Chemistry*, vol. 105, p. 453, 2005.
- [21] C.-Y. Chen and S.-H. Dong, "Exactly complete solutions of the Coulomb potential plus a new ring-shaped potential," *Physics Letters A*, vol. 335, no. 5-6, pp. 374–382, 2005.
- [22] A. D. Alhaidari, "Scattering and bound states for a class of non-central potentials," *Journal of Physics A: Mathematical and General*, vol. 38, no. 15, pp. 3409–3429, 2005.
- [23] Q. H. Liu, L. H. Tang, and D. M. Xun, "Geometric momentum: The proper momentum for a free particle on a two-dimensional sphere," *Physical Review A: Atomic, Molecular and Optical Physics*, vol. 84, no. 4, 2011.
- [24] N. Candemir and O. Bayrak, "Massive Dirac equation in asymmetric Hulthén potential," *Journal of Mathematical Physics*, vol. 54, no. 4, Article ID 042104, 2013.
- [25] Z. Sh. Zhang, Sh. F. Xiao, and D. M. Xun, "An enlarged canonical quantization scheme and quantization of a free particle on two-dimensional sphere," *Communications in Theoretical Physics*, vol. 63, p. 19, 2015.
- [26] G. Chen, "Solution of the Klein-Gordon for exponential scalar and vector potentials," *Physics Letters A*, vol. 339, no. 3-5, pp. 300–303, 2005.
- [27] A. de Souza Dutra and M. Hott, "Dirac equation exact solutions for generalized asymmetrical Hartmann potentials," *Physics Letters A*, vol. 356, no. 3, pp. 215–219, 2006.
- [28] G. Levai, "A search for the shape-invariant solvable potentials," *Journal of Physics A: Mathematical and General*, vol. 22, no. 6, pp. 689–702, 1989.
- [29] H. Panahi and Z. Bakhshi, "Solvable potentials with position-dependent effective mass and constant mass schrödinger equation," *Acta Physica Polonica B*, vol. 41, p. 11, 2010.

Research Article

Heavy-Light Mesons in the Nonrelativistic Quark Model Using Laplace Transformation Method

M. Abu-Shady ¹ and E. M. Khokha²

¹Department of Applied Mathematics, Faculty of Science, Menoufia University, Shebeen El-Kom, Egypt

²Department of Basic Science, Modern Academy of Engineering and Technology, Cairo, Egypt

Correspondence should be addressed to M. Abu-Shady; dr.abushady@gmail.com

Received 8 March 2018; Revised 15 May 2018; Accepted 3 June 2018; Published 12 July 2018

Academic Editor: Chun-Sheng Jia

Copyright © 2018 M. Abu-Shady and E. M. Khokha. This is an open access article distributed under the Creative Commons Attribution License, which permits unrestricted use, distribution, and reproduction in any medium, provided the original work is properly cited. The publication of this article was funded by SCOAP³.

An analytic solution of the N -dimensional radial Schrödinger equation with the combination of vector and scalar potentials via the Laplace transformation method (LTM) is derived. The current potential is extended to encompass the spin hyperfine, spin-orbit, and tensor interactions. The energy eigenvalues and the corresponding eigenfunctions have been obtained in the N -dimensional space. The present results are employed to study the different properties of the heavy-light mesons (HLM). The masses of the scalar, vector, pseudoscalar, and pseudovector for B , B_s , D , and D_s mesons have been calculated in the three-dimensional space. The effect of the dimensional number space is discussed on the masses of the HLM. We observed that the meson mass increases with increasing dimensional space. The decay constants of the pseudoscalar and vector mesons have been computed. In addition, the leptonic decay widths and branching ratio for the B^+ , D^+ , and B_s^+ mesons have been studied. Therefore, the used method with the current potential gives good results which are in good agreement with experimental data and are improved in comparison with recent theoretical studies.

1. Introduction

One of the most important tasks in nonrelativistic quantum mechanics is to get the solution of the Schrödinger equation. The solution of the Schrödinger equation with spherically symmetric potentials plays a significant role in many fields of physics such as hadronic spectroscopy for understanding the quantum chromodynamics theory. Numerous works have been introduced to get the solution of Schrödinger equation using different methods like the operator algebraic method [1], path integral method [2], the conventional series solution method [3, 4], Fourier transform [5, 6], shifted $(1/N)$ expansion [7, 8], point canonical transformation [9], quasi-linearization method [10], supersymmetric quantum mechanics (SUSQM) [11], Hill determinant method (HDM) [12], and other numerical methods [13–15].

Recently, the study of the different topics has received a great attention from theoretical physicists in the higher dimensional space. In addition, the study is more general and one can obtain the required results in the lower

dimensions directly, such as the hydrogen atom [16–18], harmonic oscillator [19, 20], random walks [21], Casimir effects [22], and the quantization of angular momentum [23–27]. The N -dimensional Schrödinger equation has been studied with different forms of spherically symmetric potentials [28–33]. The N -dimensional Schrödinger equation has been investigated with the Cornell potential and extended Cornell potential [34–38] using different methods such as the Nikiforov-Uvarov (NU) method [32, 36, 39, 40], power series technique (PST) [41], the asymptotic iteration method (AIM) [34], Pekeris type approximation (PTA) [41, 42], and the analytical exact iteration method (AEIM) [43, 44].

The LTM is one of the useful methods that contributed to finding the exact solution of Schrödinger equation in one-dimensional space for Morse potential [45, 46], the harmonic oscillator [47], and three-dimensional space with pseudo-harmonic and Mie-type potentials [48] and with noncentral potential [49]. The N -dimensional Schrödinger equation has been solved via the LTM in many studies for Coulomb potential [28], harmonic oscillator [50], Morse potential

[51], pseudoharmonic potential [52], Mie-type potential [53], anharmonic oscillator [54], and generalized Cornell potential [38].

The study of different properties of HLM is very vital for understanding the structure of hadrons and dynamics of heavy quarks. Thus, many theoretical and experimental efforts have been done for understanding distinct characteristics of HLM. In [4, 34, 55], the authors calculated the mass spectra of quarkonium systems as charmonium and bottomonium mesons with the quark-antiquark interaction potential using various methods in many works. Al-Jamel and Widyan [56] studied the spin-averaged mass spectra of heavy quarkonia with Coulomb plus quadratic potential using (NU) method. Abou-Salem [57] has computed the masses and leptonic decay widths of $c\bar{c}$, $b\bar{b}$, $c\bar{s}$, $b\bar{s}$, $b\bar{u}$, and $c\bar{b}$ numerically using Jacobi method. The strong decays, spectroscopy, and radiative transition of heavy-light hadrons have been computed using the quark model predictions [58]. The decay constant of HLM has been calculated using the field correlation method [59]. Moreover, the spectroscopy of HLM has been investigated in the framework of the QCD relativistic quark model [60]. The spectroscopy and Regge trajectories of HLM have been obtained using quasi-potential approach [61]. The decay constants of heavy-light vector mesons [62] and heavy-light pseudoscalar mesons [63] have been calculated with QCD sum rules. A comparative study has been introduced for the mass spectrum and decay properties for the D meson with the quark-antiquark potential using hydrogeometric and Gaussian wave function [64]. In framework of Dirac formalism the mass spectra of D_s [65] and D [66] mesons have been obtained using Martin-light potential in which the hadronic and leptonic decays of D and D_s mesons have been evaluated [67]; besides the rare decays of B^0 and B_s^0 mesons into dimuon ($\mu^+\mu^-$) [68] and the decay constants of B and B_s have been calculated [69]. The mass spectra and decay constants for ground state of pseudoscalar and vector mesons have been obtained using the variational analysis in the light quark model [70]. The spectroscopy of bottomonium and B meson has been studied using the free-form smearing in [71]. The variational method has been employed to compute the masses and decay constants of HLM in [72]. In addition, the decay properties of D and D_s mesons have been investigated using the quark-antiquark potential in [73]. The B and B_s mesons spectra and their decays have been studied with a Coulomb plus exponential type potential in [74]. The leptonic and semileptonic decays of B meson into τ have been studied [75]. The degeneracy of HLM with the same orbital angular momentum has been broken with the spin-orbit interactions [76]. The relativistic quark model has been investigated to study the properties of B and B_s mesons [77] and the excited charm and charm-strange mesons [78]. The perturbation method has been employed to determine the mass spectrum and decay properties of HLM with the mixture of harmonic and Yukawa-type potentials [79]. In [80], the authors have investigated the leptonic decays of seven types of heavy vector and pseudoscalar mesons. The spectra and wave functions of HLM have been calculated within a relativistic quark model by using the

Foldy-Wouthuysen transformation [81]. The isospin breaking of heavy meson decay constants had been compared with lattice QCD from QCD sum rules [82]. The decay constants of pseudoscalar and vector B and D mesons have been studied in the light-cone quark model with the variational method [83]. In [84], the authors have calculated the strong decays of newly observed D_J (3000) and D_{sJ} (3040) with two $2P$ (1^+) quantum number assignments. The leptonic ($D \rightarrow e^+\nu_e$) and semileptonic ($D \rightarrow K^{(*)}\ell^+\nu_\ell$, $D \rightarrow \pi\ell^+\nu_\ell$) decays have been analyzed using the covariant quark model with infrared confinement within the standard model framework [85]. The weak decays of B , B_s , and B_c into D -wave heavy-light mesons have been studied using Bethe-Salpeter equation [86]. In [87], the decay constant and distribution amplitude for the heavy-light pseudoscalar mesons have been evaluated using the light-front holographic wavefunction. By using the Gaussian wave function with quark-antiquark potential model, the Regge trajectories, spectroscopy, and decay properties have been studied for B and B_s mesons [88], D and D_s mesons [89], and also the radiative transitions and the mixing parameters of the D -meson have been obtained [90]. The dimensional space dependence of the masses of heavy-light mesons has been investigated using the string inspired potential model [91].

The goal of this work is to get the analytic solution of the N -dimensional Schrödinger equation for the mixture of vector and scalar potentials including the spin-spin, spin-orbit, and tensor interactions using LTM in order to obtain the energy eigenvalues in the N -dimensional space and the corresponding eigenfunctions. So far no attempt has been made to solve the N -dimensional Schrödinger equation using the LTM when the spin hyperfine, spin-orbit, and tensor interactions are included. To show the importance of present results, the present results are employed to calculate the mass spectra of the HLM in three-dimensional space and in the higher dimensional space. In addition, the decay constants, leptonic decay widths, and branching fractions of the HLM are calculated.

The paper is systemized as follows: the contributions of previous works are displayed in Section 1. In Section 2, a brief summary of Laplace transformation method is introduced. In Section 3, an analytic solution of the N -dimensional Schrödinger equation is derived. In Section 4, the obtained results are discussed. In Section 5, summary and conclusion are presented.

2. Overview of Laplace Transformation Method

The Laplace transform $\phi(z)$ or \mathcal{L} of a function $f(t)$ is defined by [92]

$$\phi(z) = \mathcal{L}\{f(t)\} = \int_0^\infty e^{-zt} f(t) dt. \quad (1)$$

If there is some constant $\sigma \in \mathbb{R}$ such that $|e^{-\sigma t} f(t)| \leq M$ for sufficiently large t , the integral in (1) exists for $\text{Re } z > \sigma$ for $z > 0$. The Laplace transform may fail to exist because of a

sufficiently strong singularity in the function $f(t)$ as $t \rightarrow 0$. In particular

$$\mathcal{L} \left[\frac{t^\alpha}{\Gamma(\alpha+1)} \right] = \frac{1}{z^{\alpha+1}}, \quad \alpha > -1, \quad (2)$$

where Γ is the gamma function. The Laplace transform has the derivative properties

$$\mathcal{L} \{ f^{(n)}(t) \} = z^n \mathcal{L} \{ f(t) \} - \sum_{k=0}^{n-1} z^{n-1-k} f^{(k)}(0), \quad (3)$$

$$\mathcal{L} \{ t^n f(t) \} = (-1)^n \phi^{(n)}(z), \quad (4)$$

where the superscript (n) stands for the n -th derivative with respect to t for $f^{(n)}(t)$ and with respect to z for $\phi^{(n)}(z)$. If z_0 is the singular point, the Laplace transform behaves near $z \rightarrow z_0$ as

$$\phi(z) = \frac{1}{(z-z_0)^v}, \quad (5)$$

and then for $t \rightarrow \infty$

$$f(t) = \frac{1}{\Gamma(v)} t^{v-1} e^{z_0 t}. \quad (6)$$

On the other hand, if near origin $f(t)$ behaves like t^α with $\alpha > -1$, then $\phi(z)$ behaves near $z \rightarrow \infty$ as

$$\phi(z) = \frac{\Gamma(\alpha+1)}{z^{\alpha+1}}. \quad (7)$$

3. Analytic Solution of the N -Dimensional Radial Schrödinger Equation

The N -dimensional radial Schrödinger equation that describes the interaction between quark-antiquark systems takes the form [41]

$$\left[\frac{d^2}{dr^2} + \frac{(N-1)}{r} \frac{d}{dr} - \frac{\ell(\ell+N-2)}{r^2} + 2\mu(E - V_{q\bar{q}}(r)) \right] \Psi(r) = 0, \quad (8)$$

where ℓ, N represent the angular quantum number and the dimensional number greater than one, respectively, and $\mu = m_q m_{\bar{q}} / (m_q + m_{\bar{q}})$ is the reduced mass of the quark-antiquark system.

In the nonrelativistic quark model, the quark-antiquark potential $V_{q\bar{q}}(r)$ consists of the spin independent potential $V(r)$ and the spin dependent potential $V_{SD}(r)$, respectively:

$$V_{q\bar{q}}(r) = V(r) + V_{SD}(r). \quad (9)$$

The spin independent potential is taken as a combination of vector and scalar parts [93]:

$$V(r) = V_V(r) + V_S(r), \quad (10)$$

$$V_V(r) = \eta(ar^2 + br) - \frac{c}{r}, \quad (11)$$

$$V_S(r) = (1-\eta)(ar^2 + br), \quad (12)$$

where $V_V(r)$ and $V_S(r)$ are the vector and scalar parts, respectively, and η stands for the mixing coefficient. a, b , and c are arbitrary parameters where a, b , and $c > 0$ which are fitted with experimental data. The harmonic and linear terms represent the confining part at long distance and the Coulomb term stands for the quark-antiquark interactions through one gluon exchange at short distances which gives better description of quark-antiquark interaction.

The spin dependent potential is extended to three types of interaction terms as [94]

$$V_{SD}(r) = V_{LS}(r)(\mathbf{L} \cdot \mathbf{S}) + \mathbf{S}_{12} V_T(r) + V_{SS}(r)(\mathbf{S}_1 \cdot \mathbf{S}_2), \quad (13)$$

while the spin-orbit $V_{LS}(r)$ and tensor $V_T(r)$ terms give the fine structure of the states, the spin-spin $V_{SS}(r)$ interaction term describes the hyperfine splitting of the state, and \mathbf{L} is an angular quantum operator, and \mathbf{S} is a spin operator (for detail, see [94]).

$$V_{LS}(r) = \frac{1}{2m_q m_{\bar{q}} r} \left(3 \frac{dV_V}{dr} - \frac{dV_S}{dr} \right), \quad (14)$$

$$V_T(r) = \frac{1}{12m_q m_{\bar{q}}} \left(\frac{1}{r} \frac{dV_V}{dr} - \frac{d^2 V_V}{dr^2} \right), \quad (15)$$

$$V_{SS}(r) = \frac{2}{3m_q m_{\bar{q}}} \nabla^2 V_V, \quad (16)$$

where ∇^2 is radial Laplace operator.

$$\mathbf{S}_1 \cdot \mathbf{S}_2 = \frac{1}{2} \left[S(S+1) - \frac{3}{2} \right], \quad (17)$$

$$\langle \mathbf{L} \cdot \mathbf{S} \rangle = \frac{1}{2} [J(J+1) - L(L+1) - S(S+1)], \quad (18)$$

$$\mathbf{S}_{12} = 2 \left[\mathbf{S}^2 - 3(\mathbf{S} \cdot \hat{\mathbf{r}})(\mathbf{S} \cdot \hat{\mathbf{r}}) \right]. \quad (19)$$

The diagonal elements of the \mathbf{S}_{12} are defined.

$$\langle \mathbf{S}_{12} \rangle = \frac{4}{(2L+3)(2L-1)} \left[\langle S^2 \rangle \langle L^2 \rangle - 3(\mathbf{L} \cdot \mathbf{S})^2 - \frac{3}{2} \langle \mathbf{L} \cdot \mathbf{S} \rangle \right]. \quad (20)$$

Substituting (11)-(16) into (9) then the nonrelativistic quark-antiquark potential $V_{q\bar{q}}(r)$ takes the form

$$V_{q\bar{q}}(r) = ar^2 + br + \delta + \frac{g}{r} + \frac{h}{r^3}, \quad (21)$$

where

$$\delta = \frac{2a}{m_q m_{\bar{q}}} \left[2\eta(\mathbf{S}_1 \cdot \mathbf{S}_2) + \left(2\eta - \frac{1}{2} \right) (\mathbf{L} \cdot \mathbf{S}) \right], \quad (22)$$

$$g = \frac{b}{m_q m_{\bar{q}}} \left\{ \eta \left[\frac{4}{3} (\mathbf{S}_1 \cdot \mathbf{S}_2) + \frac{1}{12} \mathbf{S}_{12} \right] + \left(2\eta - \frac{1}{2} \right) (\mathbf{L} \cdot \mathbf{S}) \right\} - c, \quad (23)$$

$$h = \frac{3c}{2m_q m_{\bar{q}}} \left[\frac{1}{6} \mathbf{S}_{12} + (\mathbf{L} \cdot \mathbf{S}) \right]. \quad (24)$$

Substituting (21) into (8), then

$$\left[\frac{d^2}{dr^2} + \frac{(N-1)}{r} \frac{d}{dr} - \frac{\ell(\ell+N-2)}{r^2} + \varepsilon - Ar^2 - Br - 2\mu\delta - \frac{G}{r} - \frac{H}{r^3} \right] \Psi(r) = 0, \quad (25)$$

where

$$\begin{aligned} \varepsilon &= 2\mu E, \\ A &= 2\mu a, \\ B &= 2\mu b, \\ G &= 2\mu g, \\ H &= 2\mu h. \end{aligned} \quad (26)$$

The complete solution of (25) takes the form

$$\Psi(r) = r^k e^{-\alpha r^2} f(r), \quad k > 0, \quad \text{with } \alpha = \sqrt{\frac{\mu a}{2}}, \quad (27)$$

where the term r^k confirms that the solution is bounded at $r = 0$. The function $f(r)$ is yet to be determined. From (27) we get

$$\Psi'(r) = r^k e^{-\alpha r^2} \left[f'(r) + \left(\frac{k}{r} - 2\alpha r \right) f(r) \right]. \quad (28)$$

$$\begin{aligned} \Psi''(r) &= r^k e^{-\alpha r^2} \left\{ f''(r) + \left(\frac{2k}{r} - 4\alpha r \right) f'(r) \right. \\ &\quad \left. + \left[\frac{k(k-1)}{r^2} + 4\alpha^2 r^2 - 4\alpha k - 2\alpha \right] f(r) \right\}. \end{aligned} \quad (29)$$

Substituting (27), (28), and (29) into (25), then,

$$\begin{aligned} r f''(r) + (\omega - 4\alpha r^2) f'(r) \\ + \left\{ \frac{\lambda}{r} - Br^2 + \zeta r - G - \frac{H}{r^2} \right\} f(r) = 0, \end{aligned} \quad (30)$$

where

$$\omega = 2k + N - 1, \quad (31)$$

$$\lambda = k(k + N - 2) - \ell(\ell + N - 2), \quad (32)$$

$$\zeta = \varepsilon - 4\alpha k - 2\alpha N - 2\mu\delta. \quad (33)$$

In order to apply the Laplace transform of the above differential equation, the parametric condition is taken as in [52, 54].

$$k(k + N - 2) - \ell(\ell + N - 2) = 0. \quad (34)$$

Thus, (32) has a solution

$$\begin{aligned} k_+ &= \ell, \\ \text{and } k_- &= -(\ell + N - 2). \end{aligned} \quad (35)$$

We take the physical solution of (32) ($k = k_+ = \ell$) as in [52, 54].

Substituting (34) into (30) yields

$$\begin{aligned} r f''(r) + (\omega - 4\alpha r^2) f'(r) \\ + \left\{ \zeta r - Br^2 - G - \frac{H}{r^2} \right\} f(r) = 0. \end{aligned} \quad (36)$$

By expanding the term H/r^2 around $y = 0$, where $y = r - v$ and v is a parameter as in [36, 56], we get

$$\frac{H}{r^2} = \frac{H}{(y+v)^2} = \frac{H}{v^4} (3r^2 - 8rv + 6v^2). \quad (37)$$

Substituting (37) into (36) yields

$$\begin{aligned} r f''(r) + (\omega - 4\alpha r^2) f'(r) + \{Qr - Pr^2 - C_0\} f(r) \\ = 0, \end{aligned} \quad (38)$$

where

$$\begin{aligned} Q &= \zeta + \frac{8H}{v^3}, \\ P &= B + \frac{3H}{v^4}, \end{aligned} \quad (39)$$

$$\text{and } C_0 = G + \frac{6H}{v^2}.$$

The Laplace transform is defined as $\phi(z) = \mathcal{L}\{f(r)\}$ and taking boundary condition $f(0) = 0$ yields

$$\begin{aligned} (z + \tau) \frac{d^2 \phi(z)}{dz^2} + \left(\frac{z^2}{4\alpha} + \rho \right) \frac{d\phi(z)}{dz} \\ + \left(\gamma z + \frac{C_0}{4\alpha} \right) \phi(z) = 0. \end{aligned} \quad (40)$$

Here

$$\begin{aligned} \tau &= \frac{P}{4\alpha}, \\ \rho &= \frac{Q}{4\alpha} + 2, \\ \gamma &= \frac{(2 - \omega)}{4\alpha}. \end{aligned} \quad (41)$$

The singular point of (40) is $z = -\tau$. By using the condition of (5), the solution of (40) takes the form

$$\phi(z) = \frac{C}{(z + \tau)^{n+1}}, \quad n = 0, 1, 2, 3, \dots \quad (42)$$

From (42),

$$\phi'(z) = \frac{-C(n+1)}{(z + \tau)^{n+2}}, \quad (43)$$

$$\phi''(z) = \frac{C(n+1)(n+2)}{(z + \tau)^{n+3}}. \quad (44)$$

Substituting (42)-(44) into (40), we obtain the following relations:

$$\gamma = \frac{n+1}{4\alpha}, \quad (45)$$

$$\gamma\tau + \frac{C_0}{4\alpha} = 0, \quad (46)$$

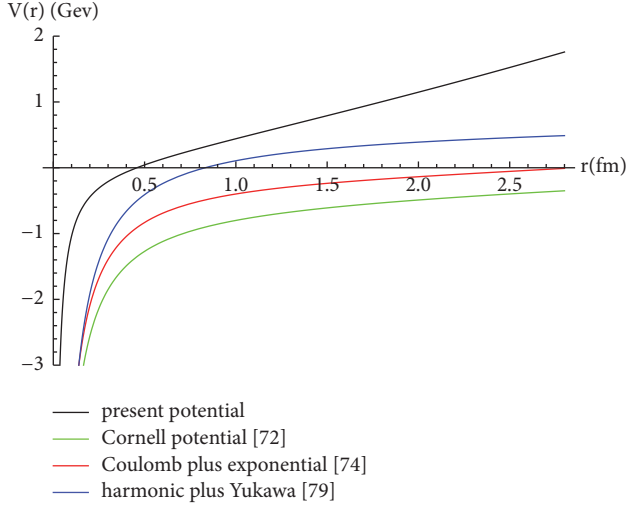


FIGURE 1: The current potential and other potential models are plotted as functions of distance r .

$$(n+1)(n+2) - \rho(n+1) + \frac{C_0\tau}{4\alpha} = 0. \quad (47)$$

Using (26), (39), and (41) and the set of (45)-(47), then, the energy eigenvalue of (8) in the N -dimensional space is given by the relation

$$E_{n\ell N} = \sqrt{\frac{a}{2\mu}} (2n + 2\ell + N) - \frac{b^2}{4a} + \delta - \frac{8h}{v^3} - \frac{h}{a} \left(\frac{9h}{4v^8} + \frac{3b}{2v^4} \right). \quad (48)$$

Take the inverse Laplace transform such that $f(r) = \mathcal{L}^{-1}\{\phi(z)\}$. The function $f(r)$ takes the following form:

$$f(r) = \frac{C}{\Gamma(n+1)} r^n e^{-\tau r}. \quad (49)$$

Using (11), (13), and (23), the eigenfunctions of (9) take the following form:

$$\Psi(r) = \frac{C}{\Gamma(n+1)} r^{n+\ell} \exp\left(-\sqrt{\frac{\mu a}{2}} r^2 - \sqrt{\frac{\mu}{2a}} br\right). \quad (50)$$

From the condition $\int_0^\infty |\Psi(r)|^2 r^{N-1} dr = 1$, the normalization constant C can be computed. In addition, the wave equation $\Psi(r)$ satisfies the boundary condition $\Psi(r=0) = \Psi(r=\infty) = 0$.

4. Discussion of Results

In Figure 1, the current potential has been plotted in comparison to other potential models; we see that the present potential is in a qualitative agreement with other potential models [72, 74, 79], in which the confining part is clearly obtained in comparison to Cornell and Coulomb plus exponential potentials. The different states of B and D mesons

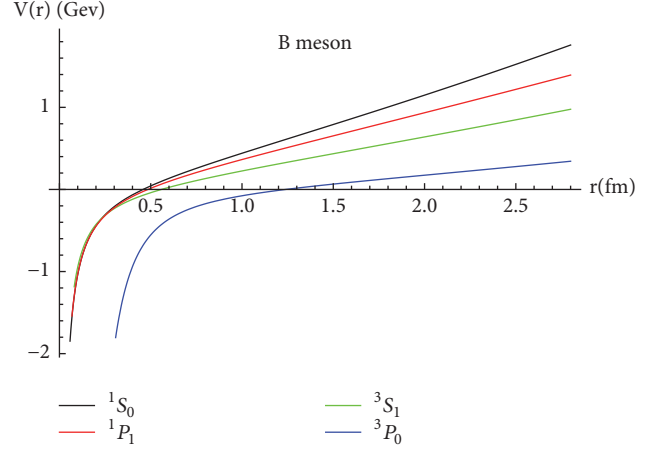


FIGURE 2: The current potential of B meson for different states.

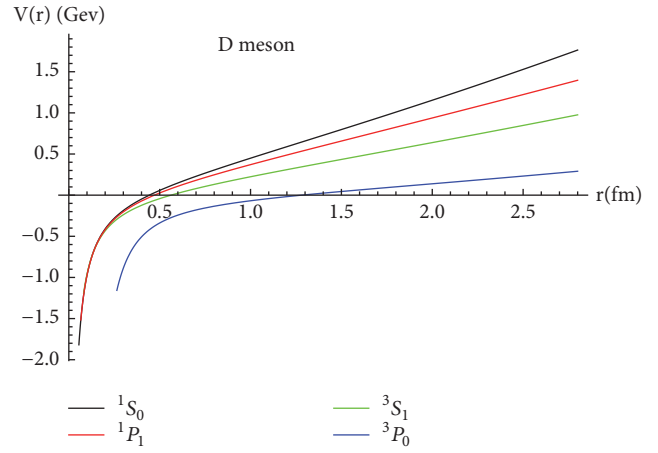


FIGURE 3: The current potential of D meson for different states.

have been shown in Figures 2 and 3, respectively, in which the principal number of states plays an important role in confining part of potential.

In the following subsections, we employ the obtained results in the previous section to determine the mass spectra of scalar, vector, pseudoscalar, and pseudovector of B , B_s , D , and D_s mesons in the N -dimensional space in comparison with the experimental data (PDG 2016) [95] and with other recent studies. In addition, the decay properties such as decay constants, leptonic decay width, and the branching ratio of HLM are calculated.

4.1. Mass Spectra of Heavy-Light Mesons. The masses of HLM in the N -dimensional space are defined [44]:

$$M_{B,D} = m_q + m_{\bar{q}} + E_{n\ell N}. \quad (51)$$

Substituting (48) into (51), then the mass spectra of HLM in the N -dimensional space can be found from the relation

$$M_{B,D} = m_q + m_{\bar{q}} + \sqrt{\frac{a}{2\mu}} (2n + 2\ell + N) - \frac{b^2}{4a} + \delta$$

TABLE 1: Parameters for HLM.

m_c	m_b	$m_{u,d}$	m_s	η	v
1.45 (GeV)	4.87 (GeV)	0.38 (GeV)	0.48 (GeV)	0.25	1 (GeV ⁻¹)

TABLE 2: Masses for pseudoscalar ($^{2S+1}L_J = {}^1S_0$) mesons in GeV. $a = 0.00085$ GeV³, $b = 0.01614$ GeV², and $c = 0.7$.

Meson	Present Work	Exp. [95]	[72]	[81]	[96]	[88, 89]	[73, 74]	N=4	N=5
D	1.864	1.864	1.895	1.871	1.859	1.884 [89]	1.864 [73]	1.902	1.939
D_s	1.960	1.968	1.962	1.964	1.949	1.965 [89]	1.978 [73]	1.989	2.023
B	5.277	5.280	5.302	5.273	5.262	5.287 [88]	5.272 [74]	5.311	5.346
B_s	5.366	5.366	5.340	5.363	5.337	5.367 [88]	5.385 [74]	5.397	5.428

TABLE 3: Masses for vector ($^{2S+1}L_J = {}^3S_1$) mesons in GeV. $a = 0.026068$ GeV³, $b = 0.218058$ GeV², and $c = 8 \times 10^{-3}$.

Meson	Present Work	Exp. [95]	[72]	[81]	[96]	[88, 89]	[73, 74]	N=4	N=5
D	2.010	2.010	2.023	2.008	2.026	2.010 [89]	2.010 [73]	2.218	2.426
D_s	2.100	2.112	2.057	2.107	2.110	2.120 [89]	2.102 [73]	2.244	2.434
B	5.374	5.325	5.356	5.329	5.330	5.323 [88]	5.327 [74]	5.567	5.759
B_s	5.415	5.415	5.384	5.419	5.405	5.413 [88]	5.409 [74]	5.588	5.760

TABLE 4: Masses for scalar ($^{2S+1}L_J = {}^3P_0$) mesons in GeV. $a = 0043$ GeV³, $b = 0.001$ GeV², and $c = 10^{-3}$.

Meson	Present Work	Exp. [95]	[72]	[81]	[96]	[88, 89]	[73, 74]	N=4	N=5
D	2.289	2.318±0.029	2.316	2.364	2.357	2.357[89]	2.539[73]	2.374	2.459
D_s	2.350	2.318	2.372	2.437	2.412	2.438[89]	2.311[73]	2.427	2.505
B	5.700	5.710	5.657	5.776	5.740	5.730[88]	5.745[74]	5.736	5.815
B_s	5.720	---	5.719	5.811	5.776	5.812[88]	5.843[74]	5.785	5.856

$$-\frac{8h}{v^3} - \frac{h}{a} \left(\frac{9h}{4v^8} + \frac{3b}{2v^4} \right). \quad (52)$$

In Tables 2–6, we have calculated the masses of the HLM in the three-dimensional space in comparison with the experimental data and other recent studies [72–74, 81, 88, 89, 96]. The parameters used in the present calculations are shown in Table 1. In addition, the masses at $N = 4$ and $N = 5$ are calculated. In Tables 2 and 3, we observe that D and B_s meson masses close to experimental data and other meson masses are in good agreement with experimental data and become better in comparison to the results in recent studies [72–74, 81, 88, 89, 96]. In comparison with [72], they used the variational method for the Cornell potential to study the HLM with including the spin-spin and spin-orbit interactions. They ignored the tensor interactions in their calculations. The present results are good in comparison to the results in [72]. In addition, we used the LTM in the present calculations. Yazarloo and Mehriban used the variational method to study D and D_s mesons for the Cornell potential [73] and used the Nikiforov-Uvarov (NU) method to study B and B_s mesons for the Coulomb plus exponential type potential [74]. The present results are in good agreement with the results of [73, 74]. Kher et al. [89] used a Gaussian wave function to calculate the mass spectra of D and D_s in addition to B and B_s mesons [88] for the Cornell potential. Jing-Bin [81, 96] obtained the spectra of the HLM in the relativistic

model from the Bethe-Salpeter equation using the Foldy-Wouthuysen transformation in his works.

We note that the present results for D and B_s meson masses become better in comparison to the results of [81, 88, 89, 96], where the values of pseudoscalar D and B_s mesons are close to the experimental data in Table 2. The values of vector D and B_s mesons close to the experimental data and the values of vector D_s and B mesons are good in comparison to the experimental results in Table 3.

The masses of the scalar mesons are presented in Table 4; the value of D meson is close to the experimental value. The values of D_s and B are in agreement with the experimental values and the value of B_s meson is in good agreement with the theoretical studies [72–74, 81, 88, 89, 96]. In Table 5, we observe that all the values of pseudovector mesons are close to the experimental results except the value of B meson which is in good agreement with the experimental value. The values of vector D_s and B mesons are in good agreement with the experimental results. In Table 6, the results of the p-wave state for the HLM are reported.

The present predictions of D , D_s , B , and B_s mesons are in agreement in comparison to the experimental data and the theoretical studies [73, 74, 81, 88, 89, 96].

In addition, we have investigated the masses of the HLM in the higher dimensions at $N=4$ and $N=5$. In Tables 2–6, the effect of the dimensional number is investigated on the masses of the HLM. One can see that the masses increase with increasing dimensional number. The influence of the

TABLE 5: Masses for pseudovector ($^{2S+1}L_J = ^1P_1$) mesons in GeV. $a = 0.01359 \text{ GeV}^3$, $b = 0.08784 \text{ GeV}^2$, and $c = 0.008$.

Meson	Present Work	Exp. [95]	[72]	[81]	[96]	[88, 89]	[73, 74]	N=4	N=5
D	2.421	2.421	2.362	2.507	2.434	2.425[89]	2.421[73]	2.571	2.722
D_s	2.460	2.460	2.409	2.558	2.528	2.529[89]	2.429[73]	2.597	2.735
B	5.797	5.726	5.760	5.719	5.736	5.733[88]	5.744[74]	5.936	6.075
B_s	5.828	5.829	5.775	5.819	5.824	5.828[88]	5.841[74]	5.952	6.077

TABLE 6: Masses for mesons with p-wave state ($^{2S+1}L_J = ^3P_2$) in GeV. $a = 0.0163 \text{ GeV}^3$, $b = 0.113 \text{ GeV}^2$, and $c = 6 \times 10^{-5}$.

Meson	Present work	Exp. [95]	[81]	[96]	[88, 89]	[73, 74]	N=4	N=5
D	2.463	2.463	2.460	2.482	2.461[89]	2.463[74]	2.628	2.792
D_s	2.500	2.537	2.570	2.575	2.569[89]	2.528[74]	2.641	2.800
B	5.817	5.740	5.739	5.754	5.740[88]	5.743[73]	5.969	6.122
B_s	5.840	5.840	5.838	5.843	5.840[88]	5.840[73]	5.976	6.113

TABLE 7: The decay constants of pseudoscalar B and D mesons in MeV.

Meson	f_p	\bar{f}_p	[72]	[83]	[87]	[97]
D	220	235	228	200 ± 24	$214.2^{+7.6}_{-7.8}$	210 ± 11
D_s	250	243	273	232 ± 17	$253.5^{+6.6}_{-7.1}$	259 ± 10
B	147	201	149	184 ± 32	$191.7^{+7.9}_{-6.5}$	192 ± 13
B_s	174	213	187	215 ± 24	$225.4^{+7.9}_{-5.3}$	230 ± 13

TABLE 8: The decay constants of vector B and D mesons in MeV.

Meson	f_v	\bar{f}_v	[83]	[73, 74]	[79]
D	290	210	247 ± 35	307 [73]	353.8
D_s	310	212	287 ± 29	344 [73]	382.1
B	196	182	210 ± 37	242.4 [74]	234.7
B_s	216	191	239 ± 29	178.8 [74]	244.2

dimensional number is not considered on the masses of the HLM in the works [72–74, 81, 88, 89, 96]. Roy and Choudhury [91] have studied the masses of heavy flavor mesons in the higher dimensional space using string inspired potential. They found that an increase of the dimensional number leads to increase the meson masses. Therefore, the present results of the mass spectra of HLM are in good agreement in comparison with the results of [91].

4.2. Decay Constants. The study of the decay constants is one of the very significant characteristics of the HLM, as it provides a direct source of information on the Cabibbo-Kobayashi-Maskawa (CKM) matrix elements. Many theoretical studies have been done for determining the decay constants with different models as relativistic quark model [97–99], lattice QCD [100–102], QCD sum rules [62, 97, 103], and nonrelativistic model [72–74, 79, 97].

The Van Royen-Weisskopf formula [104] can be used to calculate the decay constants of the pseudoscalar and vector mesons f_p and f_v , respectively, in the nonrelativistic limit which is defined as

$$f_{p/v}^2 = \frac{12 |\Psi(0)|^2}{M_{p/v}}. \quad (53)$$

The Van Royen-Weisskopf formula with the QCD radiative corrections taken into account can be written as [105]

$$\bar{f}_{p/v}^2 = \frac{12 |\Psi(0)|^2}{M_{p/v}} C^2(\alpha_s), \quad (54)$$

where

$$C(\alpha_s) = 1 - \frac{\alpha_s}{\pi} \left(\Delta_{p/v} - \frac{m_q - m_{\bar{q}}}{m_q + m_{\bar{q}}} \ln \frac{m_q}{m_{\bar{q}}} \right) \quad (55)$$

and $\Delta_p = 2$ and $\Delta_v = 8/3$, for pseudoscalar and vector mesons, respectively.

In Tables 7 and 8, we have determined the decay constants of the pseudoscalar and vector B and D mesons obtained from (53) and (54) in comparison with the results of other recent works. In [87], the authors evaluated the decay constant for the heavy-light pseudoscalar mesons using the helicity-improved light-front holographic wavefunction. In [83], the authors applied the variational method to study the decay constants of the pseudoscalar and vector B and D mesons in the light-cone quark model for the relativistic Hamiltonian with the Gaussian-type function.

In [72], the authors used the variational method to compute the decay constants of HLM from the radial Schrödinger

TABLE 9: Leptonic decay width of B^+ meson in GeV.

	Present Γ	[74]	[79]	[107]
$B^+ \rightarrow e^+ \nu_e$	2.475×10^{-24}	8.624×10^{-24}	8.094×10^{-24}	5.689×10^{-24}
$B^+ \rightarrow \mu^+ \nu_\mu$	1.086×10^{-19}	3.685×10^{-19}	3.459×10^{-19}	2.439×10^{-19}
$B^+ \rightarrow \tau^+ \nu_\tau$	2.445×10^{-17}	8.196×10^{-17}	7.697×10^{-17}	5.430×10^{-17}

TABLE 10: Leptonic decay width of D^+ meson in GeV.

	Present Γ	[79]	[108]	[66]
$D^+ \rightarrow e^+ \nu_e$	0.622×10^{-20}	1.488×10^{-20}	1.323×10^{-20}	5.706×10^{-21}
$D^+ \rightarrow \mu^+ \nu_\mu$	2.715×10^{-16}	6.322×10^{-16}	5.641×10^{-16}	2.433×10^{-16}
$D^+ \rightarrow \tau^+ \nu_\tau$	0.668×10^{-15}	1.215×10^{-15}	1.529×10^{-15}	6.157×10^{-16}

TABLE 11: Leptonic decay width of D_s^+ meson in GeV.

	Present Γ	[79]	[108]	[67]
$D_s^+ \rightarrow e^+ \nu_e$	1.529×10^{-19}	2.962×10^{-19}	3.157×10^{-19}	1.792×10^{-19}
$D_s^+ \rightarrow \mu^+ \nu_\mu$	0.668×10^{-14}	1.259×10^{-14}	1.347×10^{-14}	7.648×10^{-15}
$D_s^+ \rightarrow \tau^+ \nu_\tau$	0.586×10^{-13}	1.296×10^{-13}	1.326×10^{-13}	7.508×10^{-14}

equation with the Cornell potential. Zhi-Gang Wang [97] introduced an analysis of the decay constants of HLM with QCD sum rules. Yazarloo and Mehiraban [79] used the perturbation method to study the decay constants of D , D_s , B , and B_s mesons with the combination of harmonic and Yukawa-type potentials.

In Table 7, the obtained results are in good agreement in comparison to the results of [72, 83, 87, 97]. In Table 8, the present results are compatible with the results of [73, 74, 79, 83]. In addition, the ratio of decay constants for D mesons is ($f_{D_s}/f_D = 1.140$). This value is in good agreement with the experimental value $f_{D_s}/f_D = 1.258 \pm 0.038$ [95]. The present result is in agreement with the obtained values ($f_D/f_D = 1.195$) in [72] and ($f_{D_s}/f_D = 1.160$) in [83]. Also, we have ($f_{D_s^*}/f_{D^*} = 1.070$) which is in agreement with the calculated values ($f_{D_s^*}/f_{D^*} = 1.183$) in [87] and ($f_{D_s^*}/f_{D^*} = 1.233$) in [97]. The calculated ratio of decay constants for B mesons ($f_{B_s}/f_B = 1.184$) and ($f_{B_s^*}/f_{B^*} = 1.102$) are in good agreement in comparison with ($f_{B_s}/f_B = 1.168$) and ($f_{B_s^*}/f_{B^*} = 1.138$) in [83].

4.3. Leptonic Decay Widths and Branching Ratio. The charged HLM can decay to a charged lepton pair $l^+ \nu_l$ via a virtual W^\pm boson. The leptonic decay widths of the HLM can be obtained from the relation [106]

$$\begin{aligned} \Gamma(B^+, D_q \rightarrow l^+ \nu_l) &= \frac{G_F^2 M_{B,D_q}^2 m_l^2}{8\pi} \left(1 - \frac{m_l^2}{M_{B,D_q}^2}\right)^2 f_{B,D}^2 \\ &\times \begin{cases} |V_{ub}|^2 & \text{for } B \text{ meson} \\ |V_{cq}|^2 (q \in d, s), & \text{for } D \text{ meson} \end{cases} \end{aligned} \quad (56)$$

where $G_F = 1.664 \times 10^{-5}$ is the Fermi constant and the relevant CKM elements are taken from the PDG [95] as $|V_{ub}| = 0.004$, $|V_{cd}| = 0.227$, and $|V_{cs}| = 0.974$. The leptonic masses m_l are taken as $m_e = 0.501 \times 10^{-3}$ GeV, $m_\mu = 0.105$ GeV, and $m_\tau = 1.776$ GeV. We obtain the decay constants of the HLM from Tables 7 and 8 into (56) to compute leptonic decay widths of the HLM. The obtained results of the leptonic decay width of B^+ , D^+ , and D_s^+ mesons are shown in Tables 9, 10, and 11, respectively. Vinodkumar et al. [107] calculated the leptonic decay widths of B , B_s mesons besides, D and D_s mesons [66, 67, 108] for the Martin-like potential with Dirac formalism. We have determined the leptonic decay widths of B^+ meson in Table 9 in comparison with the results of the [74, 79, 107], as well as the leptonic decay widths of D^+ meson in Table 10 in comparison with the results of [66, 79, 108] and the leptonic decay widths of D_s^+ meson in Table 11 compared with the results of [66, 79, 108]. We note that the present results are in good agreement with the results of [66, 67, 74, 107, 108].

The branching ratio of the HLM is defined as

$$Br(B^+, D_q \rightarrow l^+ \nu_l) = \Gamma(B^+, D_q \rightarrow l^+ \nu_l) \times \tau_{B^+, D_q} \quad (57)$$

where the lifetime τ of B^+ , D^+ , and D_s^+ mesons is taken as $\tau_{B^+} = 1.638 ps$, $\tau_{D^+} = 1.040 ps$, and $\tau_{D_s^+} = 0.5 ps$ [95]. We have determined the branching ratio for the B^+ , D^+ , and D_s^+ mesons compared with the experimental data and with the results of other recent studies [72–74, 88, 89].

In Table 12, we note that the present values of the branching ratio for the B^+ meson are close to experimental data and are in agreement in comparison with the theoretical results [72, 74, 79, 88, 107]. In addition, in Tables 13 and 14, we note that the evaluated results of branching ratio for the D^+ and D_s^+ mesons are close to the experimental data and become better in comparison with works [72, 73, 79, 89, 108].

TABLE 12: Leptonic branching ratio of B^+ meson.

	Present Br	[88]	[79]	[107]	[72]	[74]	Exp. [95]
$B^+ \rightarrow e^+ \nu_e$	6.162×10^{-12}	8.640×10^{-12}	2.015×10^{-11}	1.419×10^{-11}	6.220×10^{-12}	2.147×10^{-11}	$< 9.8 \times 10^{-7}$
$B^+ \rightarrow \mu^+ \nu_\mu$	2.705×10^{-7}	0.370×10^{-7}	8.611×10^{-7}	6.085×10^{-7}	2.630×10^{-7}	9.174×10^{-7}	$< 1.0 \times 10^{-6}$
$B^+ \rightarrow \tau^+ \nu_\tau$	6.088×10^{-5}	0.822×10^{-4}	1.916×10^{-4}	1.354×10^{-4}	1.140×10^{-4}	2.040×10^{-4}	$(1.14 \pm 0.27) \times 10^{-4}$

TABLE 13: Leptonic branching ratio of D^+ meson.

	Present Br	[89]	[79]	[73]	[72]	[108]	Exp. [95]
$D^+ \rightarrow e^+ \nu_e$	0.984×10^{-8}	0.580×10^{-8}	2.351×10^{-8}	1.77×10^{-8}	1.130×10^{-8}	2.105×10^{-8}	$< 8.8 \times 10^{-6}$
$D^+ \rightarrow \mu^+ \nu_\mu$	4.293×10^{-4}	2.470×10^{-4}	9.991×10^{-4}	7.54×10^{-4}	4.770×10^{-4}	8.977×10^{-4}	$(3.74 \pm 0.17) \times 10^{-4}$
$D^+ \rightarrow \tau^+ \nu_\tau$	1.055×10^{-3}	0.860×10^{-3}	1.920×10^{-3}	1.79×10^{-3}	2.030×10^{-3}	2.933×10^{-3}	$< 1.2 \times 10^{-3}$

TABLE 14: Leptonic branching ratio of D_s^+ meson.

	Present Br	[89]	[79]	[73]	[72]	[108]	Exp. [95]
$D_s^+ \rightarrow e^+ \nu_e$	1.163×10^{-7}	0.940×10^{-7}	2.251×10^{-7}	1.82×10^{-7}	1.630×10^{-7}	1.391×10^{-7}	$< 8.3 \times 10^{-5}$
$D_s^+ \rightarrow \mu^+ \nu_\mu$	5.078×10^{-3}	4.000×10^{-3}	9.572×10^{-3}	7.74×10^{-3}	6.900×10^{-3}	5.937×10^{-3}	$(5.56 \pm 0.25) \times 10^{-3}$
$D_s^+ \rightarrow \tau^+ \nu_\tau$	4.451×10^{-3}	3.780×10^{-3}	9.864×10^{-2}	8.2×10^{-2}	6.490×10^{-2}	5.844×10^{-3}	$(5.55 \pm 0.24)\%$

5. Summary and Conclusion

In this work, we have presented an approximate-analytic solution of the N -dimensional radial Schrödinger equation for the mixture of vector and scalar potentials via the LTM. The spin-spin, spin-orbit, and tensor interactions have been included in the extended Cornell potential model. The energy eigenvalues and the corresponding eigenfunctions have been determined in the N -dimensional space. In three-dimensional space, we have employed the obtained results to study the different properties of the HLM that are not considered in many recent studies. The masses of the scalar, vector, pseudoscalar, and pseudovector for B , B_s , D , and D_s mesons have been calculated in the three-dimensional space and in the higher dimensional space in Tables 2–6. Most of the present calculations are close to the experimental data and are improved in comparison with the recent calculations [72–74, 81, 88, 89, 96]. As well, we have computed the masses of the HLM in the higher dimensional space at $N=4$ and $N=5$. The dependence of the masses of HLM on the dimensional number is discussed. We found that the masses increase with increasing dimensional number. This result is obtained in [91]. In Tables 7 and 8, the decay constants of the pseudoscalar and vector mesons have been determined in comparison with the results of [72–74, 79, 83, 87, 97]. The calculated ratios of the decay constants of D mesons ($f_{D_s^*}/f_D = 1.140$) and ($f_{D_s^*}/f_{D^*} = 1.070$) are close to the experimental ratio ($f_{D_s^*}/f_D = 1.258 \pm 0.038$).

The present results of the decay ratio of B mesons are in good agreement with the results of [72, 83]. The leptonic decay widths of B^+ meson have been studied in comparison with the results of [74, 79, 107] and the leptonic decay widths of D^+ meson in comparison with the results of [66, 79, 108]. In addition, the leptonic decay widths of D_s^+ meson have been studied in comparison with the results of [66, 79, 108].

The obtained results of the leptonic decay widths are compared with the results of [66, 67, 74, 107, 108]. We have determined the branching ratio for the B^+ , D^+ , and D_s^+ mesons that are in good agreement with the experimental data and with the recent studies [72–74, 88, 89]. Therefore, the current potential with used method gives very good predictions for the heavy-light meson properties. We hope to extend this work to include external force as a future work.

Data Availability

The data used to support the findings of this study are available from the corresponding author upon request.

Conflicts of Interest

The authors declare that they have no conflicts of interest.

References

- [1] J. J. Sakurai, *Modern Quantum Mechanics*, Addison-Wesley publishing, New York, NY, USA, 1967.
- [2] R. P. Feynman and A. R. Hibbs, *Quantum Mechanics and Path Integrals*, McGraw-Hill, New York, NY, USA, 1965.
- [3] H. Hassanabadi, M. Hamzavi, S. Zarrinkamar, and A. A. Rajabi, “Exact solutions of N -Dimensional Schrödinger equation for a potential containing coulomb and quadratic terms,” *International Journal of the Physical Sciences*, vol. 6, no. 3, pp. 583–586, 2011.
- [4] R. Kumar and F. Chand, “Series solutions to the N -dimensional radial Schrödinger equation for the quark-antiquark interaction potential,” *Physica Scripta*, vol. 85, no. 5, Article ID 055008, 2012.
- [5] S. A. Ponomarenko, “Quantum harmonic oscillator revisited: a fourier transform approach,” *American Journal of Physics*, vol. 72, article 1259, 2004.

- [6] G. Palma and U. Raff, "A novel application of a Fourier integral representation of bound states in quantum mechanics," *American Journal of Physics*, vol. 79, no. 2, pp. 201–205, 2011.
- [7] S. Erkoç and R. Sever, "1/N expansion for a Mie-type potential," *Physical Review D*, vol. 33, no. 588, 1986.
- [8] B. Roy and R. Roychoudhury, "The shifted 1/N expansion and the energy eigenvalues of the Hulthén potential for $l \neq 0$," *Journal of Physics A: Mathematical and General*, vol. 20, no. 10, pp. 3051–3055, 1987.
- [9] R. De, R. Dutt, and U. Sukhatme, "Mapping of shape invariant potentials under point canonical transformations," *Journal of Physics A: Mathematical and General*, vol. 25, no. 13, pp. L843–L850, 1992.
- [10] E. Z. Liverts, E. G. Drukarev, R. Krivec, and V. B. Mandelzweig, "Analytic presentation of a solution of the Schrödinger equation," *Few-Body Systems*, vol. 44, p. 367, 2008.
- [11] F. Cooper, A. Khare, and U. Sukhatme, "Supersymmetry and quantum mechanics," *Physics Reports*, vol. 251, no. 5–6, pp. 267–385, 1995.
- [12] R. N. Choudhury and M. Mondal, "Eigenvalues of anharmonic oscillators and the perturbed Coulomb problem in space," *Physical Review A*, vol. 52, p. 1850, 1995.
- [13] L. Gr. Ixaru, H. D. Meyer, and G. V. Berghe, "Highly accurate eigenvalues for the distorted Coulomb potential," *Physical Review E*, vol. 61, p. 3151, 2000.
- [14] T. E. Simos, "P-stable Four-Step Exponentially-Fitted Method for the Numerical Integration of the Schrödinger Equation," *Computing Letters*, vol. 1, pp. 37–45, 2005.
- [15] J. Vigo-Aguiar and T. E. Simos, "Review of multistep methods for the numerical solution of the radial Schrödinger equation," *International Journal of Quantum Chemistry*, vol. 103, no. 3, pp. 278–290, 2005.
- [16] J. Avery and D. R. Herschbach, "Hyperspherical Strumian basis functions," *International Journal of Quantum Chemistry*, vol. 41, no. 5, pp. 673–686, 1992.
- [17] A. Kirchberg, J. D. Laenge, P. A. Pisani, and A. Wipf, "Algebraic solution of the supersymmetric hydrogen atom in D-dimensions," *Annals of Physics*, vol. 303, no. 2, p. 359, 2003.
- [18] A. B. Nassar, "New quantum squeezed states for the time-dependent harmonic oscillator," *Journal of Optics B: Quantum and Semiclassical Optics*, vol. 4, no. 3, pp. S226–S228, 2002.
- [19] K. J. Oyewumi and E. A. Bangu, "Isotropic harmonic oscillator plus inverse quadratic potential in N-dimensional spaces," *Arabian Journal for Science and Engineering*, vol. 28, no. 2, pp. 173–182, 2003.
- [20] S. M. Al-Jaber, "A Confined N-dimensional Harmonic Oscillator," *International Journal of Theoretical Physics*, vol. 47, no. 7, p. 1853, 2008.
- [21] T. D. Mackay, S. D. Bartlett, L. T. Stephenson, and B. C. Sanders, "Quantum walks in higher dimensions," *Journal of Physics A: Mathematical and General*, vol. 35, no. 12, pp. 2745–2753, 2002.
- [22] C. M. Bender, S. Boettcher, and L. Lipatov, "Almost zero-dimensional quantum field theories," *Physical Review D: Particles, Fields, Gravitation and Cosmology*, vol. 46, no. 12, pp. 5557–5573, 1992.
- [23] S. M. Al-Jaber, "Quantization of angular momentum in the N-dimensional space," *Nuovo Cimento B*, vol. 110, no. 8, pp. 993–995, 1995.
- [24] S. M. Al-Jaber, "On the radial-part equation of the wave function in N dimensions," *Nuovo Cimento B*, vol. 112, no. 5, p. 761, 1997.
- [25] S. M. Al-Jaber, "Hydrogen atom in N dimensions," *International Journal of Theoretical Physics*, vol. 37, no. 4, pp. 1289–1298, 1998.
- [26] S. M. Al-Jaber, "Fermi gas in D-dimensional space," *International Journal of Theoretical Physics*, vol. 38, no. 3, pp. 919–923, 1999.
- [27] S. M. Al-Jaber, "Planck's spectral distribution law in N-dimensions," *International Journal of Theoretical Physics*, vol. 42, no. 1, pp. 111–119, 2003.
- [28] G. Chen, "Exact solutions of the N-dimensional radial Schrödinger equation with the Coulomb potential via the Laplace transform," *Zeitschrift für Naturforschung A*, vol. 59a, p. 875, 2004.
- [29] S. M. Al-Jaber, "A Confined N-Dimensional Harmonic Oscillator," *International Journal of Theoretical Physics*, vol. 47, no. 7, p. 1853, 2008.
- [30] K. J. Oyewumi, F. O. Akinpelu, and A. D. Agboola, "Exactly complete solutions of the pseudoharmonic potential in N-dimensions," *International Journal of Theoretical Physics*, vol. 47, no. 4, pp. 1039–1057, 2008.
- [31] S. Ikhdair and R. Sever, "Polynomial solutions of the Mie-type potential in the D-dimensional Schrödinger equation," *Journal of Molecular Structure*, vol. 855, p. 13, 2008.
- [32] H. Hassanabadi, S. Zarrinkamar, and A. A. Rajabi, "Exact solutions of D-dimensional Schrödinger equation for an energy dependent potential by NU method," *Communications in Theoretical Physics*, vol. 55, no. 4, pp. 541–544, 2011.
- [33] S. Ikhdair and R. Sever, "Exact solutions of the modified Kratzer potential plus ring-shaped potential in the D-dimensional Schrödinger equation by the Nikiforov-Uvarov method," *International Journal of Modern Physics C*, vol. 19, p. 221, 2008.
- [34] R. Kumar and F. Chand, "Asymptotic study to the N-dimensional radial Schrödinger equation for the quark-antiquark system," *Communications in Theoretical Physics*, vol. 59, no. 5, pp. 528–532, 2013.
- [35] S. M. Kuchin and N. V. Maksimenko, "Theoretical estimations of the spin-averaged mass spectra of heavy quarkonia and Bc mesons," *Universal Journal of Physics and Application*, vol. 7, p. 295, 2013.
- [36] M. Abu-Shady, "Heavy quarkonia and Bc-mesons in the Cornell potential with harmonic oscillator potential in the N-dimensional Schrödinger equation," *International Journal Applied Mathematics and Theoretical Physics*, vol. 2, p. 16, 2016.
- [37] E. M. Khokha, M. Abu-Shady, and T. A. Abdel-Karim, "Quarkonium masses in the N-dimensional space using the analytical exact iteration method," *International Journal of Theoretical and Applied Mathematics*, vol. 2, p. 86, 2016.
- [38] M. Abu-Shady, T. A. Abdel-Karim, and E. M. Khokha, "Exact solution of the N-dimensional radial Schrödinger equation via it with the generalized Cornell potential," *High Energy Physics - Phenomenology*, 2018.
- [39] A. N. Ikot, O. A. Awoga, and A. D. Antia, "Bound state solutions of d-dimensional Schrödinger equation with Eckart potential plus modified deformed Hylleraas potential," *Chinese Physics B*, vol. 22, no. 2, 2013.
- [40] D. Agboola, "The Hulthén potential in D-dimensions," *Physica Scripta*, vol. 80, article 065304, no. 6, 2009.
- [41] H. Hassanabadi, B. H. Yazarloo, S. Zarrinkamar, and M. Solaimani, "Approximate analytical versus numerical solutions of Schrödinger equation under molecular Hulthén potential," *International Journal of Quantum Chemistry*, vol. 112, no. 23, pp. 3706–3710, 2012.

- [42] H. Hassanabadi, E. Maghsoodi, A. N. Ikot, and S. Zarrinkamar, "Approximate arbitrary-state solutions of Dirac equation for modified deformed Hylleraas and modified Eckart potentials by the NU method," *Applied Mathematics and Computation*, vol. 219, no. 17, pp. 9388–9398, 2013.
- [43] Wahyulianti, A. Suparmi, C. Cari, and F. Anwar, "The Solutions of the D-dimensional Schrödinger Equation for the Potential $V(r) = ar^{-6} + br^{-5} + cr^{-4} + dr^{-3} + er^{-2} + fr^{-1}$," *Journal of Physics: Conference Series*, vol. 795, article 012022, 2017.
- [44] M. Abu-Shady, T. A. Abdel-Karim, and E. M. Khokha, "Binding Energies and Dissociation Temperatures of Heavy Quarkonia at Finite Temperature and Chemical Potential in the N -Dimensional Space," *Advances in High Energy Physics*, Art. ID 7356843, 12 pages, 2018.
- [45] G. Chen, "The exact solutions of the Schrödinger equation with the Morse potential via Laplace transforms," *Physics Letters A*, vol. 326, no. 1-2, pp. 55–57, 2004.
- [46] A. Arda and R. Sever, "Exact solutions of the Morse-like potential, step-up and step-down operators via Laplace transform approach," *Communications in Theoretical Physics*, vol. 58, no. 1, pp. 27–30, 2012.
- [47] D. R. M. Pimentel and A. S. de Castro, "A Laplace transform approach to the quantum harmonic oscillator," *European Journal of Physics*, vol. 34, no. 1, pp. 199–204, 2013.
- [48] A. Arda and R. Sever, "Exact solutions of the Schrödinger equation via Laplace transform approach: pseudoharmonic potential and Mie-type potentials," *Journal of Mathematical Chemistry*, vol. 50, no. 4, p. 971, 2012.
- [49] A. Arda and R. Sever, "Non-central potentials, exact solutions and Laplace transform approach," *Journal of Mathematical Chemistry*, vol. 50, no. 6, p. 1484, 2012.
- [50] C. Gang, "Exact solutions of N -dimensional harmonic oscillator via Laplace transformation," *Chinese Physics*, vol. 14, no. 6, article 1075, 2005.
- [51] S. Miraboutalebi and L. Rajaei, "Solutions of N -dimensional Schrödinger equation with Morse potential via Laplace transforms," *Journal of Mathematical Chemistry*, vol. 52, no. 4, p. 1119, 2014.
- [52] T. Das and A. Arda, "Exact analytical solution of the N -dimensional radial Schrödinger equation with pseudoharmonic potential via laplace transform approach," *Advances in High Energy Physics*, vol. 2015, Article ID 137038, 2015.
- [53] T. Das, "A Laplace transform approach to find the exact solution of the N -dimensional Schrödinger equation with Mie-type potentials and construction of Ladder operators," *Journal of Mathematical Chemistry*, vol. 53, no. 2, p. 618, 2015.
- [54] T. Das, "Treatment of N -dimensional Schrödinger Equation for Anharmonic Potential via Laplace Transform," *Electronic Journal of Theoretical Physics*, vol. 13, p. 207, 2016.
- [55] R. Kumar, D. Kumar, and F. Chand, "Mass spectra of heavy quarkonia using Cornell plus harmonic potential," in *Proceedings of the DAE Symposium on Nuclear Physics*, vol. 57, p. 664, 2012.
- [56] A. F. Al-Jamel and H. Widyan, "Heavy Quarkonium Mass Spectra in A Coulomb Field Plus Quadratic Potential Using Nikiforov-Uvarov Method," *Applied Physics Research*, vol. 4, no. 3, 2012.
- [57] L. I. Abou-Salem, "A systematic study on nonrelativistic quark-antiquark interactions," *International Journal of Modern Physics A*, vol. 20, no. 17, p. 4113, 2005.
- [58] F. E. Close and E. S. Swanson, "Dynamics and decay of heavy-light hadrons," *Physical Review D*, vol. 72, no. 9, Article ID 094004, 2005.
- [59] A. M. Badalian, B. L. Bakker, and Y. A. Simonov, "Decay constants of the heavy-light mesons from the field correlator method," *Physical Review D*, vol. 75, no. 11, Article ID 116001, 2007.
- [60] D. Ebert, R. N. Faustov, and V. O. Galkin, "Mass spectra and Regge trajectories of light mesons in the relativistic quark model," *Physical Review D*, vol. 79, no. 11, Article ID 114029, 11 pages, 2009.
- [61] D. Ebert, R. N. Faustov, and V. O. Galkin, "Heavy-light meson spectroscopy and Regge trajectories in the relativistic quark model," *The European Physical Journal C*, vol. 66, no. 1, pp. 197–206, 2010.
- [62] P. Gelhausen, A. Khodjamirian, A. A. Pivovarov, and D. Rosenthal, "Decay constants of heavy-light vector mesons from QCD sum rules," *Physical Review D*, vol. 88, article 014015, no. 9, 2013.
- [63] S. Narison, "Decay Constants of Heavy-Light Mesons from QCD," *Nuclear and Particle Physics Proceedings*, vol. 270-272, pp. 143–153, 2016.
- [64] N. Devlani and A. K. Rai, "Mass Spectrum and Decay Properties of D Meson," *International Journal of Theoretical Physics*, vol. 52, no. 7, pp. 2196–2208, 2013.
- [65] M. Shah, B. Patel, and P. C. Vinodkumar, "Mass spectra and decay properties of D_s meson in a relativistic dirac formalism," *Physical Review D*, vol. 90, article 014009, no. 1, 2014.
- [66] M. Shah, B. Patel, and P. C. Vinodkumar, "D meson spectroscopy and their decay properties using Martin potential in a relativistic Dirac formalism," *The European Physical Journal C*, vol. 76, p. 36, 2016.
- [67] P. C. Vinodkumar, M. Shah, and B. Patel, "Hadronic and Leptonic decay widths of D and D_s Mesons using Dirac formalism," in *Proceedings of the DAE Symposium on Nuclear Physics*, vol. 59, pp. 638-639, 2014.
- [68] M. Shah and P. C. Vinodkumar, "Rare decay of B_s^0 and B mesons into dimuon ($\mu + \mu$) using relativistic formalism," in *Proceedings of the DAE Symposium on Nuclear Physics*, vol. 60, pp. 674-675, 2015.
- [69] P. C. Vinodkumar, M. Shah, and B. Patel, "Pseudoscalar decay constant of B and B_s mesons using dirac formalism," in *Proceedings of the DAE Symposium on Nuclear Physics*, vol. 60, pp. 676-677, 2015.
- [70] H. M. Choi, C. R. Ji, Z. Li, and H. Y. Ryu, "Variational analysis of mass spectra and decay constants for ground state pseudoscalar and vector mesons in the light-front quark model," *Physical Review C*, vol. 92, article 055203, 2015.
- [71] M. Wurtz, R. Lewis, and R. Woloshyn, "Free-form smearing for bottomonium and B meson spectroscopy," *Physical Review D*, vol. 92, no. 5, 2015.
- [72] H. Hassanabadi, M. Ghafourian, and S. Rahmani, "Study of Heavy-Light Mesons Properties Via the Variational Method for Cornell Interaction," *Few-Body Systems*, vol. 57, no. 4, pp. 249–254, 2016.
- [73] B. H. Yazarloo and H. Mehraban, "Study of decay properties of D and D_s mesons," *The European Physical Journal*, vol. 115, no. 2, p. 21002, 2016.
- [74] B. H. Yazarloo and H. Mehraban, "Study of B and B_s mesons with a coulomb plus exponential," *The European Physical Journal*, vol. 116, article 31004, 2016.

- [75] S. Nandi, S. K. Patra, and A. Soni, “Correlating new physics signals in $B \rightarrow D^{(*)} \tau^+ \nu_\tau$ with $B \rightarrow \tau \nu_\tau$,” *High Energy Physics - Phenomenology*, 2016.
- [76] T. Matsuki, Q. F. Lü, Y. Dong, and T. Mori, “Approximate degeneracy of heavy- light mesons with the same L,” *Physics Letters B*, vol. 758, pp. 274–277, 2016.
- [77] S. Godfrey, K. Moats, and E. S. Swanson, “B and B_s meson spectroscopy,” *Physical Review D*, vol. 94, no. 5, 2016.
- [78] S. Godfrey and K. Moats, “Properties of excited charm and charm-strange mesons,” *Physical Review D*, vol. 93, article 034035, 2015.
- [79] B. H. Yazarloo and H. Mehraban, “Mass spectrum and decay properties of heavy- light mesons: D, D_s, B and B_s mesons,” *The European Physical Journal Plus*, vol. 132, no. 2, p. 80, 2017.
- [80] B.-B. Zhou, J.-J. Sun, and Y.-J. Zhang, “Leptonic decays of heavy vector and pseudoscalar mesons,” *Communications in Theoretical Physics*, vol. 67, no. 6, pp. 655–660, 2017.
- [81] J. B. Liu and C. D. Lü, “Spectra of heavy-light mesons in a relativistic model,” *The European Physical Journal C*, vol. 77, p. 312, 2017.
- [82] W. Lucha, D. Melikhov, and S. Simula, “Isospin breaking in the decay constants of heavy mesons from QCD sum rules,” *Physics Letters B*, vol. 765, pp. 365–370, 2017.
- [83] N. Dhiman and H. Dahiya, “Decay constants of pseudoscalar and vector B and D mesons in the light-cone quark model,” *The European Physical Journal Plus*, vol. 133, no. 4, 2018.
- [84] S. C. Li et al., “Strong decays of D_J (3000) and D_{sJ} (3040),” *Physical Review D*, vol. 97, Article ID 054002, 2018.
- [85] N. Soni and J. Pandya, “Decay $D \rightarrow K^{(*)} \ell^+ \nu_\ell$ in covariant quark model,” *Physical Review D*, vol. 96, no. 1, 2017.
- [86] Q. Li et al., “Decays of B, B_s and B_c to D-wave heavy-light mesons,” *The European Physical Journal C*, vol. 77, no. 12, 2017.
- [87] Q. Chang, S. Xu, and L. Chen, “Application of the light-front holographic wavefunction for heavy-light pseudoscalar meson in $B_{d,s} \rightarrow D_{d,s} P$ decays,” *Nuclear Physics B*, vol. 921, pp. 454–471, 2017.
- [88] V. Kher, N. Devlani, and A. Kumar Rai, “Spectroscopy, decay properties and Regge trajectories of the B and B_s mesons,” *Chinese Physics C*, vol. 41, no. 9, p. 093101, 2017.
- [89] V. Kher, N. Devlani, and A. K. Rai, “Excited state mass spectra, decay properties and Regge trajectories of charm and charm-strange mesons,” *Chinese Physics C*, vol. 41, no. 7, Article ID 073101, 2017.
- [90] V. H. Kher and A. K. Rai, “Radiative transitions and the mixing parameters of the D meson,” *Journal of Physics: Conference Series*, vol. 934, Article ID 012036, 2017.
- [91] S. Roy and D. K. Choudhury, “Effective string theory inspired potential and meson masses in higher dimension,” *Canadian Journal of Physics*, vol. 94, no. 12, pp. 1282–1288, 2016.
- [92] M. R. Spiegel, *Theory and Problems of Laplace Transforms*, Schaums Outline Series, McGraw-Hill, New York, NY, USA, 1965.
- [93] V. Lengyel, Y. Fekete, I. Haysak, and A. Shpenik, “Calculation of hyperfine splitting in mesons using configuration interaction approach,” *The European Physical Journal C*, vol. 21, no. 2, pp. 355–359, 2001.
- [94] W. Lucha, F. Schoberl, and D. Gromes, “Bound states of quarks,” *Physics Reports*, vol. 200, no. 4, pp. 127–240, 1991.
- [95] C. Patrignani et al., “Particle data group,” *Chinese Physics C*, vol. 40, article 100001, 2016.
- [96] J. B. Liu and M. Z. Yang, “Heavy-light mesons in a relativistic model,” *Chinese Physics C*, vol. 40, no. 7, p. 073101, 2016.
- [97] Z. Wang, “Analysis of the masses and decay constants of the heavy-light mesons with QCD sum rules,” *The European Physical Journal C*, vol. 75, no. 9, p. 427, 2015.
- [98] D. Ebert, R. N. Faustov, and V. O. Galkin, “Relativistic treatment of the decay constants of light and heavy mesons,” *Physics Letters B*, vol. 635, p. 93, 2006.
- [99] D. S. Hwang and G. Kim, “Decay constants of B, B^* and D, D^* mesons in the relativistic mock meson model,” *Physical Review D*, vol. 55, no. 11, p. 6944, 1997.
- [100] H. Na et al., “B and B_s meson decay constants from lattice QCD,” *Physical Review D*, vol. 86, Article ID 034506, 2012.
- [101] C. T. H. Davies et al., “Precision constant from full lattice QCD using very fine lattices,” *Physical Review D*, vol. 82, Article ID 114504, 2010.
- [102] A. Bazavov et al., “B- and D-meson decay constants from three-flavor lattice QCD,” *Physical Review D*, vol. 85, Article ID 114506, p. 370, 2012.
- [103] S. Narison, “A fresh look into $\overline{m}_{c,b}(\overline{m}_{c,b})$ and precise $f_{D(s),B(s)}$ from heavy-light QCD spectral sum rules,” *Physics Letters B*, vol. 718, p. 1321, 2013.
- [104] R. Van Royen and V. F. Weisskopf, “Hardon decay processes and the quark model,” *Nuovo Cimento*, vol. 50, no. 3, pp. 617–645, 1967.
- [105] E. Braaten and S. Fleming, “QCD radiative corrections to the leptonic decay rate of the Bc meson,” *Physical Review D*, vol. 52, no. 1, p. 181, 1995.
- [106] D. Silverman and H. Yao, “Relativistic treatment of light quarks in D and B mesons and W-exchange weak decays,” *Physical Review D*, vol. 38, no. 1, pp. 214–232, 1988.
- [107] M. Shah, B. Patel, and P. C. Vinodkumar, “Spectroscopy and flavor changing decays of B, B_s mesons in a Dirac formalism,” *Physical Review D*, vol. 93, no. 9, 2016.
- [108] M. Shah, B. Patel, and P. C. Vinodkumar, “Spectroscopy and Decay properties of D and D_s mesons with Martin-like confinement potential in Dirac formalism,” *Proceedings of Science*, vol. 078, 2013.

Research Article

Bottomonium Suppression in Nucleus-Nucleus Collisions Using Effective Fugacity Quasi-Particle Model

Indrani Nilima and Vineet Kumar Agotiya 

Centre for Applied Physics, Central University of Jharkhand, Ranchi 835 205, India

Correspondence should be addressed to Vineet Kumar Agotiya; agotiya81@gmail.com

Received 20 April 2018; Accepted 26 June 2018; Published 12 July 2018

Academic Editor: Chun-Sheng Jia

Copyright © 2018 Indrani Nilima and Vineet Kumar Agotiya. This is an open access article distributed under the Creative Commons Attribution License, which permits unrestricted use, distribution, and reproduction in any medium, provided the original work is properly cited. The publication of this article was funded by SCOAP³.

We have studied the equation of state and dissociation temperature of bottomonium state by correcting the full Cornell potential in isotropic medium by employing the effective fugacity quasi-particle Debye mass. We had also calculated the bottomonium suppression in an expanding, dissipative strongly interacting QGP medium produced in relativistic heavy-ion collisions. Finally we compared our results with experimental data from RHIC 200GeV/nucleon Au-Au collisions, LHC 2.76 TeV/nucleon Pb-Pb, and LHC 5.02 TeV/nucleon Pb-Pb collisions as a function of number of participants.

1. Introduction

At the Relativistic Heavy-Ion Collider (RHIC) situated at Brookhaven National Laboratory (BNL), heavy-ion collisions have been studied. After the pioneer work done in the direction of suppression by Matsui and Satz, and some other development of the potential models, suppression was observed by both SPS and RHIC [1]. Due to the Debye screening of the Quantum Chromo-Dynamic (QCD) potential between the two heavy quarks, quarkonia suppression was originally claimed to be an unambiguous signal of the formation of a quark-gluon plasma (QGP). Quarkonia suppression was suggested to be a signature of the QGP and we can measure the suppression (Y as well as J/ψ), both at RHIC and at the LHC.

In heavy-ion collisions to determine the properties of the medium formed in A+A collisions and p + p collisions, the A+A collision deviates from simple superposition of independent p + p collisions. This deviation is quantified with the nuclear modification factor (R_{AA}). This factor is the ratio of the yield in heavy-ion collisions over the yield in p + p collisions, scaled by a model of the nuclear geometry of the collision. The value of $R_{AA}=1$ indicates no modification due to the medium. We can say that the probe of interest is suppressed in heavy-ion collisions if R_{AA} is less than 1.

A quarkonia meson that forms on the outside surface will not dissociate regardless of the temperature of the medium because it does not have a chance to interact with it. This is why we never see a R_{AA} that is equal to zero. The suppression can also be affected by the QGP, the formation time of the quarkonia meson, and the QGP lifetime as well. For instance, a high p_T quarkonia meson could have a formation time long enough that it actually does not see the QGP at all and thus is not suppressed.

In the early days most of the interests were focused on the suppression of charmonium states [1–3] of collider experiments at SPS and RHIC, but several observations are yet to be understood; *namely*, the suppression of $\psi(1S)$ does not increase from SPS to RHIC, even though the centre-of-mass energy is increased by fifteen times. The heavy-ion program at the LHC may resolve those puzzles because the beam energy and luminosity are increased by ten times that of the RHIC. Moreover the CMS detector has excellent capabilities for muon detection and provides measurements of $\psi(2S)$ and the Y family, which enables the quantitative analysis of quarkonia. That is why the interest may be shifted to the bottomonium states at the LHC energy.

A potential model for the phenomenological descriptions of heavy quarkonium suppression would be quite useful

inspite of the progress of direct lattice QCD based determinations of the potential. The large mass of heavy quarks and their small relative velocity make the use of nonrelativistic quantum mechanics justifiable to describe the quarkonia in the potential models. This is one of the main goals of this present study that argues for the modification of the full Cornell potential as an appropriate potential for heavy quarkonium at finite temperature. QGP created at RHIC have a very low viscosity to entropy ratio, i.e., $\eta/\mathcal{S} \geq 1/4\pi$ [4–9], and in the nonperturbative domain of QCD, with temperature close to T_c , the quark matter in the QGP phase is strongly interacting.

In the present paper, we shall employ quasi-particle model for hot QCD equations of state [10, 11] to extract the Debye mass [12] which is obtained in terms of quasi-particle degrees of freedom. We first obtained the medium modified heavy quark potential in isotropic medium and estimate the dissociation temperature. Here, we have used the viscous hydrodynamics to define the dynamics of the system created in the heavy-ion collisions. We have included only the shear viscosity and not included the bulk viscosity. We will look the issue of bulk viscosity in near future.

Our work is organized as follows. In Section 2, we briefly discuss our recent work on medium modified potential in isotropic medium. In Sections 2.1 and 2.2 we study the real and imaginary part of the potential in the isotropic medium and effective fugacity quasi-particle model (EQPM) in Section 2.3. In Section 3 we studied binding energy and dissociation temperature of Υ , Υ' , and χ_b state considering isotropic medium. Using this effective potential and by incorporating quasi-particle Debye mass, we have then developed the equation of state for strongly interacting matter and have shown our results on pressure, energy density, and speed of sound along with the lattice data. In Section 4, we have employed the aforesaid equation of state to study the suppression of bottomonium in the presence of viscous forces and estimate the survival probability in a longitudinally expanding QGP. Results and discussion will be presented in Section 5 and finally, we conclude in Section 6.

2. Medium Modified Effective Potential in Isotropic Medium

We can obtain the medium modification to the vacuum potential by correcting its both Coulombic and string part with a dielectric function $\epsilon(p)$ encoding the effect of deconfinement [25]:

$$V(r, T) = \int \frac{d^3 \mathbf{p}}{(2\pi)^{3/2}} (e^{i\mathbf{p}\cdot\mathbf{r}} - 1) \frac{V(p)}{\epsilon(p)}. \quad (1)$$

Here the functions, $\epsilon(p)$ and $V(p)$, are the Fourier transform (FT) of the dielectric permittivity and Cornell potential, respectively. After assuming r as distribution ($r \rightarrow r \exp(-\gamma r)$) we evaluated the Fourier transform of the linear part $\sigma r \exp(-\gamma r)$ as

$$-\frac{i}{p\sqrt{2\pi}} \left(\frac{2}{(\gamma - ip)^3} - \frac{2}{(\gamma + ip)^3} \right). \quad (2)$$

While putting $\gamma = 0$, we can write the FT of the linear term σr as

$$(\overline{\sigma r}) = -\frac{4\sigma}{p^4 \sqrt{2\pi}}. \quad (3)$$

Thus the FT of the full Cornell potential becomes

$$V(p) = -\sqrt{\left(\frac{2}{\pi}\right)} \frac{\alpha}{p^2} - \frac{4\sigma}{\sqrt{2\pi} p^4}. \quad (4)$$

To obtain the real and imaginary parts of the potential, we put the temporal component of real and imaginary part in terms of retarded (or advanced) and symmetric parts in the Fourier space in isotropic medium which finally gives

$$\begin{aligned} \text{Re } D_{11}^{00}(\omega, p) &= \frac{1}{2} (D_R^{00} + D_A^{00}), \\ \text{Im } D_{11}^{00}(\omega, p) &= \frac{1}{2} D_F^{00}. \end{aligned} \quad (5)$$

Let us now discuss the real and imaginary part of the potential modified using the above define $\text{Re } D_{11}^{00}(\omega, p)$ and $\text{Im } D_{11}^{00}(\omega, p)$ along with effective fugacity quasi-particle model (EQPM) in the next subsections.

2.1. Real Part of the Potential in the Isotropic Medium. Now using the real part of retarded (advanced) propagator in isotropic medium, we get

$$\text{Re } D_{R,A}^{00}(0, p) = -\frac{1}{(p^2 + m_D^2)}, \quad (6)$$

where the real part of the dielectric permittivity (also given in [26–28]) becomes

$$\epsilon(p) = \left(1 + \frac{m_D^2}{p^2} \right). \quad (7)$$

Now using (6) and real part of dielectric permittivity (7) in (1), we get

$$\begin{aligned} \text{Re } V_{(iso)}(r, T) &= \int \frac{d^3 \mathbf{p}}{(2\pi)^{3/2}} (e^{i\mathbf{p}\cdot\mathbf{r}} - 1) \left(-\sqrt{\left(\frac{2}{\pi}\right)} \frac{\alpha}{p^2} - \frac{4\sigma}{\sqrt{2\pi} p^4} \right) \\ &\quad \times \left(\frac{p^2}{(p^2 + m_D^2)} \right) \end{aligned} \quad (8)$$

Solving the above integral, we find

$$\begin{aligned} \text{Re } V_{(iso)}(\hat{s}, T) &= \left(\frac{2\sigma}{m_D} - \alpha m_D \right) \frac{e^{-\hat{s}}}{\hat{s}} - \frac{2\sigma}{\hat{s}} + \frac{2\sigma}{m_D} \\ &\quad - \alpha m_D, \end{aligned} \quad (9)$$

where $\hat{s} = rm_D$. In the limit $\hat{s} \ll 1$, we have

$$\text{Re } V_{(iso)}(\hat{s}, T) \approx -\frac{2\sigma}{m_D \hat{s}} - \alpha m_D. \quad (10)$$

2.2. *Imaginary Part of the Potential in the Isotropic Medium.* To obtain the imaginary part of the potential in the QGP medium, the temporal component of the symmetric propagator in the static limit has been considered, which reads [29, 30]

$$\text{Im } D_{F(iso)}^{00}(0, k) = \frac{-2\pi T m_D^2}{k(k^2 + m_D^2)^2}. \quad (11)$$

Now the imaginary part of the dielectric function in the QGP medium is

$$\frac{1}{\epsilon(k)} = \pi T m_D^2 \frac{k^2}{k(k^2 + m_D^2)^2}. \quad (12)$$

Afterwards, the imaginary part of the medium potential is easy to obtain owing to the definition of the potential (1) as done in [31]:

$$\begin{aligned} \text{Im } V(r, T) = & - \int \frac{d^3 \mathbf{k}}{(2\pi)^{3/2}} (e^{i\mathbf{k}\cdot\mathbf{r}} - 1) \\ & \times \left(-\sqrt{\frac{2}{\pi}} \frac{\alpha}{k^2} - \frac{4\sigma}{\sqrt{2\pi k^4}} \right) \frac{-\pi T m_D^2 k}{(k^2 + m_D^2)^2} \end{aligned} \quad (13)$$

After performing the integration, we find

$$\text{Im } V_{(iso)}(\hat{s}, T) = T \left(\frac{\alpha \hat{s}^2}{3} - \frac{\sigma \hat{s}^4}{30 m_D^2} \right) \log \left(\frac{1}{\hat{s}} \right), \quad (14)$$

where $(\hat{s}) = rm_D$.

2.3. *Effective Fugacity Quasi-Particle Model (EQPM).* In our calculation, we use the Debye mass m_D for full QCD:

$$\begin{aligned} m_D^2 = & g^2(T) T^2 \left[\left(\frac{N_c}{3} \times \frac{6 \text{PolyLog}[2, z_g]}{\pi^2} \right) \right. \\ & \left. + \left(\frac{N_f}{6} \times \frac{-12 \text{PolyLog}[2, -z_q]}{\pi^2} \right) \right]. \end{aligned} \quad (15)$$

Here, $g(T)$ is the QCD running coupling constant, $N_c = 3$ ($SU(3)$) and N_f is the number of flavors, the function $\text{PolyLog}[2, z]$ has the form $\text{PolyLog}[2, z] = \sum_{k=1}^{\infty} (z^k/k^2)$, and z_g is the quasi-gluon effective fugacity and z_q is quasi-quark effective fugacity. These distribution functions are isotropic in nature. These fugacities should not be confused with any conservation law (number conservation) and have merely been introduced to encode all the interaction effects at high temperature QCD. Both z_g and z_q have a very complicated temperature dependence and asymptotically reach to the ideal value unity [11]. The temperature dependence of z_g and z_q fits well to the form given below:

$$z_{g,q} = a_{q,g} \exp \left(-\frac{b_{g,q}}{x^2} - \frac{c_{g,q}}{x^4} - \frac{d_{g,q}}{x^6} \right). \quad (16)$$

Here $x = T/T_c$ and $a, b, c,$ and d are fitting parameters, for both EOS1 and EOS2. Here, EoS1 is the $O(g^5)$ hot QCD [13–15] and EoS2 is the $O(g^6 \ln(1/g))$ hot QCD EoS [16] in the quasi-particle description [10, 11], respectively. Now, the expressions for the Debye mass can be rewritten in terms of effective charges for the quasi-gluons and quarks as

$$m_D^2 = \begin{cases} Q_g^2 T^2 \frac{N_c}{3} & \text{for pure gauge,} \\ T^2 \left(\frac{N_c}{3} Q_g^2 \right) + \left(\frac{N_f}{6} Q_q^2 \right) & \text{for full QCD} \end{cases} \quad (17)$$

where Q_g and Q_q are the effective charges given by the equations:

$$\begin{aligned} Q_g^2 &= g^2(T) \frac{6 \text{PolyLog}[2, z_g]}{\pi^2} \\ Q_q^2 &= g^2(T) \frac{-12 \text{PolyLog}[2, -z_q]}{\pi^2}. \end{aligned} \quad (18)$$

In our present analysis we had used the temperature dependence of the quasi-particle Debye mass, m_D^{QP} , in full QCD with $N_f = 3$ to determine charmonium suppression in an expanding, dissipative strongly interacting QGP medium. This quasi-particle Debye mass, m_D^{QP} , has the following form:

$$\begin{aligned} m_D^{\text{QP}} = & \frac{2}{\pi^2} g(T) T \left[\frac{N_c}{3} \text{PolyLog}[2, z_g] \right. \\ & \left. - N_f \text{PolyLog}[2, -z_q] \right]^{1/2}. \end{aligned} \quad (19)$$

3. Binding Energy and Dissociation Temperature

To obtain the binding energies with heavy quark potential, we need to solve the Schrödinger equation numerically. In the limiting case discussed earlier, the medium modified potential resembles to the hydrogen atom problem [1]. The solution of the Schrödinger equation gives the eigenvalues for the ground states and the first excited states in charmonium ($J/\psi, \psi'$, etc.) and bottomonium (Υ, Υ' , etc.) spectra:

$$\text{Re } E_{\text{bin}}^{\text{iso}} \stackrel{\hat{s} \gg 1}{=} \left(\frac{m_Q \sigma^2}{m_D^4 \pi^2} + \alpha m_D \right); \quad n = 1, 2, \dots \quad (20)$$

where m_Q is the mass of the heavy quark.

In our analysis, we have fixed the critical temperature ($T_c = 0.197 \text{ GeV}$) and have taken the quark masses m_Q , as $m_\Upsilon = 4.5 \text{ GeV}$, $m_{\Upsilon'} = 5.01 \text{ GeV}$, and $m_{\chi_b} = 5.18 \text{ GeV}$, as calculated in [32], and the string tension (σ) is taken as 0.184 GeV^2 . Let us now proceed to the computation of the dissociation temperatures for the above-mentioned quarkonia bound states.

As we know, dissociation of a quarkonia bound state in a thermal QGP medium will occur whenever the binding energy, E_B , of the said state will fall below the mean thermal energy of a quasi-parton. In such situations, the thermal effect can dissociate the quarkonia bound state. To obtain

TABLE 1: Dissociation temperature T_D (for a 3-flavor QGP), using quasi-particle Debye mass for bottomonium states, for EoS1.

State	τ_F	T_D	$c_s^2(\text{SIQGP})$	$c_s^2(\text{Id})$	$\epsilon_s(\text{SIQGP})$	$\epsilon_s(\text{Id})$
Υ	0.76	1.98	0.335	1/3	24.39	23.89
Υ'	1.90	1.53	0.326	1/3	8.28	8.16
χ_b	2.60	1.61	0.331	1/3	10.21	10.10

TABLE 2: Dissociation temperature T_D (for a 3-flavor QGP), using quasi-particle Debye mass for bottomonium states, for EoS2.

State	τ_F	T_D	$c_s^2(\text{SIQGP})$	$c_s^2(\text{Id})$	$\epsilon_s(\text{SIQGP})$	$\epsilon_s(\text{Id})$
Υ	0.76	2.04	0.335	1/3	27.05	27.09
Υ'	1.90	1.58	0.328	1/3	9.35	9.44
χ_b	2.60	1.65	0.331	1/3	11.21	11.34

the lower bound of the dissociation temperatures of the various quarkonia states, the (relativistic) thermal energy of the partons will be $3T$. The dissociation is supposed to occur whenever

$$\text{Re } E_{\text{bin}}^{\text{iso}} \stackrel{\hat{s} \gg 1}{\approx} E_B(T_D) = 3T_D. \quad (21)$$

T_D 's for the $b\bar{b}$ states Υ , Υ' , and χ_b with the dissociation temperature are listed in Tables 1 and 2 for EoS1 and EoS2, respectively. We observe that (on the basis of temperature dependence of binding energy) Υ' dissociates at lower temperatures as compared to Υ and χ_b for both the equations of state.

4. Formulation

In relativistic nucleus-nucleus collisions, the equation of state for the quark matter is an important observable and the properties of the matter are sensitive to it. The expansion of QGP is quite sensitive to EoS through the speed of sound and explores the sensitivity of the quarkonium suppression to the equation of state [33, 34].

For a strongly coupled QGP, Bannur [17] developed an equation of state by incorporating running coupling constant and did an appropriate modification to take account of color and flavor degrees of freedom and obtained a reasonably good fit to the lattice results. Now we will discuss briefly the equation of state which is expressed as a function of plasma parameter Γ [35]:

$$\epsilon_{\text{QED}} = \left(\frac{3}{2} + u_{\text{ex}}(\Gamma) \right) nT. \quad (22)$$

Plasma parameter Γ is the ratio of average potential energy to average kinetic energy of particles, is assumed to be weak ($\ll 1$), and is given by

$$\Gamma \equiv \frac{\langle PE \rangle}{\langle KE \rangle} = \frac{\text{Re}[V(\mathbf{r}, T)]}{T}. \quad (23)$$

We have studied the variation of plasma parameter with temperature and as well with the number of flavors that are

present in the system and shown in Figure 1 for EoS1 and EoS2, respectively. As the temperature increases, potential becomes weaker and hence the plasma parameters have started waning; albeit at very large temperature it increases slightly due to the contribution coming from the (positive) finite-range terms in the potential, unlike the decreasing trend in Bannur model [17] always due to the presence of Coulomb interaction alone in the deconfined phase.

Let us consider that hadron exists for $T < T_c$ and goes to QGP for $T > T_c$ for strongly coupled plasma in QCD. As it was assumed that confinement interactions due to QCD vacuum have been melted [17] at $T = T_c$ and thus for $T > T_c$, there are the strongly interacting plasma of quarks and gluons and no glue balls or hadrons. After inclusion of relativistic and quantum effects, the equation of state which has been obtained in the plasma parameter can be written as

$$\epsilon = (3 + u_{\text{ex}}(\Gamma)) nT. \quad (24)$$

Now, the scaled-energy density is written as in terms of ideal contribution

$$e(\Gamma) \equiv \frac{\epsilon}{\epsilon_{\text{SB}}} = 1 + \frac{1}{3} u_{\text{ex}}(\Gamma), \quad (25)$$

where ϵ_{SB} is given by

$$\epsilon_{\text{SB}} \equiv \frac{(16 + 21n_f/2) \pi^2 T^4}{30}. \quad (26)$$

Here, n_f is the number of flavors of quarks and gluons. Now, we will employ two-loop level QCD running coupling constant in $\overline{\text{MS}}$ scheme [36]:

$$g^2(T) \approx 2b_0 \ln \frac{\bar{\mu}}{\Lambda_{\overline{\text{MS}}}} \left(1 + \frac{b_1}{2b_0^2} \frac{\ln(2 \ln(\bar{\mu}/\Lambda_{\overline{\text{MS}}})}{\ln(\bar{\mu}/\Lambda_{\overline{\text{MS}}})} \right)^{-1}. \quad (27)$$

Here $b_0 = (33 - 2n_f)/(48\pi^2)$ and $b_1 = (153 - 19n_f)/(384\pi^4)$. In $\overline{\text{MS}}$ scheme, $\Lambda_{\overline{\text{MS}}}$ and $\bar{\mu}$ are the renormalization scale and the scale parameter, respectively. For the EoS to depend on the renormalization scale, the physical observables should be scale independent. We invade the problem by trading off the dependence on renormalization scale ($\Lambda_{\overline{\text{MS}}}$) to a dependence on the critical temperature T_c .

$$\bar{\mu} \exp(\gamma_E + c) = \Lambda_{\overline{\text{MS}}}(T) \quad (28)$$

$$\Lambda_{\overline{\text{MS}}}(T) \exp(\gamma_E + c) = 4\pi\Lambda_T,$$

where $\gamma_E = 0.5772156$ and $c = (n_c - 4n_f \ln 4)/(22n_c - n_f)$, which is a constant depending on colors and flavors. There are several uncertainty, associated with the scale parameter $\bar{\mu}$ and renormalization scale $\Lambda_{\overline{\text{MS}}}$, which occurs in the expression used for the running coupling constant α_s . This issue has been considered well in literature and resolved by the BLM criterion due to Brodsky, Lepage, and Mackenzie [37]. $\Lambda_{\overline{\text{MS}}}$ is allowed to vary between πT and $4\pi T$ [38]. For our motive, we choose $\Lambda_{\overline{\text{MS}}}$ close to the central value $2\pi T_c$ [39] for $n_f = 0$

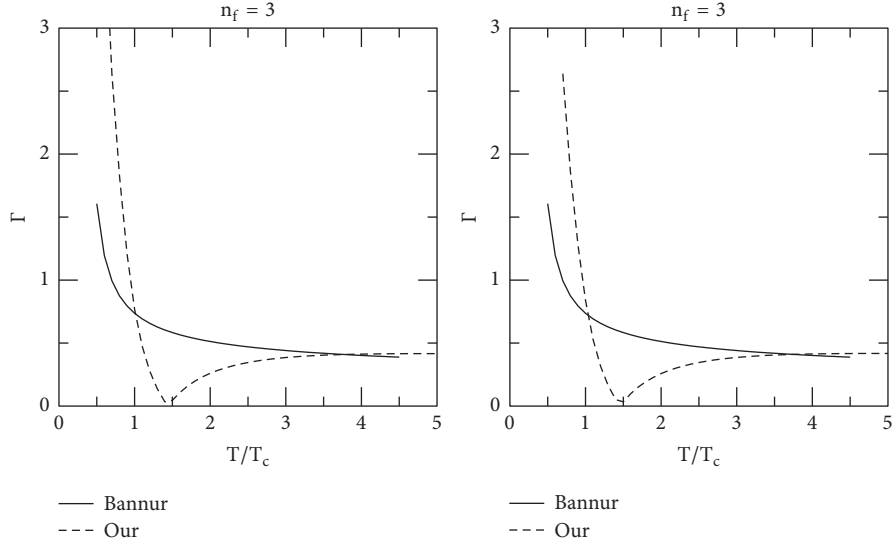


FIGURE 1: Plots of Γ as a function of T/T_c for 3-flavor QGP (extreme left figure) for EOS1 [13–15] and for EOS2 [16] (extreme right figure). In each figure, solid line represents the results obtained from Bannur EoS, and dashed line represents the results from our EoS (using quasi-particle Debye mass).

and for both $n_f=2$ and $n_f=3$ flavors the value is πT_c . If the factor $(b_1/2b_0^2)(\ln(2\ln(\bar{\mu}/\Lambda_{\overline{MS}}))/\ln(\bar{\mu}/\Lambda_{\overline{MS}}))$ is $\ll 1$, then the above expression reduces to the expression used in [17, Eq. (10)], after neglecting the higher order terms of the above factor. However, this possibility does not hold good for the temperature ranges used in the calculation and causes an error in coupling which finally makes the difference in the results between our model and Bannur model [17]. First of all, we will calculate the energy density $\epsilon(T)$ from (25) and using the thermodynamic relation

$$\epsilon = T \frac{dp}{dT} - P, \quad (29)$$

we calculated the pressure as

$$\frac{P}{T^4} = \frac{(P_0/T_0 + 3a_f \int_{T_0}^T d\tau \tau^2 e(\Gamma(\tau)))}{T^3}, \quad (30)$$

where P_0 is the pressure at some reference temperature T_0 . Now, the speed of sound $c_s^2 (= dP/d\epsilon)$ can be calculated once we know the pressure P and energy density ϵ .

5. Survival of Bottomonium State

In order to derive the Υ survival probability for an expanding QGP firstly, we explore the effects of dissipative terms up to first order in the stress-tensor. In the presence of viscous forces, the energy-momentum tensor is written as

$$T^{\mu\nu} - \pi^{\mu\nu} = (\epsilon + p) u^\mu u^\nu + g^{\mu\nu} p, \quad (31)$$

where the stress-energy tensor, $\pi^{\mu\nu}$, up to first order is given by

$$\pi^{\mu\nu} = \eta \langle \nabla^\mu u^\nu \rangle, \quad (32)$$

where η is the coefficient of the shear viscosity and $\langle \nabla^\mu u^\nu \rangle$ is the symmetrized velocity gradient.

In Bjorken expansion, the equation of motion is given by

$$\partial_\tau \epsilon + \frac{\epsilon + P}{\tau} = \frac{4\eta}{3\tau^2}. \quad (33)$$

The solution of equation of motion (33) is given as

$$\begin{aligned} \epsilon(\tau) \tau^{(1+c_s^2)} + \frac{4a}{3\bar{\tau}^2} \tau^{(1+c_s^2)} &= \epsilon(\tau_i) \tau_i^{(1+c_s^2)} + \frac{4a}{3\bar{\tau}_i^2} \\ &= \text{const}, \end{aligned} \quad (34)$$

where the constant is

$$a = \left(\frac{\eta}{s}\right) T_i^3 \tau_i \quad (35)$$

and the symbols are

$$\bar{\tau}^2 = (1 - c_s^2) \tau^2 \quad (36)$$

and

$$\bar{\tau}_i^2 = (1 - c_s^2) \tau_i^2. \quad (37)$$

The first term accounts for the contributions coming from the zeroth-order expansion (ideal fluid) and the second term is the first-order viscous corrections. We now have all the ingredients to write down the survival probability. Chu and Matsui [40] studied the transverse momentum dependence (p_T) of the survival probability by choosing the speed of sound $c_s^2 = 1/3$ (ideal EoS) and the extreme value $c_s^2 = 0$. Instead of taking arbitrary values of c_s^2 , we tabulated the values of c_s^2 in Tables 1 and 2 corresponding to the dissociation

temperatures for bottomonium states for EOS1 and EOS2. One can define initial energy density ϵ_i as

$$\epsilon_i = (1 + \beta) \langle \epsilon_i \rangle; \quad \beta = 1. \quad (38)$$

Here, β represents the proportionality of the deposited energy to the nuclear thickness where $\langle \epsilon_i \rangle$ is the average initial energy density and will be given by the modified Bjorken formula [41, 42]:

$$\langle \epsilon_i \rangle = \frac{\xi}{A_T \tau_i} \left(\frac{dE_T}{dy_h} \right)_{y_h=0}, \quad (39)$$

where A_T is the transverse overlap area of the colliding nuclei and $(dE_T/dy_h)_{y_h=0}$ is the transverse energy deposited per unit rapidity. We use the experimental value of the transverse overlap area A_T and the pseudo-rapidity distribution $dE_T/d\eta_h|_{\eta_h=0}$ [43, 44] at various values of number of participants N_{part} . These $dE_T/d\eta_h|_{\eta_h=0}$ numbers are then multiplied by a Jacobian 1.25 to yield the rapidity distribution $dE_T/dy_h|_{y_h=0}$ which will be further used to calculate the average initial energy density from Bjorken formula (39). After getting the value of average initial energy density we can obtain the initial energy density from formula (38). The scaling factor $\xi = 5$ has been introduced in order to obtain the desired values of initial energy densities [45, 46] for most central collision which are consistent with the predictions of the self-screened parton cascade model [47] and also with the requirements of hydrodynamic simulation [45, 46] to fit the pseudo-rapidity distribution of charged particle multiplicity $dN_{ch}/d\eta$ for various centralities observed in PHENIX experiments at RHIC energy. Let ϕ be the angle between the transverse momentum and position vector r_Y . Now assuming that $b\bar{b}$ is formed inside screening region at a point whose position vector is \vec{r} and moves with transverse momentum p_T making an azimuthal angle, then the condition for escape of $b\bar{b}$ without forming bottomonium states is expressed as

$$\cos \phi \geq Y; \quad Y = \frac{(r_s^2 - r_Y^2)m - \tau_F^2 p_T^2 / m}{2r_Y \tau_F p_T}, \quad (40)$$

where r_Y is the position vector at which the bottom, anti-bottom quark pair is formed, τ_F is the proper formation time required for the formation of bound states of $b\bar{b}$ from correlated $b\bar{b}$ pair, and m is the mass of bottomonia ($m = M_Y, M_{\chi_b}, M_{Y'}$ for different resonance states of bottomonium). Assume the radial probability distribution for the production of $b\bar{b}$ pair in hard collisions at transverse distance r as

$$f(r) \propto \left(1 - \frac{r^2}{R_T^2} \right)^\alpha \theta(R_T - r). \quad (41)$$

Here we take $\alpha = 0.5$ in our calculation as used in [40]. Then, in the color screening scenario, the survival probability for

the bottomonium in QGP medium can be expressed as [40, 48, 49]

$$S(p_T, N_{part}) = \frac{2(\alpha + 1)}{\pi R_T^2} \int_0^{R_T} dr r \phi_{max}(r) \left\{ 1 - \frac{r^2}{R_T^2} \right\}^\alpha, \quad (42)$$

where the maximum positive angle ϕ_{max} allowed by (26) becomes [50]

$$\phi_{max}(r) = \begin{cases} \pi & \text{if } Y \leq -1 \\ \pi - \cos^{-1}|Y| & \text{if } 0 \geq Y \geq -1 \\ \cos^{-1}|Y| & \text{if } 0 \leq Y \leq 1 \\ 0 & \text{if } Y \geq 1 \end{cases} \quad (43)$$

since the experimentalists always measure the quantity, namely, p_T integrated nuclear modification factor. We get the theoretical p_T integrated survival probability as follows:

$$S(N_{part}) = \frac{\int_{p_{Tmin}}^{p_{Tmax}} S(p_T, N_{part}) dp_T}{\int_{p_{Tmin}}^{p_{Tmax}} dp_T}. \quad (44)$$

In nucleus-nucleus collisions, it is known that only about 60% of the observed Y originate directly in hard collisions while 30% of them come from the decay of χ_b and 10% from the decay of Y' . Hence, the p_T -integrated inclusive survival probability of Y in the QGP becomes [33, 51]

$$\langle S^{incl} \rangle = 0.6 \langle S^{dir} \rangle_Y + 0.3 \langle S^{dir} \rangle_{\chi_b} + 0.1 \langle S^{dir} \rangle_{Y'}, \quad (45)$$

6. Results and Discussions

In our results, we had obtained the variation of plasma parameter with temperature and as well with the number of flavors that are present in the system and shown in Figure 1 for EoS1 and EoS2, respectively. After that, in Figure 2, we have plotted the variation of pressure (P/T^4) with temperature (T/T_c) using EoS1 and EoS2 for 3-flavor QGP along with Bannur EoS [17] and compared it with lattice results [17–21]. For each flavor, g_c and Λ_T are adjusted to get a good fit to lattice results in Bannur model. Now, energy density ϵ , speed of sound c_s^2 , and so forth can be derived since we had obtained the pressure, $P(T)$. In Figure 3, we had plotted the energy density (ϵ/T^4) with temperature (T/T_c) using EoS1 [13–15] and EoS2 for 3-flavor QGP along with Bannur EoS [17] and compared it with lattice result [17–21]. In Figure 4, the speed of sound, c_s^2 , is plotted using EoS1 and EoS2 for 3-flavor QGP along with Bannur EoS [17]. Since lattice results are not available for 3 flavors, therefore comparison has not been checked for the above-mentioned flavor. Our flavored results match excellent with the lattice results.

In this paper, we had calculated the dissociation temperatures for the bottomonium states (Y, Y', χ_b , etc.), by modifying the Cornell potential and incorporating the quasi-particle Debye mass. On that dissociation temperature, we

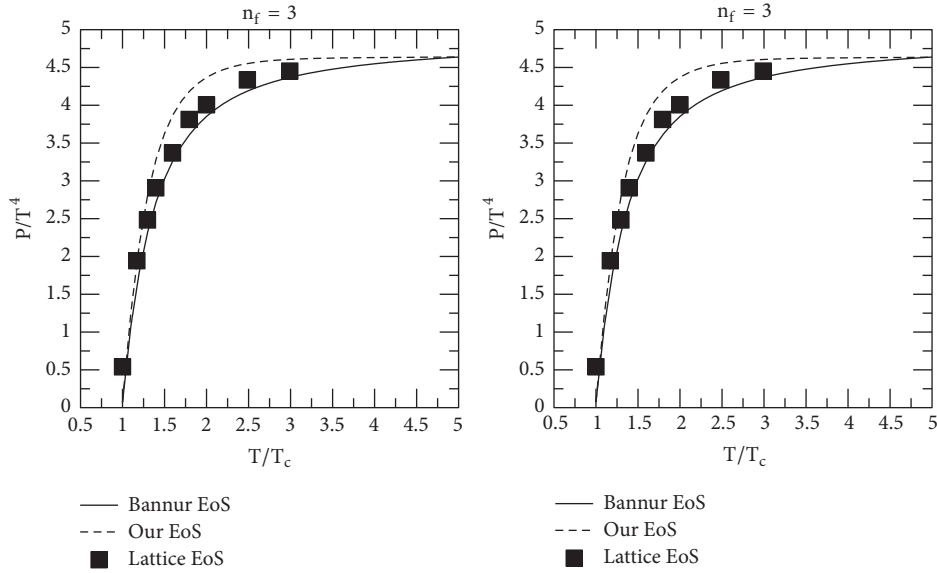


FIGURE 2: Plots of P/T^4 as a function of T/T_c for 3-flavor QGP (extreme left figure) for EOS1 [13–15] and for EOS2 [16] (extreme right figure). In each figure, solid line represents the results obtained from Bannur EoS, dashed line represents the results from our EoS, and diamond symbols represent lattice results [17–21].

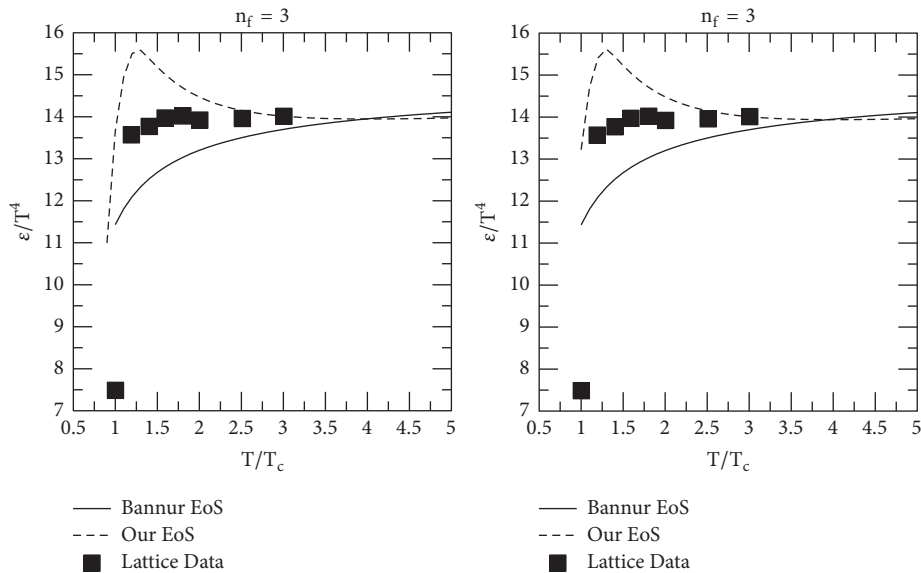


FIGURE 3: Plots of ϵ/T^4 as a function of T/T_c for our EoS (using quasi-particle Debye mass) and lattice results [17–21] for 3-flavor QGP (extreme left figure) for EoS1 [13–15] and for EOS2 [16] (extreme right figure). The notations are the same as Figure 2.

had calculated the screening energy densities, ϵ_s , and the speed of sound c_s^2 which are also listed in Tables 1 and 2 for both EoS1 and EoS2, respectively. We observe from Tables 1 and 2 that the value of ϵ_s is different for different bottomonium states and varies from one EoS to other. If $\epsilon_s \geq \epsilon_i$, initial energy density, then there will be no suppression at all, i.e., survival probability, $S(p_T)$, is equal to 1. With this physical understanding, we analyze our results, $\langle S(p_T) \rangle$, as a function of the number of participants N_{part} in an expanding QGP.

Here we are using the values as inputs listed in Tables 1 and 2, to calculate $\langle S(p_T) \rangle$ for both EOS1 and EOS2, respectively. The experimental data (the nuclear modification factor R_{AA}) are shown by the squares with error bars whereas circles represent sequential suppression. We had compared our results with the experimental results for the case of $\eta/s = 0.08$ for both EoS1 and EoS2 and found good agreement. We observe from Figures 5–10 that $\langle S(p_T) \rangle$ for both the directly and sequentially produced Upsilon (Y) are quite high with the higher values of T_D 's which is obtained from EOS2 (in

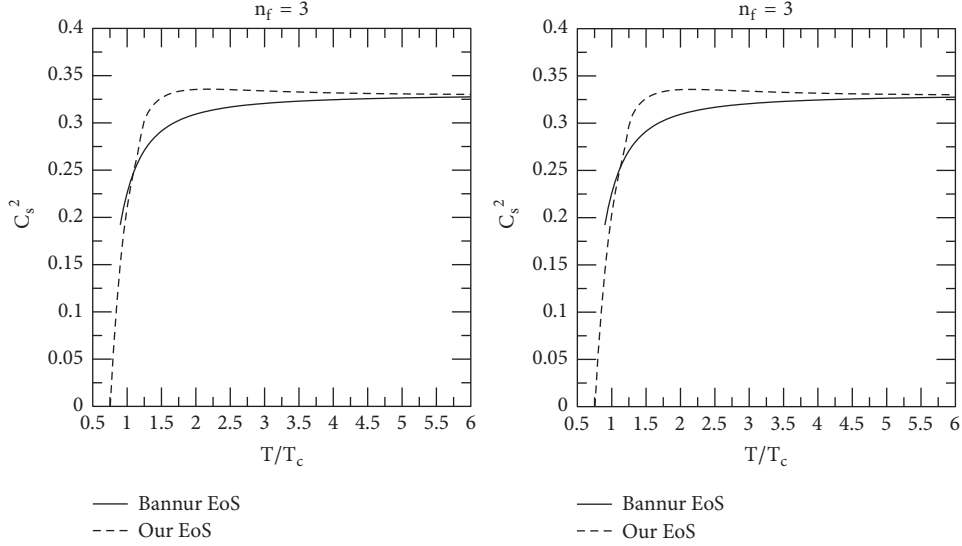


FIGURE 4: Plots of c_s^2 as a function of T/T_c for Bannur EoS, our EoS (using quasi-particle Debye mass) for 3-flavor QGP (extreme left figure) for EoS1 [13–15] and for EoS2 [16] (extreme right figure). The notations are the same as Figure 2.

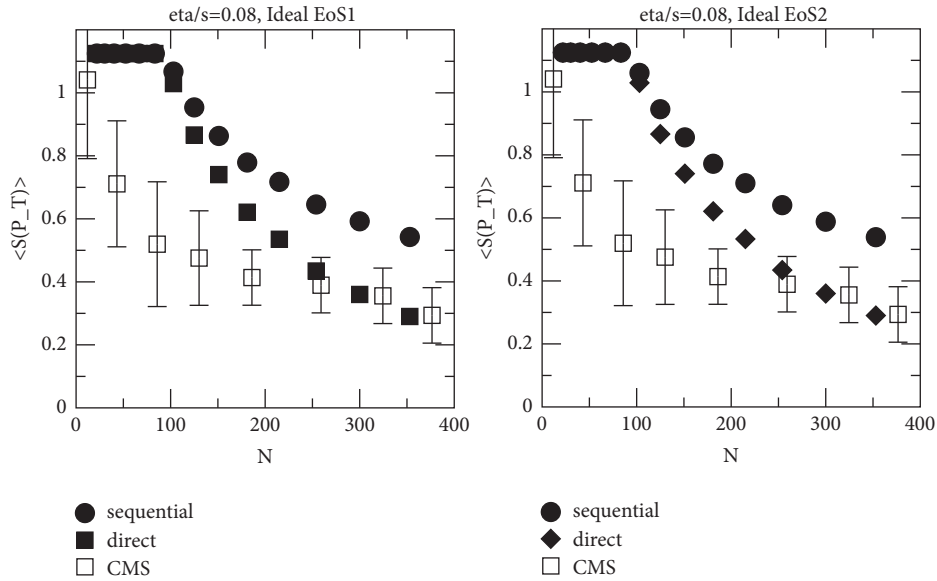


FIGURE 5: The variation of p_T integrated survival probability versus N for Y at $\sqrt{S_{NN}} = 2.76$ TeV with preliminary CMS data [22]. The experimental data are shown by the squares with error bars whereas circles and diamond represent ($\langle S^{\text{incl}} \rangle$) without ($\langle S^{\text{dir}} \rangle$) sequential melting using the value of T_D 's and related parameters from Tables 1 and 2 for ideal equation of state. Left panel shows EoS1 and right panel shows EoS2.

Table 2) compared to EOS1 (in Table 1) for both SIQGP and ideal equation of states. We find that the survival probability of sequentially produced Y is slightly higher compared to the directly produced Y and is closer to the experimental results. We also observed that sequentially produced Y nicely matches for the EOS1 compared to the EOS2. The smaller value of screening energy density ϵ_s causes an increase in the screening time and results in more suppression to match with the experimental results.

7. Conclusions

We studied the equation of state for strongly interacting quark-gluon plasma in the framework of strongly coupled plasma with appropriate modifications to take account of color and flavor degrees of freedom and QCD running coupling constant. In addition, we incorporate the nonperturbative effects in terms of nonzero string tension in the deconfined phase, unlike the Coulomb interactions alone

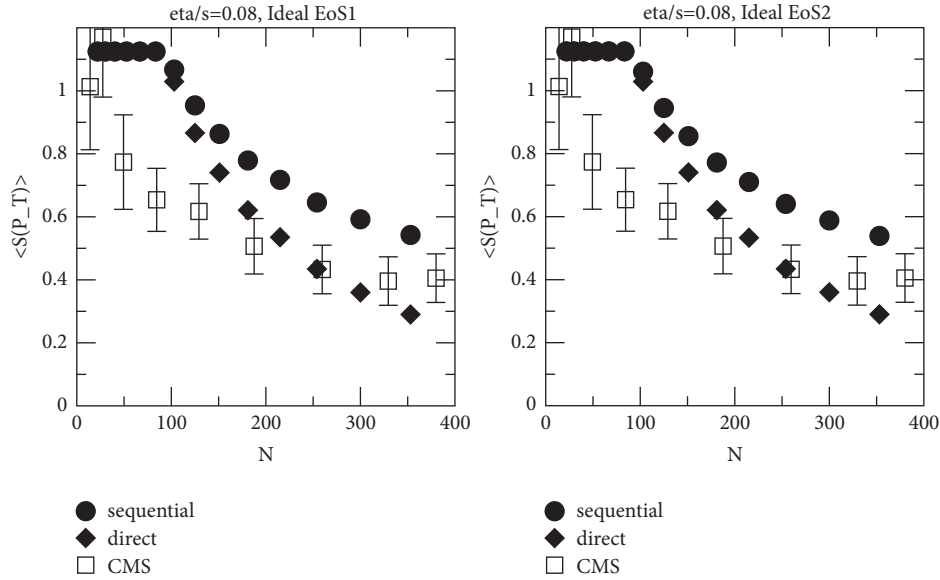


FIGURE 6: Same as Figure 5 but the variation of p_T integrated survival probability versus N for Υ at $\sqrt{s_{NN}} = 5.02$ TeV with preliminary CMS data [23].

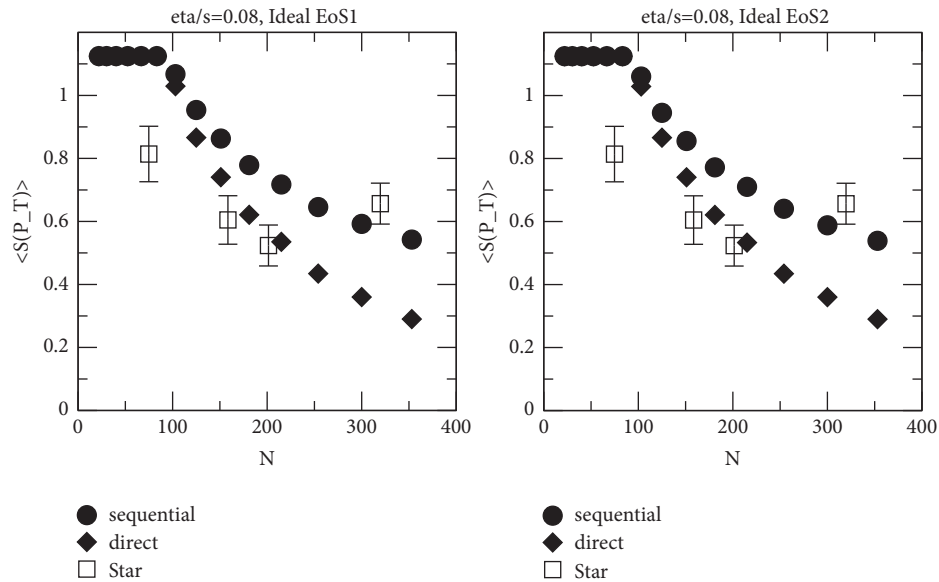


FIGURE 7: Same as Figure 5 but the variation of p_T integrated survival probability versus N for Υ at $\sqrt{s_{NN}} = 200$ GeV with preliminary STAR data [24].

in the deconfined phase beyond the critical temperature. Our results on thermodynamic observables, *namely*, pressure, energy density, and speed of sound, nicely fit the results of lattice equation of state. We had then calculated the dissociation temperatures for the bottomonium states (Υ , Υ' , χ_b , etc.), by incorporating the quasi-particle Debye mass. On that dissociation temperature, we had calculated the screening energy densities, ϵ_s , and the speed of sound c_s^2 which are listed in Tables 1 and 2 for both EoS1 and EoS2, respectively. By using the above quantities as an input, we have then studied the sequential suppression for bottomonium

states at the LHC energy in a longitudinally expanding partonic system, which underwent through the successive preequilibrium and equilibrium phases in the presence of dissipative forces. Bottomonium suppression in nucleus-nucleus collisions compared to p - p collisions couples the in-medium properties of the bottomonia states with the dynamics of the expanding medium. We have found a good agreement with the experimental data from RHIC 200GeV/nucleon Au-Au collisions, LHC 2.76 TeV/nucleon Pb-Pb, and LHC 5.02 TeV/nucleon Pb-Pb collisions [52, 53]. Here our attempt is to understand Υ suppression systematically in SIQGP in

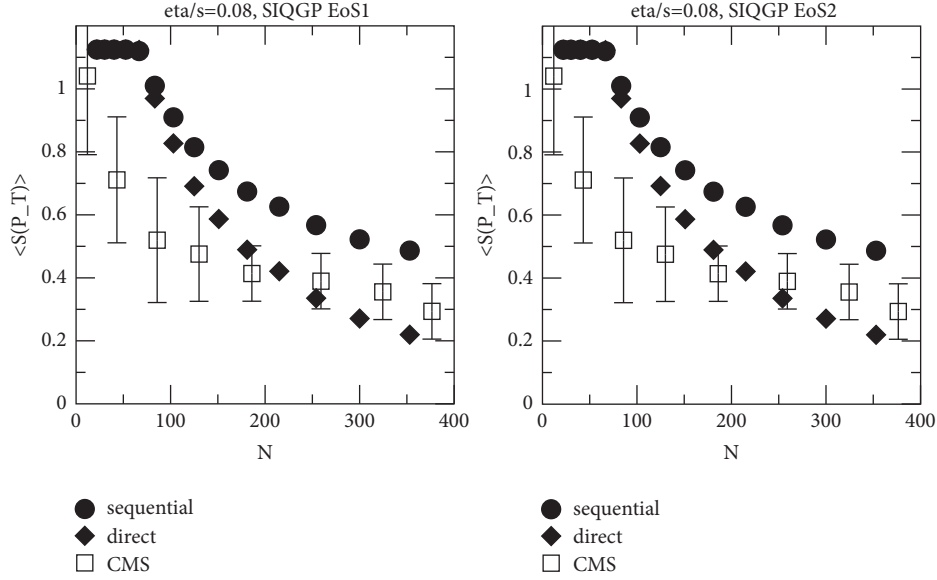


FIGURE 8: The variation of p_T integrated survival probability versus N for Υ at $\sqrt{s_{NN}} = 2.76$ TeV with preliminary CMS data [22]. The experimental data are shown by the squares with error bars whereas circles and diamond represent ($\langle S^{\text{incl}} \rangle$) without ($\langle S^{\text{dir}} \rangle$) sequential melting using the value of T_D 's and related parameters from Tables 1 and 2 for SIQGP equation of state. Left panel shows EoS1 and right panel shows EoS2.

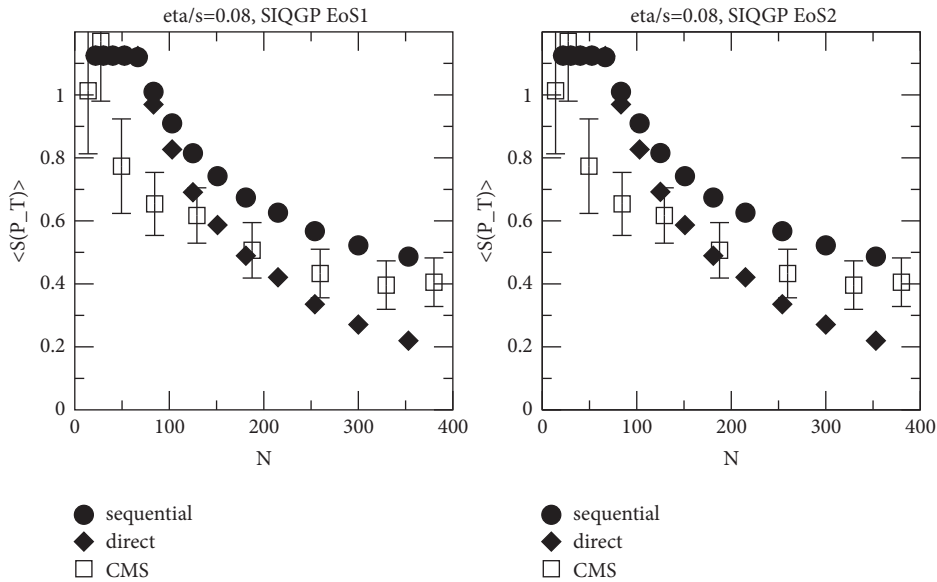


FIGURE 9: Same as Figure 8 but the variation of p_T integrated survival probability versus N for Υ at $\sqrt{s_{NN}} = 5.02$ TeV with preliminary CMS data [23].

anisotropic medium. It would be of interest to extend the present study by incorporating the contributions of the bulk viscosity. These issues will be taken up separately in the near future.

Data Availability

The data used to support the findings of this study are available from the corresponding author upon request.

Conflicts of Interest

The authors declare that they have no conflicts of interest.

Acknowledgments

Vineet Kumar Agotiya acknowledges the UGC-BSR research start up Grant no. F.30-14/2014 (BSR), New Delhi. The authors record their sincere gratitude to the people of India for their generous support for the research in basic sciences.

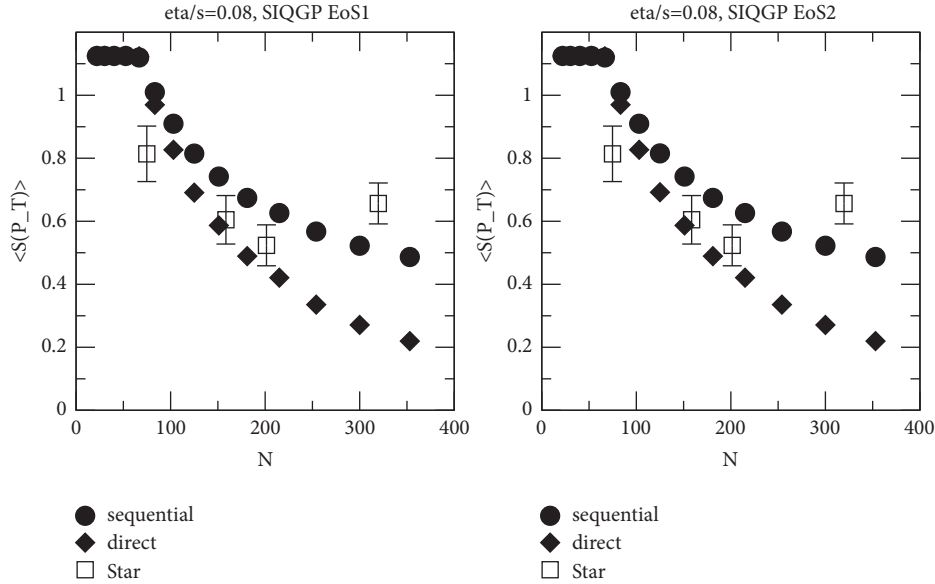


FIGURE 10: Same as Figure 8 but the variation of p_T integrated survival probability versus N for Y at $\sqrt{s_{NN}} = 200$ GeV with preliminary STAR data [24].

References

- [1] T. Matsui and H. Satz, “ J/ψ suppression by quark-gluon plasma formation,” *Physics Letters B*, vol. 178, no. 4, pp. 416–422, 1986.
- [2] F. Karsch, M. T. Mehr, and H. Satz, “Color screening and deconfinement for bound states of heavy quarks,” *Zeitschrift für Physik C Particles and Fields*, vol. 37, no. 4, pp. 617–622, 1988.
- [3] F. Karsch and H. Satz, “The spectral analysis of strongly interacting matter,” *Zeitschrift für Physik C: Particles and Fields*, vol. 51, no. 2, pp. 209–224, 1991.
- [4] STAR Collaboration, J. Adams, M. M. Aggarwal et al., “Experimental and theoretical challenges in the search for the quark-gluon plasma: The STAR Collaboration’s critical assessment of the evidence from RHIC collisions,” *Nuclear Physics A*, vol. 757, no. 1-2, pp. 102–183, 2005.
- [5] PHENIX Collaboration, K. Adcox, S. S. Adler et al., “Formation of dense partonic matter in relativistic nucleus-nucleus collisions at RHIC: Experimental evaluation by the PHENIX Collaboration,” *Nuclear Physics A*, vol. 757, no. 1-2, pp. 184–283, 2005.
- [6] B. B. Back, M. D. Baker, and M. Ballintijn, “The PHOBOS perspective on discoveries at RHIC,” *Nuclear Physics A*, vol. 757, no. 1-2, pp. 28–101, 2005.
- [7] H.-J. Drescher, A. Dumitru, C. Gombeaud, and J.-Y. Ollitrault, “Centrality dependence of elliptic flow, the hydrodynamic limit, and the viscosity of hot QCD,” *Physical Review C: Nuclear Physics*, vol. 76, no. 2, Article ID 024905, 2007.
- [8] E. Shuryak, “Toward the theory of strongly coupled quark-gluon plasma,” *Nuclear Physics A*, vol. 774, pp. 387–396, 2006.
- [9] P. K. Kovtun, D. T. Son, and A. O. Starinets, “Viscosity in strongly interacting quantum field theories from black hole physics,” *Physical Review Letters*, vol. 94, no. 11, Article ID 111601, 2005.
- [10] V. Chandra, A. Ranjan, and V. Ravishankar, “On the chromoelectric permittivity and Debye screening in hot QCD,” *European Physical Journal A*, vol. 40, no. 1, pp. 109–117, 2009.
- [11] V. Chandra, R. Kumar, and V. Ravishankar, “Hot QCD equations of state and relativistic heavy ion collisions,” *Physical Review C*, vol. 76, no. 6, Article ID 054909, 2007.
- [12] V. Chandra and V. Ravishankar, “Quasi-particle model for lattice QCD: quark-gluon plasma in heavy ion collisions,” *The European Physical Journal C*, vol. 64, no. 1, pp. 63–72, 2009.
- [13] C. Zhai and B. Kastening, “Free energy of hot gauge theories with fermions through,” *Physical Review D: Particles, Fields, Gravitation and Cosmology*, vol. 52, no. 12, pp. 7232–7246, 1995.
- [14] P. Arnold and C. Zhai, “Three-loop free energy for pure gauge QCD,” *Physical Review D: Particles, Fields, Gravitation and Cosmology*, vol. 50, no. 12, pp. 7603–7623, 1994.
- [15] P. Arnold and C. Zhai, “Three-loop free energy for high-temperature QED and QCD with fermions,” *Physical Review D: Particles, Fields, Gravitation and Cosmology*, vol. 51, no. 4, pp. 1906–1918, 1995.
- [16] K. Kajantie, M. Laine, K. Rummukainen, and Y. Schröder, “Pressure of hot QCD up to,” *Physical Review D: Particles, Fields, Gravitation and Cosmology*, vol. 67, no. 10, Article ID 105008, 2003.
- [17] V. M. Bannur, “Strongly coupled quark gluon plasma (SCQGP),” *Journal of Physics G: Nuclear and Particle Physics*, vol. 32, no. 7, article 993, 2006.
- [18] G. Boyd, J. Engels, and F. Karsch, “Equation of state for the SU(3) gauge theory,” *Physical Review Letters*, vol. 75, no. 23, pp. 4169–4172, 1995.
- [19] G. Boyd, J. Engels, F. Karsch et al., “Thermodynamics of SU(3) lattice gauge theory,” *Nuclear Physics B*, vol. 469, no. 3, pp. 419–444, 1996.
- [20] F. Karsch et al., “Lattice QCD at high temperature and density,” *Lecture Notes in Physics*, vol. 583, pp. 209–249, 2002, <https://arxiv.org/abs/hep-lat/0106019>.
- [21] A. Bazavov, T. Bhattacharya, M. Cheng et al., “Equation of state and QCD transition at finite temperature,” *Physical Review Journals*, vol. 80, Article ID 014504, 2009, <https://arxiv.org/abs/0903.4379>.

- [22] CMS Collaboration Twiki, CMS-PAS-HIN-10-006, 2015.
- [23] Chad Flores (ALICE Collaboration), “Quark matter,” 2017, <https://goo.gl/imTtmM>.
- [24] Ye. Zaochen (STAR Collaboration, URL <https://goo.gl/XgqSgG>), “Quark matter 2017.”
- [25] V. Agotiya, V. Chandra, and B. K. Patra, “Dissociation of quarkonium in a hot QCD medium: modification of the interquark potential,” *Physical Review C: Nuclear Physics*, vol. 80, no. 2, Article ID 025210, 2009.
- [26] R. A. Schneider, “Debye screening at finite temperature reexamined,” *Physical Review D*, vol. 66, Article ID 036003, 2002.
- [27] H. A. Weldon, “Covariant calculations at finite temperature: the relativistic plasma,” *Physical Review D: Particles, Fields, Gravitation and Cosmology*, vol. 26, no. 6, pp. 1394–1407, 1982.
- [28] J. I. Kapusta and C. Gale, *Finite Temperature Field Theory Principle and Applications*, Cambridge University Press, Cambridge, UK, 2nd edition, 1996.
- [29] Y. Burnier, M. Laine, and M. Vepsäläinen, “Quarkonium dissociation in the presence of a small momentum space anisotropy,” *Physics Letters B*, vol. 678, no. 1, pp. 86–89, 2009.
- [30] V. K. Agotiya, V. Chandra, M. Y. Jamal, and I. Nilima, “Dissociation of heavy quarkonium in hot QCD medium in a quasiparticle model,” *Physical Review D: Particles, Fields, Gravitation and Cosmology*, vol. 94, no. 9, Article ID 094006, 2016.
- [31] L. Thakur, U. Kakade, and B. K. Patra, “Dissociation of quarkonium in a complex potential,” *Physical Review D: Particles, Fields, Gravitation and Cosmology*, vol. 89, no. 9, Article ID 094020, 2014.
- [32] V. M. Aulchenko, KEDR Collaboration et al., “New precision measurement of the J/ψ - and ψ' -meson masses,” *Physics Letters B*, vol. 573, pp. 63–79, 2003.
- [33] D. Pal, B. K. Patra, and D. K. Srivastava, “Determination of the equation of state of quark matter from J/ψ and Υ suppression at RHIC and LHC,” *The European Physical Journal C*, vol. 17, pp. 179–186, 2000.
- [34] B. K. Patra and D. K. Srivastava, “ J/ψ suppression: gluonic dissociation vs. colour screening,” *Physics Letters B*, vol. 505, no. 1-4, pp. 113–118, 2001.
- [35] S. Ichimaru, “Statistical plasma physics,” in *Condensed Plasma*, vol. 2, Addison-Wesley Publishing Company, New York, NY, USA, 1994.
- [36] M. Laine and Y. Schroder, “Two-loop QCD gauge coupling at high temperatures,” *Journal of High Energy Physics*, vol. 2005, no. 03, pp. 067–067, 2005.
- [37] S. Huang and M. Lissia, “The relevant scale parameter in the high temperature phase of QCD,” *Nuclear Physics B*, vol. 438, no. 1-2, pp. 54–66, 1995.
- [38] E. Braaten and A. Nieto, “Free energy of QCD at high temperature,” *Physical Review D: Particles, Fields, Gravitation and Cosmology*, vol. 53, no. 6, pp. 3421–3437, 1996.
- [39] A. Vuorinen, “The pressure of QCD at finite temperature and quark number density,” 2004, <https://arxiv.org/abs/hep-ph/0402242>.
- [40] M. Chu and T. Matsui, “Pattern of J/ψ suppression in ultrarelativistic heavy-ion collisions,” *Physical Review D: Particles, Fields, Gravitation and Cosmology*, vol. 37, no. 7, pp. 1851–1855, 1988.
- [41] B. Alessandro, C. Alexa, and R. Arnaldi, “A new measurement of J/ψ suppression in Pb-Pb collisions at 158 GeV per nucleon,” *The European Physical Journal C*, vol. 39, no. 3, pp. 335–345, 2005.
- [42] F. Karsch, D. Kharzeev, and H. Satz, “Sequential charmonium dissociation,” *Physics Letters B*, vol. 637, no. 1-2, pp. 75–80, 2006.
- [43] S. S. Adler, (PHENIX Collaboration) et al., “Systematic studies of the centrality and $\sqrt{s_{NN}}$ dependence of the $dE_T/d\eta$ and $dN_{ch}/d\eta$ in heavy ion collisions at midrapidity,” *Physical Review C*, vol. 71, Article ID 034908, 2005.
- [44] S. S. Adler, (PHENIX Collaboration) et al., “Systematic studies of the centrality and $\sqrt{s_{NN}}$ dependence of the $dE_T/d\eta$ and $dN_{ch}/d\eta$ in heavy ion collisions at midrapidity,” *Physical Review C*, vol. 71, Article ID 049901(E), 2005.
- [45] T. Hirano, “Is early thermalization achieved only near midrapidity in Au + Au collisions at $\sqrt{s_{NN}}=130\text{GeV}$?” *Physical Review C*, vol. 65, Article ID 011901, 2001.
- [46] T. Hirano and K. Tsuda, “Collective flow and two-pion correlations from a relativistic hydrodynamic model with early chemical freeze-out,” *Physical Review C: Nuclear Physics*, vol. 66, no. 5, Article ID 054905, 2002.
- [47] K. J. Eskola, K. Kajantie, P. V. Ruuskanen, and K. Tuominen, “Scaling of transverse energies and multiplicities with atomic number and energy in ultrarelativistic nuclear collisions,” *Nuclear Physics*, vol. 570, pp. 379–389, 2000.
- [48] M. Mishra, C. P. Singh, V. J. Menon, and R. K. Dubey, “ J/ψ suppression in Au+Au collisions at RHIC: colour screening scenario in the bag model at variable participant numbers,” *Physics Letters B*, vol. 656, pp. 45–50, 2007.
- [49] M. Mishra, C. P. Singh, and V. J. Menon, “ J/ψ suppression vs centrality at forward and mid-rapidity in Au+Au collisions at RHIC in colour screening mechanism,” *Indian Journal of Physics*, vol. 85, no. 6, pp. 849–853, 2011.
- [50] V. Agotiya, L. Devi, U. Kakade, and B. K. Patra, “Strongly interacting QGP and quarkonium suppression at rhic and LHC energies,” *International Journal of Modern Physics A*, vol. 27, no. 2, 2012.
- [51] H. Satz, “Quarkonium binding and dissociation: the spectral analysis of the QGP,” *Nuclear Physics A*, vol. 783, pp. 249–260, 2007, <https://arxiv.org/abs/hep-ph/0609197>.
- [52] B. Krouppa, R. Ryblewski, and M. Strickland, “Bottomonium suppression in heavy-ion collisions,” *Nuclear Physics A*, vol. 967, pp. 604–607, 2017.
- [53] B. Krouppa, R. Ryblewski, and M. Strickland, “Bottomonia suppression in 2.76 TeV Pb-Pb collisions,” *Physical Review C*, vol. 92, Article ID 061901, 2015.

Research Article

New Possibilities of Hybrid Texture of Neutrino Mass Matrix

Madan Singh 

Department of Physics, National Institute of Technology Kurukshetra, Haryana 136119, India

Correspondence should be addressed to Madan Singh; singhmadan179@gmail.com

Received 15 April 2018; Revised 26 May 2018; Accepted 4 June 2018; Published 11 July 2018

Academic Editor: Andrzej Okniński

Copyright © 2018 Madan Singh. This is an open access article distributed under the Creative Commons Attribution License, which permits unrestricted use, distribution, and reproduction in any medium, provided the original work is properly cited. The publication of this article was funded by SCOAP³.

We investigate the novel possibilities of hybrid textures comprising a vanishing minor (or element) and two equal elements (or cofactors) in light neutrino mass matrix M_ν . Such type of texture structures leads to sixty phenomenological cases each, out of which only fifty-six are viable with texture containing a vanishing minor and an equality between the elements in M_ν , while fifty are found to be viable with texture containing a vanishing element and an equality of cofactors in M_ν , under the current experimental test at 3σ confidence level. Detailed numerical analysis of all the possible cases has been presented.

1. Introduction

During the last two decades, our knowledge regarding the neutrino sector has been enriched to a great extent, thanks to solar, atmospheric, reactor, and accelerator based experiments which convincingly reveal that neutrinos have nonzero and nondegenerate masses and can convert from one flavor to another. While the developments over the past two decades have brought out a coherent picture of neutrino mixing, there are still several intriguing issues without which our understanding of neutrino physics remains incomplete. For instance, the present available data does not throw any light on the neutrino mass spectrum, which may be normal/inverted and may even be degenerate. In addition, nature of neutrino mass whether Dirac or Majorana particle, determination of absolute neutrino mass, leptonic CP violation, and Dirac CP phase δ are still open issues. Also the information regarding the lightest neutrino mass has to be sharpened further to pinpoint the specific possibility of neutrino mass spectrum.

After the precise measurement of reactor mixing angle θ_{13} in T2K, MINOS, Double Chooz, Daya Bay, and RENO experiments [1–5], five parameters in the neutrino sector have been well measured by neutrino oscillation experiments. In general, there are nine parameters in the lightest neutrinos mass matrix. The remaining four unknown parameters may be taken as the lightest neutrino mass, the Dirac CP-violating

phase, and two Majorana phases. The Dirac CP-violating phase is expected to be measured in future long baseline neutrino experiments, and the lightest mass can be determined from beta decay and cosmological experiments. If neutrinoless double-beta decay ($0\nu\beta\beta$) is detected, a combination of the two Majorana phases can also be probed. Clearly, the currently available data on neutrino masses and mixing are insufficient for an unambiguous reconstruction of neutrino mass matrices.

In the lack of a convincing fermion flavor theory, several phenomenological ansatz have been proposed in the literature as some elements of neutrino mass matrix are considered to be zero or equal [6–26] or some cofactors of neutrino mass matrix are considered to be either zero or equal [6, 27–35]. The main motivation for invoking different mass matrix ansatz is to relate fermion masses and mixing angles in a testable manner which reduces the number of free parameters in the neutrino mass matrix. In particular, mass matrices with zero textures (or cofactors) have been extensively studied [10–26, 29–35] due to their connections to flavor symmetries. In addition, texture specific mass matrices with one zero element (or minor) and an equality between two independent elements (or cofactors) have also been studied in the literature [7–9, 27, 28]. Out of sixty possibilities, only fifty-four are found to be compatible with the neutrino oscillation data [9] for texture structures having one zero element and an equal matrix elements in the neutrino mass matrix (also known as

hybrid texture), while for texture with one vanishing minor and an equal cofactors in the neutrino mass matrix (also known as inverse hybrid texture) only fifty-two cases are able to survive the data [27, 28].

In the present paper, we propose the novel possibilities of hybrid textures where we assume one texture zero and an equality between the cofactors (referred as type X) or one zero minor and an equality between the elements (referred as type Y) in the Majorana neutrino mass matrix M_ν . Such type of texture structures sets two conditions on the parameter space and hence reduces the number of free parameters to seven. Therefore the proposed texture structures are as predictive as texture two zeros and any other hybrid textures.

In [6], it is demonstrated that an equality between the elements of M_ν can be realized through type-II seesaw mechanism [36–40] while an equality between cofactors of M_ν can be generated from type-I seesaw mechanism [41–44]. The zeros element (or minor) in M_ν can be obtained using Z_n flavor symmetry [29–35, 45]. Therefore the viable cases of proposed hybrid texture can be realized within the framework of seesaw mechanism.

In the present work, we have systematically investigated all the of sixty possible cases belonging to type X and type Y structures, respectively. We have studied the implication of these textures for Dirac CP-violating phase (δ) and two Majorana phases (ρ, σ). We, also, calculate the effective Majorana mass and lowest neutrino mass for all viable hybrid textures belonging to type X and type Y structures. In addition, we present the correlation plots between different parameters of the hybrid textures of neutrinos for 3σ allowed ranges of the known parameters.

The layout of the paper is planned as follows: in Section 2, we shall discuss the methodology to obtain the constraint equations. Section 3 is devoted to numerical analysis. Section 4 will summarize our result.

2. Methodology

Before proceeding further, we briefly underline the methodology relating the elements of the mass matrices to those of the mixing matrix. In the flavor basis, where the charged lepton mass matrix is diagonal, the Majorana neutrino mass matrix can be expressed as

$$M_\nu = P_l U P_\nu M^{\text{diag}} P_\nu^T U^T P_l^T, \quad (1)$$

where $M^{\text{diag}} = \text{diag}(m_1, m_2, m_3)$ is the diagonal matrix of neutrino masses and U is the flavor mixing matrix and

$$P_\nu = \begin{pmatrix} e^{i\rho} & 0 & 0 \\ 0 & e^{i\sigma} & 0 \\ 0 & 0 & 1 \end{pmatrix}, \quad (2)$$

$$P_l = \begin{pmatrix} e^{i\phi_e} & 0 & 0 \\ 0 & e^{i\phi_\mu} & 0 \\ 0 & 0 & e^{i\phi_\tau} \end{pmatrix},$$

where P_ν is diagonal phase matrix containing Majorana neutrinos ρ, σ . P_l is unobservable phase matrix and depends on phase convention. Equation (1) can be rewritten as

$$M_\nu = \begin{pmatrix} M_{ee} & M_{e\mu} & M_{e\tau} \\ M_{e\mu} & M_{\mu\mu} & M_{\mu\tau} \\ M_{e\tau} & M_{\mu\tau} & M_{\tau\tau} \end{pmatrix} \quad (3)$$

$$= P_l U \begin{pmatrix} \lambda_1 & 0 & 0 \\ 0 & \lambda_2 & 0 \\ 0 & 0 & \lambda_3 \end{pmatrix} U^T P_l^T,$$

where $\lambda_1 = m_1 e^{2i\rho}$, $\lambda_2 = m_2 e^{2i\sigma}$, and $\lambda_3 = m_3$. For the present analysis, we consider the following parameterization of U [46]:

$$U = \begin{pmatrix} c_{12}c_{13} & s_{12}c_{13} & s_{13} \\ -c_{12}s_{23}s_{13} - s_{12}c_{23}e^{-i\delta} & -s_{12}s_{23}s_{13} + c_{12}c_{23}e^{-i\delta} & s_{23}c_{13} \\ -c_{12}c_{23}s_{13} + s_{12}s_{23}e^{-i\delta} & -s_{12}c_{23}s_{13} - c_{12}s_{23}e^{-i\delta} & c_{23}c_{13} \end{pmatrix}, \quad (4)$$

where $c_{ij} = \cos \theta_{ij}$ and $s_{ij} = \sin \theta_{ij}$. Here, U is a 3×3 unitary matrix consisting of three flavor mixing angles ($\theta_{12}, \theta_{23}, \theta_{13}$) and one Dirac CP-violating phase δ .

For the illustration of type X and Y structures, we consider a case A_1 , satisfying following conditions:

$$C_{11} = M_{\mu\mu}M_{\tau\tau} - M_{\mu\tau}M_{\mu\tau} = 0, \quad (5)$$

and

$$M_{e\mu} - M_{e\tau} = 0, \quad (6)$$

for type X, while in case of type Y, it contains

$$M_{ee} = 0 \quad (7)$$

and

$$C_{12} - C_{13} = 0, \quad (8)$$

or

$$(-1) \cdot (M_{e\tau}M_{\tau\tau} - M_{\mu\tau}M_{e\tau}) - (M_{e\mu}M_{\mu\tau} - M_{\mu\mu}M_{e\tau}) = 0, \quad (9)$$

where C_{ij} denotes cofactor corresponding to i^{th} row and j^{th} column. Then A_1 can be denoted in a matrix form as

$$\begin{pmatrix} 0 & \Delta & \Delta \\ \Delta & \times & \times \\ \Delta & \times & \times \end{pmatrix}, \quad (10)$$

where “ Δ ” stands for nonzero and equal elements (or cofactors), while “0” stands for vanishing element (or minor) in neutrino mass matrix. “ \times ” stands for arbitrary elements.

2.1. *One Vanishing Minor with Two Equal Elements of M_ν .* Using (1), any element M_{pq} in the neutrino mass matrix can be expressed in terms of mixing matrix elements as

$$M_{pq} = e^{i(\phi_p + \phi_q)} \sum_{i=1,2,3} U_{pi} U_{qi} \lambda_i, \quad (11)$$

where p, q run over $e, \mu,$ and $\tau,$ and $e^{i(\phi_p + \phi_q)}$ is phase factor.

The existence of a zero minor in the Majorana neutrino mass matrix implies

$$M_{pq} M_{rs} - M_{tu} M_{vw} = 0 \quad (12)$$

The above condition yields a complex equation as

$$\sum_{i,j=1,2,3} \left(e^{i(\phi_p + \phi_q + \phi_r + \phi_s)} U_{pi} U_{qi} U_{rj} U_{sj} - e^{i(\phi_t + \phi_u + \phi_v + \phi_w)} U_{ti} U_{ui} U_{vj} U_{wj} \right) \lambda_i \lambda_j = 0, \quad (13)$$

It is observed that for any cofactor there is an inherent property as $\phi_p + \phi_q + \phi_r + \phi_s = \phi_t + \phi_u + \phi_v + \phi_w$. Thus we can extract this total phase factor from the bracket in (13).

Hence (13) can be rewritten as

$$X_3 \lambda_1 \lambda_2 + X_1 \lambda_2 \lambda_3 + X_2 \lambda_3 \lambda_1 = 0, \quad (14)$$

where

$$X_k = \left(U_{pi} U_{qi} U_{rj} U_{sj} - U_{ti} U_{ui} U_{vj} U_{wj} \right) + (i \longleftrightarrow j), \quad (15)$$

with (i, j, k) as the cyclic permutation of $(1, 2, 3)$.

On the other hand, the condition of two equal elements in M_ν yields following:

$$M_{ab} - M_{cd} = 0. \quad (16)$$

Equation (16) yields a following complex equation:

$$\sum_{i=1,2,3} (P_1 U_{ai} U_{bi} - P_2 U_{ci} U_{di}) \lambda_i = 0, \quad (17)$$

where $P_1 = e^{i(\phi_a + \phi_b)}$ and $P_2 = e^{i(\phi_c + \phi_d)}$.

Or

$$\sum_{i=1,2,3} (P U_{ai} U_{bi} - U_{ci} U_{di}) \lambda_i = 0 \quad (18)$$

where $P \equiv P_1/P_2 = e^{i(a+b-c-d)}$ and $a, b, c,$ and d run over $e, \mu,$ and τ .

Equation (18) can be rewritten as

$$Y_1 \lambda_1 + Y_2 \lambda_2 + Y_3 \lambda_3 = 0 \quad (19)$$

where $Y_1 = (P U_{a1} U_{b1} - U_{c1} U_{d1}), Y_2 = (P U_{a2} U_{b2} - U_{c2} U_{d2}),$ and $Y_3 = (P U_{a3} U_{b3} - U_{c3} U_{d3}).$

Solving (14) and (19) simultaneously leads to the following complex mass ratio in terms of $(\lambda_{13})_\pm$:

$$(\lambda_{13})_+ = \frac{-(Y_1 X_1 - Y_2 X_2 + Y_3 X_3 + \sqrt{C})}{2Y_1 X_3}, \quad (20)$$

and

$$(\lambda_{13})_- = \frac{-(Y_1 X_1 - Y_2 X_2 + Y_3 X_3 - \sqrt{C})}{2Y_1 X_3}. \quad (21)$$

Using (14), (20), and (21), we obtain the relations for complex mass ratio in terms of $(\lambda_{23})_\pm$

$$(\lambda_{23})_+ = -\frac{X_2}{X_3} \times \frac{Y_1 X_1 - Y_2 X_2 + Y_3 X_3 + \sqrt{C}}{-Y_1 X_1 - Y_2 X_2 + Y_3 X_3 + \sqrt{C}}, \quad (22)$$

and

$$(\lambda_{23})_- = -\frac{X_2}{X_3} \times \frac{Y_1 X_1 - Y_2 X_2 + Y_3 X_3 - \sqrt{C}}{-Y_1 X_1 - Y_2 X_2 + Y_3 X_3 - \sqrt{C}}, \quad (23)$$

where $C = (-Y_1 X_1 + Y_2 X_2 + Y_3 X_3)^2 - 4X_2 X_3 Y_2 Y_3$ and $(\lambda_{13})_\pm \equiv (\lambda_1/\lambda_3)_\pm$ and $(\lambda_{23})_\pm \equiv (\lambda_2/\lambda_3)_\pm$. The magnitudes of the two neutrino mass ratios in (20), (21), (22), and (23) are given by $\xi_\pm = |(\lambda_{13})_\pm|$ and $\zeta_\pm = |(\lambda_{23})_\pm|$, while the Majorana CP-violating phases ρ and σ can be given as $\rho = (1/2)\arg(\lambda_{13})_\pm$, $\sigma = (1/2)\arg(\lambda_{23})_\pm$.

2.2. *One Vanishing Element with Two Equal Cofactors of M_ν .* If one of the elements of M_ν is considered zero [e.g., $M_{\alpha\beta} = 0$], we obtain the following constraint equation:

$$\sum_{i=1,2,3} U_{\alpha i} U_{\beta i} \lambda_i = 0, \quad (24)$$

or

$$\lambda_1 A_1 + \lambda_2 A_2 + \lambda_3 A_3 = 0, \quad (25)$$

where $A_1 = U_{\alpha 1} U_{\beta 1}, A_2 = U_{\alpha 2} U_{\beta 2},$ and $A_3 = U_{\alpha 3} U_{\beta 3}.$

The condition for two equal cofactors [e.g., $C_{mn} = C_{m'n'}$] in neutrino mass matrix implies

$$(-1)^{m+n} (M_{ab} M_{cd} - M_{ef} M_{gh}) - (-1)^{m'+n'} (M_{a'b'} M_{c'd'} - M_{e'f'} M_{g'h'}) = 0, \quad (26)$$

or

$$\sum_{i,j=1,2,3} \left\{ (-1)^{m+n} (Q_3 U_{ai} U_{bi} U_{cj} U_{dj} - Q_4 U_{ei} U_{fi} U_{gj} U_{hj}) - (-1)^{m'+n'} \cdot (Q_5 U_{a'i} U_{b'i} U_{c'j} U_{d'j} - Q_6 U_{e'i} U_{f'i} U_{g'j} U_{h'j}) \right\} \lambda_i \lambda_j = 0, \quad (27)$$

where $Q_3 = Q_4$ and $Q_5 = Q_6$ due to inherent property of any cofactor. Thus we can write

$$\sum_{i,j=1,2,3} \left\{ (-1)^{m+n} Q_3 (U_{ai} U_{bi} U_{cj} U_{dj} - U_{ei} U_{fi} U_{gj} U_{hj}) - (-1)^{m'+n'} \cdot Q_5 (U_{a'i} U_{b'i} U_{c'j} U_{d'j} - U_{e'i} U_{f'i} U_{g'j} U_{h'j}) \right\} \lambda_i \lambda_j = 0, \quad (28)$$

or

$$\sum_{i,j=1,2,3} \left\{ (-1)^{m+n} Q (U_{ai} U_{bi} U_{cj} U_{dj} - U_{ei} U_{fi} U_{gj} U_{hj}) \right. \\ \left. - (-1)^{m'+n'} (U_{a'i} U_{b'i} U_{c'i} U_{d'i} - U_{e'i} U_{f'i} U_{g'i} U_{h'i}) \right\} \quad (29) \\ \cdot \lambda_i \lambda_j = 0,$$

where $Q \equiv Q_3/Q_5 = e^{i(\phi_a + \phi_b + \phi_c + \phi_d - \phi_{a'} - \phi_{b'} - \phi_{c'} - \phi_{d'})}$.

Equation (29) can be rewritten as

$$\lambda_1 \lambda_2 B_3 + \lambda_2 \lambda_3 B_1 + \lambda_3 \lambda_1 B_2 = 0, \quad (30)$$

where

$$B_k \\ = (-1)^{m+n} Q (U_{ai} U_{bi} U_{cj} U_{dj} - U_{ei} U_{fi} U_{gj} U_{hj}), \quad (31) \\ - (-1)^{m'+n'} (U_{a'i} U_{b'i} U_{c'i} U_{d'i} - U_{e'i} U_{f'i} U_{g'i} U_{h'i}) \\ + (i \longleftrightarrow j),$$

with (i, j, k) a cyclic permutation of $(1, 2, 3)$.

Solving (25) and (30) simultaneously we obtain the analytical expressions of $(\lambda_{13})_{\pm}$

$$(\lambda_{13})_+ = \frac{- (B_1 A_1 - B_2 A_2 + B_3 A_3 + \sqrt{D})}{2B_1 A_3}, \quad (32)$$

and

$$(\lambda_{13})_- = \frac{- (B_1 A_1 - B_2 A_2 + B_3 A_3 - \sqrt{D})}{2B_1 A_3}. \quad (33)$$

Using (30), (32), and (33), we get the relations for complex mass ratio in terms of $(\lambda_{23})_{\pm}$

$$(\lambda_{23})_+ = -\frac{B_2}{B_3} \times \frac{(B_1 A_1 - B_2 A_2 + B_3 A_3 + \sqrt{D})}{(-B_1 A_1 - B_2 A_2 + B_3 A_3 + \sqrt{D})}, \quad (34)$$

and

$$(\lambda_{23})_- = -\frac{B_2}{B_3} \times \frac{(B_1 A_1 - B_2 A_2 + B_3 A_3 - \sqrt{D})}{(-B_1 A_1 - B_2 A_2 + B_3 A_3 - \sqrt{D})}, \quad (35)$$

where $D = (-B_1 A_1 + B_2 A_2 + B_3 A_3)^2 - 4A_2 A_3 B_2 B_3$.

The magnitudes of the two neutrino mass ratios are given by $\xi_{\pm} = |(\lambda_{13})_{\pm}|$ and $\zeta_{\pm} = |(\lambda_{23})_{\pm}|$, while the Majorana CP-violating phases ρ and σ can be given as $\rho = (1/2)\arg(\lambda_{13})_{\pm}$, $\sigma = (1/2)\arg(\lambda_{23})_{\pm}$.

The solar and atmospheric mass-squared differences ($\delta m^2, \Delta m^2$), where δm^2 corresponds to solar mass-squared difference and Δm^2 corresponds to atmospheric mass-squared difference, can be defined as [8]

$$\delta m^2 = (m_2^2 - m_1^2), \quad (36)$$

$$\Delta m^2 = m_3^2 - \frac{1}{2} (m_1^2 + m_2^2). \quad (37)$$

The sign of Δm^2 is still unknown: $\Delta m^2 > 0$ or $\Delta m^2 < 0$ implies normal mass spectrum (NS) or inverted mass spectrum (IS). The lowest neutrino mass (m_0) is m_1 for NS and m_3 for IS. The experimentally determined solar and atmospheric neutrino mass-squared differences can be related to ξ and ζ as

$$R_{\nu} \equiv \frac{\delta m^2}{|\Delta m^2|} = \frac{2(\zeta^2 - \xi^2)}{|2 - (\zeta^2 + \xi^2)|}, \quad (38)$$

and the three neutrino masses can be determined using following relations:

$$m_3 = \sqrt{\frac{\delta m^2}{\zeta^2 - \xi^2}}, \quad (39) \\ m_2 = m_3 \zeta, \\ m_1 = m_3 \xi.$$

From the analysis, it is found that cases belonging to type X (or type Y) exhibit the identical phenomenological implications and are related through permutation symmetry [36–40, 46]. This corresponds to permutation of the 2-3 rows and 2-3 columns of M_{ν} . The corresponding permutation matrix can be given by

$$P_{23} = \begin{pmatrix} 1 & 0 & 0 \\ 0 & 0 & 1 \\ 0 & 1 & 0 \end{pmatrix}. \quad (40)$$

With the help of permutation symmetry, one obtains the following relations among the neutrino oscillation parameters:

$$\theta_{12}^l = \theta_{12}^m, \\ \theta_{23}^l = 90^\circ - \theta_{23}^m, \\ \theta_{13}^l = \theta_{13}^m, \\ \delta^l = \delta^m - 180^\circ, \quad (41)$$

where l and m denote the cases related by 2-3 permutation. The following pairs among sixty possibilities of type X (or type Y) are related via permutation symmetry:

$$(A_1, A_1); \\ (A_2, A_8); \\ (A_3, A_7); \\ (A_4, A_6); \\ (A_5, A_5); \\ (A_9, A_{10}); \\ (B_1, C_1); \\ (B_2, C_7); \\ (B_3, C_6);$$

$$\begin{aligned}
& (B_4, C_5); \\
& (B_5, C_4); \\
& (B_6, C_3); \\
& (B_7, C_2); \\
& (B_8, C_{10}); \\
& (B_9, C_9); \\
& (B_{10}, C_8); \\
& (D_1, F_2); \\
& (D_2, F_1); \\
& (D_3, F_4); \\
& (D_4, F_3); \\
& (D_5, F_5); \\
& (D_6, F_9); \\
& (D_7, F_8); \\
& (D_8, F_7); \\
& (D_9, F_6); \\
& (D_{10}, F_{10}); \\
& (E_1, E_2); \\
& (E_3, E_4); \\
& (E_5, E_5); \\
& (E_6, E_9); \\
& (E_7, E_8); \\
& (E_{10}, E_{10}).
\end{aligned} \tag{42}$$

Clearly we are left with only thirty-two independent cases. It is worthwhile mentioning that A_1, A_5, E_5 , and E_{10} are invariant under the permutations of 2- and 3-rows and columns.

3. Numerical Analysis

The experimental constraints on neutrino parameters at 3σ confidence level (CL) are given in Table 1. The effective Majorana mass relevant for neutrinoless double-beta ($0\nu\beta\beta$) decay is given by

$$|M|_{ee} = \left| m_1 c_{12}^2 c_{13}^2 e^{2i\rho} + m_2 s_{12}^2 c_{13}^2 e^{2i\sigma} + m_3 s_{13}^2 \right|. \tag{43}$$

This effective mass is just the absolute value of M_{ee} component of the neutrino mass matrix. The observation of $0\nu\beta\beta$

TABLE 1: Current neutrino oscillation parameters from global fits at 3σ confidence level (CL) [47, 48]. NS(IS) refers to normal (inverted) neutrino mass spectrum.

Parameter	Best Fit	3σ
δm^2 [$10^{-5} eV^2$]	7.50	7.03 - 8.09
$ \Delta m_{31}^2 $ [$10^{-3} eV^2$] (NS)	2.52	2.407 - 2.643
$ \Delta m_{31}^2 $ [$10^{-3} eV^2$] (IS)	2.52	2.39 - 2.63
θ_{12}	33.56°	$31.3^\circ - 35.99^\circ$
θ_{23} (NS)	41.6°	$38.4^\circ - 52.8^\circ$
θ_{23} (IS)	50.0°	$38.8^\circ - 53.1^\circ$
θ_{13} (NS)	8.46°	$7.99^\circ - 8.90^\circ$
θ_{13} (IS)	8.49°	$8.03^\circ - 8.93^\circ$
δ (NS)	261°	$0^\circ - 360^\circ$
δ (IS)	277°	$145^\circ - 391^\circ$

would establish neutrinos to be Majorana particles. Data from KamLAND-Zen experiment has presented an improved search for neutrinoless double-beta ($0\nu\beta\beta$) decay [49–51] and it is found that $|M|_{ee} < (0.061 - 0.165)eV$ at 90% (or $< 2\sigma$) CL. For recent reviews on $0\nu\beta\beta$ decay, see [49–51].

In the present analysis, we consider more conservative upper bound on $|M|_{ee}$, i.e., $|M|_{ee} < 0.5eV$ at 3σ CL [52]. We span the parameter space of input neutrino oscillation parameters ($\theta_{12}, \theta_{23}, \theta_{13}, \Delta m^2, \delta m^2$) lying in their 3σ ranges by randomly generating points of the order of 10^7 . Since the Dirac CP-violating phase δ is experimentally unconstrained at 3σ level, therefore, we vary δ within its full possible range $[0^\circ, 360^\circ]$. Using (38) and the experimental inputs on neutrino mixing angles and mass-squared differences, the parameter space of δ, ρ, σ and $|M|_{ee}$, and m_0 can be subsequently constrained.

In Figures 1, 2, 3, 4, 5, 6, 7, 8, 9, 10, 11, and 12 we demonstrate the correlations for A_1, B_2, D_7 , and E_1 cases. Since there are large numbers of viable cases, therefore it is not practically possible to show all the plots. We have simply taken arbitrary independent cases from each category for the purpose of illustration of our results. The predictions regarding three CP-violating phases (ρ, σ, δ), effective neutrino mass $|M|_{ee}$, and lowest neutrino mass m_0 for all the allowed cases of type X and type Y textures have been encapsulated in Tables 3, 4, 5, and 6. Before proceeding further, it is worth pointing out that the phenomenological results for $\rho, \sigma, \delta, |M|_{ee}$, and m_0 have been obtained using the two possible solutions of λ_{13} and λ_{23} , respectively [(20), (21), (22), and (23)]. All the sixty phenomenologically possible cases belonging to type X and type Y texture structures have been divided into six categories A, B, C, D, E, and F (Table 2). Among them a large number of cases are found to overlap in their predictions regarding $\delta, \rho, \sigma, |M|_{ee}$, and m_0 and are related via permutation symmetry as pointed out earlier. The main results and the discussion are summarized as follows.

Category A. In Category A, all the ten cases $A_1, A_2, A_3, A_4, A_5, A_6, A_7, A_8, A_9$, and A_{10} are found to be viable with the data at 3σ CL for type X structure, and normal mass spectrum (NS) remainS ruled out for all these cases (Table 3).

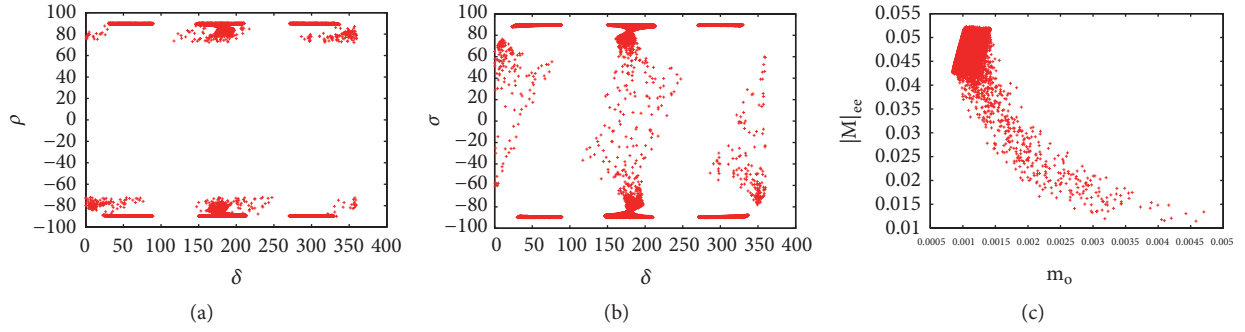


FIGURE 1: Correlation plots for texture A_1 (IS) for type X at 3σ CL. The symbols have their usual meaning. δ , ρ , and σ are measured in degrees, while $|M|_{ee}$ and m_0 are in eV units.

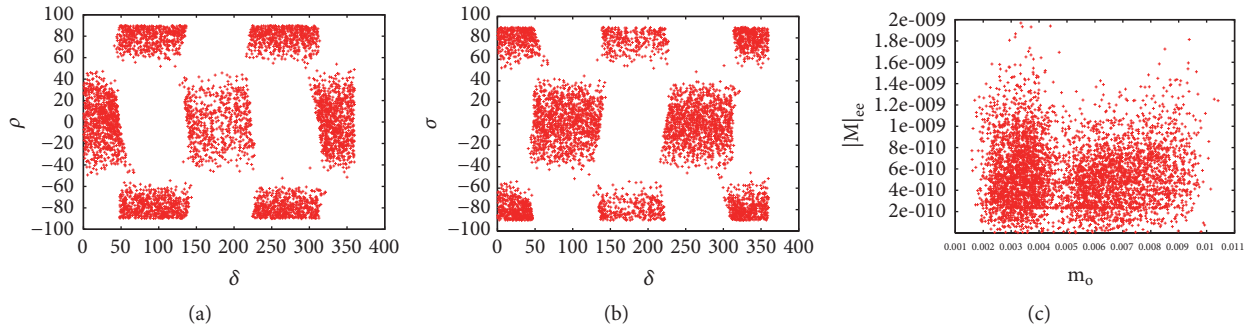


FIGURE 2: Correlation plots for texture A_1 (NS) for type Y at 3σ CL. The symbols have their usual meaning. δ , ρ , and σ are measured in degrees, while $|M|_{ee}$ and m_0 are in eV units.

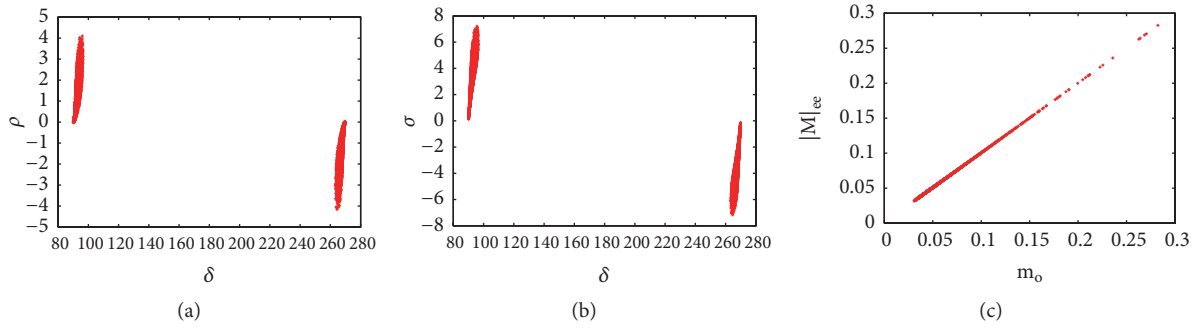


FIGURE 3: Correlation plots for texture B_2 (NS) for type X at 3σ CL. The symbols have their usual meaning. δ , ρ , and σ are measured in degrees, while $|M|_{ee}$ and m_0 are in eV units.

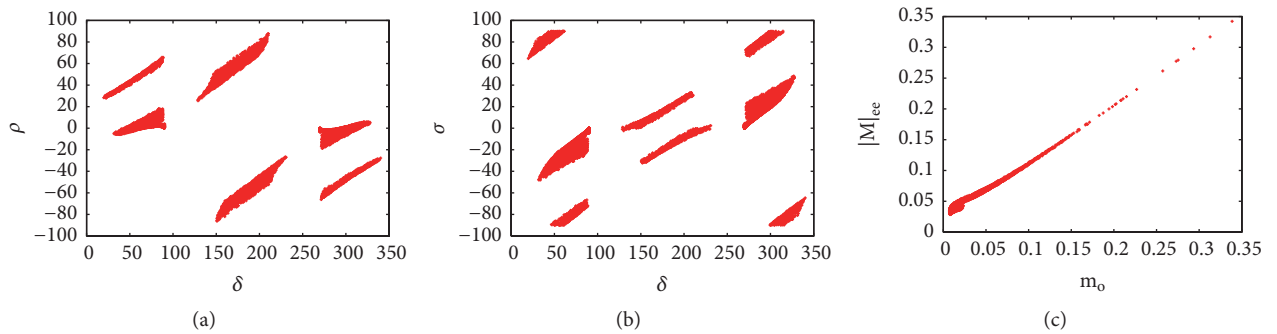


FIGURE 4: Correlation plots for texture B_2 (IS) for type X at 3σ CL. The symbols have their usual meaning. δ , ρ , and σ are measured in degrees, while $|M|_{ee}$ and m_0 are in eV units.

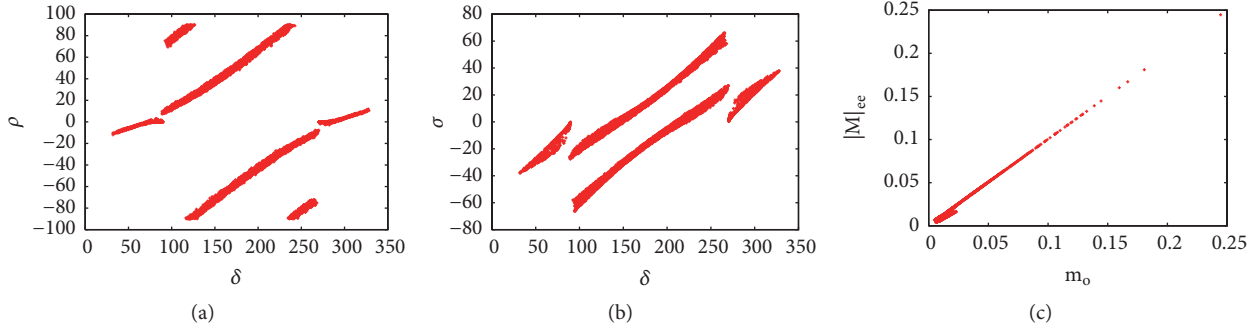


FIGURE 5: Correlation plots for texture B_2 (NS) for type Y at 3σ CL. The symbols have their usual meaning. δ, ρ , and σ are measured in degrees, while $|M|_{ee}$ and m_0 are in eV units.

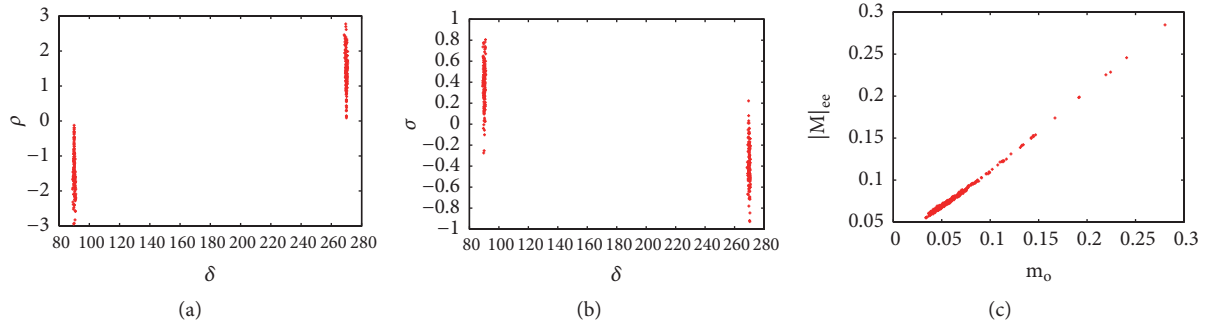


FIGURE 6: Correlation plots for texture B_2 (IS) for type Y at 3σ CL. The symbols have their usual meaning. δ, ρ , and σ are measured in degrees, while $|M|_{ee}$ and m_0 are in eV units.

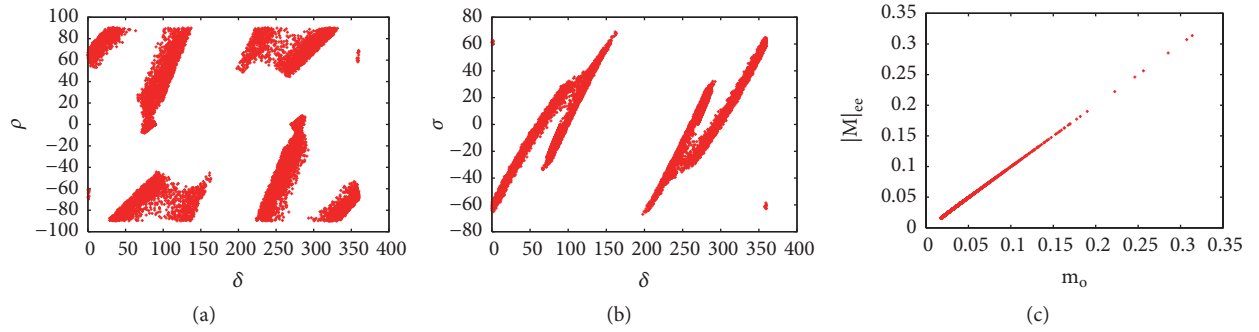


FIGURE 7: Correlation plots for texture D_7 (NS) for type X at 3σ CL. The symbols have their usual meaning. δ, ρ , and σ are measured in degrees, while $|M|_{ee}$ and m_0 are in eV units.

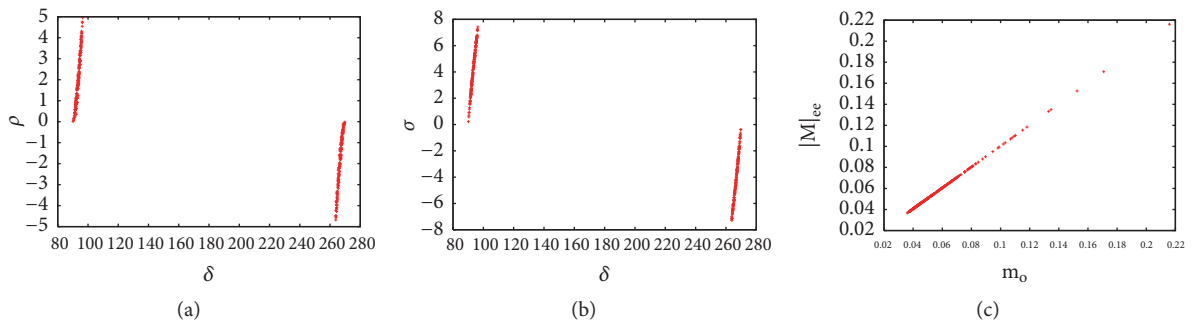


FIGURE 8: Correlation plots for texture D_7 (IS) for type X at 3σ CL. The symbols have their usual meaning. δ, ρ , and σ are measured in degrees, while $|M|_{ee}$ and m_0 are in eV units.

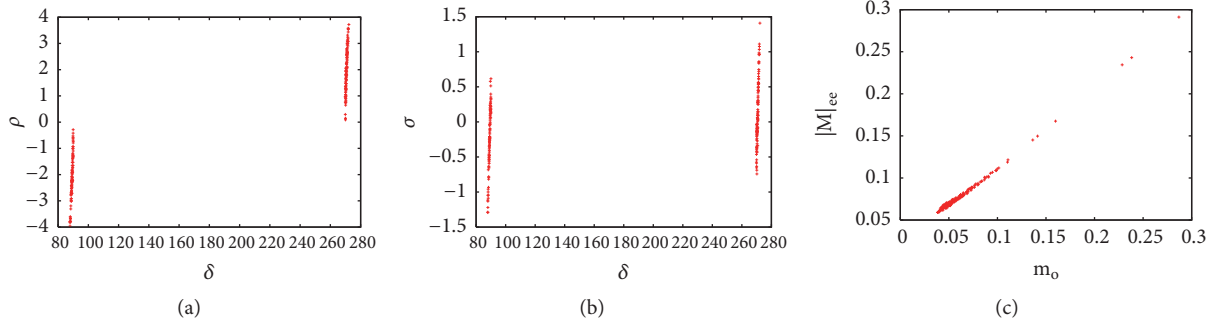


FIGURE 9: Correlation plots for texture D_7 (NS) for type Y at 3σ CL. The symbols have their usual meaning. δ , ρ , and σ are measured in degrees, while $|M|_{ee}$ and m_0 are in eV units.

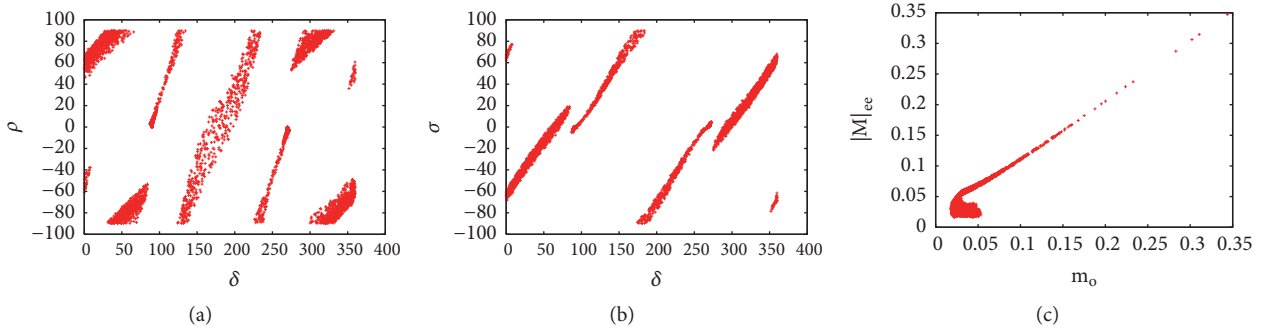


FIGURE 10: Correlation plots for texture D_7 (IS) for type Y at 3σ CL. The symbols have their usual meaning. δ , ρ , and σ are measured in degrees, while $|M|_{ee}$ and m_0 are in eV units.

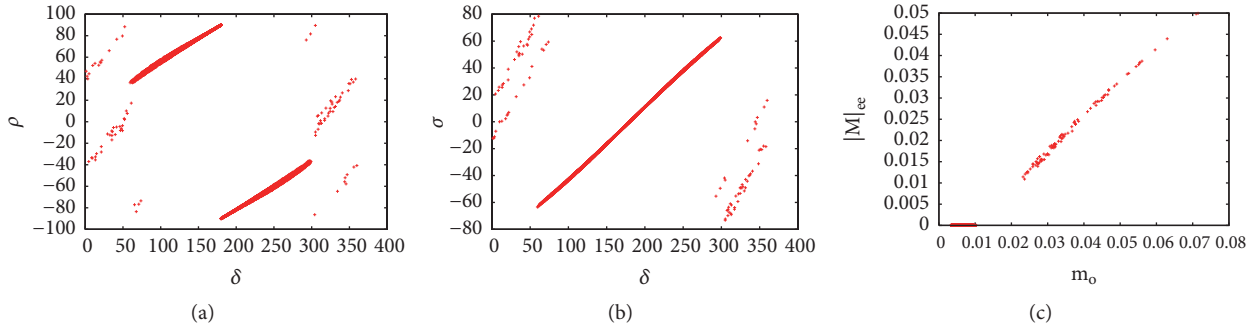


FIGURE 11: Correlation plots for texture E_1 (NS) for type X at 3σ CL. The symbols have their usual meaning. δ , ρ , and σ are measured in degrees, while $|M|_{ee}$ and m_0 are in eV units..

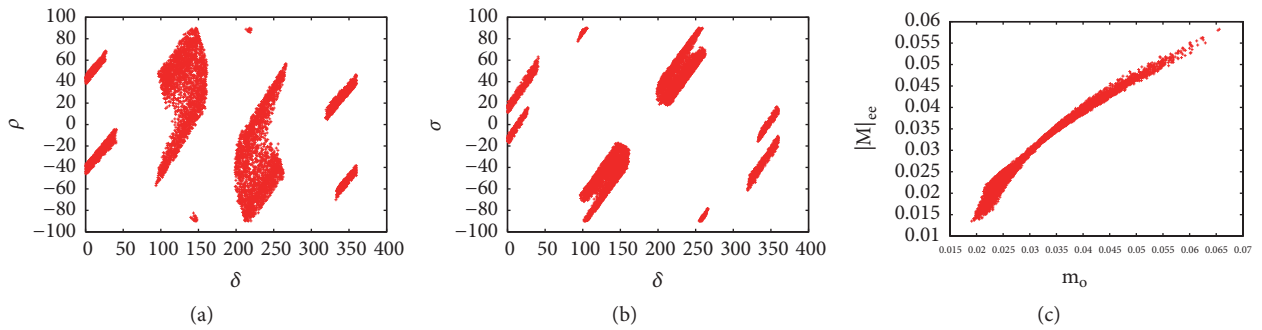


FIGURE 12: Correlation plots for texture E_1 (IS) for type Y at 3σ CL. The symbols have their usual meaning. δ , ρ , and σ are measured in degrees, while $|M|_{ee}$ and m_0 are in eV units.

TABLE 2: All the sixty phenomenological possible cases belonging to types X and Y, respectively, have been shown. P and Q are unobservable phases associated with types X and Y, respectively.

Cases	X	P	Y	Q
A_1	$C_{11} = 0, M_{12} = M_{13}$	$e^{i(\phi_\mu - \phi_\tau)}$	$M_{11} = 0, C_{12} = C_{13}$	$e^{i(\phi_\tau - \phi_\mu)}$
A_2	$C_{11} = 0, M_{12} = M_{22}$	$e^{i(\phi_e - \phi_\mu)}$	$M_{11} = 0, C_{12} = C_{22}$	$e^{i(\phi_\mu - \phi_e)}$
A_3	$C_{11} = 0, M_{13} = M_{23}$	$e^{i(\phi_e - \phi_\mu)}$	$M_{11} = 0, C_{13} = C_{23}$	$e^{i(\phi_\mu - \phi_e)}$
A_4	$C_{11} = 0, M_{22} = M_{23}$	$e^{i(\phi_\mu - \phi_\tau)}$	$M_{11} = 0, C_{22} = C_{23}$	$e^{i(\phi_\tau - \phi_\mu)}$
A_5	$C_{11} = 0, M_{22} = M_{33}$	$e^{2i(\phi_\mu - \phi_\tau)}$	$M_{11} = 0, C_{22} = C_{33}$	$e^{2i(\phi_\tau - \phi_\mu)}$
A_6	$C_{11} = 0, M_{23} = M_{33}$	$e^{i(\phi_\mu - \phi_\tau)}$	$M_{11} = 0, C_{23} = C_{33}$	$e^{i(\phi_\tau - \phi_\mu)}$
A_7	$C_{11} = 0, M_{12} = M_{23}$	$e^{i(\phi_e - \phi_\tau)}$	$M_{11} = 0, C_{12} = C_{23}$	$e^{i(\phi_\tau - \phi_e)}$
A_8	$C_{11} = 0, M_{13} = M_{33}$	$e^{i(\phi_e - \phi_\tau)}$	$M_{11} = 0, C_{13} = C_{33}$	$e^{i(\phi_\tau - \phi_e)}$
A_9	$C_{11} = 0, M_{13} = M_{22}$	$e^{i(\phi_e + \phi_\tau - 2\phi_\mu)}$	$M_{11} = 0, C_{13} = C_{22}$	$e^{i(-\phi_e - \phi_\tau + 2\phi_\mu)}$
A_{10}	$C_{11} = 0, M_{12} = M_{33}$	$e^{i(\phi_e + \phi_\mu - 2\phi_\tau)}$	$M_{11} = 0, C_{12} = C_{33}$	$e^{i(-\phi_e - \phi_\mu + 2\phi_\tau)}$
B_1	$C_{12} = 0, M_{11} = M_{13}$	$e^{i(\phi_e - \phi_\tau)}$	$M_{12} = 0, C_{11} = C_{13}$	$e^{i(\phi_\tau - \phi_e)}$
B_2	$C_{12} = 0, M_{12} = M_{22}$	$e^{i(\phi_e + \phi_\tau - 2\phi_\mu)}$	$M_{12} = 0, C_{12} = C_{22}$	$e^{i(2\phi_\mu - \phi_e - \phi_\tau)}$
B_3	$C_{12} = 0, M_{13} = M_{23}$	$e^{i(\phi_e - \phi_\mu)}$	$M_{12} = 0, C_{13} = C_{23}$	$e^{i(\phi_\mu - \phi_e)}$
B_4	$C_{12} = 0, M_{13} = M_{33}$	$e^{i(\phi_e - \phi_\tau)}$	$M_{12} = 0, C_{13} = C_{33}$	$e^{i(\phi_\tau - \phi_e)}$
B_5	$C_{12} = 0, M_{11} = M_{22}$	$e^{2i(\phi_e - \phi_\mu)}$	$M_{12} = 0, C_{11} = C_{22}$	$e^{2i(\phi_\mu - \phi_e)}$
B_6	$C_{12} = 0, M_{11} = M_{23}$	$e^{i(2\phi_e - \phi_\mu - \phi_\tau)}$	$M_{12} = 0, C_{11} = C_{23}$	$e^{i(-2\phi_e + \phi_\mu + \phi_\tau)}$
B_7	$C_{12} = 0, M_{11} = M_{33}$	$e^{2i(\phi_e - \phi_\tau)}$	$M_{12} = 0, C_{11} = C_{33}$	$e^{2i(\phi_\tau - \phi_e)}$
B_8	$C_{12} = 0, M_{22} = M_{23}$	$e^{i(\phi_\mu - \phi_\tau)}$	$M_{12} = 0, C_{22} = C_{23}$	$e^{i(\phi_\tau - \phi_\mu)}$
B_9	$C_{12} = 0, M_{22} = M_{33}$	$e^{2i(\phi_\mu - \phi_\tau)}$	$M_{12} = 0, C_{22} = C_{33}$	$e^{2i(\phi_\tau - \phi_\mu)}$
B_{10}	$C_{12} = 0, M_{23} = M_{33}$	$e^{i(\phi_\mu - \phi_\tau)}$	$M_{12} = 0, C_{23} = C_{33}$	$e^{i(\phi_\tau - \phi_\mu)}$
C_1	$C_{13} = 0, M_{11} = M_{12}$	$e^{i(\phi_e - \phi_\mu)}$	$M_{13} = 0, C_{11} = C_{12}$	$e^{i(\phi_\mu - \phi_e)}$
C_2	$C_{13} = 0, M_{11} = M_{22}$	$e^{2i(\phi_e - \phi_\mu)}$	$M_{13} = 0, C_{11} = C_{22}$	$e^{2i(\phi_\mu - \phi_e)}$
C_3	$C_{13} = 0, M_{11} = M_{23}$	$e^{i(2\phi_e - \phi_\mu - \phi_\tau)}$	$M_{13} = 0, C_{11} = C_{23}$	$e^{i(-2\phi_e + \phi_\mu + \phi_\tau)}$
C_4	$C_{13} = 0, M_{11} = M_{33}$	$e^{2i(\phi_e - \phi_\tau)}$	$M_{13} = 0, C_{11} = C_{33}$	$e^{2i(\phi_\tau - \phi_e)}$
C_5	$C_{13} = 0, M_{12} = M_{22}$	$e^{i(\phi_e - \phi_\mu)}$	$M_{13} = 0, C_{12} = C_{22}$	$e^{i(\phi_\mu - \phi_e)}$
C_6	$C_{13} = 0, M_{12} = M_{23}$	$e^{i(\phi_e - \phi_\tau)}$	$M_{13} = 0, C_{12} = C_{23}$	$e^{i(\phi_\tau - \phi_e)}$
C_7	$C_{13} = 0, M_{12} = M_{33}$	$e^{i(\phi_e - \phi_\mu - 2\phi_\tau)}$	$M_{13} = 0, C_{12} = C_{33}$	$e^{i(-\phi_e + \phi_\mu + 2\phi_\tau)}$
C_8	$C_{13} = 0, M_{22} = M_{23}$	$e^{i(\phi_\mu - \phi_\tau)}$	$M_{13} = 0, C_{22} = C_{23}$	$e^{i(\phi_\tau - \phi_\mu)}$
C_9	$C_{13} = 0, M_{22} = M_{33}$	$e^{2i(\phi_\mu - \phi_\tau)}$	$M_{13} = 0, C_{22} = C_{33}$	$e^{2i(\phi_\tau - \phi_\mu)}$
C_{10}	$C_{13} = 0, M_{23} = M_{33}$	$e^{i(\phi_\mu - \phi_\tau)}$	$M_{13} = 0, C_{23} = C_{33}$	$e^{i(\phi_\tau - \phi_\mu)}$
D_1	$C_{22} = 0, M_{11} = M_{12}$	$e^{i(\phi_e - \phi_\mu)}$	$M_{22} = 0, C_{11} = C_{12}$	$e^{i(\phi_\mu - \phi_e)}$
D_2	$C_{22} = 0, M_{11} = M_{13}$	$e^{i(\phi_e - \phi_\tau)}$	$M_{22} = 0, C_{11} = C_{13}$	$e^{i(\phi_\tau - \phi_e)}$
D_3	$C_{22} = 0, M_{11} = M_{23}$	$e^{i(2\phi_e - \phi_\mu - \phi_\tau)}$	$M_{22} = 0, C_{11} = C_{23}$	$e^{i(-2\phi_e + \phi_\mu + \phi_\tau)}$
D_4	$C_{22} = 0, M_{11} = M_{33}$	$e^{2i(\phi_e - \phi_\tau)}$	$M_{22} = 0, C_{11} = C_{33}$	$e^{2i(\phi_\tau - \phi_e)}$
D_5	$C_{22} = 0, M_{12} = M_{13}$	$e^{i(\phi_\mu - \phi_\tau)}$	$M_{22} = 0, C_{12} = C_{13}$	$e^{i(\phi_\tau - \phi_\mu)}$
D_6	$C_{22} = 0, M_{12} = M_{23}$	$e^{i(\phi_e - \phi_\tau)}$	$M_{22} = 0, C_{12} = C_{23}$	$e^{i(\phi_\tau - \phi_e)}$
D_7	$C_{22} = 0, M_{12} = M_{33}$	$e^{i(\phi_e + \phi_\mu - 2\phi_\tau)}$	$M_{22} = 0, C_{12} = C_{33}$	$e^{i(-\phi_e - \phi_\mu + 2\phi_\tau)}$
D_8	$C_{22} = 0, M_{13} = M_{23}$	$e^{i(\phi_e - \phi_\mu)}$	$M_{22} = 0, C_{13} = C_{23}$	$e^{i(\phi_\mu - \phi_e)}$
D_9	$C_{22} = 0, M_{13} = M_{33}$	$e^{i(\phi_e - \phi_\tau)}$	$M_{22} = 0, C_{13} = C_{33}$	$e^{i(\phi_\tau - \phi_e)}$
D_{10}	$C_{22} = 0, M_{23} = M_{33}$	$e^{i(\phi_\mu - \phi_\tau)}$	$M_{22} = 0, C_{23} = C_{33}$	$e^{i(\phi_\tau - \phi_\mu)}$
E_1	$C_{23} = 0, M_{11} = M_{12}$	$e^{i(\phi_e - \phi_\mu)}$	$M_{23} = 0, C_{11} = C_{12}$	$e^{i(\phi_\mu - \phi_e)}$
E_2	$C_{23} = 0, M_{11} = M_{13}$	$e^{i(\phi_e - \phi_\tau)}$	$M_{23} = 0, C_{11} = C_{13}$	$e^{i(\phi_\tau - \phi_e)}$
E_3	$C_{23} = 0, M_{11} = M_{22}$	$e^{2i(\phi_e - \phi_\mu)}$	$M_{23} = 0, C_{11} = C_{22}$	$e^{2i(\phi_\mu - \phi_e)}$
E_4	$C_{23} = 0, M_{11} = M_{33}$	$e^{2i(\phi_e - \phi_\tau)}$	$M_{23} = 0, C_{11} = C_{33}$	$e^{2i(\phi_\tau - \phi_e)}$
E_5	$C_{23} = 0, M_{12} = M_{13}$	$e^{i(\phi_\mu - \phi_\tau)}$	$M_{23} = 0, C_{12} = C_{13}$	$e^{i(\phi_\tau - \phi_\mu)}$
E_6	$C_{23} = 0, M_{12} = M_{22}$	$e^{i(\phi_e - \phi_\mu)}$	$M_{23} = 0, C_{12} = C_{22}$	$e^{i(\phi_\mu - \phi_e)}$

TABLE 2: Continued.

Cases	X	P	Y	Q
E_7	$C_{23} = 0, M_{13} = M_{33}$	$e^{i(\phi_e - \phi_\mu - 2\phi_\tau)}$	$M_{23} = 0, C_{13} = C_{33}$	$e^{i(-\phi_e + \phi_\mu + 2\phi_\tau)}$
E_8	$C_{23} = 0, M_{13} = M_{22}$	$e^{i(\phi_e - \phi_\tau - 2\phi_\mu)}$	$M_{23} = 0, C_{13} = C_{22}$	$e^{i(-\phi_e + \phi_\tau + 2\phi_\mu)}$
E_9	$C_{23} = 0, M_{13} = M_{33}$	$e^{i(\phi_e - \phi_\tau)}$	$M_{23} = 0, C_{13} = C_{33}$	$e^{i(\phi_\tau - \phi_e)}$
E_{10}	$C_{23} = 0, M_{22} = M_{33}$	$e^{2i(\phi_\mu - \phi_\tau)}$	$M_{23} = 0, C_{22} = C_{33}$	$e^{2i(\phi_\tau - \phi_\mu)}$
F_1	$C_{33} = 0, M_{11} = M_{12}$	$e^{i(\phi_e - \phi_\mu)}$	$M_{33} = 0, C_{11} = C_{12}$	$e^{i(\phi_\mu - \phi_e)}$
F_2	$C_{33} = 0, M_{11} = M_{13}$	$e^{i(\phi_e - \phi_\tau)}$	$M_{33} = 0, C_{11} = C_{13}$	$e^{i(\phi_\tau - \phi_e)}$
F_3	$C_{33} = 0, M_{11} = M_{22}$	$e^{2i(\phi_e - \phi_\mu)}$	$M_{33} = 0, C_{11} = C_{22}$	$e^{2i(\phi_\mu - \phi_e)}$
F_4	$C_{33} = 0, M_{11} = M_{23}$	$e^{i(2\phi_e - \phi_\mu - \phi_\tau)}$	$M_{33} = 0, C_{11} = C_{23}$	$e^{i(-2\phi_e + \phi_\mu + \phi_\tau)}$
F_5	$C_{33} = 0, M_{12} = M_{13}$	$e^{i(\phi_\mu - \phi_\tau)}$	$M_{33} = 0, C_{12} = C_{13}$	$e^{i(\phi_\tau - \phi_\mu)}$
F_6	$C_{33} = 0, M_{12} = M_{22}$	$e^{i(\phi_e - \phi_\mu)}$	$M_{33} = 0, C_{12} = C_{22}$	$e^{i(\phi_\mu - \phi_e)}$
F_7	$C_{33} = 0, M_{12} = M_{23}$	$e^{i(\phi_e - \phi_\tau)}$	$M_{33} = 0, C_{12} = C_{23}$	$e^{i(\phi_\tau - \phi_e)}$
F_8	$C_{33} = 0, M_{13} = M_{22}$	$e^{i(\phi_e + \phi_\tau - 2\phi_\mu)}$	$M_{33} = 0, C_{13} = C_{22}$	$e^{i(-\phi_e - \phi_\tau + 2\phi_\mu)}$
F_9	$C_{33} = 0, M_{13} = M_{23}$	$e^{i(\phi_e - \phi_\mu)}$	$M_{33} = 0, C_{13} = C_{23}$	$e^{i(\phi_\mu - \phi_e)}$
F_{10}	$C_{33} = 0, M_{22} = M_{23}$	$e^{i(\phi_\mu - \phi_\tau)}$	$M_{33} = 0, C_{22} = C_{23}$	$e^{i(\phi_\tau - \phi_\mu)}$

On the other hand, only four $A_1, A_4, A_5,$ and A_6 seem to be viable with current oscillation data for type Y, while inverted mass spectrum (IS) is ruled out for these cases.

For both types X and Y, no noticeable constraint has been found on the parameter space of CP-violating phases (ρ, σ, δ). For type X, all the viable cases predict the value of $|M|_{ee}$ in the range of 0.01eV to 0.05eV. This prediction lies well within the sensitivity limit of neutrinoless double-beta decay experiments [49–51]. On the other hand, for type Y, $|M|_{ee}$ is predicted to be zero implying that neutrinoless double-beta decay is forbidden. Also the lower bound on lowest neutrino mass (m_o) is found to be extremely small ($\sim 10^{-3}$ or less) for all the viable cases of type X and type Y structure (Table 3). For the purpose of illustration, we have presented the correlation plots for A_1 indicating the parameter space of $\rho, \sigma, \delta, |M|_{ee}$, and lowest neutrino mass (m_o) (Figures 1 and 2).

Category B (C). In Category B, all the ten possible cases are allowed for both type X and type Y structure, respectively, at 3σ CL (Table 4). Cases $B_{2,3,4,5,8,9,10}$ allow both NS and IS for type X, while cases $B_{1,2,3,4,5,8,9,10}$ allow both NS and IS for type Y. As mentioned earlier, cases of Category B are related to cases belonging to Category C via permutation symmetry; therefore we can obtain the results for Category C from B by using (41).

Type X cases B_1 (IS), B_2 (IS), B_3 (NS, IS), B_4 (IS), B_5 (NS, IS), B_7 (NS), B_8 (IS), B_9 (NS, IS), B_{10} (IS), C_1 (IS), C_2 (IS), C_4 (IS), C_5 (NS, IS), C_6 (NS, IS), C_7 (NS), C_8 (IS), C_8 (IS), C_9 (NS, IS), and C_{10} (IS) cover literally the complete range of δ . However, for B_2 (NS), B_4 (NS), B_6 (NS), B_8 (NS), B_{10} (NS), C_3 (NS), C_5 (NS), C_7 (NS), C_8 (NS), and C_{10} (NS) the parameter space of δ is found to be reduced to an appreciable extent (Table 4).

On the other hand, type Y cases B_1 (NS), B_2 (NS), B_3 (NS, IS), B_4 (NS), B_5 (NS, IS), B_7 (IS), B_8 (NS), B_9 (NS, IS), B_{10} (NS), C_1 (NS), C_2 (NS), C_4 (NS), C_5 (NS, IS), C_6 (NS, IS), C_7 (IS), C_8 (NS), C_8 (NS), C_9 (NS, IS), and C_{10} (NS) cover approximately

the complete range of δ . For B_1 (IS), B_2 (IS), B_4 (IS), B_6 (IS), B_8 (IS), B_{10} (IS), C_1 (IS), C_3 (IS), C_5 (IS), C_7 (IS), C_8 (IS), and C_{10} (IS), the parameter space of δ is found to be constricted (Table 4).

From the analysis, it is found that textures $B_2, B_4, C_5,$ and C_7 belonging to type X predict near maximal Dirac type CP violation (i.e., $\delta \approx 90^\circ$ and 270°) for NS. In addition, the Majorana phases ρ and σ are found to be very close to 0° for these cases. On the other hand, in case of type Y, $B_1, B_2, B_4, B_6, C_1, C_4, C_5$ and C_7 show almost similar constraints on the parameter space for δ however for opposite mass spectrum (Table 4). In Figures 3, 4, 5, and 6, we have compiled the correlation plots for case B_2 for both types X and Y comprising the unknown parameters $\rho, \sigma, \delta, |M|_{ee}$, and lowest neutrino mass (m_o). As explicitly shown in Figures 3(a), 3(b), and 6(b), $\delta \approx 90^\circ$ and 270° , while $\rho, \sigma \approx 0^\circ$. The correlation plots between $|M|_{ee}$ and m_o have been encapsulated in Figures 3(c), 4(c), 5(c), and 6(c). The plots indicate the strong linear relation correlation between these parameters and, in addition, the lower bound on both the parameters is somewhere in the range from 0.001 to 0.01 eV. The prediction for the allowed space of $|M|_{ee}$ for all the cases of category B is given in Table 4.

Category D (F). In Category D, only nine cases are acceptable with neutrino oscillation data at 3σ CL for both type X and type Y structures, respectively, while case D_8 is excluded for both of them (Table 5). Cases $D_1, D_2, D_4, D_5, D_6, D_7,$ and D_9 show both NS and IS for type X and type Y, respectively, while D_3 and D_{10} are acceptable for IS (NS) and NS(IS), respectively, in case of type X (type Y) structure. Similarly, the results for cases belonging to Category F can be obtained from Category D since both are related via permutation symmetry. It is found that only nine cases are allowed with data in category F, while F_7 is excluded at 3σ CL.

Cases D_1 (NS), D_2 (NS, IS), D_3 (IS), D_4 (NS), D_5 (NS, IS), D_6 (NS), D_7 (NS), D_9 (NS), D_{10} (NS), F_1 (NS), F_2 (NS, IS), F_3 (IS), F_4 (NS), F_5 (NS, IS), F_6 (NS), F_7 (NS), F_9 (NS), and

TABLE 3: The allowed ranges of Dirac CP-violating phase δ , the Majorana phases ρ, σ , effective neutrino mass $|M|_{ee}$, and lowest neutrino mass m_0 for the experimentally allowed cases of Category A at 3σ CL. The predictions corresponding to $(\lambda_{13})_-$ and $(\lambda_{23})_-$ neutrino mass ratios have been put into brackets.

Cases	NS	X	Y	IS
		IS	NS	
A_1	×	$\rho = -90^\circ - -72^\circ \oplus 72^\circ - 90^\circ$	$\rho = -90^\circ - 90^\circ$	×
	×	$= (-90^\circ - -72^\circ \oplus 72^\circ - 90^\circ)$	$= (-90^\circ - 90^\circ)$	×
	×	$\sigma = -90^\circ - 90^\circ$	$\sigma = -90^\circ - 90^\circ$	×
	×	$= (-90^\circ - 90^\circ)$	$= (-90^\circ - 90^\circ)$	×
	×	$\delta = 0^\circ - 93.2^\circ \oplus 116.6^\circ - 247.7^\circ \oplus 268.8^\circ - 360^\circ$	$\delta = 0^\circ - 360^\circ$	×
	×	$= (0^\circ - 166.27^\circ \oplus 191.98^\circ - 360^\circ)$	$= (0^\circ - 360^\circ)$	×
	×	$ M _{ee} = 0.0114 - 0.0540$	$ M _{ee} = 0.0$	×
	×	$m_0 = 0.000820 - 0.0470$	$m_0 = 0.00155 - 0.0103$	×
$A_2(A_8)$	×	$\rho = -85.6^\circ - -76.3^\circ \oplus 76.4^\circ - 85.6^\circ$	×	×
	×	$= (-85.4^\circ - -78.1^\circ \oplus 78.2^\circ - 85.1^\circ)$	×	×
	×	$\sigma = -70.1^\circ - -43.1^\circ \oplus 43.1^\circ - 70^\circ$	×	×
	×	$= (-70.1^\circ - -44.2^\circ \oplus 43.3^\circ - 76^\circ)$	×	×
	×	$\delta = 0^\circ - 360^\circ$	×	×
	×	$= (0^\circ - 360^\circ)$	×	×
	×	$ M _{ee} = 0.0273 - 0.0489$	×	×
	×	$m_0 = 0.000820 - 0.0484$	×	×
$A_3(A_7)$	×	$\rho = -81.94^\circ - -75.9^\circ \oplus 75.4^\circ - 81.93^\circ$	×	×
	×	$= (-82.4^\circ - -77.1^\circ \oplus 76.9^\circ - 82^\circ)$	×	×
	×	$\sigma = -70.1^\circ - -52.1^\circ \oplus 50.47^\circ - 66.41^\circ$	×	×
	×	$= (-72^\circ - -54.2^\circ \oplus 53.3^\circ - 73^\circ)$	×	×
	×	$\delta = 0^\circ - 360^\circ$	×	×
	×	$= (0^\circ - 360^\circ)$	×	×
	×	$ M _{ee} = 0.0308 - 0.0451$	×	×
	×	$m_0 = 0.000969 - 0.00187$	×	×
$A_4(A_6)$	×	$\rho = -89.8^\circ - -71.2^\circ \oplus 71.1^\circ - 89.9^\circ$	$\rho = -90^\circ - 90^\circ$	×
	×	$= (-90^\circ - -72.1^\circ \oplus 72^\circ - 90^\circ)$	$= (-90^\circ - 90^\circ)$	×
	×	$\sigma = -90^\circ - 90^\circ$	$\sigma = -90^\circ - 90^\circ$	×
	×	$= (-90^\circ - 90^\circ)$	$= (-90^\circ - 90^\circ)$	×
	×	$\delta = 29.78^\circ - 89.64^\circ \oplus 148.6^\circ - 208^\circ \oplus 269.8^\circ - 329^\circ$	$\delta = 0^\circ - 360^\circ$	×
	×	$= (0^\circ - 29.78^\circ \oplus 90.98^\circ - 151.64^\circ \oplus 208.6^\circ - 271^\circ \oplus 329.8^\circ - 360^\circ)$	$\delta = 0^\circ - 360^\circ$	×
	×	$ M _{ee} = 0.0108 - 0.0501$	$ M _{ee} = 0.0$	×
	×	$m_0 = 0.000904 - 0.00440$	$m_0 = 0.00143 - 0.0103$	×
$A_5(A_5)$	×	$\rho = -90^\circ - -71^\circ \oplus 71^\circ - 90^\circ$	$\rho = -90^\circ - -42.3^\circ \oplus 41.5^\circ - 90^\circ$	×
	×	$= (-90^\circ - -71.2^\circ \oplus 72^\circ - 90^\circ)$	$= (-56.6^\circ - 56.7^\circ)$	×
	×	$\sigma = -90^\circ - 90^\circ$	$\sigma = -62.5^\circ - 62.4^\circ$	×
	×	$= (-90^\circ - 90^\circ)$	$= (-90^\circ - -41.2^\circ \oplus 41.4^\circ - 90^\circ)$	×
	×	$\delta = 0^\circ - 44^\circ \oplus 92^\circ - 162^\circ \oplus 198^\circ - 268^\circ \oplus 327^\circ - 360^\circ$	$\delta = 0^\circ - 360^\circ$	×
	×	$= (27.36^\circ - 109.3^\circ \oplus 147.9^\circ - 209.37^\circ \oplus 250.7^\circ - 331^\circ)$	$= 0^\circ - 360^\circ$	×
	×	$ M _{ee} = 0.0113 - 0.0500$	$ M _{ee} = 0.0$	×
	×	$m_0 = 0.000822 - 0.00440$	$m_0 = 0.00306 - 0.0105$	×
$A_9(A_{10})$	×	$\rho = -84.2^\circ - -74.53^\circ \oplus 73.52^\circ - 84.2^\circ$	×	×
	×	$= (-84.2^\circ - -75^\circ \oplus 75^\circ - 85.1^\circ)$	×	×
	×	$\sigma = -74.83^\circ - -50.3^\circ \oplus 50.1^\circ - 73.4^\circ$	×	×
	×	$= (-75^\circ - -50.3^\circ \oplus 50.1^\circ - 75^\circ)$	×	×
	×	$\delta = 0^\circ - 360^\circ$	×	×
	×	$= (0^\circ - 360^\circ)$	×	×
	×	$ M _{ee} = 0.0293 - 0.0469$	×	×
	×	$m_0 = 0.000940 - 0.00190$	×	×

TABLE 4: The allowed ranges of Dirac CP-violating phase δ , the Majorana phases ρ, σ , effective neutrino mass $|M|_{\text{ee}}$, and lowest neutrino mass m_0 for the experimentally allowed cases of Category B(C) at 3σ CL. The predictions corresponding to $(\lambda_{13})_-$ and $(\lambda_{23})_-$ neutrino mass ratios have been put into brackets.

Cases	X			Y		
	NS	IS	IS	NS	IS	IS
$B_1(C_1)$	×	$\rho = -90^\circ - 58.7^\circ \oplus -23.8^\circ - 15^\circ \oplus 58.8^\circ - 90^\circ$ $= (-67.7^\circ - -16.6^\circ \oplus 16.6^\circ - 68.5^\circ)$	$\rho = -90^\circ - 90^\circ$ $= (-90^\circ - 90^\circ)$	$\rho = -87.04 - 86.7^\circ$ $= (-90^\circ - -3.17^\circ \oplus 2.38^\circ - 90^\circ)$		
	×	$\sigma = -87^\circ - 87.9^\circ$	$\sigma = -90^\circ - -64.8^\circ \oplus -24.98^\circ - 24.62^\circ$ $= (-72.3^\circ - -20.2^\circ \oplus 20.44^\circ - 72.44^\circ)$	$\sigma = -90^\circ - -64.96^\circ \oplus -24.8^\circ - 24.5^\circ \oplus 65^\circ - 90^\circ$ $= (-90^\circ - 90^\circ)$		
	×	$\delta = 0^\circ - 78.9^\circ \oplus 98.7^\circ - 261^\circ \oplus 282^\circ - 360^\circ$ $= (6.14^\circ - 166.27^\circ \oplus 194.7^\circ - 353.44^\circ)$	$\delta = 0^\circ - 75.9^\circ \oplus 111.4^\circ - 247^\circ \oplus 283^\circ - 360^\circ$ $= (19.7^\circ - 157^\circ \oplus 205.9^\circ - 340.5^\circ)$	$\delta = 80.8^\circ - 93.6^\circ \oplus 267.6^\circ - 279.5^\circ$ $= (87.8^\circ - 101.6^\circ \oplus 259.6^\circ - 273.5^\circ)$		
	×	$ M _{\text{ee}} = 0.0221 - 0.0371$ $m_0 = 0.00412 - 0.0139$	$ M _{\text{ee}} = 0.0 - 0.00991$ $m_0 = 0.002286 - 0.0165$	$ M _{\text{ee}} = 0.0417 - 0.0540$ $m_0 = 0.0430 - 0.0540$		
	×	$\rho = -86.6^\circ - 87.08^\circ$ $= (-90^\circ - 90^\circ)$	$\rho = -90^\circ - 90^\circ$ $= (-77.08^\circ - 76.8^\circ)$	$\rho = -2.98^\circ - 2.97^\circ$ $= (-2.14^\circ - -0.96^\circ \oplus 0.89^\circ - 2.15^\circ)$		
	×	$\sigma = -90^\circ - 90^\circ$ $= (-90^\circ - 90^\circ)$	$\sigma = -68.7 - 67.9$ $= (-90^\circ - 90^\circ)$	$\sigma = -1.01^\circ - 1.09^\circ$ $= (-1.38^\circ - -0.131^\circ \oplus 0.140^\circ - 1.28^\circ)$		
$B_2(C_7)$		$\delta = 20.1^\circ - 89.64^\circ \oplus 127.8^\circ - 229.0^\circ \oplus 268.4^\circ - 340^\circ$	$\delta = 30.59 - 328.9^\circ$	$\delta = 88.13^\circ - 92.15^\circ \oplus 267.4^\circ - 271.0^\circ$		
		$= (0.0^\circ - 53.7^\circ \oplus 86.8^\circ - 160^\circ \oplus 213.5^\circ - 271^\circ \oplus 306^\circ - 360^\circ)$	$= (0^\circ - 30.08^\circ \oplus 220.4^\circ - 360^\circ)$	$= (88.29^\circ - 97.02^\circ \oplus 267.8^\circ - 271^\circ)$		
		$ M _{\text{ee}} = 0.0213 - 0.303$ $m_0 = 0.00499 - 0.312$	$ M _{\text{ee}} = 0.00231 - 0.303$ $m_0 = 0.00203 - 0.304$	$ M _{\text{ee}} = 0.0535 - 0.445$ $m_0 = 0.0300 - 0.441$		
		$\rho = -50^\circ - 50^\circ$ $= (-62.5^\circ - 62^\circ)$	$\rho = -53.4^\circ - 53.69^\circ$ $= (-52.5^\circ - -9.48^\circ \oplus 10.46^\circ - 52.5^\circ)$	$\rho = -90^\circ - -5.48^\circ \oplus 5.46^\circ - 90^\circ$ $= (-83.4^\circ - -5.95^\circ \oplus 3.30^\circ - 84.56^\circ)$		
		$\sigma = -63.2^\circ - -38.6^\circ \oplus 38^\circ - 63.8^\circ$ $= (-56.7^\circ - 57^\circ)$	$\sigma = -80^\circ - -3.28^\circ \oplus 3.28^\circ - 80^\circ$ $= (-77.7^\circ - 79.1^\circ)$	$\sigma = -90^\circ - 2.28^\circ \oplus 2.54^\circ - 90^\circ$ $= (-90^\circ - 3.58^\circ \oplus 2.68^\circ - 90^\circ)$		
		$\delta = 0^\circ - 40.5^\circ \oplus 87.5^\circ - 156.7^\circ \oplus 158.9^\circ - 272^\circ \oplus 321^\circ - 360^\circ$	$\delta = 0^\circ - 91.6^\circ \oplus 156.8^\circ - 204^\circ \oplus 271^\circ - 360^\circ$ $(4.79^\circ - 41.6^\circ \oplus 82.5^\circ - 277.9^\circ \oplus 319^\circ - 354^\circ)$	$\delta = 82.39^\circ - 173.02^\circ \oplus 192.8^\circ - 277^\circ$ $= (6.48^\circ - 91.8^\circ \oplus 268.7^\circ - 351^\circ)$		
$B_3(C_6)$		$= (3^\circ - 90^\circ \oplus 153^\circ - 205^\circ \oplus 272^\circ - 358^\circ)$	$=$	$= (6.48^\circ - 91.8^\circ \oplus 268.7^\circ - 351^\circ)$		
		$ M _{\text{ee}} = 0.0180 - 0.500$ $m_0 = 0.0180 - 0.494$	$ M _{\text{ee}} = 0.00154 - 0.0490$ $m_0 = 0.0 - 0.484$	$ M _{\text{ee}} = 0.0441 - 0.497$ $m_0 = 0.0231 - 0.498$		
		$\rho = -80^\circ - -0.088^\circ \oplus 0.088^\circ - 80^\circ$ $= (-90^\circ - 90^\circ)$	$\rho = -50^\circ - 50^\circ$ $= (-62.5^\circ - 62^\circ)$	$\rho = -90^\circ - -5.48^\circ \oplus 5.46^\circ - 90^\circ$ $= (-83.4^\circ - -5.95^\circ \oplus 3.30^\circ - 84.56^\circ)$		
		$\sigma = -90^\circ - -0.09^\circ \oplus 0.09^\circ - 90^\circ$ $= (-90^\circ - 90^\circ)$	$\sigma = -63.2^\circ - -38.6^\circ \oplus 38^\circ - 63.8^\circ$ $= (-56.7^\circ - 57^\circ)$	$\sigma = -90^\circ - 2.28^\circ \oplus 2.54^\circ - 90^\circ$ $= (-90^\circ - 3.58^\circ \oplus 2.68^\circ - 90^\circ)$		
		$\delta = 31.49^\circ - 95.98^\circ \oplus 146^\circ - 176^\circ \oplus 184^\circ - 213^\circ \oplus 263^\circ - 329^\circ$	$\delta = 0^\circ - 40.5^\circ \oplus 87.5^\circ - 156.7^\circ \oplus 158.9^\circ - 272^\circ \oplus 321^\circ - 360^\circ$	$\delta = 82.39^\circ - 173.02^\circ \oplus 192.8^\circ - 277^\circ$		
		$= (5.5^\circ - 32^\circ \oplus 93^\circ - 150.8^\circ \oplus 208^\circ - 267^\circ)$	$= (4.79^\circ - 41.6^\circ \oplus 82.5^\circ - 277.9^\circ \oplus 319^\circ - 354^\circ)$	$= (6.48^\circ - 91.8^\circ \oplus 268.7^\circ - 351^\circ)$		

TABLE 4: Continued.

Cases	X		Y	
	NS	IS	NS	IS
$B_4(C_5)$	$\rho = -2.06^0 - 2.10^0$	$\rho = -72.4^0 - 73.2^0$	$\rho = -90^0 - -11.5^0 \oplus 2.5^0 - 90^0$	$\rho = -3.0^0 - -0.0329^0 \oplus 0.0321^0 - 3.0^0$
	\times	$= (-90^0 - 90^0)$	$= (-79.4^0 - 80.2^0)$	$= (-3.0^0 - -0.0329^0 \oplus 0.0321^0 - 3.0^0)$
	$\sigma = -7.45^0 - 7.45^0$	$\sigma = -90^0 - 90^0$	$\sigma = -71.45^0 - 70.45^0$	$\sigma = -3.22^0 - 3.29^0$
	\times	$= (-90^0 - 90^0)$	$= (-90^0 - -17.0^0 \oplus 16.2^0 - 90^0)$	$= (-3.38^0 - -1.24^0 \oplus 1.28^0 - 3.48^0)$
	$\delta = 89.2^0 - 97^0 \oplus 263.4^0 - 270.58^0$	$\delta =$ $21.19^0 - 89.6^0 \oplus 141^0 - 218^0 \oplus 276^0 - 339^0$ $= (0^0 - 33^0 \oplus 85.6^0 - 158.5^0 \oplus 214.4^0 -$ $274^0 \oplus 322^0 - 360^0)$	$\delta = 85.6^0 - 274^0$	$\delta = 88.69^0 - 92.25^0 \oplus 267.8^0 - 270.1^0$
	\times	$ M _{ee} = 0.0226 - 0.275$ $m_0 = 0.0282 - 0.284$	$ M _{ee} = 0.00532 - 0.405$ $m_0 = 0.0 - 0.404$	$= (88.9^0 - 92.57^0 \oplus 267.8^0 - 270.9^0)$ $ M _{ee} = 0.0512 - 0.0414$ $m_0 = 0.0260 - 0.410$
$B_5(C_4)$	$\rho = -61.6^0 - 60.23^0$	$\rho = -90^0 - -9^0 \oplus 9^0 - 90^0$	$\rho = -90^0 - -13.6^0 \oplus 11.8^0 - 90^0$	$\rho = -16.6^0 - 16.4^0$
	$= (-65^0 - -57^0 \oplus -19^0 - 19^0 \oplus 57^0 - 65^0)$	$= (-90^0 - -10^0 \oplus 10^0 - 90^0)$	$= (-90^0 - -8.79^0 \oplus 7.03^0 - 90^0)$	$= (-24.5^0 - -1.8^0 \oplus 1.2^0 - 23.4^0)$
	$\sigma = -64^0 - 64.08^0$	$\sigma = -90^0 - 90^0$	$\sigma = -71.8^0 - -6.6^0 \oplus 7.56^0 - 72^0$	$\sigma = -21.5^0 - 21.5^0$
	$= (-65^0 - -57^0 \oplus -19^0 - 19^0 \oplus 57^0 - 65^0)$	$= (-87^0 - -0.4^0 \oplus 0.06^0 - 88.1^0)$	$= (-90^0 - -13.6^0 \oplus 9.4^0 - 90^0)$	$= (-18.6^0 - 18.9^0)$
	$\delta = 52.5^0 - 175.6^0 \oplus 184^0 - 307^0$	$\delta =$ $28.17^0 - 87^0 \oplus 120^0 - 239.5^0 \oplus 272^0 - 331^0$	$\delta =$ $35.6^0 - 92.4^0 \oplus 140.8^0 - 220.6^0 \oplus 266^0 - 325^0$ $= (5.4^0 - 37.7^0 \oplus 87.8^0 - 144.5^0 \oplus 215^0 -$ $273^0 \oplus 328^0 - 353^0)$	$\delta =$ $58.7^0 - 96.7^0 \oplus 261.8^0 - 301.9^0$ $= (80.69^0 - 121.9^0 \oplus 238.7^0 - 273.5^0)$
	$= (6.5^0 - 63.4^0 \oplus 148^0 - 158^0 \oplus 204^0 -$ $213^0 \oplus 295^0 - 353^0)$	$=$ $(7.3^0 - 29.8^0 \oplus 56.3^0 - 165.4^0 \oplus 196^0 - 348^0)$	$ M _{ee} = 0.0417 - 0.498$ $m_0 = 0.00687 - 0.498$	$ M _{ee} = 0.0417 - 0.498$ $m_0 = 0.00687 - 0.498$
	$ M _{ee} = 0.00710 - 0.465$ $m_0 = 0.00855 - 0.478$	$ M _{ee} = 0.0114 - 0.550$ $m_0 = 0.00386 - 0.500$	$ M _{ee} = 0.0441 - 0.469$ $m_0 = 0.0540 - 0.473$	$\rho = -90^0 - 90^0$ $= (-90^0 - 90^0)$ $\sigma = -90^0 - 90^0$ $= (-90^0 - 90^0)$
$B_6(C_3)$	$\rho = -80^0 - 80^0$	\times	\times	$\rho = -90^0 - 90^0$
	$=$ $(-90^0 - -25^0 \oplus -8.27^0 - 10.26^0 \oplus 25^0 - 90^0)$	\times	\times	$= (-90^0 - 90^0)$
	$\sigma = -90^0 - 90^0$	\times	\times	$\sigma = -90^0 - 90^0$
	$= (-90^0 - -1.7^0 \oplus -1.7^0 - 1.4^0 \oplus 16.8^0 - 90^0)$	\times	\times	$= (-90^0 - 90^0)$
	$\delta = 64.29^0 - 175.6^0 \oplus 189^0 - 295^0$ $= (64.38^0 - 151^0 \oplus 207.8^0 - 296^0)$	\times	\times	$\delta = 58.7^0 - 96.7^0 \oplus 261.8^0 - 301.9^0$ $= (80.69^0 - 121.9^0 \oplus 238.7^0 - 273.5^0)$
	$ M _{ee} = 0.0121 - 0.255$ $m_0 = 0.0121 - 0.280$	\times	\times	$ M _{ee} = 0.0414 - 0.334$ $m_0 = 0.0129 - 0.332$

TABLE 4: Continued.

Cases	X			Y		
	NS	IS	NS	NS	IS	IS
$B_7(C_2)$	$\rho = -43.9^0 - 45.7^0$ $= (-18.06^0 - 2.56^0 \oplus 1.98^0 - 18.27^0)$ $\sigma = -51.27^0 - 50.63^0$ $= (-25.85^0 - 3.45^0 \oplus 2.54^0 - 26.29^0)$ $\delta = 55.28^0 - 175.6^0 \oplus 186.5^0 - 305^0$ $= (5.33^0 - 60.4^0 \oplus 300^0 - 352.3^0)$ $ M _{ee} = 0.00687 - 0.439$ $m_0 = 0.00687 - 0.439$	\times \times \times \times \times \times \times \times	\times \times \times \times \times \times \times \times	\times \times \times \times \times \times \times \times	$\rho = -18.8^0 - 18.4^0$ $= (-25.6^0 - 25.7^0)$ $\sigma = -25.7^0 - 25.8^0$ $= (-16.9^0 - 16.8^0)$ $\delta = 30^0 - 94^0 \oplus 141.6^0 - 175.6^0 \oplus$ $184.5^0 - 220.6^0 \oplus 266^0 - 325^0$ $= (13.4^0 - 35.9^0 \oplus 88.8^0 - 140.8^0 \oplus 218^0 -$ $271^0 \oplus 325^0 - 360^0)$ $ M _{ee} = 0.0417 - 0.479$ $m_0 = 0.00687 - 0.471$	$\rho = -18.8^0 - 18.4^0$ $= (-25.6^0 - 25.7^0)$ $\sigma = -25.7^0 - 25.8^0$ $= (-16.9^0 - 16.8^0)$ $\delta = 30^0 - 94^0 \oplus 141.6^0 - 175.6^0 \oplus$ $184.5^0 - 220.6^0 \oplus 266^0 - 325^0$ $= (13.4^0 - 35.9^0 \oplus 88.8^0 - 140.8^0 \oplus 218^0 -$ $271^0 \oplus 325^0 - 360^0)$ $ M _{ee} = 0.0417 - 0.479$ $m_0 = 0.00687 - 0.471$
$B_8(C_{10})$	$\rho = -90^0 - 90^0$ $= (-90^0 - 90^0)$ $\sigma = -90^0 - 90^0$ $= (-90^0 - 90^0)$ $\delta = 44.5^0 - 100^0 \oplus 139^0 - 221^0 \oplus 260.3^0 - 315^0$ $= (93^0 - 157.8^0 \oplus 201.3^0 - 267.5^0)$ $ M _{ee} = 0.0 - 0.295$ $m_0 = 0.00486 - 0.300$	\times \times \times \times \times \times \times \times	$\rho = -51.2^0 - 51^0$ $= (-52.5^0 - -40^0 \oplus 40^0 - 53^0)$ $\sigma = -90^0 - 90^0$ $= (-90^0 - 90^0)$ $\delta = 0^0 - 40.5^0 \oplus 87.5^0 - 156.7^0 \oplus 158.9^0 -$ $272^0 \oplus 321^0 - 360^0$ $= (0^0 - 80.7^0 \oplus 127^0 - 147.1^0 \oplus 210^0 -$ $234.5^0 \oplus 280^0 - 360^0)$ $ M _{ee} = 0.00968 - 0.250$ $m_0 = 0.00412 - 0.269$	\times \times \times \times \times \times \times \times	$\rho = -72.8^0 - 72.7^0$ $= (-90^0 - 90^0)$ $\sigma = -90^0 - 90^0$ $= (-67.8^0 - 67.7^0)$ $\delta = 0^0 - 360^0$ $= (0^0 - 360^0)$ $ M _{ee} = 0.000637 - 0.174$ $m_0 = 0.00136 - 0.179$	$\rho = -89.8^0 - 88.7^0$ $= (-89.8^0 - 89.7^0)$ $\sigma = -89^0 - 89^0$ $= (-89^0 - 89^0)$ $\delta = 45.6^0 - 133.6^0 \oplus 226^0 - 313^0$ $= (48.6^0 - 134.6^0 \oplus 226^0 - 313.1^0)$ $ M _{ee} = 0.0408 - 0.265$ $m_0 = 0.0 - 0.248$
$B_9(C_9)$	$\rho = -80^0 - 80^0$ $= (-90^0 - 90^0)$ $\sigma = -88^0 - 88^0$ $= (-90^0 - 90^0)$ $\delta = 22.96^0 - 92.3^0 \oplus 141^0 - 241.5^0 \oplus$ $267.3^0 - 336^0$ $= (8.47^0 - 157.8^0 \oplus 201.3^0 - 348.5^0)$ $ M _{ee} = 0.00761 - 0.250$ $m_0 = 0.00688 - 0.146$	\times \times \times \times \times \times \times \times	$\rho = -70^0 - 70^0$ $= (-69.5^0 - 69.3^0)$ $\sigma = -90^0 - 90^0$ $= (-78.9^0 - 87^0)$ $\delta = 0^0 - 81^0 \oplus 92.5^0 - 269^0 \oplus 278^0 - 360^0$ $= (0^0 - 135^0 \oplus 158.7^0 - 205.4^0 \oplus 225^0 - 360^0)$ $ M _{ee} = 0.00688 - 0.450$ $m_0 = 0.00109 - 0.476$	\times \times \times \times \times \times \times \times	$\rho = -90^0 - 90^0$ $= (-68.6^0 - 68.9^0)$ $\sigma = -72.3^0 - 72.6^0$ $= (-90^0 - 90^0)$ $\delta = 0^0 - 360^0$ $= (0^0 - 360^0)$ $ M _{ee} = 0.0 - 0.465$ $m_0 = 0.00 - 0.463$	$\rho = -90^0 - 3.7^0 \oplus 16.7^0 - 90^0$ $= (-84.7^0 - 82.3^0)$ $\sigma = -90^0 - 3.7 \oplus 18.7^0 - 90^0$ $= (-90^0 - 90^0)$ $\delta = 40.6^0 - 161.7^0 \oplus 198.7^0 - 337^0$ $= (9.68^0 - 151.1^0 \oplus 200.3^0 - 352.5^0)$ $ M _{ee} = 0.0441 - 0.207$ $m_0 = 0.00239 - 0.199$

TABLE 4: Continued.

Cases	X		Y	
	NS	IS	NS	IS
$B_{10}(C_8)$	$\rho = -90^\circ - 90^\circ$ $= (-90^\circ - 90^\circ)$ $\sigma = -90^\circ - 90^\circ$ $= (-90^\circ - 90^\circ)$	$\rho = -75.19^\circ - 75.1^\circ$ $= (-90^\circ - -55^\circ \oplus -23.1^\circ - 22.7^\circ \oplus 57^\circ - 90^\circ)$ $\sigma = -88^\circ - 88^\circ$ $= (-90^\circ - 90^\circ)$	$\rho = -90^\circ - 90^\circ$ $= (-90^\circ - 90^\circ)$ $\sigma = -90^\circ - 90^\circ$ $= (-90^\circ - 90^\circ)$ $\delta = 0^\circ - 360^\circ$ $= (0^\circ - 360^\circ)$	$\rho = -81.5^\circ - 82^\circ$ $= (-90^\circ - 90^\circ)$ $\sigma = -90^\circ - 90^\circ$ $= (-90^\circ - 90^\circ)$ $\delta = 46.6^\circ - 91.2^\circ \oplus 271.8^\circ - 314.9^\circ$ $= (89.9^\circ - 132^\circ \oplus 228^\circ - 270^\circ)$
	$\delta = 81.8^\circ - 155.3^\circ \oplus 204.5^\circ - 277.9^\circ$ $= (45.6^\circ - 85.8^\circ \oplus 144.5^\circ - 215.5^\circ \oplus 274^\circ - 315^\circ)$	$\delta = 9.2^\circ - 178^\circ \oplus 185^\circ - 352.5^\circ$ $= (0^\circ - 80.7^\circ \oplus 124^\circ - 249.1^\circ \oplus 280^\circ - 360^\circ)$		
	$ M _{ee} = 0.00581 - 0.155$ $m_{\theta} = 0.00706 - 0.153$	$ M _{ee} = 0.0138 - 0.280$ $m_{\theta} = 0.00460 - 0.134$	$ M _{ee} = 0.0 - 0.136$ $m_{\theta} = 0.0 - 0.138$	$ M _{ee} = 0.0491 - 0.0540$ $m_{\theta} = 0.0 - 0.269$

TABLE 5: The allowed ranges of Dirac CP-violating phase δ , the Majorana phases ρ , σ , effective neutrino mass $|M|_{ee}$, and lowest neutrino mass m_0 for the experimentally allowed cases of Category D(F) at 3σ CL. The predictions corresponding to $(\lambda_{13})_-$ and $(\lambda_{23})_-$ neutrino mass ratios have been put into brackets.

Cases	X		Y	
	NS	IS	NS	IS
$D_1(F_2)$	$\rho = -90^\circ - 90^\circ$	$\rho = -87.9^\circ - -30.97 \oplus 32.5 - 90^\circ$	$\rho = -84.2^\circ - -84.3^\circ$	$\rho = -86.5^\circ - 84.3^\circ$
	$= (-90^\circ - 90^\circ)$	$= (-63.8^\circ - 46.16^\circ)$	$= (-43.5^\circ - 45.3^\circ)$	$= (-90^\circ - 90^\circ)$
	$\sigma = -90^\circ - 90^\circ$	$\sigma = -44.5^\circ - 39.55^\circ$	$\sigma = -90^\circ - 90^\circ$	$\sigma = -0.0273^\circ - 0.0271^\circ$
	$= (-90^\circ - -25.6^\circ \oplus 25.5^\circ - 90^\circ)$	$= (-90^\circ - -24.6^\circ \oplus 23.5^\circ - 90^\circ)$	$= (-74.4^\circ - -15.6^\circ \oplus 11.5^\circ - 73.5^\circ)$	$= (-90^\circ - 90^\circ)$
	$\delta = 0^\circ - 360^\circ$	$\delta = 31.7^\circ - 98.4^\circ \oplus 260.8^\circ - 329^\circ$	$\delta =$ $33.3^\circ - 88.7^\circ \oplus 152.3^\circ - 207.7^\circ \oplus 274.5^\circ - 320^\circ$	$\delta =$ $0^\circ - 85.7^\circ \oplus 135.3^\circ - 224.7^\circ \oplus 272.5^\circ - 360^\circ$
$D_2(F_1)$	$= (10^\circ - 350^\circ)$	$= (100.0^\circ - 260^\circ)$	$= (89.7^\circ - 150.3^\circ \oplus 209.5^\circ - 269.4^\circ)$	$= (0^\circ - 155.3^\circ \oplus 206.5^\circ - 360^\circ)$
	$ M _{ee} = 0.0406 - 0.173$	$ M _{ee} = 0.0443 - 0.167$	$ M _{ee} = 0.0376 - 0.267$	$ M _{ee} = 0.0114 - 0.0540$
	$m_0 = 0.00137 - 0.137$	$m_0 = 0.0629 - 0.159$	$m_0 = 0.0604 - 0.384$	$m_0 = 0.00205 - 0.258$
	$\rho = -90^\circ - 90^\circ$	$\rho = -40.9^\circ - 40.1^\circ$	$\rho = -46.9^\circ - 45.9^\circ$	$\rho = -90^\circ - 90^\circ$
	$= (-90^\circ - 90^\circ)$	$= (-90^\circ - 90^\circ)$	$= (-64.5^\circ - -46.1^\circ \oplus -46.8^\circ - 65^\circ)$	$= (-90^\circ - 90^\circ)$
$D_3(F_4)$	$\sigma = -90^\circ - 90^\circ$	$\sigma = -67.5^\circ - 27^\circ \oplus 27.0^\circ - 68^\circ$	$\sigma = -74.1^\circ - -24^\circ \oplus 23.4^\circ - 70.12^\circ$	$\sigma = -90^\circ - 90^\circ$
	$= (-90^\circ - 90^\circ)$	$= (-90^\circ - 90^\circ)$	$= (-90^\circ - 70^\circ \oplus -21.0^\circ - 21^\circ \oplus 70^\circ - 90^\circ)$	$= (-90^\circ - 90^\circ)$
	$\delta = 0^\circ - 360^\circ$	$\delta = 95.78^\circ - 258.5^\circ$	$\delta = 97.78^\circ - 150^\circ \oplus 209.78^\circ - 254.6^\circ$	$\delta = 0^\circ - 31.2^\circ \oplus 93.2^\circ - 150^\circ \oplus 208.2^\circ -$ $270^\circ \oplus 328^\circ - 360^\circ$
	$= (0.0^\circ - 360^\circ)$	$= (0.0^\circ - 360^\circ)$	$= (70.5^\circ - 90.87^\circ \oplus 152^\circ - 209^\circ \oplus 271^\circ - 282^\circ)$	$= (0^\circ - 31.2^\circ \oplus 93.2^\circ - 154^\circ \oplus 208.2^\circ -$ $270^\circ \oplus 328.2^\circ - 360^\circ)$
	$ M _{ee} = 0.00771 - 0.0793$	$ M _{ee} = 0.0545 - 0.142$	$ M _{ee} = 0.0505 - 0.132$	$ M _{ee} = 0.0245 - 0.143$
$D_3(F_4)$	$m_0 = 0.00281 - 0.156$	$m_0 = 0.101 - 0.298$	$m_0 = 0.101 - 0.268$	$m_0 = 0.0124 - 0.142$
	\times	$\rho = -85.2^\circ - 85.1^\circ$	$\rho = -90^\circ - 90^\circ$	\times
	\times	$= (-90^\circ - 90^\circ)$	$\rho = -64.45^\circ - 65.6^\circ$	\times
	\times	$\sigma = -55.2^\circ - 46.8^\circ$	$\sigma = -90^\circ - 90^\circ$	\times
	\times	$= (-90^\circ - -44.8^\circ \oplus 43.6^\circ - 90^\circ)$	$= (-77.7^\circ - 78.9^\circ)$	\times
$D_3(F_4)$	\times	$\delta = 26.97^\circ - 137.87^\circ \oplus 209.3^\circ - 326.3^\circ$	$\delta =$ $0^\circ - 91.1^\circ \oplus 117.8^\circ - 245.6^\circ \oplus 266.8^\circ - 360^\circ$	\times
	\times	$= (0.0^\circ - 63^\circ \oplus 120.3^\circ - 238.8^\circ \oplus 300.8^\circ - 356.8^\circ)$	$= (31.5^\circ - 146.7^\circ \oplus 208.9^\circ - 333.6^\circ)$	\times
	\times	$ M _{ee} = 0.0461 - 0.325$	$ M _{ee} = 0.0241 - 0.243$	\times
	\times	$m_0 = 0.0499 - 0.326$	$m_0 = 0.0371 - 0.278$	\times

TABLE 5: Continued.

Cases	X			Y		
	NS	IS	IS	NS	IS	IS
$D_4(F_3)$	$\rho = -90^0 - -17^0 \oplus 18^0 - 90^0$	$\rho = -60^0 - -38.9^0 \oplus 36.75^0 - 66.66^0$	$\rho = -65.6^0 - 67.7^0$	$\rho = -90^0 - 90^0$	$\rho = -90^0 - 90^0$	$\rho = -90^0 - 90^0$
	$= (-67.7^0 \oplus 67^0)$	$= (-31.25^0 \oplus 31.5^0)$	$= (-59.8^0 - 51.6^0)$	$= (-90^0 - 90^0)$	$= (-88.9^0 - 88^0)$	$= (-88.9^0 - 88^0)$
	$\sigma = -62.5^0 \oplus 64.5^0$	$\sigma = -31.29^0 - 30.89^0$	$\sigma = -87.9^0 - 88.1^0$	$\sigma = -90^0 - 90^0$	$\sigma = -90^0 - 90^0$	$\sigma = -90^0 - 90^0$
	$= (-90^0 - -25.4^0 \oplus 25.4^0 - 90^0)$	$= (-70.38^0 - -38.1^0 \oplus 40.8^0 - 73.45^0)$	$= (-77.06^0 - 16.7^0 \oplus 13.7^0 - 76.8^0)$	$\delta = 0^0 - 360^0$	$\delta = 0^0 - 360^0$	$\delta = 0^0 - 360^0$
	$\delta = 0^0 - 360^0$	$\delta = 71.92^0 - 104.9^0 \oplus 253.8^0 - 296.3^0$	$\delta = 67.7^0 - 300^0$	$\delta = 0^0 - 360^0$	$\delta = 0^0 - 360^0$	$\delta = 0^0 - 360^0$
	$= (0^0 - 360^0)$	$= (117.1^0 - 154.4^0 \oplus 211.8^0 - 251.4^0)$	$= (97.8^0 - 157^0 \oplus 204.5^0 - 275.6^0)$	$ M _{ee} = 0.00735 - 0.158$	$ M _{ee} = 0.0120 - 0.196$	$ M _{ee} = 0.0120 - 0.196$
	$m_0 = 0.00844 - 0.310$	$m_0 = 0.114 - 0.416$	$m_0 = 0.0981 - 0.308$	$m_0 = 0.0249 - 0.387$	$m_0 = 0.0249 - 0.387$	$m_0 = 0.0249 - 0.387$
$D_5(F_5)$	$\rho = -90^0 - 90^0$	$\rho = -90^0 - 90^0$	$\rho = -90^0 - 90^0$	$\rho = -90^0 - 90^0$	$\rho = -90^0 - 90^0$	$\rho = -90^0 - 90^0$
	$= (-90^0 - 90^0)$	$= (-90^0 - 90^0)$	$= (-90^0 - 90^0)$	$= (-90^0 - 90^0)$	$= (-90^0 - 90^0)$	$= (-90^0 - 90^0)$
	$\sigma = -90^0 - 90^0$	$\sigma = -90^0 - 90^0$	$\sigma = -90^0 - 90^0$	$\sigma = -90^0 - 90^0$	$\sigma = -90^0 - 90^0$	$\sigma = -90^0 - 90^0$
	$= (-90^0 - 90^0)$	$= (-90^0 - 90^0)$	$= (-90^0 - 90^0)$	$\delta = 0^0 - 360^0$	$\delta = 0^0 - 360^0$	$\delta = 0^0 - 360^0$
	$\delta = 0^0 - 360^0$	$\delta = 76.72^0 - 284.5^0$	$\delta = 0^0 - 175.6^0 \oplus 185.6^0 - 360^0$	$\delta = 0^0 - 360^0$	$\delta = 0^0 - 360^0$	$\delta = 0^0 - 360^0$
$= (0^0 - 152.5^0 \oplus 215^0 - 360^0)$	$= (0.0^0 - 88.6^0 \oplus 275^0 - 360^0)$	$ M _{ee} = 0.0478 - 0.490$	$ M _{ee} = 0.0241 - 0.493$	$ M _{ee} = 0.00868 - 0.493$	$ M _{ee} = 0.00868 - 0.493$	
	$m_0 = 0.0478 - 0.490$	$m_0 = 0.0478 - 0.490$	$m_0 = 0.0307 - 0.501$	$m_0 = 0.0 - 0.490$	$m_0 = 0.0 - 0.490$	
$D_6(F_5)$	$\rho = -80^0 - -3.17^0 \oplus 6.54^0 - 80^0$	$\rho = -62.97^0 - 62.98^0$	$\rho = -43.6^0 - 43.1^0$	$\rho = -90^0 - 90^0$	$\rho = -57.8^0 - 54.6^0$	$\rho = -57.8^0 - 54.6^0$
	$= (-59.4^0 - 52.59^0)$	$= (-60^0 - 60^0)$	$= (-64.5^0 - -23.5^0 \oplus 24.1^0 - 64^0)$	$= (-90^0 - 90^0)$	$= (-77.1^0 - -22.89^0 \oplus 18.8^0 - 81.4^0)$	$= (-77.1^0 - -22.89^0 \oplus 18.8^0 - 81.4^0)$
	$\sigma = -66.30^0 - 66.30^0$	$\sigma = -70.1^0 - 70^0$	$\sigma = -88.9^0 - -36.7^0 \oplus 38.9^0 - 89^0$	$\sigma = -90^0 - 90^0$	$\sigma = -90^0 - -50.9^0 \oplus 48.9^0 - 90^0$	$\sigma = -90^0 - -50.9^0 \oplus 48.9^0 - 90^0$
	$= (-90^0 - 90^0)$	$= (-88.4^0 - 88.0^0)$	$= (-43.5^0 - 42.4^0)$	$\delta = 0^0 - 360^0$	$\delta = 0^0 - 360^0$	$\delta = 0^0 - 360^0$
	$\delta = 52.1^0 - 144.08^0 \oplus 218.7^0 - 306.7^0$	$\delta = 70.79^0 - 149.5^0 \oplus 210.5^0 - 290^0$	$\delta = 73.4^0 - 119.8^0 \oplus 239.8^0 - 303.5^0$	$\delta = 0^0 - 360^0$	$\delta = 130^0 - 228.9^0$	$\delta = 130^0 - 228.9^0$
$= (0^0 - 360^0)$	$= (67.9^0 - 292.08^0)$	$ M _{ee} = 0.0371 - 0.217$	$ M _{ee} = 0.0467 - 0.134$	$ M _{ee} = 0.0144 - 0.108$	$ M _{ee} = 0.0144 - 0.108$	
	$m_0 = 0.00712 - 0.101$	$m_0 = 0.0659 - 0.261$	$m_0 = 0.0610 - 0.428$	$m_0 = 0.0395 - 0.209$	$m_0 = 0.0395 - 0.209$	

TABLE 5: Continued.

Cases	X			Y		
	NS	IS	IS	NS	IS	IS
$D_7(F_8)$	$\rho = -90^\circ - 90^\circ$	$\rho = -4.12^\circ - 4.00^\circ$	$\rho = -4.69^\circ - 4.94^\circ$	$\rho = -90^\circ - 90^\circ$	$\rho = -90^\circ - 90^\circ$	$\rho = -90^\circ - 90^\circ$
	$= (-69.6^\circ - 69.4^\circ)$	$= (-2.22^\circ - -0.120^\circ \oplus 0.120^\circ - 2.25^\circ)$	$= (-3.98^\circ - 4.65^\circ)$	$= (-90^\circ - 90^\circ)$	$= (-90^\circ - 90^\circ)$	$= (-90^\circ - 90^\circ)$
	$\sigma = -69.2^\circ - 66^\circ$	$\sigma = -1.56^\circ - 1.56^\circ$	$\sigma = -7.26^\circ - 7.28^\circ$	$\sigma = -90^\circ - 90^\circ$	$\sigma = -90^\circ - 90^\circ$	$\sigma = -90^\circ - 90^\circ$
	$= (-90^\circ - 90^\circ)$	$= (-2.45^\circ - 2.34^\circ)$	$= (-7.03^\circ - 7.93^\circ)$	$= (-90^\circ - 90^\circ)$	$= (-90^\circ - 90^\circ)$	$= (-90^\circ - 90^\circ)$
$\delta = 0.0^\circ - 165^\circ \oplus 197^\circ - 360^\circ$	$\delta = 86.91^\circ - 90.69^\circ \oplus 268.65^\circ - 273^\circ$	$\delta = 89.80^\circ - 97.17^\circ \oplus 263.3^\circ - 270.4^\circ$	$\delta = 89.80^\circ - 97.17^\circ \oplus 263.3^\circ - 270.4^\circ$	$\delta = 0^\circ - 360^\circ$	$\delta = 0^\circ - 360^\circ$	$\delta = 0^\circ - 360^\circ$
$= (0^\circ - 360^\circ)$	$= (88.91^\circ - 92.69^\circ \oplus 267.65^\circ - 271^\circ)$	$= (89.13^\circ - 96.2^\circ \oplus 264.2^\circ - 270.8^\circ)$	$= (89.13^\circ - 96.2^\circ \oplus 264.2^\circ - 270.8^\circ)$	$ M _{ee} = 0.0169 - 0.0340$	$ M _{ee} = 0.0169 - 0.0340$	$ M _{ee} = 0.0169 - 0.0340$
$ M _{ee} = 0.0481 - 0.311$	$ M _{ee} = 0.0387 - 0.311$	$ M _{ee} = 0.0357 - 0.216$	$ M _{ee} = 0.0357 - 0.216$	$m_0 = 0.0153 - 0.308$	$m_0 = 0.0153 - 0.308$	$m_0 = 0.0153 - 0.308$
$m_0 = 0.0141 - 0.313$	$m_0 = 0.0312 - 0.465$	$m_0 = 0.0334 - 0.212$	$m_0 = 0.0334 - 0.212$			
$D_8(F_7)$	\times	\times	\times	\times	\times	\times
	\times	\times	\times	\times	\times	\times
	\times	\times	\times	\times	\times	\times
	\times	\times	\times	\times	\times	\times
$D_9(F_6)$	$\rho = -90^\circ - 90^\circ$	$\rho = -0.82^\circ - 2.99^\circ$	$\rho = -1.51^\circ - 0.548^\circ$	$\rho = -90^\circ - 90^\circ$	$\rho = -90^\circ - 90^\circ$	$\rho = -90^\circ - 90^\circ$
	$= (-68^\circ - 68^\circ)$	$= (-0.39^\circ - 2.53^\circ)$	$= (-7.34^\circ - 1.45^\circ)$	$= (-90^\circ - 90^\circ)$	$= (-90^\circ - 90^\circ)$	$= (-90^\circ - 90^\circ)$
	$\sigma = -66^\circ - 66^\circ$	$\sigma = -2.68^\circ - 0.46^\circ$	$\sigma = -7.34^\circ - 1.45^\circ$	$\sigma = -90^\circ - 90^\circ$	$\sigma = -90^\circ - 90^\circ$	$\sigma = -90^\circ - 90^\circ$
	$= (-90^\circ - 90^\circ)$	$= (-3.70^\circ - 2.13^\circ)$	$= (-6.34^\circ - 1.15^\circ)$	$= (-90^\circ - 90^\circ)$	$= (-90^\circ - 90^\circ)$	$= (-90^\circ - 90^\circ)$
$\delta = 0^\circ - 24.97^\circ \oplus -9.6^\circ - 1.46^\circ \oplus 20.91^\circ - 90^\circ$	$\delta = 87.87^\circ - 91.83^\circ \oplus 268.4^\circ - 272^\circ$	$\delta = 85.87^\circ - 90.83^\circ \oplus 268.4^\circ - 274.5^\circ$	$\delta = 85.87^\circ - 90.83^\circ \oplus 268.4^\circ - 274.5^\circ$	$\delta = 0^\circ - 360^\circ$	$\delta = 0^\circ - 360^\circ$	$\delta = 0^\circ - 360^\circ$
$\delta = 0^\circ - 158^\circ \oplus 200^\circ - 360^\circ$	$\delta = (88.87^\circ - 91.43^\circ \oplus 268.68^\circ - 271.6^\circ)$	$\delta = (85.57^\circ - 91.23^\circ \oplus 269^\circ - 275^\circ)$	$\delta = (85.57^\circ - 91.23^\circ \oplus 269^\circ - 275^\circ)$	$= (0^\circ - 160^\circ \oplus 198.8^\circ - 360^\circ)$	$= (0^\circ - 160^\circ \oplus 198.8^\circ - 360^\circ)$	$= (0^\circ - 160^\circ \oplus 198.8^\circ - 360^\circ)$
$= (0^\circ - 360^\circ)$	$ M _{ee} = 0.00551 - 0.277$	$ M _{ee} = 0.0564 - 0.237$	$ M _{ee} = 0.0378 - 0.343$	$ M _{ee} = 0.0239 - 0.413$	$ M _{ee} = 0.0239 - 0.413$	$ M _{ee} = 0.0239 - 0.413$
$ M _{ee} = 0.00551 - 0.277$	$m_0 = 0.00792 - 0.277$	$m_0 = 0.0351 - 0.238$	$m_0 = 0.0364 - 0.342$	$m_0 = 0.0124 - 0.412$	$m_0 = 0.0124 - 0.412$	$m_0 = 0.0124 - 0.412$

TABLE 5: Continued.

Cases	X		Y	
	NS	IS	NS	IS
$D_{10}(F_{10})$	NS	IS	NS	IS
	$\rho = -90^\circ - 90^\circ$	\times	\times	$\rho = -90^\circ - 90^\circ$
	$= (-90^\circ - 90^\circ)$	\times	\times	$= (-90^\circ - 90^\circ)$
	$\sigma = -90^\circ - 90^\circ$	\times	\times	$\sigma = -90^\circ - 90^\circ$
	$= (-90^\circ - 90^\circ)$	\times	\times	$= (-90^\circ - 90^\circ)$
	$\delta = 11.70^\circ - 348^\circ$	\times	\times	$\delta = 0^\circ - 160^\circ \oplus 209.2^\circ - 360^\circ$
	$= (0^\circ - 74.56^\circ \oplus 89.17^\circ - 275^\circ \oplus 285^\circ - 360^\circ)$	\times	\times	$= (16.5^\circ - 344^\circ)$
	$ M _{\text{ce}} = 0.0 - 0.0340$	\times	\times	$ M _{\text{ce}} = 0.0107 - 0.0268$
	$m_0 = 0.000594 - 0.0887$	\times	\times	$m_0 = 0.000649 - 0.0641$

TABLE 6: Continued.

Cases	X			Y		
	NS	IS	IS	NS	IS	IS
$E_{10}(E_{10})$	$\rho = -90^0 - 90^0$	$\rho = -90^0 - 28^0 \oplus 28^0 - 90^0$	$\rho = -87.8^0 - 31.0^0 \oplus 31.1^0 - 88.1^0$	$\rho = -87.8^0 - 31.0^0 \oplus 31.1^0 - 88.1^0$	$\rho = -89.8^0 - 89.7^0$	$\rho = -89.8^0 - 89.7^0$
	$= (-90^0 - 90^0)$	$= (-81.3^0 - 20.79^0 \oplus 25.08^0 - 83.1^0)$	$= (-85.8^0 - 38.0^0 \oplus 42.1^0 - 88.1^0)$	$= (-85.8^0 - 38.0^0 \oplus 42.1^0 - 88.1^0)$	$= (-90^0 - 90^0)$	$= (-90^0 - 90^0)$
	$\sigma = -90^0 - 90^0$	$\sigma = -87^0 - 30^0 \oplus 30^0 - 71^0$	$\sigma = -81.4^0 - 30.79^0 \oplus 30.08^0 - 82.1^0$	$\sigma = -81.4^0 - 30.79^0 \oplus 30.08^0 - 82.1^0$	$\sigma = -88.7^0 - 87.9^0$	$\sigma = -88.7^0 - 87.9^0$
	$= (-90^0 - 90^0)$	$= (-84.2^0 - 19.8^0 \oplus 23.1^0 - 88.1^0)$	$= (-81.4^0 - 30.79^0 \oplus 30.08^0 - 82.1^0)$	$= (-81.4^0 - 30.79^0 \oplus 30.08^0 - 82.1^0)$	$= (-89.8^0 - 89^0)$	$= (-89.8^0 - 89^0)$
	$\delta = 0.0^0 - 20^0 \oplus 89.59^0 - 281^0 \oplus 331^0 - 360^0$	$\delta = 21.35^0 - 71.9^0 \oplus 272.4^0 - 331.5^0$	$\delta = 25.6^0 - 28^0 \oplus 90.4^0 - 149.1^0 \oplus$	$\delta = 25.6^0 - 28^0 \oplus 90.4^0 - 149.1^0 \oplus$	$\delta =$	$\delta =$
	$= (0.0^0 - 103^0 \oplus 158^0 - 207.8^0 \oplus 254^0 - 360^0)$	$= (98.16^0 - 160.3^0 \oplus 204.5^0 - 267.8^0)$	$212.4^0 - 268.5^0 \oplus 338^0 - 339^0$	$212.4^0 - 268.5^0 \oplus 338^0 - 339^0$	$0^0 - 101.05^0 \oplus 149.2^0 - 210.2^0 \oplus 259.7^0 - 360^0$	$0^0 - 101.05^0 \oplus 149.2^0 - 210.2^0 \oplus 259.7^0 - 360^0$
	$ M _{\nu e} = 0.0 - 0.261$	$ M _{\nu e} = 0.150 - 0.430$	$= (41.84^0 - 89.65^0 \oplus 272.5^0 - 321.4^0)$	$= (41.84^0 - 89.65^0 \oplus 272.5^0 - 321.4^0)$	$ M _{\nu e} = 0.01088 - 0.432$	$ M _{\nu e} = 0.01088 - 0.432$
	$m_0 = 0.00098 - 0.276$	$m_0 = 0.147 - 0.420$	$ M _{\nu e} = 0.135 - 0.352$	$ M _{\nu e} = 0.135 - 0.352$	$m_0 = 0.00920 - 0.438$	$m_0 = 0.00920 - 0.438$
			$m_0 = 0.142 - 0.352$	$m_0 = 0.142 - 0.352$		

$F_{10}(\text{NS})$ predict literally no constraints on δ for type X texture. These cases give identical predictions for type Y as well, however for opposite mass ordering. On the other hand, for cases $D_6(\text{IS})$, $D_4(\text{IS})$, $D_7(\text{IS})$, $D_9(\text{IS})$, $F_3(\text{IS})$, $F_6(\text{IS})$, $F_8(\text{IS})$, and $F_9(\text{IS})$, δ is notably constrained for type X and similar observations have been found for these cases in type Y, however for opposite mass ordering (Table 5).

It is found that textures $D_7(\text{IS})$, $D_9(\text{IS})$, $F_6(\text{IS})$, and $F_8(\text{IS})$ belonging to type X predict near maximal Dirac CP violation (i.e., $\delta \approx 90^\circ$ and 270°). In addition, the Majorana phases ρ and σ are found to be very close to 0° for these cases. The similar predictions hold for these cases belonging to type Y structure however for opposite mass spectrum.

The prediction on the allowed range of $|M|_{ee}$ for all the cases of category D is provided in Table 5. As an illustration, in Figures 7, 8, 9, and 10 we have compiled the correlation plots for case D_7 for type X and type Y structures. Figures 7(a), 7(b), 10(a), and 10(b) indicate no constraint on δ , ρ , σ for NS(IS) corresponding to type X (type Y) structure at 3σ CL. On the other hand, $\delta \approx 90^\circ$ and 270° , while ρ and σ approach to 0° for IS in case of type X structure (Figure 8). However, similar predictions for δ , ρ , σ have been observed for type Y, however for NS (Figure 9). In Figures 7(c), 8(c), 9(c), and 10(c), we have presented the correlation plots between $|M|_{ee}$ and m_0 indicating the linear correlation.

Category E. In Category E, only eight out of ten cases are allowed with experimental data for both type X and type Y structures at 3σ CL (Table 6). Cases E_7 and E_8 are ruled out for both type X and type Y structures. Only E_5 and E_{10} favor both NS and IS, while rest of the cases favor either NS or IS for type X and type Y structure (Table 6). From Table 6, it is clear that $E_1, E_2, E_3, E_4, E_5, E_{10}$ cover literally full range of δ for type X. Same cases show identical prediction for type Y, however for opposite mass spectrum. For NS, cases $E_1, E_2, E_5, E_9, E_{10}$ belonging to type X predict the lower bound on effective mass $|M|_{ee}$ to be zero, while for IS, cases E_3, E_4, E_5, E_{10} predict larger lower bound (greater than 0.01eV) on $|M|_{ee}$ (Table 6). However for type Y, all these cases show larger lower bound on $|M|_{ee}$ ($\geq 0.01\text{eV}$) for both NS and IS.

For the purpose of illustration, we have presented the correlation plots for E_1 indicating the parameter space of $\rho, \sigma, \delta, |M|_{ee}$, and lowest neutrino mass (m_0) (Figures 11 and 12). As shown in Figures 11 and 12, ρ, σ, δ remain literally unconstrained for both type X and type Y structures. In addition, there is a linear correlation among ρ, σ , and δ at 3σ CL for type X structure (Table 6). Figure 11(c) indicates the strong linear correlation between $|M|_{ee}$ and m_0 and, in addition, the lower bound on $|M|_{ee}$ is predicted to be zero.

4. Summary and Conclusion

To summarize, we have discussed the novel possibilities of hybrid textures in the flavor basis wherein the assumption of either one zero minor and an equality between the elements or one zero element and an equality between the cofactors in the Majorana neutrino mass matrix is considered. Out of

sixty phenomenologically possible cases, only 56 are found to be viable for type X, while only 50 are viable with the present data for type Y at 3σ CL. Therefore, out of 120 only 106 cases are found to be viable with the existing data. However only 38 seems to restrict the parametric space of CP-violating phases δ, ρ , and σ , while 16 out of these predict near maximal Dirac CP violation, i.e., $\delta \approx 90^\circ, 270^\circ$. The allowed parameter space for effective mass term $|M|_{ee}$ related to neutrinoless double-beta decay and lowest neutrino mass term for all viable cases have been carefully studied. The present viable cases may be derived from the discrete symmetry. However the symmetry realization for each case in a systematic and self-consistent way deserves fine-grained research. The viability of these cases suggests that there are still rich unexplored structures of the neutrino mass matrix from both the phenomenological and the theoretical points of view.

To conclude our discussion, we would like to add that the hybrid textures comprising either one zero element and an equality between the elements or one zero minor and an equality between the cofactors lead to 106 viable cases; therefore there are now total 212 viable cases pertaining to the hybrid textures of M_ν in the flavor basis. Since most of these cases overlap in their predictions regarding the experimentally undetermined parameters, therefore we expect that only the future long baseline experiments, neutrinoless double-beta decay experiments, and cosmological observations could help us select the appropriate structure of mass texture.

Data Availability

The data used to support the findings of this study are available from the corresponding author upon request.

Conflicts of Interest

The authors declare that there are no conflicts of interest regarding the publication of this paper.

Acknowledgments

The author would like to thank the Director of the National Institute of Technology Kurukshetra, for providing the necessary facilities to work.

References

- [1] Abe, K., N. Abgrall, Y. Ajima et al., "Indication of electron neutrino appearance from an accelerator-produced off-axis muon neutrino beam," *Physical Review Letters*, vol. 107, Article ID 041801, 2011.
- [2] P. Adamson, D. J. Auty, D. S. Ayres et al., "Improved search for muon-neutrino to electron-neutrino oscillations in MINOS," *Physical Review Letters*, vol. 107, Article ID 181802, 2011.
- [3] Y. Abe, C. Aberle, T. Akiri et al., "Indication for the disappearance of reactor electron antineutrinos in the Double Chooz experiment," *Physical Review Letters*, vol. 108, Article ID 131801, 2012.

- [4] F. P. An, J. Z. Bai, A. B. Balantekin et al., “Observation of electron-antineutrino disappearance at Daya Bay,” *Physical Review Letters*, vol. 108, Article ID 171803, 2012.
- [5] J. K. Ahn, S. Chebotaryov, J. H. Choi et al., “Observation of reactor electron antineutrinos disappearance in the RENO experiment,” *Physical Review Letters*, vol. 108, Article ID 191802, 2012.
- [6] S. Dev, R. R. Gautam, and L. Singh, “Neutrino mass matrices with two equalities between the elements or cofactors,” *Physical Review D*, vol. 87, Article ID 073011, 2013.
- [7] S. Dev, S. Verma, and S. Gupta, “Phenomenological analysis of hybrid textures of neutrinos,” *Physics Letters B*, vol. 687, p. 53, 2010.
- [8] J. Y. Liu and S. Zhou, “Hybrid textures of majorana neutrino mass matrix and current experimental tests,” *Physical Review*, vol. 87, Article ID 093010, 2013.
- [9] S. Kaneko, H. Sawanaka, and M. Tanimoto, “Hybrid textures of neutrinos,” *Journal of High Energy Physics*, vol. 2005, no. 8, article 73, 2005.
- [10] P. H. Frampton, S. L. Glashow, and D. Marfatia, “Zeros of the neutrino mass matrix,” *Physics Letters B*, vol. 536, no. 1-2, pp. 79–82, 2002.
- [11] Z.-Z. Xing, “Texture zeros and majorana phases of the neutrino mass matrix,” *Physics Letters B*, vol. 530, no. 1-4, pp. 159–166, 2002.
- [12] B. R. Desai, D. P. Roy, and A. R. Vaucher, “Three-neutrino mass matrices with two texture zeros,” *Modern Physics Letters A*, vol. 18, no. 20, pp. 1355–1365, 2003.
- [13] S. Dev, S. Kumar, S. Verma, and S. Gupta, *Nuclear Physics*, vol. 784, p. 103, 2007.
- [14] G. Ahuja, S. Kumar, M. Randhawa, M. Gupta, and S. Dev, “Texture 4 zero Fritzsch-like lepton mass matrices,” *Physical Review D: Particles, Fields, Gravitation and Cosmology*, vol. 76, no. 1, Article ID 013006, 2007.
- [15] S. Kumar, “Implications of a class of neutrino mass matrices with texture zeros for nonzero θ_{13} ,” *Physical Review D: Particles, Fields, Gravitation and Cosmology*, vol. 84, no. 7, Article ID 077301, 2011.
- [16] G. Blankenburg and D. Meloni, “Fine-tuning and naturalness issues in the two-zero neutrino mass textures,” *Nuclear Physics*, vol. 867, p. 749, 2013.
- [17] W. Grimus and P. O. Ludl, “Two-parameter neutrino mass matrices with two texture zeros,” *Journal of Physics G*, vol. 40, Article ID 055003, 2013.
- [18] M. Gupta and G. Ahuja, “Flavor mixings and textures of the fermion mass matrices,” *International Journal of Modern Physics*, vol. 27, Article ID 1230033, 2012.
- [19] J. Liao, D. Marfatia, and K. Whisnant, “Texture and Cofactor Zeros of the Neutrino Mass Matrix,” *Journal of High Energy Physics*, vol. 13, 2014.
- [20] D. Meloni, A. Meroni, and E. Peinado, “Two-zero Majorana textures in the light of the Planck results,” *Physical Review D: Particles, Fields, Gravitation and Cosmology*, vol. 89, no. 5, Article ID 053009, 2014.
- [21] P. O. Ludl and W. Grimus, “A complete survey of texture zeros in the lepton mass matrices,” *Journal of High Energy Physics*, vol. 090, 2014.
- [22] P. O. Ludl and W. Grimus, “A complete survey of texture zeros in general and symmetric quark mass matrices,” *Physics Letters B*, vol. 744, pp. 38–42, 2015.
- [23] M. Borah, D. Borah, and M. K. Das, “Discriminating majorana neutrino textures in the light of baryon asymmetry,” *Physical Review D*, vol. 91, Article ID 113008, 2015.
- [24] H. Fritzsch, Z. Z. Xing, and S. Zhou, “Two-zero textures of the Majorana neutrino mass matrix and current experimental tests,” *Journal of High Energy Physics*, vol. 2011, article 83, 2011.
- [25] R. Verma, “Exploring the predictability of symmetric texture zeros in quark mass matrices,” *Physical Review*, vol. 96, Article ID 093010, 2017.
- [26] S. Dev, L. Singh, and D. Raj, “Neutrino mass matrices with two vanishing elements/cofactors,” *The European Physical Journal C*, vol. 75, no. 394, 2015.
- [27] W. Wang, “Neutrino mass textures with one vanishing minor and two equal cofactors,” *The European Physical Journal C*, vol. 73, article 2551, 2013.
- [28] S. Dev, R. R. Gautam, and L. Singh, “Hybrid textures of the right-handed Majorana neutrino mass matrix,” *Physical Review D: Particles, Fields, Gravitation and Cosmology*, vol. 88, Article ID 033008, 2013.
- [29] L. Lavoura, “Zeros of the inverted neutrino mass matrix,” *Physics Letters B*, vol. 609, no. 3-4, pp. 317–322, 2005.
- [30] E. I. Lashin and N. Chamoun, “Zero minors of the neutrino mass matrix,” *Physical Review D: Particles, Fields, Gravitation and Cosmology*, vol. 78, no. 7, Article ID 073002, 2008.
- [31] E. I. Lashin, E. Malkawi, S. Nasri, and N. Chamoun, *Physical Review D: Particles, Fields, Gravitation and Cosmology*, vol. 80, no. 11, 2009.
- [32] S. Dev, S. Gupta, R. R. Gautam, and L. Singh, “Near maximal atmospheric mixing in neutrino mass matrices with two vanishing minors,” *Physics Letters B*, vol. 706, no. 2-3, pp. 168–176, 2011.
- [33] T. Araki, J. Heeck, and J. Kubo, “Vanishing minors in the neutrino mass matrix from abelian gauge symmetries,” *Journal of High Energy Physics*, vol. 2012, no. 7, 2012.
- [34] J. Han, R. Wang, W. Wang, and X. Wei, “Neutrino mass matrices with one texture equality and one vanishing neutrino mass,” *Physical Review D: Particles, Fields, Gravitation and Cosmology*, vol. 96, no. 7, 2017.
- [35] S. Dev, D. Raj, and R. R. Gautam, “Neutrino mass matrices with three or four vanishing cofactors and nondiagonal charged lepton sector,” *Physical Review D: Particles, Fields, Gravitation and Cosmology*, vol. 96, no. 9, 2017.
- [36] W. Konetschny and W. Kummer, “Nonconservation of total lepton number with scalar bosons,” *Physics Letters B*, vol. 70, no. 4, pp. 433–435, 1977.
- [37] T. Cheng and L.-F. Li, “Neutrino masses, mixings, and oscillations in $SU(2) \times U(1)$ models of electroweak interactions,” *Physical Review D: Particles, Fields, Gravitation and Cosmology*, vol. 22, no. 11, pp. 2860–2868, 1980.
- [38] J. Schechter and J. W. F. Valle, “Neutrino masses in $SU(2) \otimes U(1)$ theories,” *Physical Review D: Particles, Fields, Gravitation and Cosmology*, vol. 22, p. 2227, 1980.
- [39] G. Lazarides, Q. Shafi, and C. Wetterich, *Nuclear Physics*, vol. 181, p. 287, 1981.
- [40] R. N. Mohapatra and G. Senjanović, “Neutrino masses and mixings in gauge models with spontaneous parity violation,” *Physical Review D: Particles, Fields, Gravitation and Cosmology*, vol. 23, article 165, 1981.
- [41] P. Minkowski, “ $\mu \rightarrow e\gamma$ at a rate of one out of 109 muon decays?” *Physics Letters B*, vol. 67, no. 4, pp. 421–428, 1977.

- [42] T. Yanagida, *Proceedings of the Workshop on the Unified Theory and the Baryon Number in the Universe*, O. Sawada and A. Sugamoto, Eds., KEK, Tsukuba, Japan, 1979.
- [43] M. Gell-Mann, P. Ramond, and R. Slansky, "Complex spinors and unified theories in supergravity," P. Van Nieuwenhuizen and D. Z. Freedman, Eds., Amsterdam, Netherlands, 1979.
- [44] R. N. Mohapatra and G. Senjanovic, "Neutrino mass and spontaneous parity nonconservation," *Physical Review Letters*, vol. 44, p. 912, 1980.
- [45] W. Grimus, A. S. Joshipura, L. Lavoura, and M. Tanimoto, "Symmetry realization of texture zeros," *The European Physical Journal C*, vol. 36, no. 2, pp. 227–232, 2004.
- [46] H. Fritzsch and Z. Xing, "How to describe neutrino mixing and CP violation," *Physics Letters B*, vol. 517, no. 3-4, pp. 363–368, 2001.
- [47] I. Esteban, M. C. Gonzalez-Garcia, M. Maltoni et al., "Updated fit to three neutrino mixing: exploring the accelerator-reactor complementarity," *Journal of High Energy Physics*, vol. 1, no. 87, 2017.
- [48] P. F. de Salas, D. V. Forero, C. A. Ternes, M. Tortola, and J. W. F. Valle, "Status of neutrino oscillations 2018: first hint for normal mass ordering and improved CP sensitivity," *Physics Letters B*, vol. 782, pp. 633–640, 2018.
- [49] J. Shirai, "Search for majorana neutrinos near the inverted mass hierarchy region with KamLAND-Zen," *Physical Review Letters*, vol. 117, Article ID 109903, 2016.
- [50] J. B. Albert, D. J. Auty, and P. S. Barbeau, "Search for Majorana neutrinos with the first two years of EXO-200 data," *Nature*, vol. 510, pp. 229–234, 2014.
- [51] S. Dell'oro, S. Marcocci, M. Viel, and F. Vissani, "Neutrinoless Double Beta Decay: 2015 Review," *Advances in High Energy Physics*, vol. 2016, Article ID 2162659, 37 pages, 2016.
- [52] W. Rodejohann and J. Mod, "Neutrino-less Double Beta Decay and Particle Physics," *International Journal of Modern Physics E*, vol. 20, no. 9, 2011.

Research Article

Expansions of the Solutions of the General Heun Equation Governed by Two-Term Recurrence Relations for Coefficients

T. A. Ishkhanyan,^{1,2,3} T. A. Shahverdyan,³ and A. M. Ishkhanyan ^{1,4}

¹Russian-Armenian University, H. Emin 123, 0051 Yerevan, Armenia

²Moscow Institute of Physics and Technology, Dolgoprudny, Moscow Region 141700, Russia

³Institute for Physical Research, NAS of Armenia, Ashtarak 0203, Armenia

⁴Institute of Physics and Technology, National Research Tomsk Polytechnic University, Tomsk 634050, Russia

Correspondence should be addressed to A. M. Ishkhanyan; aishkhanyan@gmail.com

Received 27 January 2018; Accepted 4 May 2018; Published 4 July 2018

Academic Editor: Saber Zarrinkamar

Copyright © 2018 T. A. Ishkhanyan et al. This is an open access article distributed under the Creative Commons Attribution License, which permits unrestricted use, distribution, and reproduction in any medium, provided the original work is properly cited. The publication of this article was funded by SCOAP³.

We examine the expansions of the solutions of the general Heun equation in terms of the Gauss hypergeometric functions. We present several expansions using functions, the forms of which differ from those applied before. In general, the coefficients of the expansions obey three-term recurrence relations. However, there exist certain choices of the parameters for which the recurrence relations become two-term. The coefficients of the expansions are then explicitly expressed in terms of the gamma functions. Discussing the termination of the presented series, we show that the finite-sum solutions of the general Heun equation in terms of generally irreducible hypergeometric functions have a representation through a single generalized hypergeometric function. Consequently, the power-series expansion of the Heun function for any such case is governed by a two-term recurrence relation.

1. Introduction

The general Heun equation [1–3], which is the most general second-order linear ordinary differential equation having four regular singular points, is currently widely encountered in physics and mathematics research (see, e.g., [1–14] and references therein). However, this equation is much less studied than its immediate predecessor, the Gauss hypergeometric equation, which is the most general equation having three regular singular points. A reason for the slow progress in the development of the theory is that the solutions of the Heun equation (as well as its four confluent reductions) in general are not expressed in terms of definite or contour integrals involving simpler functions [2, 3]. Furthermore, the convergence regions of power-series expansions near different singularities are rather restricted and several complications arise in studying the relevant connection problems [2, 3, 15]. Another general problematic point is that the power-series solutions of the Heun equation are governed by three-term recurrence relations between successive coefficients of expansions [1–3], instead of two-term ones appearing in

the hypergeometric case [16–18]. As a result, in general the coefficients are not determined explicitly.

In the present paper, we show that there exist some particular choices of the involved parameters for which the recurrence relations governing the power-series expansions become two-term. In these cases the solution of the general Heun equation can be written either as a linear combination of a finite number of the Gauss hypergeometric functions or in terms of a single generalized hypergeometric function. This is a main result of the present paper.

Another major result we report here is that in the case of the expansions of the solutions of the Heun equation in terms of hypergeometric functions there also exist particular choices of the involved parameters for which the governing three-term recurrence relations for expansion coefficients become two-term. In these cases the coefficients are explicitly written in terms of the gamma functions.

Expansions of the solutions of the Heun equation in terms of the Gauss hypergeometric functions ${}_2F_1$, initiated by Svartholm [19], suggest a notable extension of the series technique. This is a useful approach applicable to many

differential equations including those of more general type whose nature, outside a certain region of the extended complex plane containing only two regular singular points, is not necessary to be specified exactly. Expansions involving functions other than powers have been applied to the general and confluent Heun equations by many authors. The ordinary hypergeometric [19–25], confluent hypergeometric [26–29], Coulomb wave functions [30, 31], Bessel and Hankel functions [32], incomplete Beta and Gamma functions [33–35], Hermite functions [36, 37], Goursat and Appell generalized hypergeometric functions of two variables of the first kind [38, 39], and other known special functions have been used as expansion functions. A useful property suggested by these expansions is the possibility of deriving finite-sum solutions by means of termination of the series.

As far as the expansions of the general Heun equation in terms of the hypergeometric functions are concerned, in the early papers by Svartholm [19], Erdélyi [20, 21], and Schmidt [22], the intuitive intention was to apply hypergeometric functions with parameters so chosen as to match the Heun equation as closely as possible. For this reason they used functions of the form ${}_2F_1(\lambda + n, \mu - n; \gamma; z)$, which have matching behavior in two singular points, $z = 0$ and 1 . These functions have the following Riemann P -symbol representation:

$$P \left(\begin{array}{ccc} 0 & 1 & \infty \\ 0 & 0 & \lambda + n & z \\ 1 - \gamma & 1 - \delta & \mu - n & \end{array} \right). \quad (1)$$

Here λ and μ may adopt several values provided $1 + \lambda + \mu = \gamma + \delta$ (see [25]). It is clear that the functions have matching characteristic exponents at $z = 0$ and $z = 1$, and their behavior does not match that of the Heun function at the third singular point of the hypergeometric equation $z = \infty$.

However, it has been shown that one can also use functions that have matching behavior at only one singular point [38]. Exploring this idea, in the present paper we discuss the hypergeometric expansions of the solutions of the Heun equation in terms of functions of the form ${}_2F_1(\alpha, \beta; \gamma_0 \pm n; z)$ which have matching behavior (i.e., characteristic exponents) only at the singular point $z = \infty$. These functions are presented by the Riemann P -symbol

$$P \left(\begin{array}{ccc} 0 & 1 & \infty \\ 0 & 0 & \alpha & z \\ 1 - (\gamma_0 \pm n) & 1 - (\delta_0 \mp n) & \beta & \end{array} \right), \quad (2)$$

where $1 + \alpha + \beta = \gamma_0 + \delta_0$, and the parameters γ_0, δ_0 are chosen so that the Fuchsian condition for the general Heun equation (3), i.e., $1 + \alpha + \beta = \gamma + \delta + \varepsilon$, is fulfilled: $\gamma_0 + \delta_0 = \gamma + \delta + \varepsilon$. Note that these functions differ also from the Jacobi-polynomials used by Kalnins and Miller whose functions can be written in terms of hypergeometric functions of the form ${}_2F_1(\lambda + n, \mu - n; \gamma + 2n; z)$ [23].

In the present paper we discuss several expansions in terms of the mentioned hypergeometric functions. In general, the coefficients of the expansions obey three-term recurrence relations similar to those known from previous developments

[19–25]. However, for certain choices of the involved parameters the recurrence relations reduce to two-term ones. In these exceptional cases the coefficients of the expansions are explicitly calculated. The result is expressed in terms of the gamma functions.

Discussing the conditions for deriving finite-sum solutions by means of termination of the presented series, we show that the termination is possible if a singularity of the Heun equation is an apparent one. Furthermore, we show that any finite-sum solution of the general Heun equation derived in this way has a representation through a single generalized hypergeometric function ${}_pF_q$. The general conclusion is then that in any such case the power-series expansion of the Heun function is governed by a two-term recurrence relation (obviously, this is the relation obeyed by the corresponding power-series for ${}_pF_q$).

2. Hypergeometric Expansions

The general Heun equation written in its canonical form is [1]

$$\frac{d^2 u}{dz^2} + \left(\frac{\gamma}{z} + \frac{\delta}{z-1} + \frac{\varepsilon}{z-a} \right) \frac{du}{dz} + \frac{\alpha\beta z - q}{z(z-1)(z-a)} u = 0, \quad (3)$$

where the parameters satisfy the Fuchsian relation $1 + \alpha + \beta = \gamma + \delta + \varepsilon$. We introduce an expansion of this equation's solution of the form

$$u = \sum_{n=0}^{\infty} c_n \cdot {}_2F_1(\alpha, \beta; \gamma_0 + n; z) \quad (4)$$

with the involved Gauss hypergeometric functions obeying the equation

$$\frac{d^2 u_n}{dz^2} + \left(\frac{\gamma_0 + n}{z} + \frac{\delta + \varepsilon + \gamma - \gamma_0 - n}{z-1} \right) \frac{du_n}{dz} + \frac{\alpha\beta}{z(z-1)} u_n = 0. \quad (5)$$

Substitution of (4)-(5) into (3) gives

$$\sum_n c_n \left[\left(\frac{\gamma - \gamma_0 - n}{z} - \frac{\varepsilon + \gamma - \gamma_0 - n}{z-1} + \frac{\varepsilon}{z-a} \right) \frac{du_n}{dz} + \frac{\alpha\beta a - q}{z(z-1)(z-a)} u_n \right] = 0 \quad (6)$$

$$\text{or } \sum_n c_n \left\{ [(a-1)(\varepsilon + \gamma - \gamma_0 - n)z - a(\gamma - \gamma_0 - n)(z-1)] \frac{du_n}{dz} + (\alpha\beta a - q) \cdot u_n \right\} = 0. \quad (7)$$

Now, using the following relations between the involved hypergeometric functions [16–18]:

$$z \frac{du_n}{dz} = \gamma_{n-1} [u_{n-1} - u_n], \quad (8)$$

$$(z-1) \frac{du_n}{dz} = -\delta_{n+1} u_n + \left(\delta_{n+1} - \frac{\alpha\beta}{\gamma_n} \right) u_{n+1}, \quad (9)$$

where $\gamma_n = \gamma_0 + n$ and $\delta_n = \delta + \varepsilon + \gamma - \gamma_n$, this equation is rewritten as

$$\begin{aligned} \sum_n c_n \left[(a-1)(\varepsilon + \gamma - \gamma_n)(\gamma_n - 1) [u_{n-1} - u_n] \right. \\ \left. + a(\gamma - \gamma_n) \left((\delta_n - 1) u_n - \left(\delta_n - 1 - \frac{\alpha\beta}{\gamma_n} \right) u_{n+1} \right) \right. \\ \left. + (\alpha\beta a - q) u_n \right] = 0, \end{aligned} \quad (10)$$

from which we get a three-term recurrence relation for the coefficients of the expansion (4)

$$R_n c_n + Q_{n-1} c_{n-1} + P_{n-2} c_{n-2} = 0 \quad (11)$$

with

$$R_n = (a-1)(\varepsilon + \gamma - \gamma_n)(\gamma_n - 1), \quad (12)$$

$$Q_n = -R_n + a(\gamma - \gamma_n)(\alpha + \beta - \gamma_n) + (\alpha\beta a - q), \quad (13)$$

$$P_n = \frac{a}{\gamma_n} (\gamma - \gamma_n)(\alpha - \gamma_n)(\beta - \gamma_n). \quad (14)$$

From the initial conditions $c_0 = 1$ and $c_{-1} = c_{-2} = 0$ we get $(\varepsilon + \gamma - \gamma_0)(\gamma_0 - 1) = 0$. Since $\gamma_0 = 1$ is forbidden (it causes division by zero at $n = 1$ in P_{-1}) we obtain that the only possibility is $\gamma_0 = \varepsilon + \gamma$. Hence, the expansion finally reads

$$u = \sum_{n=0}^{\infty} c_n \cdot {}_2F_1(\alpha, \beta; \gamma + \varepsilon + n; z), \quad (15)$$

and the coefficients of the three-term recurrence relation (11) are

$$R_n = (1-a)n(\varepsilon + \gamma + n - 1), \quad (16)$$

$$Q_n = -R_n + a(1+n-\delta)(n+\varepsilon) + (\alpha\beta a - q), \quad (17)$$

$$\begin{aligned} P_n \\ = -\frac{a}{n+\varepsilon+\gamma} (n+\varepsilon)(n+\varepsilon+\gamma-\alpha)(n+\varepsilon+\gamma-\beta). \end{aligned} \quad (18)$$

The expansion applies if α, β , and $\gamma + \varepsilon$ are not zero or negative integers. The restrictions on α and β assure that the hypergeometric functions are not polynomials of fixed degree.

The derived expansion terminates if two successive coefficients vanish. If c_N is the last nonzero coefficient and $c_{N+1} =$

$c_{N+2} = 0$ for some $N = 0, 1, 2, \dots$, we obtain from (11) that it should be $P_N = 0$ so that the termination is possible if

$$\begin{aligned} \varepsilon &= -N \\ \text{or } \varepsilon + \gamma - \alpha &= -N \\ \text{or } \varepsilon + \gamma - \beta &= -N. \end{aligned} \quad (19)$$

Note that the equation $c_{N+1} = 0$ results in a polynomial equation of degree $N + 1$ for the accessory parameter q . This equation is convenient for rewriting the recurrence relation (11) in the following matrix form:

$$\begin{bmatrix} Q_0 & R_1 & 0 & & & & \\ P_0 & Q_1 & R_2 & 0 & & & \\ 0 & P_1 & Q_2 & R_3 & & & \\ & & \ddots & \ddots & \ddots & & \\ & & & 0 & P_{N-1} & Q_N & \end{bmatrix} \begin{bmatrix} c_0 \\ c_1 \\ c_2 \\ \vdots \\ c_N \end{bmatrix} = \begin{bmatrix} 0 \\ 0 \\ 0 \\ \vdots \\ 0 \end{bmatrix}. \quad (20)$$

The vanishing of the determinant of the above matrix gives the polynomial equation for q defining in general $N + 1$ values for which the termination occurs.

One may consider a mirror expansion

$$u = \sum_{n=0}^{\infty} c_n \cdot {}_2F_1(\alpha, \beta; \gamma_0 - n; z), \quad (21)$$

which differs from expansion (4) only by the sign of n in the lower parameter of the involved hypergeometric functions. This change of the sign leads to a three-term recurrence relation (11) with the coefficients

$$R_n = \frac{a}{\gamma_0 - n} (\gamma - \gamma_0 + n)(\alpha - \gamma_0 + n)(\beta - \gamma_0 + n), \quad (22)$$

$$\begin{aligned} Q_n &= -P_n + a(\gamma - \gamma_0 + n)(\alpha + \beta - \gamma_0 + n) + \alpha\beta a \\ &\quad - q, \end{aligned} \quad (23)$$

$$P_n = (a-1)(\varepsilon + \gamma - \gamma_0 + n)(\gamma_0 - n - 1), \quad (24)$$

where

$$\gamma_0 = \gamma \text{ or } \alpha \text{ or } \beta. \quad (25)$$

This expansion applies if α and β are not zero or negative integers and γ is not an integer.

In order for the series to terminate at some $n = N$ we put $P_N = 0$ so that this time we derive

$$\begin{aligned} \varepsilon, \varepsilon + \gamma - \alpha \\ \text{or } \varepsilon + \gamma - \beta &= -N \end{aligned} \quad (26)$$

for the expansions with $\gamma_0 = \gamma$ or α or β , respectively. Then the equation $c_{N+1} = 0$ again gives a $(N + 1)$ -degree polynomial equation for those values of the accessory parameter q for which the termination occurs.

3. Finite-Sum Hypergeometric Solutions

It is readily shown that the finite-sum solutions derived from the above two types of expansions by the described termination procedure coincide, as can be expected because of apparent symmetry. For example, consider the expansion (15) in the case $\varepsilon = -N$. The involved hypergeometric functions have the form $u_n = {}_2F_1(\alpha, \beta, \gamma - N + n; z)$. Since $n = 0, 1, \dots, N$, we see that the set of the involved hypergeometric functions is exactly the same as in the case of the second type expansion (21) with $\gamma_0 = \gamma : \{ {}_2F_1(\alpha, \beta, \gamma; z), {}_2F_1(\alpha, \beta, \gamma - 1; z), \dots, {}_2F_1(\alpha, \beta, \gamma - N; z) \}$. Furthermore, examination of (20) shows that the equation for the accessory parameter q and the expansion coefficients are also the same for the two expansions. The same happens to other two cases: $\varepsilon + \gamma - \alpha = -N$ and $\varepsilon + \gamma - \beta = -N$. Thus, while different in general, the expansions (15)-(18) and (21)-(25) lead to the same finite-sum closed-form solutions.

Consider the explicit forms of these solutions examining, for definiteness, the expansion (15)-(18). An immediate observation is that because of the symmetry of the Heun equation with respect to the interchange $\alpha \longleftrightarrow \beta$ the finite-sum solutions produced by the choices $\varepsilon + \gamma - \alpha = -N$ and $\varepsilon + \gamma - \beta = -N$ are of the same form. Furthermore, by applying the formula [16]

$$\begin{aligned} & {}_2F_1(\alpha, \beta; \alpha + k; z) \\ &= (1-z)^{k-\beta} {}_2F_1(k, \alpha - \beta + k; \alpha + k; z) \end{aligned} \quad (27)$$

to the involved hypergeometric functions ${}_2F_1(\alpha, \beta; \alpha - N + n; z)$ or ${}_2F_1(\alpha, \beta; \beta - N + n; z)$ we see that the sum is a quasipolynomial, namely, a product of $(1-z)^{1-\delta}$ and a polynomial in z . Here are the first two of the solutions:

$$\begin{aligned} \varepsilon + \gamma - \alpha &= 0, \\ q &= a\gamma(\delta - 1), \end{aligned} \quad (28)$$

$$\begin{aligned} u &= (1-z)^{1-\delta}, \\ \varepsilon + \gamma - \alpha &= -1, \\ q^2 + [\alpha - 1 - a(\delta - 2 + \gamma(2\delta - 3))]q - a\gamma(\delta - 2) \end{aligned} \quad (29)$$

$$\begin{aligned} & \cdot (\alpha - a(1 + \gamma)(\delta - 1)) = 0, \\ u &= (1-z)^{1-\delta} \\ & \cdot \left(1 - \frac{\alpha + 1 - \delta}{\alpha - 1}z + \frac{q - a(\alpha\beta + \varepsilon - \delta\varepsilon)}{(1-a)(\alpha - 1)}(1-z) \right). \end{aligned} \quad (30)$$

Note that, since $1 - \delta$ is a characteristic exponent of the Heun equation, the transformation $u = (1-z)^{1-\delta}w(z)$ results in another Heun equation for $w(z)$. Hence, the derived finite-sum solutions corresponding to the choices $\varepsilon + \gamma - \alpha = -N$ and $\varepsilon + \gamma - \beta = -N$ are generated from the polynomial solutions of the equation for $w(z)$.

More interesting is the case $\varepsilon = -N$, when the finite-sum solutions involve $N + 1$ hypergeometric functions irreducible, in general, to simpler functions. The case $\varepsilon = 0$ produces the

trivial result $q = a\alpha\beta$, when the Heun equation is degenerated into the hypergeometric equation with the solution $u = {}_2F_1(\alpha, \beta; \gamma; z)$. The solution for the first nontrivial case $\varepsilon = -1$ reads

$$\begin{aligned} u &= {}_2F_1(\alpha, \beta; \gamma - 1; z) + \frac{q - a\alpha\beta + a(1 - \delta)}{(1-a)(\gamma - 1)} \\ & \cdot {}_2F_1(\alpha, \beta; \gamma; z), \end{aligned} \quad (31)$$

where q is a root of the equation

$$\begin{aligned} & (q - a\alpha\beta + a(1 - \delta))(q - a\alpha\beta + (a - 1)(1 - \gamma)) \\ & - a(1 - a)(1 + \alpha - \gamma)(1 + \beta - \gamma) = 0. \end{aligned} \quad (32)$$

Note that the second term in (31) vanishes if $q - a\alpha\beta + a(1 - \delta) = 0$ so that in this degenerate case the solution involves one, not $2 = N + 1$, terms. It is seen from (32) that this situation is necessarily the case if $a = 1/2$, $\gamma + \delta = 2$ and α or β equals $\gamma - 1$. We will see that the solution in this case is a member of a family of specific solutions for which the expansion is governed by two-term recurrence relations for the coefficients.

The solutions (31) and (32) have been noticed on several occasions [40–44]. It has been shown that, for $\varepsilon = -1$, when the characteristic exponents of $z = a$ are 0, 2 so that they differ by an integer, (32) provides the condition for the singularity $z = a$ to be *apparent* (or “simple”); that is, no logarithmic terms are involved in the local Frobenius series expansion [40–42]. In fact, the Frobenius solution in this case degenerates to a Taylor series. It has further been observed that the solution (31) can be expressed in terms of the Clausen generalized hypergeometric function ${}_3F_2$ with an upper parameter exceeding a lower one by unity [40–42]:

$$\frac{u}{u(0)} = {}_3F_2(\alpha, \beta, e + 1; \gamma, e; z), \quad (33)$$

where the parameter e is given as

$$e = \frac{a\alpha\beta}{q - a\alpha\beta}. \quad (34)$$

Note that using this parameter e the solution of (32) is parameterized as [41]

$$\begin{aligned} q &= a\alpha\beta \frac{1+e}{e}, \\ a &= \frac{e(e - \gamma + 1)}{(e - \alpha)(e - \beta)}. \end{aligned} \quad (35)$$

We will now show that a similar generalized hypergeometric representation holds also for $\varepsilon = -2$ and for all $\varepsilon \in \mathbb{Z}$, $\varepsilon \neq 1$.

4. The Case $\varepsilon \leq -2$, $\varepsilon \in \mathbb{Z}$

For $\varepsilon = -2$ the termination equation $c_{N+1} = 0$ for the accessory parameter q is written as

$$\begin{aligned} & ((q - a\alpha\beta)^2 + (q - a\alpha\beta)(4a - 2 - (3 + \alpha + \beta)a + \gamma) \\ & + 2a(a - 1)\alpha\beta) \times (q - a\alpha\beta - 2(1 + \alpha + \beta)a - 2 \\ & + 2\gamma) + (q - a\alpha\beta)2a(a - 1)(\alpha\beta + 1 + \alpha + \beta) \\ & = 0. \end{aligned} \quad (36)$$

The solution of the Heun equation for a root of this equation is given as

$$u = {}_2F_1(\alpha, \beta; \gamma - 2; z) + B_1 \cdot {}_2F_1(\alpha, \beta; \gamma - 1; z) + B_2 \cdot {}_2F_1(\alpha, \beta; \gamma; z), \quad (37)$$

$$q = a\alpha\beta \frac{(1+e)(1+r)}{er}, \quad (40)$$

$$a = \frac{er(2er + (e+r+1)(2-\gamma))}{\alpha\beta((1+e)^2 + (1+r)^2 - 1) + er(2er - 4 - (e+r+3)(\alpha + \beta - 1))}. \quad (41)$$

It is further checked that this system of equations admits a unique solution e, r (up to the transposition $e \longleftrightarrow r$).

The presented result is derived in a simple way by substituting the ansatz (39) into the general Heun equation and expanding the result in powers of z . The equations resulting in cancelling the first three terms proportional to z^0 , z^1 , and z^2 are that given by (40), (41), and (36), respectively. It is then shown that these three equations are enough for the Heun equation to be satisfied identically.

A further remark is that (36) presents the condition for the singularity $z = a$ to be apparent for $\varepsilon = -2$. This is straightforwardly verified by checking the power-series solution $u = \sum_{n=0}^{\infty} c_n(z-a)^n$ with $c_0 \neq 0$ for the neighborhood of the point $z = a$. In calculating c_3 a division by zero will occur, unless q satisfies (36), in which case the equation for c_3 will be identically satisfied.

It can be checked that generalized hypergeometric representations are achieved also for $\varepsilon = -3, -4, -5$ [42]. The conjecture is that for any negative integer $\varepsilon = -N$, $N = 1, 2, 3, \dots$ there exists a generalized hypergeometric solution of the Heun equation given by the ansatz

$$u = {}_{N+2}F_{1+N}(\alpha, \beta, e_1 + 1, \dots, e_N + 1; \gamma, e_1, \dots, e_N; z) \quad (42)$$

provided the singularity at $z = a$ is an apparent one. For the latter condition to be the case, the accessory parameter q should satisfy a $(N + 1)$ -degree polynomial equation which forces the above expansions (15)-(18) and (21)-(25) to terminate at N th term. Note that (42) applies also for $N = 0$, that is, for $\varepsilon = 0$, for which the Heun function degenerates

with

$$B_1 = \frac{q - a\alpha\beta + a(1 - \delta)}{(1 - a)(\gamma - 2)}, \quad (38)$$

$$B_2 = \frac{a(1 + \alpha - \gamma)(1 + \beta - \gamma)}{(q - a\alpha\beta + 2(1 - a)(\gamma - 1))(\gamma - 1)} B_1.$$

It is now checked that this solution is presented by the hypergeometric function ${}_4F_3$ as [42]

$$\frac{u}{u(0)} = {}_4F_3(\alpha, \beta, e + 1, r + 1; \gamma, e, r; z), \quad (39)$$

where $u(0) = 1 + B_1 + B_2$ and the parameters e, r solve the equations (compare with (35))

to the Gauss hypergeometric function $u = {}_2F_1(\alpha, \beta; \gamma; z)$ provided $q = 0$.

Finally, we note that by the elementary power change $u = (z - a)^{1-\varepsilon} w$ a Heun equation with a *positive* exponent parameter $\varepsilon > 2$ is transformed into the one with a negative parameter $2 - \varepsilon < 0$. Hence, it is understood that a similar generalized hypergeometric representation of the solution of the Heun equation can also be constructed for positive integer $\varepsilon = N$, $N = 2, 3, \dots$. Thus, the only exception is the case $\varepsilon = 1$.

It is a basic knowledge that the generalized hypergeometric function ${}_pF_q$ is given by a power-series with coefficients obeying a two-term recurrence relation. Since any finite-sum solution of the general Heun equation derived via termination of a hypergeometric series expansion has a representation through a single generalized hypergeometric function ${}_pF_q$, the general conclusion is that in each such case the power-series expansion of the Heun function is governed by a two-term recurrence relation (obviously, by the relation obeyed by the corresponding power-series for ${}_pF_q$).

5. Hypergeometric Expansions with Two-Term Recurrence Relations for the Coefficients

In this section we explore if the three-term recurrence relations governing the above-presented hypergeometric expansions can be reduced to two-term ones. We will see that the answer is positive. Two-term reductions are achieved for an infinite set of particular choices of the involved parameters.

First, we mention a straightforward case which actually turns to be rather simple because in this case the Heun

equation is transformed into the Gauss hypergeometric equation by a variable change. This is the case if

$$\begin{aligned} a &= 1/2, \\ \gamma + \delta &= 2 \\ \text{and } q &= a\alpha\beta + a(1 - \delta)\varepsilon, \end{aligned} \quad (43)$$

when the coefficient Q_n in (11) identically vanishes so that the recurrence relation between the expansion coefficients straightforwardly becomes two-term for both expansions (15)-(18) and (21)-(25). The coefficients of the expansions are then explicitly calculated. For instance, expansion (15) is written as

$$\begin{aligned} u &= \sum_{k=0}^{\infty} \frac{(\varepsilon/2)_k ((\gamma + \varepsilon - \alpha)/2)_k ((\gamma + \varepsilon - \beta)/2)_k}{k! ((\gamma + \varepsilon)/2)_k ((1 + \gamma + \varepsilon)/2)_k} \\ &\cdot {}_2F_1(\alpha, \beta; \gamma + \varepsilon + 2k; z), \end{aligned} \quad (44)$$

where $(\dots)_k$ denotes the Pochhammer symbol. The values $u(0)$, $u'(0)$ and $u(1)$, and $u'(1)$ can then be written in terms of generalized hypergeometric series [17, 18]. For instance,

$$\begin{aligned} u(0) &= {}_3F_2\left(\frac{\gamma + \varepsilon - \alpha}{2}, \frac{\gamma + \varepsilon - \beta}{2}, \frac{\varepsilon}{2}; \frac{\gamma + \varepsilon}{2}, \frac{1 + \gamma + \varepsilon}{2}; \right. \\ &\left. 1\right). \end{aligned} \quad (45)$$

However, as it was already mentioned above, the case (43) is a rather simple one because the transformation

$$u(z) = z^{1-\gamma} \left(1 - \frac{z}{a}\right)^{1-\varepsilon} w(4z(1-z)) \quad (46)$$

reduces the Heun equation to the Gauss hypergeometric equation for the new function w . The solution of the general Heun equation is then explicitly written as

$$\begin{aligned} u(z) &= z^{1-\gamma} \left(1 - \frac{z}{a}\right)^{1-\varepsilon} \\ &\cdot {}_2F_1\left(\frac{1-\alpha+\delta}{2}, \frac{1-\beta+\delta}{2}; \delta; 4(1-z)z\right). \end{aligned} \quad (47)$$

Now, we will show that there exist nontrivial cases of two-term reductions of the three-term recurrence (11) with (16)-(18) or (22)-(24). These reductions are achieved by the following ansatz guessed by examination of the structure of solutions (33) and (39):

$$c_n = \left(\frac{1 \prod_{k=1}^{N+2} (a_k - 1 + n)}{n \prod_{k=1}^{N+1} (b_k - 1 + n)}\right) c_{n-1}, \quad (48)$$

where, having in mind the coefficients R_n , Q_n , and P_n given by (16)-(18), we put

$$\begin{aligned} a_1, \dots, a_N, a_{N+1}, a_{N+2} \\ = 1 + e_1, \dots, 1 + e_N, \gamma + \varepsilon - \alpha, \gamma + \varepsilon - \beta, \end{aligned} \quad (49)$$

$$b_1, \dots, b_N, b_{N+1} = e_1, \dots, e_N, \gamma + \varepsilon \quad (50)$$

with parameters e_1, \dots, e_N to be defined later. Note that this ansatz implies that e_1, \dots, e_N are not zero or negative integers.

The ratio c_n/c_{n-1} is explicitly written as

$$\begin{aligned} \frac{c_n}{c_{n-1}} &= \frac{(\gamma + \varepsilon - \alpha - 1 + n)(\gamma + \varepsilon - \alpha - 1 + n)}{(\gamma + \varepsilon - 1 + n)n} \prod_{k=1}^N \\ &\cdot \frac{e_k + n}{e_k - 1 + n}. \end{aligned} \quad (51)$$

With this, the recurrence relation (11) is rewritten as

$$\begin{aligned} R_n \frac{(\gamma + \varepsilon - \alpha - 1 + n)(\gamma + \varepsilon - \beta - 1 + n)}{(\gamma + \varepsilon - 1 + n)n} \prod_{k=1}^N \\ \cdot \frac{e_k + n}{e_k - 1 + n} + Q_{n-1} + P_{n-2} \\ \cdot \frac{(\gamma + \varepsilon - 2 + n)(n-1)}{(\gamma + \varepsilon - \alpha - 2 + n)(\gamma + \varepsilon - \beta - 2 + n)} \prod_{k=1}^N \\ \cdot \frac{e_k - 2 + n}{e_k - 1 + n} = 0. \end{aligned} \quad (52)$$

Substituting R_n and P_{n-2} from (16) and (18) and cancelling the common denominator, this equation becomes

$$\begin{aligned} (1-a)(\gamma + \varepsilon - \alpha - 1 + n)(\gamma + \varepsilon - \beta - 1 + n) \\ \cdot \prod_{k=1}^N (e_k + n) + Q_{n-1} \prod_{k=1}^N (e_k - 1 + n) \\ - a(\varepsilon + n - 2)(n-1) \prod_{k=1}^N (e_k - 2 + n) = 0. \end{aligned} \quad (53)$$

This is a polynomial equation in n . Notably, it is of degree $N+1$, not $N+2$, because the highest-degree term proportional to n^{N+2} identically vanishes. Hence, we have an equation of the form

$$\sum_{m=0}^{N+1} A_m(a, q; \alpha, \beta, \gamma, \delta, \varepsilon; e_1, \dots, e_N) n^m = 0. \quad (54)$$

Then, equating to zero the coefficients A_m warrants the satisfaction of the three-term recurrence relation (11) for all n . We thus have $N+2$ equations $A_m = 0$, $m = 0, 1, \dots, N+1$, of which N equations serve for determination of the parameters $e_{1,2,\dots,N}$ and the remaining two impose restrictions on the parameters of the Heun equation.

One of these restrictions is derived by calculating the coefficient A_{N+1} of the term proportional to n^{N+1} which is readily shown to be $2 + N - \delta$. Hence,

$$\delta = 2 + N. \quad (55)$$

The second restriction imposed on the parameters of the Heun equation is checked to be a polynomial equation of the degree $N+1$ for the accessory parameter q .

With the help of the Fuchsian condition $1 + \alpha + \beta = \gamma + \delta + \varepsilon$, we have

$$\gamma + \varepsilon - \alpha - 1 = \beta - \delta = \beta - 2 - N, \quad (56)$$

$$\gamma + \varepsilon - \beta - 1 = \alpha - \delta = \alpha - 2 - N, \quad (57)$$

$$\gamma + \varepsilon - 1 = \alpha + \beta - \delta = \alpha + \beta - 2 - N, \quad (58)$$

so that the two-term recurrence relation (51) can be rewritten as ($c_0 = 1$)

$$c_n = \left(\frac{(\alpha - 2 - N + n)(\beta - 2 - N + n)}{(\alpha + \beta - 2 - N + n)n} \prod_{k=1}^N \cdot \frac{e_k + n}{e_k - 1 + n} \right) c_{n-1}, \quad n \geq 1. \quad (59)$$

Note that it follows from this relation, since α , β , and e_1, \dots, e_N are not zero or negative integers, that c_n may vanish only if α is a positive integer such that $0 < \alpha < 2 + N$ or β is a positive integer such that $0 < \beta < 2 + N$.

Resolving the recurrence (51), the coefficients of expansion (15)-(18) are explicitly written in terms of the gamma functions as

$$c_n = \frac{\Gamma(\gamma + \varepsilon) \Gamma(n + \gamma + \varepsilon - \alpha) \Gamma(n + \gamma + \varepsilon - \beta)}{n! \Gamma(\gamma + \varepsilon - \alpha) \Gamma(\gamma + \varepsilon - \beta) \Gamma(n + \gamma + \varepsilon)} \prod_{k=1}^N \cdot \frac{e_k + n}{e_k}, \quad n \geq 1. \quad (60)$$

Here are the explicit solutions of the recurrence relation (11) for $N = 0$ and $N = 1$.

$$N = 0: \quad (61)$$

$$\delta = 2,$$

$$q = a\gamma + (\alpha - 1)(\beta - 1), \quad (62)$$

$$c_n = \frac{\Gamma(\gamma + \varepsilon) \Gamma(n + \gamma + \varepsilon - \alpha) \Gamma(n + \gamma + \varepsilon - \beta)}{n! \Gamma(\gamma + \varepsilon - \alpha) \Gamma(\gamma + \varepsilon - \beta) \Gamma(n + \gamma + \varepsilon)}. \quad (63)$$

$$N = 1: \quad (64)$$

$$\delta = 3,$$

$$q^2 - q(4 + a - 3\alpha - 3\beta + 2\alpha\beta + 3a\gamma) + (\alpha - 2) \cdot (\alpha - 1)(\beta - 2)(\beta - 1) \quad (65)$$

$$+ a(4 + 2a - 4\alpha - 4\beta + 3\alpha\beta)\gamma + 2a^2\gamma^2 = 0,$$

$$e_1 = -q + a(1 + \gamma) - 1 + (\alpha - 1)(\beta - 1), \quad (66)$$

$$c_n = \frac{\Gamma(\gamma + \varepsilon) \Gamma(n + \gamma + \varepsilon - \alpha) \Gamma(n + \gamma + \varepsilon - \beta)}{n! \Gamma(\gamma + \varepsilon - \alpha) \Gamma(\gamma + \varepsilon - \beta) \Gamma(n + \gamma + \varepsilon)} \cdot \frac{e_1 + n}{e_1}. \quad (67)$$

These results are readily checked by direct verification of the recurrence relation (11) with coefficients (16)-(18). We conclude by noting that similar explicit solutions can be straightforwardly derived for the expansion (21)-(25) as well.

6. Discussion

Thus, we have presented an expansion of the solutions of the Heun equation in terms of hypergeometric functions having the form ${}_2F_1(\alpha, \beta; \gamma_0 + n; z)$ with $\gamma_0 = \varepsilon + \gamma$ and expansions in terms of functions ${}_2F_1(\alpha, \beta; \gamma_0 - n; z)$ with $\gamma_0 = \gamma, \alpha, \beta$. For any set of parameters of the Heun equation provided that $\gamma + \varepsilon, \gamma, \alpha, \beta$ are not all simultaneously integers at least one of these expansions can be applied. Obviously, the expansions are meaningless if $\alpha\beta = 0$ since then the involved hypergeometric functions are mere constants and for the solution the summation produces the trivial result $u = 0$.

The applied technique is readily extended to the four confluent Heun equations. For instance, the solutions of the single- and double-confluent Heun equations using the Kummer confluent hypergeometric functions of the forms ${}_1F_1(\alpha_0 + n; \gamma_0 + n; s_0 z)$, ${}_1F_1(\alpha_0 + n; \gamma_0; s_0 z)$, and ${}_1F_1(\alpha_0; \gamma_0 + n; s_0 z)$ are straightforward. By slight modification, equations of more general type, e.g., of the type discussed by Schmidt [22], can also be considered. In all these cases the termination of the series results in closed-form solutions appreciated in many applications. A representative example is the determination of the exact complete return spectrum of a quantum two-state system excited by a laser pulse of Lorentzian shape and of a double level-crossing frequency detuning [45]. A large set of recent applications of the finite-sum expansions of the biconfluent Heun equation in terms of the Hermite functions to the Schrödinger equation is listed in [37] and references therein.

Regarding the closed-form solutions produced by the presented expansions, this happens in three cases: $\varepsilon = -N$, $\varepsilon + \gamma - \alpha = -N$, $\varepsilon + \gamma - \beta = -N$, $N = 0, 1, 2, 3, \dots$. In each case the general Heun equation admits finite-sum solutions in general at $N + 1$ choices of the accessory parameter q defined by a polynomial equation of the order of $N + 1$. The last two choices for ε result in quasi-polynomial solutions, while, in the first case, when ε is a negative integer, the solutions involve $N + 1$ hypergeometric functions generally irreducible to simpler functions. Discussing the termination of this series, we have shown that this is possible if a singularity of the Heun equation is an apparent one. We have further shown that the corresponding finite-sum solution of the general Heun equation has a representation through a single generalized hypergeometric function. The general conclusion suggested by this result is that in any such case the power-series expansion of the Heun function is governed by the two-term recurrence relation obeyed by the power-series for the corresponding generalized hypergeometric function ${}_pF_q$.

There are many examples of application of finite-sum solutions of the Heun equation both in physics and mathematics [46-56], for instance, the solution of a class of free boundary problems occurring in groundwater flow in liquid mechanics and the removal of false singular points

of Fuchsian ordinary differential equations in applied mathematics [43]. Another example is the derivation of the third independent exactly solvable hypergeometric potential, after the Eckart and the Pöschl-Teller potentials, which is proportional to an energy-independent parameter and has a shape that is independent of this parameter [44]. Some other recent examples can be found in references listed in [14].

Finally, we have shown that there exist infinitely many choices of the involved parameters for which the three-term recurrence relations governing the hypergeometric expansions of the solutions of the general Heun equation are reduced to two-term ones. The coefficients of the expansions are then explicitly expressed in terms of the gamma functions. We have explicitly presented two such cases.

Data Availability

No data were used to support this study.

Conflicts of Interest

The authors declare that they have no conflicts of interest.

Acknowledgments

This research has been conducted within the scope of the International Associated Laboratory IRMAS (CNRS-France & SCS-Armenia). The work has been supported by the Russian-Armenian (Slavonic) University at the expense of the Ministry of Education and Science of the Russian Federation, the Armenian State Committee of Science (SCS Grant no. 18RF-139), the Armenian National Science and Education Fund (ANSEF Grant no. PS-4986), and the project “Leading Russian Research Universities” (Grant no. FTI_24_2016 of the Tomsk Polytechnic University). T. A. Ishkhanyan acknowledges the support from SPIE through a 2017 Optics and Photonics Education Scholarship and thanks the French Embassy in Armenia for a doctoral grant as well as the Agence Universitaire de la Francophonie and Armenian State Committee of Science for a Scientific Mobility grant.

References

- [1] K. Heun, “Zur Theorie der Riemann’schen Functionen zweiter Ordnung mit vier Verzweigungspunkten,” *Mathematische Annalen*, vol. 33, no. 2, pp. 161–179, 1888.
- [2] A. Ronveaux, Ed., *Heun’s Differential Equations*, Oxford University Press, Oxford, UK, 1995.
- [3] S. Y. Slavyanov and W. Lay, *Special functions*, Oxford Mathematical Monographs, Oxford University Press, Oxford, UK, 2000.
- [4] E. Renzi and P. Sammarco, “The hydrodynamics of landslide tsunamis: Current analytical models and future research directions,” *Landslides*, vol. 13, no. 6, pp. 1369–1377, 2016.
- [5] M. Renardy, “On the eigenfunctions for Hookean and FENE dumbbell models,” *Journal of Rheology*, vol. 57, no. 5, pp. 1311–1324, 2013.
- [6] M. M. Afonso and D. Vincenzi, “Nonlinear elastic polymers in random flow,” *Journal of Fluid Mechanics*, vol. 540, pp. 99–108, 2005.
- [7] I. C. Fonseca and K. Bakke, “Quantum Effects on an Atom with a Magnetic Quadrupole Moment in a Region with a Time-Dependent Magnetic Field,” *Few-Body Systems*, vol. 58, no. 1, 2017.
- [8] Q. Xie, H. Zhong, M. T. Batchelor, and C. Lee, “The quantum Rabi model: solution and dynamics,” *Journal of Physics A: Mathematical and General*, vol. 50, no. 11, 113001, 40 pages, 2017.
- [9] C. A. Downing and M. E. Portnoi, “Massless Dirac fermions in two dimensions: Confinement in nonuniform magnetic fields,” *Physical Review B: Condensed Matter and Materials Physics*, vol. 94, no. 16, 2016.
- [10] P. Fiziev and D. Staicova, “Application of the confluent Heun functions for finding the quasinormal modes of nonrotating black holes,” *Physical Review D: Particles, Fields, Gravitation and Cosmology*, vol. 84, no. 12, 2011.
- [11] D. Batic, D. Mills-Howell, and M. Nowakowski, “Potentials of the Heun class: the triconfluent case,” *Journal of Mathematical Physics*, vol. 56, no. 5, 052106, 17 pages, 2015.
- [12] H. S. Vieira and V. B. Bezerra, “Confluent Heun functions and the physics of black holes: resonant frequencies, HAWking radiation and scattering of scalar waves,” *Annals of Physics*, vol. 373, pp. 28–42, 2016.
- [13] R. L. Hall and N. Saad, “Exact and approximate solutions of Schrödinger’s equation with hyperbolic double-well potentials,” *The European Physical Journal Plus*, vol. 131, no. 8, 2016.
- [14] M. Hortacsu, *Proc. 13th Regional Conference on Mathematical Physics*, World Scientific, Singapore, 2013.
- [15] R. Schäfke and D. Schmidt, “The connection problem for general linear ordinary differential equations at two regular singular points with applications in the theory of special functions,” *SIAM Journal on Mathematical Analysis*, vol. 11, no. 5, pp. 848–862, 1980.
- [16] A. Erdélyi, W. Magnus, F. Oberhettinger, and F. G. Tricomi, *Higher Transcendental Functions*, vol. 3, McGraw-Hill, New York, NY, USA, 1955.
- [17] L. J. Slater, *Generalized Hypergeometric Functions*, Cambridge University Press, Cambridge, UK, 1966.
- [18] W. N. Bailey, *Generalized Hypergeometric Series*, Stechert-Hafner Service Agency, 1964.
- [19] N. Svartholm, “Die Lösung der Fuchs’schen Differentialgleichung zweiter Ordnung durch Hypergeometrische Polynome,” *Mathematische Annalen*, vol. 116, no. 1, pp. 413–421, 1939.
- [20] A. Erdélyi, “The Fuchsian equation of second order with four singularities,” *Duke Mathematical Journal*, vol. 9, pp. 48–58, 1942.
- [21] A. Erdélyi, “Certain expansions of solutions of the Heun equation,” *Quarterly Journal of Mathematics*, vol. 15, pp. 62–69, 1944.
- [22] D. Schmidt, “Die Lösung der linearen Differentialgleichung 2. Ordnung um zwei einfache Singularitäten durch Reihen nach hypergeometrischen Funktionen,” *Journal für die Reine und Angewandte Mathematik*, vol. 309, pp. 127–148, 1979.
- [23] E. G. Kalnins and J. Miller, “Hypergeometric expansions of Heun polynomials,” *SIAM Journal on Mathematical Analysis*, vol. 22, no. 5, pp. 1450–1459, 1991.
- [24] S. Mano, H. Suzuki, and E. Takasugi, “Analytic solutions of the Teukolsky equation and their low frequency expansions,” *Progress of Theoretical and Experimental Physics*, vol. 95, no. 6, pp. 1079–1096, 1996.
- [25] B. D. Sleeman and V. B. Kuznetsov, “Heun Functions: Expansions in Series of Hypergeometric Functions,” <http://dlmf.nist.gov/31.11>.

- [26] T. Kurth and D. Schmidt, "On the global representation of the solutions of second-order linear differential equations having an irregular singularity of rank one in by series in terms of confluent hypergeometric functions," *SIAM Journal on Mathematical Analysis*, vol. 17, no. 5, pp. 1086–1103, 1986.
- [27] S. Mano and E. Takasugi, "Analytic solutions of the Teukolsky equation and their properties," *Progress of Theoretical and Experimental Physics*, vol. 97, no. 2, pp. 213–232, 1997.
- [28] L. J. El-Jaick and B. D. Figueiredo, "Solutions for confluent and double-confluent Heun equations," *Journal of Mathematical Physics*, vol. 49, no. 8, 083508, 28 pages, 2008.
- [29] T. A. Ishkhanyan and A. M. Ishkhanyan, "Expansions of the solutions to the confluent Heun equation in terms of the Kummer confluent hypergeometric functions," *AIP Advances*, vol. 4, Article ID 087132, 2014.
- [30] E. W. Leaver, "Solutions to a generalized spheroidal wave equation: Teukolsky's equations in general relativity, and the two-center problem in molecular quantum mechanics," *Journal of Mathematical Physics*, vol. 27, no. 5, pp. 1238–1265, 1986.
- [31] L. J. El-Jaick and B. D. Figueiredo, "Confluent Heun equations: convergence of solutions in series of Coulomb wavefunctions," *Journal of Physics A: Mathematical and General*, vol. 46, no. 8, 085203, 29 pages, 2013.
- [32] B. D. B. Figueiredo, "Generalized spheroidal wave equation and limiting cases," *Journal of Mathematical Physics*, vol. 48, Article ID 013503, 2007.
- [33] A. Ishkhanyan, "Incomplete beta-function expansions of the solutions to the confluent Heun equation," *Journal of Physics A: Mathematical and General*, vol. 38, no. 28, pp. L491–L498, 2005.
- [34] E. S. Cheb-Terrab, "Solutions for the general, confluent and biconfluent Heun equations and their connection with Abel equations," *Journal of Physics A: Mathematical and General*, vol. 37, no. 42, pp. 9923–9949, 2004.
- [35] T. A. Ishkhanyan, Y. Pashayan-Leroy, M. R. Gevorgyan, C. Leroy, and A. M. Ishkhanyan, "Expansions of the solutions of the biconfluent Heun equation in terms of incomplete Beta and Gamma functions," *Journal of Contemporary Physics (Armenian Academy of Sciences)*, vol. 51, pp. 229–236, 2016.
- [36] A. Hautot, "Sur des combinaisons linéaires d'un nombre fini de fonctions transcendentes comme solutions d'équations différentielles du second ordre," *Bulletin de la Societe Royale des Sciences de Liege*, vol. 40, pp. 13–23, 1971.
- [37] T. A. Ishkhanyan and A. M. Ishkhanyan, "Solutions of the bi-confluent Heun equation in terms of the Hermite functions," *Annals of Physics*, vol. 383, pp. 79–91, 2017.
- [38] A. Ishkhanyan and K.-A. Suominen, "New solutions of Heun's general equation," *Journal of Physics A: Mathematical and General*, vol. 36, no. 5, pp. L81–L85, 2003.
- [39] C. Leroy and A. M. Ishkhanyan, "Expansions of the solutions of the confluent Heun equation in terms of the incomplete Beta and the Appell generalized hypergeometric functions," *Integral Transforms and Special Functions*, vol. 26, no. 6, pp. 451–459, 2015.
- [40] J. Letessier, G. Valent, and J. Wimp, "Some differential equations satisfied by hypergeometric functions," in *Approximation and computation (West Lafayette, IN, 1993)*, vol. 119 of *Internat. Ser. Numer. Math.*, pp. 371–381, Birkhauser Boston, Boston, Mass, USA, 1994.
- [41] R. S. Maier, "P-symbols, Heun identities, and 3 F2 identities," in *Special Functions and Orthogonal Polynomials*, vol. 471 of *Contemp. Math.*, pp. 139–159, Amer. Math. Soc., Providence, RI, 2008.
- [42] K. Takemura, "Heun's equation, generalized hypergeometric function and exceptional Jacobi polynomial," *Journal of Physics A: Mathematical and General*, vol. 45, no. 8, 085211, 14 pages, 2012.
- [43] A. V. Shanin and R. V. Craster, "Removing false singular points as a method of solving ordinary differential equations," *European Journal of Applied Mathematics*, vol. 13, no. 6, pp. 617–639, 2002.
- [44] A. Ishkhanyan, "The third exactly solvable hypergeometric quantum-mechanical potential," *EPL (Europhysics Letters)*, vol. 115, no. 2, 2016.
- [45] A. M. Ishkhanyan and A. E. Grigoryan, "Fifteen classes of solutions of the quantum two-state problem in terms of the confluent Heun function," *Journal of Physics A: Mathematical and General*, vol. 47, no. 46, 465205, 22 pages, 2014.
- [46] L. Carlitz, "Some orthogonal polynomials related to elliptic functions," *Duke Mathematical Journal*, vol. 27, pp. 443–459, 1960.
- [47] K. Kuiken, "Heun's equation and the hypergeometric equation," *SIAM Journal on Mathematical Analysis*, vol. 10, no. 3, pp. 655–657, 1979.
- [48] J. N. Ginocchio, "A class of exactly solvable potentials. I. One-dimensional Schrödinger equation," *Annals of Physics*, vol. 152, no. 1, pp. 203–219, 1984.
- [49] G. Valent, "An integral transform involving Heun functions and a related eigenvalue problem," *SIAM Journal on Mathematical Analysis*, vol. 17, no. 3, pp. 688–703, 1986.
- [50] G. S. Joyce, "On the cubic lattice Green functions," *Proceedings of the Royal Society A Mathematical, Physical and Engineering Sciences*, vol. 445, no. 1924, pp. 463–477, 1994.
- [51] G. S. Joyce and R. T. Delves, "Exact product forms for the simple cubic lattice Green function. I," *Journal of Physics A: Mathematical and General*, vol. 37, no. 11, pp. 3645–3671, 2004.
- [52] G. S. Joyce and R. T. Delves, "Exact product forms for the simple cubic lattice Green function. II," *Journal of Physics A: Mathematical and General*, vol. 37, no. 20, pp. 5417–5447, 2004.
- [53] R. S. Maier, "On reducing the Heun equation to the hypergeometric equation," *Journal of Differential Equations*, vol. 213, no. 1, pp. 171–203, 2005.
- [54] M. van Hoeij and R. Vidunas, "Belyi functions for hyperbolic hypergeometric-to-Heun transformations," *Journal of Algebra*, vol. 441, pp. 609–659, 2015.
- [55] R. Vidunas and G. Filipuk, "Parametric transformations between the Heun and Gauss hypergeometric functions," *Funkcialaj Ekvacioj. Serio Internacia*, vol. 56, no. 2, pp. 271–321, 2013.
- [56] R. Vidunas and G. Filipuk, "A classification of coverings yielding Heun-to-hypergeometric reductions," *Osaka Journal of Mathematics*, vol. 51, no. 4, pp. 867–903, 2014.

Research Article

Integrable and Superintegrable Systems with Higher Order Integrals of Motion: Master Function Formalism

Z. Alizadeh and H. Panahi 

Department of Physics, University of Guilan, Rasht 51335-1914, Iran

Correspondence should be addressed to H. Panahi; t-panahi@guilan.ac.ir

Received 5 October 2017; Revised 28 December 2017; Accepted 5 February 2018; Published 21 June 2018

Academic Editor: Chun-Sheng Jia

Copyright © 2018 Z. Alizadeh and H. Panahi. This is an open access article distributed under the Creative Commons Attribution License, which permits unrestricted use, distribution, and reproduction in any medium, provided the original work is properly cited. The publication of this article was funded by SCOAP³.

We construct two-dimensional integrable and superintegrable systems in terms of the master function formalism and relate them to *Mielnik's* and *Marquette's* construction in supersymmetric quantum mechanics. For two different cases of the master functions, we obtain two different two-dimensional superintegrable systems with higher order integrals of motion.

1. Introduction

It is known from classical and quantum mechanics that a system with N degrees of freedom is called completely integrable if it allows N functionally independent constants of the motion [1]. From the mathematical and physical point of view, these systems play a fundamental role in description of physical systems due to their many interesting properties. A system is superintegrable if one could obtain more than N constants of the motion and if there exist $2N - 1$ constants of the motion, the system is maximally superintegrable or just superintegrable [2–5]. Recently the study of superintegrable systems has been considered for different potentials and many researches have been studied for calculating the spectrum of these systems by different methods. In [6, 7], the spectrum of these systems has been calculated by an algebraic method using the realization of some Lie groups.

For a two-dimensional quantum integrable system with Hamiltonian H , there is always one operator like A_1 which commutes with Hamiltonian of the system, that is, $[H, A_1] = 0$. For a quantum superintegrable system, one should define another operator such as A_2 which commutes with the Hamiltonian of system, that is, $[H, A_2] = 0$, but $[A_1, A_2] \neq 0$. In other words, for a two-dimensional superintegrable system, there are two integrals of the motion (A_1, A_2) in addition to the Hamiltonian. The superintegrability with the

second- and third-order integrals was the object of a series of articles [8–11]. The systems studied have second- and third-order integrals. Although superintegrability and supersymmetric quantum mechanics (SUSYQM) are two separated fields, many quantum systems, such as the harmonic oscillator, the Hydrogen atom, and the Smorodinsky-Winternitz potential, have both supersymmetry and superintegrable conditions [12–16]. These articles show that superintegrability is accurately connected with supersymmetry. For example, in [17], Marquette used the results obtained by Mielnik [18] and generated new superintegrable systems. Mielnik has shown that the factorization of second-order operators is not essentially unique. He has considered the Hamiltonian of the harmonic oscillator in one dimension as the simplest case:

$$H = -\frac{1}{2} \frac{d^2}{dx^2} + \frac{1}{2} x^2, \quad (1)$$

where it can be factorized by two types of the first-order operators of creation and annihilation as follows:

$$\begin{aligned} a_{\pm} &= \frac{1}{\sqrt{2}} \left(\mp \frac{d}{dx} + x \right), \\ b_{\pm} &= \frac{1}{\sqrt{2}} \left(\mp \frac{d}{dx} + \beta(x) \right). \end{aligned} \quad (2)$$

For two superpartner Hamiltonians H_1 and H_2 where $a_+ a_- = H - 1/2 = H_1$ and $a_- a_+ = H + 1/2 = H_2$, he has demanded

that $H_2 = b_- b_+$ and obtained the inverted product $b_+ b_-$ as a certain new Hamiltonian:

$$H' = b_+ b_- = -\frac{1}{2} \frac{d^2}{dx^2} + \frac{x^2}{2} - \varphi'(x), \quad (3)$$

where $\varphi(x)$ is a function obtained from the general solution of Riccati equation considering $\beta = x + \varphi(x)$. The creation and annihilation operators of the third order for H' are described by expressions $s_+ = b_+ a_+ b_-$, $s_- = b_+ a_- b_-$, where a_+ and a_- are the creation and annihilation operators for H_2 . Marquette [17] has taken the Hamiltonian H_2 in the x -axis and its superpartner H' given by (3) in the y -axis. Hence, he has obtained a two-dimensional superintegrable system as $H_s = H_x + H_y$, which can be separated in Cartesian coordinates with creation and annihilation operators $a_+(x)$, $a_-(x)$, $s_+(y)$, and $s_-(y)$. Also, he has shown that the Hamiltonian H_s possesses the following integrals of motion:

$$\begin{aligned} \mathcal{K} &= H_x - H_y, \\ \mathcal{A}_1 &= a_+(x) s_-(y) - a_-(x) s_+(y), \\ \mathcal{A}_2 &= a_-(x) s_+(y) + a_+(x) s_-(y), \end{aligned} \quad (4)$$

where these integrals are of order 2, 3, and 4 for shape invariant potentials [17].

On the other hand, in [19, 20], the authors have shown that the second-order differential equations and their associated differential equations in mathematical physics have the shape invariant property of supersymmetry quantum mechanics. They have shown that by using a polynomial of a degree not exceeding two, called the master function, the associated differential equations can be factorized into the product of rising and lowering operators. The master function formalism has been used in relativistic quantum mechanics for solving the Dirac equation [21, 22].

As *Mielnik's* and *Marquette's* method for generating superintegrable systems can be applied to other systems obtained in the context of supersymmetric quantum mechanics, hence, in this paper, we show that the supersymmetry method for obtaining the integrable and superintegrable systems can be related to master function formalism. In fact, we use the master function approach for 1-dimensional shape invariant potentials and generate 2-dimensional integrable systems. Also for a particular class of shape invariant systems, we generate 2-dimensional superintegrable systems. This class contains the harmonic oscillator, the singular harmonic oscillator, and their supersymmetric isospectral deformations.

The paper is presented as follows: in Section 2, we review how one can generate integrals of motion for two-dimensional superintegrable system from the creation and annihilation operators. In Section 3, we consider a particular quantum system for applying the *Mielnik's* and *Marquette's* method and obtain a superintegrable potential separable in Cartesian coordinates. In Section 4, we briefly review the master function formalism and then in Section 5, we use this approach to obtain integrable systems and particular cases of the superintegrable systems that satisfy the oscillator-like (Heisenberg) algebra with higher order integrals of motion

in terms of the master function and weight function. In Section 6, we give two examples to show how this method works in constructing oscillator-like two-dimensional superintegrable systems. Paper ends with a brief conclusion in Section 7.

2. Two-Dimensional Superintegrable System and Its Integrals of Motion

According to [17, 23, 24], for a two-dimensional Hamiltonian separable in Cartesian coordinates as

$$H(x, y, p_x, p_y) = H_x(x, p_x) + H_y(y, p_y), \quad (5)$$

where the creation and annihilation operators (polynomial in momenta) $A_+(x)$, $A_-(x)$, $A_+(y)$, and $A_-(y)$ satisfy the following equations:

$$\begin{aligned} [H_x, A_-(x)] &= -\lambda_x A_-(x), \\ [H_y, A_-(y)] &= -\lambda_y A_-(y), \\ [H_x, A_+(x)] &= \lambda_x A_+(x), \\ [H_y, A_+(y)] &= \lambda_y A_+(y), \end{aligned} \quad (6)$$

one can show that the operators $f_1 = A_+^m(x) A_-^n(y)$ and $f_2 = A_-^m(x) A_+^n(y)$ commute with the Hamiltonian H : that is,

$$[H, f_1] = [H, f_2] = 0, \quad (7)$$

if

$$m\lambda_x - n\lambda_y = 0, \quad m, n \in \mathbb{Z}^+. \quad (8)$$

Also the following sums of f_1 and f_2 commute with the Hamiltonian

$$\begin{aligned} I_1 &= A_+^m(x) A_-^n(y) - A_-^m(x) A_+^n(y), \\ I_2 &= A_+^m(x) A_-^n(y) + A_-^m(x) A_+^n(y); \end{aligned} \quad (9)$$

that is, I_1 and I_2 are the integrals of motion. The order of these integrals of motion depends on the order of the creation and annihilation operators. On the other hand, the Hamiltonian H possesses a second-order integral as $K = H_x - H_y$, such that the integral I_2 is the commutator of I_1 and K . Thus, the Hamiltonian H is a superintegrable system and H , I_1 , and K are its integrals of motion.

3. Mielnik-Marquette Method and Superintegrable Model Obtained from Shifted Oscillator Hamiltonian

In this section, for reviewing the *Mielnik-Marquette* method, we consider shifted oscillator Hamiltonian as

$$H = -\frac{d^2}{dx^2} + \frac{1}{4}\omega^2 \left(x - \frac{2b}{\omega}\right)^2 - \frac{\omega}{2}. \quad (10)$$

We introduce the following first-order operators:

$$a_- = \frac{d}{dx} + \frac{1}{2}\omega x - b, \quad (11)$$

$$a_+ = -\frac{d}{dx} + \frac{1}{2}\omega x - b,$$

where the supersymmetric partner Hamiltonians are calculated as

$$\begin{aligned} H_1 &= a_- a_+ = H + \omega, \\ H_2 &= a_+ a_- = H. \end{aligned} \quad (12)$$

It is obvious that H_1 and H_2 have the shape invariant properties. Now, according to (2), we define the new operators b_- and b_+ such that

$$H_1 = H + \omega = b_- b_+. \quad (13)$$

The above equation gives the following Riccati equation:

$$\beta^2 + \beta' = \frac{1}{4}\omega^2 x^2 - b\omega x + b^2 + \frac{\omega}{2}, \quad (14)$$

where a particular solution is

$$\beta(x) = \beta_0(x) = \frac{1}{2}\omega x - b. \quad (15)$$

Now, if we consider

$$\beta(x) = \beta_0(x) + \varphi(x), \quad (16)$$

then we can obtain the following first-order linear inhomogeneous equation:

$$z' + (-2\beta_0)z = 1, \quad (17)$$

where $z = 1/\varphi(x)$. After solving the above equation, we get

$$\begin{aligned} \varphi(x) &= \frac{1}{z(x)} \\ &= \frac{e^{-(\omega/2)x^2 + 2bx}}{\sqrt{\pi/2\omega} e^{2b^2/\omega} \operatorname{erf}\left(\sqrt{\omega/2}(x - 2b/\omega)\right) + C}, \end{aligned} \quad (18)$$

where C is the constant of integration. Using the function $\varphi(x)$, we obtain

$$H' = b_+ b_- = H_1 - \varphi'(x), \quad (19)$$

where its creation and annihilation operators are given by the following expressions:

$$\begin{aligned} s_+ &= b_+ a_+ b_-, \\ s_- &= b_+ a_- b_-. \end{aligned} \quad (20)$$

According to Marquette method, we take the x -axis for Hamiltonian H_1 and the y -axis for its superpartner H' and we have the following two-dimensional superintegrable system:

$$\begin{aligned} H_s &= H_x + H_y = H_1 + H' \\ &= -\frac{d^2}{dx^2} - \frac{d^2}{dy^2} + \frac{1}{4}\omega^2 \left(x - \frac{2b}{\omega}\right)^2 \\ &\quad + \frac{1}{4}\omega^2 \left(y - \frac{2b}{\omega}\right)^2 - \omega - \frac{d\varphi}{dy}. \end{aligned} \quad (21)$$

This Hamiltonian possesses the integral of motion given by (4), which are of order 2, 3, and 4.

4. The Master Function Formalism

According to [19, 20], the general form of the differential equation in master function approach is written as

$$\begin{aligned} A(x) \Phi_n'' + \frac{(A(x)w(x))'}{w(x)} \Phi_n'(x) \\ - \left(n \left(\frac{(A(x)w(x))'}{w(x)} \right)' + \frac{n(n-1)}{2} A''(x) \right) \Phi_n(x) \\ = 0, \end{aligned} \quad (22)$$

where $A(x)$ as master function is at most a second-order polynomial and $w(x)$ is the nonnegative weight function in interval (a, b) . By differentiating (22) m times and then multiplying it by $(-1)^m A^{m/2}(x)$, we get the following associated second-order differential equation in terms of the master function and weight function:

$$\begin{aligned} A(x) \Phi_{n,m}'' + \frac{(A(x)w(x))'}{w(x)} \Phi_{n,m}'(x) \\ + \left[-\frac{1}{2}(n^2 + n - m^2) A'' \right. \\ \left. + (m-n) \left(\frac{(A(x)w'(x))'}{w(x)} \right)' - \frac{m^2 (A'(x))^2}{4 A(x)} \right. \\ \left. - \frac{m A'(x) w'(x)}{2 w(x)} \right] \Phi_{n,m}(x) = 0, \end{aligned} \quad (23)$$

where

$$\Phi_{n,m}(x) = (-1)^m A^{m/2} \left(\frac{d}{dx} \right)^m \Phi_n(x). \quad (24)$$

Changing the variable $dx/dr = \sqrt{A(x)}$ and defining the new function $\Psi_n^m(r) = A^{1/4}(x)w^{1/2}(x)\Phi_{n,m}(x)$, one can obtain the Schrodinger equation as

$$\begin{aligned} -\frac{d^2}{dr^2} \Psi_n^m(r) + v_m(x(r)) \Psi_n^m(r) = E(n, m) \Psi_n^m(r), \\ m = 0, 1, 2, \dots, n, \end{aligned} \quad (25)$$

where the most general shape invariant potential is

$$\begin{aligned} v_m(x(r)) = & -\frac{1}{2} \left(\frac{A(x) w'(x)}{w(x)} \right)' - \frac{2m-1}{4} A''(x) \\ & + \frac{1}{4A(x)} \left(\frac{A(x) w'(x)}{w(x)} \right)^2 \\ & + \frac{m A'(x) w'(x)}{2 w(x)} + \frac{4m^2 - 1}{16} \frac{A'^2(x)}{A(x)}, \end{aligned} \quad (26)$$

and the energy spectrum $E(n, m)$ is as

$$\begin{aligned} E(n, m) = & -(n - m + 1) \\ & \cdot \left[\left(\frac{A(x) w'(x)}{w(x)} \right)' + \frac{1}{2} (n + m) A''(x) \right]. \end{aligned} \quad (27)$$

According to [19, 20] the first-order deferential operators are written as

$$A_{\pm} = \mp \frac{d}{dr} + W_m(x(r)), \quad (28)$$

where the superpotential $W_m(x(r))$ is expressed in terms of the master function $A(x)$ and weigh function $w(x)$ as

$$\begin{aligned} W_m(x(r)) \\ = & -\frac{A(x) w'(x) / 2w(x) + ((2m-1)/4) A'(x)}{\sqrt{A(x)}}. \end{aligned} \quad (29)$$

The Hamiltonian H_1 and H_2 called the superpartner Hamiltonians are written as

$$\begin{aligned} H_1 = A_- A_+ = & -\frac{d^2}{dr^2} + W_m^2(r) + W_m'(r) \\ = & -\frac{d^2}{dr^2} + v_1(r), \\ H_2 = A_+ A_- = & -\frac{d^2}{dr^2} + W_m^2(r) - W_m'(r) \\ = & -\frac{d^2}{dr^2} + v_2(r), \end{aligned} \quad (30)$$

where $v_1(r)$ and $v_2(r)$ are called the partner potentials in the concept of supersymmetry in nonrelativistic quantum mechanics. Furthermore, if the partner potentials have the same shape and differ only in parameters, then potentials $v_1(r)$ and $v_2(r)$ are called the shape invariant potentials that satisfy

$$v_1(r, a_0) = v_2(r, a_1) + R(a_1), \quad (31)$$

where $R(a_1)$ is independent of any dynamical variable and a_1 is a function of a_0 . Potentials which satisfy in this condition are exactly solvable, although shape invariance is not the most general integrability or superintegrability condition.

5. Integrable and Superintegrable Systems Obtained from the Master Function Formalism

In this section, we try to relate the Mielnik-Marquette method to the master function approach. Hence, we define the following new operators:

$$B_{\pm} = \mp \frac{d}{dr} + \omega(r), \quad (32)$$

where $\omega(r)$ as the new superpotential must be related to the general form of the master function superpotential $W_m(x(r))$. Their product yields to Hamiltonians as

$$\begin{aligned} B_- B_+ = & -\frac{d^2}{dr^2} + \omega^2(r) + \omega'(r), \\ B_+ B_- = & -\frac{d^2}{dr^2} + \omega^2(r) - \omega'(r). \end{aligned} \quad (33)$$

Now if we demand $A_- A_+ = B_- B_+$ then we can obtain the following Riccati equation in terms of master function:

$$\omega^2(r) + \omega'(r) = W_m^2(r) + W_m'(r), \quad (34)$$

where a particular solution is $\omega(r) = W_m(r)$. The general solution can be obtained like

$$\omega(r) = W_m(r) + \lambda(r), \quad (35)$$

which yields

$$\lambda^2(r) + 2W_m(r) \lambda(r) + \lambda'(r) = 0. \quad (36)$$

We consider the transformation $f(r) = 1/\lambda(r)$ and obtain a first-order linear inhomogeneous differential equation as

$$f'(r) - 2W_m(r) f(r) = 1, \quad (37)$$

where the general solution is

$$\begin{aligned} f(r) = & \exp \left[2 \int W_m(r) dr \right] \\ & \cdot \left(C + \int \exp \left[2 \int W_m(r') dr' \right] dr \right), \end{aligned} \quad (38)$$

where C is constant. Hence,

$$\omega(r) = W_m(r) + \frac{e^{-\int 2W_m(r) dr}}{C + \int e^{\int 2W_m(r') dr'} dr}. \quad (39)$$

Using the function $f(r)$ given by (38), the superpartner Hamiltonian is given by

$$\begin{aligned} H' = & H_2 - \lambda'(r) \\ = & -\frac{d^2}{dr^2} + W_m^2(r) - W_m'(r) - \lambda'(r), \end{aligned} \quad (40)$$

which is the general form of Hamiltonian in terms of master function. Now if we catch $H_r = H_2$ and $H_{r'} = H'$

(the Hamiltonian H' is thus given in terms of the variable r' vertical to r), then we obtain a new two-dimensional integrable Hamiltonian as

$$\begin{aligned} H_s &= H_r + H_{r'} \\ &= -\frac{d^2}{dr^2} - \frac{d^2}{dr'^2} + W_m^2(r) + W_m^2(r') - W_m'(r) \\ &\quad - W_m'(r') - \lambda'(r'). \end{aligned} \quad (41)$$

Therefore, we have obtained the general form of the 2-dimensional integrable Hamiltonian in terms of master function which can be separated in radial coordinates. This separation of variable implies the existence of a second-order integral as $K = H_r - H_{r'}$. Hence, H_s is an integrable system. Now, for generating superintegrable systems, we can obtain the creation and annihilation operators for H' from H_2 as

$$\begin{aligned} S_+ &= B_+ A_+ B_-, \\ S_- &= B_+ A_- B_-, \end{aligned} \quad (42)$$

where A_\pm and B_\pm are given in (28) and (32). It is necessary to mention that these ladder operators satisfy (6) only for a particular class of shape invariant systems and in general, the 2-dimensional system H_s , obtained from a given master function, is not a superintegrable system. In other words, we cannot obtain 2-dimensional superintegrable system for all of the shape invariant cases given in [19, 20]. This particular class contains the harmonic oscillator, the singular harmonic oscillator, and their supersymmetric isospectral deformations.

Hence, if relation (6) exists, according to (9) we can obtain the integrals of motion for Hamiltonian (41) as

$$\begin{aligned} K &= H_r - H_{r'}, \\ A_1 &= A_+^m(r) S_-^n(r') - A_-^m(r) S_+^n(r'), \\ A_2 &= A_+^m(r) S_-^n(r') + A_-^m(r) S_+^n(r'). \end{aligned} \quad (43)$$

In the next section, we apply this formalism for some particular cases of shape invariant potentials in terms of master function.

6. Examples of Two-Dimensional Superintegrable Systems as a Result of Master Function Approach

In this section, we would apply the master function formalism of the previous section for two examples and show how these results allow us to obtain 2-dimensional superintegrable systems with higher order integrals.

Example 1. Let $A(x) = 1$; then according to [19], $w(x) = e^{-(\beta/2)x^2}$ that $x = r - 2\alpha/\beta$, $\beta > 0$ and the interval is $(-\infty, +\infty)$. Using (29), we obtain the superpotential as

$$W_m(r) = -\frac{\beta}{2} \left(r - \frac{2\alpha}{\beta} \right). \quad (44)$$

According to (27), the energy spectrum is as

$$E = n - m + 1, \quad (45)$$

and also the ladder operators given by (28) related to (44) satisfy a Heisenberg algebras (6). Now, substituting expression $W_m(r)$ in (38) yields the following relation in terms of the error function:

$$\lambda(r) = \frac{e^{-\beta(r^2/2)+2\alpha r}}{C + \sqrt{\pi/2}\beta e^{2\alpha^2/\beta} \operatorname{erf}(\sqrt{\beta/2}(r - 2\alpha/\beta))}, \quad (46)$$

and so

$$\begin{aligned} \omega(r) &= W_m(r) + \lambda(r) \\ &= \frac{\beta}{2} \left(r - \frac{2\alpha}{\beta} \right) \\ &\quad + \frac{e^{\beta(r^2/2)+\alpha r}}{C + \sqrt{\pi/2}\beta e^{2\alpha^2/\beta} \operatorname{erf}(\sqrt{\beta/2}(r - 2\alpha/\beta))}. \end{aligned} \quad (47)$$

Substituting this expression in (40) and (41) yields the family of superpartner H' and a two-dimensional superintegrable Hamiltonian H_s , respectively, as

$$\begin{aligned} H' &= H_2 - \lambda'(r), \\ H_s &= -\frac{d^2}{dr^2} - \frac{d^2}{dr'^2} \\ &\quad + \frac{\beta^2}{4} \left\{ \left(r - \frac{2\alpha}{\beta} \right)^2 + \left(r' - \frac{2\alpha}{\beta} \right)^2 \right\} - \beta \\ &\quad - \lambda'(r'), \end{aligned} \quad (48)$$

where

$$\begin{aligned} \lambda'(r') &= \frac{(\beta r' + \alpha) e^{(\beta/2)r'^2 + \alpha r'}}{C + \sqrt{\pi/2}\beta e^{2\alpha^2/\beta} \operatorname{erf}(\sqrt{\beta/2}(r' - 2\alpha/\beta))} \\ &\quad - \frac{(e^{(\beta/2)r'^2 + \alpha r'}) (e^{2\alpha^2/\beta} e^{-(1/2)\beta(r' - 2\alpha/\beta)^2})}{[C + \sqrt{\pi/2}\beta e^{2\alpha^2/\beta} \operatorname{erf}(\sqrt{\beta/2}(r' - 2\alpha/\beta))]^2}, \\ H_2 &= -\frac{d^2}{dr^2} + \frac{\beta^2}{4} \left(r - \frac{2\alpha}{\beta} \right)^2 - \frac{\beta}{2}. \end{aligned} \quad (49)$$

It is seen that 2-dimensional superintegrable Hamiltonian (48) is the same as (21). We can find the general form of the operators S_+ and S_- in terms of the master function for this oscillator-like potential as follows:

$$\begin{aligned} S_+ &= -\frac{d^3}{dr^3} - W_m \frac{d^2}{dr^2} + (-2\omega' - W_m' + \omega^2) \frac{d}{dr} \\ &\quad + (-\omega'' - W_m' \omega - W_m \omega' + \omega \omega' + W_m \omega^2), \end{aligned}$$

$$S_- = \frac{d^3}{dr^3} - W_m \frac{d^2}{dr^2} + (-2\omega' - W_m' - \omega^2) \frac{d}{dr} + (\omega'' - W_m' \omega - W_m \omega' + \omega \omega' + W_m \omega^2). \quad (51)$$

Thus, we have obtained a 2-dimensional superintegrable system with integrals given by (43) as

$$K = H_r - H_{r'}, \quad (52)$$

$$A_1 = A_+(r) S_-(r') - A_-(r) S_+(r'),$$

$$A_2 = A_+(r) S_-(r') + A_-(r) S_+(r'),$$

where

$$K = -\frac{d^2}{dr^2} + \frac{d^2}{dr'^2} + W_m^2(r) - W_m^2(r') - W_m'(r) + W_m'(r') + \lambda'(r'), \quad (53)$$

$$A_1 = 2W_m(r) \frac{d^3}{dr'^3} + 2W_m(r') \frac{d^3}{dr dr'^2} - 2(-2\omega'(r') - W_m'(r')) \frac{d^2}{dr dr'} - 2(-W_m'(r') \omega(r') - W_m(r') \omega'(r')) + \omega(r') \omega'(r') + W_m(r') \omega^2(r') \frac{d}{dr} - 2W_m(r) \omega^2(r') \frac{d}{dr'} + 2W_m(r) \omega''(r'),$$

$$A_2 = -2 \frac{d^4}{dr dr'^3} + 2\omega^2(r') \frac{d^2}{dr dr'} - 2W_m(r) \cdot W_m(r') \frac{d^2}{dr'^2} - 2\omega''(r') \frac{d}{dr} + 2W_m(r) \cdot (-2\omega'(r') - W_m'(r')) \frac{d}{dr'} + 2W_m(r) \cdot (-W_m'(r') \omega(r') - W_m(r') \omega'(r')) + \omega(r') \omega'(r') + W_m(r') \omega^2(r').$$

These integrals are of order 2, 3, and 4.

Example 2. According to [19] for $A(x) = x$, we have $w(x) = x^\alpha e^{-\beta x}$, $x = r^2/4$, $\alpha > -1$, $\beta > 0$ and the interval is $[0, +\infty)$. Now, using (29), the superpotential and the energy spectrum are as

$$W_m(r) = -\frac{1}{r} \left(\alpha + m - \frac{1}{2} \right) + \frac{\beta}{4} r, \quad (54)$$

$$E = \beta(n - m + 1).$$

This system has also the ladder operators that satisfy the form of (6); hence, substituting expression $W_m(r)$ in (38) yields the following relation in terms of Whittaker function:

$$f(r) = \frac{\beta^{-(\alpha+m)}}{(\alpha+m)} \left(\frac{r}{2} \right)^{-(2\alpha+2m-1)} e^{(1/4)\beta r^2} \left(C + e^{-(1/8)\beta r^2} \left[\frac{1}{(\alpha+m+1)} \left(\frac{\beta r^2}{4} \right)^{\alpha/2+m/2} \cdot M_{(1/2)\alpha+(1/2)m, (1/2)\alpha+(1/2)m+1/2} \left(\frac{1}{4}\beta r^2 \right) + \left(\frac{\beta r^2}{4} \right)^{\alpha/2+m/2-1} \cdot M_{(1/2)\alpha+(1/2)m+1, (1/2)\alpha+(1/2)m+1/2} \left(\frac{1}{4}\beta r^2 \right) \right] \right), \quad (55)$$

where the Whittaker function $M_{\mu,\nu}(z)$ is the solution of the following differential equation:

$$y'' + \left(-\frac{1}{4} + \frac{\mu}{z} + \frac{1/4 - \nu^2}{z^2} \right) y = 0. \quad (56)$$

It can be also defined in terms of the confluent hypergeometric function as

$$M_{\mu,\nu}(z) = e^{-(1/2)z} z^{(1/2+\nu)} {}_1F_1 \left(\frac{1}{2} + \nu - \mu, 1 + 2\nu, z \right). \quad (57)$$

The family of superpartner Hamiltonians H' and the two-dimensional superintegrable Hamiltonian H_s are thus calculated by (40) and (41), respectively. The creation and annihilation operators for the Hamiltonian H_2 are as

$$M_+(r) = A_+^2(r) A_-(r), \quad (58)$$

$$M_-(r) = A_+(r) A_-^2(r),$$

where $A_\pm(r)$ is given in (28) and from (42), we have the creation and annihilation operators of the Hamiltonian H' as

$$R_+(r') = B_+(r') M_+(r') B_-(r'), \quad (59)$$

$$R_-(r') = B_+(r') M_-(r') B_-(r'),$$

where $B_\pm(r)$ is given by (32) and (39). We can also find the integrals of motion of the Hamiltonian H_s from (43) as

$$K = H_r - H_{r'}, \quad (60)$$

$$A_1 = M_+(r) R_-(r') - M_-(r) R_+(r'),$$

$$A_2 = M_+(r) R_-(r') + M_-(r) R_+(r'),$$

that are of the order 2, 7, and 8.

7. Conclusion

In this article, we have used the results obtained by Mielnik in the concept of SUSYQM and related it to master function formalism for constructing two-dimensional integrable and superintegrable systems with higher order integrals of motion. From this procedure, we have generated the superintegrable systems for two different cases of master functions $A(x) = 1$ and $A(x) = x$ and have shown that the higher integrals of motion are in order 2, 3, 4 and 2, 7, 8, respectively.

Conflicts of Interest

The authors declare that they have no conflicts of interest.

References

- [1] V. I. Arnold, *Mathematical Methods of Classical Mechanics*, Graduate Texts in Mathematics, Springer-Verlag, 1978.
- [2] E. G. Kalnins, J. M. Kress, J. Miller, and P. Winternitz, "Superintegrable systems in Darboux spaces," *Journal of Mathematical Physics*, vol. 44, no. 12, pp. 5811–5848, 2003.
- [3] E. Ramos, "A comment on the odd flows for the supersymmetric KdV equation," *Modern Physics Letters A*, vol. 9, no. 35, pp. 3235–3243, 1994.
- [4] G. Sparano, "Superintegrable systems and recursion operators," *Modern Physics Letters A*, vol. 18, no. 33–35, pp. 2501–2507, 2003.
- [5] J. Bérubé and P. Winternitz, "Integrable and superintegrable quantum systems in a magnetic field," *Journal of Mathematical Physics*, vol. 45, no. 5, pp. 1959–1973, 2004.
- [6] J. A. Calzada, J. Negro, and M. A. Del Olmo, "Dynamical symmetries for superintegrable quantum systems," *Physics of Atomic Nuclei*, vol. 70, no. 3, pp. 496–504, 2007.
- [7] J. A. Calzada, J. Negro, and M. A. del Olmo, "Intertwining symmetry algebras of quantum superintegrable systems," *SIGMA*, vol. 5, Paper 039, 23 pages, 2009.
- [8] S. Gravel and P. Winternitz, "Superintegrability with third-order integrals in quantum and classical mechanics," *Journal of Mathematical Physics*, vol. 43, no. 12, pp. 5902–5912, 2002.
- [9] I. Marquette, "Superintegrability with third order integrals of motion, cubic algebras, and supersymmetric quantum mechanics. I. Rational function potentials," *Journal of Mathematical Physics*, vol. 50, no. 1, 012101, 23 pages, 2009.
- [10] M. Visinescu, "Higher order first integrals of motion in a gauge covariant Hamiltonian framework," *Modern Physics Letters A*, vol. 25, no. 5, pp. 341–350, 2010.
- [11] I. Marquette, "Superintegrability with third order integrals of motion, cubic algebras, and supersymmetric quantum mechanics. II. Painlevé transcendent potentials," *Journal of Mathematical Physics*, vol. 50, no. 9, 095202, 18 pages, 2009.
- [12] G. Junker, *Supersymmetric Methods in Quantum and Statistical Physics*, Springer, Berlin, Germany, 1996.
- [13] W. Skiba, "Dynamical supersymmetry breaking," *Modern Physics Letters A*, vol. 12, no. 11, pp. 737–750, 1997.
- [14] C. Quesne, "Comments on dihedral and supersymmetric extensions of a family of Hamiltonians on a plane," *Modern Physics Letters A*, vol. 25, no. 27, pp. 2373–2380, 2010.
- [15] A. V. Bratchikov, "Gauge algebra of irreducible theories in the $Sp(2)$ -symmetric BRST formalism," *Modern Physics Letters A*, vol. 27, no. 30, 1250170, 10 pages, 2012.
- [16] I. Marquette, "An infinite family of superintegrable systems from higher order ladder operators and supersymmetry," *Journal of Physics: Conference Series*, vol. 284, Article ID 012047, 2011.
- [17] I. Marquette, "Supersymmetry as a method of obtaining new superintegrable systems with higher order integrals of motion," *Journal of Mathematical Physics*, vol. 50, no. 12, 122102, 10 pages, 2009.
- [18] B. Mielnik, "Factorization method and new potentials with the oscillator spectrum," *Journal of Mathematical Physics*, vol. 25, no. 12, pp. 3387–3389, 1984.
- [19] M. A. Jafarizadeh and H. Fakhri, "Supersymmetry and shape invariance in differential equations of mathematical physics," *Physics Letters A*, vol. 230, no. 3–4, pp. 164–170, 1997.
- [20] M. A. Jafarizadeh and H. Fakhri, "Parasupersymmetry and shape invariance in differential equations of mathematical physics and quantum mechanics," *Annals of Physics*, vol. 262, no. 2, pp. 260–276, 1998.
- [21] H. Panahi and L. Jahangiry, "Rodrigues solutions of the Dirac equation for shape-invariant potentials: Master function approach," *Theoretical and Mathematical Physics*, vol. 164, no. 2, pp. 1081–1088, 2010.
- [22] Z. Bakhshi and H. Panahi, "Rodrigues solution of the Dirac equation for fields obtained from the master function formalism," *Physica Scripta*, vol. 85, no. 2, 2012.
- [23] I. Marquette, "Construction of classical superintegrable systems with higher order integrals of motion from ladder operators," *Journal of Mathematical Physics*, vol. 51, no. 7, 072903, 9 pages, 2010.
- [24] I. Marquette, "Generalized Kaluza-Klein monopole, quadratic algebras and ladder operators," *Journal of Physics A: Mathematical and General*, vol. 44, no. 23, 235203, 12 pages, 2011.

Research Article

Heun Functions Describing Bosons and Fermions on Melvin's Spacetime

Marina-Aura Dariescu  and Ciprian Dariescu

Faculty of Physics, "Alexandru Ioan Cuza" University of Iași, Bd. Carol I, No. 11, 700506 Iași, Romania

Correspondence should be addressed to Marina-Aura Dariescu; marina@uaic.ro

Received 13 January 2018; Accepted 29 April 2018; Published 11 June 2018

Academic Editor: Saber Zarrinkamar

Copyright © 2018 Marina-Aura Dariescu and Ciprian Dariescu. This is an open access article distributed under the Creative Commons Attribution License, which permits unrestricted use, distribution, and reproduction in any medium, provided the original work is properly cited. The publication of this article was funded by SCOAP³.

Employing a pseudo-orthonormal coordinate-free approach, the solutions to the Klein–Gordon and Dirac equations for particles in Melvin spacetime are derived in terms of Heun's biconfluent functions.

1. Introduction

The study of relativistic particles in static magnetic fields has a long history and is still attracting considerable attention, especially for cases where someone deals with curved manifolds.

Even though on Minkowski spacetime the relativistic behavior of an electron in various magnetostatic configurations is well understood (see, for example, Johnson and Lippmann's paper [1]), a weakness on curved spacetime regards the explicit gauge covariant formulation.

Recently, when dealing with slowly rotating neutron stars which have been termed as magnetars [2], it has been assumed that their huge magnetic induction in the core and crust, $B \sim 10^{14} - 10^{15}$ (G), is affecting the spacetime geometry. A way out could be the search for general relativistic solutions with the magnetic field considered as a perturbation of the spherically symmetric background [3]. Another way is to assume that magnetized metrics, as the one belonging to the Melvin class [4, 5], may be reliable candidates for describing these highly compact astrophysical objects with a dominant axial magnetic field [6].

Within a coordinate-dependent formulation, switching between canonical and pseudo-orthonormal basis, the above-mentioned authors are integrating the system of four coupled first-order differential equations, in the first approximation, neglecting the terms in higher orders of the polar radial coordinate ρ . Their solutions are expressed in terms of

generalized Laguerre polynomials, similarly to the case of the Dirac equation in cylindrical coordinates on a flat manifold [7].

In the present work, we are applying a coordinates-free method to analyze the Klein–Gordon and Dirac equations describing particles evolving in Melvin's spacetime. Employing Cartan's formalism, we are computing all the essential geometrical objects for writing down the corresponding matter fields and Einstein's equations.

It turns out that the $SO(3,1) \times U(1)$ -gauge covariant Klein–Gordon equation can be exactly solved, its solutions being given by the Heun biconfluent functions [8–10]. The same happens with the approximate expression of the second-order differential system derived from the Dirac equation.

The Heun functions, either general or confluent, are main targets of recent investigations and have been obtained for massless particles evolving in a Universe described by the metric function written as a nonlinear mixture of Schwarzschild, Melvine, and Bertotti-Robinson solutions [11].

2. The Geometry

Recently, in [12], the procedure of transforming a known static symmetric solution to Einstein-hydrodynamic equations into a magnetized metric was presented, by (nonlinearly) adding the magnetic field. In spherical coordinates, this has the general form

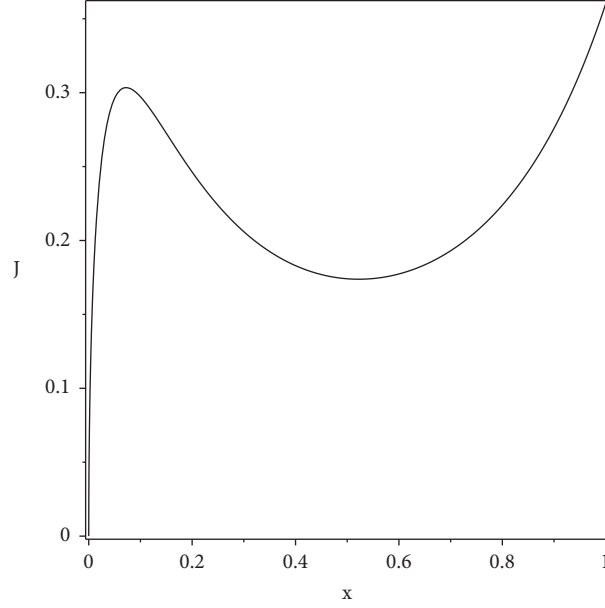


FIGURE 1: The radial current (50) in terms of the variable $x \approx \sqrt{2}MB_*^2\rho^2/(8\omega)$.

$$ds^2 = \Lambda^2 g_{11} (dr)^2 + \Lambda^2 r^2 (d\theta)^2 + \frac{r^2 \sin^2 \theta}{\Lambda^2} (d\varphi)^2 - \Lambda^2 g_{00} (dt)^2, \quad (1)$$

with the metric functions g_{11} and g_{00} depending only on r and

$$\Lambda = 1 + \frac{B_*^2}{4} r^2 \sin^2 \theta, \quad (2)$$

where, for the moment, B_* is a parameter related to the magnetic field intensity.

In the pseudo-orthonormal Cartan frame corresponding to the metric (1),

$$\begin{aligned} \omega^1 &= \Lambda \sqrt{g_{11}} dr, \\ \omega^2 &= \Lambda r d\theta, \\ \omega^3 &= \frac{r \sin \theta}{\Lambda} d\varphi, \\ \omega^4 &= \Lambda \sqrt{g_{00}} dt, \end{aligned} \quad (3)$$

for the potential

$$A_2 = \frac{B_0 r \sin \theta}{2}, \quad (4)$$

where B_0 is the strength of the magnetic field on the axis, and the Maxwell tensor components, corresponding to a poloidal magnetic field with B_ρ and B_θ , are given by the relations

$$\begin{aligned} F_{23} &= \frac{B_0 \cos \theta}{\Lambda^2}, \\ F_{13} &= \frac{B_0 \sin \theta}{\Lambda^2 \sqrt{g_{11}}}, \end{aligned} \quad (5)$$

pointing out a prolate (in shape) star.

Once we assume $g_{00} = g_{11} = 1$, we can switch to cylindrical coordinates $\{\rho, \varphi, z, t\}$, by

$$\begin{aligned} \rho &= r \sin \theta, \\ z &= r \cos \theta, \end{aligned} \quad (6)$$

so that the magnetized metric (1) turns into the simple Melvin expression

$$ds^2 = \Lambda^2 (d\rho)^2 + \frac{\rho^2}{\Lambda^2} (d\varphi)^2 + \Lambda^2 (dz)^2 - \Lambda^2 (dt)^2, \quad (7)$$

with

$$\Lambda = 1 + \frac{B_*^2 \rho^2}{4}. \quad (8)$$

Within an $SO(3,1)$ -gauge covariant formulation, we introduce the pseudo-orthonormal frame

$$\begin{aligned} e_1 &= \frac{1}{\Lambda} \partial_\rho, \\ e_2 &= \frac{\Lambda}{\rho} \partial_\varphi, \\ e_3 &= \frac{1}{\Lambda} \partial_z, \\ e_4 &= \frac{1}{\Lambda} \partial_t, \end{aligned} \quad (9)$$

whose corresponding dual base is

$$\begin{aligned}\omega^1 &= \Lambda d\rho, \\ \omega^2 &= \frac{\rho}{\Lambda} d\varphi, \\ \omega^3 &= \Lambda dz, \\ \omega^4 &= \Lambda dt,\end{aligned}\quad (10)$$

so that the metric (7) gets the Minkowskian form $ds^2 = \eta_{ab}\omega^a\omega^b$, with $\eta_{ab} = [1, 1, 1, -1]$. The first Cartan equation,

$$d\omega^a = \Gamma_{[bc]}^a \omega^b \wedge \omega^c, \quad (11)$$

with $1 \leq b < c \leq 4$ and $\Gamma_{[bc]}^a = \Gamma_{.bc}^a - \Gamma_{.cb}^a$, leads to the following connection one-form:

$$\begin{aligned}\Gamma_{12} &= \left(\frac{\Lambda'}{\Lambda^2} - \frac{1}{\rho\Lambda} \right) \omega^2, \\ \Gamma_{13} &= -\frac{\Lambda'}{\Lambda^2} \omega^3, \\ \Gamma_{14} &= \frac{\Lambda'}{\Lambda^2} \omega^4,\end{aligned}\quad (12)$$

where Λ' is the derivative of Λ with respect to ρ .

Employing the second Cartan equation

$$\mathcal{R}_{ab} = d\Gamma_{ab} + \Gamma_{ac} \wedge \Gamma_{cb}, \quad (13)$$

one derives the curvature two-forms $\mathcal{R}_{ab} = R_{abcd}\omega^c \wedge \omega^d$, with $1 \leq c < d \leq 4$, leading to the curvature components

$$\begin{aligned}R_{1212} &= \frac{2B_*^2}{\Lambda^4} \left[1 - \frac{B_*^2 \rho^2}{8} \right], \\ R_{3434} &= \frac{B_*^4 \rho^2}{4\Lambda^4}, \\ R_{1313} &= R_{2323} = -\frac{B_*^2}{2\Lambda^4} \left[1 - \frac{B_*^2 \rho^2}{4} \right] = -R_{1414} \\ &= -R_{2424},\end{aligned}\quad (14)$$

pointing out the special radius value $\rho_* = 2/B_*$, for which only the components $R_{1212} = B_*^2/\Lambda^4 = R_{3434}$ are surviving and the Weyl tensor vanishes.

Since the scalar curvature is zero, the Einstein tensor components are given by the Ricci tensor components, as

$$G_{11} = G_{22} = -G_{33} = G_{44} = \frac{B_*^2}{\Lambda^4}. \quad (15)$$

In the pseudo-orthonormal frame whose dual bases are (10), it turns out that the potential (4), generating the magnetic induction along Oz , gets the familiar expression

$$A_2 = \frac{B_0 \rho}{2}, \quad (16)$$

and the essential component of the Maxwell tensor reads

$$F_{12} = A_{2|1} + \Gamma_{212} A_2 = \frac{B_0}{\Lambda^2}, \quad (17)$$

where $f_{|1} = e_1(f)$.

Using the energy-momentum tensor components

$$T_{11} = T_{22} = -T_{33} = T_{44} = \frac{1}{2} F_{12}^2 = \frac{1}{2} \frac{B_0^2}{\Lambda^4}, \quad (18)$$

in the Einstein equations $G_{ab} = \kappa_0 T_{ab}$, one gets the following relation between the parameters B_* and B_0 :

$$B_*^2 = \frac{\kappa_0 B_0^2}{2}, \quad (19)$$

with $\kappa_0 = 8\pi G/c^4$.

3. Exactly Solvable Klein–Gordon Equation

In this section, we are going to construct the wave function of the charged bosons, considered as test particles evolving in the crust of a relativistic magnetar. The complex scalar field of mass μ , minimally coupled to gravity, is described by the $SO(3, 1) \times U(1)$ gauge covariant Klein–Gordon equation

$$\eta^{ab} \Phi_{|ab} - \eta^{ab} \Phi_{|c} \Gamma_{ab}^c = \mu^2 \Phi + 2iqA_2 \Phi_{|2} + q^2 A_2^2 \Phi, \quad (20)$$

which, in the pseudo-orthonormal frame with the dual bases (10), reads

$$\begin{aligned}\frac{1}{\rho} \frac{\partial}{\partial \rho} \left[\rho \frac{\partial \Phi}{\partial \rho} \right] + \frac{\Lambda^4}{\rho^2} \frac{\partial^2 \Phi}{\partial \varphi^2} + \frac{\partial^2 \Phi}{\partial z^2} - \frac{\partial^2 \Phi}{\partial t^2} \\ = \left[\mu^2 \Lambda^2 + iqB_0 \Lambda^3 \frac{\partial \Phi}{\partial \varphi} + \left(\frac{qB_0 \rho \Lambda}{2} \right)^2 \right] \Phi.\end{aligned}\quad (21)$$

The above form suggests the variables separation

$$\Phi = \phi(\rho) e^{im\varphi} e^{ip_z z} e^{-i\omega t}, \quad (22)$$

which leads to the following differential equation for the unknown function ϕ ,

$$\begin{aligned}\frac{1}{\rho} \frac{\partial}{\partial \rho} \left[\rho \frac{\partial \phi}{\partial \rho} \right] + \left[\omega^2 - p_z^2 - \frac{m^2}{\rho^2} \Lambda^4 - \mu^2 \Lambda^2 + mqB_0 \Lambda^3 \right. \\ \left. - \left(\frac{qB_0 \rho \Lambda}{2} \right)^2 \right] \phi = 0,\end{aligned}\quad (23)$$

with Λ defined in (8).

This can be exactly integrated, its solution being expressed in terms of the Heun biconfluent function as [9, 10]

$$\phi(y) \sim \exp \left[-\frac{y^2}{2} - \frac{\beta y}{2} \right] y^{\alpha/2} \text{HeunB}[\alpha, \beta, \gamma, \delta, y], \quad (24)$$

where the variable and the parameters are, respectively, given by

$$y = \frac{\sqrt{b}B_*\rho^2}{4}, \quad (25)$$

$$b = qB_0 - \frac{mB_*^2}{2} \approx qB_0,$$

$$\alpha = \pm m,$$

$$\beta \approx 2 \frac{\sqrt{qB_0}}{B_*},$$

$$\gamma \approx m - \frac{\mu^2}{qB_0}, \quad (26)$$

$$\delta \approx -\frac{2[\omega^2 - p_z^2 - \mu^2 + mqB_0]}{B_*\sqrt{qB_0}}.$$

Let us point out that the Heun biconfluent equation has one regular singularity at the origin and one irregular at ∞ and can be obtained, from the Heun general equation, by a process of successive confluences [10].

Regarding the asymptotic behavior of the function (24), solution to (23), that has a singularity in $\rho \rightarrow 0$, due to the exponential term, this is vanishing for large y -values. On the other hand, for a regular solution at the origin $y = 0$ (where $\text{HeunB}(0) = 1$), one has to choose the plus sign of α in (26).

4. The $SO(3, 1) \times U(1)$ -Gauge Covariant Dirac Equation

For relativistic fermions of mass M , coupled to the external magnetic field generated by (16), the Dirac equation has the $SO(3, 1) \times U(1)$ -gauge covariant expression

$$\gamma^a \Psi_{;a} + M\Psi = 0, \quad (27)$$

where “;” stands for the covariant derivative

$$\Psi_{;a} = e_a \Psi + \frac{1}{4} \Gamma_{bca} \gamma^b \gamma^c \Psi - iqA_a \Psi. \quad (28)$$

In view of the relations (12), the term expressing the Ricci spin-connection in (27) reads

$$\frac{1}{4} \Gamma_{bca} \gamma^a \gamma^b \gamma^c = \frac{f}{\Lambda} \gamma^1, \quad (29)$$

where we have introduced the function

$$f = \frac{1}{2} \left[\frac{1}{\rho} + \frac{\Lambda'}{\Lambda} \right]. \quad (30)$$

With the explicit form of the Dirac equation (27) being

$$\frac{1}{\Lambda} \left[\gamma^1 (\partial_\rho + f) + \frac{\Lambda^2}{\rho} \gamma^2 \partial_\phi + \gamma^3 \partial_z + \gamma^4 \partial_t + M\Lambda - iq\gamma^2 \Lambda A_2 \right] \Psi = 0, \quad (31)$$

one may use the variables separation

$$\Psi = e^{i(m\phi + p_z z - \omega t)} \psi(\rho), \quad (32)$$

to derive the differential equation satisfied by the part depending on ρ ; i.e.,

$$\gamma^1 [\psi' + f\psi] + i \left\{ \gamma^2 \Lambda \left[\frac{m\Lambda}{\rho} - \frac{qB_0 \rho}{2} \right] + p_z \gamma^3 - \omega \gamma^4 - iM\Lambda \right\} \psi = 0. \quad (33)$$

With the following function substitution

$$\psi = \frac{1}{2\sqrt{\rho\Lambda}} \chi, \quad (34)$$

the above equation becomes

$$\gamma^1 \chi' + i \left\{ \gamma^2 F + p_z \gamma^3 - \omega \gamma^4 - iM\Lambda \right\} \chi = 0, \quad (35)$$

where

$$F(\rho) = \Lambda \left[\frac{m\Lambda}{\rho} - \frac{qB_0 \rho}{2} \right], \quad (36)$$

and we are going to use the Dirac representation for the γ^μ matrices,

$$\begin{aligned} \gamma^\mu &= -i\beta\alpha^\mu, \\ \gamma^4 &= -i\beta, \\ \mu &= \overline{1, 3}, \end{aligned} \quad (37)$$

with

$$\begin{aligned} \beta &= \begin{pmatrix} \mathcal{J} & 0 \\ 0 & -\mathcal{J} \end{pmatrix}, \\ \alpha^\mu &= \begin{pmatrix} 0 & \sigma^\mu \\ \sigma^\mu & 0 \end{pmatrix}, \end{aligned} \quad (38)$$

where σ^μ denotes the usual Pauli matrices.

In the following, we are assuming that the particle is not moving along the magnetic field direction, i.e., $p_z = 0$, and the bispinor χ is of the form

$$\chi(\rho) = \begin{bmatrix} \zeta(\rho) \\ \eta(\rho) \end{bmatrix}, \quad (39)$$

so that (35) decouples in two equations for the (two-component) spinors ζ and η ; i.e.,

$$\begin{aligned} \sigma^1 \zeta' + iF\sigma^2 \zeta &= i(\omega + M\Lambda) \eta, \\ \sigma^1 \eta' + iF\sigma^2 \eta &= i(\omega - M\Lambda) \zeta. \end{aligned} \quad (40)$$

Applying the usual procedure, one gets the following differential equations:

$$\begin{aligned} \zeta_A'' - \frac{M\Lambda'}{\omega + M\Lambda} \zeta_A' \\ + \left\{ \omega^2 - M^2\Lambda^2 - F^2 \mp \left[F' - \frac{MF\Lambda'}{\omega + M\Lambda} \right] \right\} \zeta_A = 0, \\ \eta_A'' + \frac{M\Lambda'}{\omega - M\Lambda} \eta_A' \\ + \left\{ \omega^2 - M^2\Lambda - F^2 \mp \left[F' + \frac{MF\Lambda'}{\omega - M\Lambda} \right] \right\} \eta_A = 0, \end{aligned} \quad (41)$$

which cannot be analytically solved. However, by imposing the condition $B_*^2 \ll qB_0$ and neglecting the powers of ρ larger than 3, (41) get the simpler forms:

$$\begin{aligned} \zeta_A'' - \frac{MB_*^2\rho}{2(\omega + M)} \left[1 - \frac{MB_*^2\rho^2}{4(\omega + M)} \right] \zeta_A' + \left\{ \omega^2 - M^2 \right. \\ \left. + \left(m \pm \frac{1}{2} \right) qB_0 - \frac{m(m \mp 1)}{\rho^2} - \left(\frac{qB_0\rho}{2} \right)^2 \right\} \zeta_A = 0, \\ \eta_A'' + \frac{MB_*^2\rho}{2(\omega - M)} \left[1 + \frac{MB_*^2\rho^2}{4(\omega - M)} \right] \eta_A' + \left\{ \omega^2 - M^2 \right. \\ \left. + \left(m \pm \frac{1}{2} \right) qB_0 - \frac{m(m \mp 1)}{\rho^2} - \left(\frac{qB_0\rho}{2} \right)^2 \right\} \eta_A = 0. \end{aligned} \quad (42)$$

The corresponding solutions, i.e.,

$$\begin{aligned} \zeta_1 &= \{ \sqrt{\rho}, \rho^m \} u_1, \\ \zeta_2 &= \{ \sqrt{\rho}, \rho^{m+1} \} u_2, \\ \eta_1 &= \{ \sqrt{\rho}, \rho^m \} v_1, \\ \eta_2 &= \{ \sqrt{\rho}, \rho^{m+1} \} v_2, \end{aligned} \quad (43)$$

are expressed in terms of Heun's biconfluent functions [8–10]

$$\begin{aligned} u_1 &= \text{HeunB} [\alpha_1, \beta, \gamma^+, \delta_1^+, x_u], \\ u_2 &= \text{HeunB} [\alpha_2, \beta, \gamma^+, \delta_2^+, x_u]; \\ v_1 &= \text{HeunB} [\alpha_1, \beta, \gamma^-, \delta_1^-, x_v]; \\ v_2 &= \text{HeunB} [\alpha_2, \beta, \gamma^-, \delta_2^-, x_v], \end{aligned} \quad (44)$$

of variables

$$\begin{aligned} x_u &= -\frac{\sqrt{2}MB_*^2\rho^2}{8(\omega + M)}, \\ x_v &= \frac{\sqrt{2}MB_*^2\rho^2}{8(\omega - M)} \end{aligned} \quad (45)$$

and parameters

$$\begin{aligned} \alpha_1 &= m - \frac{1}{2}, \\ \alpha_2 &= m + \frac{1}{2}, \\ \beta &= \sqrt{2}, \\ \gamma^\pm &= -2 \left[\frac{qB_0(\omega \pm M)}{MB_*^2} \right]^2, \\ \delta_1^\pm &= \pm \frac{2\sqrt{2}}{MB_*^2} (\omega \pm M) \left[\omega^2 - M^2 + \left(m + \frac{1}{2} \right) qB_0 \right], \\ \delta_2^\pm &= \pm \frac{2\sqrt{2}}{MB_*^2} (\omega \pm M) \left[\omega^2 - M^2 + \left(m - \frac{1}{2} \right) qB_0 \right], \end{aligned} \quad (46)$$

and therefore the components of the bispinor ψ in (34) are given by

$$\begin{aligned} \psi_1 &= \frac{1}{2\sqrt{\Lambda}} \{ 1, \rho^{m-1/2} \} u_1, \\ \psi_2 &= \frac{1}{2\sqrt{\Lambda}} \{ 1, \rho^{m+1/2} \} u_2, \\ \psi_3 &= \frac{1}{2\sqrt{\Lambda}} \{ 1, \rho^{m-1/2} \} v_1, \\ \psi_4 &= \frac{1}{2\sqrt{\Lambda}} \{ 1, \rho^{m+1/2} \} v_2. \end{aligned} \quad (47)$$

Using the expressions (47) in (32), one may compute the radial current density, meaning particles per unit time and per unit covariant 2-surface

$$d\Sigma_1 = \omega^2 \wedge \omega^3 = \rho d\varphi \wedge dz, \quad (48)$$

as

$$j^1 = i\bar{\Psi}\gamma^1\Psi = \Psi^\dagger \alpha^1 \Psi = \frac{1}{2\Lambda} [u_1 v_2 + u_2 v_1] \quad (49)$$

and the corresponding (radial) current,

$$I(\rho) = \int_{-L_z/2}^{L_z/2} \int_0^{2\pi} e_a^1 j^a d\Sigma_1 = \frac{\pi L_z \rho}{\Lambda^2} [u_1 v_2 + u_2 v_1], \quad (50)$$

represented in Figure 1, as a function of

$$x \approx \frac{\sqrt{2}MB_*^2\rho^2}{8\omega}. \quad (51)$$

One may notice that, for $x \ll 1$, the current is suddenly increasing from zero to a maximum value, which depends on the ratio M/ω and on the magnetic field intensity.

The case corresponding to massless fermions is significantly less complicated. Thus, the equation

$$\begin{aligned} \frac{1}{\Lambda} \left[\gamma^1 (\partial_\rho + f) + \frac{\Lambda^2}{\rho} \gamma^2 \partial_\varphi + \gamma^3 \partial_z + \gamma^4 \partial_t \right] \Psi_0 \\ - iq\gamma^2 A_2 \Psi_0 = 0, \end{aligned} \quad (52)$$

with the variables separation (32), leads to the following differential equation satisfied by the part depending on ρ ; i.e.,

$$\gamma^1 [\psi'_0 + f\psi_0] + i \left\{ \gamma^2 \Lambda \left[\frac{m\Lambda}{\rho} - \frac{qB_0\rho}{2} \right] + p\gamma^3 - \omega\gamma^4 \right\} \psi_0 = 0. \quad (53)$$

As customary for massless fermions, we are going to use the Weyl representation for the γ matrices,

$$\begin{aligned} \gamma^\mu &= -i\beta\alpha^\mu, \\ \gamma^4 &= -i\beta, \\ \mu &= \overline{1, 3}, \end{aligned} \quad (54)$$

with

$$\alpha^\mu = \begin{pmatrix} \sigma^\mu & 0 \\ 0 & -\sigma^\mu \end{pmatrix}, \quad (55)$$

and the bispinor ψ_0 will be taken as

$$\psi_0(\rho) = \begin{bmatrix} \zeta(\rho) \\ \eta(\rho) \end{bmatrix}. \quad (56)$$

Once (53) decouples in two equations for ζ and η , one gets, for the up spinor's components, the second-order differential equations

$$\begin{aligned} \zeta''_A + 2f\zeta'_A + [\omega^2 - p_z^2 + f^2 - F^2 + \partial_\rho(f \mp F)] \zeta_A \\ = 0, \end{aligned} \quad (57)$$

and similarly for η_A . Within the same approximation $B_*^2 \ll qB_0$ and neglecting the powers of ρ larger than 2, (57) turns into the simpler forms

$$\begin{aligned} \frac{d^2\zeta_A}{d\rho^2} + \left[\frac{1}{\rho} + \frac{B_*\rho}{2} \right] \frac{d\zeta_A}{d\rho} + \left[\omega^2 - p_z^2 + qB_0 \left(m \pm \frac{1}{2} \right) \right. \\ \left. - \left(m \mp \frac{1}{2} \right)^2 \frac{1}{\rho^2} - \left(\frac{qB_0\rho}{2} \right)^2 \right] \zeta_A = 0, \end{aligned} \quad (58)$$

whose solutions can be expressed either in terms of confluent hypergeometric functions, as [13]

$$\begin{aligned} \zeta_1 &= x^{(1/2)(m-1/2)} e^{-x/2} U \left[-\frac{\omega^2 - p_z^2}{2qB_0} + \frac{B_*^2}{4qB_0}, m \right. \\ &\quad \left. + \frac{1}{2}, x \right]; \\ \zeta_2 &= x^{-(1/2)(m+1/2)} e^{-x/2} U \left[-\frac{\omega^2 - p_z^2}{2qB_0} + \frac{B_*^2}{4qB_0} \right. \\ &\quad \left. - \left(m - \frac{1}{2} \right), -\left(m - \frac{1}{2} \right), x \right], \end{aligned} \quad (59)$$

or in terms of Whittaker functions [13], as

$$\zeta_1 = \frac{1}{\sqrt{x}} W_{\lambda_1, \mu_1}(x), \quad (60)$$

$$\zeta_2 = \frac{1}{\sqrt{x}} W_{\lambda_2, \mu_2}(x),$$

with the dimensionless variable

$$x = \frac{B_*^2 \rho^2}{4} \sqrt{1 + \left(\frac{2qB_0}{B_*^2} \right)^2} \approx \frac{qB_0 \rho^2}{2} \quad (61)$$

and parameters

$$\begin{aligned} \lambda_1 &\approx \frac{\omega^2 - p_z^2}{2qB_0} - \frac{B_*^2}{4qB_0} + \frac{1}{2} \left(m + \frac{1}{2} \right), \\ \mu_1 &= \frac{1}{2} \left(m - \frac{1}{2} \right); \\ \lambda_2 &\approx \frac{\omega^2 - p_z^2}{2qB_0} - \frac{B_*^2}{4qB_0} + \frac{1}{2} \left(m - \frac{1}{2} \right), \\ \mu_2 &= \frac{1}{2} \left(m + \frac{1}{2} \right). \end{aligned} \quad (62)$$

5. Conclusions

Within the framework of the gauge-invariant geometry, based on the semi-direct product of the local groups $SO(3, 1)$ and $U(1)$, the present paper is focusing on the Klein–Gordon and Dirac equations describing particles evolving in a background endowed with Melvin's metric.

By making use of Cartan's formalism, we have derived the corresponding Einstein–Melvin equations leading to the essential relation between the model's parameters (19). As a remark, switching to the canonical bases, the third covariant induction component is given by the expression

$$B_z = \sqrt{|g|} F_{(c)}^{12} = \sqrt{|g|} e_a^1 e_b^2 F^{ab} \equiv B_0. \quad (63)$$

In case of bosons, the Klein–Gordon equation can be integrated exactly, its solution being given by the Heun biconfluent functions of parameters (26).

Equations (41) coming from the Dirac equation (31) have rather complicated expressions, containing several additional terms which were neglected in [6]. In the assumption $B_*^2 \ll qB_0$, we have been able to find solutions for (42), expressed in terms of Heun's biconfluent functions (44). The corresponding radial particle-current (50), represented in Figure 1, is starting from zero, at the origin $\rho = 0$, and exhibits a rather nontrivial behavior, characterized by a sudden growth to a maximum value. This one is followed by a local minimum which might signal, in the approximation we have used, the presence of a plateau. The seemingly far away unlimited increasing is a result of the violation of the approximation holding condition which demands $x < 1$.

Data Availability

No data were used to support this study.

Conflicts of Interest

The authors declare that there are no conflicts of interest regarding the publication of this paper.

Acknowledgments

This work was supported by a grant of Ministry of Research and Innovation, CNCS-UEFISCDI, Project no. PN-III-P4-ID-PCE-2016-0131, within PNCDI III.

References

- [1] M. H. Johnson and B. A. Lippmann, "Relativistic Motion in a Magnetic Field," *Physical Review A: Atomic, Molecular and Optical Physics*, vol. 77, no. 5, pp. 702–705, 1950.
- [2] R. C. Duncan and C. Thompson, "Formation of very strongly magnetized neutron stars: implications for gamma-ray bursts," *The Astrophysical Journal Letters*, vol. 392, no. 1, pp. L9–L13, 1992.
- [3] R. Ciolfi, V. Ferrari, L. Gualtieri, and J. A. Pons, "Relativistic models of magnetars: the twisted-torus magnetic field configuration," *Monthly Notices of the Royal Astronomical Society*, vol. 397, no. 2, pp. 913–924, 2009.
- [4] M. A. Melvin, "Pure magnetic and electric geons," *Physics Letters B*, vol. 8, pp. 65–68, 1964.
- [5] M. A. Melvin, "Dynamics of cylindrical electromagnetic universes," *Physical Review A: Atomic, Molecular and Optical Physics*, vol. 139, p. B225, 1965.
- [6] L. C. N. Santos and C. C. Barros, "Dirac equation and the Melvin metric," *The European Physical Journal C*, vol. 76, p. 560, 2016.
- [7] D. B. Melrose and A. J. Parle, "Quantum electrodynamics in strong magnetic fields. I Electron states," *Australian Journal of Physics*, vol. 36, pp. 755–774, 1983.
- [8] K. Heun, "Beiträge zur Theorie der Lamé'schen Functionen," *Mathematische Annalen*, vol. 33, pp. 180–196, 1889.
- [9] A. Ronveaux, *Heuns Differential Equations*, Ronveaux, Ed., Oxford Univ. Press, New York, NY, USA, 1995.
- [10] S. Y. Slavyanov and W. Lay, *Special Functions, A Unified Theory Based on Singularities*, Oxford Mathematical Monographs, Oxford, 2000.
- [11] T. Birkandan and M. Hortacsu, "Heun-type solutions for Schwarzschild metric with electromagnetic fields," *Europhysics Letters*, vol. 119, no. 2, Article ID 20002, 2017, <https://arxiv.org/abs/1704.00294?context=gr-qc>.
- [12] P. G. Nedkova and S. S. Yazadjiev, "Magnetized black hole on the Taub-NUT instanton," *Physical Review D: Covering Particles, Fields, Gravitation, and Cosmology*, vol. 85, 2012.
- [13] S. Gradshteyn and I. M. Ryzhik, *Table of Integrals, Series, and Products*, Academic, New York, NY, USA, 4th edition, 1965.

Research Article

Nonrelativistic Arbitrary l -States of Quarkonium through Asymptotic Iteration Method

Hakan Ciftci ¹ and Hasan Fatih Kisoglu ²

¹Gazi Üniversitesi, Fen-Edebiyat Fakültesi, Fizik Bölümü, 06500 Teknikokullar-Ankara, Turkey

²Department of Basic Sciences, Faculty of Maritime, Mersin University, Mersin, Turkey

Correspondence should be addressed to Hakan Ciftci; hciftci@gazi.edu.tr and Hasan Fatih Kisoglu; hasanfatihk@mersin.edu.tr

Received 15 February 2018; Accepted 27 March 2018; Published 29 May 2018

Academic Editor: Chun-Sheng Jia

Copyright © 2018 Hakan Ciftci and Hasan Fatih Kisoglu. This is an open access article distributed under the Creative Commons Attribution License, which permits unrestricted use, distribution, and reproduction in any medium, provided the original work is properly cited. The publication of this article was funded by SCOAP³.

The energy eigenvalues with any $l \neq 0$ states and mass of heavy quark-antiquark system (quarkonium) are obtained by using Asymptotic Iteration Method in the view of nonrelativistic quantum chromodynamics, in which the quarks are considered as spinless for easiness and are bounded by Cornell potential. A semianalytical formula for energy eigenvalues and mass is achieved via the method in scope of the perturbation theory. The accuracy of this formula is checked by comparing the eigenvalues with the ones numerically obtained in this study and with exact ones in literature. Furthermore, semianalytical formula is applied to $c\bar{c}$, $b\bar{b}$, and $c\bar{b}$ meson systems for comparing the masses with the experimental data.

1. Introduction

Investigation of an atomic or subatomic system is done by achieving an energy spectrum of the system. This is carried out, generally, for the events in which the system is bounded by a potential function. Besides, the scattering states or resonance states can also be observed in the investigation of the system. The eigenvalues (or eigenenergies) of Hamiltonian of this system is obtained for a given potential function. In order to do this, various mathematical methods are used in quantum mechanics. One of these, named Asymptotic Iteration Method (AIM), has been commonly used since 2003 [1]. AIM can be used for analytically as well as numerically (or approximately) solvable problems [2–4]. Moreover, it can be used for obtaining the perturbative energy eigenvalues of the system without any need of the unperturbative eigenstate [5, 6].

As a subatomic system, a quarkonium that is composed of a heavy quark-antiquark ($q\bar{q}$) pair has attracted attention of particle physicists since the first half of 1970, and [7–11] are just a few studies of them. In most of these studies, for easiness, the system is examined via Schrödinger equation in nonrelativistic quantum chromodynamics (NRQCD), assuming that the quarks are spinless [12–15]. Cornell potential is one of the potential functions that represent

interactions between the quarks in such a $q\bar{q}$ system. It is used for obtaining the mass and energy spectrum of the quarkonium and obtaining the hadron decay widths [7–9, 16]. Cornell potential is given as

$$V(r) = -\frac{A}{r} + B^2 r \quad (1)$$

where A and B are positive constants (B is in energy dimension). As is seen in (1), Cornell potential has two parts: one is the Coulombic term and the other is the linear part. For obtaining the energy levels and mass of the quarkonium, A and B may be fitted to the first-few states. Therefore, the full spectrum of the quarkonium can be constructed through these potential parameters.

In literature, it is possible to find many studies in which the solutions of Schrödinger equation for Cornell potential have been obtained. For example, in [17], Hall has found an approximate energy formula to construct an energy spectrum of Schrödinger equation for Cornell potential, under some conditions. Jacobs et al. [13] have compared the eigenvalues of Schrödinger and spinless Salpeter equations in the cases of Cornell potential and Wisconsin potential [18]. Vega and friends have obtained, for $l=0$ states, the energy spectrum,

mass, and wavefunctions at the origin for $c\bar{c}$, $b\bar{b}$, and $b\bar{c}$ mesons by using the usual variation method in the scope of supersymmetric quantum mechanics (SUSYQM) [19, 20], in [12]. They have also compared their results with the exact ones in literature and with the experimental data.

In this study, we attempted to get the energy eigenvalues (for any $l \neq 0$ states) and masses of heavy mesons by using Asymptotic Iteration Method in the view of NRQCD, in which the quarks are considered as spinless for easiness and are bounded by Cornell potential. We achieved a semianalytical formula for constructing the energy spectrum and obtaining the masses of the mesons, using the method in scope of the perturbation theory. The accuracy of this formula was cross-checked by comparing the eigenvalues with the ones numerically obtained in this study and with the exact ones in literature. Furthermore, semianalytical formula was applied to $c\bar{c}$, $b\bar{b}$, and $b\bar{c}$ heavy mesons for comparing the masses with the experimental data.

AIM has been firstly applied to Schrödinger equation for Cornell potential by Hall and Saad in [21]. They have used Airy function as an asymptotic form of the wavefunction and have got highly-accurate numerical results in their study. Alternatively, we obtained a semianalytical mass-energy formula for quarkonium by having differential equation which gives polynomial solutions for asymptotic forms of the wavefunction of the system.

This paper is organized as follows: we give a short summary of AIM in Section 2, while Section 3 includes the main problem. In Section 4, we give numerical results for the eigenenergies and obtain semianalytical energy formula by applying perturbation theory to our problem in the view of AIM. Furthermore, in Section 4, we compare our energy spectrum and masses with the exact ones in literature and with the experimental data. Finally, Section 5 includes some comments about our results.

2. The Asymptotic Iteration Method (AIM)

According to the organization of the paper, we summed up AIM in this section, while it is comprehensively introduced in [1]. The AIM is used to solve second-order homogeneous linear differential equations in the following form:

$$y''(x) = \lambda_0(x) y'(x) + s_0(x) y(x) \quad (2)$$

where $\lambda_0(x)$ and $s_0(x)$ have continuous derivatives in the defined interval of the x independent variable. If there is an asymptotic condition such as

$$\frac{s_n}{s_{n-1}} = \frac{\lambda_n}{\lambda_{n-1}} \equiv \alpha \quad (3)$$

for $n \in \mathbb{Z}^+$, where n is large enough, the general solution of (2) is obtained as

$$y(x) = \exp\left(-\int^x \alpha(t) dt\right) \cdot \left[C_2 + C_1 \int^x \exp\left(\int^t (\lambda_0(\tau) + 2\alpha(\tau)) d\tau\right) dt \right] \quad (4)$$

with the functions

$$\begin{aligned} \lambda_n &= \lambda'_{n-1} + s_{n-1} + \lambda_0 \lambda_{n-1} \\ s_n &= s'_{n-1} + s_0 \lambda_{n-1} \end{aligned} \quad (5)$$

As a field of application, AIM can be used to deal with Schrödinger equation (or energy eigenvalue problem) in mathematical physics. The eigenvalues can be obtained through the following quantization condition:

$$\begin{aligned} \delta_n(x, E) &= s_n(x, E) \lambda_{n-1}(x, E) - \lambda_n(x, E) s_{n-1}(x, E) \\ &= 0 \end{aligned} \quad (6)$$

If the energy eigenvalues (E) can be obtained from (6), independently from the x variable, the problem is exactly solvable. In this case, the eigenvalue and eigenfunction of n th energy level can be derived in explicit algebraic form via n iterations. However, there are limited numbers of suitable potentials for this case.

As for the approximately (or numerically) solvable problems, δ_n depends on both x and E . In this case, an appropriate value, $x \equiv x_0$, should be determined to solve $\delta_n(x, E) = 0$ with respect to E [2, 6]. The energy eigenvalue of an n th level is obtained through q iterations where $q \geq n$.

3. Formulation of the Problem

Consider the following Cornell potential:

$$V(r) = -\frac{A}{r} + B^2 r \quad (7)$$

where A, B are real and positive constants (B is in energy dimension) and $r \in (0, \infty)$. If we substitute $V(r)$ into Schrödinger equation in three dimensions, we have

$$\left\{ \frac{d^2}{dr^2} + \varepsilon - \left[-\frac{\alpha}{r} + \rho r + \frac{l(l+1)}{r^2} \right] \right\} \Psi(r) = 0 \quad (8)$$

where $\varepsilon = 2\mu E_n$, $\alpha = 2\mu A$, and $\rho = 2\mu B^2$. E_n and $\mu = m_1 m_2 / (m_1 + m_2)$ are energy eigenvalue of n th level and reduced mass of the $q\bar{q}$ system, respectively (m_1 and m_2 are quark masses). Besides, we study in natural units (i.e., $\hbar, c = 1$) for the system. After changing the variable, in (8), as $r = u^2$, then substituting $\Psi(u) = u^{1/2} g(u)$, we get

$$\begin{aligned} g''(u) + \left[4\varepsilon u^2 + 4\alpha - 4\rho u^4 - \frac{4l(l+1) + 3/4}{u^2} \right] g(u) \\ = 0 \end{aligned} \quad (9)$$

If one puts $g(z) = z^{\gamma+1} e^{-z^3/3} f(z)$ into (9), in accordance with the domain of the problem, we have

$$\begin{aligned} f''(z) &= 2 \left[z^2 - \frac{\gamma+1}{z} \right] f'(z) \\ &+ \left[2(\gamma+2)z - \sigma z^2 - \omega \right] f(z) \end{aligned} \quad (10)$$

TABLE 1: Comparisons of the perturbative energy eigenvalues (E_{pert}) (in GeV) with those obtained by direct application of AIM (E_{nl}) for the potential parameters $A = 1$ and $B = 1$ GeV, and for the reduced mass $\mu = 1/2$ GeV.

n	E_{n0}	E_{pert}	l	E_{0l}	E_{pert}
0	1.39788	1.41015	0	1.39788	1.41015
1	3.47509	3.47509	1	2.82565	2.82690
2	5.03291	5.03224	2	3.85058	3.85089
3	6.37015	6.36948	3	4.72675	4.72687
4	7.57493	-	4	5.51698	-
5	8.68791	-	5	6.24840	-

where $\omega = 4\alpha/(4\rho)^{1/3}$, $\sigma = 4\epsilon/(4\rho)^{2/3}$, $\gamma = 2l + 1/2$, and $z = (4\rho)^{1/6}u$. The final equation is suitable for applying AIM. After this point, we can apply AIM to the problem in two different ways: one is direct application (i.e., approximate solution) to get the numerical results and the other is usage of the method in scope of perturbation theory to obtain perturbative energies through a perturbation expansion as follows:

$$\sigma = \sigma_0 + \omega\sigma_1 + \omega^2\sigma_2 + \dots \quad (11)$$

where $\sigma_0, \sigma_1, \sigma_2, \dots$ are perturbation expansion coefficients. These can be obtained independently from the potential parameters. Thus, we can get a semianalytical formula for the energy eigenvalues. One can also achieve the mass-energy of the system by using this formula, as given in Section 4.

3.1. Numerical Results. In this section, we directly apply AIM to (10) to get the energy eigenvalues for different potential parameters, and we compare our results with the perturbative energies, for which (28) in the next section has been used.

$$f''(z) = 2 \left[z^2 - \frac{\gamma+1}{z} \right] f'(z) + [2(\gamma+2)z - \sigma z^2 - \omega] f(z) \quad (12)$$

From (12), it is easily seen that $\lambda_0(z) = 2[z^2 - (\gamma+1)/z]$ and $s_0(z) = 2(\gamma+2)z - \sigma z^2 - \omega$ according to (2). We tabulate the results of direct application of AIM in Tables 1, 2, and 3. For simplicity, in the calculations, the reduced mass has been considered $\mu = 1/2$ GeV. In Table 1 the potential parameters have been chosen as $A = 1$ and $B = 1$ GeV while $A = 1$, $B = 0.1$ GeV in Table 2, and $A = 1$, $B = 10$ GeV in Table 3. E_{pert} , seen in the tables, is for the comparison and has been obtained by using (28).

As can be seen from Tables 1–3, the perturbative energy eigenvalues are in very good agreement with the numerically obtained ones, even for small values of the parameter B . Furthermore, they are in accordance with each other for $B \geq 1$ GeV, while $A = 1$ (see in Tables 1 and 3). Additionally, this agreement is much better for higher quantum states. The perturbative eigenvalues are a little bit different from that obtained as numerically, for $B < 1$ GeV, $A = 1$, and the lower quantum states (see in Table 2). However, they are in agreement for the higher levels.

TABLE 2: Comparisons of the perturbative energy eigenvalues (E_{pert}) (in GeV) with those obtained by direct application of AIM (E_{nl}) for the potential parameters, $A = 1$ and $B = 0.1$ GeV, and for the reduced mass $\mu = 1/2$ GeV.

n	E_{n0}	E_{pert}	l	E_{0l}	E_{pert}
0	-0.221031	-0.164433	0	-0.221031	-0.164433
1	0.0347222	0.033627	1	0.0174006	0.023501
2	0.141913	0.138477	2	0.102472	0.104008
3	0.220287	0.217229	3	0.159831	0.160406
4	0.286111	-	4	0.206238	-
5	0.344602	-	5	0.246681	-

TABLE 3: Comparisons of the perturbative energy eigenvalues (E_{pert}) (in GeV) with those obtained by direct application of AIM (E_{nl}) for the potential parameters, $A = 1$ and $B = 10$ GeV, and for the reduced mass $\mu = 1/2$ GeV.

n	E_{n0}	E_{pert}	l	E_{0l}	E_{pert}
0	46.4022	46.4047	0	46.4022	46.4047
1	85.3393	85.3394	1	70.0161	70.0165
2	116.729	116.729	2	89.7154	89.7154
3	144.315	144.315	3	107.334	107.334
4	169.461	-	4	123.562	-
5	192.851	-	5	138.761	-

4. Perturbation Theory

Although the usage of perturbation method in the frame of AIM is comprehensively introduced in [5], we give a summary about the methodology in this section, assuming that the potential of a system is written as

$$V(x) = V_0(x) + \eta V_p(x) \quad (13)$$

where $V_0(x)$ is solvable (unperturbed Hamiltonian) potential. $V_p(x)$ and η are potential of the perturbed Hamiltonian and perturbation expansion parameter, respectively. The Schrödinger equation then reads

$$\left(-\frac{d^2}{dx^2} + V_0(x) + \eta V_p(x) \right) \Psi(x) = E \Psi(x) \quad (14)$$

where E_n eigenvalues are written as a series expansion of j th-order correction $E_n^{(j)}$ as follows:

$$E_n = E_n^{(0)} + \eta E_n^{(1)} + \eta^2 E_n^{(2)} + \dots = \sum_{j=0}^{\infty} \eta^j E_n^{(j)} \quad (15)$$

After substituting $\psi(x) = \psi_0(x)f(x)$ in (14), one can obtain the following equation for $f(x)$:

$$f''(x) = \lambda_0(x, \eta, E) f'(x) + s_0(x, \eta, E) f(x) \quad (16)$$

and the termination condition in this case can be written as

$$\begin{aligned} \delta_n(x, \eta, E) &= s_n(x, \eta, E) \lambda_{n-1}(x, \eta, E) \\ &\quad - \lambda_n(x, \eta, E) s_{n-1}(x, \eta, E) = 0 \end{aligned} \quad (17)$$

Once $\delta_n(x, \eta, E)$ is expanded about $\eta = 0$, we obtain

$$\begin{aligned} \delta_n(x, \eta, E) &= \delta_n(x, 0, E) + \frac{\eta}{1!} \frac{\partial \delta_n(x, \eta, E)}{\partial \eta} \Big|_{\eta=0} \\ &+ \frac{\eta^2}{2!} \frac{\partial^2 \delta_n(x, \eta, E)}{\partial \eta^2} \Big|_{\eta=0} + \dots \\ &= \sum_{k=0}^{\infty} \eta^k \delta_n^{(k)}(x, E) = 0 \end{aligned} \quad (18)$$

where $\delta_n^{(k)}(x, E) = (1/k!) (\partial^k \delta_n(x, \eta, E) / \partial \eta^k) |_{\eta=0}$.

According to perturbation method in the framework of AIM, solving the equation $\delta_n(x, 0, E) = 0$ with respect to (unknown) E gives $E_n^{(0)}$ (eigenvalues of unperturbed Hamiltonian), equation $\delta_n^{(1)}(x, E) = 0$ gives $E_n^{(1)}$ (first-order correction to E_n), $\delta_n^{(2)}(x, E)$ gives $E_n^{(2)}$ (second-order correction to E_n), and so on. Besides, the perturbative eigenfunctions can be achieved in the same vein with the eigenvalues. This is an alluring feature of the AIM usage in the perturbation theory for obtaining the eigenfunctions $f_n(x)$ given as follows:

$$f_n(x) = \exp\left(-\int^x \alpha_n(t, \eta) dt\right) \quad (19)$$

where $\alpha_n(t, \eta) \equiv s_n(t, \eta) / \lambda_n(t, \eta)$. $\alpha_n(t, \eta)$ is expanded about $\eta = 0$ in a similar manner, done for obtaining the eigenvalues. So,

$$\alpha_n(t, \eta) = \sum_{k=0}^{\infty} \eta^k \alpha_n^{(k)}(t) \quad (20)$$

where $\alpha_n^{(k)} = (1/k!) (\partial^k \alpha_n(x, \eta) / \partial \eta^k) |_{\eta=0}$. Thus, perturbation expansion of $f_n(x)$ is written as follows:

$$\begin{aligned} f_n(x) &= \exp\left[\sum_{k=0}^{\infty} \eta^k \left(-\int^x \alpha_n^{(k)}(t) dt\right)\right] \\ &= \prod_{k=0}^{\infty} f_n^{(k)}(x) \end{aligned} \quad (21)$$

where k th-order correction $f_n^{(k)}(x)$ to $f_n(x)$ is

$$f_n^{(k)}(x) = \eta^k \left(-\int^x \alpha_n^{(k)}(t) dt\right) \quad (22)$$

4.1. Perturbation Theory for the Cornell Potential. For our problem, we may apply the perturbation expansion which has been elucidated in previous section to the following differential equation:

$$\begin{aligned} f''(z) &= 2 \left[z^2 - \frac{\gamma+1}{z} \right] f'(z) \\ &+ [2(\gamma+2)z - \sigma z^2 - \omega] f(z) \end{aligned} \quad (23)$$

Suppose that σ is written as follows:

$$\sigma(n, l) = \sigma_0(n, l) + \sigma_1(n, l) \omega + \sigma_2(n, l) \omega^2 + \dots \quad (24)$$

where ω is the perturbation expansion parameter. So, the energy eigenvalue is yielded as

$$E_{pert} = \left(\frac{(4\rho)^{2/3}}{8\mu} \right)^{2/3} \sigma(n, l) \quad (25)$$

and more clearly

$$\begin{aligned} E_{pert} &= \frac{(4\rho)^{2/3}}{8\mu} \sigma_0(n, l) + \frac{(4\rho)^{1/3}}{2\mu} \alpha \sigma_1(n, l) \\ &+ \frac{2\alpha^2}{\mu} \sigma_2(n, l) + \dots \end{aligned} \quad (26)$$

In the above expansion, the general form of the zeroth-order correction σ_0 is obtained via

$$\delta^{(0)}(z, 0, \sigma_0) = 0 \quad (27)$$

The first-order correction, σ_1 , is obtained by using the equation $\delta^{(1)}(z, 0, \sigma_1) = 0$ in the same manner with σ_0 , while $\delta^{(2)}(z, 0, \sigma_2) = 0$ is used for σ_2 . Numerical results of σ_0 , σ_1 , and σ_2 coefficients, obtained by AIM, are reported in Table 4 for some energy levels. Besides, for $\mu = 1/2$ GeV, comparisons of the perturbative energy eigenvalues with the ones obtained by direct application of AIM have been given in Tables 1, 2, and 3, in previous section. We emphasize, in Table 4, that corrections to the perturbation expansion do not depend on the potential parameters.

As a practice, we have applied our perturbation expansion formula (up to second-order correction) to get the ground-state energies of quarkonium in Table 5, for various values of the parameter A , while $B = 1$ GeV and $\mu = 1/2$ GeV. In Table 5, we also report comparisons of the perturbative energy eigenvalues with the ones of s-wave heavy quarkonium from [10, 21].

As is seen from Table 5, the results for which our perturbation expansion (up to second-order correction) has been used are in very good agreement with [10, 21] for small values of A . However, our analytical results are a little bit different from the exact ones as A gets larger values. It seems that the perturbation expansion, which includes third-order correction, may give more accurate results. The more correction term we add to the perturbative expansion, the more compatible results we get. Nevertheless, we can say that (26) can be used as an eigenvalue formula of the Schrödinger equation in case of Cornell potential, for practical purposes. So, one can use the following formula:

$$E_{pert} = \frac{(4\rho)^{2/3}}{8\mu} \sigma_0(n, l) + \frac{(4\rho)^{1/3}}{2\mu} \alpha \sigma_1(n, l) \quad (28)$$

$$+ \frac{2\alpha^2}{\mu} \sigma_2(n, l)$$

for obtaining the eigenvalues and mass of the quarkonium for Cornell potential. Besides, it can be fit to mass formula of experimental values for determining the potential parameters A and B . The advantage of (28) is that the coefficients σ_0 , σ_1 , and σ_2 are independent of the potential parameters.

TABLE 4: Perturbation coefficients of the expansion given as (24) and (26). Notice that corrections to the perturbation expansion do not depend on the potential parameters.

l	n	$\sigma_0(n,l)$	$\sigma_1(n,l)$	$\sigma_2(n,l)$
0	0	3.71151	-0.525933	-0.0232729
	1	6.48922	-0.366743	-0.00767365
	2	8.76334	-0.297538	-0.00400191
	3	10.7732	-0.256486	-0.00251618
1	0	5.33566	-0.322683	-0.00554189
	1	7.75358	-0.258925	-0.00282569
	2	9.85399	-0.222298	-0.00176295
	3	11.7558	-0.197751	-0.00122526
2	0	6.74357	-0.244191	-0.00241586
	1	8.93661	-0.208300	-0.00148846
	2	10.9037	-0.184664	-0.00102765
	3	12.7146	-0.167585	-0.000761053
3	0	8.01784	-0.200753	-0.00134507
	1	10.0516	-0.177251	-0.000921458
	2	11.9129	-0.160449	-0.000679139
	3	13.6471	-0.147666	-0.000525832

TABLE 5: Comparisons of energy eigenvalues (in GeV) obtained by using the perturbation expansion formula in (26) (E_{pert}) with the ones of s-wave heavy quarkonium from [10, 21]. The potential parameter B is taken as $B = 1$ GeV, while the reduced mass is $\mu = 1/2$ GeV in this case. The eigenvalues of [10, 21] are exact results.

A	E_{00} (Ref. [10])	E_{00} (Ref. [21])	E_{pert}	A	E_{00} (Ref. [10])	E_{00} (Ref. [21])	E_{pert}
0.2	2.16732	2.16732	2.16741	0.1	2.25368	2.25368	2.25369
0.4	1.98850	1.98850	1.98923	0.3	2.07895	2.07895	2.07927
0.6	1.80107	1.80107	1.80367	0.5	1.89590	1.89590	1.89740
0.8	1.60441	1.60441	1.61063	0.7	1.70394	1.70393	1.70808
1	1.39788	1.39788	1.41015	0.9	1.50242	1.50242	1.51132
1.2	1.18084	1.18083	1.20221	1.1	1.29071	1.29071	1.30711
1.4	0.95264	0.95264	0.98683	1.3	1.06817	1.06817	1.09545
1.6	0.71266	0.71266	0.76400	1.5	0.83416	0.83416	0.87635
1.8	0.46027	0.46026	0.53373	1.7	0.58805	0.58805	0.64980

4.2. Energy Eigenvalues and Mass Spectrum for Heavy Quarkonium. In this section, we tested our formula through cross-checking with the exact results in literature and with the experimental data. For comparing our energy eigenvalues with the exact ones, the parameters of Cornell potential have been considered $A = 0.52$ and $B = 0.43$ GeV. Besides, we have chosen the quark masses as $m_c = 1.84$ GeV and $m_b = 5.18$ GeV, in this case [12].

Also, we tested our formula by comparing our results, for the masses of heavy mesons, with the experimental data. For doing this, we have taken the quark masses as $m_c = 1.44$ GeV and $m_b = 4.87$ GeV and the potential parameters as $A = 0.64$ and $B = 0.39$ GeV. All these values have been obtained by fitting our formula to the experimental data in [22].

In Table 6, we compared our energy eigenvalues calculated by using (28) with the ones of [12]. Furthermore, in Table 7, we gave our results for the masses of the mesons obtained by the same equation. Table 7 also includes the experimental data got from [22].

It can be seen from Table 6 that the energy eigenvalues of the mesons $c\bar{c}$, $b\bar{b}$, and $b\bar{c}$, obtained by (28), are more compatible with the exact ones, than those of [12]. The difference between AIM and [12] becomes clearer as the energy level increases. Similar things can be said for the masses in Table 7: the results obtained via AIM are closer to the experimental data than those of [12].

5. Conclusion

We have used AIM to obtain both, the eigenvalues of Schrödinger equation and mass of $q\bar{q}$ system for Cornell potential, in three dimensions. AIM has some advantages such as being used for either exactly or numerically (or approximately) solvable problems. Furthermore, one can use AIM in the frame of perturbation theory. Once it is performed to obtain perturbative solutions, the wavefunction of unperturbed Hamiltonian is not needed to get the corrections to the perturbation expansion.

TABLE 6: Comparisons of the energy eigenvalues (in GeV) of the mesons $c\bar{c}$, $b\bar{b}$, and $b\bar{c}$ calculated by using (28) with the exact ones of [12]. The parameters of Cornell potential are $A = 0.52$ and $B = 0.43$ GeV, while the quark masses are $m_c = 1.84$ GeV and $m_b = 5.18$ GeV.

E_n	$c\bar{c}$			$b\bar{b}$			$b\bar{c}$		
	Exact [12]	Ref. [12]	AIM	Exact [12]	Ref. [12]	AIM	Exact [12]	Ref. [12]	AIM
1s	0.2575	0.2578	0.2660	-0.1704	-0.1702	-0.1216	0.1110	0.1113	0.1269
2s	0.8482	0.8096	0.8481	0.4214	0.3579	0.4203	0.6813	0.6324	0.6803
3s	1.2720	1.1427	1.2715	0.7665	0.5612	0.7635	1.0686	0.9065	1.0668

TABLE 7: Comparisons of the masses (in GeV), obtained via AIM, of the heavy mesons $c\bar{c}$, $b\bar{b}$, and $b\bar{c}$ with the ones of [12], and with the experimental data from [22]. In this case, we have taken the quark masses as $m_c = 1.44$ GeV and $m_b = 4.87$ GeV, and the potential parameters as $A = 0.64$ and $B = 0.39$ GeV, for our calculations. All these parameters have been obtained by fitting our formula, given in (28), to the experimental data.

M_n	$c\bar{c}$			$b\bar{b}$			$b\bar{c}$		
	Exp.	Ref. [12]	AIM	Exp.	Ref. [12]	AIM	Exp.	Ref. [12]	AIM
1s	3.097	3.097	3.096	9.460	9.350	9.462	6.275	6.291	6.362
2s	3.686	3.649	3.672	10.023	9.878	10.027	6.842	6.812	6.911
3s	4.039	3.963	4.085	10.355	10.081	10.361	-	7.087	7.284
4s	-	-	4.433	10.579	-	10.624	-	-	7.593
1p	3.511	-	3.521	9.899	-	9.963	-	-	6.792
2p	3.927	-	3.951	10.260	-	10.299	-	-	7.178
3p	-	-	4.310	10.512	-	10.564	-	-	7.494
1d	-	-	3.800	10.164	-	10.209	-	-	7.051

In the present study, the energy eigenvalues in the case of Cornell potential have been achieved by direct application of the method. Besides, we have performed perturbation theory in the view of AIM for the problem and found a semianalytical formula for energy eigenvalues. Numerical results obtained by using this formula, for the reduced mass $\mu = 1/2$ GeV, conform with the exact results of [10, 21], in a wide spectrum of the potential parameters A and B (especially for $B > A$). Furthermore, the results are compatible with the ones obtained directly, in Section 3. It is also possible to see from the results that the perturbative eigenvalues fit in with the exact ones for higher quantum states, even for the large values of A . For any values of A and B , the higher quantum states are more consonant with the exact ones than the lower states. The perturbation expansion, which includes third-order correction, may give more accurate results. The more correction terms we add to the perturbative expansion, the more compatible results we may get.

We have also tested our semianalytical formula, by cross-checking it with the exact results in literature and with the experimental data. It can be seen, from Table 6, that our energy eigenvalues calculated by using (28) are more compatible with the exact ones than those of [12]. Furthermore, the difference between our results and [12] becomes clearer as the energy level increases. By using AIM, we have also obtained mass results which are closer to the experimental data than [12].

As a consequence, semianalytical formula achieved for energy eigenvalues and mass of quarkonium can be used for practical purposes in the case of Cornell potential. If our formula is fitted to the experimental data, the potential

parameters (and masses of the quarks, if it is needed) can also be obtained.

Data Availability

The data used to support the findings of this study are available from the corresponding author upon request.

Conflicts of Interest

The authors declare that they have no conflicts of interest.

Acknowledgments

This academic work was supported by the Mersin Technology Transfer Office Academic Writing Center of Mersin University.

References

- [1] H. Çiftçi, R. L. Hall, and N. Saad, "Asymptotic iteration method for eigenvalue problems," *Journal of Physics A: Mathematical and General*, vol. 36, no. 47, pp. 11807–11816, 2003.
- [2] N. Saad, R. L. Hall, and N. Saad, "Exact and approximate solutions of Schrödinger's equation for a class of trigonometric potentials," *Central European Journal of Physics*, vol. 11, no. 1, pp. 37–48, 2013.
- [3] E. Olğar, R. Koç, and H. Tütüncüler, "The exact solution of the s-wave Klein-Gordon equation for the generalized Hulthén potential by the asymptotic iteration method," *Physica Scripta*, vol. 78, no. 1, Article ID 015011, 2008.

- [4] F. M. Fernández, “On an iteration method for eigenvalue problems,” *Journal of Physics A: Mathematical and General*, vol. 37, no. 23, pp. 6173–6180, 2004.
- [5] H. Ciftci, R. L. Hall, and N. Saad, “Perturbation theory in a framework of iteration methods,” *Physics Letters A*, vol. 340, no. 5-6, pp. 388–396, 2005.
- [6] H. Ciftci and H. F. Kisoglu, “Accidental Degeneracies in N dimensions for Potential Class $\alpha r^{2d-2} - \beta r^{d-2}$ via Asymptotic Iteration Method (AIM),” *Communications in Theoretical Physics*, vol. 67, p. 350, 2017.
- [7] E. Eichten, K. Gottfried, T. Kinoshita, J. Kogut, K. D. Lane, and T.-M. Yan, “Spectrum of charmed quark-antiquark bound states,” *Physical Review Letters*, vol. 34, no. 6, pp. 369–372, 1975.
- [8] E. Eichten, K. Gottfried, T. Kinoshita, K. D. Lane, and T. -. Yan, “Charmonium: The model,” *Physical Review D: Particles, Fields, Gravitation and Cosmology*, vol. 17, no. 11, pp. 3090–3117, 1978.
- [9] E. Eichten, K. Gottfried, T. Kinoshita, K. D. Lane, and T. M. Yan, “Charmonium: comparison with experiment,” *Physical Review D: Particles, Fields, Gravitation and Cosmology*, vol. 21, no. 1, pp. 203–233, 1980.
- [10] H. Chung S and J. Lee, “Cornell potential parameters for S-wave heavy quarkonia,” *Journal of the Korean Physical Society*, vol. 52, p. 1151, 2008.
- [11] M. Hamzavi and A. A. Rajabi, “Scalar–vector–pseudoscalar Cornell potential for a spin-1/2 particle under spin and pseudospin symmetries: 1 + 1 dimensions,” *Annals of Physics*, vol. 334, pp. 316–320, 2013.
- [12] A. Vega and J. Flores, “Heavy quarkonium properties from Cornell potential using variational method and supersymmetric quantum mechanics,” *Pramana – Journal of Physics*, vol. 87, 2016, Article ID 73.
- [13] S. Jacobs, M. G. Olsson, and C. Suchyta, “Comparing the Schrödinger and spinless Salpeter equations for heavy-quark bound states,” *Physical Review D: Particles, Fields, Gravitation and Cosmology*, vol. 33, no. 11, pp. 3338–3348, 1986.
- [14] B. Grinstein, “A modern introduction to quarkonium theory,” *International Journal of Modern Physics A*, vol. 15, p. 461, 2000.
- [15] W. Lucha, F. Schoberl, and D. Gromes, “Bound states of quarks,” *Physics Reports*, vol. 200, no. 4, pp. 127–240, 1991.
- [16] P. Evans, C. Allton, and J. Skullerud, *Physical Review D: Particles, Fields, Gravitation and Cosmology*, vol. 89, no. 7, 2014.
- [17] R. L. Hall, “Simple eigenvalue formula for the Coulomb-plus-linear potential,” *Physical Review D*, vol. 30, p. 433, 1984.
- [18] K. Hagiwara J and S. Jacobs, “Probing QCD with heavy quark bound states,” *Physics Letters B*, vol. 131, pp. 455–460, 1983.
- [19] E. Gozzi, M. Reuter, and W. Thacker D, “Variational methods via supersymmetric techniques,” *Physics Letters A*, vol. 183, p. 29, 1993.
- [20] F. Cooper, A. Khare, and U. Sukhatme, “Supersymmetry and quantum mechanics,” *Physics Reports*, vol. 251, no. 5-6, pp. 267–385, 1995.
- [21] L. R. Hall and S. Nasser, “Schrödinger spectrum generated by the Cornell potential,” *Open Physics*, vol. 13, p. 83, 2015.
- [22] C. Patrignani and etal. (Particle Data Group), “Review of Particle Physics,” *Chinese Physics C*, vol. 40, 2016, 100001.

Research Article

Solutions of the D -Dimensional Schrödinger Equation with the Hyperbolic Pöschl-Teller Potential plus Modified Ring-Shaped Term

Ibsal A. Assi,¹ Akpan N. Ikot ,² and E. O. Chukwuocha²

¹Department of Physics and Physical Oceanography, Memorial University of Newfoundland, St. John's, NL, Canada A1B 3X7

²Department of Physics, University of Port Harcourt, PMB 5323, Choba, Port Harcourt, Nigeria

Correspondence should be addressed to Akpan N. Ikot; ndemikotphysics@gmail.com

Received 9 November 2017; Accepted 26 February 2018; Published 22 May 2018

Academic Editor: Shi-Hai Dong

Copyright © 2018 Ibsal A. Assi et al. This is an open access article distributed under the Creative Commons Attribution License, which permits unrestricted use, distribution, and reproduction in any medium, provided the original work is properly cited. The publication of this article was funded by SCOAP³.

We solve the D -dimensional Schrödinger equation with hyperbolic Pöschl-Teller potential plus a generalized ring-shaped potential. After the separation of variable in the hyperspherical coordinate, we used Nikiforov-Uvarov (NU) method to solve the resulting radial equation and obtain explicitly the energy level and the corresponding wave function in closed form. The solutions to the energy eigenvalues and the corresponding wave functions are obtained using the NU method as well.

1. Introduction

The noncentral potentials in recent times have been an active field of research in physics and quantum chemistry [1–3]. For instance, the occurrence of accidental degeneracy and hidden symmetry in the noncentral potentials and their application in quantum chemistry and nuclear physics are used to describe ring-shaped molecules like benzene and the interaction between deformed pair of nuclei [4, 5]. It is known that this accidental degeneracy occurring in the ring-shaped potential was explained by constructing an SU(2) algebra [6]. Owing to these applications, many authors have investigated a number of real physical problems on non-spherical oscillator [7], ring-shaped oscillator (RSO) [8], and ring-shaped nonspherical oscillator [9]. Berkdemir [10] had shown that either Coulomb or harmonic oscillator will give a better approximation for understanding the spectroscopy and structure of diatomic molecules in the ground electronic state. Other applications of the ring-shaped potential can be found in ring-shaped organic molecules like cyclic polyenes and benzene [11, 12].

On the other hand, Chen and Dong studied the Schrödinger equation with a new ring-shaped potential [3].

Cheng and Dai investigated modified Kratzer potential plus the new ring-shaped potential using Nikiforov-Uvarov method [13]. Recently, Ikot et al. [14–16] investigated the Schrödinger equation with Hulthen potential plus a new ring-shaped potential [3], nonspherical harmonic and Coulomb potential [15], and pseudo-Coulomb potential in the cosmic string space-time [16]. Many authors have used different methods to obtain exact solutions of the wave equation such as the methods of Supersymmetric Quantum Mechanics (SUSY-QM) [17–19], the Tridiagonal Representation Approach (TRA) [20–23], and Nikiforov-Uvarov (NU) method [24–28].

Motivated by the recent studies of the ring-shaped potential [29–32], we proposed a novel hyperbolic Pöschl-Teller potential plus generalized ring-shaped potential of the form (see Figure 1)

$$V(r, \theta) = A \tanh^2(\lambda r) + \frac{B}{\tanh^2(\lambda r)} + \frac{\gamma \cot^2 \theta + \zeta \cot \theta \csc \theta + \kappa \csc^2 \theta}{r^2}, \quad (1)$$

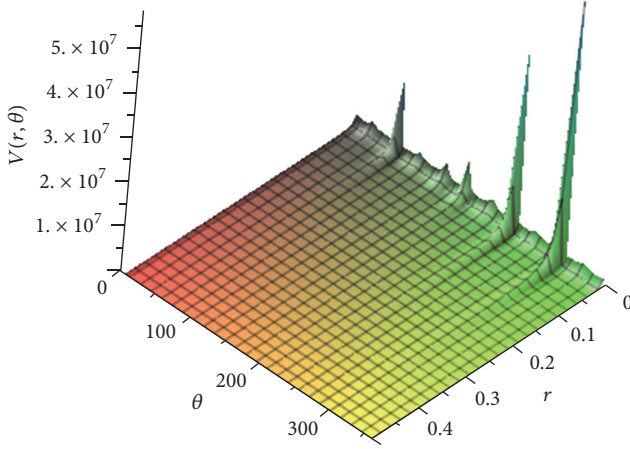


FIGURE 1: The plot of the novel Pöschl-Teller plus ring-shaped potential as a function of r and θ for $A = 1$, $B = 2$, $\lambda = 0.1$, $\gamma = 2$, $\zeta = 4$, and $\kappa = 3$.

where λ is the screening parameter and A , B , γ , ζ , and κ are real potential parameters. As a special case when $\lambda r \rightarrow 0$ with $A \rightarrow m\omega^2/2\lambda^2 - (\hbar^2\alpha/30m)\lambda^2$, $B \rightarrow (\hbar^2\alpha/2m)\lambda^2$, and $E \rightarrow E + 2B/3$; the potential of (1) turns to nonspherical harmonic oscillator plus generalized ring-shaped potential.

$$V(r, \theta) = \frac{1}{2}m\omega^2 r^2 + \frac{\hbar^2\alpha}{2mr^2} + \frac{\gamma \cot^2\theta + \zeta \cot\theta \csc\theta + \kappa \csc^2\theta}{r^2}. \quad (2)$$

2. D -Dimensional Schrödinger Equation in Hyperspherical Coordinates

The D -dimensional Schrödinger equation is given as follows [33, 34]:

$$\left\{ \nabla_D^2 + \frac{2\mu}{\hbar^2} [E - U] \right\} \Psi_{l_1, l_2, \dots, l_{D-2}}^{l=l_{D-1}}(\vec{X}) = 0, \quad (3)$$

where μ is the effective mass of two interacting particles, \hbar is Planck's constant, E is the energy eigenvalue, U is the potential energy function, $\vec{X} = (r, \theta_1, \theta_2, \dots, \theta_{D-1})^T$ is the position vector in D -dimensions, where $\vec{\theta} = \{\theta_1, \theta_2, \dots, \theta_{D-1}\}$ is the angular position vector written in terms of hyperspherical coordinates [35, 36], and ∇_D^2 is the D -dimensional Laplacian operator given in Appendix B.

The solvable potentials that allow separation of variable in (3) must be of the form

$$U(\vec{X}) = V_1(r) + \frac{V_2(\theta_{D-1})}{r^2}. \quad (4)$$

The separable wave function takes the following form:

$$\Psi_{l_1, l_2, \dots, l_{D-2}}^{l=l_{D-1}}(\vec{X}) = r^{-(D-1)/2} g(r) Y_{l_1, l_2, \dots, l_{D-2}}^{l=l_{D-1}}(\vec{\theta}). \quad (5)$$

Applying (5) to (3) with the use of (4), we obtain the following radial and angular wave equations:

$$\left[\frac{d^2}{dr^2} - \frac{(D+2l-2)^2-1}{4r^2} + \frac{2\mu}{\hbar^2} [E - V_1(r)] \right] g(r) = 0, \quad (6)$$

$$\left[\frac{d^2}{d\theta_j^2} + (j-1) \frac{\cos\theta_j}{\sin\theta_j} \frac{d}{d\theta_j} + \Lambda_j - \frac{\Lambda_{j-1}}{\sin^2\theta_j} \right] H(\theta_j) = 0, \quad (7)$$

$$\left[\frac{d^2}{d\theta_{D-1}^2} + (D-2) \frac{\cos\theta_{D-1}}{\sin\theta_{D-1}} \frac{d}{d\theta_{D-1}} + l(l+D-2) - \frac{\Lambda_{D-2}}{\sin^2\theta_{D-1}} + \frac{2\mu}{\hbar^2} V_2(\theta_{D-1}) \right] H(\theta_{D-1}) = 0, \quad (8)$$

where $Y_{l_1, l_2, \dots, l_{D-2}}^{l=l_{D-1}}(\vec{\theta}) = (1/\sqrt{2\pi}) e^{\pm im\theta} \prod_{j=2}^{D-1} H(\theta_j)$, (8) holds for $j \in [2, D-2]$, with $D > 3$, and $\Lambda_j = l_j(l_j + j - 1)$. Solutions of (8) will not be affected by the presence of the proposed potential and thus are common to different systems and they were done before using different approaches [37]. Consequently, we will only solve (6) and (8) using the Nikiforov-Uvarov method [24, 25].

3. Nikiforov-Uvarov Method

Many problems in physics lead to the following second-order linear differential equation [24]:

$$\left[\frac{d^2}{dx^2} + \frac{\tilde{\tau}(x)}{\sigma(x)} \frac{d}{dx} + \frac{\tilde{\sigma}(x)}{\sigma^2(x)} \right] u(x) = 0, \quad (9)$$

where $\sigma(x)$ and $\tilde{\sigma}(x)$ are polynomials of degree 2 at most and $\tilde{\tau}(x)$ is at most linear in x . Equation (9) is sometimes called of hypergeometric type. Let us consider $u(x) = \phi(x)y(x)$; this will transform (9) to the following differential equation for $y(x)$:

$$\left[\frac{d^2}{dx^2} + \frac{\tau(x)}{\sigma(x)} \frac{d}{dx} + \frac{\bar{\sigma}(x)}{\sigma^2(x)} \right] y(x) = 0, \quad (10)$$

where we assumed the following conditions:

$$\frac{\phi'(x)}{\phi(x)} = \frac{\pi(x)}{\sigma(x)}, \quad (11a)$$

$$\tau(x) = \tilde{\tau}(x) + 2\pi(x), \quad (11b)$$

$$\bar{\sigma}(x) = \tilde{\sigma}(x) + \pi^2(x) + \pi(x) [\tilde{\tau}(x) - \sigma'(x)] + \pi'(x)\sigma(x), \quad (11c)$$

$$\pi(x) = \frac{\sigma'(x) - \tilde{\tau}(x)}{2} \pm \sqrt{\left(\frac{\sigma'(x) - \tilde{\tau}(x)}{2} \right)^2 - \tilde{\sigma}(x) + k\sigma(x)}, \quad (11d)$$

$$k = \eta - \pi'(x), \quad (11e)$$

where k and η are constants chosen such that $\pi(x)$ is polynomial which is at most linear in x and $\bar{\sigma}(x) = \eta\sigma(x)$. This will transform (10) to the following:

$$\left[\sigma(x) \frac{d^2}{dx^2} + \tau(x) \frac{d}{dx} + \eta \right] y(x) = 0, \quad (12)$$

where $\sigma(x)$ and $\tau(x)$ are polynomials of degrees 2 and 1, respectively. In this case, solutions to (12) are polynomials of degree n ; $y(x) = y_n(x, \eta_n)$, where η_n is given as follows:

$$\eta_n = -n\tau' - \frac{1}{2}n(n-1)\sigma''. \quad (13)$$

Equation (13) will be used to obtain the energy spectrum formula of the quantum mechanical system. We should point out here that the polynomial solutions to (12) for $\tau' < 0$ and $\tau = 0$ on the boundaries of the finite space (the latter case is omitted for infinite space) are the classical orthogonal polynomials. It is well known that each set of polynomials is associated with a weight function $\rho(x)$. For the polynomial solutions to (12), this function must be bounded on the domain of the system and must satisfy $(\sigma\rho)' = \tau\rho$. This weight function will be used to construct the Rodrigues formula for these polynomials, which reads

$$y_n(x) = \frac{B_n}{\rho(x)} \frac{d^n}{dx^n} [\sigma^n(x) \rho(x)], \quad (14)$$

where B_n is just a constant obtained by the normalization conditions and $n = 0, 1, 2, \dots$

4. The Solutions of the D -Dimensional Radial Equation

We use the NU method to solve (6); in the presence of our potential,

$$\frac{d^2 g(r)}{dr^2} + \frac{2\mu}{\hbar^2} \left[E - A \tanh^2(\lambda r) - \frac{B}{\tanh^2(\lambda r)} - \frac{\gamma_D \hbar^2}{2\mu} \frac{1}{r^2} \right] g(r) = 0, \quad (15)$$

where $\gamma_D = ((D+2l-2)^2 - 1)/4$. Equation (15) cannot be solved analytically due to the centrifugal term $1/r^2$. Different authors used different approximation techniques to allow an approximate analytical solution of (15) and these methods rely on Taylor expansion of the centrifugal potential in terms of the other components of the potential of interest [38]. In this work, we use the following approximation obtained by Taylor expansion [39]:

$$\frac{1}{\lambda^2 r^2} \approx -\frac{2}{3} - \frac{1}{3} \tanh^2(\lambda r) + \frac{1}{\tanh^2(\lambda r)}. \quad (16)$$

The advantage of this approximation is that it is valid not only for $\lambda r \ll 1$ but also for $0 \leq \lambda r \leq 2$ with high accuracy. Also, it satisfies the limits on $1/r^2$ at zero and infinity; that is, $\lim_{r \rightarrow 0} \text{RHS} = 1/\lambda^2 r^2$ and $\lim_{r \rightarrow \infty} \text{RHS} = 0$, where RHS denotes the right-hand side of (16). Now, Using (16) back in (15), we get

$$\left[\frac{d^2}{dr^2} - 4\lambda^2 \tilde{A} \tanh^2 \lambda r - \frac{4\lambda^2 \tilde{B}}{\tanh^2 \lambda r} + 4\lambda^2 \tilde{E} \right] g(r) = 0, \quad (17)$$

where $4\lambda^2 \tilde{E} = (2\mu/\hbar^2)[E + \gamma_D \hbar^2 \lambda^2 / 3\mu]$, $4\lambda^2 \tilde{A} = (2\mu/\hbar^2)(A - \gamma_D \hbar^2 \lambda^2 / 6\mu)$, and $4\lambda^2 \tilde{B} = (2\mu/\hbar^2)[B + \gamma_D \hbar^2 \lambda^2 / 2\mu]$. Making change of variable $s = \tanh^2 \lambda r$ and by writing $g(s) = \phi(s)y(s)$, this transforms (17) to (9) with the polynomials being $\sigma = s - s^2$, $\tilde{\tau} = -(3s - 1)/2$, and $\tilde{\sigma} = \tilde{E}s - \tilde{A}s^2 - \tilde{B}$. We now use (11d) to calculate $\pi(s)$, which reads

$$\pi(s) = \frac{1-s}{4} \pm \sqrt{\left(\frac{1-s}{4}\right)^2 + \tilde{A}s^2 - \tilde{E}s + \tilde{B} + k(s-s^2)}. \quad (18)$$

The choice of k that makes (18) a polynomial of first degree must satisfy $c_1^2 = c_2 c_3$, where $c_1 = 16k - 8 - 16\tilde{E}$, $c_2 = 1 + 16\tilde{A} - 16k$, and $c_3 = 4(1 + 16\tilde{B})$. This gives

$$\pi(s) = \frac{1-s}{4} \pm \frac{1}{4} \sqrt{c_2} \left(s + \frac{c_1}{2c_2} \right), \quad (19)$$

where we will pick the negative part in (19) which makes $\tau' < 0$. The function $\tau(s)$ can be easily calculated using (11b):

$$\tau(s) = 1 - 2s - \frac{1}{2} \sqrt{c_2} \left(s + \frac{c_1}{2c_2} \right). \quad (20)$$

Using (19) and (20) in (13) and (11e), we get

$$\left[\frac{4k}{(2n+1)} - (2n+1) \right]^2 = (1 + 16\tilde{A} - 16k). \quad (21)$$

Solutions of (21) for k are

$$4k = -(2n+1)^2 \pm (2n+1) \sqrt{1 + 16\tilde{A}}. \quad (22)$$

The next step is to use the value of c_2 in (21) with the constraint on k mentioned in (18), which is $c_1^2 = c_2 c_3$; we obtain

$$[8 + 16\tilde{E} - 16k]^2 = 4(1 + 16\tilde{B})(1 + 16\tilde{A} - 16k). \quad (23)$$

The conditions for bound states are $k \leq 0$ and $\tilde{A}, \tilde{B} \geq -1/16$. Using (22) in (23), we write the bound states formula as follows:

$$\tilde{E}_{nl}^D = -\frac{1}{4}(2n+1)^2 - \frac{1}{4}(2n+1) \sqrt{1 + 16\tilde{A}} - \frac{1}{2} \pm \frac{1}{8} \cdot \sqrt{(1 + 16\tilde{B}) \left(1 + 16\tilde{A} + 4(2n+1)^2 + 4(2n+1) \sqrt{1 + 16\tilde{A}} \right)}. \quad (24)$$

In terms of the original parameters A , B , and E , the spectrum formula in D -dimensions reads

$$\begin{aligned} \frac{2\mu}{\hbar^2} E_{nl}^D = & -\frac{2\gamma_D \lambda^2}{3} - \lambda^2 (2n+1)^2 - \lambda^2 (2n+1) \sqrt{1 + \frac{8\mu}{\lambda^2 \hbar^2} \left(A - \frac{\gamma_D \hbar^2 \lambda^2}{6\mu} \right)} - 2\lambda^2 \pm \frac{\lambda^2}{2} \sqrt{\left(1 + \frac{8\mu}{\lambda^2 \hbar^2} \left[B + \frac{\gamma_D \hbar^2 \lambda^2}{2\mu} \right] \right)} \\ & \times \sqrt{1 + \frac{8\mu}{\lambda^2 \hbar^2} \left(A - \frac{\gamma_D \hbar^2 \lambda^2}{6\mu} \right) + 4(2n+1)^2 + 4(2n+1) \sqrt{1 + \frac{8\mu}{\lambda^2 \hbar^2} \left(A - \frac{\gamma_D \hbar^2 \lambda^2}{6\mu} \right)}}, \end{aligned} \quad (25)$$

where conditions for bound states become $A \geq (\lambda^2 \hbar^2 / 2\mu)(\gamma_D/3 - 1/4)$ and $B \geq -(\lambda^2 \hbar^2 / 2\mu)(\gamma_D + 1/4)$. We will only take the (-) sign in (25) as explained below. The s -wave spectrum formula in three dimensions is the only exact solution that is obtained by setting $\gamma_D = 0$ in (25). However, for other higher states, the above solution is acceptable with high accuracy as far as the condition $0 \leq \lambda r \leq 2$ is satisfied.

The transformation $s = \tanh^2 \lambda x$ makes the domain of the function be $[0, 1]$. This suggests a change of variable $z = 2s - 1$ to bring the domain to that of Jacobi polynomials which are well-known classical orthogonal polynomials. By using (18) in (11a), we obtain $\phi(z) = 2^{c_4 - 2c_5} (1+z)^{c_5} (1-z)^{c_5 - c_4}$, where $4c_4 = 1 + \sqrt{c_2}$ and $8c_5 = 2 - c_1/\sqrt{c_2}$. The weight function can be easily calculated using (20) in $(\sigma\rho)' = \tau\rho$, which gives $\rho(z) = 2^{2c_7 + c_6} (1+z)^{-c_7} (1-z)^{-c_6 - c_7}$, where $2c_6 = 8 + \sqrt{c_2}$ and $4c_7 = c_1/\sqrt{c_2}$. The solution of (12) in our case is written in the following Rodrigues formula:

$$\begin{aligned} y_n(z) = & C_n (1+z)^{c_7} \\ & \cdot (1-z)^{c_6 + c_7} \frac{d^n}{dz^n} \left[(1+z)^{-c_7 + n} (1-z)^{n - c_6 - c_7} \right]. \end{aligned} \quad (26)$$

By comparison to Jacobi polynomials, we conclude that $y_n(z) = P_n^{(-c_6 - c_7, -c_7)}(z)$, where $P_n^{(-c_6 - c_7, -c_7)}(z)$ is the Jacobi polynomial of order n in z . Thus, the bound state solution of the radial wave equation now reads

$$\begin{aligned} g_n(r) = & \Omega_n (\tanh \lambda r)^{-c_6 - c_7 + 1/2} (\operatorname{sech} \lambda r)^{-c_7} \\ & \cdot P_n^{(-c_6 - c_7, -c_7)} \left[2 \tanh(\lambda r)^2 - 1 \right], \end{aligned} \quad (27)$$

where Ω_n is just a normalization constant. We must clarify here that, for Jacobi polynomials, we have to have $(-c_6 - c_7), -c_7 > -1$. Thus, the parameters c_1 and c_2 are chosen to satisfy $c_1 < 4\sqrt{c_2}$ and $2c_2 + c_1 < -12\sqrt{c_2}$. Moreover, since those parameters depend on the energy as we mentioned previously, this yields us to reject the (+) sign in (24) and (25). Consequently, bound states occur for $\bar{B} > 35/16$ (which does not violate the old restriction $\bar{B} \geq -1/16$) and $|\bar{E}| > |k - 1/2|$. The latter condition on E is already satisfied as we can see in (25), so we do not have to worry about it.

To calculate the normalization constant Ω_n , we first use the following identity of Jacobi polynomials [40]:

$$\begin{aligned} P_n^{(a,b)}(y) & \\ = & \frac{1}{2^n} \sum_{m=0}^n \binom{n+a}{m} \binom{n+b}{n-m} (1-y)^{m-n} (1+y)^m. \end{aligned} \quad (28)$$

Next, we use the normalization constraint $\int_0^\infty |g(r)|^2 dr = \int_{-1}^+ |g(y)|^2 (dy/\sqrt{2\lambda}\sqrt{1+y}(1-y)) = 1$, where $y = 2 \tanh^2(\lambda r) - 1$; this gives

$$\begin{aligned} (|\Omega_n|^2 / \lambda 2^{n+1/2}) \sum_{m=0}^n \binom{n+a}{m} \binom{n+b}{n-m} \\ \cdot \int_{-1}^+ (1-y)^{2a+m-n-1} (1+y)^{b+m} P_n^{(a,b)}(y) dy = 1. \end{aligned} \quad (29)$$

To calculate the integral in (29), we will use the following very useful integral formula [41]:

$$\begin{aligned} \int_{-1}^+ (1-y)^c (1+y)^d P_n^{(a,b)}(y) dy \\ = \frac{2^{c+d+1} \Gamma(c+1) \Gamma(d+1) \Gamma(n+a+1)}{\Gamma(n+1) \Gamma(c+d+2) \Gamma(a+1)} \\ \times {}_3F_2(-n, n+a+b+1, c+1; a+1, c+d+2; 1), \end{aligned} \quad (30)$$

where ${}_3F_2(a, b, c; d, e; f)$ is the generalized hypergeometric function [41]. By direct comparison between (29) and (30) we get $\Omega_n = 1/\sqrt{\Lambda_n}$, where Λ_n is given as follows:

$$\begin{aligned} \Lambda_n = & \frac{1}{\lambda 2^{n+1/2}} \sum_{m=0}^n \binom{n+a}{m} \binom{n+b}{n-m} \\ & \cdot \frac{2^{2a+2m-n+b} \Gamma(2a+m-n) \Gamma(b+m+1) \Gamma(n+a+1)}{\Gamma(n+1) \Gamma(2a+2m-n+b+1) \Gamma(a+1)} \\ & \times {}_3F_2(-n, n+a+b+1, 2a+m-n; a+1, 2a+2m \\ & -n+b+1; 1), \end{aligned} \quad (31)$$

where $a = -c_6 - c_7$ and $b = -c_7$.

The only issue that is left for discussion in this section is that the solutions of the radial wave equation $\{g_n(r)\}_{n=0}^N$, where N denotes the maximum number in which we get bound states, are not orthogonal! But they are normalized as we discussed above. We know that Hermitian operators with distinct eigenvalues must have orthogonal eigenvectors [42]. To solve this problem, one must use the Gram-Schmidt (GS) method to obtain an orthonormal set $\{\phi_n(r)\}_{n=0}^N$ by linear combinations [43]. The latter set will be the solutions of the radial wave equation. The process is a bit lengthy and we will not be able to do it here. However, we encourage the interested reader to do these calculations by referring to the process of GS.

5. Solutions of the Angular Equations

It is well known from literature that solutions of (7) are written in terms of Jacobi polynomials as follows [41]:

$$H(y) = N_n (1-y)^\alpha (1+y)^\beta P_n^{(c,d)}(y), \quad (32)$$

where N_n is just a constant factor, $2\beta + j/2 = d + 1$, and $2\alpha + j/2 = c + 1$. Moreover, the latter parameters are written in terms of the quantum numbers as $c = d = c_j = l_{j-1} + (j-2)/2$, which yields $\alpha = \beta = l_{j-1}/2$ and $n = l_j - l_{j-1}$. The above solution was obtained using different methods including the NU technique [24]. Hence, solutions of (7) are written below:

$$H(\theta_j) = N_n (\sin \theta_j)^{l_{j-1}} P_n^{(c_j, c_j)}(\cos \theta_j). \quad (33)$$

To solve (8), we introduce coordinate transformation as $y = \cos \theta_{D-1}$, which gives

$$\left[(1-y^2) \frac{d^2}{dy^2} - (D-1)y \frac{d}{dy} + l(l+D-2) - \frac{\Lambda_{D-2}}{1-y^2} + U(y) \right] H(y) = 0, \quad (34)$$

where $U(y) = (2\mu/\hbar^2)V_2(y) = (\gamma'y^2 + \zeta'y + \kappa')/(1-y^2)$ for real parameters $\{\gamma', \zeta', \kappa'\}$ are related to $\{\gamma, \zeta, \kappa\}$ by a factor of $2\mu/\hbar^2$. Equation (34) is of hypergeometric type with the polynomials being $\sigma(y) = 1 - y^2$, $\bar{\tau}(y) = -(D-1)y$, and $\bar{\sigma}(y) = \eta_2 y^2 + \eta_1 y + \eta_0$, where $\eta_2 = \gamma' - l(l+D-2)$, $\eta_1 = \zeta'$, and $\eta_0 = \kappa' + l(l+D-2) - \Lambda_{D-2}$. The solutions of (34) are written as $H(y) = \phi(y)Y(y)$, where $\phi(y)$ satisfies (11a). Next, we need to find the function $\pi(y)$ using (11d); we find that this function takes the following form:

$$\pi(y) = \frac{(D-3-2u_0)y}{2} + \frac{\eta_1}{2u_0}, \quad (35)$$

where $u_0 = \sqrt{((D-3)/2)^2 - \eta_2 - k}$ and the parameter k defined in (11e) must satisfy $4k - 4\eta_0 = \eta_1^2/u_0^2$. The latter constraint will be used later to obtain the eigenvalues of (34). Now, we use (35) in (11b); we get $\tau(y) = -2(1+u_0)y + \eta_1/u_0$, which satisfies $d\tau(y)/dy < 0$. Using (11a), we can obtain $\phi(y)$ to be $\phi(y) = (1-y)^{-(u_1+u_2)/2} (1+y)^{(u_2-u_1)/2}$, where $2u_1 = (D-3-2u_0)$ and $\eta_1 = 2u_0 u_2$. We can also calculate the weight function by solving $(\sigma\rho)' = \tau\rho$, which gives $\rho(y) = (1-y)^{u_0-u_2} (1+y)^{u_0+u_2}$. The Rodrigues formula of the polynomials $Y(y)$ reads

$$Y_n(y) = \frac{\xi_n}{(1-y)^{u_0-u_2} (1+y)^{u_0+u_2}} \cdot \frac{d^n}{dy^n} \left[(1-y)^{n+u_0-u_2} (1+y)^{n+u_0+u_2} \right], \quad (36)$$

where ξ_n is just a constant. By direct comparison with the Rodrigues formula of Jacobi polynomials [xx], we conclude that $Y_n(y) = P_n^{(u_0-u_2, u_0+u_2)}(y)$. As required by Jacobi polynomials, we must impose that $u_0 \pm u_2 > -1$. Now, we use (35)

and (13) in (11e) to obtain the following quadratic formula for k :

$$\left[k - n^2 - n + \frac{(D-3)}{2} \right]^2 = (2n+1)^2 \left[\left(\frac{D-3}{2} \right)^2 - \eta_2 - k \right]. \quad (37)$$

The solutions of (37) are given below:

$$k = \frac{1}{2} \left[2 - D - 2n - 2n^2 \pm (1+2n) \sqrt{(D-2)^2 - 4\eta_2} \right]. \quad (38)$$

Moreover, we use $4k - 4\eta_0 = \eta_1^2/((D-3)/2)^2 - \eta_2 - k$ to obtain another solution for k :

$$8k = 9 + D^2 - 6D + 4\eta_0 - 4\eta_2 \pm \sqrt{((D-3)^2 + 4\eta_0 - 4\eta_2)^2 - 16(\eta_1^2 + \eta_0((D-3)^2 - 4\eta_2))}. \quad (39)$$

Direct comparison between (38) and (39) gives

$$(2n+1)^2 = -\frac{(D-1)^2 + 4\eta_0 - 4\eta_2 - 2}{2}, \quad (40)$$

$$(2n+1)^2 \left[(D-2)^2 - 4\eta_2 \right] = \frac{((D-3)^2 + 4\eta_0 - 4\eta_2)^2}{16} - (\eta_1^2 + \eta_0((D-3)^2 - 4\eta_2)). \quad (41)$$

In the next section, we will consider different examples and try to obtain the unknown parameters for each case.

6. Results and Discussions

In this section, we will discuss different examples that are considered as special cases of the potential in (1).

As a first example, we consider the case when $\gamma' = \zeta' = 0$ and $\kappa' \neq 0$, which is equivalent to the following noncentral hyperbolic potential:

$$V(r, \theta) = A \tanh^2(\lambda r) + \frac{B}{\tanh^2(\lambda r)} + \frac{\kappa \csc^2 \theta}{r^2}. \quad (42)$$

In this case, we have $u_2 = 0$. Thus, solution of (34) reads

$$H_n(\theta_{D-1}) = N_n (\sin \theta_{D-1})^{-u_1} P_n^{(u_0, u_0)}(\cos \theta_{D-1}), \quad (43)$$

where $2u_1 = (D - 3 - 2u_0)$, $u_0 = \sqrt{((D-3)/2)^2 + l(l+D-2) - k}$, and k is given below:

$$8k = 9 + D^2 - 6D + 4\eta_0 + 4l(l+D-2) \pm \sqrt{\left((D-3)^2 + 4\eta_0 + 4l(l+D-2)\right)^2 - 16\left(\eta_0\left((D-3)^2 + 4l(l+D-2)\right)\right)} \quad (44)$$

and the corresponding eigenvalue is obtain from (41) as

$$\begin{aligned} & (2n+1)^2 \left[(D-2)^2 + 4l(l+D-2) \right] \\ &= \frac{\left((D-3)^2 + 4\eta_0 + 4l(l+D-2) \right)^2}{16} \\ & - \left(\eta_0 \left((D-3)^2 + 4l(l+D-2) \right) \right). \end{aligned} \quad (45)$$

(2) The next special case of our potential model is considered when we choose the ring-shaped parameters $\gamma = \pm\zeta$ and $\kappa \neq 0$, which corresponds to the following potential:

$$\begin{aligned} V(r, \theta) = & A \tanh^2(\lambda r) + \frac{B}{\tanh^2(\lambda r)} \\ & + \frac{\gamma \left(\cot^2 \theta \pm \cot \theta \csc \theta \right) + \kappa \csc^2 \theta}{r^2}. \end{aligned} \quad (46)$$

$8k$

$$\begin{aligned} &= 9 + D^2 - 6D + 4\eta_0 \mp 4\zeta + 4l(l+D-2) \\ & \pm \sqrt{\left((D-3)^2 + 4\eta_0 \mp 4\zeta + 4l(l+D-2) \right)^2 - 16\left(\zeta^2 + \eta_0 \left((D-3)^2 \mp 4\zeta + 4l(l+D-2) \right) \right)}, \\ & (2n+1)^2 \left[(D-2)^2 \mp 4\zeta + 4l(l+D-2) \right] \\ &= \frac{\left((D-3)^2 + 4\eta_0 \mp 4\zeta + 4l(l+D-2) \right)^2}{16} - \left(\zeta^2 + \eta_0 \left((D-3)^2 \mp 4\zeta + 4l(l+D-2) \right) \right). \end{aligned} \quad (48)$$

The associated nonnormalized wave function is obtained as

$$\begin{aligned} H_n(\theta_{D-1}) = & N_n (1 - \cos \theta_{D-1})^{-(u_1+u_2)/2} \\ & \cdot (1 + \cos \theta_{D-1})^{(u_2-u_1)/2} \\ & \cdot P_n^{(u_0-u_2, u_0+u_2)}(\cos \theta_{D-1}) \end{aligned} \quad (49)$$

(3) Another special case of our study is when $\zeta = 0$ and $\gamma, \kappa \neq 0$, which corresponds to the following potential:

$$\begin{aligned} V(r, \theta) = & A \tanh^2(\lambda r) + \frac{B}{\tanh^2(\lambda r)} \\ & + \frac{(\gamma + \kappa) \cot^2 \theta + \kappa}{r^2}. \end{aligned} \quad (50)$$

Under these conditions, we have

$$\begin{aligned} \eta_1 &= \zeta, \\ \eta_2 &= \pm\zeta - l(l+D-2), \\ u_1 &= \frac{(D-3-2u_0)}{2}, \\ u_2 &= \frac{\zeta}{2u_0}, \\ u_0 &= \sqrt{\left(\frac{D-3}{2} \right)^2 \mp (\zeta - l(l+D-2)) - k}. \end{aligned} \quad (47)$$

The k values and the corresponding eigenvalues are obtained as follows:

With these assumptions, we have

$$\begin{aligned} \eta_1 &= 0, \\ \eta_1 &= \kappa + l(l+D-2) - \Lambda_{D-2}, \\ \eta_2 &= \gamma - l(l+D-2), \\ u_1 &= \frac{D-3-2u_0}{2}, \\ u_2 &= 0, \\ u_0 &= \sqrt{\left(\frac{D-3}{2} \right)^2 - \gamma + l(l+D-2) + k}. \end{aligned} \quad (51)$$

Under this special case, we obtain the k parameter, the eigenvalues, and the corresponding wave function as follows:

$$\begin{aligned}
8k &= 9 + D^2 - 6D + 4(\kappa + l(l + D - 2) - \Lambda_{D-2}) - 4(\gamma - l(l + D - 2)) \\
&\pm \sqrt{\left((D - 3)^2 + 4(\kappa + l(l + D - 2) - \Lambda_{D-2}) - 4(\gamma - l(l + D - 2))\right)^2 - 16(\eta_0((D - 3)^2 - 4\eta_2))}, \\
(2n + 1)^2 \left[(D - 2)^2 - 4(\gamma - l(l + D - 2)) \right] &= \frac{\left((D - 3)^2 + 4(\kappa + l(l + D - 2) - \Lambda_{D-2}) - 4(\gamma - l(l + D - 2))\right)^2}{16} \quad (52) \\
&- \left((\kappa + l(l + D - 2) - \Lambda_{D-2}) \left((D - 3)^2 - 4(\gamma - l(l + D - 2)) \right) \right), \\
H_n(\theta_{D-1}) &= N_n (\sin \theta_{D-1})^{-u_1} P_n^{(u_0, u_0)}(\cos \theta_{D-1}).
\end{aligned}$$

However, one needs to be careful here as, for $\gamma = -\kappa$, there will be no ring-shaped term and one ends up with hyperbolic PT potential plus pseudo centrifugal term:

$$V(r, \theta) = A \tanh^2(\lambda r) + \frac{B}{\tanh^2(\lambda r)} + \frac{\kappa}{r^2}. \quad (53)$$

(4) We consider the last special case for $\gamma = 0$ and $\kappa = \pm\zeta$, which corresponds to the potential of the form

$$\begin{aligned}
V(r, \theta) &= A \tanh^2(\lambda r) + \frac{B}{\tanh^2(\lambda r)} \\
&+ \frac{\zeta [\cot \theta \csc \theta \pm \csc^2 \theta]}{r^2}. \quad (54)
\end{aligned}$$

The following parameters are obtained under this case:

$$\eta_1 = \pm\zeta,$$

$$\eta_2 = -l(l + D - 2),$$

$$\eta_0 = \pm\zeta + l(l + D - 2) - \Lambda_{D-2},$$

$$u_1 = \left(\frac{D - 3 - 2u_0}{2} \right),$$

$$u_0 = \sqrt{\left(\frac{D - 3}{2} \right)^2 + l(l + D - 2) - k},$$

$$u_2 = \frac{\pm\zeta}{2u_0}.$$

(55)

Using (55), we obtain the k parameter, the eigenvalues, and the corresponding wave function for this special case as follows:

$$\begin{aligned}
8k &= 9 + D^2 - 6D + 4(\pm\zeta + l(l + D - 2) - \Lambda_{D-2}) + 4l(l + D - 2) \\
&\pm \sqrt{\left((D - 3)^2 + 4(\pm\zeta + l(l + D - 2) - \Lambda_{D-2}) + 4l(l + D - 2)\right)^2 - 16\left((\pm\zeta)^2 + (\pm\zeta + l(l + D - 2) - \Lambda_{D-2})\left((D - 3)^2 + 4l(l + D - 2)\right)\right)}, \\
(2n + 1)^2 \left[(D - 2)^2 + 4l(l + D - 2) \right] &= \frac{\left((D - 3)^2 + 4(\pm\zeta + l(l + D - 2) - \Lambda_{D-2}) + 4l(l + D - 2)\right)^2}{16} \quad (56) \\
&- \left((\pm\zeta)^2 + (\pm\zeta + l(l + D - 2) - \Lambda_{D-2}) \left((D - 3)^2 + 4l(l + D - 2) \right) \right), \\
H_n(\theta_{D-1}) &= N_n (1 - \cos \theta_{D-1})^{-(u_1 + u_2)/2} (1 + \cos \theta_{D-1})^{(u_2 - u_1)/2} P_n^{(u_0 - u_2, u_0 + u_2)}(\cos \theta_{D-1}).
\end{aligned}$$

7. Conclusions

In this paper, we have obtained analytically the solutions of the D -dimensional Schrödinger potential with hyperbolic

Pöschl-Teller potential plus a generalized ring-shaped term. We employed NU and trial function methods to solve the radial and angular parts of the Schrödinger equation, respectively. This result is new and has never been reported in the

available literature to the best of our knowledge. Finally, this result can find many applications in atomic and molecular physics and thermodynamic properties [43].

Appendix

A. Jacobi Polynomials

Jacobi polynomials $P_n^{(\mu,\nu)}(y)$ defined on $[-1, 1]$ are solutions of the following second-order linear differential equation [8]:

$$\left\{ (1-y^2) \frac{d^2}{dy^2} - [(\mu+\nu+2)y + \mu - \nu] \frac{d}{dy} + n(n+\mu+\nu+1) \right\} P_n^{(\mu,\nu)}(y) = 0. \quad (\text{A.1})$$

We also mention their orthogonality relation:

$$\int_{-1}^1 (1-y)^\mu (1+y)^\nu P_n^{(\mu,\nu)} P_m^{(\mu,\nu)} dy = \frac{2^{\mu+\nu+1}}{2n+\mu+\nu+1} \frac{\Gamma(n+\mu+1)\Gamma(n+\nu+1)}{\Gamma(n+\mu+\nu+1)n!} \delta_{n,m}. \quad (\text{A.2})$$

B. Hyperspherical Coordinates

The D -dimensional position vector $\vec{x} = (r, \theta_1, \dots, \theta_{D-1})$ is defined in terms of hyperspherical Cartesian coordinates below [36]:

$$\begin{aligned} x_1 &= r \cos \theta_1 \sin \theta_2 \cdots \sin \theta_{D-1}, \\ x_2 &= r \sin \theta_1 \sin \theta_2 \cdots \sin \theta_{D-1}, \\ x_j &= r \cos \theta_{j-1} \sin \theta_j \cdots \sin \theta_{D-1}, \end{aligned} \quad (\text{B.1})$$

where $j = 3, 4, \dots, D-1$, $x_D = r \cos \theta_{D-1}$, and $\sum_{j=1}^D x_j^2 = r^2$. For $D = 2$, this is the case of polar coordinates (r, φ) with $x_1 = x = r \cos \varphi$ and $x_2 = y = r \sin \varphi$, whereas $D = 3$ represents the spherical coordinates (r, φ, θ) , where $x_1 = x = r \cos \varphi \sin \theta$, $x_2 = y = r \cos \varphi \sin \theta$, and $x_3 = z = r \cos \theta$.

The volume element in D -dimension is defined as $dV = r^{D-1} dr \prod_{j=1}^{D-1} (\sin \theta_j)^{j-1} d\theta_j$, where $r \in [0, \infty[$, $\theta_1 \in [0, 2\pi[$, and $\theta_j \in [0, \pi[$ for $j \geq 2$. The Laplacian operator in D dimensions is defined below:

$$\begin{aligned} \nabla_D^2 &= \frac{\partial^2}{\partial r^2} + \frac{D-1}{r} \frac{\partial}{\partial r} + \frac{1}{r^2} \\ &\times \left[\frac{1}{\sin^{D-2} \theta_{D-1}} \frac{\partial}{\partial \theta_{D-1}} \left(\sin^{D-2} \theta_{D-1} \frac{\partial}{\partial \theta_{D-1}} \right) \right. \\ &\left. - \frac{L_{D-2}^2}{\sin^2 \theta_{D-1}} \right]. \end{aligned} \quad (\text{B.2})$$

Finally, we mention the normalization conditions of the wave function in D -dimensions:

$$\begin{aligned} \int_0^\infty |g_n(r)|^2 dr &= 1, \\ \prod_{j=2}^{D-1} \int_0^\pi |H(\theta_j)|^2 (\sin \theta_j)^{j-1} d\theta_j &= 1. \end{aligned} \quad (\text{B.3})$$

Conflicts of Interest

The authors declare that they have no conflicts of interest.

References

- [1] M. C. Zhang, G. H. Sun, and S.-H. Dong, "Exactly complete solutions of the Schrödinger equation with a spherically harmonic oscillatory ring-shaped potential," *Physics Letters A*, vol. 374, no. 5, pp. 704–708, 2010.
- [2] A. D. Alhaidari, "Scattering and bound states for a class of non-central potentials," *Journal of Physics A: Mathematical and General*, vol. 38, no. 15, pp. 3409–3429, 2005.
- [3] C.-Y. Chen and S.-H. Dong, "Exactly complete solutions of the Coulomb potential plus a new ring-shaped potential," *Physics Letters A*, vol. 335, no. 5-6, pp. 374–382, 2005.
- [4] C. Berkdemir and R. Sever, "Modified ℓ -states of diatomic molecules subject to central potentials plus an angle-dependent potential," *Journal of Mathematical Chemistry*, vol. 46, no. 4, pp. 1122–1136, 2009.
- [5] H. Hartmann and D. Schuch, "Spin-orbit coupling for the motion of a particle in a ring-shaped potential," *International Journal of Quantum Chemistry*, vol. 18, pp. 125–141, 1980.
- [6] G. E. Draganescu, C. Campigotto, and M. Kibler, "On a generalized Aharonov-Bohm plus Coulomb system," *Physics Letters A*, vol. 170, no. 5, pp. 339–343, 1992.
- [7] C.-Y. Chen, D.-S. Sun, and F.-L. Lu, "The relativistic bound states of the Hartmann potentials," *Physica Scripta*, vol. 74, no. 4, pp. 405–409, 2006.
- [8] C. Quesne, "An $sl(4, \mathbb{R})$ Lie algebraic treatment of the first family of Pöschl-Teller potentials," *Journal of Physics A: Mathematical and General*, vol. 21, no. 24, pp. 4487–4500, 1988.
- [9] S.-H. Dong, G.-H. Sun, and M. Lozada-Cassou, "An algebraic approach to the ring-shaped non-spherical oscillator," *Physics Letters A*, vol. 328, no. 4-5, pp. 299–305, 2004.
- [10] C. Berkdemir, "A novel angle-dependent potential and its exact solution," *Journal of Mathematical Chemistry*, vol. 46, no. 1, pp. 139–154, 2009.
- [11] H. Hassanabadi, A. N. Ikot, and S. Zarrinkamar, "Exact solution of Klein-Gordon with the Pöschl-Teller double-ring-shaped Coulomb potential," *Acta Physica Polonica A*, vol. 126, no. 3, pp. 647–651, 2014.
- [12] M.-C. Zhang, B. An, and H.-F. Guo-Qing, "Exact solutions of a new Coulomb ring-shaped potential," *Journal of Mathematical Chemistry*, vol. 48, no. 4, pp. 876–882, 2010.
- [13] Y.-F. Cheng and T.-Q. Dai, "Exact solution of the Schrödinger equation for the modified Kratzer potential plus a ring-shaped potential by the Nikiforov-Uvarov method," *Physica Scripta. An International Journal for Experimental and Theoretical Physics*, vol. 75, no. 3, pp. 274–277, 2007.

- [14] A. N. Ikot, E. Olgar, and H. Hassanabadi, "The analytical solutions of the Schrödinger equation with generalized hulten plus a new ring shaped like potential," *Gazi University Journal of Science*, vol. 29, no. 4, pp. 937–946, 2016.
- [15] A. N. Ikot, I. O. Akpan, T. M. Abbey, and H. Hassanabadi, "Exact Solutions of Schrödinger Equation with Improved Ring-Shaped Non-Spherical Harmonic Oscillator and Coulomb Potential," *Communications in Theoretical Physics*, vol. 65, no. 5, pp. 569–574, 2016.
- [16] A. N. Ikot, T. M. Abbey, E. O. Chukwuocha, and M. C. Onyeaju, "Solutions of the Schrödinger equation for pseudo-Coulomb potential plus a new improved ring-shaped potential in the cosmic string space-time," *Canadian Journal of Physics*, vol. 94, no. 5, pp. 517–521, 2016.
- [17] G. Lévai, "SUSYQM and other symmetries in quantum mechanics," *Journal of Physics A: Mathematical and General*, vol. 37, no. 43, pp. 10179–10191, 2004.
- [18] A. N. Ikot, S. Zarrinkamar, S. Zare, and H. Hassanabadi, "Relativistic Dirac-attractive radial problem with Yukawa-like tensor interaction via SUSYQM," *Chinese Journal of Physics*, vol. 54, no. 6, pp. 968–977, 2016.
- [19] R. Butt, A. Khare, and U. P. Sukhatme, "Supersymmetry, shape invariance, and exactly solvable potentials," *American Journal of Physics*, vol. 56, pp. 163–168, 1988.
- [20] A. D. Alhaidari, "An extended class of L^2 -series solutions of the wave equation," *Annals of Physics*, vol. 317, no. 1, pp. 152–174, 2005.
- [21] H. Bahlouli and A. D. Alhaidari, "Extending the class of solvable potential:III:the hyperbolic single wave," *Physica Scripta*, vol. 81, 2010, 025008.
- [22] A. D. Alhaidari, H. Bahlouli, and I. A. Assi, "Solving Dirac equation using the tridiagonal matrix representation approach," *Physics Letters A*, vol. 380, no. 18–19, pp. 1577–1581, 2016.
- [23] I. A. Assi, H. Bahlouli, and A. D. Alhaidari, "Solvable potentials for the 1D Dirac equation using the tridiagonal matrix representations," in *Proceedings of the 5th Saudi International Meeting on Frontiers of Physics, SIMFP 2016*, Saudi Arabia, February 2016.
- [24] A. F. Nikiforov and V. B. Uvarov, *Special Functions of Mathematical Physics*, Birkhäuser, Basel, Switzerland, 1988.
- [25] A. Ikot, E. Maghsoodi, E. Ibanga, E. Ituen, and H. Hassanabadi, "Bound States of the Dirac Equation for Modified Mobius Square Potential Within the Yukawa-Like Tensor Interaction," *Proceedings of the National Academy of Sciences India Section A - Physical Sciences*, vol. 86, no. 3, pp. 433–440, 2016.
- [26] A. D. Antia, A. N. Ikot, H. Hassanabadi, and E. Maghsoodi, "Bound state solutions of Klein-Gordon equation with Mobius square plus Yukawa potentials," *Indian Journal of Physics*, vol. 87, no. 11, pp. 1133–1139, 2013.
- [27] C. Berkdemir, A. Berkdemir, and R. Sever, "Polynomial Solution of the Schrödinger equation for the generalized Woods-Saxon potential," *Physical Review C: Nuclear Physics*, vol. 74, no. 3, Article ID 039902, 2006.
- [28] F. Yasuk, A. Durmus, and I. Boztosun, "Exact analytical solution to the relativistic Klein-Gordon equation with noncentral equal scalar and vector potentials," *Journal of Mathematical Physics*, vol. 47, no. 8, Article ID 082302, 082302, 8 pages, 2006.
- [29] C. Y. Chen, F. L. Lu, D. S. Sun, Y. You, and S. H. Dong, "Exact solutions to a class of differential and some new mathematical properties for the universal associated-legendre polynomials," *Appl.Math.Lett.*40(2015)90.
- [30] D. S. Sun, Y. You, F. L. Lu, C. Y. Chen, and S. H. Dong, "The quantum characteristics of a class of complicated double ring shaped non-central potential," *Physica Scripta*, vol. 89, 2014, 045002.
- [31] C. Y. Chen, F. L. Lu, D. S. Sun, and S. H. Dong, "Analytical solutions of the double ring shaped Coulomb potential in quantum mechanics," *Chinese Physics B*, vol. 22, Article ID 100302, 2013.
- [32] C. Y. Chen, F. L. Lu, and D. S. Sun, "Relativistic scattering states of Coulomb plus a new ring shaped potential," *Communications in Theoretical Physics*, vol. 45, p. 889, 2016.
- [33] L. Y. Wang, X. Y. Gu, Z. Q. Ma, and S. H. Dong, "Exact solutions to D -dimensional Schrödinger equation with a pseudoharmonic oscillator," *Foundations of Physics Letters*, vol. 15, no. 6, pp. 569–576, 2002.
- [34] S. H. Dong, "The realization of dynamic group for the pseudo-harmonic oscillator," *Appl.Math.Lett.*, vol. 16, p. 199, 2013.
- [35] H. Bateman et al., *Higher Transcendental Functions*, vol. 2, McGraw-Hill, New York, NY, USA, 1955.
- [36] J. D. Louck, "Theory Of Angular Momentum in N -Dimensional Space," in *Los Alamos Scientific Lab.N.Mex*, 1960, No.LA-2451.
- [37] I. A. Assi, A. J. Sous, and A. N. Ikot, "Using the AIM for solving the non-relativistic wave equation for a new class of infinite one-dimensional well with non-flat bottom," *The European Physical Journal Plus*, vol. 132, no. 12, article no. 525, 2017.
- [38] F. J. Ferreira and F. V. Prudente, "Pekeris approximation—another perspective," *Physics Letters A*, vol. 377, no. 42, pp. 3027–3032, 2013.
- [39] S. I. Zlatev, *Pekeris-type approximation for the l -wave in a Pöschl-Teller potential*, 2013.
- [40] N. M. Temme, *Special Functions: An Introduction to Classical Functions of Mathematical Physics*, John Wiley and Sons, New York, NY, USA, 1996.
- [41] W. Magnus, F. Onerhetttinger, and R. P. Soni, *Formulas and Theorem for the special Functions of Mathematical Physics*, Springer, Berlin, 1966.
- [42] J. Griffiths David, *Introduction to quantum mechanics*, Cambridge University Press, 2016.
- [43] P. Q. Wang, L. H. Zhang, C. S. Jia, and J. Y. Liu, "Equivalence of the three empirical potential energy models for diatomic molecules," *Journal of Molecular Spectroscopy*, vol. 274, 5 pages, 2012.

Research Article

Spinors and Rodrigues Representations Associated with Orthogonal Polynomials

Zahra Bakhshi 

Department of Physics, Faculty of Basic Sciences, Shahed University, Tehran, Iran

Correspondence should be addressed to Zahra Bakhshi; z.bakhshi@shahed.ac.ir

Received 26 December 2017; Revised 18 March 2018; Accepted 26 March 2018; Published 20 May 2018

Academic Editor: Shi-Hai Dong

Copyright © 2018 Zahra Bakhshi. This is an open access article distributed under the Creative Commons Attribution License, which permits unrestricted use, distribution, and reproduction in any medium, provided the original work is properly cited. The publication of this article was funded by SCOAP³.

An effective approach is presented to produce Schrödinger-like equation for the spinor components from Dirac equation. Considering electrostatic potential as a constant value yields a second-order differential equation that is comparable with the well-known solvable models in the nonrelativistic quantum mechanics for the certain bound state energy spectrum and the well-known potentials. By this comparison, the gauge field potential and the relativistic energy can be written by the nonrelativistic models and the spinors will be related to the orthogonal polynomials. It has also shown that the upper spinors wave functions based on the orthogonal polynomials can be given in terms of the Rodrigues representations. Association with the Rodrigues representations of orthogonal polynomials has also been investigated in the lower spinor components, since they are related to the upper spinor components according to first-order differential equation that is attained from Dirac equation.

1. Introduction

In recent years, there has been a developing interest in search for exactly solvable systems in nonrelativistic and relativistic quantum mechanics. The expression exactly solvable means the eigenvalues and the eigenfunctions of the Hamiltonian operator of the physical system can be derived analytically in closed form. Solvable models are noteworthy because understanding of physics can only be brought with such solutions. Moreover, exact solutions are valuable tools for testing and improving numerical methods introduced to solve problems physically more interesting [1]. Since relativistic extensions of the exact solvable potentials are very useful to study the relativistic effects, various methods were employed to obtain the exact solution of the problem. Point canonical transformation [2–4], dynamical group [5, 6], factorization method [7], supersymmetric quantum mechanics, and shape invariance [8–10] are methods among many which were used in the search for exact solutions of wave function. Also, there are a lot of investigations that show how methods used to obtain analytical solutions of the Schrödinger equation can be extended to Dirac case [11–15].

Alhaidari [11–13] applies a unitary transformation to Dirac equation such that the resulting second-order differential equation becomes Schrödinger-like equation so that comparison with the well-known nonrelativistic problems is transparent. If the electrostatic potential is assumed as a constant value, the second-order differential equation can be constituted for upper component by eliminating lower component, without applying a general local unitary transformation that eliminates the first-order derivative such as what Alhaidari has considered.

In this method, by assuming electrostatic potential as a constant value, the second-order differential equation can be compared with the well-known solvable Schrödinger equation in the nonrelativistic quantum models. The wave functions in Schrödinger equation for the well-known potentials have been obtained on the orthogonal polynomials, such as Jacobi, generalized Laguerre, and Hermite polynomials and the energy eigenvalues spectrum can be accessible for each case. By comparing the second-order differential equation that has been obtained from Dirac equation with Schrödinger equation for the well-known potential such as Scarff-II, Pöshel-Teller, Möse, 3D-oscillator, and shift-oscillator

potentials, the gauge field potential can be written based on the well-known superpotentials that are related to the mentioned potentials. Therefore, the second-order differential is transformed to the solvable models with the exact solutions; it means that the relativistic energy eigenvalues can be gotten based on the nonrelativistic models, and also the spinors will be related to the orthogonal polynomials according to the nonrelativistic models. Then, Rodrigues representations and the differential equation of them are calculated for orthogonal polynomials. Moreover, the second-order differential equation also can be considered as a product of two first-order differential operators and the spinor wave function related to the differential equation that is expressed in terms of Rodrigues representations related to the orthogonal polynomials. Therefore, the solution of second-order differential equation can be considered with the determined relativistic energy and association with Rodrigues representations can be gotten for each orthogonal polynomial.

This paper is organized as followed: In Section 2, by using the point canonical transformations, the second-order differential equation is constituted with the gauge field potential and the energy spectrum that will be introduced based on the nonrelativistic models. Then, the association of Rodrigues representation with orthogonal polynomials is shown in the Sections 3, 4, and 5 for Jacobi, generalized Laguerre, and Hermite polynomials, respectively. In each section, all of the gauge field potentials are considered to have the ability to constitute the solvable models with the certain energy eigenvalues, for each orthogonal polynomial. Therefore, in the each section, Rodrigues representations of the orthogonal polynomials have been calculated for some gauge field potentials. In Section 6, the paper ends with a brief conclusion.

2. The Three-Dimensional Dirac Equation for a Free Structure

Particle of spin 1/2 reads $(i\hbar\gamma^\mu\partial_\mu - mc)\Phi = 0$, where m is the rest mass of the particle, c is the speed of light, and Φ is a four-component wave function. The four matrices $\{\gamma^\mu\}_{\mu=0}^3$ are given the following standard representation [16]:

$$\begin{aligned}\gamma^0 &= \begin{pmatrix} I & 0 \\ 0 & -I \end{pmatrix}, \\ \vec{\gamma} &= \begin{pmatrix} 0 & \vec{\sigma} \\ -\vec{\sigma} & 0 \end{pmatrix},\end{aligned}\quad (1)$$

where I is the 2×2 unit matrix and σ are the usual 2×2 Pauli spin matrices. In atomic units ($m = e = \hbar = 1$), Dirac equation reads $(i\gamma^\mu\partial_\mu - \alpha^{-1})\Phi = 0$, where $\alpha = \hbar/mc = 1/c$ is the Compton wavelength of the particle. In the presence of the electromagnetic potential, $A_\mu = (A_0, \vec{A})$, gauge invariant coupling to the charged spinor is accomplished by the minimal substitution $\partial_\mu \rightarrow \partial_\mu + i\alpha A_\mu$, which transforms free Dirac equation into

$$[i\gamma^\mu(\partial_\mu + i\alpha A_\mu) - \alpha^{-1}]\Phi = 0. \quad (2)$$

For time independent potential, (2) gives the following matrix representation of Dirac Hamiltonian (in units of $mc^2 = \alpha^2$) [14]:

$$H = \begin{pmatrix} \alpha^2 A_0 + 1 & -i\alpha\vec{\sigma} \cdot \vec{\nabla} + \alpha\vec{\sigma} \cdot \vec{A} \\ -i\alpha\vec{\sigma} \cdot \vec{\nabla} + \alpha\vec{\sigma} \cdot \vec{A} & \alpha^2 A_0 - 1 \end{pmatrix}. \quad (3)$$

Taking into consideration gauge invariance, the form of electromagnetic potential for static charge distribution with spherical symmetry is

$$(A_0, \vec{A}) = (v(r), \hat{r}\omega(r)), \quad (4)$$

where \hat{r} is radial unit vector; $v(r)$ and $\omega(r)$ are electrostatic potential and gauge field potential, respectively. By substituting the two off-diagonal terms $\alpha\vec{\sigma} \cdot \vec{A}$ by $\pm i\alpha\vec{\sigma} \cdot \vec{A}$ in (3), the Hamiltonian leads to the following two-component radial Dirac equation [17]:

$$\begin{aligned}& \begin{pmatrix} \alpha^2 v(r) + 1 & \alpha \left(\frac{k}{r} + \omega(r) - \frac{d}{dr} \right) \\ \alpha \left(\frac{k}{r} + \omega(r) + \frac{d}{dr} \right) & \alpha^2 v(r) - 1 \end{pmatrix} \begin{pmatrix} \varphi(r) \\ \theta(r) \end{pmatrix} \\ &= \varepsilon \begin{pmatrix} \varphi(r) \\ \theta(r) \end{pmatrix},\end{aligned}\quad (5)$$

where ε are the relativistic energy eigenvalues and k is the spin-orbit coupling parameter defined as $k = \pm(j+1/2)$ for $l = j \pm 1/2$. Equation (5) gives two coupled first-order differential equations for the radial spinor components. By eliminating lower spinor component and by assuming the electrostatic potential $v(r)$ to be a constant value η , the second-order differential equation can be gotten for upper spinor wave function as

$$\begin{aligned}-\frac{d^2\varphi}{dr^2} + \left[\left(\omega(r) + \frac{k}{r} \right)^2 - \left(\frac{d\omega}{dr} - \frac{k}{r^2} \right) \right. \\ \left. - \left(\frac{(\alpha^2\eta - \varepsilon)^2 - 1}{\alpha^2} \right) \right] \varphi(r) = 0.\end{aligned}\quad (6)$$

Equation (5) also gives the lower spinor component in terms of the upper component as follows:

$$\theta(r) = \left[\alpha\eta - \left(\frac{\varepsilon + 1}{\alpha} \right) \right]^{-1} \left\{ \left[\omega(r) + \frac{k}{r} \right] \varphi(r) + \frac{d\varphi}{dr} \right\}. \quad (7)$$

By comparing (6) with the solvable Schrödinger equation in the nonrelativistic models, the relation can be considered between the well-known potential in the nonrelativistic quantum models and the gauge field potential in the relativistic system as $V_m(r) = (\omega(r) + k/r)^2 - (d\omega/dr - k/r^2)$. Also, nonrelativistic energy eigenvalues can be related to the relativistic energy eigenvalues as $E = ((\alpha^2\eta - \varepsilon)^2 - 1)/\alpha^2$. So, the gauge field potential and the relativistic energy due to solvability of Dirac equation based on the nonrelativistic quantum mechanics are easily available.

3. Association of Rodrigues Representation with Jacobi Polynomials

Let us consider the gauge field potentials where their wave functions are related to Jacobi polynomials such as Pöschl-Teller potential $\omega^{(1)}(r) = -A \coth r + B/\sinh r - k/r$ and Scarf-II potential $\omega^{(2)}(r) = -A \tanh r - B/\cosh r - k/r$, where A and B are real parameters. For each potential, respectively, (6) gives the following second-order differential equations for upper spinor component:

$$-\frac{d^2\varphi_{n,m}^{(1)}(r)}{dr^2} + \left[A^2 + \frac{(B^2 - A^2 + A)}{\sinh^2 r} + \frac{(B - 2AB) \cosh r}{\sinh^2 r} \right] \varphi_{n,m}^{(1)}(r) = \left[\frac{(\alpha^2 \eta - \varepsilon)^2 - 1}{\alpha^2} \right] \varphi_{n,m}^{(1)}(r), \quad (8)$$

$$-\frac{d^2\varphi_{n,m}^{(2)}(r)}{dr^2} + \left[A^2 + \frac{(B^2 - A^2 + A)}{\cosh^2 r} + \frac{(2AB - B) \sinh r}{\cosh^2 r} \right] \varphi_{n,m}^{(2)}(r) = \left[\frac{(\alpha^2 \eta - \varepsilon)^2 - 1}{\alpha^2} \right] \varphi_{n,m}^{(2)}(r), \quad (9)$$

where $A = (\lambda + \gamma + 2m - 1)/2$ and $B = (\gamma - \lambda)/2$ such that $\lambda, \gamma > -1$ in (8) and $A = m + \lambda - 1/2$ and $B = \gamma/2$ such that $\lambda > -1$ and $-\infty > \gamma > +\infty$ in (9). There will be the well-known nonrelativistic energy spectrum as $E_{n,m}^{(1)} = (\lambda + \gamma + n + m)(m - n - 1)$ and $E_{n,m}^{(2)} = (2\lambda + n + m)(n - m + 1)$ for Pöschl-Teller potential and Scarf-II potential, respectively. As mentioned before, they can be used to calculate relativistic energy spectrum of Dirac equation as the following forms:

$$\varepsilon_n^{(1)} = \alpha^2 \eta \mp \left[-\alpha^2 (\lambda + \gamma + n + m)(n - m + 1) + 1 \right]^{1/2}, \quad (10)$$

$$\varepsilon_n^{(2)} = \alpha^2 \eta \mp \left[-\alpha^2 (2\lambda + n + m)(n - m + 1) + 1 \right]^{1/2}.$$

The bound states wave functions of the nonrelativistic problem [6] are mapped into the following upper spinor components wave functions:

$$\varphi_{n,m}^{(1)}(x) \propto (x-1)^{(2\lambda+2m-1)/4} \times (x+1)^{(2\gamma+2m-1)/4} \cdot P_n^{(\lambda+m-1, \gamma+m-1)}(x), \quad (11)$$

$$\varphi_{n,m}^{(2)}(x) \propto (1+x^2)^{-1/2} \times \exp\left(\frac{\gamma}{2} \tanh^{-1} x\right) \cdot P_n^{(i(\gamma/2)+m+\lambda-1/4, -i(\gamma/2)+m+\lambda-1/4)}(x), \quad (12)$$

where $P_n^{(\mu, \nu)}(x)$ is Jacobi polynomial with $\mu, \nu > -1$, and $x = \cosh r$, $\mu = \lambda + m - 1$, and $\nu = \gamma + m - 1$ in (11) and $x = \sinh r$, $\mu + i(\gamma/2) + m + \lambda - 1/4$, and $\nu = -i(\gamma/2) + m + \lambda - 1/4$ in (12). By substituting upper spinor components (11) and (12) into (7) and using recursion properties of Jacobi polynomials, lower spinor components are given as

$$\begin{aligned} \theta_{n,m}^{(1)}(x) &\propto \left(\frac{1}{\alpha} \mp \left[\frac{1}{\alpha^2} - n^2 - n(\lambda + \gamma + 2m - 1) \right]^{1/2} \right)^{-1} \\ &\times \left(\left[nx - \left(\frac{\lambda - \gamma}{2n + 2m + \lambda + \gamma - 2} \right) \right] (x^2 - 1)^{-1/2} \right. \\ &\cdot \varphi_{n,m}^{(1)}(x) - \left[\frac{2(n + m + \lambda - 1)(n + m + \gamma - 1)}{2n + 2m + \lambda + \gamma - 2} \right] \\ &\cdot (x^2 - 1)^{-1/2} \varphi_{n-1,m}^{(1)}(x) \Big), \\ \theta_{n,m}^{(2)}(x) &\propto \left(\frac{1}{\alpha} \mp \left[\frac{1}{\alpha^2} + (n - m + 1)(m - n + 2\lambda - 2) \right]^{1/2} \right)^{-1} \\ &\times \left(\left[-\left(n + \lambda + \frac{3}{4} \right) x + \frac{\gamma}{2} \left(\frac{2n - 3m - \lambda + 3}{-n + 2m - 2} \right) \right] \right. \\ &\cdot (x^2 + 1)^{-1/2} + \frac{\gamma}{2} (1 - x)^{-1} (x^2 + 1)^{1/2} \varphi_{n,m}^{(2)}(x) \\ &- \left[\frac{i(-n + 2m + \lambda - 2)^2 + \gamma^2/8}{-n + 2m + \lambda - 2} \right] (x^2 + 1)^{-1/2} \\ &\cdot \varphi_{n-1,m}^{(2)}(x) \Big). \end{aligned} \quad (13)$$

Raising and lowering operators $B_{\pm}(m) = \pm d/dr + W_m(x(r))$, where the superpotential $W_m(x(r))$ satisfies in the Riccati equation $V_m = W_m^2 \pm W_m'$, can be written as the following forms according to Pöschl-Teller and Scarf-II potentials, respectively:

$$B_+^{(1)} = \frac{d}{dr} + \left[-A \coth r + \frac{B}{\sinh r} \right], \quad (14)$$

$$B_-^{(1)} = -\frac{d}{dr} + \left[-A \coth r + \frac{B}{\sinh r} \right],$$

$$B_+^{(2)} = \frac{d}{dr} + \left[-A \tanh r - \frac{B}{\cosh r} \right], \quad (15)$$

$$B_-^{(2)} = -\frac{d}{dr} + \left[-A \tanh r + \frac{B}{\cosh r} \right].$$

It is obvious that the second-order differential equations can always be considered in a factorization form as a product of a pair of linear differential operators (14) and (15). Therefore,

$$\begin{aligned} & B_+^{(1),(2)}(m) B_-^{(1),(2)}(m) \varphi_{n,m}^{(1),(2)}(r) \\ &= E^{(1),(2)}(n, m) \varphi_{n,m}^{(1),(2)}(r), \\ & B_-^{(1),(2)}(m) B_+^{(1),(2)}(m) \varphi_{n,m-1}^{(1),(2)}(r) \\ &= E^{(1),(2)}(n, m) \varphi_{n,m-1}^{(1),(2)}(r). \end{aligned} \quad (16)$$

In the above equations, for a given n , the operator $B_+(m)$ raises the index m while the operator $B_-(m)$ lowers it. We can also obtain the highest state $\varphi_{n,n}$ by solving the first-order differential equation $B_+(n+1)\varphi_{n,n}(r) = 0$ because the nonrelativistic energy spectrum $E(n, m)$ vanishes for $m = n + 1$ [10], since by introducing a new function as $\varphi_{n,m}(x) = A^{1/4}(x)W^{1/2}(x)\psi_{n,m}(x)$ and changing the variable $dx/dr = \sqrt{A(x)}$ Schrödinger equation (6) has been obtained from the general form associated with second-order differential equation in terms of master function $A(x)$ and the wave function $W(x)$ as follows [18–20]:

$$\begin{aligned} & A(x) \ddot{\psi}_{n,m}(x) + \frac{(A(x)W(x))'}{W(x)} \dot{\psi}_{n,m}(x) \\ &+ \left[-\frac{1}{2}(n^2 + n - m^2) \ddot{A}(x) \right. \\ &+ (m-n) \left(\frac{A(x)\dot{W}(x)}{W(x)} \right)' - \frac{m^2 \dot{A}(x)^2}{4A(x)} \\ &\left. - \frac{m \dot{A}(x)\dot{W}(x)}{2W(x)} \right] \psi_{n,m}(x) = 0, \end{aligned} \quad (17)$$

where $\psi_{n,m}(x)$ is Rodrigues representation of the orthogonal polynomials in (17). For a positive integer n , $\psi_{n,m}(x)$ as Rodrigues representation is given by

$$\begin{aligned} \psi_{n,m}(x) &= (-1)^m A^{m/2}(x) \left(\frac{d}{dx} \right)^m \psi_n(x), \\ & m = 0, 1, 2, \dots, n, \end{aligned} \quad (18)$$

where

$$\psi_n(x) = \frac{N}{W(x)} \left(\frac{d}{dx} \right)^n (A^n(x)W(x)), \quad (19)$$

with N which is normalization constant. So, for each case of the gauge field potentials, the Rodrigues representations of upper and lower spinors and differential equations associated with them are available. Furthermore, it can be shown that they are clear examples of connection between Jacobi polynomials and Rodrigues representations in Dirac equation. Thus, the wave functions $\psi_{n,m}(x)$ are related to the upper spinors as the following forms:

$$\psi_{n,m}^{(1)}(x) = (x-1)^{-(\lambda/2+1/4)} (x+1)^{-(\gamma/2+1/4)} \varphi_{n,m}^{(1)}(x), \quad (20)$$

for $A^{(1)}(x) = x^2 - 1$ and $W^{(1)}(x) = (x-1)^\lambda (x+1)^\gamma$ in Pöschl-Teller potential and

$$\begin{aligned} & \psi_{n,m}^{(2)}(x) \\ &= (x^2 + 1)^{-(\lambda/2+1/4)} \exp\left(-\frac{\gamma}{2} \tan^{-1}(x)\right) \varphi_{n,m}^{(2)}(x), \end{aligned} \quad (21)$$

when $A^{(2)}(x) = x^2 + 1$ and $W^{(2)}(x) = (x^2 + 1)^\lambda \exp(\gamma \tan^{-1}(x))$ in Scarf-II potential. Since the lower spinors can be connected to the upper spinors according to (13), therefore, Rodrigues representations of upper spinors also can be associated with lower spinors. If the wave function $\Theta_{n,m}(x)$ is introduced for lower spinor $\theta_{n,m}(x)$, it can be written based on Rodrigues representations $\psi_{n,m}(x)$. The wave function $\Theta_{n,m}(x)$ that is connected to the lower spinors $\theta_{n,m}(x)$ can be written as follows for Pöschl-Teller and Scarf-II potentials, proportionately:

$$\begin{aligned} & \Theta_{n,m}^{(1)}(x) \propto \left(\frac{1}{\alpha} \right. \\ & \left. \mp \left[\frac{1}{\alpha^2} - n^2 - n(\lambda + \gamma + 2m - 1) \right]^{1/2} \right)^{-1} \\ & \times \left(\left[nx - \left(\frac{\lambda - \gamma}{2n + 2m + \lambda + \gamma - 2} \right) \right] (x^2 - 1)^{-1/2} \right. \\ & \cdot \psi_{n,m}^{(1)}(x) - \left[\frac{2(n+m+\lambda-1)(n+m+\gamma-1)}{2n+2m+\lambda+\gamma-2} \right] \\ & \cdot (x^2 - 1)^{-1/2} \psi_{n-1,m}^{(1)}(x) \Big), \\ & \Theta_{n,m}^{(2)}(x) \propto \left(\frac{1}{\alpha} \right. \\ & \left. \mp \left[\frac{1}{\alpha^2} + (n-m+1)(m-n+2\lambda-2) \right]^{1/2} \right)^{-1} \\ & \times \left(\left[-\left(n + \lambda + \frac{3}{4} \right) x + \frac{\gamma}{2} \left(\frac{2n-3m-\lambda+3}{-n+2m-2} \right) \right] \right. \\ & \cdot (x^2 + 1)^{-1/2} + \frac{\gamma}{2} (1-x)^{-1} (x^2 + 1)^{1/2} \psi_{n,m}^{(2)}(x) \\ & - \left[\frac{i(-n+2m+\lambda-2)^2 + \gamma^2/8}{-n+2m+\lambda-2} \right] (x^2 + 1)^{-1/2} \\ & \cdot \psi_{n-1,m}^{(2)}(x) \Big). \end{aligned} \quad (22)$$

The wave functions $\psi_{n,m}(x)$ can be also satisfied in the second-order differential equations for each potential, correlatively:

$$\begin{aligned} & (x^2 - 1) \ddot{\psi}_{n,m}^{(1)}(x) + \left[\frac{1}{2} (1 - \gamma - \lambda) x^3 + \frac{1}{2} (\gamma - \lambda) x^2 \right. \\ & \left. - 1 \right] \dot{\psi}_{n,m}^{(1)}(x) + \left[(1 - m)(\lambda + \gamma + m) x^2 \right. \end{aligned}$$

$$\begin{aligned}
& + (m-2)(\gamma-\lambda)x + \frac{(\lambda+\gamma+n+m)(m-n-1)}{x^2-1} \\
& + \left[\frac{(\lambda+\gamma+2m-1)^2}{2} - m+1 \right] \psi_{n,m}^{(1)}(x) = 0,
\end{aligned} \tag{23}$$

$$\begin{aligned}
& (x^2+1)\ddot{\psi}_{n,m}^{(2)}(x) + [2(\lambda+1)x+\gamma]\dot{\psi}_{n,m}^{(2)}(x) \\
& + \left[(m^2-n^2-n) + 2\lambda(m-n) \right. \\
& \left. - \frac{(m^2+2m\lambda)x^2-\gamma mx}{x^2+1} \right] \psi_{n,m}^{(2)}(x) = 0.
\end{aligned} \tag{24}$$

Rodrigues representations of the associated polynomials $\psi_{n,m}(x)$ are given by

$$\begin{aligned}
\psi_{n,m}^{(1)}(x) &= (-1)^m (x^2-1)^{m/2} \left(\frac{d}{dx} \right)^m \psi_n^{(1)}(x), \\
& m = 0, 1, 2, \dots, n,
\end{aligned} \tag{25}$$

$$\begin{aligned}
\psi_{n,m}^{(2)}(x) &= (-1)^m (x^2+1)^{m/2} \left(\frac{d}{dx} \right)^m \psi_n^{(2)}(x), \\
& m = 0, 1, 2, \dots, n,
\end{aligned}$$

where $\psi_n(x)$ satisfies in Jacobi differential equation whose Rodrigues representations, respectively, are

$$\begin{aligned}
\psi_n^{(1)}(x) &= N(x-1)^{-\lambda}(x+1)^{-\gamma} \left(\frac{d}{dx} \right)^n \\
& \cdot \left((x-1)^{n+\lambda}(x+1)^{n+\gamma} \right),
\end{aligned} \tag{26}$$

$$\begin{aligned}
\psi_n^{(2)}(x) &= N(x^2+1)^{-\lambda} \exp(-\gamma \tan^{-1}x) \left(\frac{d}{dx} \right)^n \\
& \cdot \left((x^2+1)^{n+\lambda} \exp(-\gamma \tan^{-1}x) \right),
\end{aligned} \tag{27}$$

where N is a normalization constant. Since the wave functions $\Theta_{n,m}(x)$ connected to the lower spinor $\theta_{n,m}(x)$ that have been calculated based on upper spinors $\varphi_{n,m}(x)$ and Rodrigues representations of upper spinors can be generalized to the wave function $\Theta_{n,m}(x)$ as $\psi_{n,m}(x)$ and $\psi_{n-1,m}(x)$, therefore, the above Rodrigues representation can also be related to the lower spinor components.

4. Association of Rodrigues Representation with Generalized Laguerre Polynomials

When Mörse potential $\omega^{(1)}(r) = -(\gamma/2)e^{-r} - m - \lambda/2 + 1/2 - k/r$ and 3-dimensional oscillator potential $\omega^{(2)}(r) = (\gamma/4)r - (\lambda+m-1/2)(2/r) - k/r$ are considered as the gauge field potentials, the upper spinor components are associated with generalized Laguerre polynomials. So, the second-order

differential equations for the upper spinor components are written according to (6):

$$\begin{aligned}
& - \frac{d^2 \varphi_{n,m}^{(1)}(r)}{dr^2} + \left[\frac{\gamma^2}{4} e^{-2r} + \gamma \left(m + \frac{\lambda}{2} - 1 \right) e^{-r} \right] \\
& \cdot \varphi_{n,m}^{(1)}(r) = \left[\frac{(\alpha^2 \eta - \varepsilon)^2 - 1}{\alpha^2} \right] \varphi_{n,m}^{(1)}(r), \\
& - \frac{d^2 \varphi_{n,m}^{(2)}(r)}{dr^2} + \left[\frac{\gamma^2}{16} r^2 \right. \\
& \left. + \left(\lambda + m - \frac{1}{2} \right) \left(\lambda + m - \frac{3}{2} \right) \frac{1}{r^2} \frac{\gamma}{2} (\lambda + m) \right] \\
& \cdot \varphi_{n,m}^{(2)}(r) = \left[\frac{(\alpha^2 \eta - \varepsilon)^{(2)} - 1}{\alpha^2} \right] \varphi_{n,m}^{(2)}(r).
\end{aligned} \tag{28}$$

According to the nonrelativistic energy spectrum $E_{n,m}^{(1)} = -(n-m+1)(\lambda+n+m)$ and $E_{n,m}^{(2)} = \gamma(n-m+1)$, the relativistic energy spectrums are obtained as

$$\begin{aligned}
\varepsilon_n^{(1)} &= \alpha^2 \eta \mp \left[-\alpha^2 (n-m+1)(\lambda+n+m) + 1 \right]^{1/2}, \\
\varepsilon_n^{(2)} &= \alpha^2 \eta \mp \left[-\alpha^2 \gamma (n-m+1) + 1 \right]^{1/2}.
\end{aligned} \tag{29}$$

Second-order differential equations (28) are due to the solutions based on the generalized Laguerre polynomials as upper spinor wave functions

$$\begin{aligned}
\varphi_{n,m}^{(1)}(x) &\propto \left(\frac{\gamma}{x} \right)^{-(n+\lambda/2+1/2)} \\
&\times \exp\left(-\frac{\gamma}{2x} \right) L_n^{(-2n-\lambda-1)} \left(\frac{\gamma}{x} \right),
\end{aligned} \tag{30}$$

$$\begin{aligned}
\varphi_{n,m}^{(2)}(x) &\propto (\gamma x)^{(\lambda+m-1/2)/2} \\
&\times \exp\left(-\frac{\gamma x}{2} \right) L_n^{(\lambda+m-1/4)}(\gamma x),
\end{aligned} \tag{31}$$

where $L_n^\alpha(x)$ is generalized Laguerre polynomial with $\alpha > -1$. In the upper spinor (30), $x = e^r$ and $\alpha = -2n-\lambda-1$ and, in the other upper spinor (31), $x = r^2/4$ and $\alpha = \lambda+m-1/4$. Lower spinor components can be attained by (7) for each potential

$$\begin{aligned}
\theta_{n,m}^{(1)}(x) &\propto \left(\frac{1}{\alpha} \right. \\
&\left. \mp \left[\frac{1}{\alpha^2} + (n-m+1)(-m-n-\lambda) \right]^{1/2} \right)^{-1} \\
&\times \left[\frac{(-2m-\lambda+1) - (n-m+1)}{\gamma} \right] x \varphi_{n-1,m}^{(1)}(x),
\end{aligned}$$

$$\begin{aligned} \theta_{n,m}^{(2)}(x) &\propto \left(\frac{1}{\alpha} \mp \left[\frac{1}{\alpha^2} + \gamma(n-m+1) \right]^{1/2} \right)^{-1} \\ &\times x^{-1/2} \left[(n-m+1) \varphi_{n,m}^{(2)}(\gamma x) \right. \\ &\left. - \left(n + \lambda + \frac{3}{4} \right) \varphi_{n-1,m}^{(2)}(\gamma x) \right]. \end{aligned} \quad (32)$$

As mentioned in pervious section, the raising and lowering B_+ and B_- operators based on the superpotentials are given as

$$\begin{aligned} B_+^{(1)} &= \frac{d}{dr} - \frac{\gamma}{2} e^{-r} - m - \frac{\lambda}{2} + \frac{1}{2}, \\ B_-^{(1)} &= -\frac{d}{dr} - \frac{\gamma}{2} e^{-r} - m - \frac{\lambda}{2} + \frac{1}{2}, \\ B_+^{(2)} &= \frac{d}{dr} + \frac{\gamma}{4} r - \left(\lambda + m - \frac{1}{2} \right) \frac{2}{r}, \\ B_-^{(2)} &= -\frac{d}{dr} + \frac{\gamma}{4} r - \left(\lambda + m - \frac{1}{2} \right) \frac{2}{r}. \end{aligned} \quad (33)$$

The pair of linear differential operators can factorize Schrödinger equation for each potential. Similar to the pervious section, in Mörse potential, if $A^{(1)}(x) = x^2$ and $W^{(1)}(x) = x^\lambda e^{-\gamma/x}$, the wave function $\psi_{n,m}^{(1)}(x)$ is written based on upper spinor as

$$\psi_{n,m}^{(1)}(x) = \left(\frac{\exp(\gamma/2x)}{x} \right) \varphi_{n,m}^{(1)}(x), \quad (34)$$

and, in 3-dimensional oscillator potential, when $A^{(2)}(x) = x$ and $W^{(2)}(x) = x^\lambda e^{-\gamma x}$, the wave function $\psi_{n,m}^{(2)}(x)$ is obtained as

$$\psi_{n,m}^{(2)}(x) = x^{-(\lambda/2+1/4)} \exp\left(\frac{\gamma x}{2}\right) \varphi_{n,m}^{(2)}(x). \quad (35)$$

Therefore, they are also related to the generalized Laguerre polynomials. It is clear that both of them are examples of associating generalized Laguerre polynomial with Rodrigues representation in Dirac equation. Also, Rodrigues representation of lower spinors $\theta_{n,m}(x)$ that are called $\Theta_{n,m}(x)$ will be in the following forms based on $\psi_{n,m}(x)$ and $\psi_{n-1,m}(x)$, for Mörse and 3-dimensional oscillator potentials:

$$\begin{aligned} \Theta_{n,m}^{(1)}(x) &\propto \left(\frac{1}{\alpha} \mp \left[\frac{1}{\alpha^2} + (n-m+1)(-m-n-\lambda) \right]^{1/2} \right)^{-1} \\ &\times x \left[-\frac{(m+n+\lambda)}{\gamma} \right] \psi_{n-1,m}^{(1)}(x), \\ \Theta_{n,m}^{(2)}(x) &\propto \left(\frac{1}{\alpha} \mp \left[\frac{1}{\alpha^2} + \gamma(n-m+1) \right]^{1/2} \right)^{-1} \\ &\times x^{(\lambda+1)/2} \left[(n-m+1) \psi_{n,m}^{(2)}(x) \right. \\ &\left. + \left(n + \lambda + \frac{3}{4} \right) \psi_{n-1,m}^{(2)}(x) \right]. \end{aligned} \quad (36)$$

The wave functions $\psi_{n,m}(x)$ can be also satisfied in second-order differential equations for each potential, proportionately:

$$\begin{aligned} x^2 \ddot{\psi}_{n,m}^{(1)}(x) + (\lambda x + \gamma + 2) \dot{\psi}_{n,m}^{(1)}(x) + \left(-\frac{m\gamma}{x} + m^2 \right. \\ \left. - m - 2n^2 - n(\lambda + 1) \right) \psi_{n,m}^{(1)}(x) = 0, \end{aligned} \quad (37)$$

$$\begin{aligned} x \ddot{\psi}_{n,m}^{(2)}(x) + \left(2 \left(\lambda + \frac{1}{2} \right) - \gamma x \right) \dot{\psi}_{n,m}^{(2)}(x) \\ + \left(\gamma \left(n - m + \frac{1}{2} \right) - \frac{\gamma \lambda}{2} \right. \\ \left. - \frac{(m-1)(2\lambda+1)}{4} x^{-1/2} \right) \psi_{n,m}^{(2)}(x) = 0. \end{aligned} \quad (38)$$

Rodrigues representations of associated polynomials $\psi_{n,m}(x)$ are given as

$$\begin{aligned} \psi_{n,m}^{(1)}(x) &= (-1)^m x^m \left(\frac{d}{dx} \right)^m \psi_n^{(1)}(x), \\ & \quad m = 0, 1, 2, \dots, n, \end{aligned} \quad (39)$$

$$\begin{aligned} \psi_{n,m}^{(2)}(x) &= (-1)^m x^{m/2} \left(\frac{d}{dx} \right)^m \psi_n^{(2)}(x), \\ & \quad m = 0, 1, 2, \dots, n, \end{aligned}$$

where $\psi_n(x)$ satisfies in Laguerre differential equation whose Rodrigues representations are, respectively,

$$\begin{aligned} \psi_n^{(1)}(x) \\ = N x^{-\lambda} \exp\left(\frac{\gamma}{x}\right) \left(\frac{d}{dx} \right)^n \left(x^{2n+\lambda} \exp\left(-\frac{\gamma}{x}\right) \right), \end{aligned} \quad (40)$$

$$\psi_n^{(2)}(x) = N x^{-\lambda} \exp(\gamma x) \left(\frac{d}{dx} \right)^n \left(x^{\lambda+n} \exp(-\gamma x) \right). \quad (41)$$

The above Rodrigues representations can be also related to lower spinor components, because there are the wave function $\Theta_{n,m}(x)$ based on the wave function $\psi_{n,m}(x)$ and $\psi_{n-1,m}(x)$ according to the lower spinor components.

5. Association of Rodrigues Representation with Hermite Polynomials

The upper spinor component will be considered as Hermite polynomials, if the gauge field potential $\omega(r) = (\gamma/2)r - \lambda - k/r$ is written based on shift-oscillator potential. This upper spinor component satisfies in (6) as

$$\begin{aligned} -\frac{d^2 \varphi_{n,m}(r)}{dr^2} + \left[\left(\frac{\gamma}{2} r - \lambda \right)^2 - \frac{\gamma}{2} \right] \varphi_{n,m}(r) \\ = \left[\frac{(\alpha^2 \eta - \varepsilon)^2 - 1}{\alpha^2} \right] \varphi_{n,m}(r). \end{aligned} \quad (42)$$

For this potential, the nonrelativistic energy $E_{n,m} = \gamma(n-m+1)$ can be used in the following relativistic energy spectrum:

$$\varepsilon_n = \alpha^2 \eta \mp \left[\alpha^2 \gamma (n-m+1) + 1 \right]^{1/2}. \quad (43)$$

The upper spinor wave function based on the Hermite polynomials can be obtained from (42):

$$\varphi_{n,m}(x) \propto \exp\left(-\frac{\gamma}{4}x^2\right) \times H_n\left(\left(\frac{\gamma}{2}\right)^{1/2}x\right), \quad (44)$$

where $H_n(x)$ is Hermite polynomial. In the wave function (44) $x = r - 2\lambda/\gamma$ and $-\infty < x < +\infty$. According to (7), the lower spinor wave function is calculated as

$$\begin{aligned} \theta_{n,m}(x) \propto & \left(\frac{1}{\alpha} \mp \left[\frac{1}{\alpha^2} + \gamma(n-m+1) \right]^{1/2} \right)^{-1} \\ & \times \left[(2\gamma)^{1/2} (n-m+1) \right] \varphi_{n-1,m}(x). \end{aligned} \quad (45)$$

To factorize Schrödinger equation, there are pairs of linear differential operator as

$$\begin{aligned} B^+ &= \frac{d}{dr} + \frac{\gamma}{2}r - \lambda, \\ B^- &= -\frac{d}{dr} + \frac{\gamma}{2}r - \lambda. \end{aligned} \quad (46)$$

As mentioned before, the wave function $\psi_{n,m}(x)$ that is related to upper spinor is gotten by

$$\psi_{n,m}(x) = \exp\left(\frac{\gamma}{4}x^2\right) \varphi_{n,m}(x), \quad (47)$$

for $A(x) = 1$ and $W(x) = \exp(-(\gamma/2)x^2)$. In this potential, Hermite polynomial can be associated with Rodrigues representation in Dirac equation. Also, similar to pervious section, the wave function $\Theta_{n,m}(x)$ that is connected to lower spinor $\theta_{n,m}(x)$ can be written based on Rodrigues representation:

$$\begin{aligned} \Theta_{n,m}(x) \propto & \left(\frac{1}{\alpha} \mp \left[\frac{1}{\alpha^2} + \gamma(n-m+1) \right]^{1/2} \right)^{-1} \\ & \times \left[(2\gamma)^{1/2} (n-m+1) \right] \psi_{n-1,m}(x). \end{aligned} \quad (48)$$

The second-order differential equation for shift-oscillator potential will be

$$\ddot{\psi}_{n,m}(x) + (-\gamma x) \dot{\psi}_{n,m}(x) - \gamma(m-n) \psi_{n,m}(x) = 0, \quad (49)$$

where Rodrigues representation of the associated polynomial $\psi_{n,m}(x)$ is considered by

$$\psi_{n,m}(x) = (-1)^m \left(\frac{d}{dx} \right)^m \psi_n(x), \quad m = 0, 1, 2, \dots, n \quad (50)$$

and Rodrigues representation of $\psi_n(x)$, will be in the following form:

$$\psi_n(x) = N \exp\left(\frac{\gamma}{2}x^2\right) \left(\frac{d}{dx} \right)^n \left(\exp\left(-\frac{\gamma}{2}x^2\right) \right). \quad (51)$$

Since $\Theta_{n,m}(x)$ has been used for lower spinor $\theta_{n,m}(x)$ and it has been associated with $\psi_{n-1,m}(x)$ according to (48), therefore, (49), (50), and (51) can be considered for the lower spinor component in shift-oscillator potential.

6. Conclusion

A procedure for connecting the methods used in the analysis of exactly solvable potentials in the nonrelativistic quantum mechanics with the solution of Dirac equation has presented. A gauge field potential and the bound states energy spectrum have been defined for the Dirac equation with a constant electrostatic potential that can be constituted by a Schrödinger-like equation. Since orthogonal polynomials are considered as the solution of Schrödinger-like equation that have been obtained from Dirac equation, Rodrigues representations of the orthogonal polynomials can be associated with upper and lower spinor components.

Conflicts of Interest

The author declares that she has no conflicts of interest.

References

- [1] A. D. Alhaidari, "Exact solutions of dirac and schrödinger equations for a large class of power-law potentials at zero energy," *International Journal of Modern Physics A*, vol. 17, no. 30, p. 4551, 2002.
- [2] J. W. Dabrowska, A. Khare, and U. Sukhatme, "Explicit wave-functions for shape-invariant potentials by operator techniques," *Journal of Physics A: Mathematical and General*, vol. 21, p. L195, 1988.
- [3] G. Levai, "A search for shape-invariant solvable potentials," *Journal of Physics A: Mathematical and General*, vol. 22, no. 6, pp. 689-702, 1989.
- [4] R. De, R. Dut, and U. Sukhatme, "Mapping of shape invariant potentials under point canonical transformations," *Journal of Physics A: Mathematical and General*, vol. 25, pp. L843-L850, 1992.
- [5] Y. Alhassid, F. Gursey, and F. Iachello, "Group theory approach to scattering. II. The euclidean connection," *Annals of Physics*, vol. 167, no. 1, p. 181, 1986.
- [6] G. Levai, "Solvable potentials associated with su(1,1) algebras: a systematic study," *Journal of Physics A: Mathematical and General*, vol. 27, p. 3809, 1994.
- [7] L. Infeld and T. E. Hull, "The factorization method," *Reviews of Modern Physics*, vol. 23, no. 1, pp. 21-68, 1951.
- [8] E. Witten, "Dynamical breaking of supersymmetry," *Nuclear Physics B*, vol. 185, pp. 513-554, 1981.
- [9] L. E. Gendenshtein, "Derivation of exact spectra of the schrodinger equation by means of supersymmetry," *JETP Letters*, vol. 38, pp. 356-359, 1983.
- [10] F. Cooper, A. Khare, and U. Sukhatme, "Supersymmetry and quantum mechanics," *Physics Reports*, vol. 251, no. 5-6, pp. 267-385, 1995.
- [11] A. D. Alhaidari, "Relativistic extension of shape-invariant potentials," *Journal of Physics A: Mathematical and General*, vol. 34, p. 9827, 2001.

- [12] A. D. Alhaidari, "CORRIGENDUM: Relativistic extension of shape-invariant potentials," *Journal of Physics A: Mathematical and General*, vol. 35, p. 6207, 2002.
- [13] A. D. Alhaidari, "Solution of the Relativistic Dirac-Morse Problem," *Physical Review Letters*, vol. 87, no. 24, 2001.
- [14] H. Panahi and Z. Bakhshi, "Dirac equation and ground state of solvable potentials: supersymmetry method," *International Journal of Theoretical Physics*, vol. 50, no. 9, pp. 2811–2818, 2011.
- [15] H. Panahi and Z. Bakhshi, "Dirac equation with position-dependent effective mass and solvable potentials in the Schrödinger equation," *Journal of Physics A: Mathematical and Theoretical*, vol. 44, p. 175304, 2011.
- [16] L. H. Ryder, *Quantum Field Theory*, Cambridge University Press, Cambridge, UK, 1985.
- [17] W. Greiner, *Relativistic Quantum Mechanics*, Springer-Verlag, Berlin, Germany, 1981.
- [18] M. A. Jafarizadeh and H. Fakhri, "Calculation of the determinant of shape invariant operators," *Physics Letters A*, vol. 230, pp. 157–163, 1997.
- [19] M. A. Jafarizadeh and H. Fakhri, "Supersymmetry and shape invariance in differential equations of mathematical physics," *Physics letters A*, vol. 230, pp. 164–170, 1997.
- [20] M. A. Jafarizadeh and H. Fakhri, "Parasupersymmetry and shape invariance in differential equations of mathematical physics and quantum mechanics," *Annals of Physics*, vol. 262, no. 2, pp. 260–276, 1998.

Research Article

Energy Dependence of Particle Ratios in High Energy Nucleus-Nucleus Collisions: A USTFM Approach

Inam-ul Bashir, Rameez Ahmad Parra , Hamid Nanda, and Saeed Uddin

Department of Physics, Jamia Millia Islamia (Central University), New Delhi, India

Correspondence should be addressed to Rameez Ahmad Parra; rameezparra@gmail.com

Received 7 February 2018; Accepted 1 April 2018; Published 13 May 2018

Academic Editor: Chun-Sheng Jia

Copyright © 2018 Inam-ul Bashir et al. This is an open access article distributed under the Creative Commons Attribution License, which permits unrestricted use, distribution, and reproduction in any medium, provided the original work is properly cited. The publication of this article was funded by SCOAP³.

We study the identified particle ratios produced at mid-rapidity ($|y| < 0.5$) in heavy-ion collisions, along with their correlations with the collision energy. We employ our earlier proposed unified statistical thermal freeze-out model (USTFM), which incorporates the effects of both longitudinal and transverse hydrodynamic flow in the hot hadronic system. A fair agreement seen between the experimental data and our model results confirms that the particle production in these collisions is of statistical nature. The variation of the chemical freeze-out temperature and the baryon chemical potential with respect to collision energies is studied. The chemical freeze-out temperature is found to be almost constant beyond the RHIC energy and is found to be close to the QCD predicted phase-transition temperature suggesting that the chemical freeze-out occurs soon after the hadronization takes place. The vanishing value of chemical potential at LHC indicates very high degree of nuclear transparency in the collision.

1. Introduction

Relative hadron yields and their correlations are observable which can provide information on the nature, composition, and size of the medium from which they originate in high energy heavy-ion collisions where a strongly interacting nuclear matter at high energy density and temperatures is formed. Within the framework of the statistical model, it is assumed that a hot and dense fireball is formed over an extended region for a brief period of time (\sim a few fm/c) after the initial collision which undergoes collective expansion leading to a decrease in its temperature and finally to the hadronization. After the hadronization of the hot fireball, the hadrons keep interacting with each other and the particle number changing (inelastic) reaction processes continue to take place till the temperature drops to a certain value where a given reaction process almost comes to a stop. Those particle number changing reaction processes (e.g., strangeness exchange process) stop earlier for which the threshold energy is larger. The temperature at which the particle number changing process for a given hadron almost stops is called the “chemical freeze-out” temperature of that

hadronic specie. However, the (elastic) rescattering still takes place and continues to build up the collective (hydrodynamic) expansion. Consequently, the matter becomes dilute and the mean free path for the elastic reaction processes of given hadronic species becomes comparable with the system size. At this stage the scattering processes stop and the given hadron decouples from the rest of the system. This is called the “kinetic or thermal freeze-out” after which the hadron’s energy/momentum spectrum is frozen in time [1]. As the inelastic cross sections are only a small fraction of the total cross section at lower (thermal) energies, the inelastic processes stop well before the *elastic* ones. Thus chemical freeze-out precedes kinetic or thermal freeze-out [2].

Statistical thermal models have successfully reproduced the essential features of particle production in heavy-ion collisions [3] as well as in many types of elementary collisions [4–7] at LHC energies suggesting a statistical nature of particle production in these collisions. Systematic studies of particle yields using experimental results at different beam energies have revealed a clear underlying freeze-out pattern for particle yields in heavy-ion collisions [8, 9]. The success of the statistical (thermal) models in describing the ratios of

hadron yields produced in heavy-ion collisions is remarkable. The agreement of the particle ratios with simple predictions of the statistical models is a key argument for the thermalization of the system formed in heavy-ion collisions. Measurements of antiparticle to particle ratios in these collisions give information on the net baryon density or baryon chemical potential achieved and are thus of interest in characterizing the environment created in these collisions. It has also been suggested that the measurement of strange antibaryon to baryon ratios could help distinguish between a hadron gas and deconfined plasma of quarks and gluons [10]. For a boost invariant system at mid-rapidity for the RHIC and LHC energies, the particle yields dN/dy change only by a few percentages in the rapidity window $|y| < 1$. The particles ratios detected at mid-rapidity are the integrated yield from various parts of the fireball.

In this paper, we attempt to reproduce the particle ratios and to study their correlations and the energy dependence in the hadron gas (HG) scenario by using our phenomenological boost invariant unified statistical thermal freeze-out model (USTFM) [1, 13–17] which assumes that at freeze-out all the hadrons in the hadron gas resulting from a high energy nuclear collision follow an equilibrium distribution. The local particle phase space densities have the form of the Fermi-Dirac or Bose-Einstein statistical distributions.

2. Model Description

The nuclear matter created in high energy heavy-ion collisions is assumed to form an ideal gas that can be described by Grand Canonical Ensemble. The density of the particle i can then be written as

$$n_i = \frac{g_i}{2\pi^2} \int_0^\infty \frac{k^2 dk}{\exp[(E_i(k) - \mu_i)/T] \pm 1}, \quad (1)$$

where $E_i = \sqrt{(k^2 + m_i^2)}$ is the energy, k is the momentum of the particle specie, $g_i = (2J_i + 1)$ is the spin degeneracy factor, μ_i is the chemical potential of the particle species i , and T is the temperature. The (+) sign is for fermions and (–) sign is for bosons. For high temperatures and energies, the Bose-Einstein or Fermi-Dirac statistics can be replaced with the Boltzmann statistics by dropping the ± 1 term. The chemical freeze-out relates to the equilibrium between different flavors. If the hadron gas reaches chemical equilibrium, the particle abundance is described by chemical potentials and temperatures. The information of the chemical freeze-out can be extracted from particle ratios in the measurement. Relative particle production can be studied by particle ratios of the integrated dN/dy yields. If we neglect the decay contributions and consider only the primordial yield, the antiparticle to particle ratios are found to be controlled only by their respective fugacities. That is,

$$\frac{n_i}{\bar{n}_i} = \exp \frac{\mu_i - \bar{\mu}_i}{T} = \exp \left(\frac{2\mu_i}{T} \right). \quad (2)$$

Ratios of particles with the same mass, but different quark content, such as \bar{p}/p and K^-/K^+ , are sensitive to the balance

between matter and antimatter, characterized by the baryon chemical potential μ_B . As strange quarks are created during the collision and are not transported from the incoming nuclei, strangeness production is expected to be a good estimator of the degree of equilibration of the produced fireball [18]. The \bar{p}/p ratio in accordance with (2) can be written as follows:

$$\frac{\bar{p}}{p} = \exp \left(-2 \frac{\mu_B}{T} \right). \quad (3)$$

The other particle ratios of thermal yields (i.e., without feed-down contributions from the heavier resonances) can be correlated accordingly with the \bar{p}/p ratio as follows:

$$\frac{K^-}{K^+} = \exp \left(2 \frac{\mu_s}{T} \right) \left(\frac{\bar{p}}{p} \right)^{1/3}, \quad (4)$$

$$\frac{\bar{\Lambda}}{\Lambda} = \exp \left(-2 \frac{\mu_s}{T} \right) \left(\frac{\bar{p}}{p} \right)^{2/3}, \quad (5)$$

$$\frac{\bar{\Sigma}}{\Sigma} = \exp \left(-2 \frac{\mu_s}{T} \right) \left(\frac{\bar{p}}{p} \right)^{2/3}, \quad (6)$$

$$\frac{\bar{\Xi}}{\Xi} = \exp \left(-4 \frac{\mu_s}{T} \right) \left(\frac{\bar{p}}{p} \right)^{1/3}, \quad (7)$$

$$\frac{\bar{\Omega}}{\Omega} = \exp \left(-6 \frac{\mu_s}{T} \right). \quad (8)$$

Incidentally, the above given relations of the mid-rapidity equal mass particle ratios, emitted from a hadronic fireball maintaining a high degree of thermal and chemical equilibration, hold even when the resonance decay contributions are included [18]. In (8), the \bar{p}/p ratio is absent because of the complete strange quark content of Omega mesons.

In our model [1, 13–17], it is assumed that the rapidity axis is populated with hot hadronic regions moving along the beam axis with monotonically increasing rapidity y_0 . This essentially emerges from the situation where the colliding nuclei exhibit transparency effects. Hence the regions away from the mid-region also consist of the constituent partons of the colliding nucleons, which suffer less rapidity loss due to partial nuclear transparency. Due to this, these regions have an excess of quarks over the antiquarks and hence maintain larger baryon chemical potentials on either side of the mid-region in a symmetric manner. For this reason, a quadratic-type rapidity-dependent chemical potential μ_B has been considered in our model as follows:

$$\mu_B = a + by_0^2, \quad (9)$$

where the model parameter a defines the chemical potential at mid-rapidity and the parameter b gives the variation of the chemical potential along the rapidity axis. We focus on the mid-rapidity data (dN/dy), for which a bulk of published hadrons yields is available. We have also employed the strangeness conservation criteria in a way such that the total strangeness in the fireball is zero.

TABLE 1: The values of chemical potential obtained at different collision energies in our model are compared to the values obtained in references [11, 12].

$\sqrt{s_{\text{NN}}}$ (GeV)	$\mu_B = a$ (MeV) (our model)	μ_B (MeV) Ref. [11, 12]
9.2	290 ± 3	300 ± 12
62.4	45 ± 5	62.7 ± 6
130	25 ± 3	29 ± 4.6
200	23 ± 2	22 ± 4.4
2760	0.5 ± 0.5	0.75

We have tabulated above the different values of chemical potentials obtained in our previous papers [1, 13–17] for different center-of-mass energies, as shown in Table 1, by using our unified statistical thermal freeze-out model. For the sake of comparison, we have also mentioned the values of μ_B obtained at different SPS and RHIC energies by STAR collaboration [11] and by ALICE at LHC [12].

3. Results and Discussion

In order to reproduce the variation of various particle ratios, at all possible energies up to the LHC, we need to obtain the dependence of the chemical potential and the chemical freeze-out temperature on the collision energies. For this purpose, we use the following parameterization [19]:

$$\mu_B = \frac{c}{1 + d\sqrt{s_{\text{NN}}}}. \quad (10)$$

Using the set of extracted values of μ_B from our model at five different energies we obtain $c = 1304$ MeV and $d = 0.38$ GeV⁻¹ when μ_B is in the units of MeV. These values are found to be in a close vicinity with the values of the parameters $c = 1308 \pm 0.028$ MeV and $d = 0.273 \pm 0.008$ GeV⁻¹ obtained by Cleymans et al. [20]. Similarly, in order to obtain the values of freeze-out temperatures at various energies, we first fit the \bar{p}/p and $\bar{\Lambda}/\Lambda$ ratios at five different collision energies by using the corresponding values of the chemical potentials obtained through our model as mentioned in Table 1. The five different values of freeze-out temperatures obtained in this way are shown in Table 2. To obtain the chemical freeze-out temperature at all possible energies we use the following parameterization:

$$T = T_0 \left[1 - \frac{1}{(\log \sqrt{s_{\text{NN}}} - e)/f} \right]. \quad (11)$$

Using the set of chemical freeze-out temperature obtained at five different collision energies we obtain the values of the parameters in (11) as $T_0 = 172$ MeV, $e = 1.10$ GeV, and $f = 0.14$ GeV. The result of these parameterizations ((10) and (11)) is shown in Figure 1. The solid red curves represent the best fit and the black square shapes represent the values of chemical potentials and the freeze-out temperatures as obtained previously in our model.

In Table 2, we have also shown the values of kinetic freeze-out temperatures T_{kin} obtained by reproducing the

TABLE 2: The values of chemical and kinetic freeze-out temperatures obtained at different collision energies in our model.

$\sqrt{s_{\text{NN}}}$ (GeV)	T (MeV) (our model)	T_{kin} (MeV) (our model)
9.2	149 ± 4	150 ± 2
62.4	167 ± 5	170 ± 5
130	165 ± 4	163 ± 2
200	166 ± 3	162 ± 2
2760	169 ± 3	103 ± 1

transverse momentum distributions of protons and kaons at the five different collision energies in our model [1, 13–17]. It is seen that the values of chemical freeze-out temperature T and the kinetic freeze-out temperature T_{kin} are almost the same at $\sqrt{s_{\text{NN}}} = 9.2$ GeV while, at RHIC, the values of chemical freeze-out temperature T are a little higher than the values of kinetic freeze-out temperature T_{kin} . At LHC, this difference is even larger. Thus it seems that the time duration between the two types of freeze-outs is dependent on the collision energy. This duration is larger for the larger collision energies. This may be understood as a result of the larger particle production (and hence a larger system size) at higher energies, which results in the development of the larger collective flow effects at the cost of thermal temperature. We find in Figure 1 that the extracted temperature values generally increase rapidly whereas the baryon chemical potential decreases monotonically with the collision energy and tends to saturate at RHIC and LHC energies. In general, these values are found to lie close to the ideal gas values. Using these values of μ_B and T , we reproduce the energy dependence of various antiparticle to particle ratios by using (3)–(8).

These particle ratios are plotted in Figures 2–4. The experimental data shown by red colored shapes in Figures 2 and 3 is taken from [19] and the references therein, while, for Figure 4, the data is taken from [21] and the references therein. In heavy-ion collisions the increase in the antimatter to matter ratio with the center-of-mass energy of the system has been observed earlier by the NA49 and the STAR collaborations. The increase of \bar{p}/p ratio towards unity with an increase in the center-of-mass energy from SPS to LHC is shown in Figure 2(a). Our model results are in good agreement with the experimental data. The increase in \bar{p}/p ratio with an increase in collision energy reflects the decrease in net baryon density towards higher collision energies, thus making the collision system partially transparent at RHIC and almost completely transparent at LHC. The ratio k^-/k^+ plotted in Figure 2(b) shows a significant dependence on the center-of-mass energy. Our model prediction shows a close agreement with the experimental data points. Hence the overall feature of the experimental data in both cases is in good agreement with our model calculations. The decrease in k^-/k^+ ratio with a decrease in collision energy is due to an increase in net baryon density which leads to the associated production of kaons, thus favoring the production of k^+ over k^- . In Figures 3 and 4(a), we have plotted the energy

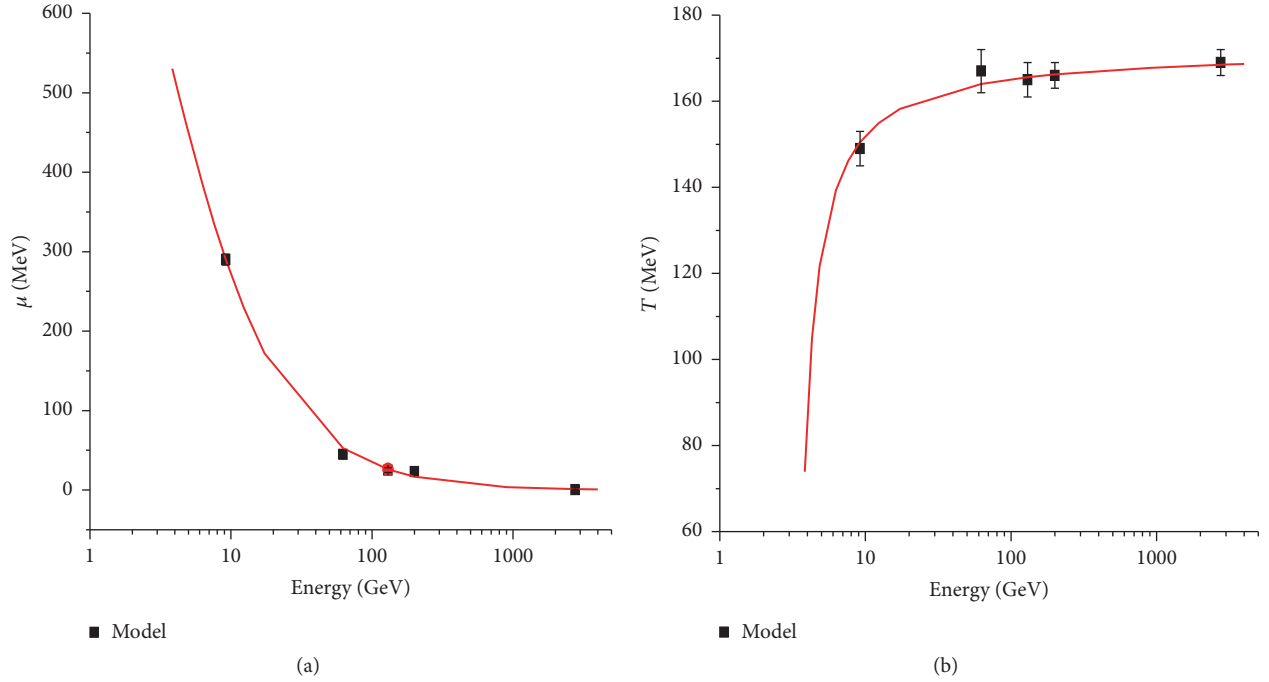


FIGURE 1: The energy dependence of baryon chemical potential (a) and chemical freeze-out temperature (b) in our model.

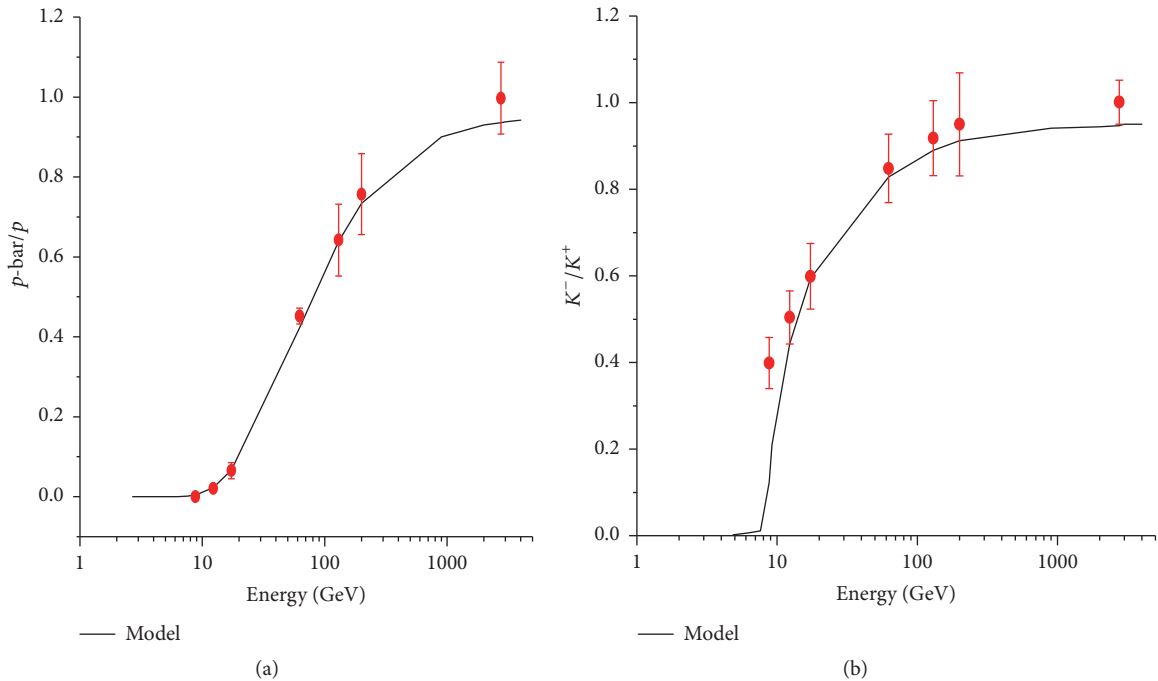
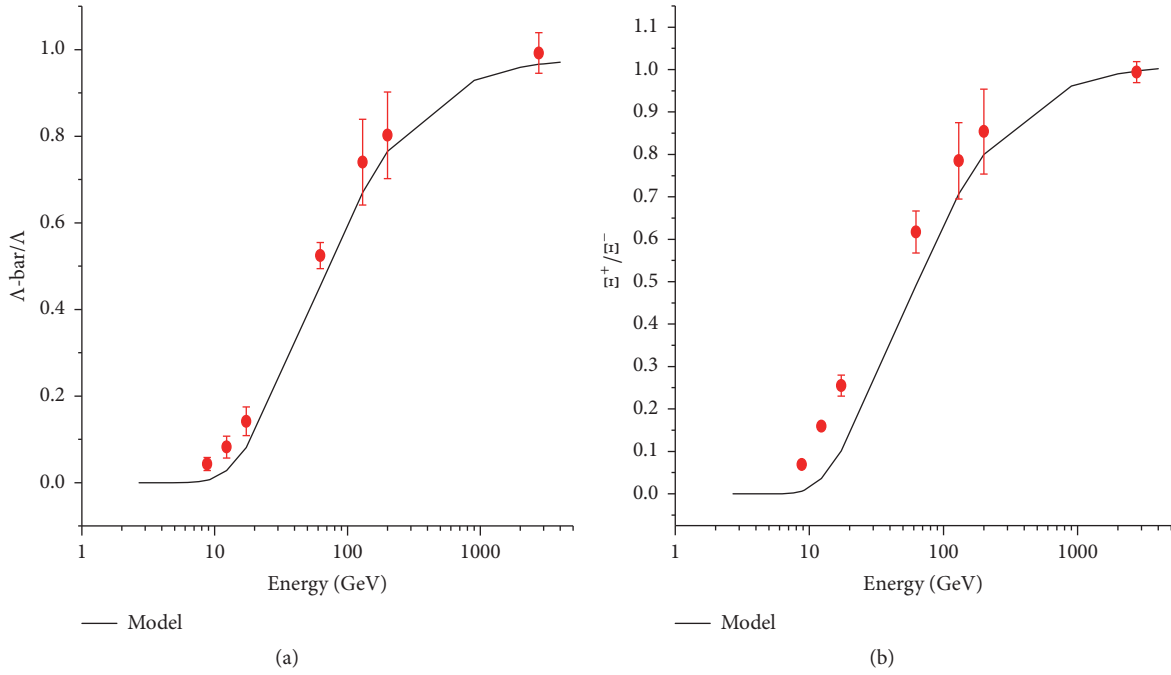
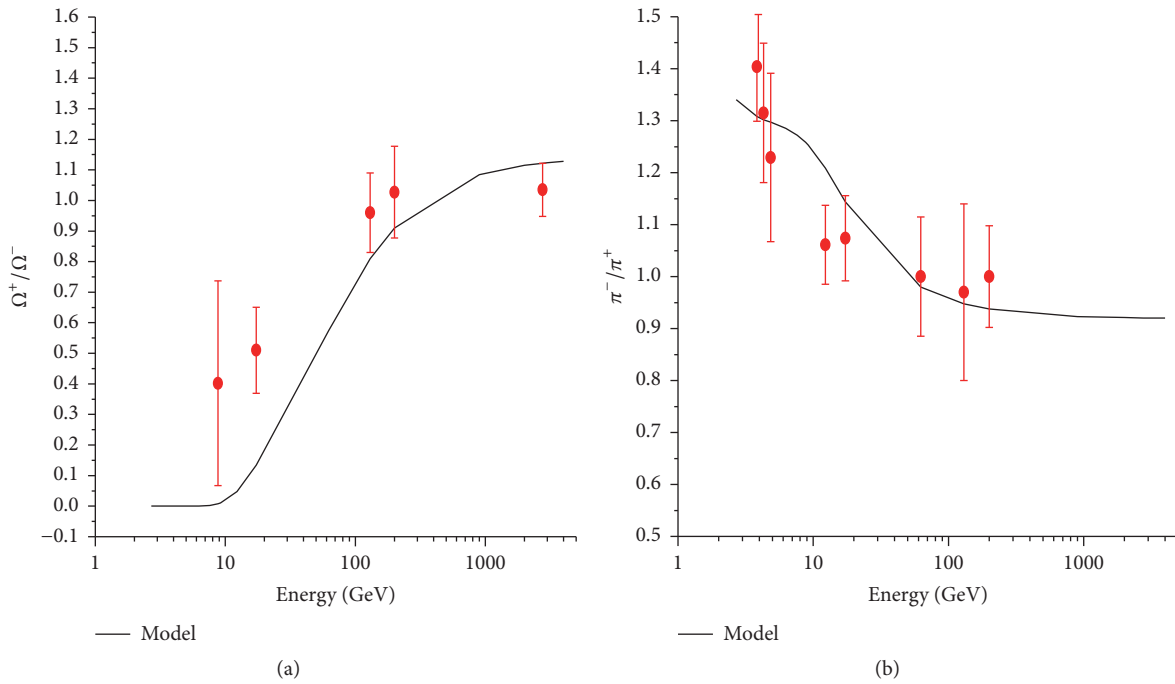


FIGURE 2: Energy dependence of \bar{p}/p (a) and k^-/k^+ (b) ratios.

dependence of singly, doubly, and triply strange antibaryon to baryon ratios. We find a fairly good agreement between our model results and the experimental data. It is seen that the ratios increase towards unity with the increase in collision energies. The ratios appear ordered with the strangeness quantum number, that is, the higher the strangeness quantum number, the smaller the difference between antibaryon and

baryon content. This is so called “mass-hierarchy” where the saturation value (i.e., 1) of the ratio is achieved earlier for the more massive hyperons species [21]. It is interesting to note that even the yield of rarely produced strange particles like Ω is also fairly well described by our USTF model. In Figure 4(b), we have shown the energy dependence of π^-/π^+ ratio. This is also reproduced with a fairly good agreement.


 FIGURE 3: Energy dependence of $\bar{\Lambda}/\Lambda$ (a) and $\bar{\Xi}/\Xi$ (b) ratios.

 FIGURE 4: Energy dependence of $\bar{\Omega}/\Omega$ (a) and π^-/π^+ (b) ratios.

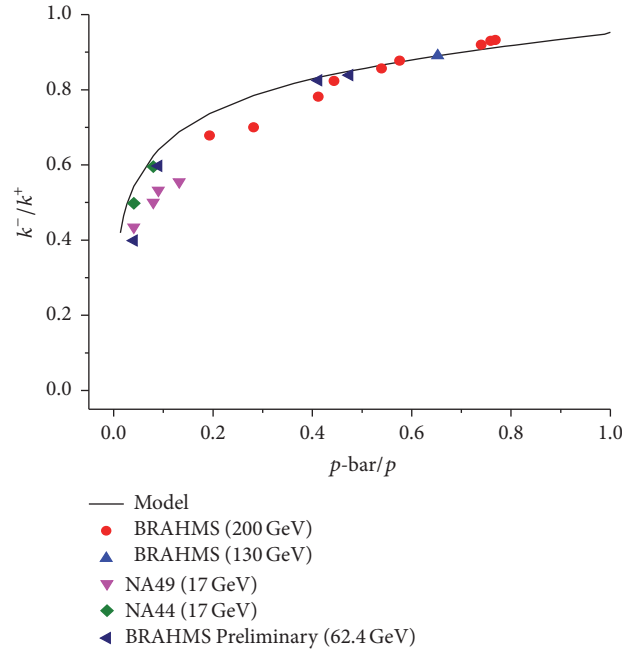
It is seen that the distribution characteristics of π^-/π^+ ratio are different as compared to other particle ratios studied in this manuscript. This seems to be because of the associated production of π^- over π^+ at lower energies. The ratio is greater than 1 at lower energies and goes to unity at LHC energies where the pair production mechanism dominates and complete nuclear transparency effects are observed. It is seen that

antibaryon/baryon ratios have more sharp dependence on collision energy.

Figure 5 shows the correlation of k^-/k^+ (representing net strange chemical potential μ_s) with the \bar{p}/p ratio (representing net baryon chemical potential μ_B). This is an attempt to prove the validity of our model. The black solid curve, which is a result of (4) ($k^-/k^+ \sim (\bar{p}/p)^{1/3}$), represents our model

TABLE 3: Model predictions for hadron ratios at LHC ($T = 168.65$ MeV, $\mu_B = 0.85$ MeV). Decay contributions are included.

K^-/K^+	\bar{p}/p	$\bar{\Lambda}/\Lambda$	Ξ^+/Ξ^-	$\bar{\Omega}/\Omega$	π^-/π^+	p/π^+	K^+/π^+	K^-/π^-	Λ/π^-	Ξ^-/π^-	Ω^-/π^-	ϕ/K^-
0.947	0.936	0.966	0.996	1.121	0.94	0.060	0.184	0.135	0.039	0.061	0.087	0.147

FIGURE 5: Correlation of k^-/k^+ ratio with \bar{p}/p ratio at mid-rapidity for central collisions.

prediction whereas the colored shapes represent the different experimental data points as mentioned in the Figure 5. This correlation could give information on how the kaon production is related to the net baryon density. At lower energies, the kaon production is dominated by the associated production which results in more k^+ production compared to k^- . Also the \bar{p}/p ratio is much less than unity, indicating that there is a large baryon stopping at the lower energies. As we go towards higher energies, the pair production mechanism starts to dominate and the ratios tend to become closer to unity.

We have further reproduced the energy dependence of various other particle yields relative to pions as shown in Figure 6. The experimental data is taken from [19, 21] and the references therein. Unlike in case of antiparticle to particle ratios, here we have to include the effects of resonance decay contributions, as discussed in the first section. Our model results are seen to be in a fair agreement with the experimental data points. At lower energies, a peak has been observed in k^+/π^+ ratio at around 8 GeV [22–24]. However this is not reproduced very well in our analysis. The k^-/π^- ratio exhibits no sharp structure and instead a smooth evolution with the collision energy is seen. Our model results for the k^-/π^- ratio slightly overpredict the experimental data points at lower energies. However, the main features of the data showing a steady decrease towards lower energies are well reproduced. Also we find that all the particle ratios seem to saturate at RHIC and LHC energies. This saturation seems to arise due to almost constant chemical freeze-out

temperatures at RHIC and LHC energies. The steep decrease of the p/π^+ ratio towards higher energies reflects a decrease in the baryon chemical potential and hence an increase in the nuclear transparency, though the increase of pion production also plays a role in this. Beyond $\sqrt{s_{NN}} = 100$ GeV the flattening of the curves takes place.

We have predicted the various hadron ratios produced in central Pb-Pb collisions at LHC ($\sqrt{s_{NN}} = 2.76$ TeV) and they are presented in Table 3. The antiparticle by particle ratios are close to unity reflecting a very small chemical potential at LHC. Also the yields relative to pions are very similar to the values measured at RHIC energy.

In Figure 7, we have plotted the chemical freeze-out temperature on the vertical axis and the chemical potential on the horizontal axis obtained at different collision energies. The value of chemical freeze-out temperature at RHIC and LHC lies in the vicinity of lattice QCD predicted phase-transition temperature of ~ 170 MeV [19], indicating that the freeze-out occurs almost simultaneously after the phase-transition. The red squares in Figure 7 represent the values of chemical potentials obtained at various collision energies as mentioned in Table 1.

4. Summary and Conclusion

We have used our model (USTFM) to analyze the variations of the ratios of particles, produced in the high energy nucleus-nucleus collisions, with center-of-mass energy and their

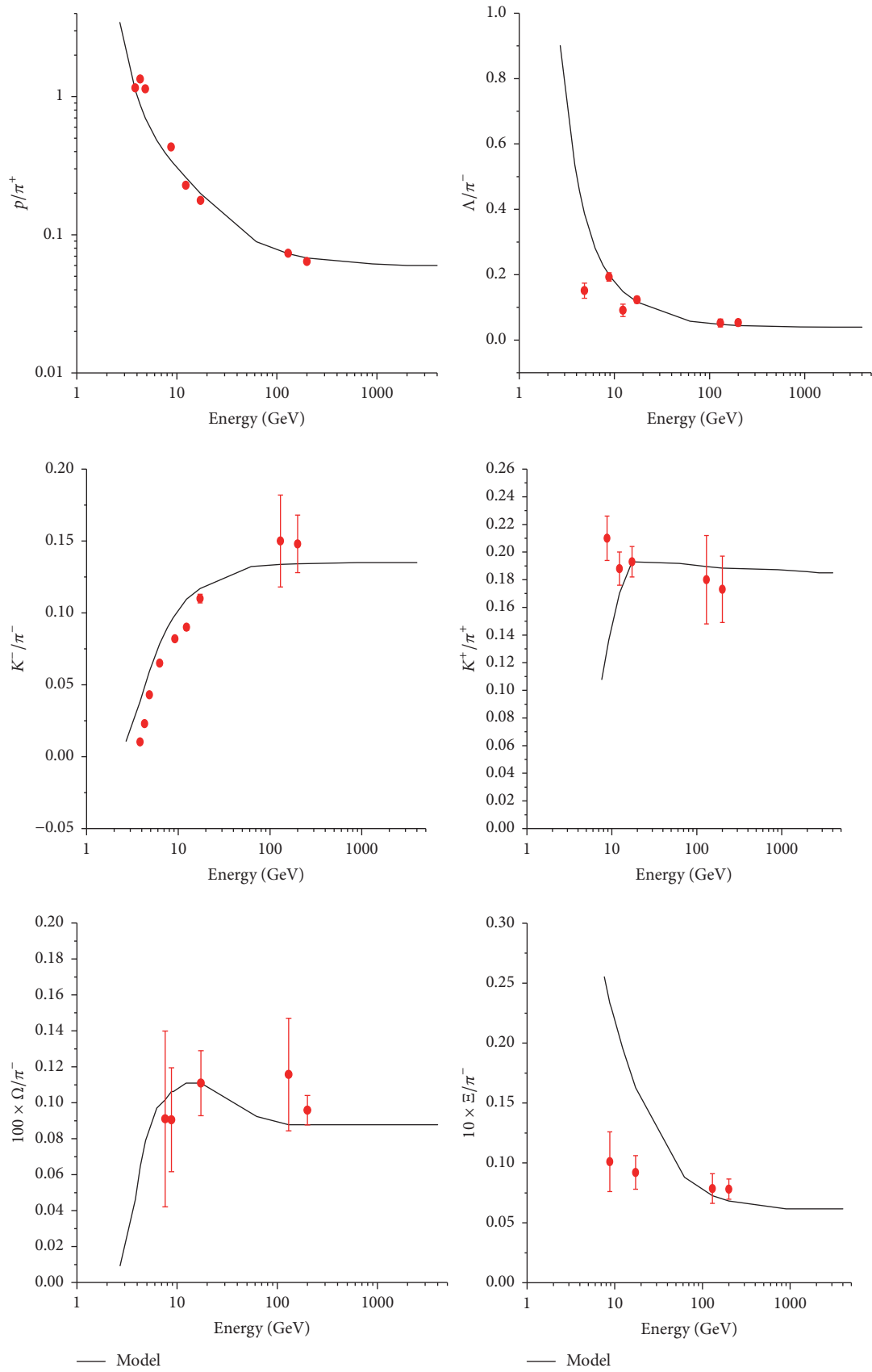


FIGURE 6: Continued.

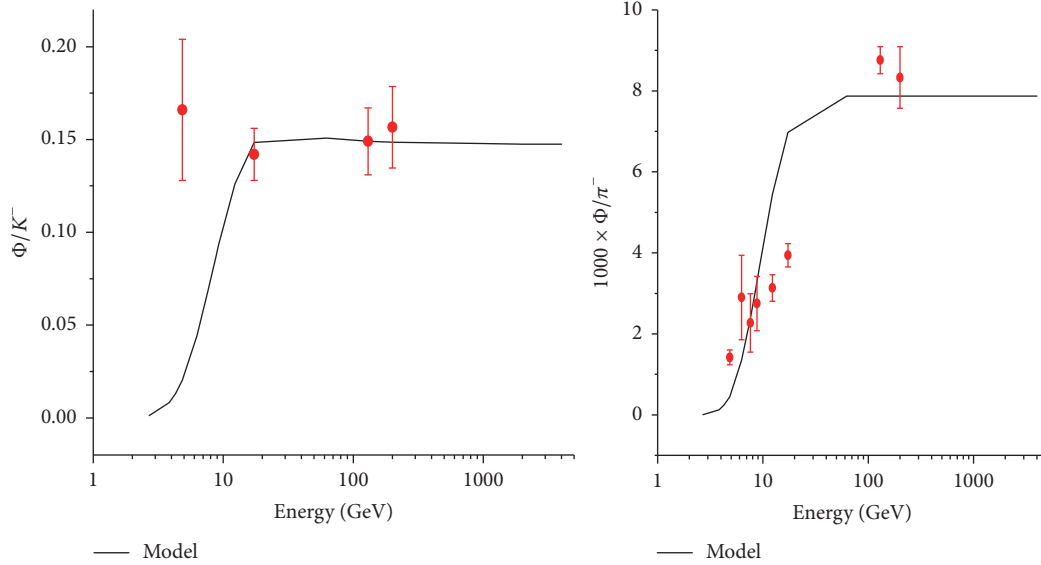


FIGURE 6: Energy dependence of various unlike particle ratios.

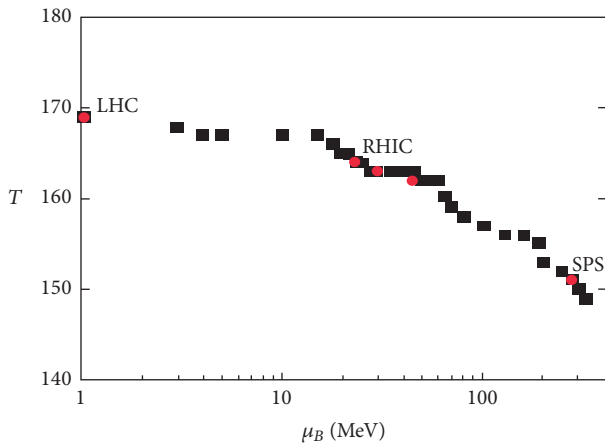


FIGURE 7: Chemical freeze-out temperature T versus mid-rapidity baryon chemical potential μ_B at different collision energies. The red squares represent the values of chemical potentials obtained at various collision energies as mentioned in Table 1. The black squares are the results from the present analysis.

correlations. We have compared our results with the experimental data. A good agreement between our model results and experimental data shows that thermal model used in the analysis gives a satisfactory description of the data. The dependence of the baryon chemical potential and the chemical freeze-out temperature on the energy is studied. For this purpose, a parameterization is used for each case. It is found that the extracted values of chemical freeze-out temperatures at RHIC and LHC are almost constant and are close to the lattice QCD predicted phase-transition temperature, suggesting that chemical freeze-out happens in the vicinity of the phase boundary, that is, shortly after hadronization process is completed. Also the difference between the chemical freeze-out and the kinetic (thermal)

freeze-out temperatures is found to increase with the collision energy.

Conflicts of Interest

The authors declare that they have no conflicts of interest.

Acknowledgments

The authors acknowledge the financial support from Council of Scientific and Industrial Research (CSIR) for this work.

References

- [1] S. Uddin et al., “Transverse Momentum Distributions of Hadrons Produced in Pb-Pb Collisions at LHC Energy $\sqrt{s_{NN}} = 2.76$ TeV,” *Advances in High Energy Physics*, vol. 2015, Article ID 154853, 7 pages, 2015.
- [2] U. W. Heinz, “Concepts of heavy-ion physics,” in *Proceedings of the 2003 CERN-CLAF School of High-Energy Physics*, San Miguel Regla, Mexico, <http://arxiv.org/abs/hep-ph/0407360>.
- [3] U. W. Heinz, “Primordial hadrosynthesis in the little bang,” *Nuclear Physics A*, vol. 661, no. 1-4, pp. 140–149.
- [4] F. Becattini and et al., “Multiplicity distributions in a thermodynamical model of hadron production in e^+e^- collisions,” *Zeitschrift für Physik C*, vol. 72, p. 485, 1996.
- [5] F. Becattini and U. Heinz, “Thermal hadron production in pp and $p\bar{p}$,” *Zeitschrift für Physik C*, vol. 76, pp. 269–286, 1997.
- [6] F. Becattini and G. Passaleva, “Statistical hadronization model and transverse momentum spectra of hadrons in high energy collisions,” *The European Physical Journal C*, vol. 23, pp. 551–583, 2002.
- [7] F. Becattini, “Statistical hadronisation phenomenology,” *Nuclear Physics A*, vol. 702, no. 1-4, pp. 336–340, 2002.
- [8] J. Cleymans and K. Redlich, “Unified description of freeze-out parameters in relativistic heavy ion collisions,” *Physical Review Letters*, vol. 81, article 5284, 1998.

- [9] J. Cleymans and K. Redlich, “Chemical and thermal freeze-out parameters from 1A to 200A GeV,” *Physical Review C: Nuclear Physics*, vol. 60, no. 5, 1999.
- [10] B. Biedron and W. Broniowski, “Rapidity-dependent spectra from a single-freeze-out model of relativistic heavy-ion collisions,” *Physical Review C: Nuclear Physics*, vol. 75, no. 5, Article ID 054905, 2007.
- [11] B. I. Abelev et al., “STAR Collaboration,” *Physical Review C*, vol. 79, Article ID 034909, 2009.
- [12] J. Cleymans, I. Kraus, H. Oeschler, K. Redlich, and S. Wheaton, “Statistical model predictions for particle ratios at $s_{NN} = 5.5$ TeV,” *Physical Review C Nuclear Physics*, vol. 74, no. 3, Article ID 034903, 2006.
- [13] S. Uddin, J. S. Ahmad, W. Bashir, and R. Ahmad Bhat, “A unified approach towards describing rapidity and transverse momentum distributions in a thermal freeze-out model,” *Journal of Physics G: Nuclear and Particle Physics*, vol. 39, no. 1, Article ID 015012, 2012.
- [14] S. Uddin, R. A. Bhat, I.-U. Bashir, W. Bashir, and J. S. Ahmad, “Systematic of particle thermal freeze-out in a hadronic fireball at RHIC,” *Nuclear Physics A*, vol. 934, no. 1, pp. 121–132, 2015.
- [15] R. A. Bhat, S. Uddin, and I.-U. Bashir, “Unified thermal freeze-out model and its parameters at RHIC,” *Nuclear Physics A*, vol. 935, pp. 43–51, 2015.
- [16] I.-U. Bashir et al., “Identified charged particle distributions in Au + Au collisions at $s_{NN} = 9.2$ GeV,” *International Journal of Modern Physics A*, vol. 30, no. 24, Article ID 1550139, 2015.
- [17] I.-U. Bashir, R. A. Bhat, and S. Uddin, “Transverse momentum distributions of strange hadrons produced in p–p collisions at $\sqrt{s_{NN}} = 200$ GeV,” *Journal of Experimental and Theoretical Physics*, vol. 121, no. 2, pp. 206–211, 2015.
- [18] V. Baban, A. Jipa, O. Ristea et al., “Centrality determination in 15 GeV/u Au-Au collisions in CBM experiment,” *Romanian Reports in Physics*, vol. 56, no. 4, pp. 659–666, 2004.
- [19] S. K. Tiwari and C. P. Singh, “Particle production in ultrarelativistic heavy-ion collisions: a statistical-thermal model review,” *Advances in High Energy Physics*, vol. 2013, Article ID 805413, 27 pages, 2013.
- [20] J. Cleymans, H. Oeschler, K. Redlich, and S. Wheaton, “Status of chemical freeze-out,” *Journal of Physics G: Nuclear and Particle Physics*, vol. 32, no. 12, pp. S165–S169, 2006.
- [21] A. Andronic et al., “Hadron production in central nucleus–nucleus collisions at chemical freeze-out,” *Nuclear Physics A*, vol. 772, no. 3-4, pp. 167–199, 2006.
- [22] M. Mishra and C. P. Singh, “Particle multiplicities and ratios in excluded volume models,” *Physical Review C: Nuclear Physics*, vol. 78, no. 2, 2008.
- [23] P. Braun-Muzinger, J. Cleymans, H. Oeschler, and K. Redlich, “Nuclear Physics,” A697, 902, 2002.
- [24] J. Cleymans, H. Oeschler, K. Redlich, and S. Wheaton, “Transition from baryonic to mesonic freeze-out,” *Physics Letters B*, vol. 615, no. 1-2, pp. 50–64, 2005.

Research Article

Hermitian–Non-Hermitian Interfaces in Quantum Theory

Miloslav Znojil 

Nuclear Physics Institute of the CAS, 250 68 Řež, Czech Republic

Correspondence should be addressed to Miloslav Znojil; znojil@ujf.cas.cz

Received 10 January 2018; Accepted 18 February 2018; Published 24 April 2018

Academic Editor: Saber Zarrinkamar

Copyright © 2018 Miloslav Znojil. This is an open access article distributed under the Creative Commons Attribution License, which permits unrestricted use, distribution, and reproduction in any medium, provided the original work is properly cited. The publication of this article was funded by SCOAP³.

In the global framework of quantum theory, the individual quantum systems seem clearly separated into two families with the respective manifestly Hermitian and hiddenly Hermitian operators of their Hamiltonian. In the light of certain preliminary studies, these two families seem to have an empty overlap. In this paper, we will show that whenever the interaction potentials are chosen to be weakly nonlocal, the separation of the two families may disappear. The overlaps *alias* interfaces between the Hermitian and non-Hermitian descriptions of a unitarily evolving quantum system in question may become nonempty. This assertion will be illustrated via a few analytically solvable elementary models.

1. Introduction

In virtually any representation of quantum theory, the states can be perceived as constructed in a suitable user-friendly Hilbert space \mathcal{H} . By a number of authors [1–4], it has been recommended to enhance the flexibility of the formalism by making use of an ad hoc, quantum-system-adapted physical inner product in \mathcal{H} , that is, by an introduction of a nontrivial, stationary metric operator $\Theta \neq \Theta(t)$. All of the other, relevant “physical” operators Λ of the observables in \mathcal{H} (i.e., say, $\Lambda_1 = Q$ representing a coordinate or $\Lambda_2 = H$ representing the energy, etc.) must be then chosen, in Diedonné’s terminology [5], quasi-Hermitian,

$$\Lambda^\dagger \Theta = \Theta \Lambda. \quad (1)$$

These observables become Hermitian if and only if we reach the conventional textbook limit with $\Theta \rightarrow I$. Otherwise, our candidates for the observables remain manifestly non-Hermitian in our friendly Hilbert space \mathcal{H} . The latter space (with artificial $\Theta = I$) must be declared, therefore, auxiliary and unphysical, $\mathcal{H} \rightarrow \mathcal{H}^{(\text{unphysical})}$. Only the reincorporation of the amended metric will reinstall the space as physical, $\mathcal{H} \rightarrow \mathcal{H}^{(\text{redefined})}$.

In certain very promising recent high-energy physics applications of the formalism, say, in neutrino physics [6, 7], people usually restrict attention to the special form of

$\Theta = \mathcal{P}\mathcal{C}$, where \mathcal{P} is parity while \mathcal{C} denotes charge. In such a setting the stationarity of the theory represents a serious obstacle for experimentalists, mainly because the adiabatic changes and tuning of the parameter-dependence of the observables may lead to multiple counterintuitive no-go theorems [3, 8, 9]. At the same time, the new degree of the kinematical freedom represented by the nontrivial metric $\Theta \neq I$ may find its efficient use, say, in the manipulations leading to the experimental realizations of various quantum phase transitions in the theory [6, 10–16] as well as in the laboratory [17].

The consistent mathematical formulation of the theories with innovative $\Theta \neq I$ and traditional $H = T + V(x)$ proved to be truly challenging [18]. In practice, the main source of difficulties can be seen in the “smearing” feature of the use of generic $\Theta \neq I$ [19]. Jones noticed that “we have to start with x ” (i.e., with $\Theta \neq I$) “because that is how the potential is defined” [20]. His analysis was then aimed at the search for natural interfaces (*alias* operational connections) between the hypothetical non-Hermitian dynamics (using $\Theta \neq I$) and the available experimental setups (at $\Theta = I$).

In a way based on a detailed study of certain over-restricted family of models (for purely technical reasons the interaction potentials were kept local), Jones arrived, not too surprisingly, at a heavily sceptical conclusion that the theory cannot be unitary. In his own words “the only

satisfactory resolution of the dilemma is to treat the non-Hermitian potential as an effective one, and [to] work in the standard framework of quantum mechanics, accepting that this effective potential may well involve the loss of unitarity” [21].

Jones’ conclusions were partially opposed and weakened in [19, 22, 23] where the assumption of “starting with x ” (i.e., of our working with the potentials which are local in x) has been shown unfounded (because the value of the lowercase x is not observable) and misleading (because one need not give up the unitarity in general). At the same time, the underlying, deep, and important conceptual problem of the possible existence of suitable Hermitian–non-Hermitian interfaces remained open.

An affirmative answer will be given in what follows. In order to formulate the problem more clearly we will have to recall, in the next section, a few well-known aspects of forming a nontrivial feasible contact and of a smooth transition between several versions of quantum dynamics. In the subsequent sections, we shall then point out that a formal key to the realization of the project of construction of the smooth interfaces lies in the properties of the inner-product metric operators Θ which have to degenerate smoothly, in their turn, to the trivial limit $\Theta = I$. Furthermore, in Section 5 several technical aspects of such a general interface-construction recipe will be illustrated by an elementary toy model-Hamiltonian example admitting a nonnumerical and nonperturbative analytical treatment. Some of the possible impacts upon quantum phenomenology will finally be mentioned in Section 6.

2. Quantum Dynamics in Schrödinger Picture

During the birth of quantum theory, its oldest (namely, the Heisenberg’s “matrix”) picture was quickly followed by Schrödinger’s “wave-function” formulation which proved less intuitive but more economical [24]. The conventional, “textbook” *alias* “Hermitian” Schrödinger picture (HSP, [25]) was later complemented by its “non-Hermitian” Schrödinger picture (NHSP) alternative (cf. the works by Dyson [1] or by nuclear physicists [2]). In this direction, the recent wave of new activities was inspired by Carl Bender with coauthors [4, 10–12]. The emerging, more or less equivalent innovated versions of the NHSP description of quantum dynamics were characterized as “quantum mechanics in pseudo-Hermitian representation” [3] or as “quantum mechanics in the Dyson’s three-Hilbert-space formulation” [1, 26], and so forth [18].

The availability of the two alternative representations of the laws of quantum evolution in Schrödinger picture inspired Jones to ask the above-cited questions about the existence of an “overlap of their applicability” in an “interface” [27]. His interest was predominantly paid to the scattering [20] and his answers were discouraging [21]. In papers [22, 23, 28] we opposed his scepticism. We argued that the difficulties with the HSP-NHSP interface may be attributed to the ultralocal, point-interaction toy model background of his methodical analysis. We introduced certain weakly non-local interactions and via their constructive description we reopened the possibility of practical realization of a smooth

transition between the Hermitian and non-Hermitian theoretical treatment of scattering experiments.

Now we intend to return to the challenge of taking advantage of the specific merits of *both* of the respective HSP and NHSP representations inside their interface. We shall only pay attention to the technically less complicated quantum systems with bound states. Our old belief in the existence, phenomenological relevance, and, perhaps, even fundamental-theory usefulness of a domain of coexistence of alternative Schrödinger picture descriptions of quantum dynamics will be given an explicit formulation supported by constructive arguments and complemented by elementary, analytically solvable illustrative examples.

2.1. The Concept of Hidden Hermiticity. An optimal formulation of quantum theory is, obviously, application-dependent [24]. Still, the so-called Schrödinger picture seems exceptional. Besides historical reasons this is mainly due to the broad applicability as well as maximal economy of the complete description of quantum evolution using the single Schrödinger equation

$$i \frac{d}{dt} \psi(t) = \mathfrak{h} \psi(t), \quad \psi(t) \in \mathcal{H}^{(\text{textbook})}. \quad (2)$$

Whenever the evolution is assumed unitary, the generator \mathfrak{h} (called Hamiltonian) must be, due to Stone’s theorem [29], self-adjoint in $\mathcal{H}^{(\text{textbook})}$,

$$\mathfrak{h} = \mathfrak{h}^{(\text{Hermitian})} = \mathfrak{h}^\dagger. \quad (3)$$

Recently it has been emphasized that even in the unitary evolution scenario the latter Hamiltonian-Hermiticity constraint may be omitted or, better, circumvented. The idea, dating back to Dyson [1], relies upon a suitable preconditioning of wave functions. This induces the replacement of the “Hermitian,” lowercase Schrödinger equations (2) + (3) by their “non-Hermitian” uppercase alternative

$$i \frac{d}{dt} \Psi(t) = H \Psi(t), \quad (4)$$

$$\Psi(t) \in \mathcal{H}^{(\text{unphysical})}, \quad \psi(t) = \Omega \Psi(t).$$

The preconditioning operator Ω is assumed to be invertible but nonunitary, $\Omega^\dagger \Omega \neq I$ [2]. Thus, the standard textbook version of the Schrödinger picture splits into its separate Hermitian and non-Hermitian versions (cf. influential reviews [3, 4] and/or mathematical commentaries in [18]).

The slightly amended forms of Dyson’s version of the NHSP formalism proved successful in phenomenological applications, for example, in nuclear physics [2]. As we already indicated, the “non-Hermitian” philosophy of (4) was made widely popular by Bender [4]. Its appeal seems to result from the observation that the nonunitarity of Ω makes the respective geometries in the two Hilbert spaces $\mathcal{H}^{(\text{textbook})}$ and $\mathcal{H}^{(\text{unphysical})}$ mutually nonequivalent. As a consequence, the uppercase Hamiltonian H acting in $\mathcal{H}^{(\text{unphysical})}$ and entering the upgrade (4) of Schrödinger

equation becomes manifestly non-self-adjoint *alias* non-Hermitian in $\mathcal{H}^{(\text{unphysical})}$,

$$H = H^{(\text{non-Hermitian})} = \Omega^{-1} \mathfrak{h} \Omega \neq H^\dagger = \Theta H \Theta^{-1}, \quad (5)$$

$$\Theta = \Omega^\dagger \Omega \neq I.$$

Still, it is obvious that *both* the NHSP version (4) of Schrödinger equation *and* its HSP predecessor (2) represent *the same* quantum dynamics.

2.2. The Choice between the HSP and NHSP Languages. Several reviews in monograph [18] may be recalled for an extensive account of multiple highly nontrivial mathematical details of the NHSP formalism. In applications, quantum physicists take it for granted, nevertheless, that we have a choice between the *two* alternative descriptions of the standard *unitary* evolution of wave functions. People are already persuaded that the basic mathematics of the HSP and NHSP constructions is correct and that the two respective Schrödinger equations are, for any practical purposes, equally reliable.

The accepted abstract HSP-NHSP equivalence still does not mean that the respective practical ranges of the two recipes are the same. The preferences really *depend* very strongly on the quantum system in question. Thus, the choice of the HSP language is made whenever the corresponding self-adjoint Hamiltonian possesses the most common form of superposition of a kinetic energy term with a suitable *local-interaction* potential,

$$\mathfrak{h}_{(\text{local})} = -\frac{d^2}{dq^2} + \mathfrak{v}(q) = \mathfrak{h}_{(\text{local})}^\dagger. \quad (6)$$

Similarly, the recent impressive success of the NHSP phenomenological models is almost exclusively related to the use of the non-Hermitian local-interaction Hamiltonians

$$H = -\frac{d^2}{dx^2} + W(x) \neq H^\dagger, \quad (7)$$

which are only required to possess the strictly real spectra of energies [3, 4].

2.3. The Concept of the HSP-NHSP Interface. The two local-interaction operators (6) and (7) should be perceived as just the two illustrative elements of the two respective general families $\mathcal{F}^{(H)}$ and $\mathcal{F}^{(\text{NH})}$ of the eligible, that is, practically tractable and sufficiently user-friendly HSP and NHSP Hamiltonians. In a way influenced by this exemplification one has a natural tendency to assume that the latter two families are distinct and clearly separated, nonoverlapping [4],

$$\mathcal{F}^{(H)} \cap \mathcal{F}^{(\text{NH})} = \emptyset. \quad (8)$$

During the early stages of testing and weakening such as a priori assumption, Jones [27] introduced the concept of an interface as a potentially nonempty set of Hamiltonians,

$$\mathcal{F}^{(\text{interface})} = \mathcal{F}^{(H)} \cap \mathcal{F}^{(\text{NH})}. \quad (9)$$

Basically, he had in mind a domain of a technically feasible and phenomenologically consistent interchangeability of the two pictures. He also outlined some of the basic features and possible realizations of such a Hermitian/non-Hermitian interface in [20]. Incidentally, the continued study of the problem made him more sceptical [21]. In a way based on a detailed analysis of a schematic though, presumably, generic toy model local-interaction Hamiltonian

$$H = H_{(\text{local})}^{(\text{non-Hermitian})} = -\frac{d^2}{dx^2} + V^{(\text{Hermitian})}(x) + W^{(\text{non-Hermitian})}(x), \quad (10)$$

he came to the conclusion that the merits of families $\mathcal{F}^{(H)}$ and $\mathcal{F}^{(\text{NH})}$ are really specific and that, in the case of scattering at least, their respective domains of applicability really lie far from each other, that is, $\mathcal{F}^{(\text{interface})}_{(\text{scattering})} = \emptyset$. Even at the most favorable parameters and couplings, in his own words, “the physical picture [of scattering] changes drastically when going from one picture to the other” [21].

In our first paper [28] on the subject, we pointed out that Jones’ discouraging “no-interface” conclusions remain strongly model-dependent. For another, weakly nonlocal choice of $H_{(\text{weakly nonlocal})}^{(\text{non-Hermitian})}$, we encountered a much less drastic effect of the interchange of the mathematically equivalent Schrödinger equations (2) and (4) upon the predicted physical outcome of the scattering (see also the related footnote added in [21]). In our subsequent papers [22, 23] we further amended the model and demonstrated that in the context of scattering the overlaps $\mathcal{F}^{(\text{interface})}_{(\text{scattering})}$ may be nonempty. We showed that there may exist the sets of parameters for which the causality as well as the unitarity would be guaranteed for *both* of the Hamiltonians in (3) and (5). Thus, Jones’ ultimate recommendations of giving up the scattering models in $\mathcal{F}^{(\text{NH})}$ and/or of “accepting . . . the loss of unitarity” while treating any “non-Hermitian scattering potential as an effective one” [21] may be requalified as oversceptical (cf. also [3]).

3. Repulsion of Eigenvalues

The presentation of our results is to be preceded by a compact summary of some of the key specific features of spectra in the separate HSP and NHSP frameworks. This review may be found complemented, in Appendix A, by a brief explanation why the NHSP Hamiltonians H which are *non-Hermitian* (though only in an auxiliary, *unphysical* Hilbert space) still do generate the *unitary* evolution (naturally, via wave functions in another, nonequivalent, physical Hilbert space).

Quantum dynamics of the one-dimensional motion described by an ordinary differential local-interaction Hamiltonian (6) is a frequent target of conceptual analyses. These models stay safely inside Hermitian class $\mathcal{F}^{(H)}$ but still a brief summary of some of their properties and simplifications will facilitate a compact clarification of the purpose of our present study.

3.1. Discrete Coordinates. The kinetic plus interaction structure of models (6) reflects their classical physics origin. It may also facilitate the study of bound states, say, by the perturbation-theory techniques [21] and/or by the analytic-construction methods [30]. Still, for our present purposes it is rather unfortunate that any transition to the hidden-Hermiticity language of the alternative model-building family $\mathcal{F}^{(\text{NH})}$ would be counterproductive. One of the main obstacles of a hidden-Hermiticity reclassification of model (6) is technical because the associated Hamiltonians (5) are, in general, strongly non-local [31]. Another, subtler mathematical obstacle may be seen in the unbounded-operator nature of the kinetic energy $T = -d^2/dx^2$ (see [2] for a thorough though still legible explanation).

In [22, 23, 28], we proposed that one of the most efficient resolutions of at least some of the latter problems might be sought and found in the discretization of the coordinates. Thus, one replaces the real line of $q \in (-\infty, \infty)$ by a discrete lattice of grid points q_j such that $q_j = q_0 + hj$, with $j = \dots, -1, 0, 1, \dots$ and with any suitable constant $h > 0$. This leads to the kinetic energy represented by the difference-operator Laplacean

$$T = \begin{bmatrix} \ddots & \ddots & & & \\ \ddots & 0 & -1 & & \\ & -1 & 0 & -1 & \\ & & -1 & 0 & \ddots \\ & & & \ddots & \ddots \end{bmatrix}. \quad (11)$$

In parallel, one can argue that the sparse-matrix structure of this component of the Hamiltonian makes it very natural to replace also the strictly local (i.e., diagonal-matrix) interaction $\mathbf{v}(q_j)$ by its weakly nonlocal tridiagonal-matrix generalization [32].

3.2. Elementary Example. Once we restrict our attention to the analysis of bound states, the above-mentioned doubly infinite tridiagonal matrices $\mathfrak{h}_{(\text{weakly-local})}$ may be truncated yielding an N by N matrix Hamiltonian. Let us assume here that the latter matrix varies with a single real coupling strength ϵ and with a single real parameter λ modifying the interaction,

$$\mathfrak{h}^{(\epsilon, \lambda)} = T + \epsilon \mathbf{v}^{(\lambda)} = [\mathfrak{h}^{(\epsilon, \lambda)}]^\dagger, \quad \epsilon, \lambda \in \mathbb{R}. \quad (12)$$

This will enable us to assume that our parameters can vary, typically, with time (i.e., $\epsilon = \epsilon(t)$ and/or $\lambda = \lambda(t)$) and that, subsequently, also the energy levels E_n of our quantum system form a set which can, slowly or quickly, vary. Thus, at a time of preparation $t = t_0$ of a Gedankenexperiment the energy of our system may be selected as equal to one of the real and time-dependent eigenvalues of our Hamiltonian \mathfrak{h} . Naturally, the latter operator represents a quantum observable and must be self-adjoint in the underlying physical Hilbert space $\mathcal{H}^{(\text{textbook})}$.

The first nontrivial tridiagonal matrix (12) with $N = 4$ may represent, for example, a schematic quantum system with Hermitian-matrix interaction

$$\mathbf{v}^{(\lambda)} = \begin{bmatrix} 0 & i & 0 & 0 \\ -i & 0 & i\lambda & 0 \\ 0 & -i\lambda & 0 & i \\ 0 & 0 & -i & 0 \end{bmatrix}. \quad (13)$$

The spectrum of energies may be then easily calculated and was sampled in Figure 1. The parameter-dependence of the energies seems to be such that they avoid ‘‘collisions.’’ As long as we choose $\lambda = 1$, that is, Hamiltonian

$$\mathfrak{h}^{(\epsilon, 1)} = \begin{bmatrix} 0 & -1 + i\epsilon & 0 & 0 \\ -1 - i\epsilon & 0 & -1 + i\epsilon & 0 \\ 0 & -1 - i\epsilon & 0 & -1 + i\epsilon \\ 0 & 0 & -1 - i\epsilon & 0 \end{bmatrix}, \quad (14)$$

the quadruplet of the energy eigenvalues becomes available also in the closed form

$$E_{\pm, \pm} = \pm \frac{1}{2} \sqrt{(6 \pm 2\sqrt{5})(1 + \epsilon^2)}. \quad (15)$$

This formula explains not only the hyperbolic shapes of the curves in Figure 1 but also their closest-approach values $E_{\pm, +} \approx \pm 1.618033988$ and $E_{\pm, -} \approx \pm 0.6180339880$ at $\epsilon = 0$.

The details of the generic avoided-crossing phenomenon are model-dependent but an analogous observation will be made using *any* Hermitian-matrix Hamiltonian. The explanation may be found in Kato’s book [33]. In essence, Kato’s mathematical statement is that once a given matrix is self-adjoint *alias* Hermitian, then in the generic case (i.e., without any additional symmetries) an arbitrary pair of the eigenvalues can only merge at the so-called exceptional-point (EP) value of the parameter. In the Hermitian diagonalizable (i.e., physical) cases, these EP values are all necessarily complex so that whenever the parameter remains real, the distances between the separate real eigenvalues behave as if controlled by a mutual ‘‘repulsion’’ (A deeper analysis may be found in the Kato’s book [33]). From Figure 1 we may then extract one of the key messages mediated by the model, namely, the observation that the unitary evolution is ‘‘robust.’’ One may expect that whenever we need to achieve an unavailed crossing of the eigenvalues, the more adequate description of the phenomenon will be provided by the transition to non-Hermitian Hamiltonians in $\mathcal{F}^{(\text{NH})}$ for which the EP values may be real.

4. Attraction of Eigenvalues

The phenomenon of the existence of a minimal distance between the energy levels of a Hermitian matrix is generic. After one tries to move from family $\mathcal{F}^{(H)}$ to family $\mathcal{F}^{(\text{NH})}$, the robust nature of such an obstruction is lost. The reason lies in the above-mentioned change of the geometry of the Hilbert spaces in question. The resulting new freedom of

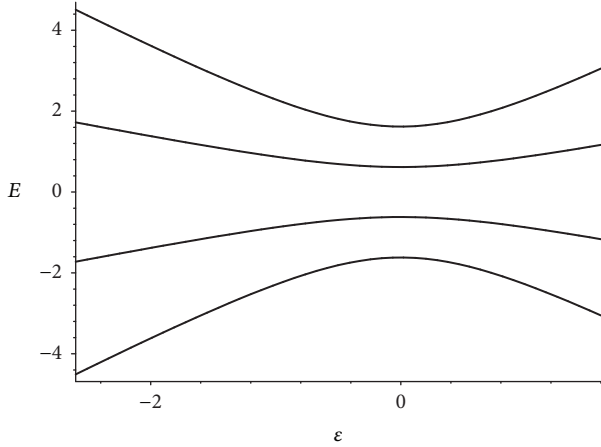


FIGURE 1: The repulsion of the eigenvalues of the Hermitian matrix (12) + (13) with $\lambda = 1$ and $N = 4$ near $\epsilon = 0$.

models in $\mathcal{F}^{(\text{NH})}$ may find applications, for example, in an effective description of nonunitarities in open quantum systems [34] or, in cosmology, in an elementary explanation of the possibility of a consistently quantized Big Bang [35, 36].

4.1. Local Interactions. One of the reasons of the recent turn of attention to the hidden Hermitian local-interaction models (cf. their sample (10) above) is that the mapping $H \rightarrow \mathfrak{h}$ of (5) produces, in general, strongly nonlocal generalizations of the conventional local Hamiltonians (6). The same argument works in both directions and it enriched the scope of the conventional quantum theory [3, 4]. Several impressive constructive illustrations of such a type of enrichment of the class of the tractable quantum models (treating the direct use of local-interaction models (7) as an important extension of the applied quantum theory) may be found, for example, in [31]. One may conclude that the local-interaction nature and constructive tractability of the alternative models (10) contained in class $\mathcal{F}^{(\text{NH})}$ would render their isospectral partners (3) nonlocal. Thus, some of the weaker forms of the nonlocalities as sampled, for example, in [22, 23, 28] may be expected necessary for the constructive search for the nonempty interfaces $\mathcal{F}^{(H)} \cap \mathcal{F}^{(\text{NH})}$.

4.2. Weakly Nonlocal Interactions. For the purposes of the most elementary though still sufficiently rich illustration of some technical aspects of the transition from $\mathcal{F}^{(H)}$ to $\mathcal{F}^{(\text{NH})}$, one may perform the straightforward de-Hermitization of (13). This yields the two-parametric pencil of Hamiltonian matrices

$$\begin{aligned}
 H^{(\eta, \lambda)} &= T + \eta W^{(\lambda)} \\
 &= \begin{bmatrix} 0 & -1 + \eta & 0 & 0 \\ -1 - \eta & 0 & -1 + \eta\lambda & 0 \\ 0 & -1 - \eta\lambda & 0 & -1 + \eta \\ 0 & 0 & -1 - \eta & 0 \end{bmatrix} \\
 &\neq [H^{(\eta, \lambda)}]^\dagger,
 \end{aligned} \tag{16}$$

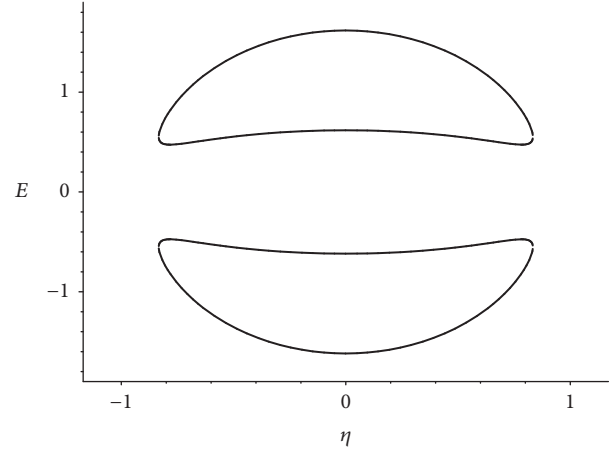


FIGURE 2: The attraction (followed by the loss of reality) in the case of the eigenvalues of the manifestly non-Hermitian matrix (16) at $\lambda = 6/5$.

characterized by a minimal, tridiagonal-matrix nonlocality of their interaction component. For real η and λ the related energy spectra only remain real (i.e., observable and phenomenologically meaningful) in certain physical parametric intervals.

The simplicity of our toy model (16) enables us to illustrate the latter statement by recalling the explicit formula for the eigenvalues,

$$\begin{aligned}
 E_{(\pm, \pm)}(\epsilon, \lambda) &= \pm \frac{1}{\sqrt{2}} \\
 &\cdot \sqrt{3 - (\lambda^2 + 2)\epsilon^2 \pm \sqrt{[5 - (\lambda^2 + 4)\epsilon^2](1 - \lambda^2\epsilon^2)}}.
 \end{aligned} \tag{17}$$

The knowledge of this formula enables us to separate the interval of the interaction-controlling parameters λ into three qualitatively different subintervals.

4.2.1. $\lambda > 1$ (Strong Non-Hermiticities). The first, $\lambda > 1$ sample of the energy spectrum is displayed here in Figure 2. The picture shows that at the two real exceptional points $\eta = \eta^{(\text{EP})}$ such that $|\eta| = |\eta^{(\text{EP})}| < 1$ the (real-energy) quadruplets of energies degenerate and, subsequently, acquire imaginary components. These complexifications proceed pairwise; that is, our four-level model effectively decays into two almost independent, weakly coupled two-level systems. The full descriptive wealth of our model will only manifest itself at the smaller values of λ .

4.2.2. $\lambda < 1$ (Weak Non-Hermiticities). In Figure 3 using a smaller $\lambda < 1$ a much more interesting scenario is displayed in which all of the four energy levels are mutually attracted. Firstly we notice that the complexifications of the eigenvalues occur at the EP values $\eta_{(\text{first kind})}^{(\text{EP})}$ which are “large”, that is, $|\eta_{(\text{first kind})}^{(\text{EP})}| > 1$. The domain of the observability of the energies is larger than interval $(-1, 1)$. Still, the latter interval has natural boundaries because of the emergence of the other two

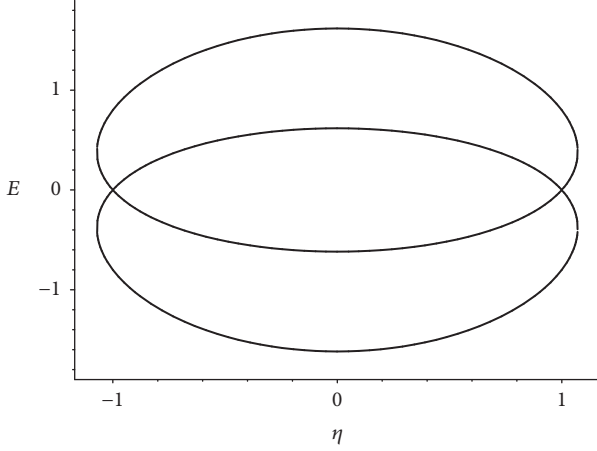


FIGURE 3: Same as Figure 2, with smaller $\lambda = 3/5$.

EP degeneracies at $\eta_{(\text{second kind})}^{(\text{EP})} = \pm 1$. These new singularities are characterized by the unavoided level crossings without a complexification. Their occurrence splits the interval of η into separate subintervals. The consequences for the quantum phenomenology are remarkable, for example, for the reasons which were discussed, recently, in [13–16].

$$\Theta_{(c,d,f,g)}^{(\eta,\lambda)} = \begin{bmatrix} A(f,c) & \frac{(g-d)(1+\eta)}{1-\eta\lambda} & \frac{c}{1-\eta} & d \\ \frac{(g-d)(1+\eta)}{1-\eta\lambda} & \frac{f}{1-\eta\lambda} & g & \frac{c}{1+\eta} \\ \frac{c}{1-\eta} & g & \frac{f}{1+\eta\lambda} & \frac{(g-d)(1-\eta)}{1+\eta\lambda} \\ d & \frac{c}{1+\eta} & \frac{(g-d)(1-\eta)}{1+\eta\lambda} & F(f,c) \end{bmatrix}, \quad (19)$$

where

$$A(f,c) = \frac{f - f\eta^2 - c + c\eta^2\lambda^2}{(1-\eta)^2(1-\eta\lambda)}, \quad (20)$$

$$F(f,c) = \frac{f - f\eta^2 - c + c\eta^2\lambda^2}{(1+\eta)^2(1+\eta\lambda)}.$$

Thus, one can summarize that unless we add more requirements, the specification of the mere Hamiltonian leads to the four-parametric family of the inner-product metric operators (19). Obviously, this opens the possibility of the choice of the additional observables which would have to satisfy (A.1) and, thereby, restrict the freedom in our choice of the parameters c , d , f , and g .

One of the possible formal definitions of an “interface” between the alternative descriptions (2) and (4) of a quantum system may be based on the presence of a variable parameter or parameters (say, of a real $\sigma \in (-\infty, \infty)$) such that $\mathfrak{h} = \mathfrak{h}(\sigma)$ and $H = H(\sigma)$. One may then reveal that there exists a point σ_0 or a non-empty closed vicinity $I_0 = (\sigma_-, \sigma_+)$ of this point

4.2.3. $\lambda = 1$ (*The Instant of Degeneracy*). The shared boundary between the two dynamical regimes is characterized by Figure 4. The algebraic representation of the $\lambda = 1$ spectrum is elementary,

$$E_{\pm,\pm} = \pm \frac{1}{2} \sqrt{(6 \pm 2\sqrt{5})(1-\eta^2)}. \quad (18)$$

The formula may be read as an analytic continuation of (15).

5. The Model with Interface

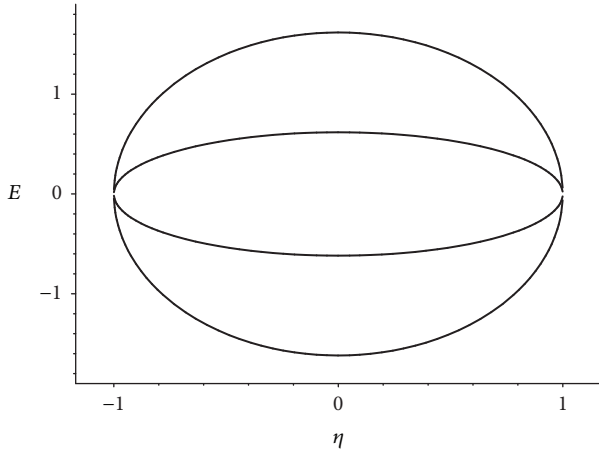
5.1. *Hilbert-Space Metric*. In comparison with the conventional textbook family $\mathcal{F}^{(H)}$, the practical use of the non-Hermitian phenomenological Hamiltonians in $\mathcal{F}^{(\text{NH})}$ is certainly much more difficult. One of the key complications is to be seen in the (in general, non-unique) reconstruction of the metric from the given observables or, in the simplest case, from Hamiltonian H .

The ambiguity of the reconstruction may be illustrated by the insertion of our two-parametric toy model $N = 4$ Hamiltonian $X = H^{(\eta,\lambda)}$ of (16) in the quasi-Hermiticity constraint (A.1) in Appendix A interpreted as an implicit definition of $\Theta^{(\eta,\lambda)} = \Theta(H^{(\eta,\lambda)})$. After a tedious but straightforward algebra one obtains the general result

such that the formally equivalent Schrödinger equations (2) and (4) are also more or less equally user-friendly when $\sigma \in I_0$. Naturally, such a concept will make sense when just the solution of one of the Schrödinger equations remains feasible and practically useful far from σ_0 .

Whenever one tries to treat σ as a function of time, a number of technical complications immediately emerge (the most recent account of some of them may be found in [37]). One has to assume, therefore, that the time-variation of σ as well as the σ -variation of the Hamiltonians remains sufficiently slow, that is, so slow that the corresponding time-derivatives of σ and the σ -derivatives of the Hamiltonians remain negligible. Under these assumptions, the passage of certain quantum systems through their respective HSP-NHSP interfaces can be shown possible.

5.2. *Illustrative Hamiltonian*. One of the most straightforward implementations of the above idea may be based on the identification of the above-introduced parameter σ with the parameter ϵ of (12) (and, say, of Figure 1) along the negative real half-axis, and with the parameter η of (16) (and


 FIGURE 4: The confluence of exceptional points at $\lambda = 1$.

of Figure 4) along the positive real half-axis. In such an arrangement the interval of a large and negative $\sigma \ll -1$ will be the domain in which the use of the non-Hermitian picture $\mathcal{F}^{(\text{NH})}$ (with any nontrivial metric) would prove absolutely useless. In parallel, any attempt of working with the Hermitian picture $\mathcal{F}^{(H)}$ will necessarily fail close to $\sigma \approx +1$ and further to the right. At the same time, in practically any interval of the positive $\sigma = \eta \in I_0 = (0, \sigma_+)$ with $\sigma_+ < 1$, we would be able to work, more or less equally easily, with both of the non-Hermitian and Hermitian versions of the matrix.

The main advantage of the work in simultaneous pictures, that is, with the Hamiltonian matrix defined in $\mathcal{F}^{(\text{interface})}$, may be seen in the smoothness of the transitions to both of the neighboring pictures $\mathcal{F}^{(H)}$ and $\mathcal{F}^{(\text{NH})}$. This smoothness is nontrivial because the respective behaviors of the quantum system in question will be different, in spite of the unified definition of the dynamics. Thus, once we set

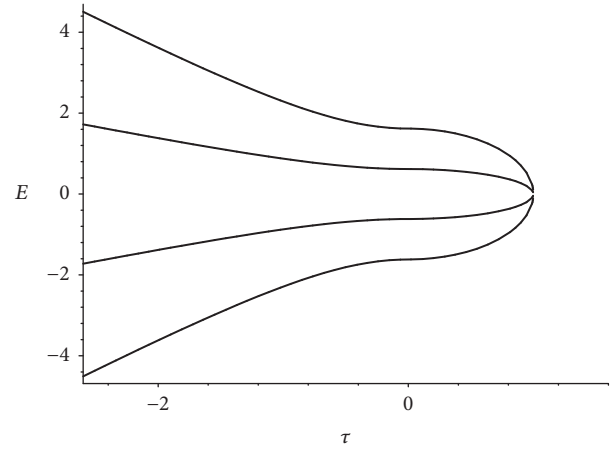
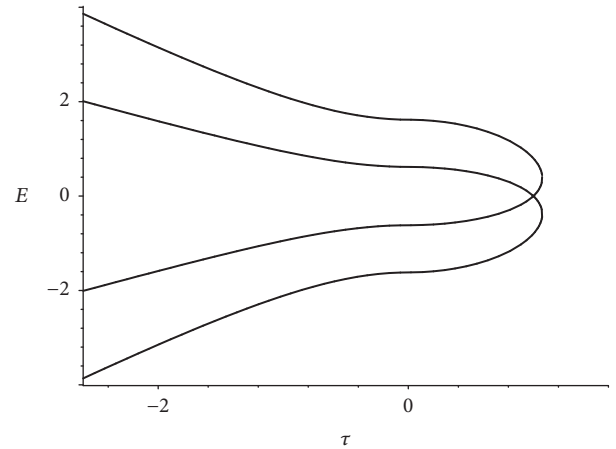
$$H^{(\text{unified})} = \begin{bmatrix} 0 & -1 + \gamma(\tau) & 0 & 0 \\ -1 - \gamma(\tau) & 0 & -1 + \gamma(\tau) & 0 \\ 0 & -1 - \gamma(\tau) & 0 & -1 + \gamma(\tau) \\ 0 & 0 & -1 - \gamma(\tau) & 0 \end{bmatrix}, \quad (21)$$

with

$$\gamma(\tau) = \sqrt{\tau^2 \cdot \text{sign } \tau} = \begin{cases} i\tau, & \tau < 0, \\ \tau, & \tau \geq 0, \end{cases} \quad (22)$$

we will be able to interpolate, smoothly, between the eigenvalue repulsion to the left and the eigenvalue attraction to the right (see Figure 5).

In addition, one may also appreciate the asymmetry of the spectrum. In the purely phenomenological setting it could be interpreted, for example, as a transition from the conventional and robust dynamical regime to the emergence of an instability and collapse at positive $\tau = 1$. Marginally, let us also note that our choice of notation is indicative because τ


 FIGURE 5: Monotonic convergence of eigenvalues of matrix (21) with the growth of τ .

 FIGURE 6: Same as Figure 5 but with a slightly smaller $\lambda = 3/5$.

might have been perceived as a time variable, in an adiabatic regime at least [37]. Another marginal comment is that at $\tau > \tau^{(\text{EP})} = 1$, that is, at $\tau = \sqrt{1 + \varrho^2} > 1$, the eigenvalues form the two purely imaginary complex-conjugate pairs

$$\pm \frac{i\varrho}{2} \sqrt{(6 \pm 2\sqrt{5})} \approx \begin{cases} \pm 1.618033988 i\varrho \\ \pm 0.6180339880 i\varrho. \end{cases} \quad (23)$$

In the light of our preceding analysis it is not too surprising that for the larger values of $\lambda > 1$ the simultaneous complexification of the eigenvalues would occur at a slightly smaller EP singularity $\tau^{(\text{EP})} < 1$ and that the model would effectively decay into the two two-level subsystems. Such an observation might be contrasted with the more interesting spectral pattern obtained at $\lambda = 3/5$ and displayed in Figure 6.

5.3. The Interface-Compatible Metrics. The physical interpretation of the parameter σ need not be specified at all. Its interface values $\sigma_0 \in I_0$ might mark a critical time or the position of a spatial boundary or a critical value of the strength of influence of an environment, and so forth.

In our present illustrative model the specification of the left boundary point $\sigma_- = 0$ is unique because of the natural choice of $\Theta = I$ along the whole negative half-axis of σ . In contrast, our choice of the right boundary point $\sigma_+ < 1$ remains variable because we always have $\Theta \neq I$ for all of the positive physical values of σ .

We have to match the Hermitian choice of $\Theta = I$ valid at the negative half-axis of $\sigma \leq 0$ to the hidden-Hermiticity choice of $\Theta \neq I$ at the small and positive $\sigma > 0$. We may recall formula (19) and deduce that

$$\lim_{\eta \rightarrow 0} \Theta_{(c,d,f,g)}^{(\eta,\lambda)} = \begin{bmatrix} f-c & g-d & c & d \\ g-d & f & g & c \\ c & g & f & g-d \\ d & c & g-d & f-c \end{bmatrix}. \quad (24)$$

Even if we admit that the values of the parameters in the metric may be η -dependent, $c = c(\eta)$, $d = d(\eta)$, $f = f(\eta)$, and $g = g(\eta)$, we must demand that $d(0) = c(0) = g(0) = 0$ and normalize, say, $f(0) = 1$. This yields the metric which is diagonal at $\eta = 0$ and which remains diagonal after we require that the parameters remain constant, η -independent. The elements forming the diagonal of such a special Hilbert-space metric Θ read

$$\left\{ \frac{1+\eta}{(1-\eta)(1-\eta\lambda)}, \frac{1}{1-\eta\lambda}, \frac{1}{1+\eta\lambda}, \frac{1-\eta}{(1+\eta)(1+\eta\lambda)} \right\}. \quad (25)$$

In Figure 7 we may see the coincidence of these elements in the limit $\eta \rightarrow 0$, demonstrating the smooth variation of the metric Θ in the both-sided vicinity of $\eta = 0$.

The construction of the kinetic energy part T of all of our toy model matrix Hamiltonians H with $N = 4$ was based on the assumption that there exist coordinates q forming a spatial grid-point lattice. In the present context this means that once the metric (25) remains diagonal, in an interval of small $\sigma = \eta > 0$ at least, we may conclude that the strong-non-locality effects as caused by the metric Θ and observed, say, in [21, 31] are absent here. In this sense, our present model shares the weak-nonlocality merits of its predecessors in [22, 23, 28].

Our diagonal metric remains positive and invertible, at the sufficiently small η at least. Naturally, it also has the EP-related singularities at $\eta_{(\text{first kind})}^{(\text{EP})} = \pm 1/\lambda$. Their occurrence and λ -dependence are illustrated here in Figure 8. Naturally, for $\lambda < 1$ there emerge also the singularities at $\eta_{(\text{second kind})}^{(\text{EP})} = \pm 1$ (see the dedicated references [13–16] for a more thorough explanation of this terminology).

6. Summary and Conclusions

In the conventional applications to quantum theory, the description of the unitary evolution of a given system \mathcal{S} need not necessarily be performed in Schrödinger picture (cf., e.g., the compact review of its eight eligible alternatives in [24]). Naturally, once people decide to prefer the work in Schrödinger picture, they usually recall Stone's theorem [29] and conclude that the Hamiltonian (i.e., in our present

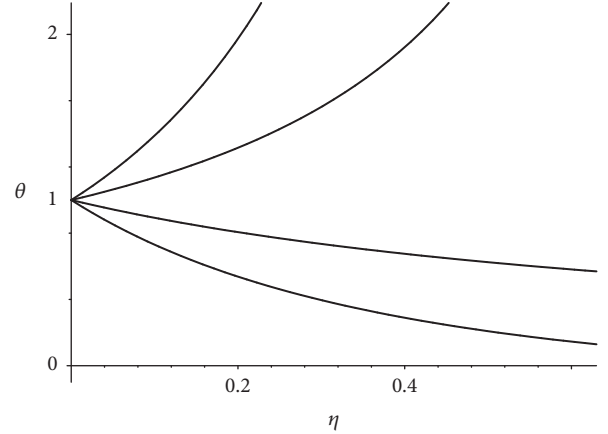


FIGURE 7: The η -dependence of the eigenvalues of the metric Θ of (25) at $\lambda = 6/5$.

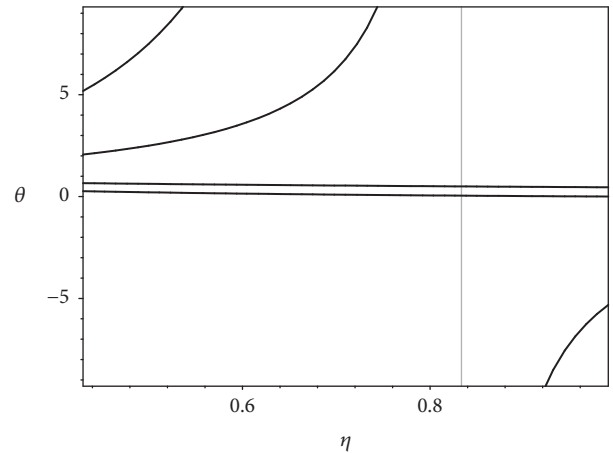


FIGURE 8: The prolongation of Figure 7 beyond $\eta^{(\text{EP})} = 5/6$.

notation, operator $\mathfrak{H} \in \mathcal{F}^{(H)}$ acting in the conventional Hilbert space $\mathcal{H}^{(\text{textbook})}$) must necessarily be Hermitian (for the sake of brevity we spoke here about the HSP realization of Schrödinger picture).

Along a complementary, different line of thinking which dates back to Dyson [1] and which recently climaxed with Bender [4] and Mostafazadeh [3], the community of physicists already accepted the consistency of the alternative, NHSP realization of the same Schrödinger picture. In the NHSP version and language the Hamiltonian (i.e., the upper-case operator $H \in \mathcal{F}^{(\text{NH})}$ with real spectrum) is naturally self-adjoint in the physical Hilbert space $\mathcal{H}^{(\text{redefined})}$ which is, unfortunately, highly unconventional. The same operator H only *appears* manifestly non-Hermitian in the other, auxiliary, “redundant” Hilbert space $\mathcal{H}^{(\text{unphysical})}$ which is, by assumption, “the friendliest” one.

It is unfortunate that the latter, historically developed terminology is so confusing. This is one of the explanations why the methodically important question of the possible HSP/NHSP overlap of applicability has not yet been properly addressed and clarified in the literature. In our present paper

we filled the gap by showing that such an overlap (called, by Jones [21], an “interface”) may exist. We also emphasized that the construction of the interface should start from the uppercase (and, typically, one-parametric) family of the hiddenly Hermitian NHSP Hamiltonians operators $H = H(\sigma) \in \mathcal{F}^{(\text{NH})}$ and that it has to be based on the analysis of the related family of the Hermitizing metric operators $\Theta = \Theta[H(\sigma)]$.

In such a framework one can conclude that Hamiltonian $H = H(\sigma)$ with $\sigma \in (\sigma_-, \sigma_+)$ can be perceived as an element of an HSP/NHSP overlap $\mathcal{F}^{(\text{interface})} \neq \emptyset$, provided only that the Hermitizing metric operator at our disposal (i.e., operator $\Theta = \Theta[H(\sigma)]$) is such that

$$\lim_{\sigma \rightarrow \sigma_-} \Theta[H(\sigma)] = I. \quad (26)$$

In other words, once we have $H(\sigma_-) = H^\dagger(\sigma_-)$, we may now introduce the quantum Hamiltonians $\mathfrak{h}(\sigma)$ (which lie, by construction, in $\mathcal{F}^{(H)}$) in such a way that they are connected with $H(\sigma)$ (i.e., defined) by relation (5) at $\sigma \in (\sigma_-, \sigma_+)$ while their definition may be continued to $\sigma < \sigma_-$ arbitrarily (e.g., by the most straightforward constant-operator prescription $\mathfrak{h}(\sigma) = H(\sigma_-)$).

The lower boundary σ_-0 of the interval of the interface-compatible parameters carries an immediate physical meaning of a point of transition from the HSP eigenvalue repulsion regime (guaranteeing the robust reality of the spectrum) to the NHSP eigenvalue attraction (and, possibly, complexification). Via an elementary illustrative example, we demonstrated that the resulting “mixed” dynamics could enrich the current phenomenological considerations in quantum theory. Naturally, this is a task for future research because our present, methodically motivated and analytically solvable example is only too schematic for such a purpose.

Appendix

A. Unitary Evolution via Non-Hermitian H

A.1. The Third Hilbert Space. Strictly speaking, the real spectra of eigenvalues of $H \neq H^\dagger$ as well as of any other operator $X \neq X^\dagger$ of the observable characterizing the quantum system in question cannot be assigned any immediate physical meaning because the underlying Hilbert space $\mathcal{H}^{(\text{unphysical})}$ is, by definition, just auxiliary and “incorrect.” The “correct” meaning of the observables can only be established in the “correct” Hilbert space $\mathcal{H}^{(\text{textbook})}$. Whenever needed, any experimental prediction may be reconstructed using the correspondences $\psi(t) = \Omega\Psi(t)$, $\mathfrak{h} = \Omega H \Omega^{-1}$, and $\mathfrak{x} = \Omega X \Omega^{-1}$.

One of the benefits of the NHSP representation is that in the generic stationary case the full knowledge of Dyson’s operator Ω is not necessary. What controls the predictions are just the mean values of the operators of observables. For them, the translations of the relevant formulae from $\mathcal{H}^{(\text{textbook})}$ to $\mathcal{H}^{(\text{unphysical})}$ may be shown to contain only the so-called Hilbert-space metric, that is, the Dyson-map product $\Theta = \Omega^\dagger \Omega$ (see, e.g., [2] for more details). This

implies that in a close parallel to (5), all of the observables of a system in question may be represented by the diagonalizable operators $X \neq X^\dagger$ with real spectra which only have to satisfy the generalized Hermiticity relation

$$X^\dagger \Theta = \Theta X. \quad (\text{A.1})$$

Any Hilbert-space metric Θ which is “mathematically acceptable” (see [3] for details) may be interpreted as redefining the inner product in $\mathcal{H}^{(\text{unphysical})}$. This redefinition of the inner product may be reread as a redefinition of the Hilbert space itself,

$$\mathcal{H}^{(\text{unphysical})} \longrightarrow \mathcal{H}^{(\text{redefined})}. \quad (\text{A.2})$$

By construction, the new space becomes unitarily equivalent to $\mathcal{H}^{(\text{textbook})}$. This means that we may reinterpret Hamiltonians H (sampled by (10) and non-Hermitian in auxiliary $\mathcal{H}^{(\text{unphysical})}$) as self-adjoint in the new Hilbert space $\mathcal{H}^{(\text{redefined})}$. Thus, using the notation of [26] we may write $H = H^\ddagger$, with the definition of $H^\ddagger = \Theta^{-1} H^\dagger \Theta$ being deduced from (5).

In opposite direction, our quantum-model-building may start from a given N -plet $\{X_n\}$ of candidates for the observables. As long as all of these operators (defined in $\mathcal{H}^{(\text{unphysical})}$) must satisfy the respective hidden Hermiticity condition (A.1), there must exist a metric candidate $\Theta = \Theta(X_1, \dots, X_N)$ compatible with all of these hidden-Hermiticity conditions. Thus, the metric need not exist at all (see an example in [38]). If it does exist, it may be either ambiguous (see an example in [31]) or unique (see, e.g., a large number of examples in [4]).

A.2. Physical Inner Products. The non-Hermiticity property of operators might cause complications in calculations. Also the assumptions of the user-friendliness of $\mathcal{H}^{(\text{unphysical})}$ and/or of $H(t)$ seem highly nontrivial. On the level of theory one must keep in mind that the new, friendlier Hilbert space is, by itself, merely auxiliary and unphysical. In principle, a return to $\mathcal{H}^{(\text{textbook})}$ is needed whenever experiment-related predictions are asked for. Still, whenever the structures of such a space and/or of the observables (defined in this space and sampled by Hamiltonian \mathfrak{h}) appear prohibitively complicated, the evaluation of the predictions of the theory is to be made also directly in $\mathcal{H}^{(\text{unphysical})}$. Due care must only be paid to the insertions of the metric operator $\Theta = \Omega^\dagger \Omega \neq I$ (i.e., to the amendments of the inner products) whenever applicable [3].

People do not always notice that after the latter amendment of the inner product our auxiliary Hilbert space $\mathcal{H}^{(\text{unphysical})}$ becomes redefined and converted into another, third Hilbert space $\mathcal{H}^{(\text{redefined})}$ which is, by construction, physical, that is, unitarily equivalent to $\mathcal{H}^{(\text{textbook})}$. Thus, whenever we start from (4), the quantum system in question becomes *simultaneously* represented in a *triplet* of Hilbert spaces (the pattern is displayed in Figure 9).

Naturally, Stone’s theorem does not get violated due to the one-to-one, Ω -mediated correspondence between H and \mathfrak{h} . Due to the property $\Omega^\dagger \Omega = \Theta \neq I$ of Dyson’s nonunitary

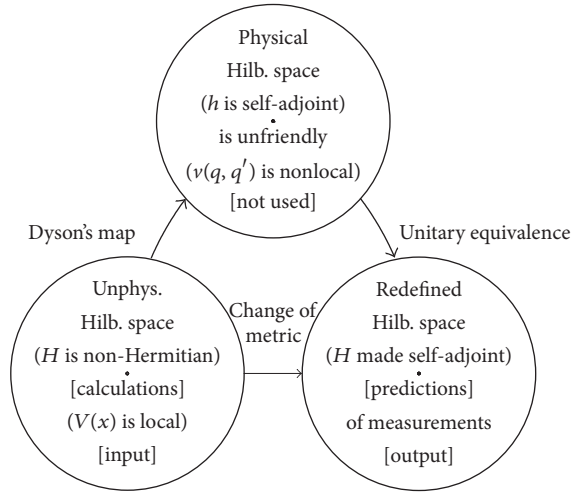


FIGURE 9: The three-Hilbert-space representation pattern.

mappings, the Hermiticity of the conventional Hamiltonian \mathfrak{h} in the physical space $\mathcal{H}^{(\text{textbook})}$ becomes replaced, in the auxiliary and manifestly unphysical Hilbert space $\mathcal{H}^{(\text{unphysical})}$, by the hidden-Hermiticity *alias* Θ -pseudo-Hermiticity [3] property $H = \Theta^{-1}H^\dagger\Theta$ of the uppercase non-Hermitian Hamiltonian with real spectrum (cf. (4)). In the related literature one can also read about the closely related concepts of quasi-Hermiticity (see [2]), unbroken \mathcal{PT} -symmetry [4], or crypto-Hermiticity [26, 39] of H and/or, last but not least, about the quasi-similarity between H and H^\dagger [40].

A.3. The Hermitian-Theory Point of View. Technically, it is usually easier to work with the elements of the “Hermitian” family $\mathcal{F}^{(H)}$ comprising the traditional quantum systems and the traditional textbook self-adjoint Hamiltonians $\mathfrak{h} = \mathfrak{h}^\dagger$. Dyson [1] merely proposed that sometimes it may still make sense to make use of the other, innovative family $\mathcal{F}^{(\text{NH})}$ which works with the “non-Hermitian” Schrödinger equations (4). Certainly, the latter family is not small. Pars pro toto it contains Hamiltonians of relativistic quantum mechanics [41, 42], the well-known \mathcal{PT} -symmetric imaginary cubic oscillator [43–46] (which appears, after a more detailed scrutiny, strongly nonlocal [31, 47]), its power-law generalizations [10–12, 48] as well as exactly solvable models [49–52], models with methodical relevance in the context of supersymmetry [53, 54], realistic and computation-friendly interacting-boson models of heavy nuclei [2], benchmark candidates for classification of quantum catastrophes [55–57], and so forth.

In the majority of the above-listed models defined in $\mathcal{F}^{(\text{NH})}$ one may still keep in mind that their physical contents can always be sought in their equivalence to the partner Hamiltonians (and/or other observables) in $\mathcal{F}^{(H)}$. Thus, the use of the less usual representation in $\mathcal{F}^{(\text{NH})}$ is treated as a mere technical trick.

The main argument against the latter, fairly widespread point of view may be formulated as an objection against the overintimate, history-produced relationship between the

way of our thinking in classical physics and the related production of the “conventional” quantum models in $\mathcal{F}^{(H)}$ by the techniques of the so-called “quantization.” In principle, we should have been much more humble, taking rather the classical world as a result of making its quantum picture “dequantized” [58].

Data Availability

There are no relevant data to be made available.

Conflicts of Interest

The author declares that there are no conflicts of interest.

Acknowledgments

The work was supported by the GAČR Grant No. 16-22945S.

References

- [1] F. J. Dyson, “General theory of spin-wave interactions,” *Physical Review A: Atomic, Molecular and Optical Physics*, vol. 102, no. 5, pp. 1217–1230, 1956.
- [2] F. G. Scholtz, H. B. Geyer, and F. J. Hahne, “Quasi-Hermitian operators in quantum mechanics and the variational principle,” *Annals of Physics*, vol. 213, no. 1, pp. 74–101, 1992.
- [3] A. Mostafazadeh, “Pseudo-Hermitian representation of quantum mechanics,” *International Journal of Geometric Methods in Modern Physics*, vol. 7, no. 7, pp. 1191–1306, 2010.
- [4] C. M. Bender, “Making sense of non-Hermitian Hamiltonians,” *Reports on Progress in Physics*, vol. 70, no. 6, pp. 947–1018, 2007.
- [5] J. Dieudonné, “Quasi-Hermitian operators,” in *Proceedings of the International Symposium on Linear Spaces (Jerusalem, 1960)*, pp. 115–122, Oxford, Pergamon, 1961.
- [6] J. Alexandre, C. M. Bender, and P. Millington, “Non-Hermitian extension of gauge theories and implications for neutrino physics,” *Journal of High Energy Physics*, vol. 2015, no. 11, article no. 111, pp. 1–24, 2015.
- [7] J. Alexandre, C. M. Bender, and P. Millington, “Light neutrino masses from a non-Hermitian Yukawa theory,” *Journal of Physics: Conference Series*, vol. 873, p. 012047, 2017.
- [8] T. J. Milburn, J. Doppler, C. A. Holmes, S. Portolan, S. Rotter, and P. Rabl, “General description of quasiadiabatic dynamical phenomena near exceptional points,” *Physical Review A: Atomic, Molecular and Optical Physics*, vol. 92, no. 5, Article ID 052124, 2015.
- [9] A. Mostafazadeh, “Time-Dependent Pseudo-Hermitian Hamiltonians Defining a Unitary Quantum System and Uniqueness of the Metric Operator,” *Physics Letters B*, vol. 650, pp. 208–212, 2007.
- [10] C. M. Bender and S. Boettcher, “Real spectra in non-Hermitian Hamiltonians having \mathcal{PT} symmetry,” *Physical Review Letters*, vol. 80, no. 24, pp. 5243–5246, 1998.
- [11] C. M. Bender, D. C. Brody, and H. F. Jones, “Complex extension of quantum mechanics,” *Physical Review Letters*, vol. 89, Article ID 270401, 2002.
- [12] C. M. Bender, D. C. Brody, and H. F. Jones, “Erratum: Complex Extension of Quantum Mechanics,” *Physical Review Letters*, vol. 92, no. 11, Article ID 119902, 2004.

- [13] D. I. Borisov, "Eigenvalue collision for PT-symmetric waveguide," *Acta Polytechnica*, vol. 54, no. 2, pp. 93–100, 2014.
- [14] D. I. Borisov, F. Růžička, and M. Znojil, "Multiply degenerate exceptional points and quantum phase transitions," *International Journal of Theoretical Physics*, vol. 54, no. 12, pp. 4293–4305, 2015.
- [15] M. Znojil, "Solvable model of quantum phase transitions and the symbolic-manipulation-based study of its multiply degenerate exceptional points and of their unfolding," *Annals of Physics (NY)*, vol. 336, pp. 98–111, 2013.
- [16] D. I. Borisov and M. Znojil, "Mathematical and physical meaning of the crossings of energy levels in PT-symmetric systems," in *Non-Hermitian Hamiltonians in Quantum Physics*, F. Bagarello, R. Passante, and C. Trapani, Eds., pp. 201–217, Springer, 2016.
- [17] C. E. Rüter, K. G. Makris, R. El-Ganainy, D. N. Christodoulides, M. Segev, and D. Kip, "Observation of parity-time symmetry in optics," *Nature Physics*, vol. 6, no. 3, pp. 192–195, 2010.
- [18] F. Bagarello, J. P. Gazeau, F. H. Szafraniec, and M. Znojil, Eds., *Non-Selfadjoint Operators in Quantum Physics*, John Wiley & Sons, Inc., Hoboken, NJ, 2015.
- [19] M. Znojil, "Scattering theory using smeared non-Hermitian potentials," *Physical Review D: Particles, Fields, Gravitation and Cosmology*, vol. 80, no. 4, 045009, 12 pages, 2009.
- [20] H. F. Jones, "Scattering from localized non-Hermitian potentials," *Physical Review D*, vol. 76, Article ID 125003, 2007.
- [21] H. F. Jones, "Interface between Hermitian and non-Hermitian Hamiltonians in a model calculation," *Physical Review D*, vol. 78, Article ID 065032, 2008.
- [22] M. Znojil, "Discrete PT-symmetric models of scattering," *Journal of Physics A: Mathematical and Theoretical*, vol. 41, no. 29, Article ID 292002, 2008.
- [23] M. Znojil, "Cryptohermitian Picture of Scattering Using Quasilocal Metric Operators," *Symmetry Integrability and Geometry Methods and Applications*, vol. 5, Article ID 085, 2009.
- [24] D. F. Styer et al., "Nine formulations of quantum mechanics," *American Journal of Physics*, vol. 70, no. 3, pp. 288–297, 2002.
- [25] A. Messiah, *Quantum Mechanics*, vol. I, North Holland, Amsterdam, 1961.
- [26] M. Znojil, "Three-Hilbert-space formulation of quantum mechanics," *Symmetry Integrability and Geometry Methods and Applications*, vol. 5, Article ID 001, 2009.
- [27] H. F. Jones, in *Proceedings of the*, <http://www.staff.city.ac.uk/~fring/PT/Timetable>.
- [28] M. Znojil, "Scattering theory with localized non-Hermiticities," *Physical Review D: Particles, Fields, Gravitation and Cosmology*, vol. 78, no. 2, 025026, 10 pages, 2008.
- [29] M. H. Stone, "On One-Parameter Unitary Groups in Hilbert Space," in *Annals of Mathematics*, vol. 33 of 2nd, pp. 643–648, 1932.
- [30] S. Flügge, *Practical Quantum Mechanics II*, Springer, Berlin, 1971.
- [31] A. Mostafazadeh, "Metric operator in pseudo-Hermitian quantum mechanics and the imaginary cubic potential," *Journal of Physics A: Mathematical and General*, vol. 39, no. 32, pp. 10171–10188, 2006.
- [32] M. Znojil, "Bound states emerging from below the continuum in a solvable PT-symmetric discrete Schrödinger equation," *Physical Review A: Atomic, Molecular and Optical*, vol. 96, Article ID 012127, 2017.
- [33] T. Kato, *Perturbation Theory for Linear Operators*, vol. 132 of *Grundlehren der Mathematischen Wissenschaften*, Springer, New York, NY, USA, 1966.
- [34] U. Günther and B. F. Samsonov, "Naimark-dilated PT-symmetric brachistochrone," *Physical Review Letters*, vol. 101, no. 23, Article ID 230404, 2008.
- [35] M. Znojil, "Quantum Big Bang without fine-tuning in a toy-model," *Journal of Physics: Conference Series*, vol. 343, Article ID 012136, 2012.
- [36] M. Znojil, "Quantization of big bang in crypto-hermitian heisenberg picture," in *Non-Hermitian Hamiltonians in Quantum Physics*, F. Bagarello, R. Passante, and C. Trapani, Eds., pp. 383–399, Springer, 2016.
- [37] M. Znojil, "Non-Hermitian interaction representation and its use in relativistic quantum mechanics," *Annals of Physics*, vol. 385, pp. 162–179, 2017.
- [38] M. Znojil, I. Semorádová, F. Růžička, H. Moulla, and I. Leghrib, "Problem of the coexistence of several non-Hermitian observables in PT -symmetric quantum mechanics," *Physical Review A: Atomic, Molecular and Optical Physics*, vol. 95, no. 4, Article ID 042122, 2017.
- [39] A. V. Smilga, "Cryptogauge symmetry and cryptoghosts for crypto-Hermitian HAMILtonians," *Journal of Physics A: Mathematical and General*, vol. 41, no. 24, Article ID 244026, 2008.
- [40] J.-P. Antoine and C. Trapani, "Metric Operators, Generalized Hermiticity and Lattices of Hilbert Spaces," in *Non-Selfadjoint Operators in Quantum Physics*, pp. 345–402, John Wiley & Sons, Hoboken, chapter 7 edition, 2015.
- [41] A. Mostafazadeh, "Quantum mechanics of Klein-Gordon-type fields and quantum cosmology," *Annals of Physics*, vol. 309, no. 1, pp. 1–48, 2004.
- [42] V. Jakubský and J. Smejkal, "A positive-definite scalar product for free Proca particle," *Czechoslovak Journal of Physics*, vol. 56, no. 9, pp. 985–997, 2006.
- [43] E. Caliceti, S. Graffi, and M. Maioli, "Perturbation theory of odd anharmonic oscillators," *Communications in Mathematical Physics*, vol. 75, no. 1, pp. 51–66, 1980.
- [44] G. Alvarez, "Bender-Wu branch points in the cubic oscillator," *Journal of Physics A: Mathematical and General*, vol. 27, pp. 4589–4598, 1995.
- [45] D. Bessis, "private communication," 1992.
- [46] G. Alvarez, "private communication," 1994.
- [47] P. Siegl and D. Krejčířik, "On the metric operator for the imaginary cubic oscillator," *Physical Review D*, vol. 86, Article ID 121702(R), 2012.
- [48] M. Znojil, "Topology-controlled spectra of imaginary cubic oscillators in the large- ℓ approach," *Physics Letters A*, vol. 374, pp. 807–812, 2010.
- [49] M. Znojil, "PT- symmetric harmonic oscillators," *Physics Letters A*, vol. 259, no. 3-4, pp. 220–223, 1999.
- [50] G. Lévai and M. Znojil, "Systematic search for PT symmetric potentials with real energy spectra," *Journal of Physics A: Mathematical and General*, vol. 33, no. 40, pp. 7165–7180, 2000.
- [51] M. Znojil, "PT-symmetric square well," *Phys. Lett. A*, vol. 285, no. 1-2, pp. 7–10, 2001.
- [52] M. Znojil and G. Lévai, "Spontaneous breakdown of PT symmetry in the solvable square-well model," *Modern Physics Letters A*, vol. 16, no. 35, pp. 2273–2280, 2001.
- [53] B. K. Bagchi, *Supersymmetry in Quantum And Classical Mechanics*, Chapman & Hall/CRC, 2000.

- [54] M. Znojil, “Non-Hermitian SUSY and singular, PT-symmetrized oscillators,” *Journal of Physics A: Mathematical and General*, vol. 35, no. 9, pp. 2341–2352, 2002.
- [55] M. Znojil, “Maximal couplings in PT-symmetric chain models with the real spectrum of energies,” *Journal of Physics A: Mathematical and Theoretical*, vol. 40, pp. 4863–4875, 2007.
- [56] M. Znojil, “Tridiagonal PT-symmetric N-by-N Hamiltonians and a fine-tuning of their observability domains in the strongly non-Hermitian regime,” *Journal of Physics A: Mathematical and Theoretical*, vol. 40, pp. 13131–13148, 2007.
- [57] M. Znojil, “Quantum catastrophes: a case study,” *Journal of Physics A: Mathematical and Theoretical*, vol. 45, Article ID 444036, 2012.
- [58] D. C. Brody and L. P. Hughston, “Geometric quantum mechanics,” *Journal of Geometry and Physics*, vol. 38, no. 1, pp. 19–53, 2001.

Research Article

The Visualization of the Space Probability Distribution for a Particle Moving in a Double Ring-Shaped Coulomb Potential

Yuan You ¹, Fa-Lin Lu,¹ Dong-Sheng Sun,¹ Chang-Yuan Chen ¹ and Shi-Hai Dong ²

¹New Energy and Electronic Engineering, Yancheng Teachers University, Yancheng 224002, China

²Laboratorio de Información Cuántica, CIDETEC, Instituto Politécnico Nacional, Unidad Profesional Adolfo López Mateos, 07700 Ciudad de México, Mexico

Correspondence should be addressed to Yuan You; yuanyou.w@163.com, Chang-Yuan Chen; yctccc@163.net, and Shi-Hai Dong; dongsh2@yahoo.com

Received 1 October 2017; Accepted 20 February 2018; Published 24 April 2018

Academic Editor: Saber Zarrinkamar

Copyright © 2018 Yuan You et al. This is an open access article distributed under the Creative Commons Attribution License, which permits unrestricted use, distribution, and reproduction in any medium, provided the original work is properly cited. The publication of this article was funded by SCOAP³.

The analytical solutions to a double ring-shaped Coulomb potential (RSCP) are presented. The visualizations of the space probability distribution (SPD) are illustrated for the two- (contour) and three-dimensional (isosurface) cases. The quantum numbers (n, l, m) are mainly relevant for those *quasi*-quantum numbers (n', l', m') via the double RSCP parameter c . The SPDs are of circular ring shape in spherical coordinates. The properties for the relative probability values (RPVs) P are also discussed. For example, when we consider the special case $(n, l, m) = (6, 5, 0)$, the SPD moves towards two poles of z -axis when P increases. Finally, we discuss the different cases for the potential parameter b , which is taken as negative and positive values for $c > 0$. Compared with the particular case $b = 0$, the SPDs are shrunk for $b = -0.5$, while they are spread out for $b = 0.5$.

1. Introduction

Since the ring-shaped noncentral potentials (RSNCPs) are used to describe the molecular structure of Benzene as well as the interaction between the deformed nuclei, they have attracted much attention of many authors [1–14]. Generally, these RSNCPs are chosen as the sum of the Coulomb or harmonic oscillator and the single ring-shaped part $1/(r^2 \sin^2 \theta)$ or the double ring-shaped part $1/(r^2 \sin^2 \theta) + 1/(r^2 \cos^2 \theta)$. In this work, what we are only interested in is the double RSCP, which may be used to describe the properties of ring-shaped organic molecule. The corresponding bound states were investigated by SUSY quantum mechanics and shape invariance [15]. Recently, other complicated double RSCPs have also been proposed [16–25]. Many authors have obtained their solutions in [7, 8, 13, 14, 26]. Among them, the SPDs have been carried out, but their studies are treated either for the radial part in spherical shell $(r, r + dr)$ or for the angular parts [27, 28]. The discussions mentioned above are only concerned with one or two of three variables (r, θ, φ) . To show the SPD in all position spaces, we have studied

the SPD of a single RSCP for two- and three-dimensional visualizations [29]. In this work, our aim is to focus on the more comprehensive SPD for the particle moving in a double RSCP.

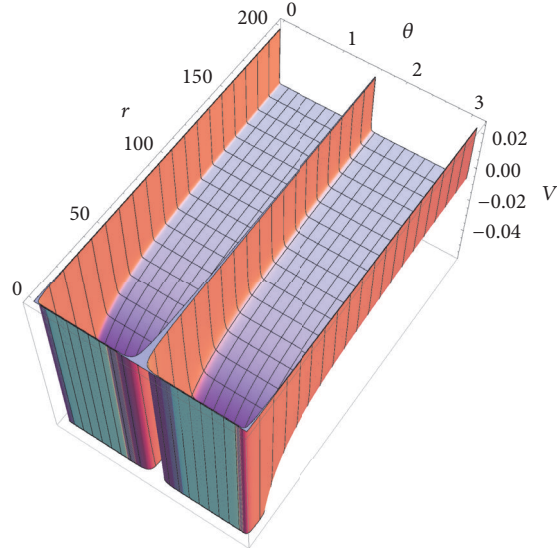
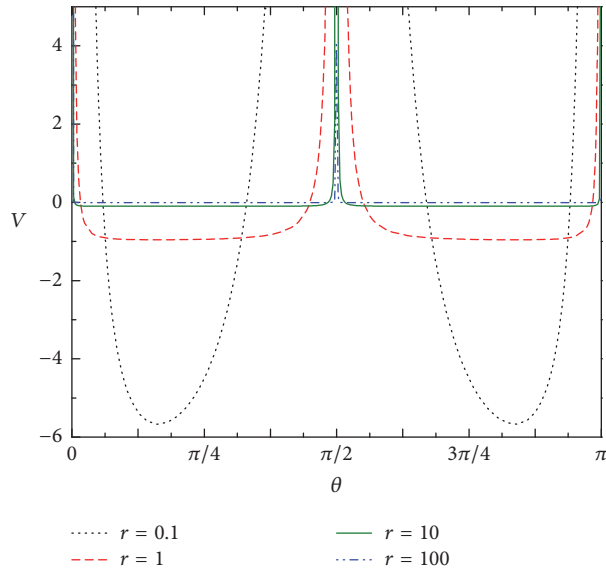
The plan of this paper is as follows. We present the exact solutions to the system in Section 2. In Section 3, we apply the SPD formula to show the visualizations using the similar technique in [29] getting over the difficulty appearing in the calculation skill when using MATLAB program. We discuss their variations on the number of radial nodes, the RPV P , and the RSCP parameter b (positive and negative) when $c \neq 0$ in Section 4. We give our concluding remarks in Section 5.

2. Exact Solutions to a Double RSCP

In the spherical coordinates, the double RSCP is given by

$$V(r, \theta) = -\frac{Ze^2}{r} + \frac{\hbar^2}{2Mr^2} \left(\frac{b}{\sin^2 \theta} + \frac{c}{\cos^2 \theta} \right) \quad (1)$$

as plotted in Figures 1–3.

FIGURE 1: $V(r, \theta)$ as the functions of variables θ and r .FIGURE 2: Potential function $V(r, \theta)$ versus θ at $r = 0.1, 1, 10, 100$.

The Schrödinger equation with this potential is written as ($\hbar = M = e = 1$)

$$\left[-\frac{1}{2}\nabla^2 - \frac{Z}{r} + \frac{1}{2r^2} \left(\frac{b}{\sin^2\theta} + \frac{c}{\cos^2\theta} \right) \right] \Psi(\vec{r}) = E\Psi(\vec{r}). \quad (2)$$

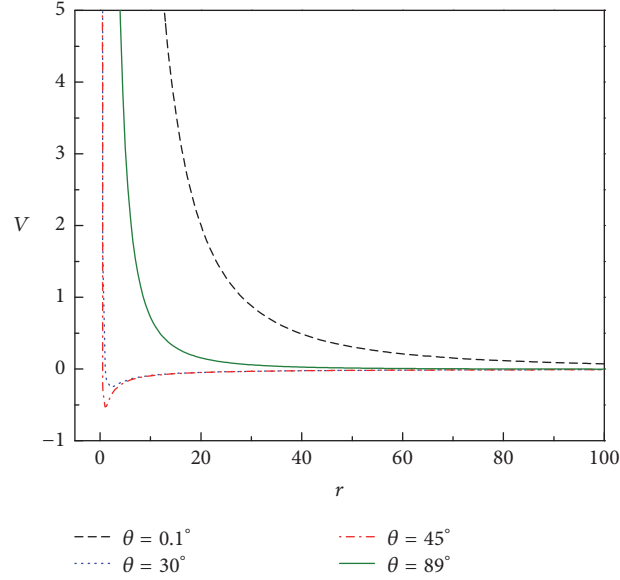
Take wave function as

$$\Psi(\vec{r}) = \frac{1}{\sqrt{2\pi}} \frac{u(r)}{r} H(\theta) e^{\pm im\varphi}, \quad m = 0, 1, 2, \dots \quad (3)$$

Substitute this into (2) and obtain the following differential equations:

$$\frac{d^2 u(r)}{dr^2} + \left(2E + \frac{2Z}{r} - \frac{\lambda}{r^2} \right) u(r) = 0, \quad (4a)$$

$$\frac{1}{\sin\theta} \frac{d}{d\theta} \left(\sin\theta \frac{dH(\theta)}{d\theta} \right) + \left(\lambda - \frac{b+m^2}{\sin^2\theta} - \frac{c}{\cos^2\theta} \right) H(\theta) = 0, \quad (4b)$$


 FIGURE 3: Potential function $V(r, \theta)$ versus r at $\theta = 0.1^\circ, 30^\circ, 45^\circ, 89^\circ$.

where λ is a separation constant. Define $x = \cos \theta$; (4b) is modified as

$$(1-x^2) \frac{d^2 H(x)}{dx^2} - 2x \frac{dH(x)}{dx} + \left(l'(l'+1) - \frac{(m')^2}{1-x^2} - \frac{c}{x^2} \right) H(x) = 0. \quad (5)$$

Its solutions are given by [30]

$$H_{l'm'}(x) = N_{l'm'} P_{l'}^{m'}(\gamma_1, x) = N_{l'm'} (1-x^2)^{m'/2} \cdot x^{\gamma_1} \sum_{\nu=0}^k \frac{(-1)^\nu \Gamma(k+\gamma_1-\nu+1) \Gamma(2l'-2\nu+1)}{2^\nu \nu! (k-\nu)! \Gamma(2k+2\gamma_1-2\nu+1) \Gamma(l'-\nu+1)} x^{2k-2\nu}, \quad (6)$$

where

$$N_{l'm'} = 2^{\gamma_1} \sqrt{\frac{k! (2l'+1) \Gamma(2k+2\gamma_1+1) \Gamma(l'-k+1)}{2\Gamma(l'-k-\gamma_1+1) \Gamma(k+\gamma_1+1) \Gamma(2l'-2k+1)}}, \quad (7)$$

$$m' = \sqrt{b+m^2}, \quad l' = n_\theta + m' = 2k + \gamma_1 + \sqrt{b+m^2}, \quad \lambda = l'(l'+1), \quad |m|, k = 0, 1, 2, \dots,$$

$$\gamma_1 = \begin{cases} 0 \text{ or } 1, & c = 0 \\ \frac{(1 + \sqrt{1+4c})}{2}, & c > 0. \end{cases} \quad (8)$$

We are now in the position to consider (4a). Substituting $\lambda = l'(l'+1)$ into (4a) and taking $\chi = \tau r$, $s = 2Z$, and $\tau = Z\sqrt{-1/(2E)}$, from (4a) we have

$$\frac{d^2 u(\chi)}{d\chi^2} + \left(\frac{s}{\chi} - \frac{1}{4} - \frac{l'(l'+1)}{\chi^2} \right) u(\chi) = 0, \quad (9)$$

whose solutions are given by [18]

$$u_{n'l'}(r) = \frac{1}{\Gamma(2l'+2)} \left[\frac{Z}{a_0} \frac{\Gamma(n'+l'+1)}{n_r! (n')^2} \right]^{1/2}$$

$$\cdot \left(\frac{2Zr}{a_0 n'} \right)^{l'+1} \cdot e^{-Zr/a_0 n'} F \left(-n_r, 2l'+2, \frac{2Zr}{a_0 n'} \right), \quad (10)$$

where

$$n' = n_r + l' + 1 = \begin{cases} n_r + 2k + m' + \frac{(3 + \sqrt{1+4c})}{2}, & c > 0, \quad n_r, m, k = 0, 1, 2, \dots \\ n_r + k + m' + 1, & c = 0, \quad n_r, m, k = 0, 1, 2, \dots \end{cases} \quad (11)$$

TABLE I: The isosurface SPDs with a section plane.

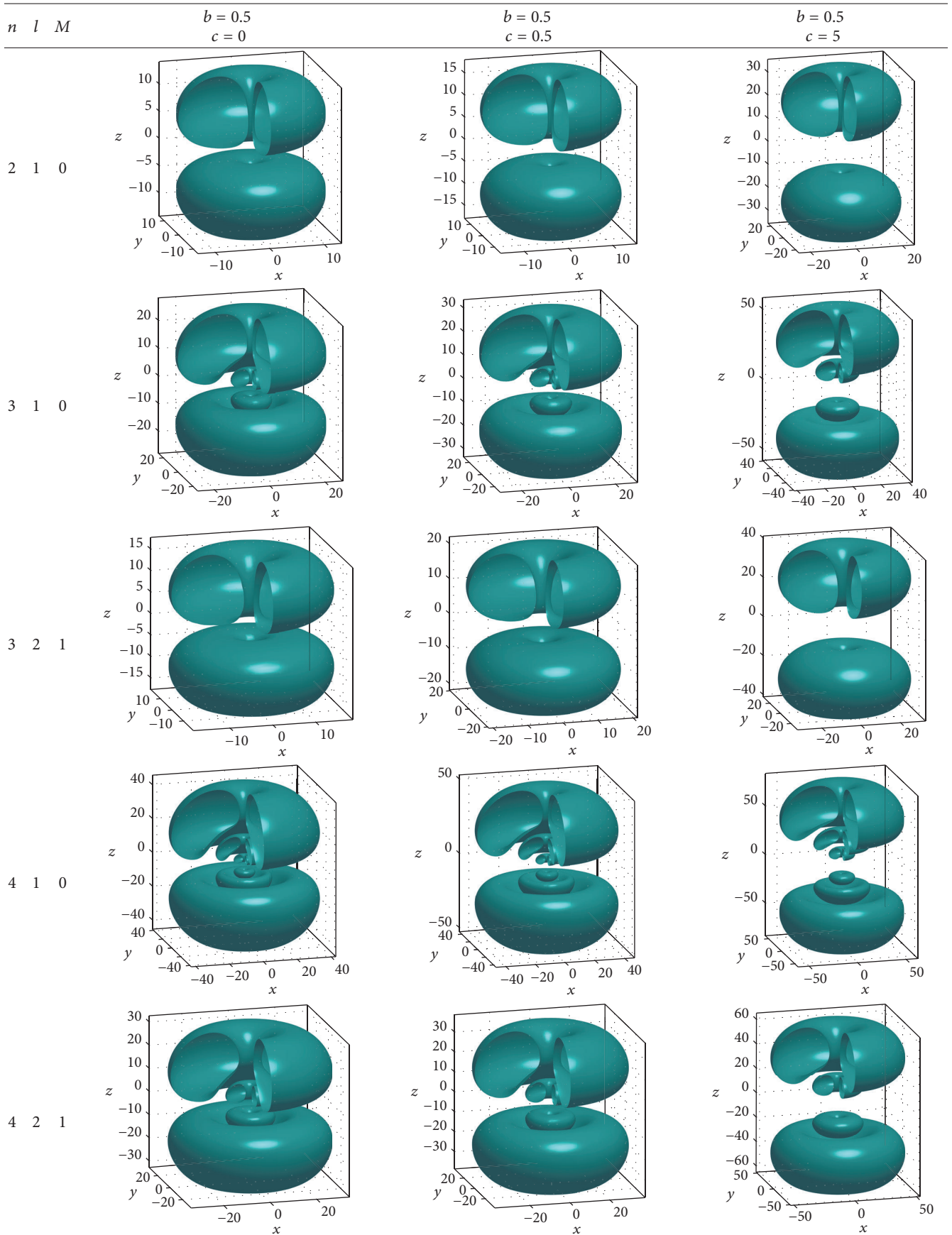


TABLE I: Continued.

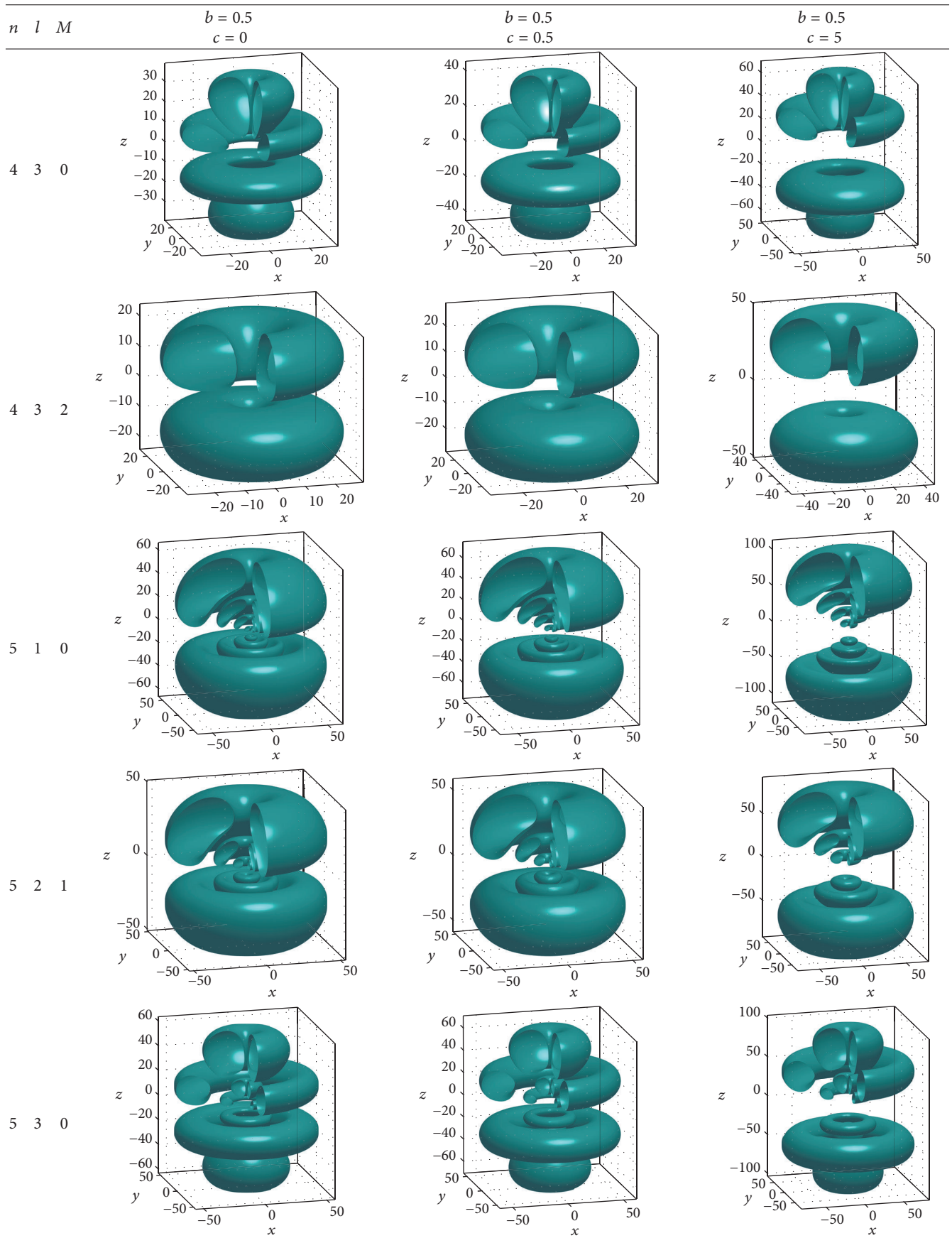


TABLE I: Continued.

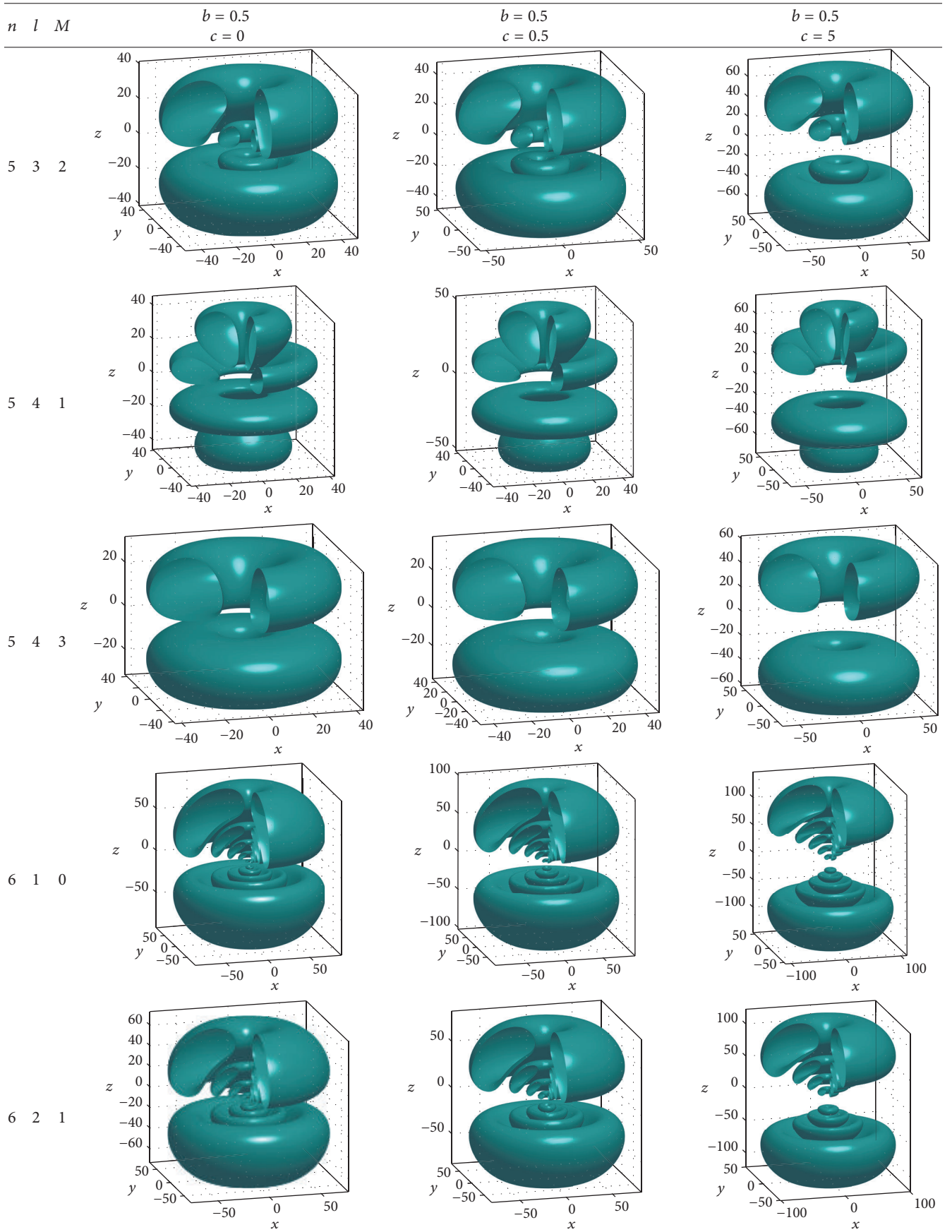
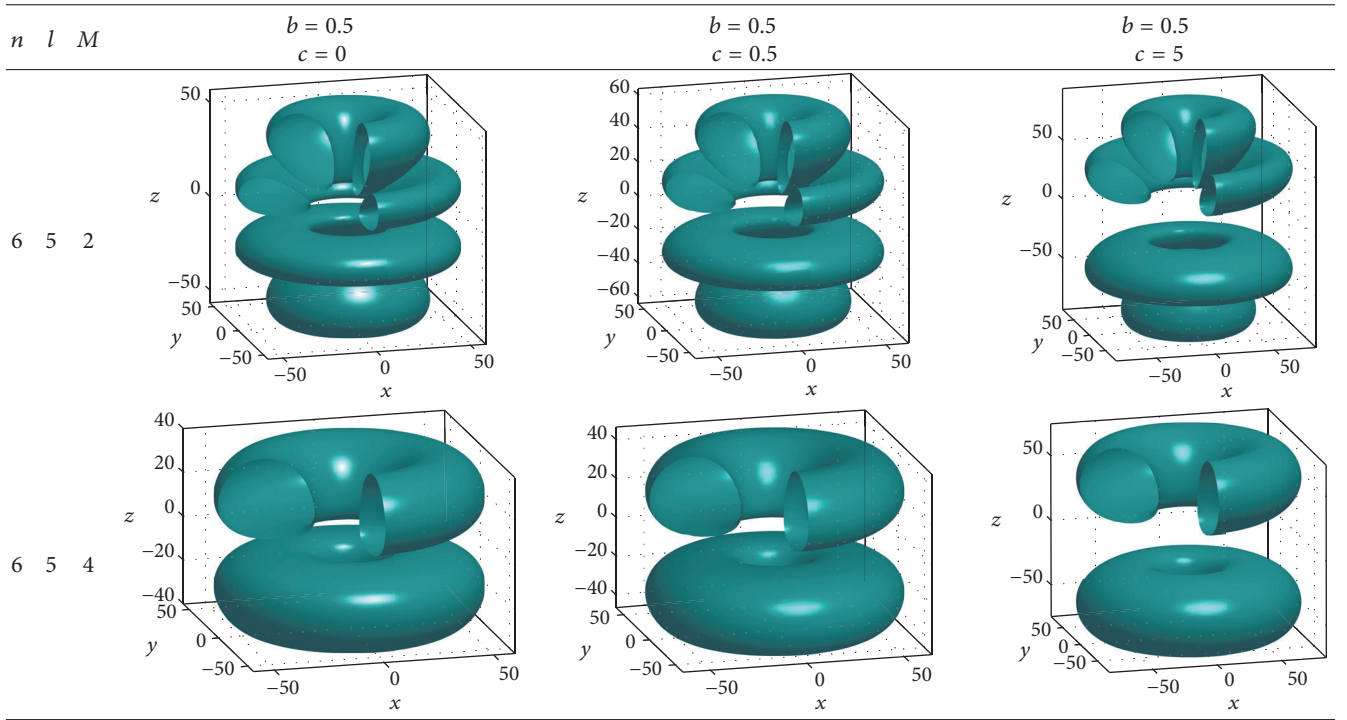


TABLE I: Continued.

n	l	M	$b = 0.5$ $c = 0$	$b = 0.5$ $c = 0.5$	$b = 0.5$ $c = 5$
6	3	0			
6	3	2			
6	4	1			
6	4	3			
6	5	0			

TABLE I: Continued.



and the Bohr radius $a_0 = \hbar^2/Me^2 = 1$. The complete wave function has the form

$$\Psi_{n'l'm'}(\vec{r}) = \frac{1}{\sqrt{2\pi}} \frac{u_{n'l'}(r)}{r} H_{l'm'}(\cos\theta) e^{\pm im\varphi}. \quad (12)$$

3. Two- and Three-Dimensional Visualizations of SPDs

As we know, the SPDs at the position $\vec{r} = (r, \theta, \varphi)$ are calculated by

$$\rho = |\Psi_{n'l'm'}(\vec{r})|^2 = \frac{1}{2\pi} \frac{u_{n'l'}^2(r)}{r^2} H_{l'm'}^2(\cos\theta). \quad (13)$$

To show the SPD, let us transform (13) to popular Cartesian coordinates via the relations $r = \sqrt{x^2 + y^2 + z^2}$ and $\cos\theta = z/r$. Thus, one is able to find the corresponding SPD $\rho(x, y, z)$.

Taking a series of discrete positions, we may study the values of the respective SPD by numerical calculation. In order to make the graphic resolution better, one takes N discrete positions in the Cartesian space (x, y, z) and studies density block, say $\text{den}(N, N, N)$, which is composed of all values $w_{n'l'm'}$ for all $N \times N \times N$ positions. Here, N is taken as 151. For states denoted by (n', l', m') , we display their two- and three-dimensional visualizations for different states ($n \leq 6$) using MATLAB program as shown in Tables 1 and 2.

4. Discussions on the SPD

4.1. Variation Caused by the Radial Nodes. We show the SPDs for various cases $b = 0.5$ and $c = 0, 0.5, 5$ (see Table 1). The case $c = 0$ corresponds to a single RSCP, which was discussed in our previous works [29, 30]. We take the unit in axis as the Bohr radial a_0 . It should be pointed out that we plot the figures only for the value of $n_r = n - l - 1$ equal to integer. To display the inside structure of the graphics, we create a section plane but need not consider SPDs numerical values in the regions $x < 0, y < 0, z > 0$.

Compared to the cases $c = 0$ and $b \neq 0$, it is seen that the graphics are expanded. That is to say, the SPDs enlarge towards z -axis and the hole is expanded outside when the potential parameter c increases. We may understand it through considering (8). As we know, m' will increase relatively for a fixed m . For $l \neq m$, their isosurfaces are of circular ring shape.

We project the SPDs to a plane yoz and find that they are symmetric to the y -axis and z -axis (see Table 2). In this work, the graphics are plotted only in the first quadrant by enlarging proportionally the probability $|\Psi_{n'l'm'}(\vec{r})|^2$ and by making the maximum value as 100, in which the interval is taken as 10. A corresponding balance among the density distributions exists in the directions of axes x , y , and z because the sum of density distributions has to be equal to one when considering the normalization condition. It is clear that each figure becomes expanded along with y -axis and z -axis.

TABLE 2: The contour of the SPDs in the plane yoz .

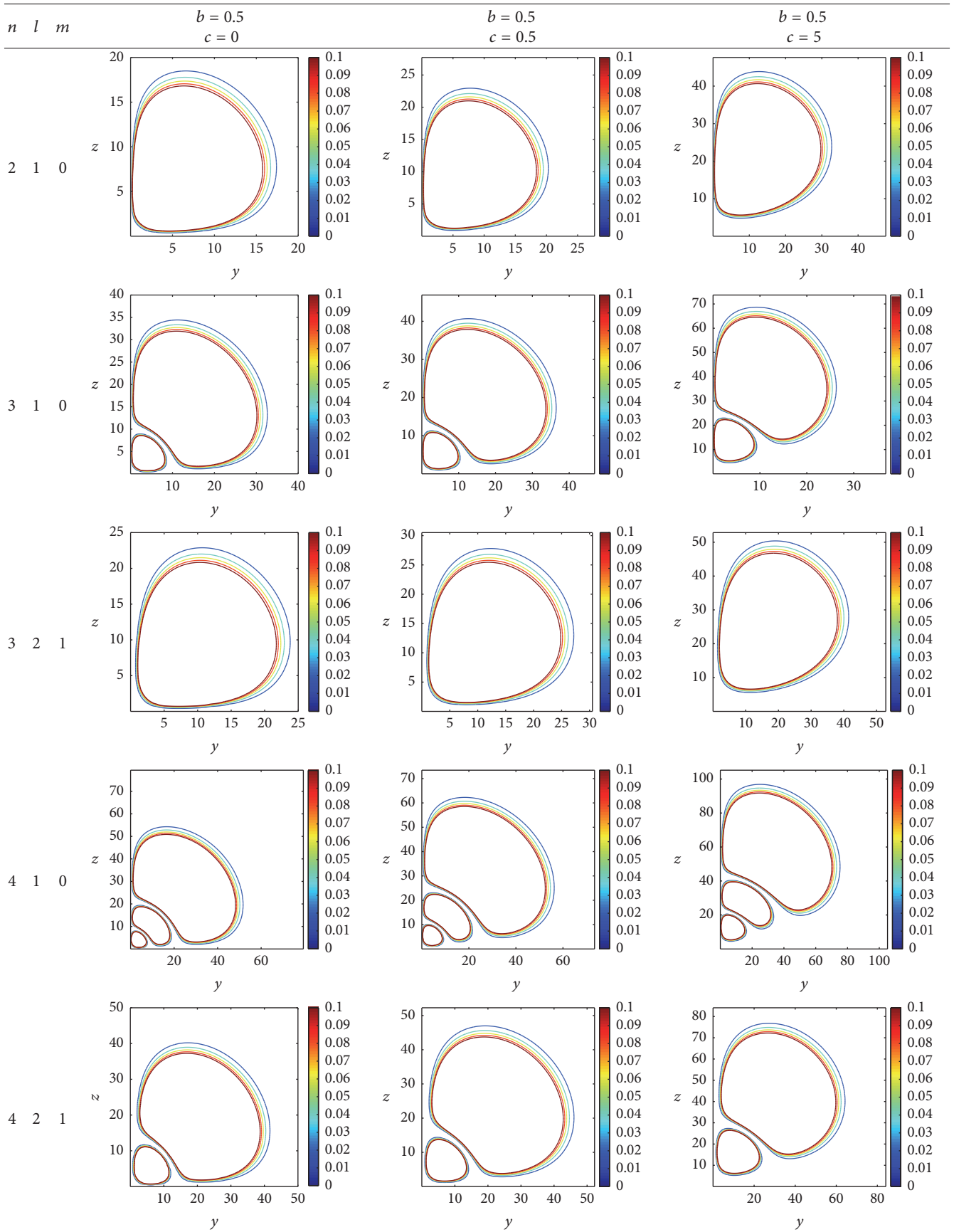


TABLE 2: Continued.

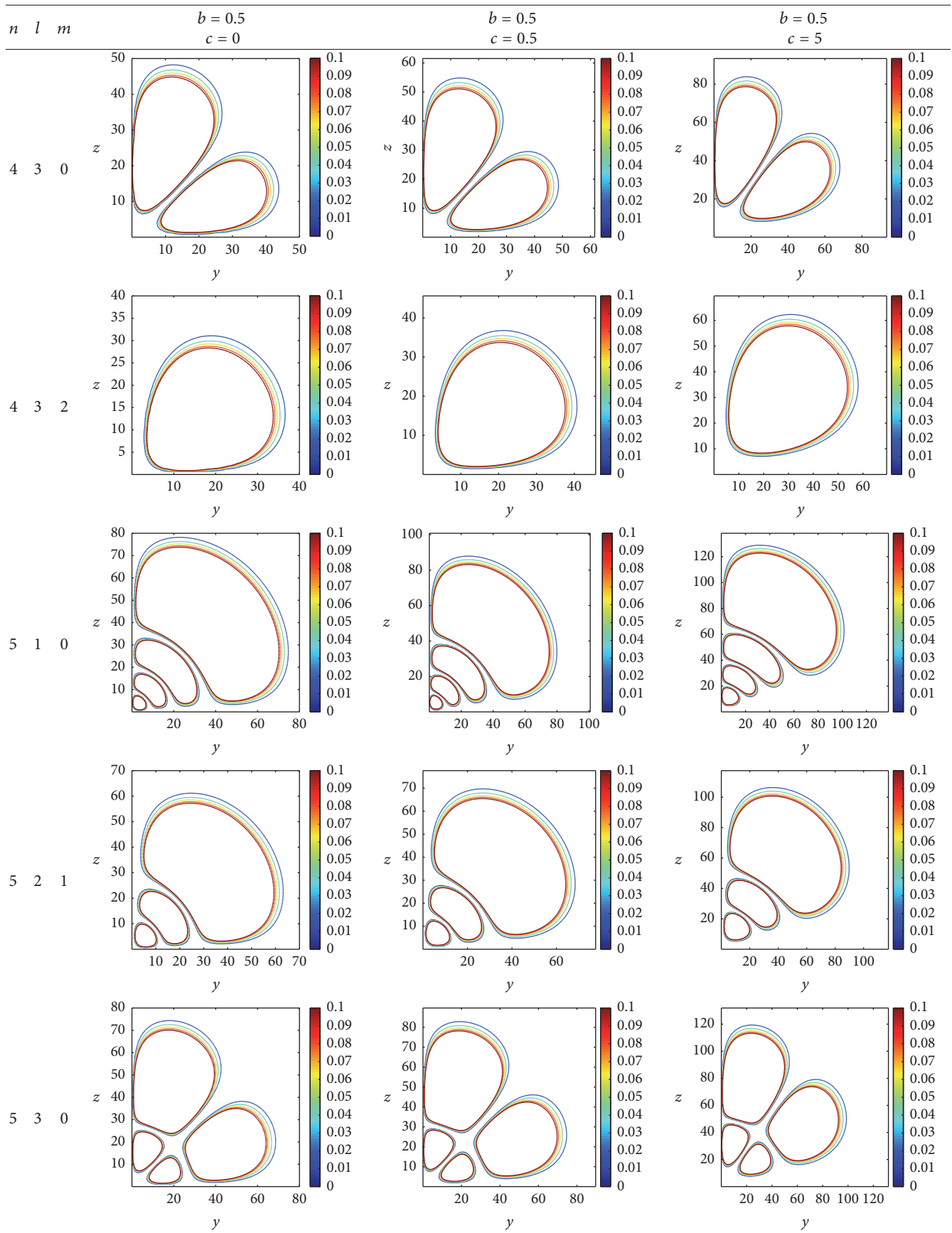


TABLE 2: Continued.

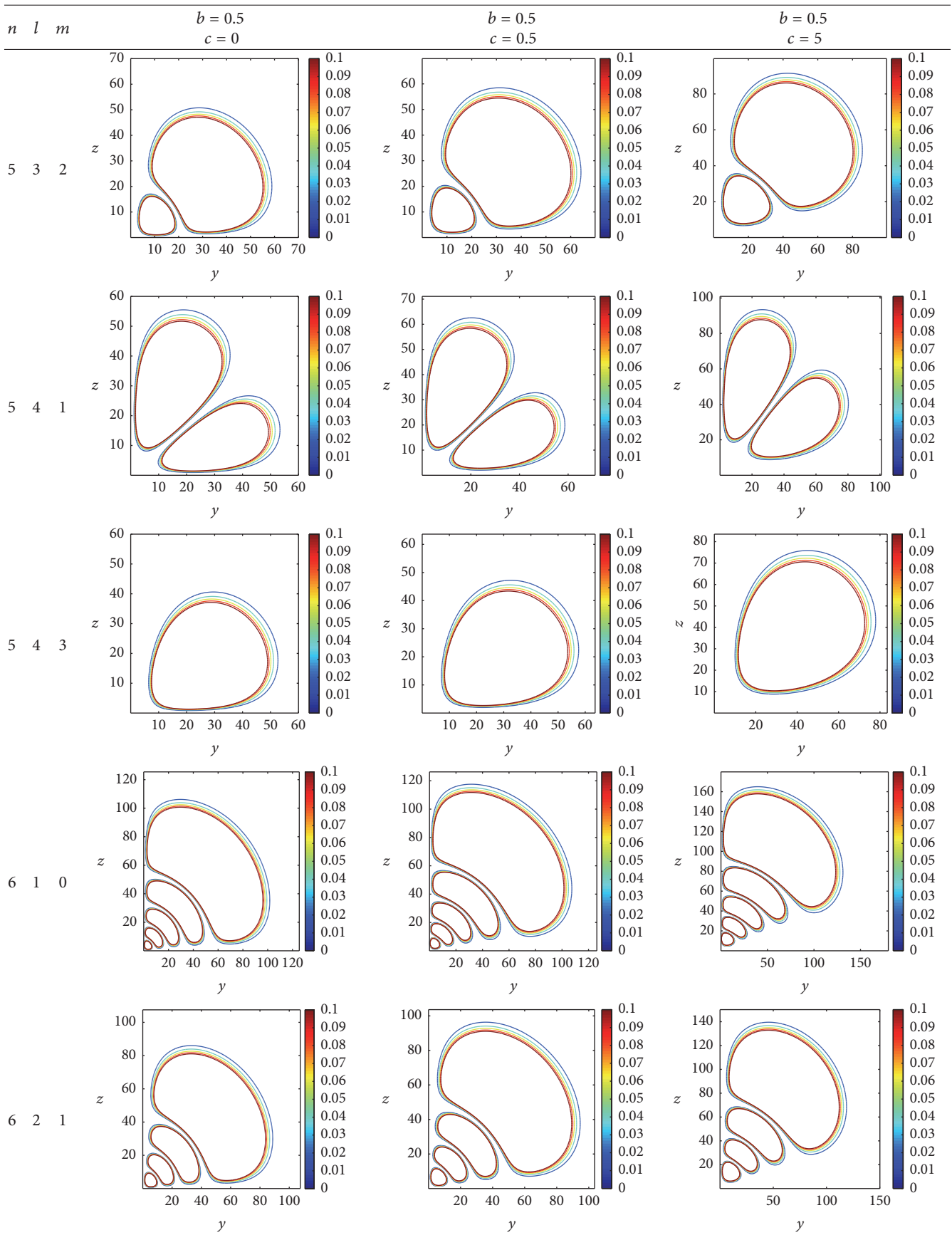


TABLE 2: Continued.

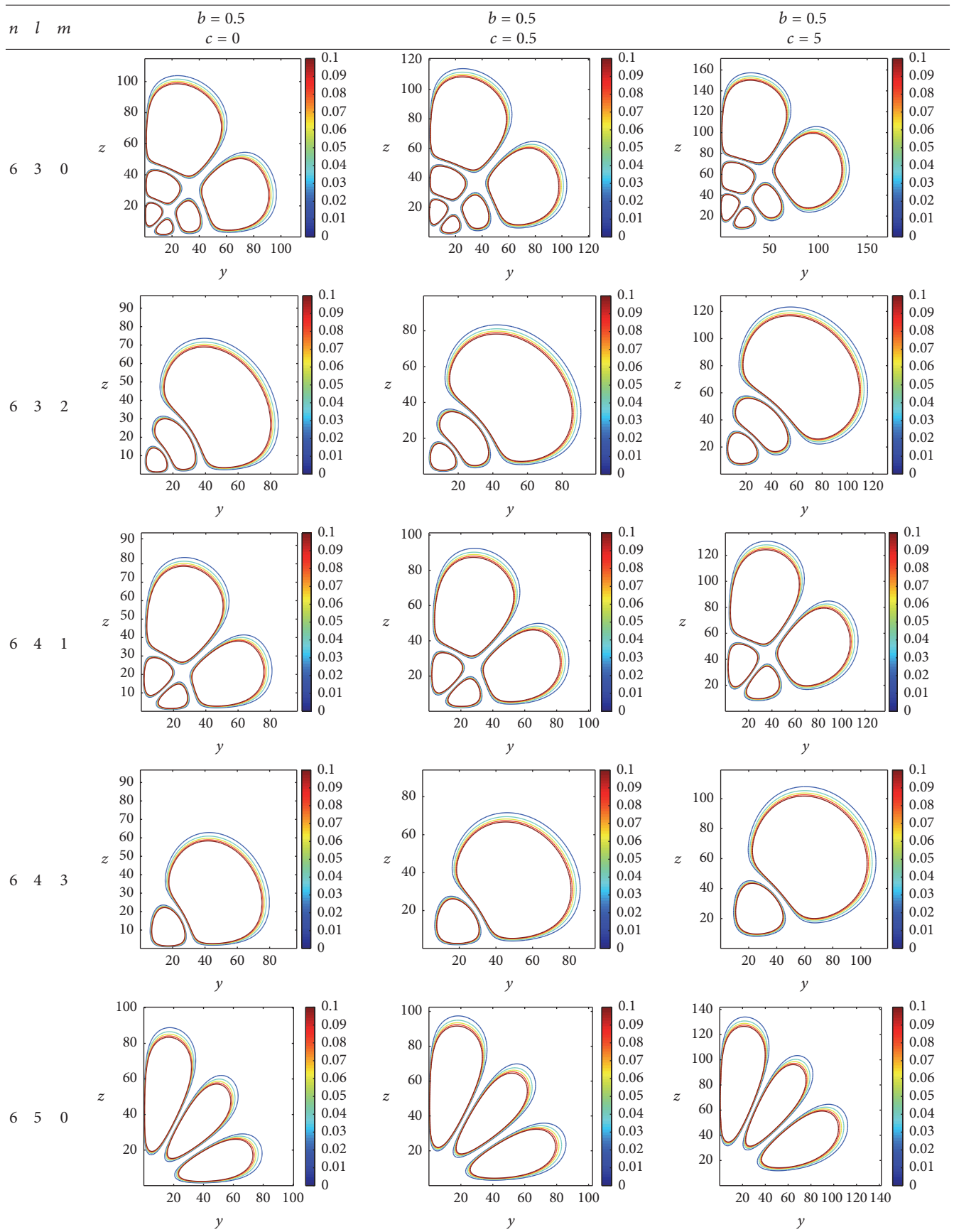
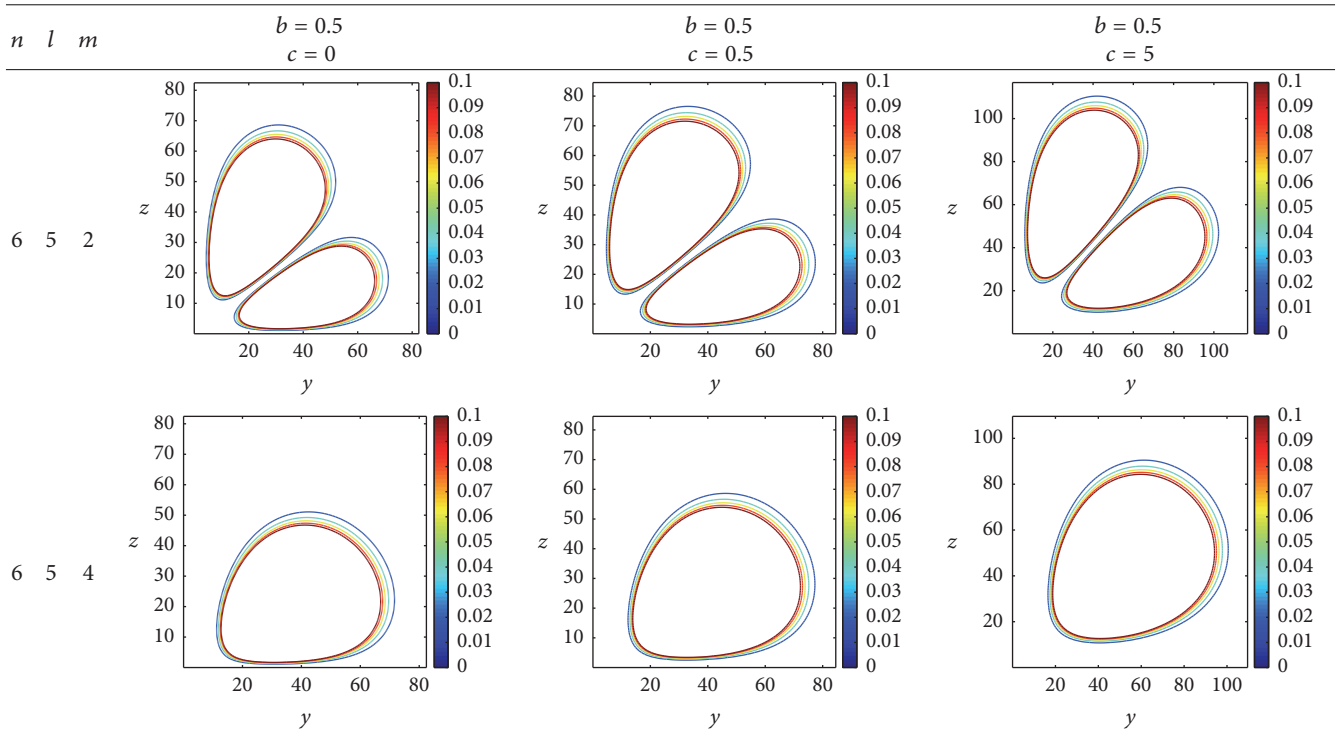


TABLE 2: Continued.



4.2. *Variation on RPV P .* To show the isosurface of the SPDs for various RPVs $P \in (0, 100)\%$, the quantum numbers $(n, l, m) = (6, 5, 0)$ for two different cases $b = 0.5$ and $c = 0.5, 10$ are taken as seen in Table 3. It is shown that the particle for smaller P will be distributed to almost all spaces. However, the particle for larger P will move to the poles in z -axis.

4.3. *Variations on Various Potential Parameters b and c .* Considering given quantum numbers m and n_θ , we know from (8) that m' will become bigger as b increases and the parameter γ_1 also becomes larger with increasing c . As a result, this will result in increasing l' . In Table 4, the SPDs are plotted for state $(n, l, m) = (5, 1, 0)$ in the cases of $c = 0.5$ and $b = 0, 5, 10, 25, 40, 80$ and $b = 0.5$ and $c = 0, 5, 10, 25, 40, 80$, respectively. Obviously, we see a big difference between them. When the potential parameter b increases, the expansions of the SPDs along with x -axis and y -axis and the number of radial nodes are changed. However, when the parameter c increases, the expansions of the SPDs are along with z -axis.

The comparison is done for positive and negative $b < 0$ and $b > 0$ when $c = 0.5$ (see Table 5). It is shown that the SPDs for the negative $b = -0.5$ compared with the case $b = 0$ are shrunk into the origin. However, the SPDs for $b = 0.5$ are enlarged outside. We can understand it very well by studying the contributions of the potential parameter b made on the Coulomb potential. The choice of the negative or positive b determines the attractive Coulomb potential that is bigger or

smaller relatively. Thus, the attractive force that acts on the particle will be larger or smaller. Finally, this will result in the SPDs that are shrunk or expanded.

5. Conclusions

The analytical solutions to the double RSCP have been obtained and then the visualization of the SPDs for this potential is performed. The contour and isosurface visualizations have been illustrated for quantum numbers (n', l', m') by taking various values of the parameter c . It is shown that the SPDs are of circular ring shape. On the other hand, the properties of the RPVs P of the SPDs have also been discussed. As an example, we have studied the particular case, that is, $(n, l, m) = (6, 5, 0)$, and found that the SPDs will move towards the poles of z -axis when the RPVs P increase.

Conflicts of Interest

The authors declare that there are no conflicts of interest.

Acknowledgments

This work is supported by the National Natural Science Foundation of China under Grant no. 11275165, partially by 20180677-SIP-IPN, and by CONACYT, Mexico, under Grant no. 288856-CB-2016. Professor Yuan You acknowledges Jiangsu Overseas Research & Training Program for

TABLE 3: The SPDs for various RPVs P for $(n, l, m) = (6, 5, 0)$ ($b = 0.5, c = 0.5, 10$).

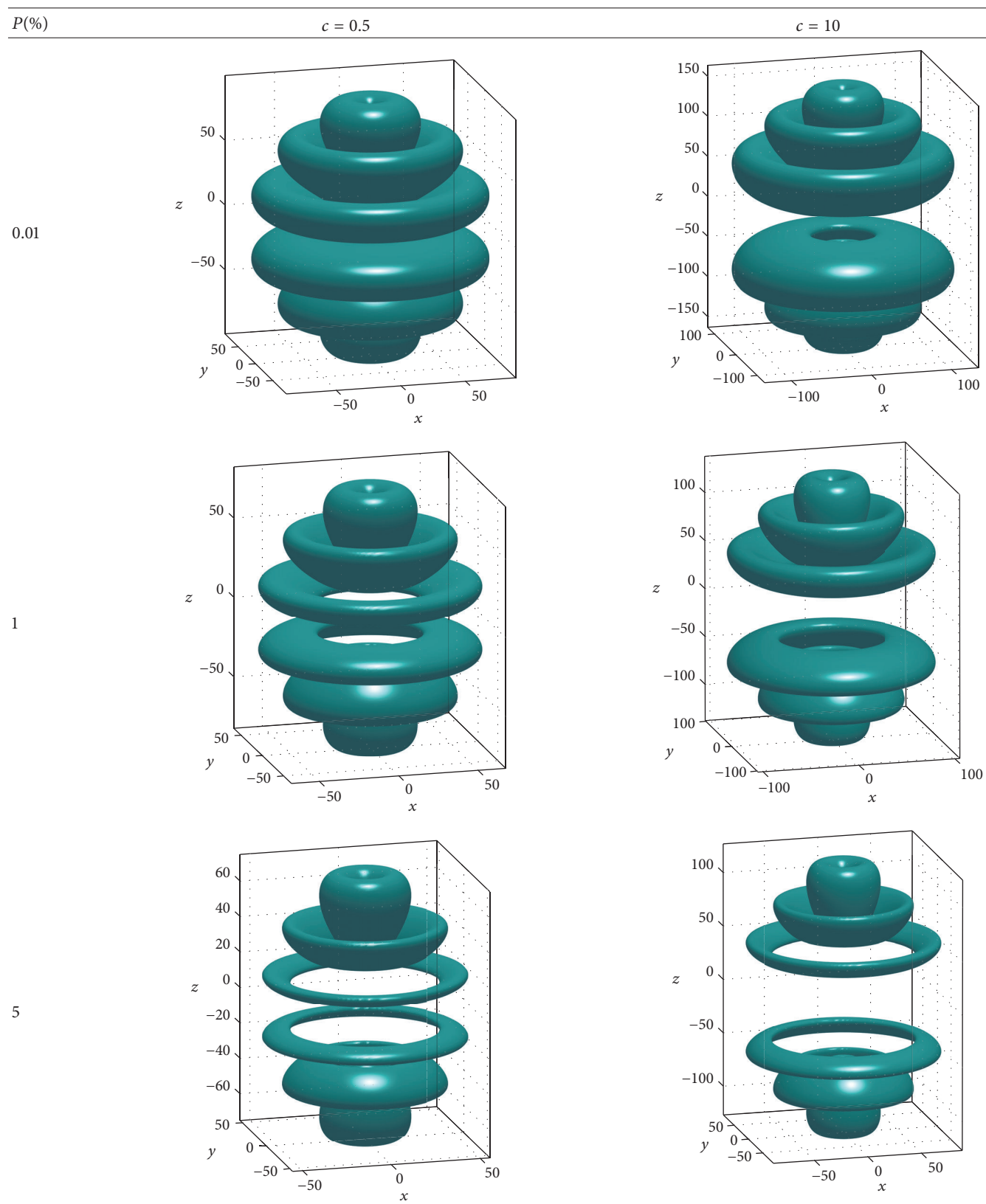


TABLE 3: Continued.

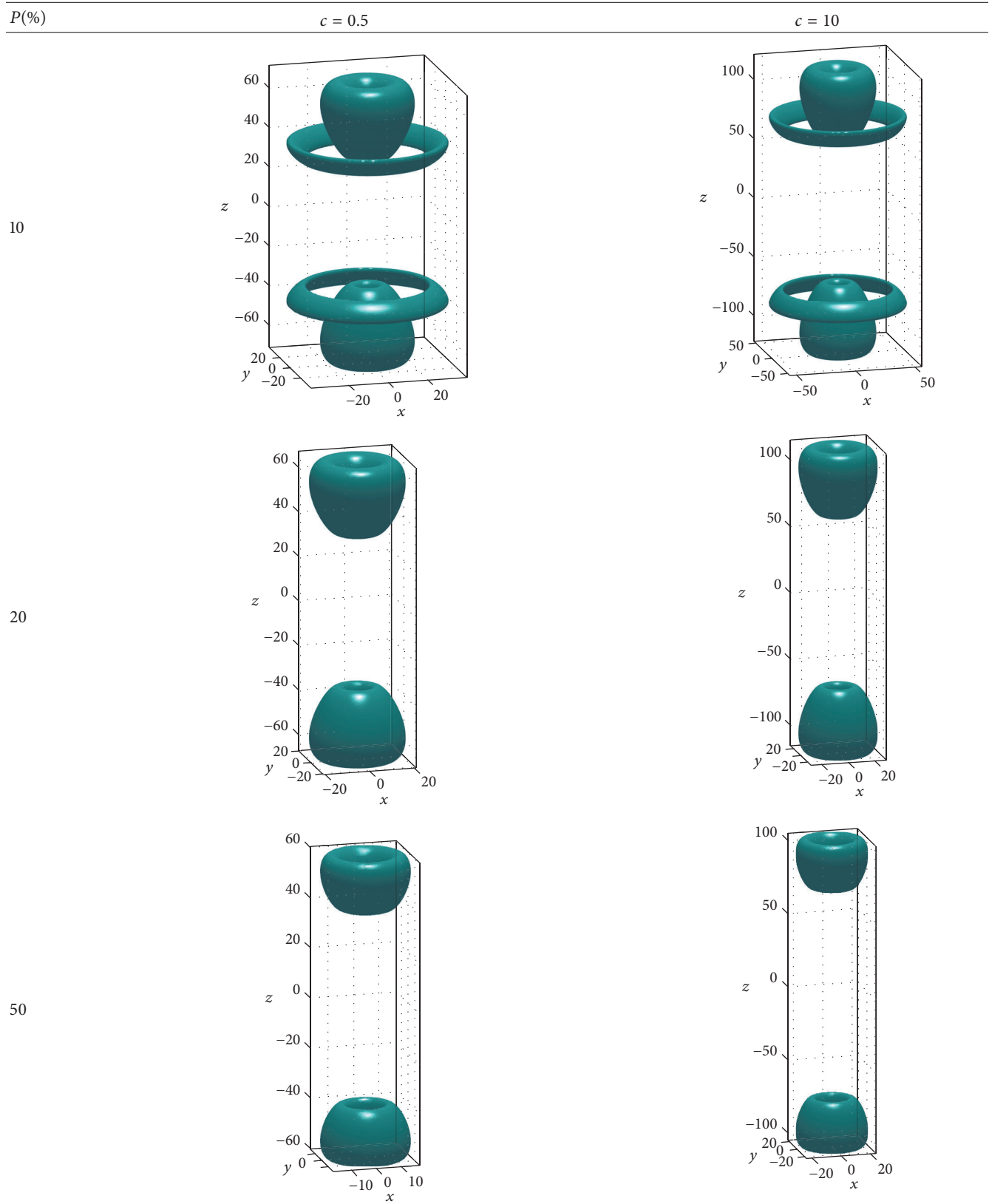


TABLE 3: Continued.

$P(\%)$	$c = 0.5$	$c = 10$
70		
90		
99		

TABLE 4: The isosurface illustration of the state (5, 1, 0) with various values of b and c .

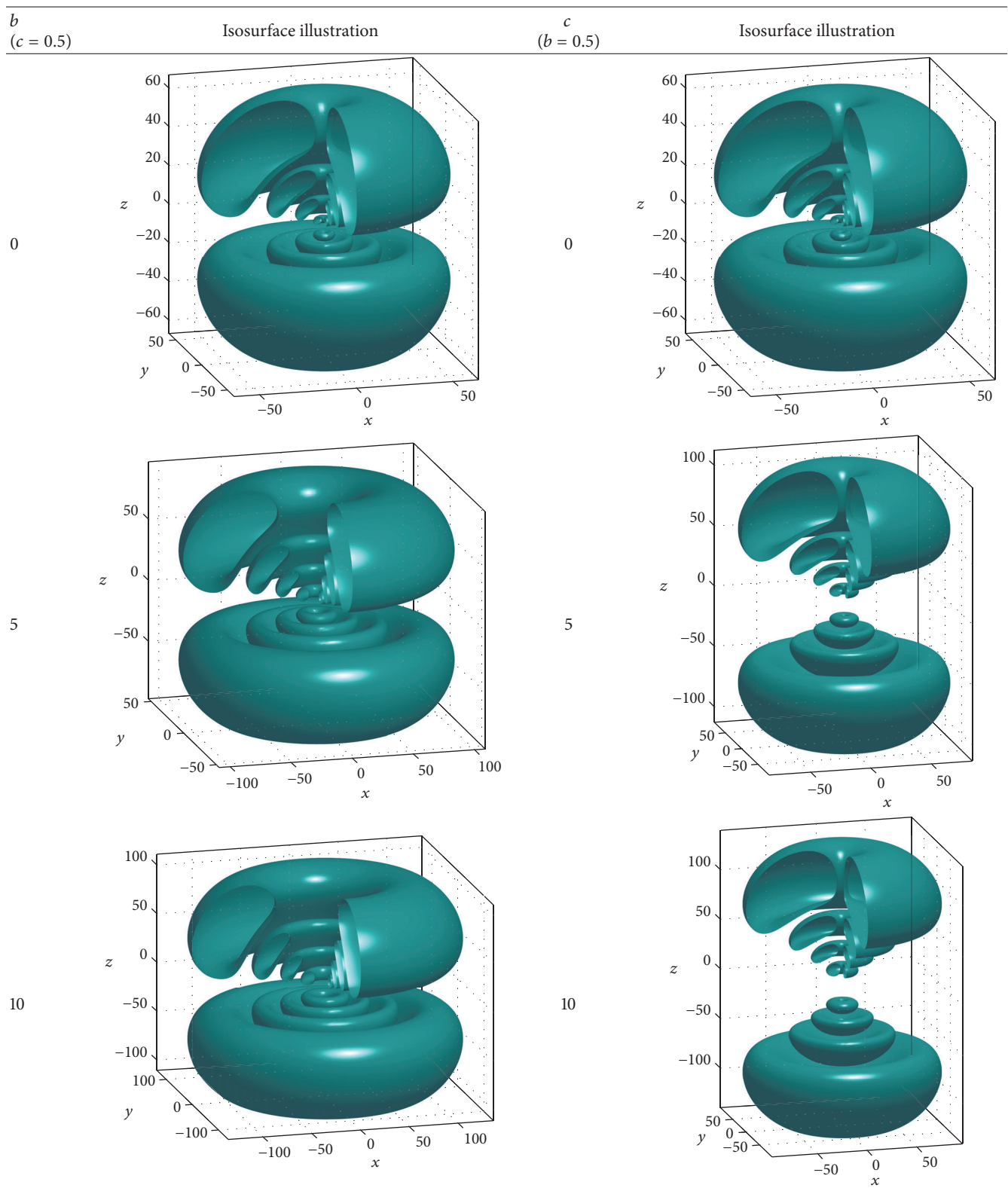
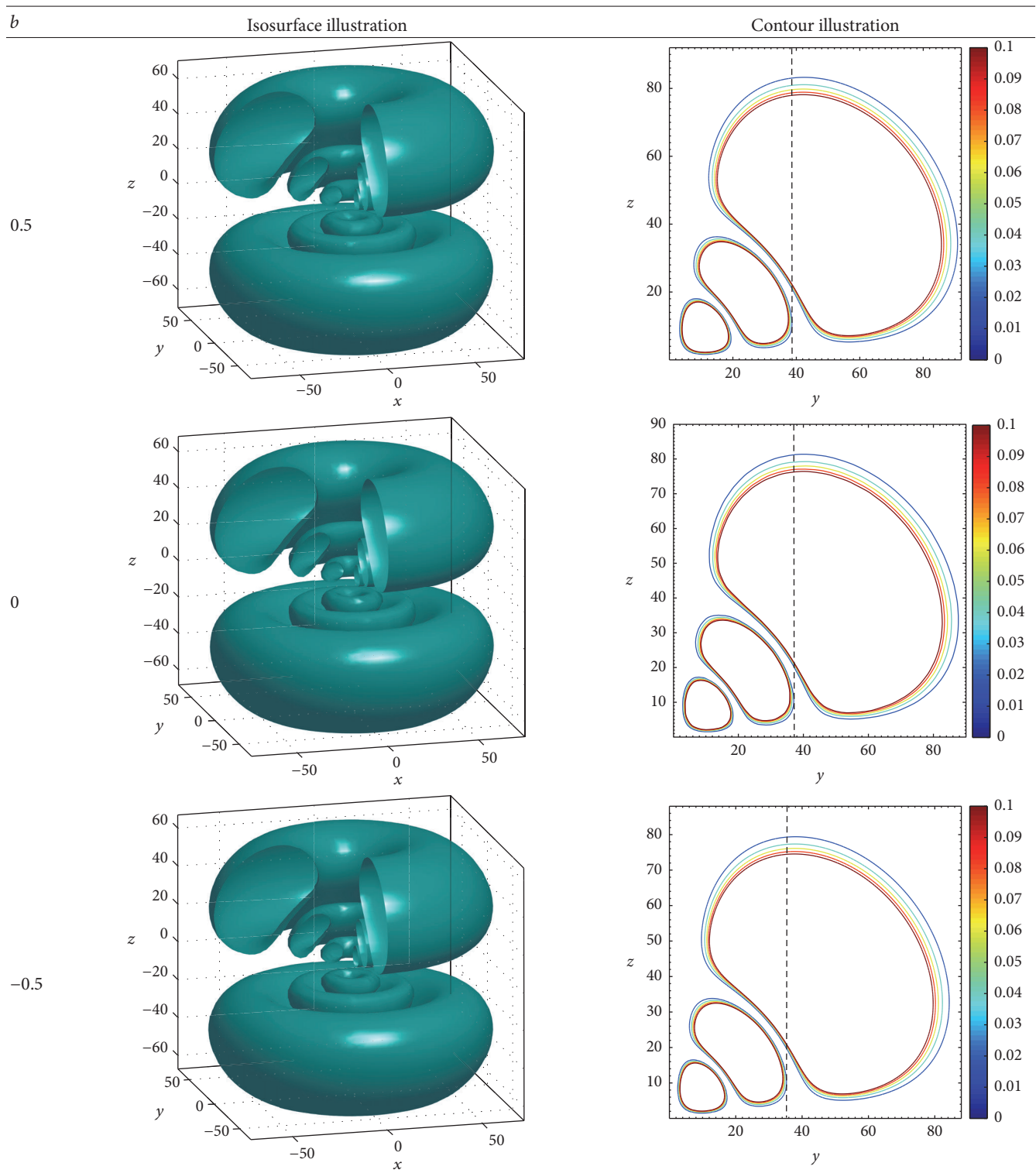


TABLE 4: Continued.

b ($c = 0.5$)	Isosurface illustration	c ($b = 0.5$)	Isosurface illustration
25		25	
40		40	
80		80	

TABLE 5: SPDs for different cases of the value of b for $(4, 1, 0)$ when $c = 0.5$.



University Prominent Young & Middle-Aged Teachers and Presidents for support.

References

- [1] C. Quesne, "A new ring-shaped potential and its dynamical invariance algebra," *Journal of Physics A: Mathematical and General*, vol. 21, no. 14, pp. 3093–3101, 1988.
- [2] Y. C. Chen and S. D. Sun, "Exact solutions of a ring-shaped oscillator," *Acta Photonica Sinica*, vol. 30, no. 104, 2001.
- [3] C. Y. Chen, "General formulas and recurrence formulas for radial matrix elements of ring shaped oscillator," *Acta Physica Sinica*, vol. 30, no. 539, 2001.
- [4] S.-H. Dong, G.-H. Sun, and M. Lozada-Cassou, "An algebraic approach to the ring-shaped non-spherical oscillator," *Physics Letters A*, vol. 328, no. 4-5, pp. 299–305, 2004.
- [5] J.-Y. Guo, J.-C. Han, and R.-D. Wang, "Pseudospin symmetry and the relativistic ring-shaped non-spherical harmonic oscillator," *Physics Letters A*, vol. 353, no. 5, pp. 378–382, 2006.
- [6] A. S. Zhedanov, "Hidden symmetry algebra and overlap coefficients for two ring-shaped potentials," *Journal of Physics A: Mathematical and General*, vol. 26, no. 18, pp. 4633–4641, 1993.
- [7] H. Hartmann and R. Schuck, "Spin-orbit coupling for the motion of a particle in a ring-shaped potential," *International Journal of Quantum Chemistry*, vol. 18, no. 1, pp. 125–141, 1980.
- [8] H. Hartmann, "Die Bewegung eines Körpers in einem ringförmigen Potentialfeld," *Theoretical Chemistry Accounts*, vol. 24, no. 2-3, pp. 201–206, 1972.
- [9] C. C. Gerry, "Dynamical group for a ring potential," *Physics Letters A*, vol. 118, no. 9, pp. 445–447, 1986.
- [10] G. G. Blado, "Supersymmetric treatment of a particle subjected to a ring-shaped potential," *International Journal of Quantum Chemistry*, vol. 58, no. 5, pp. 431–439, 1996.
- [11] L. Chetouani, L. Guechi, and T. F. Hammann, "Algebraic treatment of a general noncentral potential," *Journal of Mathematical Physics*, vol. 33, no. 10, pp. 3410–3418, 1992.
- [12] B. P. Mandal, "Path integral solution of noncentral potential," *International Journal of Modern Physics A*, vol. 15, no. 8, pp. 1225–1234, 2000.
- [13] C.-Y. Chen, D.-S. Sun, and C.-L. Liu, "The general calculation formulas and the recurrence relations of radial matrix elements for Hartmann potential," *Physics Letters A*, vol. 317, no. 1-2, pp. 80–86, 2003.
- [14] C.-Y. Chen, C.-L. Liu, and D.-S. Sun, "The normalized wavefunctions of the Hartmann potential and explicit expressions for their radial average values," *Physics Letters A*, vol. 305, no. 6, pp. 341–348, 2002.
- [15] L. F. Lu, C. G. Zhuang, and Y. C. Chen, "Exact solutions of the Schrödinger equation with double ring-shaped potential," *Journal of Physics B: Atomic and Molecular Physics*, vol. 23, p. 493, 2006.
- [16] A. Hautot, "Exact motion in noncentral electric fields," *Journal of Mathematical Physics*, vol. 14, no. 10, pp. 1320–1327, 1973.
- [17] A. de Souza Dutra and M. Hott, "Dirac equation exact solutions for generalized asymmetrical Hartmann potentials," *Physics Letters A*, vol. 356, no. 3, pp. 215–219, 2006.
- [18] C. Berkdemir, "A novel angle-dependent potential and its exact solution," *Journal of Mathematical Chemistry*, vol. 46, no. 1, pp. 139–154, 2009.
- [19] F. L. Lu and C. Y. Chen, "Bound states of the Schrödinger equation for the Pöschl-Teller double-ring-shaped Coulomb potential," *Chinese Physics B*, vol. 19, no. 10, Article ID 100309, 2010.
- [20] G.-H. Sun and S.-H. Dong, "Exact solutions of dirac equation for a new spherically asymmetrical singular oscillator," *Modern Physics Letters A*, vol. 25, no. 33, pp. 2849–2857, 2010.
- [21] F. T. Chen and M. C. Zhang, "Exact solutions of the Schrödinger equation for a ring-shaped non-central potential," *Acta Physica Sinica*, vol. 59, no. 6819, 2010.
- [22] H. Hassanabadi, Z. Molaee, and S. Zrrinkamar, "Relativistic vector bosons under pöschl-teller double-ring-shaped coulomb potential," *Modern Physics Letters A*, vol. 27, no. 39, Article ID 1250228, 2012.
- [23] S. Bskkeshizadeh and V. Vahidi, "Exact solution of the Dirac equation for the Coulomb potential plus NAD potential by using the Nikiforov-Uvarov method," *Adv. Studies Theor. Phys.*, vol. 6, p. 733, 2012.
- [24] A. g. Arda and R. Sever, "Non-central potentials, exact solutions and Laplace transform approach," *Journal of Mathematical Chemistry*, vol. 50, no. 6, pp. 1484–1494, 2012.
- [25] E. Maghsoodi, H. Hassanabadi, and S. Zarrinkamar, "Exact solutions of the Dirac equation with Pöschl—Teller double-ring-shaped Coulomb potential via the Nikiforov—Uvarov method," *Chinese Physics B*, vol. 22, no. 3, Article ID 030302, 2013.
- [26] C.-Y. Chen, F.-L. Lu, D.-S. Sun, Y. You, and S.-H. Dong, "Exact solutions to a class of differential equation and some new mathematical properties for the universal associated-Legendre polynomials," *Applied Mathematics Letters*, vol. 40, pp. 90–96, 2015.
- [27] R. A. Sari, A. Suparmi, and C. Cari, "Solution of Dirac equation for Eckart potential and trigonometric Manning Rosen potential using asymptotic iteration method," *Chinese Physics B*, vol. 25, no. 1, Article ID 010301, 2015.
- [28] D.-S. Sun, Y. You, F.-L. Lu, C.-Y. Chen, and S.-H. Dong, "The quantum characteristics of a class of complicated double ring-shaped non-central potential," *Physica Scripta*, vol. 89, no. 4, Article ID 045002, 2014.
- [29] Y. You, F. Lu, D. Sun, C. Chen, and S. Dong, "The Visualization of the Space Probability Distribution for a Moving Particle: In a Single Ring-Shaped Coulomb Potential," *Advances in High Energy Physics*, vol. 2017, pp. 1–19, 2017.
- [30] C.-Y. Chen, F.-L. Lu, D.-S. Sun, and S.-H. Dong, "Analytic solutions of the double ring-shaped Coulomb potential in quantum mechanics," *Chinese Physics B*, vol. 22, no. 10, Article ID 100302, 2013.

Research Article

The Texture One-Zero Neutrino Mass Matrix with Vanishing Trace

Madan Singh 

Department of Physics, National Institute of Technology Kurukshetra, Haryana 136119, India

Correspondence should be addressed to Madan Singh; singhmadan179@gmail.com

Received 14 October 2017; Accepted 6 December 2017; Published 5 April 2018

Academic Editor: Andrzej Okniński

Copyright © 2018 Madan Singh. This is an open access article distributed under the Creative Commons Attribution License, which permits unrestricted use, distribution, and reproduction in any medium, provided the original work is properly cited. The publication of this article was funded by SCOAP³.

In the light of latest neutrino oscillation data, we have investigated the one-zero Majorana neutrino mass matrix M_ν , with zero sum condition of mass eigenvalues in the flavor basis, where charged lepton mass matrix is diagonal. Among the six possible one-zero cases, it is found that only five can survive the current experimental data, while case with (1, 1) vanishing element of M_ν , is ruled out, if zero trace condition is imposed at 3σ confidence level (CL). Numerical and some approximate analytical results are presented.

1. Introduction

The Double Chooz, Daya Bay, and RENO Collaborations [1–3] have finally established the nonzero and relatively large value of the reactor mixing angle θ_{13} ; hence the number of known available neutrino oscillation parameters approaches five, namely, two mass-squared differences ($\delta m^2, \Delta m^2$) and three neutrino mixing angles ($\theta_{12}, \theta_{23}, \theta_{13}$). However, any general 3×3 neutrino mass matrix contains more parameters than can be measured in realistic experiments. In fact, assuming the Majorana-type nature of neutrinos, the neutrino mass matrix contains nine real free parameters: three neutrino masses (m_1, m_2, m_3), three flavor mixing angles ($\theta_{12}, \theta_{23}, \theta_{13}$), and three CP violating phases (δ, ρ, σ).

In order to reduce the number of free parameters, several phenomenological ideas, in particular texture zeros [4–26], have been widely adopted in the literature. The imposition of texture zeros in neutrino mass matrix leads to some important phenomenological relations between flavor mixing angles and fermion mass ratios [24–27]. In the flavor basis, where charged lepton mass matrix is diagonal, at most two zeros are allowed in neutrino mass matrix, which are consistent with neutrino oscillation data [25, 26]. The analysis of two texture zero neutrino mass matrices limits the number of experimentally viable cases to seven. The phenomenological implications of one texture zero neutrino mass matrix have

also been studied in the literature [20–23] and it has been observed that all the six cases are viable with experimental data. However, the imposition of single texture zero condition in neutrino mass matrix makes larger parametric space for viability with the data available compared with two-zero texture. In order to impart predictability to one-zero texture, additional constraints in the form of vanishing determinant [28] or trace can be incorporated. The phenomenological implication of determinantless condition on one-zero texture have been rigorously studied in [20, 28–32]. The implication of traceless condition was first put forward in [33] wherein the anomalies of solar and atmospheric neutrino oscillation experiments as well as the LSND experiment were simultaneously explained in the framework of three neutrinos. In [34], Zee has particularly investigated the case of CP conserving traceless neutrino mass matrix for explaining the solar and atmospheric neutrino deficits. Further motivation of traceless mass matrices can be provided by models wherein neutrino mass matrix can be constructed through a commutator of two matrices, as what happens in models of radiative mass generation [35]. In [36], Alhendi et al. have studied the case of two trackless submatrices of Majorana mass matrix in the flavor basis and carried out a detailed numerical analysis at 3σ confidence level. The phenomenological implications of traceless neutrino mass matrix on neutrino masses, CP violating phases, and effective neutrino mass term are also

studied in [37], for both normal and inverted mass ordering and in case of CP conservation and violation, respectively. In the present work we impose the traceless condition on texture one-zero Majorana mass matrix and investigate the outcomes of such condition on the parametric space of neutrino masses (m_1, m_2, m_3) and CP violating phases (δ, ρ, σ).

Assuming the Majorana nature of neutrinos, neutrino mass matrix is complex symmetric. In the flavor basis, if one of the elements is considered to be zero, the number of possible cases turns out to be six, which are given below:

$$\begin{aligned}
 T_1: & \begin{pmatrix} 0 & \times & \times \\ \times & \times & \times \\ \times & \times & \times \end{pmatrix}, \\
 T_2: & \begin{pmatrix} \times & \times & \times \\ \times & 0 & \times \\ \times & \times & \times \end{pmatrix}, \\
 T_3: & \begin{pmatrix} \times & \times & \times \\ \times & \times & \times \\ \times & \times & 0 \end{pmatrix}; \\
 T_4: & \begin{pmatrix} \times & 0 & \times \\ 0 & \times & \times \\ \times & \times & \times \end{pmatrix}, \\
 T_5: & \begin{pmatrix} \times & \times & 0 \\ \times & \times & \times \\ 0 & \times & \times \end{pmatrix}, \\
 T_6: & \begin{pmatrix} \times & \times & \times \\ \times & \times & 0 \\ \times & 0 & \times \end{pmatrix},
 \end{aligned} \tag{1}$$

where “ \times ” stands for nonzero element and complex matrix element.

Among these possible cases, there exists a permutation symmetry between certain pair of cases, namely, (T_2, T_3) and (T_4, T_5), while cases T_1 and T_6 transform onto themselves independently. The origin of permutation symmetry is explained from the fact that these pairs are related by exchange of 2-3 rows and 2-3 columns of neutrino mass matrix. The corresponding permutation matrix is given by

$$P_{23} = \begin{pmatrix} 1 & 0 & 0 \\ 0 & 0 & 1 \\ 0 & 1 & 0 \end{pmatrix}, \tag{2}$$

which leads to the following relations among the neutrino oscillation parameters:

$$\begin{aligned}
 \theta_{12}^X &= \theta_{12}^Y, \\
 \theta_{23}^X &= 90^\circ - \theta_{23}^Y,
 \end{aligned}$$

$$\begin{aligned}
 \theta_{13}^X &= \theta_{13}^Y, \\
 \delta^X &= \delta^Y \pm 180^\circ,
 \end{aligned} \tag{3}$$

where X and Y superscripts denote the cases related by 2-3 permutation symmetry.

The rest of the work is planned as follows: In Section 2, we discuss the methodology used to reconstruct the Majorana neutrino mass matrix and subsequently obtain some useful phenomenological relations of neutrino mass ratios and Majorana phases by incorporating texture one-zero and zero trace conditions simultaneously. In Section 3, we present the numerical analysis using some approximate analytical relations. In Section 4, we summarize our work.

2. Formalism

In the flavor basis, the Majorana neutrino mass matrix M_ν , depending on three neutrino masses (m_1, m_2, m_3) and the flavor mixing matrix can be expressed as

$$M_\nu = V \begin{pmatrix} m_1 & 0 & 0 \\ 0 & m_2 & 0 \\ 0 & 0 & m_3 \end{pmatrix} V^T. \tag{4}$$

The mixing matrix V can be written as $V = UP$, where U denotes the neutrino mixing matrix consisting of three flavor mixing angles and one Dirac-like CP violating phase, whereas the matrix P is a diagonal phase matrix; that is, $P = \text{diag}(e^{i\rho}, e^{i\sigma}, 1)$ with ρ and σ being the two Majorana CP violating phases. The neutrino mass matrix M_ν can then be rewritten as

$$M_\nu = \begin{pmatrix} M_{ee} & M_{e\mu} & M_{e\tau} \\ M_{e\mu} & M_{\mu\mu} & M_{\mu\tau} \\ M_{e\tau} & M_{\mu\tau} & M_{\tau\tau} \end{pmatrix} = U \begin{pmatrix} \lambda_1 & 0 & 0 \\ 0 & \lambda_2 & 0 \\ 0 & 0 & \lambda_3 \end{pmatrix} U^T, \tag{5}$$

where $\lambda_1 = m_1 e^{2i\rho}$, $\lambda_2 = m_2 e^{2i\sigma}$, and $\lambda_3 = m_3$.

For the purpose of calculations, we have adopted the parameterization of the mixing matrix U considered by [5]; for example,

$$U = \begin{pmatrix} c_{12}c_{13} & s_{12}c_{13} & s_{13} \\ -c_{12}s_{23}s_{13} - s_{12}c_{23}e^{-i\delta} & -s_{12}s_{23}s_{13} + c_{12}c_{23}e^{-i\delta} & s_{23}c_{13} \\ -c_{12}c_{23}s_{13} + s_{12}s_{23}e^{-i\delta} & -s_{12}c_{23}s_{13} - c_{12}s_{23}e^{-i\delta} & c_{23}c_{13} \end{pmatrix}, \tag{6}$$

where $c_{ij} = \cos \theta_{ij}$, $s_{ij} = \sin \theta_{ij}$ for $i, j = 1, 2, 3$, and δ is the CP violating phase.

If one of the elements of M_ν is considered zero, that is, $M_{lm} = 0$, it leads to the following constraint equation:

$$U_{l1}U_{m1}\lambda_1 + U_{l2}U_{m2}\lambda_2 + U_{l3}U_{m3}\lambda_3 = 0, \tag{7}$$

where l, m run over e, μ , and τ .

TABLE 1: Current neutrino oscillation parameters from global fits at 1σ , 2σ , and 3σ confidence level [39]. No (IO) refers to normal (inverted) neutrino mass ordering.

Parameter	Best fit	1σ	2σ	3σ
δm^2 [10^{-5}eV^2]	7.60	7.42–7.79	7.26–7.99	7.11–8.18
$ \Delta m_{31}^2 $ [10^{-3}eV^2] (NO)	2.48	2.41–2.53	2.35–2.59	2.30–2.65
$ \Delta m_{31}^2 $ [10^{-3}eV^2] (IO)	2.38	2.32–2.43	2.26–2.48	2.20–2.54
θ_{12}	34.6°	33.6° – 35.6°	32.7° – 36.7°	31.8° – 37.8°
θ_{23} (NO)	48.9°	41.7° – 50.7°	40.0° – 52.1°	38.8° – 53.3°
θ_{23} (IO)	49.2°	46.9° – 50.7°	41.3° – 52.0°	39.4° – 53.1°
θ_{13} (NO)	8.6°	8.4° – 8.9°	8.2° – 9.1°	7.9° – 9.3°
θ_{13} (IO)	8.7°	8.5° – 8.9°	8.2° – 9.1°	8.0° – 9.4°
δ (NO)	254°	182° – 353°	0° – 360°	0° – 360°
δ (IO)	266°	210° – 322°	0° – $16^\circ \oplus 155^\circ$ – 360°	0° – 360°

The traceless condition implies that sum of the mass eigenvalues in neutrino mass matrix is zero; that is,

$$\lambda_1 + \lambda_2 + \lambda_3 = 0. \quad (8)$$

Using (7) and (8), we obtain

$$\frac{\lambda_1}{\lambda_3} = \frac{U_{12}U_{m2} - U_{13}U_{m3}}{U_{11}U_{m1} - U_{12}U_{m2}}, \quad (9)$$

$$\frac{\lambda_2}{\lambda_3} = \frac{U_{13}U_{m3} - U_{11}U_{m1}}{U_{11}U_{m1} - U_{12}U_{m2}}.$$

The magnitudes of neutrino mass ratios are given by

$$\xi \equiv \frac{m_1}{m_3} = \left| \frac{U_{12}U_{m2} - U_{13}U_{m3}}{U_{11}U_{m1} - U_{12}U_{m2}} \right|, \quad (10)$$

$$\zeta \equiv \frac{m_2}{m_3} = \left| \frac{U_{13}U_{m3} - U_{11}U_{m1}}{U_{11}U_{m1} - U_{12}U_{m2}} \right|.$$

Using (9), we find the following analytical relations for Majorana phases (ρ, σ):

$$\rho = \frac{1}{2} \arg \left(\frac{U_{12}U_{m2} - U_{13}U_{m3}}{U_{11}U_{m1} - U_{12}U_{m2}} \right), \quad (11)$$

$$\sigma = \frac{1}{2} \arg \left(\frac{U_{13}U_{m3} - U_{11}U_{m1}}{U_{11}U_{m1} - U_{12}U_{m2}} \right).$$

Thus neutrino mass ratios (ξ, ζ) and two Majorana-type CP violating phases (ρ, σ) can fully be determined in terms of three mixing angles ($\theta_{12}, \theta_{23}, \theta_{13}$) and the Dirac-type CP violating phase (δ). The ratio of two neutrino mass-squared differences in terms of neutrino mass ratios ξ and ζ is given by

$$R_\nu = \frac{\delta m^2}{|\Delta m^2|} = \frac{2(\zeta^2 - \xi^2)}{|2 - (\zeta^2 + \xi^2)|}, \quad (12)$$

where $\delta m^2 = (m_2^2 - m_1^2)$ and $\Delta m^2 = |m_3^2 - (1/2)(m_1^2 + m_2^2)|$ [38] corresponds to solar and atmospheric neutrino squared differences, respectively. The sign of Δm^2 is still not known

experimentally; that is, $\Delta m^2 > 0$ or $\Delta m^2 < 0$ corresponds to the normal or inverted mass ordering of neutrinos.

The expressions for three neutrino masses (m_1, m_2, m_3) can be given as

$$m_3 = \sqrt{\frac{\delta m^2}{(\zeta^2 - \xi^2)}}, \quad (13)$$

$$m_2 = m_3 \zeta,$$

$$m_1 = m_3 \xi.$$

Thus the neutrino mass spectrum can be fully determined.

The expression for Jarlskog rephasing parameter J_{CP} , which is a measure of CP violation, is given by

$$J_{\text{CP}} = s_{12}c_{12}s_{23}c_{23}s_{13}c_{13}^2 \sin \delta. \quad (14)$$

3. Numerical Results and Discussion

The experimental constraints on neutrino parameters at 1σ , 2σ , and 3σ confidence level (CL) are given in Table 1.

The effective Majorana mass term relevant for neutrinoless double beta ($0\nu\beta\beta$) decay is given by

$$|M|_{ee} = |m_1c_{12}^2c_{13}^2e^{2i\rho} + m_2s_{12}^2c_{13}^2e^{2i\sigma} + m_3s_{13}^2|. \quad (15)$$

The future observation of $0\nu\beta\beta$ decay would imply lepton number violation and Majorana character of neutrinos. For recent reviews see [40–43]. There are a large number of projects such as CUORICINO [44], CUORE [45], GERDA [46], MAJORANA [47], SuperNEMO [48], EXO [49], and GENIUS [50] which target achieving a sensitivity up to 0.01 eV for $|M|_{ee}$. For the present analysis, we assume the upper limit on $|M|_{ee}$ to be less than 0.5 eV at 3σ CL [43]. The data collected from the Planck satellite [51] combined with other cosmological data put a limit on the sum of neutrino masses as

$$\Sigma = \sum_{i=1}^3 m_i < 0.23 \text{ eV} \quad \text{at } 95\% \text{ CL}. \quad (16)$$

Here, we take rather more conservative limit on sum of neutrino masses (Σ) (i.e., $\Sigma < 1 \text{ eV}$) at 3σ CL. We span

TABLE 2: The exact expression of neutrino mass ratios ξ and ζ of all the six one-zero textures with vanishing trace is shown. The symbols $c_{2(ij)} \equiv \cos 2\theta_{ij}$, $s_{2(ij)} \equiv \sin 2\theta_{ij}$ are defined.

Cases	Analytical expressions for ξ and ζ
T_1	$\xi = +\sec 2\theta_{12} (s_{12}^2 - t_{13}^2)$ $\zeta = -\sec 2\theta_{12} (c_{12}^2 - t_{13}^2)$
T_2	$\xi = \frac{(s_{12}^2 s_{13}^2 - c_{13}^2) s_{23}^2 + c_{12} c_{23} (c_{12} c_{23} e^{-i\delta} - 2s_{12} s_{23} s_{13}) e^{-i\delta}}{(s_{23}^2 s_{13}^2 - c_{23}^2 e^{-2i\delta}) c_{2(12)} + s_{2(12)} s_{2(23)} s_{13} e^{-i\delta}}$ $\zeta = \frac{(-c_{12}^2 s_{13}^2 + c_{13}^2) s_{23}^2 - s_{12} c_{23} (s_{12} c_{23} e^{-i\delta} + 2c_{12} s_{23} s_{13}) e^{-i\delta}}{(s_{23}^2 s_{13}^2 - c_{23}^2 e^{-2i\delta}) c_{2(12)} + s_{2(12)} s_{2(23)} s_{13} e^{-i\delta}}$
T_3	$\xi = \frac{(s_{12}^2 s_{13}^2 - c_{13}^2) c_{23}^2 + c_{12} s_{23} (c_{12} s_{23} e^{-i\delta} + 2s_{12} c_{23} s_{13}) e^{-i\delta}}{(c_{23}^2 s_{13}^2 - s_{23}^2 e^{-2i\delta}) c_{2(12)} - s_{2(12)} s_{2(23)} s_{13} e^{-i\delta}}$ $\zeta = \frac{(-c_{12}^2 s_{13}^2 + c_{13}^2) c_{23}^2 - s_{12} s_{23} (s_{12} s_{23} e^{-i\delta} - 2c_{12} c_{23} s_{13}) e^{-i\delta}}{(c_{23}^2 s_{13}^2 - s_{23}^2 e^{-2i\delta}) c_{2(12)} - s_{2(12)} s_{2(23)} s_{13} e^{-i\delta}}$
T_4	$\xi = \frac{-s_{12} c_{12} c_{23} e^{-i\delta} + s_{23} s_{13} (1 + s_{12}^2)}{s_{23} s_{13} (c_{12}^2 - s_{12}^2) + 2s_{12} c_{12} c_{23} e^{-i\delta}}$ $\zeta = \frac{-s_{12} c_{12} c_{23} e^{-i\delta} - s_{23} s_{13} (1 + c_{12}^2)}{s_{23} s_{13} (c_{12}^2 - s_{12}^2) + 2s_{12} c_{12} c_{23} e^{-i\delta}}$
T_5	$\xi = \frac{s_{12} c_{12} s_{23} e^{-i\delta} + c_{23} s_{13} (1 + s_{12}^2)}{c_{23} s_{13} (c_{12}^2 - s_{12}^2) - 2s_{12} c_{12} s_{23} e^{-i\delta}}$ $\zeta = \frac{s_{12} c_{12} s_{23} e^{-i\delta} - c_{23} s_{13} (1 + c_{12}^2)}{c_{23} s_{13} (c_{12}^2 - s_{12}^2) - 2s_{12} c_{12} s_{23} e^{-i\delta}}$
T_6	$\xi = \frac{s_{23} c_{23} (s_{12}^2 s_{13}^2 - c_{13}^2 - c_{12}^2 e^{-2i\delta}) - c_{12} s_{12} s_{13} (c_{23}^2 - s_{23}^2) e^{-i\delta}}{s_{23} c_{23} (s_{13}^2 + e^{-2i\delta}) c_{2(12)} e^{-i\delta} + 2s_{12} c_{12} s_{13} c_{2(23)} e^{-i\delta}}$ $\zeta = \frac{s_{23} c_{23} (-c_{12}^2 s_{13}^2 + c_{13}^2 + s_{12}^2 e^{-2i\delta}) - c_{12} s_{12} s_{13} (c_{23}^2 - s_{23}^2) e^{-i\delta}}{s_{23} c_{23} (s_{13}^2 + e^{-2i\delta}) c_{2(12)} e^{-i\delta} + 2s_{12} c_{12} s_{13} c_{2(23)} e^{-i\delta}}$

the parameter space of input neutrino oscillation parameters ($\theta_{12}, \theta_{23}, \theta_{13}, \delta m^2, \Delta m^2$) by choosing the randomly generated points of the order of 10^{6-7} . Using Eq. (12), the parameter space of CP violating phases (δ, ρ, σ), effective mass term $|M|_{ee}$, neutrino masses (m_1, m_2, m_3) can be subsequently constrained. In order to interpret the phenomenological results, some approximate analytical relations (up to certain leading order term of s_{13}) have been used in the following discussion. The exact analytical relations of neutrino mass ratios (ξ, ζ) have been provided in Table 2.

3.1. Case T_1 . Using (6) and (9), in the leading order term of θ_{13} , we obtain the following analytical relations:

$$\frac{\lambda_1}{\lambda_3} \approx \sec 2\theta_{12} s_{12}^2,$$

$$\frac{\lambda_2}{\lambda_3} \approx -\sec 2\theta_{12} c_{12}^2. \quad (17)$$

For NO, using (12), we obtain $R_\nu \approx \zeta^2 - \xi^2 \approx \sec 2\theta_{12}$. Using 3σ experimental range of oscillation parameters, we find $2.23 \leq R_\nu \leq 4.02$, which excludes the experimental range of R_ν , and for IO we have

$$R_\nu \approx \frac{\sec 2\theta_{12}}{\sec^2 2\theta_{12} c_{12}^4 - 1}, \quad (18)$$

which is again inconsistent with current experimental data as $R_\nu > 0.75$. Therefore, Case T_1 is ruled out with the latest neutrino oscillation data at 3σ CL.

3.2. Case T_2 . Using (6) and (9), we obtain the following analytical relations in the leading order approximation of θ_{13} :

$$\frac{\lambda_1}{\lambda_3} \approx -\sec 2\theta_{12} (c_{12}^2 - t_{23}^2 e^{2i\delta}),$$

$$\frac{\lambda_2}{\lambda_3} \approx \sec 2\theta_{12} (s_{12}^2 - t_{23}^2 e^{2i\delta}). \quad (19)$$

From (19), one can obtain the neutrino mass ratios

$$\xi \approx \sec 2\theta_{12} \sqrt{c_{12}^4 + t_{23}^4 - 2c_{12}^2 t_{23}^2 \cos 2\delta},$$

$$\zeta \approx \sec 2\theta_{12} \sqrt{s_{12}^4 + t_{23}^4 - 2s_{12}^2 t_{23}^2 \cos 2\delta} \quad (20)$$

and the Majorana CP violating phases

$$\rho \approx \frac{1}{2} \tan^{-1} \left(-\frac{t_{23}^2 \sin 2\delta}{c_{12}^2 - t_{23}^2 \cos 2\delta} \right) + O(s_{13}),$$

$$\sigma \approx \frac{1}{2} \tan^{-1} \left(-\frac{t_{23}^2 \sin 2\delta}{s_{12}^2 - t_{23}^2 \cos 2\delta} \right) + O(s_{13}). \quad (21)$$

The correlation plots for case T_2 have been compiled in Figures 1(a), 1(b), 1(c), and 1(d) and Figures 2(a), 2(b), 2(c),

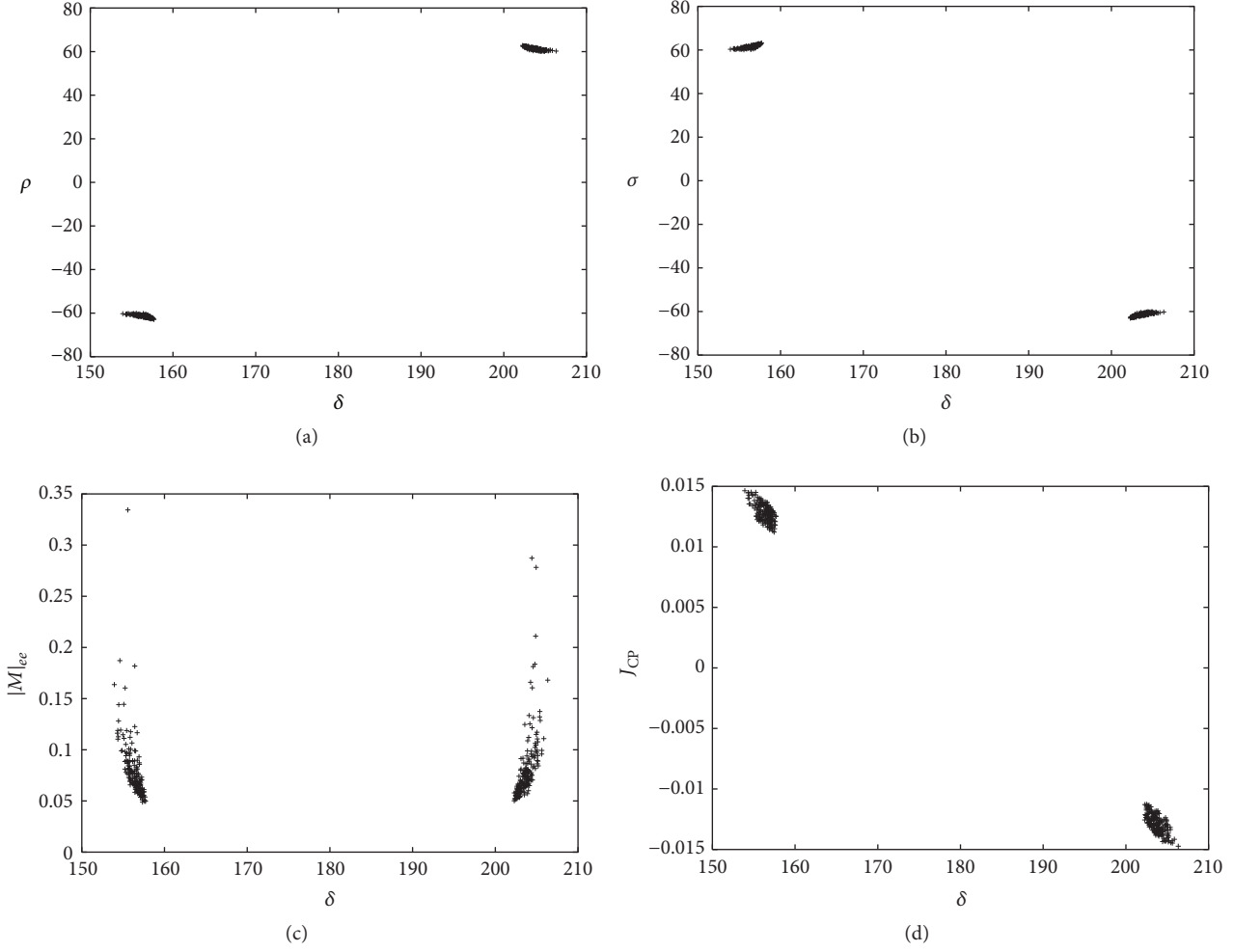


FIGURE 1: Case T_2 (NO): scattering plots of Majorana phases, Dirac CP violating phase (δ), effective neutrino mass $|M|_{ee}$, and Jarlskog rephrasing invariant (J_{CP}) have been shown. All the phase angles (δ, ρ, σ) are measured in degrees and $|M|_{ee}$ is in eV unit.

and 2(d), respectively. It is found from the analysis that case T_2 favors both normal (NO) and inverted mass ordering (IO) at 3σ CL. The parameter space of CP violating phases δ, ρ, σ is found to be constrained to very small ranges for NO (Figures 1(a) and 1(b)). However, for IO, comparatively significant allowed parameter space is available for δ, ρ, σ (Figures 2(a) and 2(b)).

In the leading order approximation of s_{13} , the effective mass term in $0\nu\beta\beta$ decay turns out to be

$$|M|_{ee} \approx m_3 t_{23}^2 \approx 2.32 \times 10^{-2} \text{ eV}, \quad (22)$$

which lies well within the sensitivity limit of neutrinoless double beta decay experiments. Figures 1(c) and 2(c) show the correlation plot between $|M|_{ee}$ and δ for NO and IO, respectively. The Jarlskog rephrasing parameter J_{CP} is found to be nonvanishing for NO (Figure 1(d)); however, $J_{CP} = 0$ cannot be excluded for IO (Figure 2(d)).

3.3. Case T_3 . With the help of (6) and (9), we deduce the following analytical expressions in the leading order of s_{13} term.

$$\begin{aligned} \frac{\lambda_1}{\lambda_3} &\approx \sec 2\theta_{12} \left(c_{12}^2 - \frac{1}{t_{23}^2} e^{2i\delta} \right), \\ \frac{\lambda_2}{\lambda_3} &\approx \sec 2\theta_{12} \left(s_{12}^2 - \frac{1}{t_{23}^2} e^{2i\delta} \right). \end{aligned} \quad (23)$$

From (23), one can obtain the neutrino mass ratios

$$\begin{aligned} \xi &\approx \sec 2\theta_{12} \sqrt{c_{12}^4 + \frac{1}{t_{23}^4} - 2c_{12}^2 \frac{1}{t_{23}^2} \cos 2\delta}, \\ \zeta &\approx \sec 2\theta_{12} \sqrt{s_{12}^4 + \frac{1}{t_{23}^4} - 2s_{12}^2 \frac{1}{t_{23}^2} \cos 2\delta} \end{aligned} \quad (24)$$

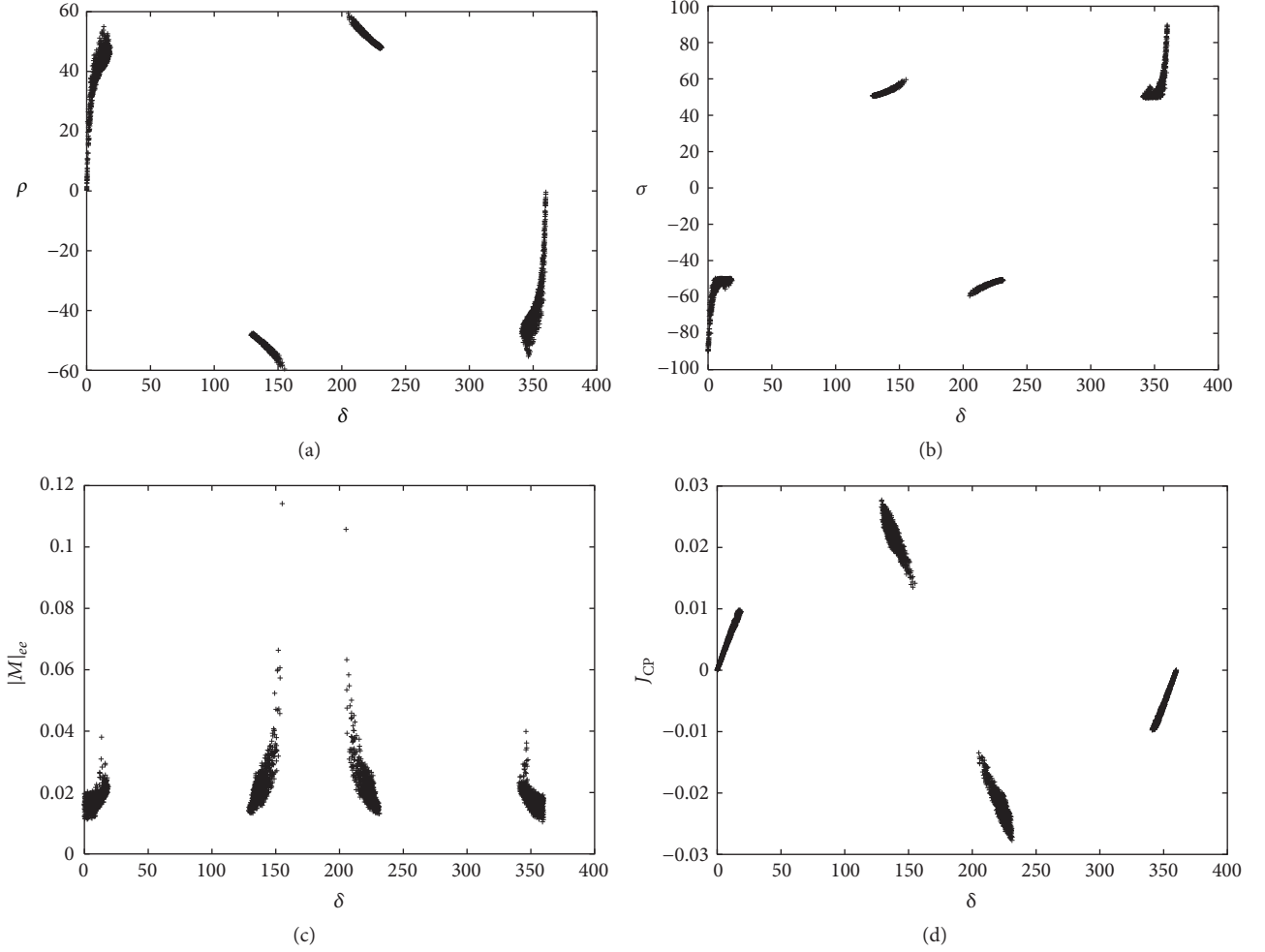


FIGURE 2: Case T_2 (IO): scattering plots of Majorana phases, Dirac CP violating phase (δ), effective neutrino mass $|M|_{ee}$, and Jarlskog rephrasing invariant (J_{CP}) have been shown. All the phase angles (δ, ρ, σ) are measured in degrees and $|M|_{ee}$ is in eV unit.

and the Majorana CP violating phases

$$\begin{aligned}\rho &\approx \frac{1}{2} \tan^{-1} \left(-\frac{\sin 2\delta}{c_{12}^2 t_{23}^2 - \cos 2\delta} \right) + O(s_{13}), \\ \sigma &\approx \frac{1}{2} \tan^{-1} \left(-\frac{\sin 2\delta}{s_{12}^2 t_{23}^2 - t_{23}^2 \cos 2\delta} \right) + O(s_{13}).\end{aligned}\quad (25)$$

Cases T_2 and T_3 are related via permutation symmetry; therefore the phenomenological results for case T_3 can be obtained from case T_2 by using (3). The correlation plots for case T_3 have been compiled in Figures 3(a), 3(b), 3(c), and 3(d) (NO) and Figures 4(a), 4(b), 4(c), and 4(d) (IO), indicating the parameter space of $\rho, \sigma, \delta, |M|_{ee}, J_{CP}$.

3.4. Case T_4 . Using (6) and (9), we deduce the following analytical expressions in the leading order of s_{13} term:

$$\begin{aligned}\frac{\lambda_1}{\lambda_3} &\approx \frac{\lambda_2}{\lambda_3} \approx -0.5, \\ \xi &\approx \zeta \approx 0.5.\end{aligned}\quad (26)$$

Since $R_\nu = 0$ in the leading order approximation of s_{13} , we have to work next to leading order, and we get

$$\begin{aligned}\frac{\lambda_1}{\lambda_3} &\approx -\frac{1}{2} \left(1 - \frac{3}{2} \frac{s_{23}s_{13}}{c_{12}s_{12}c_{23}} e^{i\delta} \right) + O(s_{13}^2), \\ \frac{\lambda_2}{\lambda_3} &\approx -\frac{1}{2} \left(1 + \frac{3}{2} \frac{s_{23}s_{13}}{c_{12}s_{12}c_{23}} e^{i\delta} \right) + O(s_{13}^2).\end{aligned}\quad (27)$$

Using (27), the neutrino mass ratios can be given as

$$\begin{aligned}\xi &\approx \frac{1}{2} \sqrt{1 + \frac{9}{4} \frac{s_{23}^2 s_{13}^2}{c_{12}^2 s_{12}^2 c_{23}^2} - \frac{3s_{23}s_{13}}{c_{12}s_{12}c_{23}} \cos \delta}, \\ \zeta &\approx \frac{1}{2} \sqrt{1 + \frac{9}{4} \frac{s_{23}^2 s_{13}^2}{c_{12}^2 s_{12}^2 c_{23}^2} + \frac{3s_{23}s_{13}}{c_{12}s_{12}c_{23}} \cos \delta},\end{aligned}\quad (28)$$

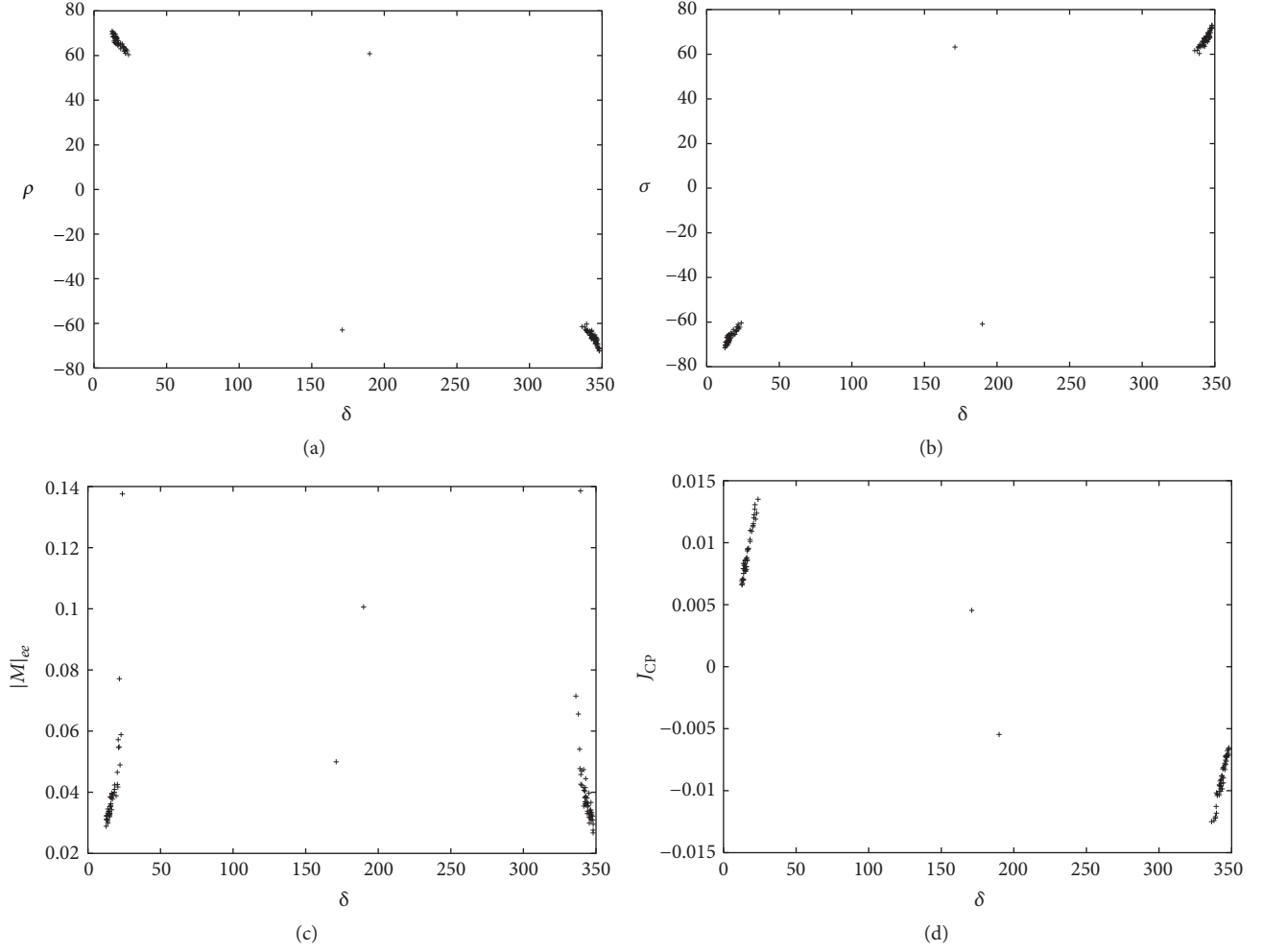


FIGURE 3: Case T_3 (NO): scattering plots of Majorana phases, Dirac CP violating phase (δ), effective neutrino mass $|M|_{ee}$, and Jarlskog rephrasing invariant (J_{CP}) have been shown. All the phase angles (δ, ρ, σ) are measured in degrees and $|M|_{ee}$ is in eV unit.

and the Majorana CP violating phases are as

$$\begin{aligned} \rho &\approx \frac{1}{2} \tan^{-1} \left(\frac{3s_{23}s_{13} \sin \delta}{3s_{23}s_{13} \cos \delta - 2c_{12}s_{12}c_{23}} \right) + O(s_{13}^2), \\ \sigma &\approx \frac{1}{2} \tan^{-1} \left(\frac{3s_{23}s_{13} \sin \delta}{3s_{23}s_{13} \cos \delta + 2c_{12}s_{12}c_{23}} \right) + O(s_{13}^2). \end{aligned} \quad (29)$$

Using the best fit values from latest global fits on neutrino oscillation data (Table 1), the neutrino mass spectrum can be given as follows:

$$\begin{aligned} m_3 &= \sqrt{\frac{\delta m^2}{(\zeta^2 - \xi^2)}} \approx 4.87 \times 10^{-2} \text{ eV}, \\ m_2 &= m_3 \zeta \approx 2.85 \times 10^{-2} \text{ eV}, \\ m_1 &= m_3 \xi \approx 2.71 \times 10^{-2} \text{ eV}, \end{aligned} \quad (30)$$

implying that only NO is allowed. Figures 5(a) and 5(b) show the correlation plot between Majorana phases (ρ, σ) and Dirac CP violating phase (δ). The parameter space for δ is found to be restricted near 90° and 270° . The prediction is significant considering the latest hint on δ near 270° in the recent global fits on neutrino oscillation data (Table 1). The Majorana phases (ρ, σ) are found to be constrained near -90° and 90° . In Figure 5(d), it is explicitly shown that J_{CP} is nonzero implying that case T_5 is necessarily CP violating.

In the leading order of s_{13} , the effective mass term in $0\nu\beta\beta$ decay can be approximated as

$$|M|_{ee} \approx \frac{m_3}{2} \approx 2.43 \times 10^{-2} \text{ eV}, \quad (31)$$

which is well within the accessible limit of next generation neutrinoless double decay experiments. The correlation plot between $|M|_{ee}$ and δ has been provided for case T_4 in Figure 5(c).

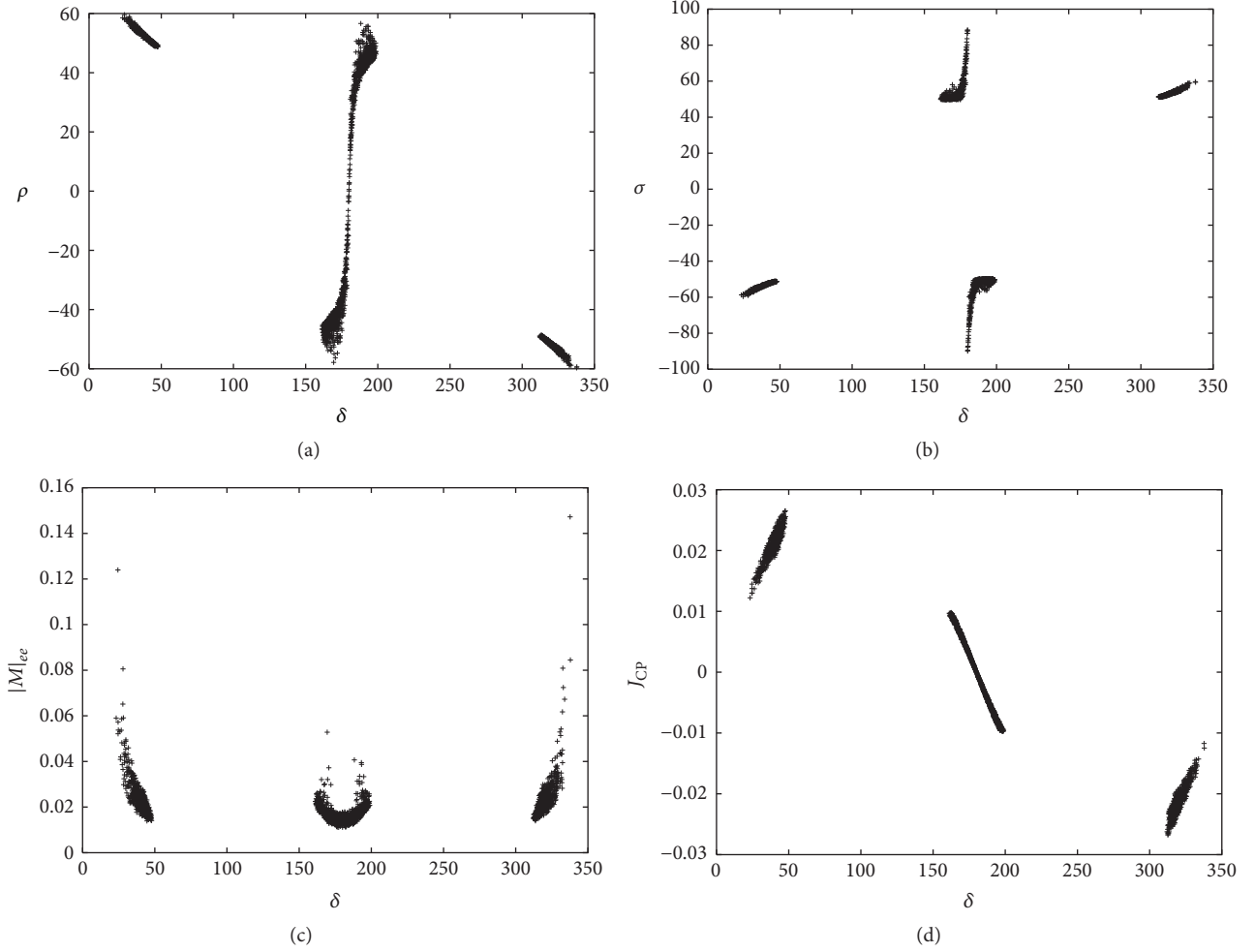


FIGURE 4: Case T_3 (IO): scattering plots of Majorana phases, Dirac CP violating phase (δ), effective neutrino mass $|M|_{ee}$, and Jarlskog rephrasing invariant (J_{CP}) have been shown. All the phase angles (δ, ρ, σ) are measured in degrees and $|M|_{ee}$ is in eV unit.

3.5. Case T_5 . With the help of (6) and (9), we obtain the following analytical expressions in the leading order of s_{13} term:

$$\begin{aligned} \frac{\lambda_1}{\lambda_3} &\approx \frac{\lambda_2}{\lambda_3} \approx 0.5, \\ \xi &\approx \zeta \approx 0.5. \end{aligned} \quad (32)$$

Since $R_\nu = 0$ in the leading order approximation of s_{13} , we have to work next to leading order, and we obtain

$$\begin{aligned} \frac{\lambda_1}{\lambda_3} &\approx -\frac{1}{2} \left(1 + \frac{3}{2} \frac{c_{23}s_{13}}{c_{12}s_{12}s_{23}} e^{i\delta} \right) + O(s_{13}^2), \\ \frac{\lambda_2}{\lambda_3} &\approx -\frac{1}{2} \left(1 - \frac{3}{2} \frac{c_{23}s_{13}}{c_{12}s_{12}s_{23}} e^{i\delta} \right) + O(s_{13}^2). \end{aligned} \quad (33)$$

From (33), the neutrino mass ratios can be given as follows:

$$\begin{aligned} \xi &\approx \frac{1}{2} \sqrt{1 + \frac{9}{4} \frac{c_{23}^2 s_{13}^2}{c_{12}^2 s_{12}^2 s_{23}^2} - \frac{3c_{23}s_{13}}{c_{12}s_{12}s_{23}} \cos \delta}, \\ \zeta &\approx \frac{1}{2} \sqrt{1 + \frac{9}{4} \frac{c_{23}^2 s_{13}^2}{c_{12}^2 s_{12}^2 s_{23}^2} + \frac{3c_{23}s_{13}}{c_{12}s_{12}s_{23}} \cos \delta}, \end{aligned} \quad (34)$$

and the Majorana CP violating phases are given as

$$\begin{aligned} \rho &\approx \frac{1}{2} \tan^{-1} \left(\frac{3c_{23}s_{13} \sin \delta}{3c_{23}s_{13} \cos \delta + 2c_{12}s_{12}s_{23}} \right) + O(s_{13}^2), \\ \sigma &\approx \frac{1}{2} \tan^{-1} \left(\frac{3c_{23}s_{13} \sin \delta}{3c_{23}s_{13} \cos \delta - 2c_{12}s_{12}s_{23}} \right) + O(s_{13}^2). \end{aligned} \quad (35)$$

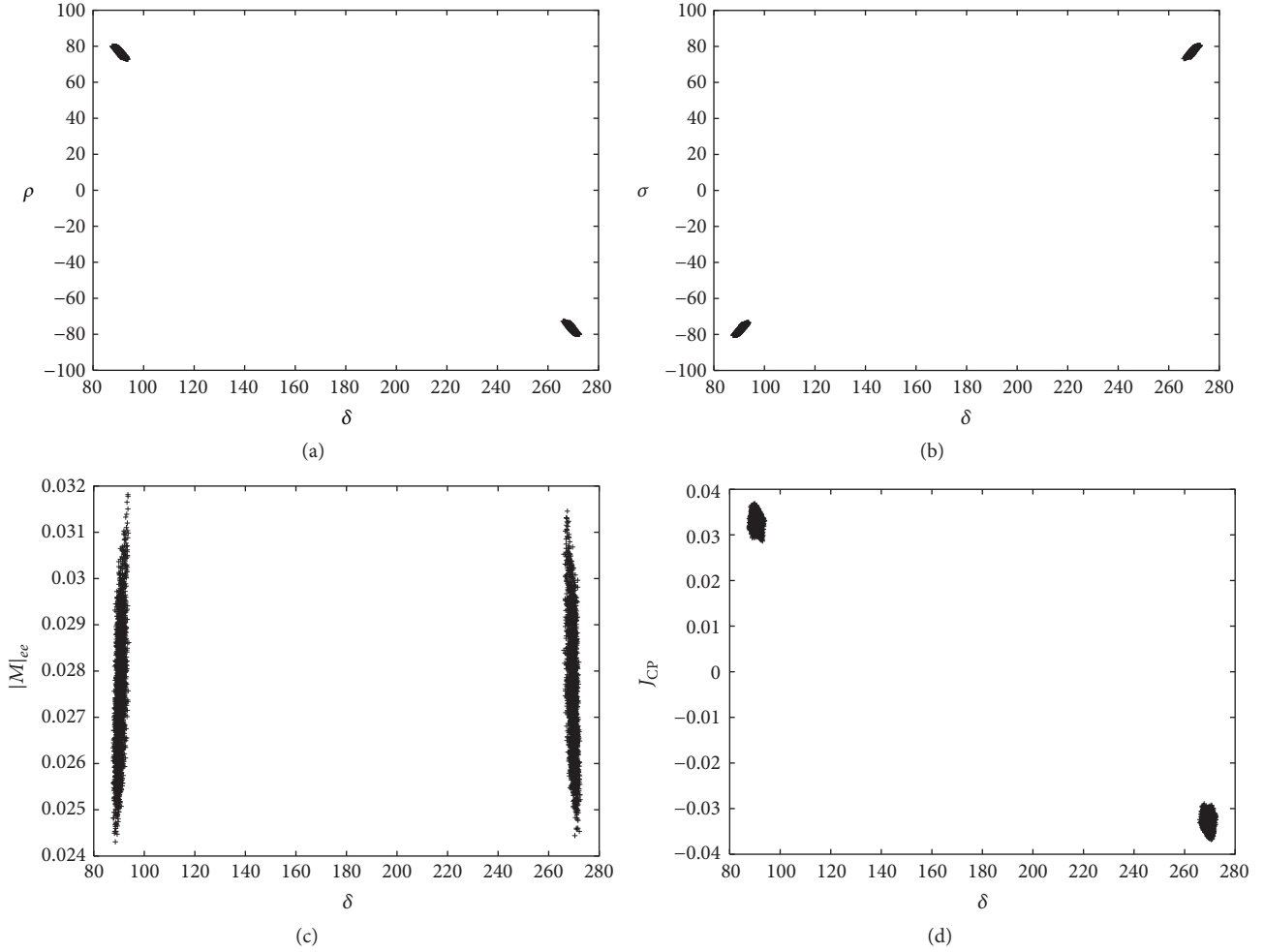


FIGURE 5: Case T_4 (NO): scattering plots of Majorana phases, Dirac CP violating phase (δ), effective neutrino mass $|M|_{ee}$, and Jarlskog rephrasing invariant (J_{CP}) have been shown. All the phase angles (δ, ρ, σ) are measured in degrees and $|M|_{ee}$ is in eV unit.

Using the best fits from latest global neutrino oscillation data, the neutrino mass spectrum can be given as follows:

$$\begin{aligned}
 m_3 &= \sqrt{\frac{\delta m^2}{(\zeta^2 - \xi^2)}} \approx 4.87 \times 10^{-2} \text{ eV}, \\
 m_2 &= m_3 \zeta \approx 2.85 \times 10^{-2} \text{ eV}, \\
 m_1 &= m_3 \xi \approx 2.71 \times 10^{-2} \text{ eV},
 \end{aligned}
 \tag{36}$$

indicating that only NO is allowed. Since T_4 and T_5 are related due to permutation symmetry, therefore their phenomenological implications are similar. The phenomenological results for case T_5 can be derived from case T_4 using (3). The correlation plots for $\rho, \sigma, \delta, |M|_{ee}, J_{CP}$ have been compiled in Figure 6.

In the leading order of s_{13} term, the effective mass term in $0\nu\beta\beta$ decay can be approximated as

$$|M|_{ee} \approx \frac{m_3}{2} \approx 2.43 \times 10^{-2} \text{ eV}, \tag{37}$$

which lies within the sensitivity limits of future $0\nu\beta\beta$ decay experiments.

3.6. Case T_6 . With the help of (6) and (9), we deduce the following analytical expressions in the leading order of s_{13} term

$$\begin{aligned}
 \frac{\lambda_1}{\lambda_3} &\approx -\sec 2\theta_{12} (c_{12}^2 + e^{2i\delta}) e^{i\delta}, \\
 \frac{\lambda_2}{\lambda_3} &\approx \sec 2\theta_{12} (s_{12}^2 + e^{2i\delta}) e^{i\delta}.
 \end{aligned}
 \tag{38}$$

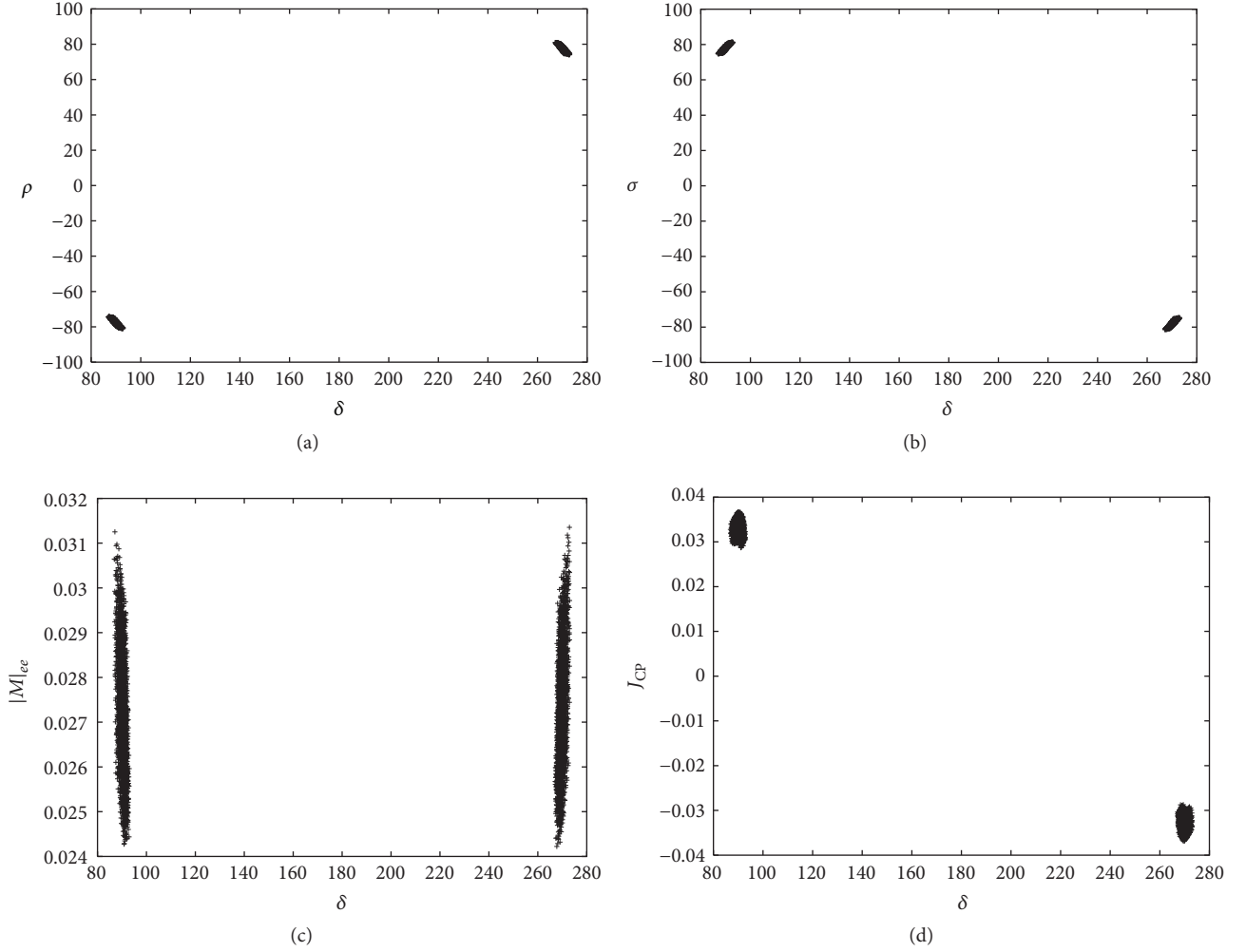


FIGURE 6: Case T_5 (NO): scattering plots of Majorana phases, Dirac CP violating phase (δ), effective neutrino mass $|M|_{ee}$, and Jarlskog rephrasing invariant (J_{CP}) have been shown. All the phase angles (δ, ρ, σ) are measured in degrees and $|M|_{ee}$ is in eV unit.

Using (38), we obtain the approximate relations for neutrino mass ratios

$$\begin{aligned} \xi &\approx \sec 2\theta_{12} \sqrt{c_{12}^4 + 2c_{12}^2 \cos 2\delta + 1}, \\ \zeta &\approx \sec 2\theta_{12} \sqrt{s_{12}^4 + 2s_{12}^2 \cos 2\delta + 1}, \end{aligned} \quad (39)$$

and the Majorana CP violating phases

$$\begin{aligned} \rho &\approx \frac{1}{2} \tan^{-1} \left(\frac{\sin \delta (\cos 2\delta + c_{12}^2) + \sin 2\delta \cos \delta}{\cos \delta (\cos 2\delta + c_{12}^2) - \sin 2\delta \sin \delta} \right) \\ &+ O(s_{13}^2), \end{aligned}$$

$$\begin{aligned} \sigma &\approx \frac{1}{2} \tan^{-1} \left(\frac{\sin \delta (\cos 2\delta + s_{12}^2) + \sin 2\delta \cos \delta}{\cos \delta (\cos 2\delta + s_{12}^2) - \sin 2\delta \sin \delta} \right) \\ &+ O(s_{13}^2). \end{aligned} \quad (40)$$

The correlation plots for $\rho, \sigma, \delta, |M|_{ee}, J_{CP}$ have been compiled in Figures 7(a), 7(b), 7(c), and 7(d). In Figures 7(a) and 7(b) the parameter space of δ is found to be confined to very small regions. Also the Majorana phases ρ and σ also get restricted to $-54.7^\circ - -44.7^\circ \oplus 45.3^\circ - 54.5^\circ$. However, $J_{CP} = 0$ as evident in Figure 7(d), which implies case T_6 points out the CP conservation.

From the analysis, out of six cases, only T_1 is found to be inconsistent with the experimental data for both normal and inverted mass ordering. For remaining cases the parameter space of CP violating phases (δ, σ, ρ), effective mass term $|M|_{ee}$, and neutrino masses (m_1, m_2, m_3) is found to be

TABLE 3: The allowed ranges of Dirac-like CP violating phase δ , the Majorana phases ρ, σ , and three neutrino masses m_1, m_2, m_3 for the experimentally viable cases at 3σ CL. Masses are in eV.

Cases	Normal mass ordering (NO)		Inverted mass ordering (IO)	
T_1	\times	\times	\times	\times
	\times	\times	\times	\times
	\times	\times	\times	\times
T_2	$\delta = 153.7^\circ - 158.4^\circ \oplus 204.1^\circ - 206.3^\circ$	$m_1 = 0.0680 - 0.311$	$\delta = 0^\circ - 21.06^\circ \oplus 126^\circ - 156^\circ$	$m_1 = 0.0425 - 0.357$
	$\rho = -64.9^\circ - -58.5^\circ \oplus 58.6^\circ - 64.3^\circ$	$m_2 = 0.0712 - 0.314$	\oplus	$m_2 = 0.0435 - 0.359$
	$\sigma = -64.5^\circ - -58.89^\circ \oplus 57.8^\circ - 64.3^\circ$	$m_3 = 0.0842 - 0.343$	$204^\circ - 2\ 33^\circ$	$m_3 = 0.00098 - 0.359$
T_3	$\delta = 12.49^\circ - 25.9^\circ \oplus 334.9^\circ - 348.8^\circ$	$m_1 = 0.0291 - 0.690$	\oplus	$m_1 = 0.0422 - 0.377$
	$\rho = -71.49^\circ - -60.3^\circ \oplus 59.36^\circ - 69.7^\circ$	$m_2 = 0.0307 - 0.690$	$159.6^\circ - 201.2^\circ$	$m_2 = 0.0435 - 0.377$
	$\sigma = -73.34^\circ - -59.62^\circ \oplus 57.87^\circ - 72.7^\circ$	$m_3 = 0.0480 - 0.690$	\oplus	$m_3 = 0.00095 - 0.377$
T_4	$\delta = 86.68^\circ - 94.95^\circ \oplus 264.8^\circ - 273.3^\circ$	$m_1 = 0.0269 - 0.0406$	\times	\times
	$\rho = -82.87^\circ - -1.29^\circ \oplus 69.57^\circ - 82.08^\circ$	$m_2 = 0.0280 - 0.0417$	\times	\times
	$\sigma = -82.87^\circ - -71.7^\circ \oplus 70.5^\circ - 82.08^\circ$	$m_3 = 0.0516 - 0.0682$	\times	\times
T_5	$\delta = 85.99^\circ - 94.48^\circ \oplus 266.45^\circ - 274.49^\circ$	$m_1 = 0.0269 - 0.0406$	\times	\times
	$\rho = -82.87^\circ - -72.22^\circ \oplus 71.88^\circ - 83.01^\circ$	$m_2 = 0.0280 - 0.0417$	\times	\times
	$\sigma = -82.87^\circ - -72.22^\circ \oplus 71.88^\circ - 83.01^\circ$	$m_3 = 0.0516 - 0.0682$	\times	\times
T_6	\times	\times	$\delta = 53.25^\circ - 68.5^\circ$	$m_1 = 0.0449 - 0.0664$
	\times	\times	\oplus	$m_2 = 0.0456 - 0.0672$
	\times	\times	$110.2^\circ - 125^\circ$	$m_3 = 0.0099 - 0.0400$
	\times	\times	\oplus	
	\times	\times	$235.7^\circ - 250^\circ$	
	\times	\times	\oplus	
			$291.3^\circ - 309^\circ$	
			$\rho = -54.73^\circ - -44.7^\circ \oplus 45.36^\circ - 54.5^\circ$	
			$\sigma = -54.73^\circ - -44.7^\circ \oplus 45.36^\circ - 54.5^\circ$	

constrained to an appreciable extent at 3σ CL. The allowed ranges of all the five viable cases for Dirac CP violating phase (δ), Majorana phases (ρ, σ), and neutrino masses (m_1, m_2, m_3) have been summarized in Table 3.

4. Summary and Conclusion

In the present work, we have systematically analyzed the texture one-zero Majorana mass matrix along with zero trace condition. In our analysis, we find that case T_1 with vanishing (1, 1) element of M_ν is ruled out with current experimental

data. Therefore, out of six possible cases of one-zero texture with zero trace, only five, namely, T_2, T_3, T_4, T_5 , and T_6 , can survive the current experimental tests at 3σ CL. The ongoing and future neutrino based experiments including neutrinoless double beta decay and cosmological experiments would test the validity of present texture zero analysis.

Conflicts of Interest

The authors declare that there are no conflicts of interest regarding the publication of this paper.

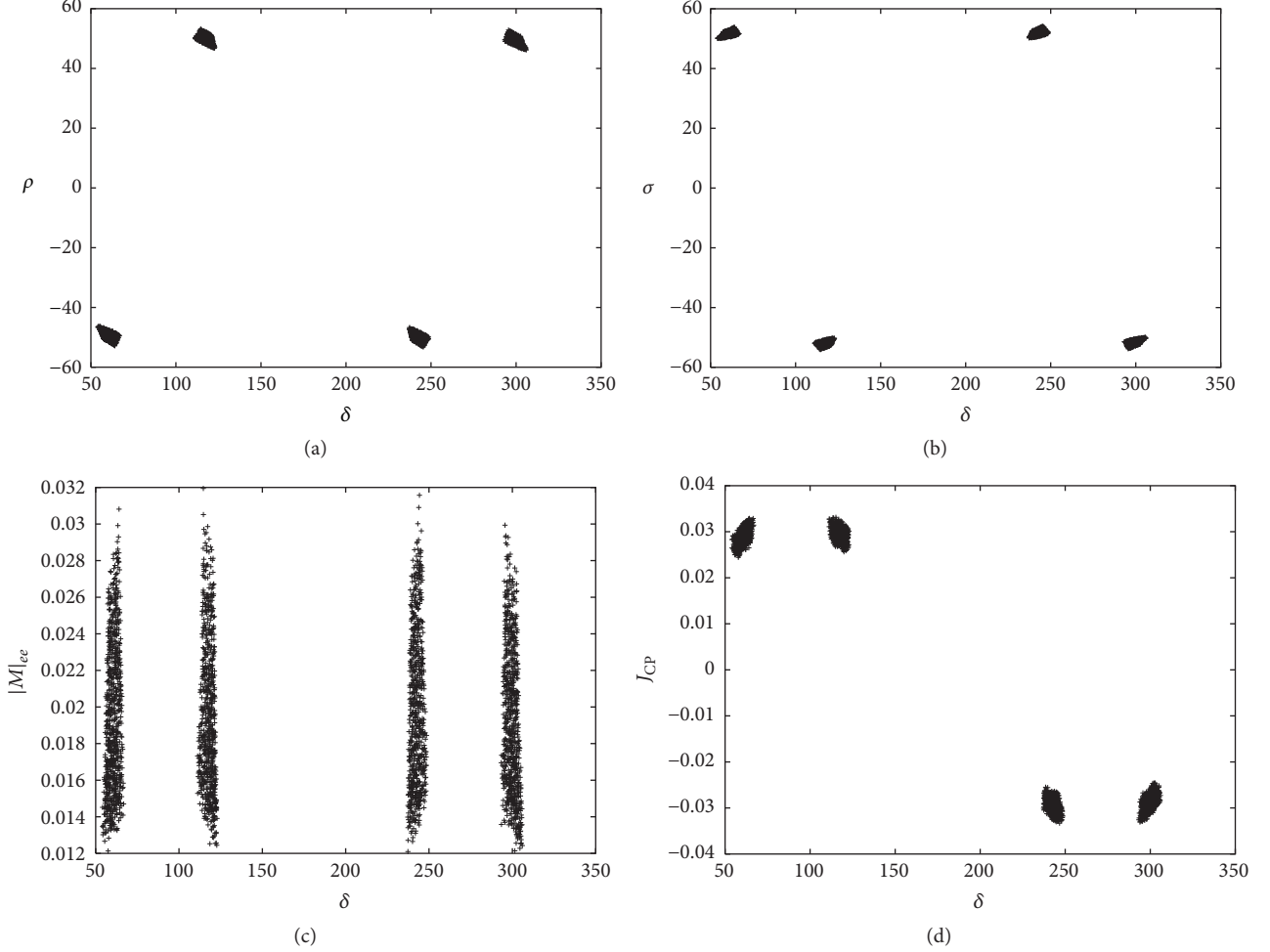


FIGURE 7: Case T_6 (IO): scattering plots of Majorana phases, Dirac CP violating phase (δ), effective neutrino mass $|M|_{ee}$, and Jarlskog rephrasing invariant (J_{CP}) have been shown. All the phase angles (δ, ρ, σ) are measured in degrees and $|M|_{ee}$ is in eV unit.

Acknowledgments

The author would like to thank the Director of National Institute of Technology Kurukshetra, for providing the necessary facilities to work.

References

- [1] Y. Abe, T. Akiri, J. Dos Anjos et al., "Indication of reactor $\bar{\nu}_e$ disappearance in the double chooz experiment," *Physical Review Letters*, vol. 108, no. 13, 2012.
- [2] F. P. An, J. Z. Bai, A. B. Balantekin et al., "Observation of electron-antineutrino disappearance at daya bay," *Physical Review Letters*, vol. 108, no. 17, 2012.
- [3] S.-B. Kim and RENO collaboration, "Observation of reactor electron antineutrinos disappearance in the RENO experiment," *Physical Review Letters*, vol. 108, p. 191802, 2012.
- [4] P. H. Frampton, S. L. Glashow, and D. Marfatia, "Zeroes of the neutrino mass matrix," *Physics Letters B*, vol. 536, no. 1-2, pp. 79–82, 2002.
- [5] Z.-Z. Xing, "Texture zeros and majorana phases of the neutrino mass matrix," *Physics Letters B*, vol. 530, no. 1-4, pp. 159–166, 2002.
- [6] R. Bipin, R. Desai, D. P. Roy, R. Alexander, and R. Vaucher, "Three-neutrino mass matrices with two texture zeros," *Modern Physics Letters A*, vol. 18, no. 20, pp. 1355–1365, 2003.
- [7] A. Merle and W. Rodejohann, "Elements of the neutrino mass matrix: allowed ranges and implications of texture zeros," *Physical Review D*, vol. 73, no. 7, Article ID 073012, 11 pages, 2006.
- [8] S. Dev, S. Kumar, S. Verma, and S. Gupta, "Phenomenological implications of a class of neutrino mass matrices," *Nuclear Physics B*, vol. 784, no. 1-2, pp. 103–117, 2007.
- [9] S. Dev, S. Kumar, S. Verma, and S. Gupta, "Phenomenology of two-texture zero neutrino mass matrices," *Physical Review D*, vol. 76, no. 1, Article ID 013002, 15 pages, 2007.
- [10] M. Randhawa, G. Ahuja, and M. Gupta, "Implications of Fritzsch-like lepton mass matrices," *Physics Letters B*, vol. 643, no. 3-4, pp. 175–181, 2006.
- [11] G. Ahuja, S. Kumar, M. Randhawa, M. Gupta, and S. Dev, "Texture 4 zero Fritzsch-like lepton mass matrices," *Physical Review D*, vol. 76, no. 1, Article ID 013006, 2007.
- [12] S. Kumar, "Implications of a class of neutrino mass matrices with texture zeros for nonzero θ_{13} ," *Physical Review D*, vol. 84, no. 7, Article ID 077301, 2011.

- [13] P. O. Ludl, S. Morisi, and E. Peinado, “The reactor mixing angle and CP violation with two texture zeros in the light of T2K,” *Nuclear Physics B*, vol. 857, no. 3, pp. 411–423, 2012.
- [14] H. Itoyama and N. Maru, “Flavor mixings and textures of the fermion mass matrices,” *International Journal of Modern Physics A*, vol. 27, no. 31, Article ID 1250159, 2012.
- [15] D. Meloni and G. Blankenburg, “Fine-tuning and naturalness issues in the two-zero neutrino mass textures,” *Nuclear Physics B*, vol. 867, no. 3, pp. 749–762, 2013.
- [16] W. Grimus and J. Ludl, “Two-parameter neutrino mass matrices with two texture zeros,” *Journal of Physics G: Nuclear and Particle Physics*, vol. 40, Article ID 125003, p. 055003, 2013.
- [17] S. Sharma, P. Fakay, G. Ahuja, and M. Gupta, “Majorana neutrinos and non minimal lepton mass textures,” <https://arxiv.org/abs/1402.1598>.
- [18] P. O. Ludl and W. Grimus, “A complete survey of texture zeros in the lepton mass matrices,” *Journal of High Energy Physics*, vol. 2014, 2014.
- [19] H. Fritzsch, Z. Z. Xing, and S. Zhou, “Two-zero textures of the Majorana neutrino mass matrix and current experimental tests,” *Journal of High Energy Physics*, vol. 2011, no. 09, p. 083, 2011.
- [20] E. I. Lashin and N. Chamoun, “One-zero textures of Majorana neutrino mass matrix and current experimental tests,” *Physical Review D*, vol. 85, no. 11, p. 113011, 2012.
- [21] K. N. Deepthi, S. Gollu, and R. Mohanta, “Neutrino mixing matrices with relatively large θ_{13} and with texture one-zero,” *The European Physical Journal C*, vol. 72, no. 2, pp. 1–18, 2012.
- [22] J. Liao, D. Marfatia, and K. Whisnant, “Seesaw mechanism with four texture zeros in the neutrino Yukawa matrix,” *Physical Review D: Particles, Fields, Gravitation and Cosmology*, vol. 87, no. 7, p. 073013, 2013.
- [23] J. Liao, D. Marfatia, and K. Whisnant, “One diagonal texture or cofactor zero of the neutrino mass matrix,” *Physical Review D*, vol. 88, no. 3, p. 033011, 2013.
- [24] H. Fritzsch and Z. Z. Xing, “Mass and flavor mixing schemes of quarks and leptons,” *Progress in Particle and Nuclear Physics*, vol. 45, no. 1, 2000, arXiv: hep-ph/9912358.
- [25] Z. Z. Xing, “Texture zeros and CP-violating phases in the neutrino mass matrix,” arXiv: hep-ph/0406049.
- [26] M. Singh, G. Ahuja, and M. Gupta, “Revisiting the texture zero neutrino mass matrices,” *PTEP*, vol. 2016, no. 8, p. 123, 2016.
- [27] X. Sun and W. Liu, “Improved black hole entropy calculation without cutoff,” *Modern Physics Letters A*, vol. 19, no. 9, 2004.
- [28] G. C. Branco, R. González Felipe, F. R. Joaquim, and T. Yanagida, “Removing ambiguities in the neutrino mass matrix,” *Physics Letters B*, vol. 562, no. 3-4, pp. 265–272, 2003.
- [29] Z. Z. Xing, “The majorana neutrino mass matrix with one texture zero and one vanishing eigenvalue,” *Physical Review D*, vol. 69, p. 013006, 2004, arXiv: hep-ph/0307007.
- [30] W. Rodejohann, M. Tanimoto, and A. Watanabe, “Relating large U_{e3} to the ratio of neutrino mass-squared differences,” *Physics Letters B*, vol. 710, no. 4-5, 2012.
- [31] L. Lavoura, W. Rodejohann, and A. Watanabe, “Reproducing lepton mixing in a texture zero model,” *Physics Letters B*, vol. 726, no. 1-3, 2013.
- [32] R. R. Gautam, M. Singh, and M. Gupta, “Neutrino mass matrices with one texture zero and a vanishing neutrino mass,” *Physical Review D*, vol. 92, no. 1, Article ID 024001, p. 013006, 2015.
- [33] D. Black, A. H. Fariborz, S. Nasri, and J. Schechter, “Complementary ansatz for the neutrino mass matrix,” *Physical Review D*, vol. 62, p. 073015, 2000, arXiv: hep-ph/0004105.
- [34] X. G. He and A. Zee, “Neutrino masses with “zero sum” condition: $m_{\nu 1} + m_{\nu 2} + m_{\nu 3} = 0$,” *Physical Review D*, vol. 68, p. 037302, 2003, arXiv: hep-ph/0302201.
- [35] A. Zee, “A theory of lepton number violation and neutrino Majorana masses,” *Physics Letters B*, vol. 93, no. 4, pp. 389–393, 1980.
- [36] H. A. Alhendi, E. I. Lashin, and A. A. Mudlej, “Textures with two traceless submatrices of the neutrino mass matrix,” *Physical Review D*, vol. 77, no. 1, p. 013009, 2008.
- [37] W. Rodejohann, “Neutrino mass matrices leaving no trace,” *Physics Letters B*, vol. 579, no. 1-2, pp. 127–139, 2004.
- [38] G. L. Fogli, E. Lisi, A. Marrone et al., “Evidence of $\theta_{13} > 0$ from global neutrino data analysis,” *Physical Review D*, vol. 84, no. 5, 2011.
- [39] D. V. Forero, M. Tórtola, and J. W. F. Valle, “Neutrino oscillations refitted,” *Physical Review D*, vol. 90, no. 9, p. 093006, 2014.
- [40] F. T. Avignone III, S. R. Elliott, and J. Engel, “Double beta decay, Majorana neutrinos, and neutrino mass,” *Reviews of Modern Physics*, vol. 80, no. 2, p. 481, 2008.
- [41] J. J. Gomez-Cadenas, J. Martin-Albo, M. Mezzetto, F. Monrabal, and M. Sorel, “The search for neutrinoless double beta decay,” *Italian Physical Science*, no. 2, 2012.
- [42] S. M. Bilenyk and C. Giunti, “Neutrinoless double-beta decay: a brief review,” *Modern Physics Letters A*, vol. 27, no. 13, Article ID 1230015, 2012.
- [43] W. Rodejohann, “Neutrino-less double beta decay and particle physics,” *International Journal of Modern Physics E*, vol. 20, no. 9, p. 1833, 2011.
- [44] C. Arnaboldi et al., “First results on neutrinoless double beta decay of ^{130}Te with the calorimetric CUORICINO experiment,” *Physics Letters B*, vol. 584, p. 260, 2004.
- [45] C. Arnaboldi et al., “CUORE: a cryogenic underground observatory for rare events,” *Nuclear Instruments and Methods in Physics Research A*, vol. 518, p. 775.
- [46] I. Abt et al., “A new ^{76}Ge double beta decay experiment at LNGS,” [GERDA Collaboration] hep-ex/0404039.
- [47] R. Gaitskell et al., “A new evaluation of the pion weak form factors,” [Majorana Collaboration] nucl-ex/0311013.
- [48] A. S. Barabash, “Average (recommended) half-life values for two neutrino double beta decay,” *Czechoslovak Journal of Physics*, vol. 52, p. 567, 2002.
- [49] M. Danilov, R. DeVoec, A. Dolgolenkod et al., “Detection of very small neutrino masses in double-beta decay using laser tagging,” *Physics Letters B*, vol. 480, no. 1-2, pp. 12–18, 2000.
- [50] H. V. Klapdor-Kleingrothaus, A. Dietz, G. Baudis et al., “Latest results from the HEIDELBERG-MOSCOW double beta decay experiment,” *The European Physical Journal A - Hadrons and Nuclei*, vol. 12, no. 2, pp. 147–154, 2001.
- [51] P. A. R. Ade, N. Aghanim, C. Armitage-Caplan et al., “Planck 2013 results. XVI. cosmological parameters,” *Astronomy & Astrophysics: World Wide Astronomical and Astrophysical Research*, vol. 571, 2014.

Research Article

Study of Rare Semileptonic $B_c^+ \rightarrow D^+ \nu \bar{\nu}$ Decay in the Light-Cone Quark Model

Nisha Dhiman and Harleen Dahiya 

Department of Physics, Dr. B. R. Ambedkar National Institute of Technology, Jalandhar 144011, India

Correspondence should be addressed to Harleen Dahiya; dahiya@nitj.ac.in

Received 7 November 2017; Accepted 4 March 2018; Published 3 April 2018

Academic Editor: Luca Stanco

Copyright © 2018 Nisha Dhiman and Harleen Dahiya. This is an open access article distributed under the Creative Commons Attribution License, which permits unrestricted use, distribution, and reproduction in any medium, provided the original work is properly cited. The publication of this article was funded by SCOAP³.

We study the exclusive semileptonic rare $B_c^+ \rightarrow D^+ \nu \bar{\nu}$ decay in the framework of light-cone quark model. The transition form factors $f_+(q^2)$ and $f_T(q^2)$ are evaluated in the timelike region using the analytic continuation method in $q^+ = 0$ frame. The analytic solutions of these form factors are compared with the results obtained from the double pole parametric form. The branching ratio for $B_c^+ \rightarrow D^+ \nu \bar{\nu}$ decay is calculated and compared with the other theoretical model predictions. The predicted results in this model can be tested at the LHCb experiments in near future which will help in testing the unitarity of CKM quark mixing matrix, thus providing an insight into the phenomenon of CP violation.

1. Introduction

In the past few years, great progress has been made in understanding the semileptonic decays in the B sector as these are among the cleanest probes of the flavor sector of the Standard Model (SM) which not only provide valuable information to explore the SM but also are powerful means for probing different new physics (NP) scenarios beyond the SM (BSM) [1–3]. Due to the Glashow-Iliopoulos-Maiani (GIM) mechanism [4], flavor changing neutral current (FCNC) induced semileptonic B decays are rare in the SM because these decays are forbidden at tree level and can proceed at the lowest order only via electroweak penguin and box diagrams [5, 6]. Therefore, these decay processes provide sensitive probes to look into physics BSM [7]. They also play a significant role in providing a new framework to study the mixing between different generations of quarks by extracting the most accurate values of Cabibbo-Kobayashi-Maskawa (CKM) matrix elements which help us to test the charge-parity (CP) violation in the SM and to dig out the status of NP [8, 9].

The theoretical analysis of CP violating effects in rare semileptonic B decays requires knowledge of the transition form factors that are model dependent quantities and are

scalar functions of the square of momentum transfer [10]. These form factors also interrelate to the decay rates and branching ratios of all the observed decay modes of B mesons and their calculation requires a nonperturbative treatment. Various theoretical approaches, such as relativistic constituent quark model [11–15], QCD sum rules [16–20], lattice QCD calculations [21–23], chiral perturbation theory [24, 25], and the light-front quark model (LFQM) [26–34], have been applied to the calculations of hadronic form factors for rare semileptonic B decays. Experimentally, a significant effort has been made for the advancement of our knowledge of the flavor structure of the SM through the studies of inclusive [35] as well as exclusive [36] rare B decays. The violation of CP symmetry in B meson decays was first observed in 2001 (other than in neutral K meson decays) by two experiments: the Belle experiment at KEK and the Babar experiment at SLAC [37]. Both these experiments were constructed and operated on similar time scales and were able to take flavor physics into a new realm of discovery [38]. The Babar and Belle experiments completed taking data in 2008 and 2010, respectively. Recently, numerous measurements of B decays have been performed by the LHC experiments at CERN; in particular, the dedicated B physics experiment LHCb makes a valuable contribution in the understanding of

CP violation through the precise determination of the flavor parameters of the SM [39–41].

In particular, there has been an enormous interest in studying the decay properties of the B_c meson due to its outstanding properties [42]. Unlike the symmetric heavy quark bound states $b\bar{b}$ (bottomonium) and $c\bar{c}$ (charmonium), B_c meson is the lowest bound state of two heavy quarks (b and c) with different flavors and charge. Due to the explicit flavor numbers, B_c mesons can decay only through weak interaction and are stable against strong and electromagnetic interactions, thereby providing us an opportunity to test the unitarity of CKM quark mixing matrix. The study of an exclusive semileptonic rare $B_c^+ \rightarrow D^+ \nu \bar{\nu}$ decay is prominent among all the B_c meson decay modes as it plays a significant role for precision tests of the flavor sector in the SM and its possible NP extensions. At quark level, the decay $B_c^+ \rightarrow D^+ \nu \bar{\nu}$ proceeds via $b \rightarrow d$ FCNC transition with the intermediate u , c , and t quarks and most of the contribution comes from the intermediate t quark. Also, due to the neutral and massless final states ($\nu \bar{\nu}$), it provides an unique opportunity to study the Z penguin effects [10]. As a theoretical input, hadronic matrix elements of quark currents will be required to calculate the transition form factors [43] in order to study the decay rates and branching ratios of the above-mentioned decay.

The semileptonic rare $B_c^+ \rightarrow D^+ \nu \bar{\nu}$ decay has been studied by various theoretical approaches such as constituent quark model (CQM) [44] and QCD sum rules [45]. In this work, we choose the framework of light-cone quark model (LCQM) [46] for the analysis of this decay process. LCQM deals with the wave function defined on the four-dimensional space-time plane given by the equation $x^+ = x^0 + x^3$ and includes the important relativistic effects that are neglected in the traditional CQM [47, 48]. The kinematic subgroup of the light-cone formalism has the maximum number of interaction-free generators in comparison with the point form and instant form [49]. The most phenomenal feature of this formalism is the apparent simplicity of the light-cone vacuum, because the vacuum state of the free Hamiltonian is an exact eigen state of the total light-cone Hamiltonian [50]. The light-cone Fock space expansion constructed on this vacuum state provides a complete relativistic many-particle basis for a hadron [51]. The light-cone wave functions providing a description about the hadron in terms of their fundamental quark and gluon degrees of freedom are independent of the hadron momentum making them explicitly Lorentz invariant [52].

The paper is organized as follows. In Section 2, we discuss the formalism of light-cone framework and calculate the transition form factors for $B_c^+ \rightarrow D^+ \nu \bar{\nu}$ decay process in $q^+ = 0$ frame. In Section 3, we present our numerical results for the form factors and branching ratios and compare them with other theoretical results. Finally, we conclude in Section 4.

2. Light-Cone Framework

In the light-cone framework, we can write the bound state of a meson M consisting of a quark q_1 and an antiquark \bar{q} with total momentum P and spin S as [53]

$$|M(P, S, S_z)\rangle = \int \frac{d^2 p_{q_1}^+ d^2 p_{q_1\perp}}{16\pi^3} \frac{d^2 p_{\bar{q}}^+ d^2 p_{\bar{q}\perp}}{16\pi^3} \cdot 16\pi^3 \delta^3(\tilde{P} - \tilde{p}_{q_1} - \tilde{p}_{\bar{q}}) \times \sum_{\lambda_{q_1}, \lambda_{\bar{q}}} \Psi^{SS_z}(\tilde{p}_{q_1}, \tilde{p}_{\bar{q}}, \lambda_{q_1}, \lambda_{\bar{q}}) \cdot |q_1(p_{q_1}, \lambda_{q_1}) \bar{q}(p_{\bar{q}}, \lambda_{\bar{q}})\rangle, \quad (1)$$

where p_{q_1} and $p_{\bar{q}}$ denote the on-mass shell light-front momenta of the constituent quarks. The four-momentum \tilde{p} is defined as

$$\begin{aligned} \tilde{p} &= (p^+, \mathbf{p}_\perp), \\ \mathbf{p}_\perp &= (p^1, p^2), \\ p^- &= \frac{m^2 + \mathbf{p}_\perp^2}{p^+}, \\ |q_1(p_{q_1}, \lambda_{q_1}) \bar{q}(p_{\bar{q}}, \lambda_{\bar{q}})\rangle &= b^\dagger(p_{q_1}, \lambda_{q_1}) d^\dagger(p_{\bar{q}}, \lambda_{\bar{q}}) |0\rangle, \\ \{b(p', \lambda'), b^\dagger(p, \lambda)\} &= \{d(p', \lambda'), d^\dagger(p, \lambda)\} \\ &= 2(2\pi)^3 \delta^3(\tilde{p}' - \tilde{p}) \delta_{\lambda'\lambda}. \end{aligned} \quad (2)$$

The momenta p_{q_1} and $p_{\bar{q}}$ in terms of light-cone variables are

$$\begin{aligned} p_{q_1}^+ &= x_1 P^+, \\ p_{\bar{q}}^+ &= x_2 P^+, \\ \mathbf{p}_{q_1\perp} &= x_1 \mathbf{P}_\perp + \mathbf{k}_\perp, \\ \mathbf{p}_{\bar{q}\perp} &= x_2 \mathbf{P}_\perp - \mathbf{k}_\perp, \end{aligned} \quad (3)$$

where x_i ($i = 1, 2$) represent the light-cone momentum fractions satisfying $x_1 + x_2 = 1$ and \mathbf{k}_\perp is the relative transverse momentum of the constituent.

The momentum-space light-cone wave function Ψ^{SS_z} in (1) can be expressed as

$$\Psi^{SS_z}(\tilde{p}_{q_1}, \tilde{p}_{\bar{q}}, \lambda_{q_1}, \lambda_{\bar{q}}) = R_{\lambda_{q_1} \lambda_{\bar{q}}}^{SS_z}(x, \mathbf{k}_\perp) \phi(x, \mathbf{k}_\perp), \quad (4)$$

where $\phi(x, \mathbf{k}_\perp)$ describes the momentum distribution of the constituents in the bound state and $R_{\lambda_{q_1} \lambda_{\bar{q}}}^{SS_z}$ constructs a state of definite spin (S, S_z) out of the light-cone helicity ($\lambda_{q_1}, \lambda_{\bar{q}}$) eigenstates. For convenience, we use the covariant form of $R_{\lambda_{q_1} \lambda_{\bar{q}}}^{SS_z}$ for pseudoscalar mesons which is given by

$$\begin{aligned} R_{\lambda_{q_1} \lambda_{\bar{q}}}^{SS_z}(x, \mathbf{k}_\perp) &= \frac{\sqrt{p_{q_1}^+ p_{\bar{q}}^+}}{\sqrt{2} \sqrt{M_0^2 - (m_{q_1} - m_{\bar{q}})^2}} \bar{u}(p_{q_1}, \lambda_{q_1}) \gamma_5 v(p_{\bar{q}}, \lambda_{\bar{q}}), \end{aligned} \quad (5)$$

where

$$M_0^2 = \frac{m_{q_1}^2 + \vec{k}_\perp^2}{x_1} + \frac{m_{\bar{q}}^2 + \vec{k}_\perp^2}{x_2}. \quad (6)$$

The meson state can be normalized as

$$\begin{aligned} & \langle M(P', S', S'_z) | M(P, S, S_z) \rangle \\ & = 2(2\pi)^3 P^+ \delta^3(\vec{P}' - \vec{P}) \delta_{S'S} \delta_{S'_z S_z}, \end{aligned} \quad (7)$$

so that

$$\int \frac{dx d^2\mathbf{k}_\perp}{2(2\pi)^3} |\phi(x, \mathbf{k}_\perp)|^2 = 1. \quad (8)$$

We choose the Gaussian-type wave function to describe the radial wave function ϕ :

$$\phi(x, \mathbf{k}_\perp) = \sqrt{\frac{1}{\pi^{3/2} \beta^3}} \exp\left(-\frac{\mathbf{k}^2}{2\beta^2}\right), \quad (9)$$

where β is a scale parameter and $\mathbf{k}^2 = \mathbf{k}_\perp^2 + k_z^2$ denotes the internal momentum of meson. The longitudinal component k_z is defined as

$$k_z = \left(x - \frac{1}{2}\right) M_0 + \frac{m_{q_1}^2 - m_{\bar{q}}^2}{2M_0}. \quad (10)$$

2.1. Form Factors for the Semileptonic $B_c^+ \rightarrow D^+ \nu \bar{\nu}$ Decay in LCQM. The form factors $f_+(q^2)$ and $f_T(q^2)$ can be obtained in $q^+ = 0$ frame with the ‘‘good’’ component of current, that is, $\mu = +$, from the hadronic matrix elements given by [53]

$$\langle D^+ | \bar{d} \gamma^\mu b | B_c^+ \rangle = f_+(q^2) P^\mu + f_-(q^2) q^\mu, \quad (11)$$

$$\begin{aligned} & \langle D^+ | \bar{d} i \sigma^{\mu\nu} q_\nu b | B_c^+ \rangle \\ & = \frac{f_T(q^2)}{(M_{B_c^+} + M_{D^+})} \left[q^2 P^\mu - (M_{B_c^+}^2 - M_{D^+}^2) q^\mu \right]. \end{aligned} \quad (12)$$

It is more convenient to express the matrix element defined by (11) in terms of $f_+(q^2)$ and $f_0(q^2)$ as

$$\begin{aligned} \langle D^+ | \bar{d} \gamma^\mu b | B_c^+ \rangle & = F_+(q^2) \left[P^\mu - \frac{M_{B_c^+}^2 - M_{D^+}^2}{q^2} q^\mu \right] \\ & + f_0(q^2) \frac{M_{B_c^+}^2 - M_{D^+}^2}{q^2} q^\mu, \end{aligned} \quad (13)$$

with

$$\begin{aligned} F_+(q^2) & = f_+(q^2), \\ f_0(q^2) & = f_+(q^2) + \frac{q^2}{M_{B_c^+}^2 - M_{D^+}^2} f_-(q^2). \end{aligned} \quad (14)$$

Here $P = P_{B_c^+} + P_{D^+}$ and $q = P_{B_c^+} - P_{D^+}$ and $0 \leq q^2 \leq (M_{B_c^+} - M_{D^+})^2$.

Using the parameters of b and d quarks, the form factors $f_+(q^2)$ and $f_T(q^2)$ can be, respectively, expressed in the quark explicit forms as follows [46]:

$$\begin{aligned} f_+(q^2) & = \int_0^1 dx \int d^2\mathbf{k}_\perp \sqrt{\frac{\partial k'_z}{\partial x}} \sqrt{\frac{\partial k_z}{\partial x}} \phi_d(x, \mathbf{k}'_\perp) \phi_b(x, \mathbf{k}_\perp) \\ & \cdot \frac{A_b A_d + \mathbf{k}_\perp \cdot \mathbf{k}'_\perp}{\sqrt{A_b^2 + \mathbf{k}_\perp^2} \sqrt{A_d^2 + \mathbf{k}'_\perp^2}}, \\ f_T(q^2) & = - \int_0^1 dx \int d^2\mathbf{k}_\perp \sqrt{\frac{\partial k'_z}{\partial x}} \sqrt{\frac{\partial k_z}{\partial x}} \phi_d(x, \mathbf{k}'_\perp) \phi_b(x, \mathbf{k}_\perp) \\ & \times \frac{x(M_{B_c^+} + M_{D^+}) \left[(m_d - m_b) (\mathbf{k}_\perp \cdot \mathbf{q}_\perp / q_\perp^2) + A_b \right]}{\sqrt{A_b^2 + \mathbf{k}_\perp^2} \sqrt{A_d^2 + \mathbf{k}'_\perp^2}}, \end{aligned} \quad (15)$$

where $\mathbf{k}'_\perp = \mathbf{k}_\perp - x\mathbf{q}_\perp$ represents the final state transverse momentum, $A_b = xm_b + (1-x)m_{\bar{q}}$, and $A_d = xm_d + (1-x)m_{\bar{q}}$. The term $\partial k_z / \partial x$ denotes the Jacobian of the variable transformation $\{x, \mathbf{k}_\perp\} \rightarrow \mathbf{k} = (k_z, \mathbf{k}_\perp)$.

The LCQM calculations of form factors have been performed in the $q^+ = 0$ frame [54, 55], where $q^2 = q^+ q^- - \mathbf{q}_\perp^2 = -\mathbf{q}_\perp^2 < 0$ (spacelike region). The calculations are analytically continued to the $q^2 > 0$ (timelike) region by replacing \mathbf{q}_\perp to $i\mathbf{q}_\perp$ in the form factors. To obtain the numerical results of the form factors, we use the change of variables as follows:

$$\begin{aligned} \mathbf{k}_\perp & = \boldsymbol{\ell}_\perp + \frac{x\beta_{B_c^+}^2}{\beta_{B_c^+}^2 + \beta_{D^+}^2} \mathbf{q}_\perp, \\ \mathbf{k}'_\perp & = \boldsymbol{\ell}_\perp - \frac{x\beta_{D^+}^2}{\beta_{B_c^+}^2 + \beta_{D^+}^2} \mathbf{q}_\perp. \end{aligned} \quad (16)$$

The detailed procedure of analytic solutions for the weak form factors in timelike region has been discussed in literature [56].

For the sake of completeness and to compare our analytic solutions, we use a double pole parametric form of form factors expressed as follows [44]:

$$f(q^2) = \frac{f(0)}{1 + \mathcal{A}s + \mathcal{B}s^2}, \quad (17)$$

where $s = q^2/M_{B_c^+}^2$, $f(q^2)$ denotes any of the form factors, and $f(0)$ denotes the form factors at $q^2 = 0$. Here \mathcal{A} , \mathcal{B} are the parameters to be fitted from (17). While performing calculations, we first compute the values of $f_+(q^2)$ and $f_T(q^2)$ from (15) in $0 \leq q^2 \leq (M_{B_c^+} - M_{D^+})^2$, followed by extraction of the parameters \mathcal{A} and \mathcal{B} using the values of $M_{B_c^+}$ and $f(0)$, and then finally fit the data in terms of parametric form.

2.2. Decay Rate and Branching Ratio for $B_c^+ \rightarrow D^+ \nu \bar{\nu}$ Decay. At the quark level, the rare semileptonic $B_c^+ \rightarrow D^+ \nu \bar{\nu}$ decay

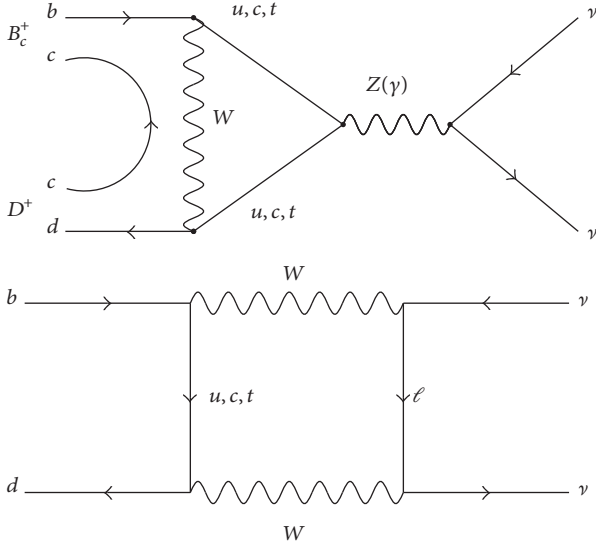


FIGURE 1: Loop diagrams for $B_c^+ \rightarrow D^+ \nu \bar{\nu}$ decay process.

is described by the $b \rightarrow d$ FCNC transition. As mentioned earlier, these kinds of transitions are forbidden at the tree level in the SM and occur only through loop diagrams as shown in the Figure 1. They receive contributions from the penguin and box diagrams [44]. Theoretical investigation of these rare transitions usually depends on the effective Hamiltonian density. The effective interacting Hamiltonian density responsible for $b \rightarrow d$ transition is given by [57]

$$\begin{aligned} \mathcal{H}_{\text{eff}}(b \rightarrow d \nu \bar{\nu}) &= \frac{G_F}{\sqrt{2}} \frac{\alpha V_{tb} V_{td}^*}{2\pi \sin^2 \theta_W} X(x_t) \bar{d} \gamma_\mu (1 - \gamma_5) b \bar{\nu} \gamma^\mu (1 - \gamma_5) \nu, \end{aligned} \quad (18)$$

where G_F is the Fermi constant, α is the electromagnetic fine structure constant, θ_W is the Weinberg angle, V_{ij} ($i = t, j = b$ and d) are the CKM matrix elements, and $x_t = m_t^2/M_W^2$.

The function $X(x_t)$ denotes the top quark loop function, which is given by

$$X(x_t) = \frac{x_t}{8} \left(\frac{2 + x_t}{x_t - 1} + \frac{3x_t - 6}{(x_t - 1)^2} \ln x_t \right). \quad (19)$$

The differential decay rate for $B_c^+ \rightarrow D^+ \nu \bar{\nu}$ can be expressed in terms of the form factors as [46]

$$\frac{d\Gamma}{ds} = \frac{M_{B_c}^5 G_F^2}{2^8 \pi^5 \sin^4 \theta_W} \alpha^2 |V_{tb} V_{td}^*|^2 |X(x_t)|^2 \phi_{D^+}^{3/2} |f_+|^2, \quad (20)$$

where $\phi_{D^+} = (1 - r_{D^+})^2 - 2s(1 + r_{D^+}) + s^2$ with $s = q^2/M_{B_c}^2$ and $r_{D^+} = M_{D^+}^2/M_{B_c}^2$.

The differential branching ratio ($d\text{BR}/ds$) can be obtained by dividing the differential decay rate ($d\Gamma/ds$) by the total width (Γ_{total}) of the B_c^+ meson and then, by integrating the differential branching ratio over $s = q^2/M_{B_c}^2$, we can obtain the branching ratio (BR) for $B_c^+ \rightarrow D^+ \nu \bar{\nu}$ decay.

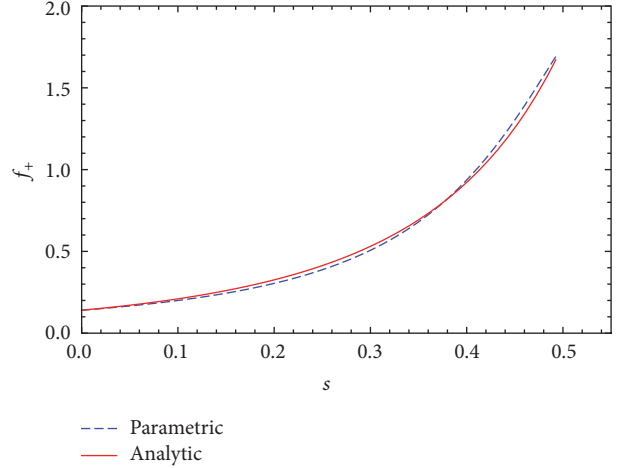


FIGURE 2: Analytic solutions of f_+ (thick solid curve) compared with the parametric results (dashed curve), with definition $s = q^2/M_{B_c}^2$.

3. Numerical Results

Before obtaining the numerical results of the form factors for the semileptonic $B_c^+ \rightarrow D^+ \nu \bar{\nu}$ decay, we first specify the parameters appearing in the wave functions of the hadrons. We have used the constituent quark masses as [53, 58]

$$\begin{aligned} m_b &= 4.8 \text{ GeV}, \\ m_d &= 0.25 \text{ GeV}, \\ m_c &= 1.4 \text{ GeV}. \end{aligned} \quad (21)$$

The parameter β that describes the momenta distribution of constituent quarks can be fixed by the meson decay constants $f_{B_c^+}$ and f_{D^+} , respectively. The β parameters that we have used in our work are given as [44]

$$\begin{aligned} \beta_{B_c^+} &= 0.81 \text{ GeV}, \\ \beta_{D^+} &= 0.46 \text{ GeV}. \end{aligned} \quad (22)$$

Using the above parameters, we present the analytic solutions of the form factors f_+ and f_T (thick solid curve) for $0 \leq q^2 \leq (M_{B_c^+} - M_{D^+})^2$ in Figures 2 and 3, respectively. We have also shown the results obtained from the parametric formula (dashed curve) given by (17). We would like to mention here that the point $q^2 = 0$ represents the maximum recoil point and the point $q^2 = q_{\text{max}}^2 = (M_{B_c^+} - M_{D^+})^2$ represents the zero recoil point where the produced meson is at rest. As we can see from Figures 2 and 3, the form factors f_+ and f_T increase and decrease exponentially with respect to q^2 . The analytic solutions of form factors given by (15) are well approximated by the parametric form in the physical decay region $0 \leq q^2 \leq (M_{B_c^+} - M_{D^+})^2$. For a deeper understanding of the results, we have listed the numerical results for the form factors f_+ and f_T at $q^2 = 0$ and the parameters \mathcal{A} and \mathcal{B} of the double pole form in Table 1. For the sake of comparison, we have also presented the results of other theoretical models.

TABLE 1: Form factors for $B_c^+ \rightarrow D^+ \nu \bar{\nu}$ decay process at $q^2 = 0$ and the parameters \mathcal{A} and \mathcal{B} defined by (17) and their comparison with other theoretical model predictions.

Model	$f_+(0)$	\mathcal{A}	\mathcal{B}	$f_T(0)$	\mathcal{A}	\mathcal{B}
This work	0.140	-3.263	2.846	-0.234	-3.430	3.174
CQM [44]	0.123	-3.35	3.03	-0.186	-3.52	3.38
SR [45]	0.22	-1.10	-2.48	-0.27	-0.72	-3.24
Linear [46]	0.086	-3.50	3.30	-0.120	-3.35	3.06
HO [46]	0.079	-3.20	2.81	-0.108	-3.18	2.77

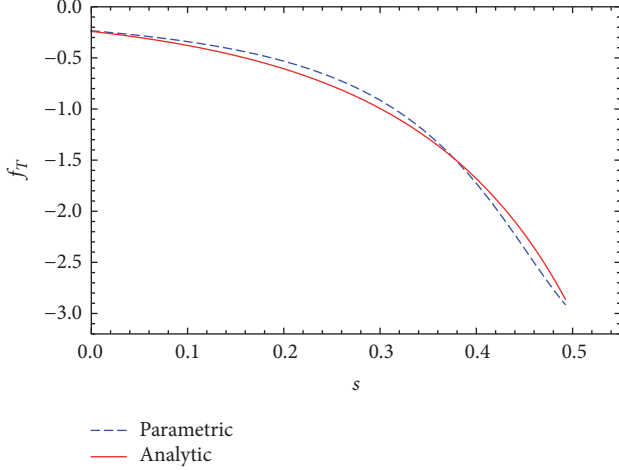


FIGURE 3: Analytic solutions of f_T (thick solid curve) compared with the parametric results (dashed curve), with definition $s = q^2/M_{B_c^+}^2$.

TABLE 2: Branching ratio for $B_c^+ \rightarrow D^+ \nu \bar{\nu}$ decay in LCQM and its comparison with the other models.

Model	Branching ratios (in units of 10^{-8})
This work	3.33
CQM [44]	2.74
QCD sum rules [45]	3.38
Linear [46]	1.31
HO [46]	0.81

It can be seen from the table that the values of form factors f_+ and f_T at $q^2 = 0$ in our model agree quite well with the CQM. The difference in the values with respect to other models might be due to the different assumptions of the models or different choices of parameters.

To estimate the numerical value of the branching ratio for $B_c^+ \rightarrow D^+ \nu \bar{\nu}$ decay (defined in (20)), the various input parameters used are [46] $\alpha^{-1} = 129$, $|V_{tb}V_{td}^*| = 0.008$, $M_W = 80.43$ GeV, $m_t = 171.3$ GeV, and $\sin^2\theta_W = 0.2233$. The lifetime of B_c^+ ($\tau_{B_c^+} = 0.507$ ps) is taken from the Particle Data Group [59]. Our results for the differential branching ratio as a function of s is shown in Figure 4.

Our prediction for the decay branching ratio of $B_c^+ \rightarrow D^+ \nu \bar{\nu}$ decay is listed in Table 2 and compared with the other theoretical predictions. As we can see from Table 2, the result predicted by LCQM approximately agrees with the prediction

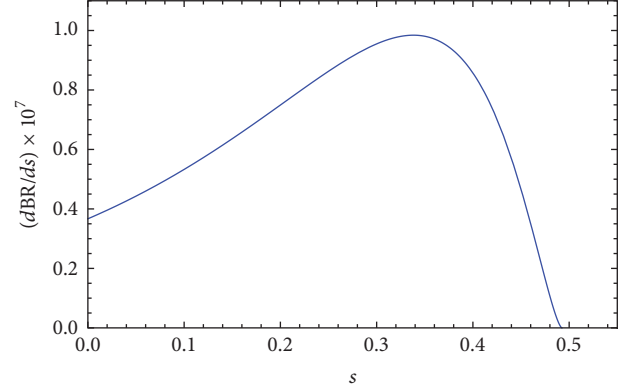


FIGURE 4: Differential branching ratios as a function of s for $B_c^+ \rightarrow D^+ \nu \bar{\nu}$ decay.

given by QCD sum rules whereas it is slightly larger when compared with the results of CQM. At present, we do not have any deep understanding of these values; however they do indicate that these results may be important even in a more rigorous model. The measurements can perhaps be substantiated by measurement of the decay width of B mesons. Several experiments at LHCb are contemplating the possibility of searching for more B meson decays.

4. Conclusions

We have studied the exclusive semileptonic rare $B_c^+ \rightarrow D^+ \nu \bar{\nu}$ decay within the framework of LCQM. In our analysis, we have evaluated the transition form factors $f_+(q^2)$ and $f_T(q^2)$ in the $q^+ = 0$ frame and then extended them from the spacelike region ($q^2 < 0$) to the timelike region ($q^2 > 0$) through the method of analytical continuation using the constituent quark masses (m_b , m_d , and m_c) and the parameters describing the momentum distribution of the constituent quarks ($\beta_{B_c^+}$ and β_{D^+}), respectively. The numerical values of $\beta_{B_c^+}$ and β_{D^+} have been fixed from the meson decay constants $f_{B_c^+}$ and f_{D^+} , respectively. We have also compared the analytic solutions of transition form factors with the results obtained for the form factors using the double pole parametric form. Using the numerical results of transition form factors, we have calculated the decay branching ratio and compared our result with the other theoretical predictions. The LCQM result for the decay branching ratio of $B_c^+ \rightarrow D^+ \nu \bar{\nu}$ decay comes out to be 3.33×10^{-8} which approximately agrees with the prediction given by QCD

sum rules [45]. This result can also be tested at the LHCb experiments in near future.

To conclude, new experiments aimed at measuring the decay branching ratios are not only needed for the profound understanding of B decays but also to restrict the model parameters for getting better knowledge on testing the unitarity of CKM quark mixing matrix. This will provide us with a useful insight into the phenomenon of CP violation.

Conflicts of Interest

The authors declare that they have no conflicts of interest.

Acknowledgments

The authors would like to acknowledge Chueng-Ryong Ji (North Carolina State University, Raleigh, NC) for the helpful discussions and Department of Science and Technology (Ref no. SB/S2/HEP-004/2013), Government of India, for financial support.

References

- [1] J. Dingfelder and T. Mannel, “Leptonic and semileptonic decays of B mesons,” *Reviews of Modern Physics*, vol. 88, no. 3, Article ID 035008, 2016.
- [2] H.-M. Choi and C.-R. Ji, “Semileptonic and radiative decays of the B_c meson in the light-front quark model,” *Physical Review D*, vol. 80, Article ID 054016, 2009.
- [3] W. Jaus, “Semileptonic decays of B and D mesons in the light-front formalism,” *Physical Review D: Particles, Fields, Gravitation and Cosmology*, vol. 41, no. 11, Article ID 3394, 1990.
- [4] S. L. Glashow, J. Iliopoulos, and L. Maiani, “Weak interactions with lepton-hadron symmetry,” *Physical Review D: Particles, Fields, Gravitation and Cosmology*, vol. 2, no. 7, pp. 1285–1292, 1970.
- [5] A. Ali, “ B decays in the standard model — status and perspectives,” *Acta Physica Polonica B*, vol. 27, p. 3529, 1996.
- [6] G. Buchalla and A. Buras, “QCD corrections to rare K - and B -decays for arbitrary top quark mass,” *Nuclear Physics B*, vol. 400, pp. 225–239, 1993.
- [7] T. Blake, G. Lanfranchi, and R. Khosravi, “Rare B decays as tests of the Standard Model,” *Progress in Particle and Nuclear Physics*, vol. 92, pp. 50–91, 2017.
- [8] C. S. Kim, T. Morozumi, and A. I. Sanda, “ $B \rightarrow X_q l^+ l^-$ ($q = d, s$) and determination of $|V_{td}/V_{ts}|$,” *Physical Review D*, vol. 56, pp. 7240–7246, 1997.
- [9] T. Aliev, C. Kim, and M. Savcı, “Exclusive $B \rightarrow M \ell^+ \ell^-$ ($M = \pi, K, \rho, K^*$) decays and determinations of V_{ts} (and V_{td}/V_{ts}),” *Physics Letters B*, vol. 441, no. 1-4, pp. 410–418, 1998.
- [10] M. Wick, *Ph.D. thesis*, Technical University of Munich, 2010.
- [11] D. Melikhov, “Form factors of meson decays in the relativistic constituent quark model,” *Physical Review D: Particles, Fields, Gravitation and Cosmology*, vol. 53, no. 5, pp. 2460–2479, 1996.
- [12] D. Melikhov, N. Nikitin, and S. Simula, “Rare exclusive semileptonic,” *Physical Review D: Particles, Fields, Gravitation and Cosmology*, vol. 57, no. 11, pp. 6814–6828, 1998.
- [13] D. Melikhov and B. Stech, “Weak form factors for heavy meson decays: an update,” *Physical Review D: Particles, Fields, Gravitation and Cosmology*, vol. 62, no. 1, Article ID 014006, 2000.
- [14] M. Wirbel, B. Stech, and M. Bauer, “Exclusive semileptonic decays of heavy mesons,” *Zeitschrift für Physik C*, vol. 29, no. 4, pp. 637–642, 1985.
- [15] W. Jaus and D. Wyler, “Rare decays,” *Physical Review D: Particles, Fields, Gravitation and Cosmology*, vol. 41, no. 11, pp. 3405–3413, 1990.
- [16] P. Ball, V. M. Braun, and H. G. Dosch, “Form factors of semileptonic D decays from QCD sum rules,” *Physical Review D: Particles, Fields, Gravitation and Cosmology*, vol. 44, no. 11, pp. 3567–3581, 1991.
- [17] P. Ball, “ $B \rightarrow \pi$ and $B \rightarrow K$ and $B \rightarrow K$ transitions from QCD sum rules on the light-cone,” *Journal of High Energy Physics*, vol. 9, p. 5, 1998.
- [18] P. Ball and V. M. Braun, “Exclusive semileptonic and rare,” *Physical Review D: Particles, Fields, Gravitation and Cosmology*, vol. 58, no. 9, Article ID 094016, 1998.
- [19] P. Colangelo, F. De Fazio, P. Santorelli, and E. Scrimieri, “QCD sum rule analysis of the decays $B \rightarrow K \ell^+ \ell^-$ and $B \rightarrow K^* \ell^+ \ell^-$,” *Physical Review D: Particles, Fields, Gravitation and Cosmology*, vol. 53, no. 7, pp. 3672–3686, 1996.
- [20] V. V. Kiselev, A. E. Kovalsky, and A. K. Likhoded, “ B_c decays and lifetime in QCD sum rules,” *Nuclear Physics B*, vol. 585, no. 1-2, pp. 353–382, 2000.
- [21] J. M. Flynn and C. T. Sachrajda, “Heavy quark physics from lattice QCD,” *Journal of High Energy Physics*, vol. 15, pp. 402–452, 1998.
- [22] A. Abada, D. Becirevic, P. Boucaud et al., “Decays of heavy mesons,” *Nuclear Physics B—Proceedings Supplements*, vol. 83-84, no. 1-3, pp. 268–270, 2000.
- [23] K. C. Bowler et al., “Improved $B \rightarrow \pi l \nu_l$ form factors from the lattice,” *Physics Letters B*, vol. 486, pp. 111–117, 2000.
- [24] R. Casalbuoni, A. Deandrea, N. Di Bartolomeo, R. Gatto, F. Feruglio, and G. Nardulli, “Phenomenology of heavy meson chiral lagrangians,” *Physics Reports*, vol. 281, no. 3, pp. 145–238, 1997.
- [25] D. Du, C. Liu, and D. Zhang, “The rare decay $B \rightarrow K_{T^+ T^-}$ in heavy meson chiral perturbation theory,” *Physics Letters B*, vol. 317, pp. 179–182, 1993.
- [26] H. Choi and C. Ji, “Nonleptonic two-body decays of the B_c meson in the light-front quark model and the QCD factorization approach,” *Physical Review D: Particles, Fields, Gravitation and Cosmology*, vol. 80, Article ID 114003, 2009.
- [27] H.-M. Choi and C.-R. Ji, “Kaon electroweak form factors in the light-front quark model,” *Physics Letters D*, vol. 59, Article ID 034001, 1999.
- [28] H.-M. Choi, “Decay constants and radiative decays of heavy mesons in light-front quark model,” *Physical Review D*, vol. 75, Article ID 073016, 2007.
- [29] H.-M. Choi and C.-R. Ji, “Light-front quark model analysis of exclusive $0^- \rightarrow 0^-$ semileptonic heavy meson decays,” *Physics Letters B*, vol. 460, pp. 461–466, 1999.
- [30] H. Cheng, C. Chua, and C. Hwang, “Covariant light-front approach for s-wave and p-wave mesons: Its application to decay constants and form factors,” *Physical Review D: Particles, Fields, Gravitation and Cosmology*, vol. 69, no. 7, 2004.
- [31] C. Q. Geng, C. W. Hwang, C. C. Lih, and W. M. Zhang, “Mesonic tensor form factors with the light front quark model,” *Physical Review D: Particles, Fields, Gravitation and Cosmology*, vol. 64, no. 11, Article ID 114024, 2001.
- [32] C. Y. Cheung, C. W. Hwang, and W. M. Zhang, “ $B \rightarrow \pi l N$ form factors calculated on the light-front,” *Zeitschrift für Physik C Particles and Fields*, vol. 75, pp. 657–664, 1997.

- [33] C. Q. Geng, C. C. Lih, and W. Zhang, “Radiative leptonic,” *Physical Review D: Particles, Fields, Gravitation and Cosmology*, vol. 57, no. 9, pp. 5697–5702, 1998.
- [34] C. C. Lih, C. Q. Geng, and W.-M. Zhang, “Study of $B_c^+ \rightarrow l^+ \nu_l \gamma$ decays in the light front model,” *Physical Review D*, vol. 59, Article ID 114002, 1999.
- [35] M. S. Alam et al., “First measurement of the rate for the inclusive radiative penguin decay $b \rightarrow s \gamma$,” *Physical Review Letters*, vol. 74, Article ID 2885, 1995.
- [36] R. Ammar et al., “Evidence for penguin-diagram decays: first observation of $B \rightarrow K^*(892)\gamma$,” *Physical Review Letters*, vol. 71, p. 674, 1993.
- [37] A. J. Bevan et al., “The physics of the B factories,” *The Physics of the B Factories*, vol. 74, p. 3026, 2014.
- [38] A. J. Bevan, “B factories,” *Comptes Rendus Physique*, vol. 13, no. 2, pp. 145–151, 2012.
- [39] C. Langenbruch, LHCb Collaboration et al., “Contribution to the proceedings of the 51st Rencontres de Moriond,” QCD Session, 2016.
- [40] B. Adeva, LHCb Collaboration et al., “Flavour physics at LHCb,” in *Proceedings of the 4th International Conference on New Frontiers in Physics*, vol. 126, 2016.
- [41] J. He et al., “Electroweak penguins at LHCb,” *Nuclear and Particle Physics Proceedings*, vol. 273, pp. 1370–1375, 2016.
- [42] S. S. Gershtein, V. V. Kiselev, A. K. Likhoded, and A. V. Tkabladze, “Reviews of topical problems: physics of B_c -mesons,” *Physics-Uspokhi*, vol. 38, no. 1, pp. 1–37, 1995.
- [43] H. Cheng, C. Cheung, and C. Hwang, “Mesonic form factors and the Isgur-Wise function on the light front,” *Physical Review D: Particles, Fields, Gravitation and Cosmology*, vol. 55, no. 3, pp. 1559–1577, 1997.
- [44] C. Q. Geng, C. W. Hwang, and C. C. Liu, “Study of rare $B_c^+ \rightarrow D_{ds}^{(*)+} \bar{l} l$ decays,” *Physical Review D: Particles, Fields, Gravitation and Cosmology*, vol. 65, Article ID 094037, 2002.
- [45] K. Azizi and R. Khosravi, “Analysis of the rare semileptonic,” *Physical Review D: Particles, Fields, Gravitation and Cosmology*, vol. 78, no. 3, 2008.
- [46] H.-M. Choi, “Light-front quark model analysis of the exclusive rare $B_c \rightarrow D_{(s)}(\ell^+ \ell^-, \nu_\ell \bar{\nu}_\ell)$ decays,” *Physical Review D*, vol. 81, Article ID 054003, 2010.
- [47] S. J. Brodsky, H.-C. Pauli, and S. S. Pinsky, “Quantum chromodynamics and other field theories on the light cone,” *Physics Reports*, vol. 301, no. 4-6, pp. 299–486, 1998.
- [48] G. P. Lepage and S. J. Brodsky, “Exclusive processes in perturbative quantum chromodynamics,” *Physical Review D: Particles, Fields, Gravitation and Cosmology*, vol. 22, article 2157, 1980.
- [49] P. A. Dirac, “Forms of relativistic dynamics,” *Reviews of Modern Physics*, vol. 21, pp. 392–399, 1949.
- [50] S. J. Brodsky and H. C. Pauli, “Light-cone quantization of quantum chromodynamics,” *Lecture Notes in Physics*, vol. 396, pp. 51–121, 1991.
- [51] S. J. Brodsky, “SLAC-PUB-8627 Presented at VII Hadron Physics 2000,” Caraguatutuba, Sao Paulo, Brazil, April 10-15, 2000.
- [52] S. J. Brodsky, “QCD phenomenology and light-front wavefunctions,” *Acta Physica Polonica B*, vol. 32, pp. 4013–4068, 2001.
- [53] C.-D. Lu, W. Wang, and Z.-T. Wei, “Heavy-to-light form factors on the light cone,” *Physical Review D*, vol. 76, Article ID 014013, 2007.
- [54] S. D. Drell and T.-M. Yan, “Connection of elastic electromagnetic nucleon form factors at large Q^2 and deep inelastic structure functions near threshold,” *Physical Review Letters*, vol. 24, p. 181, 1970.
- [55] G. B. West, “Phenomenological model for the electromagnetic structure of the proton,” *Physical Review Letters*, vol. 24, no. 21, pp. 1206–1209, 1970.
- [56] H. Choi, C. Ji, and L. S. Kisslinger, “Light-front quark model analysis of rare,” *Physical Review D: Particles, Fields, Gravitation and Cosmology*, vol. 65, no. 7, 2002.
- [57] B. Grinstein, M. B. Wise, and M. J. Savage, “ $B \rightarrow X_s e^+ e^-$ in the six-quark model,” *Nuclear Physics B*, vol. 319, no. 2, pp. 271–290, 1989.
- [58] T. Wang, T. Liu, D. Zhang, and B. Ma, “ B_c meson rare decays in the light-cone quark model,” *The European Physical Journal C*, vol. 71, no. 9, p. 1758, 2011.
- [59] C. Patrignani, Particle Data Group et al., “Review of particle physics,” *Chinese Physics C*, vol. 40, no. 10, Article ID 100001, 2016.

Research Article

Standard Model Effective Potential from Trace Anomalies

Renata Jora 

National Institute of Physics and Nuclear Engineering, P.O. Box MG-6, Bucharest-Magurele, Romania

Correspondence should be addressed to Renata Jora; crjora@yahoo.com

Received 15 November 2017; Revised 18 January 2018; Accepted 24 January 2018; Published 12 March 2018

Academic Editor: Andrzej Okniński

Copyright © 2018 Renata Jora. This is an open access article distributed under the Creative Commons Attribution License, which permits unrestricted use, distribution, and reproduction in any medium, provided the original work is properly cited. The publication of this article was funded by SCOAP³.

By analogy with the low energy QCD effective linear sigma model, we construct a standard model effective potential based entirely on the requirement that the tree level and quantum level trace anomalies must be satisfied. We discuss a particular realization of this potential in connection with the Higgs boson mass and Higgs boson effective couplings to two photons and two gluons. We find that this kind of potential may describe well the known phenomenology of the Higgs boson.

1. Introduction

With the discovery of the electroweak Higgs boson by the ATLAS [1] and CMS [2] experiments, the standard model has entered an era of unprecedented experimental confirmation with few hints with regard to its possible extensions to accommodate other particles, interactions, or symmetries. Even in its early years, the standard model Higgs boson has been the subject of a flurry of theoretical papers that dealt with its properties [3–9], the effective one or two loops' potential [10–12], naturalness of the electroweak scale [13], or the vacuum stability of the standard model [14–16].

It is relatively straightforward to compute the effective potential for a theory with spontaneous symmetry breaking [11, 12]. This potential then may be renormalization group improved [14, 15], constrained to be scale invariant, and the associated vacuum expectation value or effective mass computed.

Historically, the electroweak model with spontaneous symmetry breaking and the $SU(2)_L \times SU(2)_R$ linear sigma model for low energy QCD have been strongly related. The latter also displays spontaneous symmetry breaking associated with the formation of quark condensates and possessed also three Goldstone bosons, the pions. However the QCD linear sigma model was not straightforwardly derived in some loop order from the more basic QCD as the hadron detailed structure is as of yet unknown but rather based on the specific properties and symmetries already observed in the hadron spectrum. It is worth mentioning that linear

sigma models have long been a basic tool for some effective description for low energy QCD and were generalized to the more comprehensive global group $SU(3)_L \times SU(3)_R$ [17–20] and also to include four quark states [21–25] that can accommodate two scalar and two pseudoscalar nonets. Moreover without the specific knowledge of the detailed interaction, one can add phenomenological terms that mock up the axial [26] and the trace anomalies [27] with significant role in the hadron properties and good agreement with the experimental data.

In this work, we will construct an effective potential based entirely on the trace anomaly terms at tree and quantum level. First in Section 2, we will propose a general version where the parameters are constrained only by the requirement of mocking up exactly the trace anomaly. Then the model will contain a number of unknown parameters which should be determined from the phenomenological data. Further on, in Section 3 based on the analogy with low energy QCD, we introduce a particular version of the same potential where all the parameters are specified. We will study in this context the minimum equations and the mass of the Higgs boson. In Section 4 we analyze in the same framework the Higgs effective couplings to two photons and two gluons, relevant for the associated decay. Section 5 is dedicated to conclusions.

2. Trace Anomaly Induced Potential

We start by considering the relevant part of the standard model Lagrangian apart from the kinetic terms for the

fermions and for the Higgs doublet. Our choice is motivated by the fact that these terms are scale invariant at the tree level and for the quantum renormalized Lagrangian there is no contribution to the trace anomaly since there is no coupling constant in front of these terms. The gauge fields however behave differently; we can always transform the gauge field as $gA_\mu^a \rightarrow A_\mu^a$, where A_μ^a is generic arbitrary gauge field and g is its coupling constant. Then the corresponding kinetic term in the Lagrangian will appear with a factor $1/g^2$ which will contribute to the trace anomaly through its beta function. The relevant part of the Lagrangian is then

$$\begin{aligned} \mathcal{L}_s = & -\frac{1}{4g^2} F^{\alpha\mu\nu} F_{\mu\nu}^a - \frac{1}{4g'^2} G^{\mu\nu} G_{\mu\nu} + (y\bar{q}_L \tilde{\Phi} t_R + \text{h.c.}) \\ & - \frac{m^2}{2} \Phi^\dagger \Phi - \frac{\lambda}{6} (\Phi^\dagger \Phi)^2, \end{aligned} \quad (1)$$

where Φ is the Higgs doublet and

$$\begin{aligned} F_{\mu\nu}^a &= \partial_\mu A_\nu^a - \partial_\nu A_\mu^a + g\epsilon^{abc} A_\mu^b A_\nu^c, \\ G_{\mu\nu} &= \partial_\mu B_\nu - \partial_\nu B_\mu \end{aligned} \quad (2)$$

and $F_{\mu\nu}^a$ is the $SU(2)$ field tensor and $G_{\mu\nu}$ is the $U(1)_Y$ one. Moreover since all fermions except for the top quark have small masses compared to the electroweak scale, we considered only the term pertaining to the top quark and its associated left handed doublet. By definition, all the terms in (1) are gauge invariant.

The next step is to take into account all trace anomalies known at both tree and quantum levels. It is known that the mass terms break scale invariance at tree level. However the quantum breaking of the scale transformation deserves a more detailed discussion. The trace anomaly refers to the renormalized Lagrangian. Then for a general Lagrangian depending on the fields Φ_i (fermions or bosons) and coupling constants λ_i the quantum corrections to the trace anomalies are given by

$$\theta_\mu^\mu = \left[\sum_i \frac{\partial \mathcal{L}}{\partial \Phi_i} \frac{\partial \Phi_i}{\partial \sigma} + \sum_i \frac{\partial \mathcal{L}}{\partial \lambda_i} \frac{\partial \lambda_i}{\partial \sigma} \right] \sigma, \quad (3)$$

where $x' = \exp[\sigma]x$ and σ is the scale associated with the scale transformation. One may write

$$\sum_i \frac{\partial \mathcal{L}}{\partial \lambda_i} \frac{\partial \lambda_i}{\partial \sigma} \sigma = \frac{\partial \mathcal{L}}{\partial \lambda_i} \beta(\lambda_i). \quad (4)$$

Next we observe that in functional sense as it is the case:

$$\left. \frac{\partial \mathcal{L}}{\partial \Phi_i} \right|_f = \frac{\partial \mathcal{L}}{\partial \Phi_i} - \partial_\mu \left(\frac{\partial \mathcal{L}}{\partial_\mu \Phi_i} \right), \quad (5)$$

which is zero by the equation of motion (the subscript f indicates the functional sense). Since the trace anomaly calculations implicitly assume that the equation of motion for the renormalized field is satisfied, then clearly $(\partial \mathcal{L} / \partial \Phi_i)|_f = 0$.

Consequently only the terms that contain coupling constants contribute to the trace anomaly whereas the contribution from the dependence of the renormalized fields with the scale is cancelled by the equation of motion. For a general gauge theory with fermions and scalars, one can make from the beginning the change of variable $A_\mu^a g \rightarrow A_\mu^a$ such that the coupling constant is eliminated from all gauge covariant derivatives. Thus the gauge invariant kinetic terms of the matter fermions or bosons bring no contribution to the trace anomaly.

We shall start with the $U(1)_Y$ gauge group that we will analyze in detail and just write down the results for $SU(2)_L$ and $SU(3)_C$ that can be easily obtained by applying the same procedure. All our calculations and definitions are inspired by the work in [17–20] by analogy with low energy QCD. Thus for a generic Lagrangian of the type,

$$\mathcal{L} = -\frac{1}{2} \partial^\mu \eta \partial_\mu \eta - V(\eta), \quad (6)$$

the new improved energy momentum tensor is defined as

$$\theta_{\mu\nu} = \delta_{\mu\nu} \mathcal{L} + \partial_\mu \eta \partial_\nu \eta - \frac{1}{6} (\partial_\mu \partial_\nu - \delta_{\mu\nu} \square) \eta^2. \quad (7)$$

This leads upon applying the equation of motion for the field η to the following trace of the energy momentum tensor:

$$\theta_{\mu\mu} = \eta \frac{\partial V}{\partial \eta} - 4V. \quad (8)$$

We will apply (8) consistently in all our subsequent calculations of course adjusted to the specific Lagrangian.

The trace anomaly for $U(1)_Y$ reads [28, 29]

$$\theta_\mu^\mu = \frac{\beta(g')}{2g'^3} G^{\mu\nu} G_{\mu\nu}. \quad (9)$$

We rescale the gauge fields back to their original form $B_\mu \rightarrow B_\mu g'$ which leads to

$$\theta_\mu^\mu = \frac{\beta(g')}{2g'} G^{\mu\nu} G_{\mu\nu}. \quad (10)$$

Then we consider Φ a slowly varying background Higgs field and introduce the term

$$\begin{aligned} V_1 = & b_1 G^{\mu\nu} G_{\mu\nu} \ln \left[\frac{x_1 G^{\mu\nu} G_{\mu\nu}}{\Lambda^4} \right] \\ & + b_2 G^{\mu\nu} G_{\mu\nu} \ln \left[\frac{y_1 \Phi^4}{\Lambda^4} \right], \end{aligned} \quad (11)$$

where Λ is some arbitrary scale and b_1 , b_2 , x_1 , and y_1 are arbitrary dimensionless coefficients. We compute the trace of the energy momentum tensor for the potential in (11) as

$$\theta_\mu^\mu = \frac{\partial V_1}{\partial (G^{\mu\nu} G_{\mu\nu})} 4G^{\mu\nu} G_{\mu\nu} + \frac{\partial V_1}{\partial \Phi} \Phi - 4V, \quad (12)$$

to determine that it is

$$\theta_\mu^\mu = (4b_1 + 4b_2) G^{\mu\nu} G_{\mu\nu}, \quad (13)$$

which leads to the constraint $4b_1 + 4b_2 = \beta(g')/2g'$. Then we apply the equation of motion

$$\begin{aligned} \frac{\partial V_1}{\partial (G^{\mu\nu})} &= 2 \left[b_1 G_{\mu\nu} \ln \left[\frac{x_1 G^{\mu\nu} G_{\mu\nu}}{\Lambda^4} \right] + b_1 G_{\mu\nu} \right. \\ &\quad \left. + b_2 G_{\mu\nu} \ln \left[\frac{y_1 \Phi^4}{\Lambda^4} \right] \right] = 0 \end{aligned} \quad (14)$$

and extract the field $G^{\mu\nu}$ from the potential V_1 :

$$G^{\mu\nu} G_{\mu\nu} = \frac{y_1}{x_1} \Phi^4 \exp \left[-1 - \left(\frac{b_2}{b_1} \right) \ln \left[\frac{y_1 \Phi^4}{\Lambda^4} \right] \right]. \quad (15)$$

We introduce the result in (15) into the expression for the potential in (11) to obtain

$$V_1 = -b_1 \frac{y_1}{x_1} \Phi^4 \exp \left[-1 - \left(\frac{b_2}{b_1} + 1 \right) \ln \left[\frac{y_1 \Phi^4}{\Lambda^4} \right] \right]. \quad (16)$$

A similar expression can be determined for $SU(2)_L$:

$$V_2 = -c_1 \frac{y_2}{x_2} \Phi^4 \exp \left[-1 - \left(\frac{c_2}{c_1} + 1 \right) \ln \left[\frac{y_2 \Phi^4}{\Lambda^4} \right] \right], \quad (17)$$

where $4c_1 + 4c_2 = \beta(g)/2g$, y_2 and x_2 are arbitrary dimensionless coefficients, and g is the weak coupling constant. Then the potential induce by $SU(3)_C$ is just

$$V_3 = -d_1 \frac{y_3}{x_3} \Phi^4 \exp \left[-1 - \left(\frac{d_2}{d_1} + 1 \right) \ln \left[\frac{y_3 \Phi^4}{\Lambda^4} \right] \right], \quad (18)$$

with $4d_1 + 4d_2 = \beta(g_3)/2g_3$, y_3 and x_3 arbitrary dimensionless coefficients, and g_3 the strong coupling constant.

One can associate with the trace anomaly corresponding to the top Yukawa term in the Lagrangian the potential

$$\begin{aligned} V_4 &= k_1 (\bar{\Psi}_L \tilde{\Phi} t_R + \text{h.c.}) \ln \left[\frac{(x_4 (\bar{\Psi}_L \tilde{\Phi} t_R + \text{h.c.}))}{\Lambda^4} \right] \\ &\quad + k_2 (\bar{\Psi}_L \tilde{\Phi} t_R + \text{h.c.}) \ln \left[\frac{y_4 \Phi^4}{\Lambda^4} \right], \end{aligned} \quad (19)$$

where the anomaly requires that $4k_1 + 4k_2 = \beta(y)/\sqrt{2}$, where y is the top Yukawa coupling. Here again k_1 and k_2 are arbitrary dimensionless coefficients.

The most interesting and complicated term to evaluate is however that of the mass of the Higgs bosons in conjunction with that of the quadrilinear coupling λ . The mass term is not scale invariant already at tree level and the trace of the

energy momentum tensor will receive corrections also at the quantum level. A suitable potential is then

$$\begin{aligned} V_5 &= \frac{1}{2} \left(m^2 - \frac{\beta(m^2)}{2} \right) \Phi^\dagger \Phi \\ &\quad + r_1 [\Phi^\dagger \Phi]^2 \ln \left[\frac{x_5 [\Phi^\dagger \Phi]^2}{\Lambda^4} \right] \\ &\quad + r_2 [\Phi^\dagger \Phi]^2 \ln \left[\frac{y_5 \Phi^4}{\Lambda^4} \right]. \end{aligned} \quad (20)$$

Here Φ is the regular Higgs doublet and r_1 and r_2 are arbitrary dimensionless coefficients. First term gives the correct mass anomaly and the second and third terms give the correct λ anomaly provided that $4r_1 + 4r_2 = \beta(\lambda)/24$. The equation of motion $\partial V_5 / \partial \Phi = 0$ leads to

$$\begin{aligned} &2r_1 [\Phi^\dagger \Phi] \ln \left[\frac{x_5 [\Phi^\dagger \Phi]^2}{\Lambda^4} \right] + 2r_1 [\Phi^\dagger \Phi] \\ &\quad + 2r_2 [\Phi^\dagger \Phi] \ln \left[\frac{y_5 \Phi^4}{\Lambda^4} \right] + \frac{1}{2} \left(m^2 - \frac{\beta(m^2)}{2} \right) \\ &= 0. \end{aligned} \quad (21)$$

Equation (21) is a transcendental equation. To solve it, we first make the notations:

$$\begin{aligned} X &= [\Phi^\dagger \Phi], \\ a &= 4d_1, \\ b &= 2d_1 \ln \left[\frac{x_5}{\Lambda^4} \right] + 2d_2 \ln \left[\frac{y_5 \Phi^4}{\Lambda^4} \right] + 2d_1, \\ c &= \frac{1}{2} \left(m^2 - \frac{\beta(m^2)}{2} \right). \end{aligned} \quad (22)$$

Then (21) may be rewritten as

$$aX \ln [X] + bX + c = 0. \quad (23)$$

We denote $Y = \exp[b/a]X$ to determine

$$Y = W \left[-\frac{c}{a} \exp \left[\frac{b}{a} \right] \right], \quad (24)$$

where $W(x)$ is the Lambert function. We can assume $x = -(c/a) \exp[b/a]$ to be small (making the final choice of the coefficients as such), in which case $W(x) \approx x$. This leads to

$$X = \exp \left[-\frac{b}{a} - \frac{c}{a} \exp \left[\frac{b}{a} \right] \right]. \quad (25)$$

We introduce (25) into (20) to determine

$$V_5 = c \exp \left[-\frac{b}{a} \right] - \frac{a}{4} \exp \left[-\frac{2b}{a} \right], \quad (26)$$

or by using (22)

$$\begin{aligned} V_5 = & \frac{1}{2} \left(m^2 - \frac{\beta(m^2)}{2} \right) \frac{\sqrt{y_5}}{\sqrt{x_5}} \\ & \cdot \exp \left[-\frac{1}{2} - \frac{1}{2} \left(1 + \frac{r_2}{r_1} \right) \ln \left[\frac{y_5 \Phi^4}{\Lambda^4} \right] \right] - d_1 \frac{y_5}{x_5} \\ & \cdot \Phi^4 \exp \left[-1 - \left(1 + \frac{r_2}{r_1} \right) \ln \left[\frac{y_5 \Phi^4}{\Lambda^4} \right] \right]. \end{aligned} \quad (27)$$

The full potential is then

$$V = V_1 + V_2 + V_3 + V_4 + V_5 + \frac{1}{24} \lambda \Phi^4. \quad (28)$$

Note that we could safely introduce the λ term because it is scale invariant.

3. Trace Anomaly Inspired Particular Potential

The effective potential in (28) is constructed by analogy with low energy QCD effective models and contains in its most general form 20 parameters and 5 constraints. In order to substantiate that nevertheless this is a good phenomenological model, we need to stress out three important points: (1) The effective potential built here is an all orders potential and even if it contains a proliferation of parameters, these parameters encapsulate the intrinsic dependence on higher order loops without making any explicit calculations. Since computing beta functions and anomalous dimensions is far more amenable than calculating an effective potential or other processes at the same loop order, the apparent complexity leads in essence to an effective simplification. (2) The potential in (28) is completely independent of the nature elementary or composite of the Higgs boson and it is a reliable description also for the case when some strong dynamics are at play in the electroweak symmetry breaking. Note that the composite scenario is not completely excluded by the LHC or other experimental data [30]. (3) The number of parameters may be greatly reduced by making an educated guess of some of the parameters by analogy with low energy QCD [28] or even with the standard construction of the Higgs one-loop effective potential as described in the literature [14, 15]. Thus one can choose from physical arguments related to the

relative renormalization of the wave function of the Higgs field the following expression for the constrained parameters:

$$\begin{aligned} b_1 &= \frac{1}{4} \left[\frac{\beta(g')}{2g'} - \frac{\gamma}{2} \right], \\ c_1 &= \frac{1}{4} \left[\frac{\beta(g)}{2g} - \frac{\gamma}{2} \right], \\ d_1 &= \frac{1}{4} \left[\frac{\beta(g_3)}{2g_3} - \frac{\gamma}{2} \right], \\ b_2 = c_2 = d_2 &= \frac{\gamma}{8}, \\ k_1 &= \frac{1}{4} \left[\frac{\beta(y)}{\sqrt{2}} - \frac{\gamma y}{\sqrt{2}} \right], \\ k_2 &= \frac{1}{4} \frac{\gamma y}{\sqrt{2}}, \\ r_1 &= \frac{1}{4} \left[\frac{\beta(\lambda)}{24} - \frac{4\gamma\lambda}{24} \right], \\ r_2 &= \frac{1}{4} \frac{4\gamma\lambda}{24}. \end{aligned} \quad (29)$$

Here $\beta(g')$, $\beta(g)$, $\beta(g_3)$, $\beta(y)$, and $\beta(\lambda)$ are the beta functions for the coupling constants of the $U(1)_Y$, $SU(2)_L$, and $SU(3)_c$ groups, the quadrilinear term in the Higgs potential, and the top Yukawa coupling, respectively (we use the results in [11]). Moreover γ is the anomalous dimension of the Higgs field.

Moreover the parameters x_i and y_i are redundant because they are already associated with a factor in front of the respective terms so they may be chosen as

$$\begin{aligned} x_1 &= y_1 = \frac{1}{4}, \\ x_2 &= y_2 = \frac{1}{4}, \\ x_3 &= y_3 = \frac{1}{4}, \\ x_4 &= y_4 = \frac{y}{\sqrt{2}}, \\ x_5 &= y_5 = \frac{\lambda}{24}. \end{aligned} \quad (30)$$

Here we took into account as arguments of the logarithm the natural expressions of the scalar polynomials as they appear in the Lagrangian.

Next we will set Φ constant and apply the standard approach for constructing effective potentials. We denote [14, 15]

$$\Phi(t) = \xi(t) \Phi, \quad (31)$$

where t is the running parameter $\mu(t) = m_Z \exp[t]$ and

$$\xi(t) = \exp \left[- \int_0^t \gamma(t') dt' \right]. \quad (32)$$

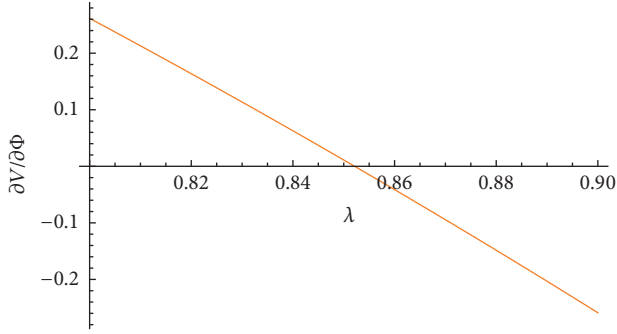


FIGURE 1: Plot of $(\partial V/\partial\Phi)|_{\Phi=\nu}$ as function of the parameter λ in the effective potential V .

Note that, for $\mu(t) = m_Z$, $t_Z = 0$. We consider all the parameters computed at this scale and apply the minimum equation:

$$\left. \frac{\partial V}{\partial\Phi} \right|_{t=t_Z} = 0. \quad (33)$$

In (33), all couplings are known except for λ . We further require that the minimum is obtained for $\Phi = \nu = 246.22$ GeV and solve the minimum equation for the parameter λ . Here we make the underlying assumption that if the potential is phenomenologically viable as an effective potential, then it should lead to a mass of the Higgs boson very close to the actual mass (this is actually exact in the on-shell subtraction scheme where the renormalized mass is equal to the pole one).

In Figure 1, we plot $(\partial V/\partial\Phi)|_{\Phi=\nu}$ in terms of the parameter λ to determine $\lambda = 0.852$. We use this value to further calculate

$$\frac{\partial^2 V}{\partial\Phi^2} = m_h^2. \quad (34)$$

Then the resulting mass of $m_h = 126.15$ GeV is very close to the actual experimental mass of the Higgs boson $m_{h\text{exp}} = 125.09$ GeV. By varying the top Yukawa coupling (here we took $y = m_t/\sqrt{2}\nu$ with the mass of the top quark $m_t = 174.135$ GeV [30]), one can reproduce the exact pole mass of the Higgs boson.

4. Higgs Effective Couplings to Two Photons and Two Gluons

An unusual feature of the potential obtained in Section 2 and particularized in Section 3 is that it contains terms of the type $\ln[G^{\mu\nu}G_{\mu\nu}/\Lambda^4]$ (exemplified here for $U(1)_Y$). These terms are finally integrated out. The logarithms introduce singularities if the fields are close to zero but we fixed the scale of our potential, the electroweak scale, so we expect values of the fields around that scale. For all range of values, however one would need to regularize the corresponding terms. Things can also be regarded differently. Depending on the nature of their beta functions, the couplings of the gauge fields may become strong at higher or lower scales. Then it is

possible that at that scale a phase transition occurs and gauge condensates forms. Neglecting the anomalous dimensions of the gauge fields, then it makes sense to expand the logarithms against the scale where the coupling becomes strong which virtually would be identified with the scale of the condensate. This approach which we will consider here is very helpful in determining the Higgs couplings to two photons and two gluons for the potential in Section 3.

To illustrate this, we first consider the decay of the Higgs boson to two photons discussed in detail in the literature [31–33]. For a Higgs coupling with two photons of the type

$$\frac{1}{2}F_h F^{\mu\nu} F_{\mu\nu} h, \quad (35)$$

where $F^{\mu\nu}$ is the electromagnetic tensor, h is the Higgs boson, and F_h is the coupling, the amplitude of the two-photon decay of the Higgs is [32]

$$\begin{aligned} A(h \rightarrow \gamma\gamma) \\ = F_h (k_{1\mu}\epsilon_{1\nu} - k_{1\nu}\epsilon_{1\mu}) (k_{2\mu}\epsilon_{2\nu} - k_{2\nu}\epsilon_{2\mu}), \end{aligned} \quad (36)$$

where k_1 and k_2 are the momenta of the two photons and ϵ_1 and ϵ_2 are their polarization. In the standard model at one loop [33]

$$F_h = \frac{e^2 g}{(4\pi)^2 m_W} \frac{1}{2} F, \quad (37)$$

where

$$F = F_W(\beta_W) + \sum_f N_c Q_f^2 F_f(\beta_f). \quad (38)$$

Here N_c is the color factor ($N_c = 2$ for leptons and $N_c = 3$ for quarks) and

$$\begin{aligned} \beta_W &= \frac{4m_W^2}{m_h^2}, \\ \beta_f &= \frac{4m_f^2}{m_h^2}. \end{aligned} \quad (39)$$

Furthermore,

$$\begin{aligned} F_W(\beta) &= 2 + 3\beta + 3\beta(2 - \beta)f(\beta), \\ F_f(\beta) &= -2\beta[1 + (1 - \beta)f(\beta)], \end{aligned} \quad (40)$$

with

$$\begin{aligned} f(\beta) &= \arcsin^2(\beta^{-1/2}) \quad \text{for } \beta \geq 1, \\ f(\beta) &= -\frac{1}{4} \left[\ln \left[\frac{1 + \sqrt{1 - \beta}}{1 - \sqrt{1 - \beta}} \right] - i\pi \right]^2. \end{aligned} \quad (41)$$

For the values of the parameters at the electroweak scale and considering only the top quark, the couplings F (of Higgs to two photons) and F_t (of Higgs to two gluons) have the values

$$\begin{aligned} F_t &= -1.376, \\ F &= 6.5. \end{aligned} \quad (42)$$

For comparison, we will determine the Higgs couplings in our potential before integrating out the gauge fields. We will explain in detail how this works for the decay to two photons of the Higgs boson and apply briefly our results to the two-gluon decay of the Higgs boson because the results are very similar. The relevant term in the Lagrangian is

$$\begin{aligned} \mathcal{L}_s = & -b_1 G^{\mu\nu} G_{\mu\nu} \ln \left[\frac{G^{\mu\nu} G_{\mu\nu}}{4m_Z^4} \right] \\ & - b_2 G^{\mu\nu} G_{\mu\nu} \ln \left[\frac{\Phi^4}{4m_Z^4} \right] \\ & - c_1 F^{a\mu\nu} F_{\mu\nu}^a \ln \left[\frac{F_{\mu\nu}^a F^{a\mu\nu}}{4m_Z^4} \right] \\ & - c_2 F^{a\mu\nu} F_{\mu\nu}^a \ln \left[\frac{\Phi^4}{4m_Z^4} \right]. \end{aligned} \quad (43)$$

We expand around the Higgs vev:

$$\ln \left[\frac{\Phi^4}{4m_Z^4} \right] = \ln \left[\frac{(v+h)^4}{4m_Z^4} \right] = \ln \left[\frac{v^4}{4m_Z^4} \right] + \frac{h}{v} + \dots, \quad (44)$$

where we retained only the relevant terms. We use

$$\begin{aligned} G^{\mu\nu} G_{\mu\nu} &= \cos^2 \theta_W F^{\mu\nu} F_{\mu\nu} + \dots, \\ F^{a\mu\nu} F_{\mu\nu}^a &= \sin^2 \theta_W F^{\mu\nu} F_{\mu\nu} + \dots, \end{aligned} \quad (45)$$

where $F^{\mu\nu}$ is the electromagnetic tensor.

The logarithms of the gauge fields are then expanded around the scale where the coupling constant is strong which is $g'^2 = 1$ for the $U(1)_Y$ group (such that $e_a^2 = \cos^2 \theta_W g'^2 = \cos^2 \theta_W$, where e_a^2 is the electric charge at that scale) and $g^2 = 1$ for $SU(2)_L$ (such that $e_b^2 = \sin^2 \theta_W$, where e_b^2 is the electric charge at the second scale). One can use the beta function for the electromagnetic coupling,

$$\frac{de}{d \ln(\mu)} = \frac{1}{16\pi^2} \frac{11}{3} e^3, \quad (46)$$

to integrate it out:

$$\frac{1}{2e_Z^2} - \frac{1}{2e_1^2} = \frac{1}{16\pi^2} \frac{11}{3} \ln \left[\frac{\mu_1}{\mu_Z} \right], \quad (47)$$

where $\mu_Z = m_Z$ is the electroweak scale and μ_1 is the strong coupling scale to find

$$\begin{aligned} \ln \left[\frac{\mu_{1a}^4}{m_Z^4} \right] &= \frac{6}{11} 16\pi^2 \left[\frac{1}{e_Z^2} - \frac{1}{\cos^2 \theta_W} \right], \\ \ln \left[\frac{\mu_{1b}^4}{m_Z^4} \right] &= \frac{6}{11} 16\pi^2 \left[\frac{1}{e_Z^2} - \frac{1}{\sin^2 \theta_W} \right], \end{aligned} \quad (48)$$

where μ_{1a} is the scale where $g'^2 \approx 1$ and μ_{1b} is the scale where $g^2 \approx 1$. Then one can rewrite (43) as

$$\begin{aligned} \mathcal{L}_s = & -b_1 \cos^2 \theta_W F^{\mu\nu} F_{\mu\nu} \ln \left[\frac{\mu_{1a}^4}{m_Z^4} \right] \\ & - c_1 \sin^2 \theta_W F^{\mu\nu} F_{\mu\nu} \ln \left[\frac{\mu_{1b}^4}{m_Z^4} \right] \\ & - b_2 F^{\mu\nu} F_{\mu\nu} \ln \left[\frac{v^4}{4m_Z^4} \right] - b_2 F^{\mu\nu} F_{\mu\nu} \frac{h}{v} + \dots, \end{aligned} \quad (49)$$

where we omitted the irrelevant terms which are assimilated with interactions. Here we also used the fact that $b_2 = c_2$.

Consequently, the kinetic terms for the electromagnetic field receive a factor s

$$\begin{aligned} s = & 4b_1 \cos^2 \theta_W \frac{6}{11} 16\pi^2 \left[\frac{1}{e_Z^2} - \frac{1}{\cos^2 \theta_W} \right] \\ & + 4c_1 \sin^2 \theta_W \frac{6}{11} 16\pi^2 \left[\frac{1}{e_Z^2} - \frac{1}{\sin^2 \theta_W} \right] \\ & + 4b_2 \ln \left[\frac{v^4}{4m_Z^4} \right], \end{aligned} \quad (50)$$

which leads to an amplitude of Higgs decay to two photons as follows:

$$\begin{aligned} A_V(h \rightarrow \gamma\gamma) &= \frac{-8b_2}{vs} (k_{1\mu}\epsilon_{1\nu} - k_{1\nu}\epsilon_{1\mu}) (k_{2\mu}\epsilon_{2\nu} - k_{2\nu}\epsilon_{2\mu}). \end{aligned} \quad (51)$$

From (36), (37), and (51), we obtain the correspondence:

$$\frac{-8b_2}{s} \rightarrow F, \quad (52)$$

where, for our model,

$$\frac{-8b_2}{s} = 6.821. \quad (53)$$

The result in (53) is very close to the value for the one loop in the standard model computed in (42).

The same method can be applied to the two-gluon decay of the Higgs boson at the scale of reference Λ_{QCD} such that

$$\ln \frac{\Lambda_{\text{QCD}}^4}{m_Z^4} = 16\pi^2 \left(-\frac{7}{2} \frac{1}{g_{3Z}^2} \right), \quad (54)$$

where g_{3Z} is the strong coupling constant at the electroweak scale m_Z . The kinetic term for the gluon field will receive a factor:

$$s' = 4d_1 \left(-\frac{2}{7} 16\pi^2 \frac{1}{g_{3Z}^2} \right) + 4d_2 \ln \left[\frac{v^4}{4m_Z^4} \right]. \quad (55)$$

The amplitude of Higgs decaying to two gluons is

$$\begin{aligned} A(h \rightarrow gg) &= \frac{-8d_2}{s'v} (k_{1\mu}\epsilon_{1\nu}^a - k_{1\nu}\epsilon_{1\mu}^a) (k_{2\mu}\epsilon_{2\nu}^a - k_{2\nu}\epsilon_{2\mu}^a). \end{aligned} \quad (56)$$

Here k_1 and k_2 are the momenta of the two gluons and ϵ_1^a and ϵ_2^a are their polarization. Then from (37) and (56), the following correspondence is obtained:

$$\frac{-8d_2}{s'} \longrightarrow f_2, \quad (57)$$

where for our model $-8d_2/s' = -1.091$ again very close to the standard model value computed at one loop in (37).

In this section, we computed the decay widths to two photons and two gluons of the Higgs boson in the context of an effective model. These decay widths as stated here depend on four parameters b_2 , d_2 , s , and s' which in their turn depend on the top Yukawa and the gauge coupling constants. Again from low energy QCD [26, 27], we learn that in the context of an effective theory one should not expect that the parameters that describe the effective widths should be directly related to those employed in standard tree level or one-loop calculations or to those employed in other types of models that describe the same processes. For a phenomenological model to be viable, it is necessary and sufficient only that the phenomenological result is aligned to the experimental data or other consistent theoretical results.

5. Conclusions

In this work, we proposed an effective Higgs model constructed not by integrating out at one or two loops the gauge, fermion, and scalar degrees of freedom but by analogy with the low energy QCD linear sigma models. Thus this kind of model may be suitable for both when the Higgs boson is elementary and also when it is the result of some unknown strong dynamics. All terms in this potential apart from the λ term are directly derived from the trace anomaly expressed as the product between the beta function of the coupling constant and the two-dimensional or four-dimensional operators characterized by it. First we constructed a general potential that contained a number of 20 parameters along with 5 constraints. In this case, available phenomenological data might be used to fix the parameters.

Next we consider a particular case of the potential again inspired by the construction of low energy QCD effective models [28] and also from the construction of the standard one-loop effective Higgs models [14, 15]. Moreover we eliminated all redundant parameters. We fixed the scale of our model at $\mu = m_Z$ and applied the minimum condition $\partial V/\partial\Phi = 0$ for $\Phi = \nu$ to determine the value of the quadrilinear coupling constant λ . With this value, we further computed the Higgs mass as $\partial^2 V/\partial\Phi^2 = m_h^2$. Our result of $m_h = 126.15$ GeV agreed well with the known experimental value of the Higgs boson $m_{h_{\text{exp}}} = 125.09 \pm 0.24$ GeV.

In the same framework but before integrating out the gauge degrees of freedom, we determined the effective Higgs couplings to two photons and two gluons again in good accordance with what we know from one-loop calculations. This shows that the particular case of the model we proposed already describes very well at least a few phenomenological quantities. The potential derived here can be used to extract other possible couplings along the same lines.

The presence of a large number of parameters in the most general version of the model constructed here should not be regarded as a lack of predictability as compared to standard calculations at some loop order of the effective potential but as a way of encapsulating our lack of knowledge with regard to higher loop corrections to the phenomenological parameters. Since in general it is easier to compute beta functions and anomalous dimensions than intricate processes, this kind of model, especially if one uses physical arguments to further constrain or determine some of the parameters, may have important applications.

One potential application of our model would be to study the vacuum stability of the standard model. This topic was thoroughly studied in the framework of regular one-loop or two-loop renormalization improved effective potentials [11, 12]. Some authors [34, 35] argued that since the actual mass of the Higgs boson discovered at the LHC situates the standard model at the border between absolute stability and metastability, the lack of gauge invariance of usual effective model may play a negative role in this issue. Of course any effective potential expressed in terms of the classical field is nongauge invariant but any physical quantities obtained from it should be gauge invariant. Not only does the potential constructed here satisfy in detail the trace anomaly, but also, in its primitive form before integrating out the gauge, fermions and scalars degrees of freedom have all the terms gauge invariant again apart from the classical field. Then one can extract useful gauge invariant effective couplings of the Higgs boson with the other fields in the standard model Lagrangian.

Other possible aspects and applications of our method will be investigated in further work.

Conflicts of Interest

The author declares that they have no conflicts of interest.

References

- [1] G. Aad, T. Abajyan, B. Abbott et al., "Observation of a new particle in the search for the Standard Model Higgs boson with the ATLAS detector at the LHC," *Physics Letters B*, vol. 716, no. 1, pp. 1–29, 2012.
- [2] S. Chatrchyan, V. Khachatryan, A. M. Sirunyan et al., "Observation of a new boson at a mass of 125 gev with the cms experiment at the lhc," *Physics Letters B*, vol. 716, no. 1, pp. 30–61, 2012.
- [3] S. L. Glashow, "Partial-symmetries of weak interactions," *Nuclear Physics A*, vol. 22, no. 4, pp. 579–588, 1961.
- [4] S. Weinberg, "A model of leptons," *Physical Review Letters*, vol. 19, no. 21, pp. 1264–1266, 1967.
- [5] A. Salam, "Elementary particle theory," N. Svartholm, Ed., p. 367, Almquist and Wiksells, Stockholm, Sweden, 1969.
- [6] J. Goldstone, A. Salam, and S. Weinberg, "Broken symmetries," *Physical Review A: Atomic, Molecular and Optical Physics*, vol. 127, no. 3, pp. 965–970, 1962.
- [7] F. Englert and R. Brout, "Broken symmetry and the mass of gauge vector mesons," *Physical Review Letters*, vol. 13, pp. 321–323, 1964.

- [8] P. W. Higgs, “Broken symmetries and the masses of gauge bosons,” *Physical Review Letters*, vol. 13, pp. 508–509, 1964.
- [9] G. S. Guralnik, C. R. Hagen, and T. W. B. Kibble, “Global conservation laws and massless particles,” *Physical Review Letters*, vol. 13, no. 20, pp. 585–587, 1964.
- [10] M. Sher, “Electroweak Higgs potential and vacuum stability,” *Physics Reports*, vol. 179, no. 5–6, pp. 273–418, 1989.
- [11] C. Ford, D. R. T. Jones, and W. Stephenson, “The effective potential and the renormalisation group,” *Nuclear Physics B*, vol. 395, pp. 17–34, 1993.
- [12] M. B. Einhorn and D. R. T. Jones, “The effective potential, the renormalization group and vacuum stability,” *Journal of High Energy Physics*, vol. 2007, no. 4, 051 pages, 2007.
- [13] M. J. G. Veltman, “The infrared-ultraviolet connection,” *Acta Physica Polonica Series B*, vol. 12, no. 5, pp. 437–457, 1981.
- [14] J. A. Casas, J. R. Espinosa, and M. Quirós, “Improved Higgs mass stability bound in the standard model and implications for supersymmetry,” *Physics Letters B*, vol. 342, no. 1–4, pp. 171–179, 1995.
- [15] J. A. Casas, J. R. Espinosa, M. Quirós, and A. Riotto, “The lightest Higgs boson mass in the Minimal Supersymmetric Standard Model,” *Nuclear Physics B*, vol. 436, no. 1–2, pp. 3–29, 1995.
- [16] G. Degrandi, S. Di Vita, J. Elias-Miró et al., “Higgs mass and vacuum stability in the Standard Model at NNLO,” *Journal of High Energy Physics*, vol. 2012, no. 8, article 98, 2012.
- [17] J. Schechter and Y. Ueda, “General Treatment of the Breaking of Chiral Symmetry and Scale Invariance in the,” *Physical Review D: Particles, Fields, Gravitation and Cosmology*, vol. 3, no. 11, pp. 2874–2893, 1971.
- [18] C. Rosenzweig, J. Schechter, and C. G. Trahern, “Is the effective Lagrangian for quantum chromodynamics a model?” *Physical Review D: Particles, Fields, Gravitation and Cosmology*, vol. 21, no. 12, pp. 3388–3392, 1980.
- [19] C. Rosenzweig, A. Salomone, and J. Schechter, “Pseudoscalar glueball, the axial-vector anomaly, and the mixing problem for pseudoscalar mesons,” *Physical Review D: Particles, Fields, Gravitation and Cosmology*, vol. 24, no. 9, pp. 2545–2548, 1981.
- [20] D. Black, A. H. Fariborz, S. Moussa, S. Nasri, and J. Schechter, “Unitarized pseudoscalar meson scattering amplitudes from three flavor linear sigma models,” *Physical Review D: Particles, Fields, Gravitation and Cosmology*, vol. 64, no. 1, 2001.
- [21] A. H. Fariborz, R. Jora, and J. Schechter, “Toy model for two chiral nonets,” *Physical Review D: Particles, Fields, Gravitation and Cosmology*, vol. 72, no. 3, 2005.
- [22] A. H. Fariborz, R. Jora, and J. Schechter, “Two chiral nonet model with massless quarks,” *Physical Review D: Particles, Fields, Gravitation and Cosmology*, vol. 77, no. 3, 2008.
- [23] A. H. Fariborz, R. Jora, and J. Schechter, “Model for light scalar mesons in QCD,” *Physical Review D: Particles, Fields, Gravitation and Cosmology*, vol. 76, no. 1, 2007.
- [24] A. H. Fariborz, R. Jora, and J. Schechter, “Note on a sigma model connection with instanton dynamics,” *Physical Review D: Particles, Fields, Gravitation and Cosmology*, vol. 77, no. 3, 2008.
- [25] A. H. Fariborz, R. Jora, and J. Schechter, “Global aspects of the scalar meson puzzle,” *Physical Review D: Particles, Fields, Gravitation and Cosmology*, vol. 79, no. 7, 2009.
- [26] A. H. Fariborz and R. Jora, “Generalized fermion symmetry, its currents algebra, and Ward-Takahashi identities,” *Physical Review D: Particles, Fields, Gravitation and Cosmology*, vol. 95, no. 11, 2017.
- [27] A. H. Fariborz and R. Jora, “Electromagnetic trace anomaly in a generalized linear sigma model,” *Physical Review D: Covering Particles, Fields, Gravitation, and Cosmology*, vol. 96, 2017.
- [28] J. Schechter, “A two glueball effective Lagrangian,” *Syracuse University preprint*, 23 pages, 1979, SU-4217-155, COO-3533-155.
- [29] M. E. Peskin and D. V. Schroeder, *An Introduction to Quantum Field Theory*, Westview Press, Reading, Mass, USA, 1995.
- [30] C. Patrignani (Particle Data Group) et al., “The review of particle physics,” *Chinese Physics C*, vol. 40, no. 10, 2016.
- [31] J. Ellis, M. K. Gaillard, and D. V. Nanopoulos, “A phenomenological profile of the Higgs boson,” *Nuclear Physics B*, vol. 106, pp. 292–340, 1976.
- [32] M. A. Shifman, A. I. Vainshtein, M. B. Voloshin, and V. I. Zakharov, “Low energy theorems for Higgs boson coupling with photons,” *Sov. J. Nucl. Phys.*, vol. 30, pp. 711–716, 1979.
- [33] W. J. Marciano, C. Zhang, and S. Willenbrock, “Higgs decay to two photons,” *Physical Review D: Particles, Fields, Gravitation and Cosmology*, vol. 85, no. 1, 2012.
- [34] A. Andreassen, W. Frost, and M. D. Schwartz, “Precision decay rate calculations in quantum field theory,” *Physical Review D: Particles, Fields, Gravitation and Cosmology*, vol. 95, no. 8, 2017.
- [35] A. Andreassen, W. Frost, and M. D. Schwartz, “Direct Approach to Quantum Tunneling,” *Physical Review Letters*, vol. 117, no. 23, 2016.